

*Compact and Broadband Microstrip Antennas.* Kin-Lu Wong  
Copyright © 2002 John Wiley & Sons, Inc.  
ISBNs: 0-471-41717-3 (Hardback); 0-471-22111-2 (Electronic)

# **Compact and Broadband Microstrip Antennas**

---

# **Compact and Broadband Microstrip Antennas**

---

**KIN-LU WONG**



A WILEY-INTERSCIENCE PUBLICATION  
**JOHN WILEY & SONS, INC.**

Designations used by companies to distinguish their products are often claimed as trademarks. In all instances where John Wiley & Sons, Inc., is aware of a claim, the product names appear in initial capital or ALL CAPITAL LETTERS. Readers, however, should contact the appropriate companies for more complete information regarding trademarks and registration.

Copyright © 2002 by John Wiley & Sons, Inc., New York. All rights reserved.

No part of this publication may be reproduced, stored in a retrieval system or transmitted in any form or by any means, electronic or mechanical, including uploading, downloading, printing, decompiling, recording or otherwise, except as permitted under Sections 107 or 108 of the 1976 United States Copyright Act, without the prior written permission of the Publisher. Requests to the Publisher for permission should be addressed to the Permissions Department, John Wiley & Sons, Inc., 605 Third Avenue, New York, NY 10158-0012, (212) 850-6011, fax (212) 850-6008, E-Mail: PERMREQ@WILEY.COM.

This publication is designed to provide accurate and authoritative information in regard to the subject matter covered. It is sold with the understanding that the publisher is not engaged in rendering professional services. If professional advice or other expert assistance is required, the services of a competent professional person should be sought.

**ISBN 0-471-22111-2**

This title is also available in print as ISBN 0-471-41717-3.

For more information about Wiley products, visit our web site at [www.Wiley.com](http://www.Wiley.com).

# Contents

---

<b>Preface</b>	<b>ix</b>
<b>1 Introduction and Overview</b>	<b>1</b>
1.1 Introduction	1
1.2 Compact Microstrip Antennas	1
1.3 Compact Broadband Microstrip Antennas	7
1.4 Compact Dual-Frequency Microstrip Antennas	8
1.5 Compact Dual-Polarized Microstrip Antennas	10
1.6 Compact Circularly Polarized Microstrip Antennas	10
1.7 Compact Microstrip Antennas with Enhanced Gain	12
1.8 Broadband Microstrip Antennas	12
1.9 Broadband Dual-Frequency and Dual-Polarized Microstrip Antennas	14
1.10 Broadband and Dual-Band Circularly Polarized Microstrip Antennas	15
<b>2 Compact Microstrip Antennas</b>	<b>22</b>
2.1 Introduction	22
2.2 Use of a Shorted Patch with a Thin Dielectric Substrate	23
2.3 Use of a Meandered Patch	26
2.4 Use of a Meandered Ground Plane	28
2.5 Use of a Planar Inverted-L Patch	33
2.6 Use of an Inverted U-Shaped or Folded Patch	39
<b>3 Compact Broadband Microstrip Antennas</b>	<b>45</b>
3.1 Introduction	45

3.2	Use of a Shorted Patch with a Thick Air Substrate	46
3.2.1	Probe-Fed Shorted Patch or Planar Inverted-F Antenna (PIFA)	46
3.2.2	Aperture-Coupled Shorted Patch	48
3.2.3	Microstrip-Line-Fed Shorted Patch	50
3.2.4	Capacitively Coupled or L-Probe-Fed Shorted Patch	53
3.3	Use of Stacked Shorted Patches	54
3.4	Use of Chip-Resistor and Chip-Capacitor Loading Technique	55
3.4.1	Design with a Rectangular Patch	55
3.4.2	Design with a Circular Patch	59
3.4.3	Design with a Triangular Patch	70
3.4.4	Design with a Meandered PIFA	76
3.5	Use of a Slot-Loading Technique	78
3.6	Use of a Slotted Ground Plane	79
<b>4</b>	<b>Compact Dual-Frequency and Dual-Polarized Microstrip Antennas</b>	<b>87</b>
4.1	Introduction	87
4.2	Some Recent Advances in Regular-Size Dual-Frequency Designs	88
4.2.1	Dual-Frequency Operation with Same Polarization Planes	88
4.2.2	Dual-Frequency Operation with Orthogonal Polarization Planes	104
4.2.3	Dual-Frequency Feed Network Designs	108
4.3	Compact Dual-Frequency Operation with Same Polarization Planes	111
4.3.1	Design with a Pair of Narrow Slots	112
4.3.2	Design with a Shorted Microstrip Antenna	115
4.3.3	Design with a Triangular Microstrip Antenna	121
4.4	Compact Dual-Frequency Operation	129
4.4.1	Design with a Rectangular Microstrip Antenna	129
4.4.2	Design with a Circular Microstrip Antenna	140
4.4.3	Design with a Triangular Microstrip Antenna	146
4.5	Dual-Band or Triple-Band PIFA	149
4.6	Compact Dual-Polarized Designs	149
4.6.1	Design with a Slotted Square Patch	149
4.6.2	Design with a Slotted Ground Plane	154
4.6.3	Design with a Triangular Patch	156
<b>5</b>	<b>Compact Circularly Polarized Microstrip Antennas</b>	<b>162</b>
5.1	Introduction	162
5.2	Designs with a Cross-Slot of Unequal Arm Lengths	162
5.3	Designs with a Y-Shaped Slot of Unequal Arm Lengths	168

5.4	Designs with Slits	172
5.4.1	With a Slit	172
5.4.2	With a Pair of Slits	177
5.4.3	With Four Inserted Slits	181
5.5	Designs with Spur Lines	192
5.6	Designs with Truncated Corners	193
5.6.1	With a Triangular Patch	194
5.6.2	With a Square-Ring Patch	194
5.6.3	With a Triangular-Ring Patch	198
5.6.4	With a Slotted Square Patch	201
5.7	Designs with Peripheral Cuts	203
5.8	Designs with a Tuning Stub	205
5.8.1	With a Circular Patch	205
5.8.2	With a Square-Ring Patch	209
5.8.3	With a Triangular Patch	211
5.9	Designs with a Bent Tuning Stub	213
5.10	Compact CP Designs with an Inset Microstrip-Line Feed	215
<b>6</b>	<b>Compact Microstrip Antennas with Enhanced Gain</b>	<b>221</b>
6.1	Introduction	221
6.2	Compact Microstrip Antennas with High-Permittivity Superstrate	221
6.2.1	Gain-Enhanced Compact Broadband Microstrip Antenna	221
6.2.2	Gain-Enhanced Compact Circularly Polarized Microstrip Antenna	223
6.3	Compact Microstrip Antennas with Active Circuitry	225
<b>7</b>	<b>Broadband Microstrip Antennas</b>	<b>232</b>
7.1	Introduction	232
7.2	Use of Additional Microstrip Resonators	233
7.3	Microstrip Antennas with an Air Substrate	236
7.3.1	Design with a Modified Probe Feed	236
7.3.2	Design with a U-Slotted Patch	237
7.3.3	Design with an E-Shaped Patch	241
7.3.4	Design with a Three-Dimensional V-Shaped Patch	249
7.4	Broadband Slot-Loaded Microstrip Antennas	251
7.4.1	Design with a Rectangular Patch	251
7.4.2	Design with a Circular Patch	260
7.5	Broadband Microstrip Antennas with an Integrated Reactive Loading	261
7.5.1	Design with a Rectangular Patch	261
7.5.2	Design with a Circular Patch	263

7.5.3	Design with a Bow-Tie Patch	267
7.5.4	Design with a Triangular Patch	270
7.6	Broadband Microstrip Antennas with Reduced Cross-Polarization Radiation	273
<b>8</b>	<b>Broadband Dual-Frequency and Dual-Polarized Microstrip Antennas</b>	<b>279</b>
8.1	Introduction	279
8.2	Broadband Dual-Frequency Microstrip Antennas	279
8.2.1	A Two-Element Microstrip Antenna	279
8.2.2	A Three-Dimensional V-Shaped Microstrip Antenna	280
8.3	Broadband Dual-Polarized Microstrip Antennas	282
8.3.1	Use of Two Aperture-Coupled Feeds	282
8.3.2	Use of a Gap-Coupled Probe Feed and an H-Slot Coupled Feed	287
8.3.3	Use of an L-Strip Coupled Feed and an H-Slot Coupled Feed	288
<b>9</b>	<b>Broadband and Dual-Band Circularly Polarized Microstrip Antennas</b>	<b>294</b>
9.1	Introduction	294
9.2	Broadband Single-Feed Circularly Polarized Microstrip Antennas	295
9.3	Broadband Two-Feed Circularly Polarized Microstrip Antennas	298
9.3.1	Use of Two Gap-Coupled Probe Feeds with a Wilkinson Power Divider	298
9.3.2	Use of Two Capacitively Coupled Feeds with a Wilkinson Power Divider	299
9.3.3	Use of Two Capacitively Coupled Feeds with a Branch-Line Coupler	305
9.4	Broadband Four-Feed Circularly Polarized Microstrip Antennas	307
9.5	Dual-Band Circularly Polarized Microstrip Antennas	309
9.5.1	A Probe-Fed Circular Patch with Two Pairs of Arc-Shaped Slots	309
9.5.2	A Probe-Fed Square Patch with a Center Slot and Inserted Slits	312
9.5.3	A Probe-Fed Stacked Elliptic Patch	321
<b>Index</b>		<b>325</b>

# Preface

---

In order to meet the miniaturization requirements of portable communication equipment, researchers have given much attention recently to compact microstrip antennas. Many related compact designs with broadband dual-frequency operation, dual-polarized radiation, circularly polarized radiation, and enhanced antenna gain have been reported. Many significant advances in improving the inherent narrow operating bandwidth of microstrip antennas have been published in the open literature since 1997. By using presently available techniques, one can easily achieve an impedance bandwidth (1:2 voltage standing wave ratio) of larger than 25% for a probe-fed single-patch microstrip antenna. Other feeding methods such as the use of an aperture-coupled feed, a capacitively coupled feed, or a three-dimensional microstrip transition feed can yield impedance bandwidths greater than 40% with good radiation characteristics for a single-patch microstrip antenna. In addition, various designs for achieving broadband circularly polarized radiation, broadband dual-frequency operation, and broadband dual-polarized radiation have been demonstrated. Taking broadband circularly polarized radiation as an example, some recently reported designs exhibit a 3-dB axial-ratio bandwidth greater than 40% for a single-patch microstrip antenna.

Since 1997, the author and his graduate students at National Sun Yat-Sen University, Kaohsiung, Taiwan, have published more than 100 refereed journal papers on the subject of compact and broadband microstrip antennas. These results along with many other advanced designs reported recently by antenna researchers are scattered in many technical journals, and it is the intention of this book to organize these advanced designs in the areas of compact and broadband microstrip antennas.

The microstrip antenna designs covered in this book are divided into two groups: compact microstrip antennas and broadband microstrip antennas. The book is organized into nine chapters. Chapter 1 presents an introduction and overview of recent advances in the design of both compact and broadband microstrip antennas. Chapters 2–6 describe in detail advanced designs for compact microstrip antennas,

compact broadband microstrip antennas, compact dual-frequency and dual-polarized microstrip antennas, compact circularly polarized microstrip antennas, and compact microstrip antennas with enhanced gain, respectively. Chapters 7–9 are devoted respectively to advanced designs for broadband microstrip antennas, broadband dual-frequency and dual-polarized microstrip antennas, and broadband and dual-band circularly polarized microstrip antennas.

Chapter 2 introduces recent advances in compact microstrip antennas. Based on recent compact design techniques, such as using a shorted patch, a meandered patch, a meandered ground plane, an inverted U-shaped patch, a planar inverted-L patch, among others, microstrip antenna designs are discussed in the different sections of this chapter. Details of antenna designs and experimental results are presented.

Chapter 3 discusses compact broadband microstrip antenna designs. Design techniques for achieving broadband operation with a reduced antenna size are described. Related techniques include the use of a shorted patch with a thick air substrate, stacked shorted patches, chip-resistor loading, chip-resistor and chip-capacitor loading, and slot loading in the radiating patch or ground plane. Chapter 4 presents designs for compact dual-frequency and dual-polarized microstrip antennas. Recent advances in regular-size dual-frequency designs are first discussed, and then designs for achieving compact dual-frequency operation with same-polarization and orthogonal polarization planes are described in detail. Both regular-size and compact dual-frequency designs are discussed, which should give the reader a more complete view of recent developments in dual-frequency design. Advances in compact dual-polarized design are also reviewed, and design examples are given.

Advances in compact circularly polarized (CP) microstrip antennas are considered in Chapter 5. Examples of compact CP designs, including those using a probe feed, an edge-fed microstrip-line feed, or an inset-microstrip-line feed, are presented. Designs for achieving gain-enhanced compact microstrip antennas are included in Chapter 6. Some design examples for active compact microstrip antennas and gain-enhanced compact circularly polarized microstrip antennas are given.

Chapter 7 is devoted to recent advances in broadband microstrip antennas. Advances in broadband microstrip antennas with, for example, additional microstrip resonators, an air or a foam substrate, slot loading, or integrated reactive loading are presented and discussed in detail. Broadband designs with reduced cross-polarization radiation are presented. Chapter 8 presents broadband dual-frequency and dual-polarized microstrip antennas. Various design examples are presented, and design considerations for achieving high isolation and low cross-polarization for broadband dual-polarized radiation are addressed.

Finally, in Chapter 9, advances in broadband and dual-band circularly polarized microstrip antennas are discussed. Related broadband designs with single-feed excitation, two-feed excitation with a  $90^\circ$  phase shift, and four-feed excitation with  $0^\circ$ – $90^\circ$ – $180^\circ$ – $270^\circ$  phase shifts are studied. In addition to obtaining a wide axial-ratio bandwidth, it is shown how to improve CP quality in the entire radiation pattern to achieve wide-angle CP coverage, and related designs are presented. Recent advances in dual-band CP radiation are included in this chapter.

This book is intended to organize new advanced designs of compact and broadband microstrip antennas, mainly those reported since 1997. Over 100 advanced microstrip antenna designs and their detailed experimental results are included. It is believed that this book can be a very useful design reference on compact and broadband microstrip antennas for antenna scientists and engineers.

KIN-LU WONG

*Kaohsiung, Taiwan*

# **Compact and Broadband Microstrip Antennas**

# Index

---

- Active circuitry, 225  
Air substrate, *see* Substrate  
Annular-ring patch, 177  
Annular-ring slot, *see* Slot  
Aperture-coupled feed, *see* feed  
Arc-shaped slot, *see* Slot  
  
Bent slot, *see* Slot  
Bent tuning stub, 11, 213  
Bow-tie patch  
    shorted, *see* Shorted patch  
    with integrated reactive loading, *see* Integrated reactive loading  
Branchlike slot, *see* slot  
Branch-line coupler, 305  
Broadband microstrip antenna  
    circularly polarized, 15, 298  
    dual-frequency, 14, 279  
    dual-polarized, 14, 279  
  
Capacitively coupled feed, *see* Feed  
Ceramic substrate, *see* Substrate  
Chip-capacitor loading, 55  
Chip-resistor loading  
    circular patch, 59  
    meandered PIFA, 76  
    rectangular patch, 55  
    triangular patch, 70  
Circular E-patch, 245, 247  
Circularly polarized microstrip antenna  
    broadband, *see* Broadband microstrip antenna  
    compact, *see* Compact microstrip antenna  
    dual-band, 15, 294, 309  
    four-feed, 307  
    single-feed, 295  
    two-feed, 298  
  
Compact microstrip antenna  
    circularly polarized, 10, 162  
    dual-frequency, 8, 88  
    dual-polarized, 10, 88  
    gain-enhanced, 12, 221  
Cross slot of equal arm length, *see* Slot  
Cross slot of unequal arm length, *see* Slot  
Cross strip, *see* Strip  
  
DCS (Digital Communication System), 13  
Directly coupled parasitic patch, *see* Parasitic patch  
Double-folded patch, 5  
Dual-band PIFA, *see* Planar inverted-F antenna (PIFA)  
Dual-frequency feed network, 108  
Dual-frequency microstrip antenna  
    compact, *see* Compact microstrip antenna  
    with orthogonal polarization planes, 104  
    with same polarization planes, 88  
Dual-polarized microstrip antenna  
    broadband, *see* Broadband microstrip antenna  
    compact, *see* Compact microstrip antenna  
Dual-frequency microstrip array, 101  
  
Elliptic patch, 321  
E-shaped patch, 241  
  
Feed  
    aperture-coupled, 282  
    capacitively coupled, 53, 299, 305  
    gap-coupled probe, 287, 298  
    H-slot coupled, 287, 288  
    hybrid, 287, 288  
    inset microstrip-line, 215  
    L-probe, 53

- Feed (*Continued*)
  - L-strip coupled, 273, 288
  - microstrip-line, 50, 215
  - three-dimensional microstrip transition, 236
- Folded patch, 5
- Folded slit, *see* Slit
- Gain-enhanced compact microstrip antenna, *see* Compact microstrip antenna
- Gap-coupled parasitic patch, *see* Parasitic patch
- Gap-coupled probe feed, *see* Feed
- Global Positioning System (GPS), 2
- Ground plane
  - meandered, 28
  - slotted, 79
- GSM (Global System for Mobile Communication), 13
- High-permittivity superstrate, 221
- H-shaped slot, *see* Slot
- H-slot coupled feed, *see* Feed
- Inset microstrip-line feed, *see* Feed
- Integrated reactive loading
  - bow-tie patch, 267
  - circular patch, 263
  - rectangular patch, 261
  - triangular patch, 270
- Inserted slit, *see* Slit
- Inverted U-shaped patch, 39
- Isolation, 152
- L-probe feed, *see* Feed
- L-shaped slit, *see* Slit
- L-strip coupled feed, *see* Feed
- Meandered ground plane, *see* Ground plane
- Meandered patch, 4, 26, 76, 112
- Microstrip antenna
  - broadband, *see* Broadband microstrip antenna
  - circularly polarized, *see* Circularly polarized microstrip antenna
  - compact, *see* Compact microstrip antenna
  - dual-frequency, *see* Dual-frequency microstrip antenna
- Notched square patch, 108
- Offset circular slot, *see* Slot
- Open-ring slot, *see* Slot
- Parasitic patches
  - directly coupled, 233
  - gap-coupled, 233
- Patch surface current distribution, 84
- PCS (Personal Communication System), 13
- Peripheral cuts, 203
- Planar inverted F antenna (PIFA)
  - dual-band, 149
  - triple band, 149
- Planar inverted-L antenna (PILA), 33
- Polarization diversity, 87
- Quarter-wavelength structure, 2
- Reduced cross-polarization radiation, 273
- Shorted patch
  - air substrate, 46
  - aperture-coupled, 48
  - bow-tie patch, 122
  - capacitively coupled, 53
  - circular patch, 118
  - L-probe-fed, 53
  - microstrip-line-fed, 50
  - probe-fed, 46
  - rectangular patch, 115
  - stacked, 54
  - thin dielectric substrate, 23
  - triangular patch, 120
- Shorting pin, 3
- Shorting strip, 3
- Shorting wall, 3
- Slit(s)
  - folded, 9
  - inserted, 4, 6, 9, 112, 173, 175
  - L-shaped, 9, 46
  - T-shaped, 313
  - Y-shaped, 313
- Slot
  - annular-ring, 298
  - arc-shaped, 16, 95
  - bent, 4, 134, 150, 201
  - branchlike, 79
  - circular, 145
  - cross
    - equal arm lengths, 162, 203, 207
    - unequal arm lengths, 163, 164, 213
  - H-shaped, 280, 285
  - modified U-shaped, 255
  - offset circular, 145
  - open-ring, 103, 260
  - square, 141
  - step, 92
  - toothbrush-shaped, 252
  - T-shaped, 139
  - U-shaped, 237

- V-shaped, 126
- Y-shaped, 170
- Slot-loaded microstrip antenna
  - circular patch, 260
  - rectangular patch, 251
- Slotted ground plane, *see* Ground plane
- Slotted radiating patch, 5
- Spur lines, 93, 192
- Stacked elliptic patch, 321
- Stacked shorted patch, *see* Shorted patch
- Step slot, *see* Slot
- Strip
  - cross, 210
  - Y-shaped, 199
- Substrate
  - air, 46
  - ceramic, 2
  - thin dielectric, 23
- Three-dimensional microstrip transition feed,
  - see* Feed
- Three-dimensional V-shaped patch, 280
- Toothbrush-shaped slot, *see* Slot
- Triangular E-patch, 248
- Truncated corners
  - slotted square patch, 188
  - square-ring patch, 197
- Truncated tip
  - square-ring patch, 197
  - triangular patch, 194, 199
- T-shaped slit, *see* Slit
- T-shaped slot, *see* Slot
- Tuning stub, 206, 207, 210, 213
- UMTS (Universal Mobile Telecommunication System), 13
- U-shaped slot, *see* Slot
- U-slotted patch, 237
- V-shaped slot, *see* Slot
- Wedge-shaped patch, 251
- Wilkinson power divider, 298, 299
- Y-shaped slit, *see* Slit
- Y-shaped slot, *see* Slot
- Y-shaped strip, *see* Strip

---

## **WILEY SERIES IN MICROWAVE AND OPTICAL ENGINEERING**

---

**KAI CHANG**, Editor  
Texas A&M University

- FIBER-OPTIC COMMUNICATION SYSTEMS, Second Edition • *Govind P. Agrawal*
- COHERENT OPTICAL COMMUNICATIONS SYSTEMS • *Silvello Betti, Ciancarlo De Marchis and Eugenio Iannone*
- HIGH-FREQUENCY ELECTROMAGNETIC TECHNIQUES: RECENT ADVANCES AND APPLICATIONS • *Asoke K. Bhattacharyya*
- COMPUTATIONAL METHODS FOR ELECTROMAGNETICS AND MICROWAVES •  
*Richard C. Booton, Jr.*
- MICROWAVE RING CIRCUITS AND ANTENNAS • *Kai Chang*
- MICROWAVE SOLID-STATE CIRCUITS AND APPLICATIONS • *Kai Chang*
- RF AND MICROWAVE WIRELESS SYSTEMS • *Kai Chang*
- DIODE LASERS AND PHOTONIC INTEGRATED CIRCUITS • *Larry Coldren and Scott Corzine*
- RADIO FREQUENCY CIRCUIT DESIGN • *W. Alan Davis and Krishna Agarwal*
- MULTICONDUCTOR TRANSMISSION-LINE STRUCTURES: MODAL ANALYSIS TECHNIQUES •  
*J. A. Brandão Faria*
- PHASED ARRAY-BASED SYSTEMS AND APPLICATIONS • *Nick Fourikis*
- FUNDAMENTALS OF MICROWAVE TRANSMISSION LINES • *Jon C. Freeman*
- OPTICAL SEMICONDUCTOR DEVICES • *Mitsuo Fukuda*
- MICROSTRIP CIRCUITS • *Fred Cardiol*
- HIGH-SPEED VLSI INTERCONNECTIONS: MODELING, ANALYSIS, AND SIMULATION •  
*A. K. Goel*
- FUNDAMENTALS OF WAVELETS: THEORY, ALGORITHMS, AND APPLICATIONS •  
*Jaideva C. Goswami and Andrew K. Chan*
- ANALYSIS AND DESIGN OF INTEGRATED CIRCUIT ANTENNA MODULES • *K. C. Gupta and Peter S. Hall*
- PHASED ARRAY ANTENNAS • *R. C. Hansen*
- HIGH-FREQUENCY ANALOG INTEGRATED CIRCUIT DESIGN • *Ravender Goyal (ed.)*
- MICROSTRIP FILTERS FOR RF/MICROWAVE APPLICATIONS • *Jia-Sheng Hong and M. J. Lancaster*
- MICROWAVE APPROACH TO HIGHLY IRREGULAR FIBER OPTICS • *Huang Hung-Chia*
- NONLINEAR OPTICAL COMMUNICATION NETWORKS • *Eugenio Iannone, Francesco Matera, Antonio Mecozzi, and Marina Settembre*
- FINITE ELEMENT SOFTWARE FOR MICROWAVE ENGINEERING • *Tatsuo Itoh, Giuseppe Pelosi and Peter P. Silvester (eds.)*
- INFRARED TECHNOLOGY: APPLICATIONS TO ELECTROOPTICS, PHOTONIC DEVICES, AND SENSORS • *A. R. Jha*
- SUPERCONDUCTOR TECHNOLOGY: APPLICATIONS TO MICROWAVE, ELECTRO-OPTICS, ELECTRICAL MACHINES, AND PROPULSION SYSTEMS • *A. R. Jha*
- OPTICAL COMPUTING: AN INTRODUCTION • *M. A. Karim and A. S. S. Awwal*
- INTRODUCTION TO ELECTROMAGNETIC AND MICROWAVE ENGINEERING • *Paul R. Karmel, Gabriel D. Colef, and Raymond L. Camisa*
- MILLIMETER WAVE OPTICAL DIELECTRIC INTEGRATED GUIDES AND CIRCUITS •  
*Shiban K. Koul*

MICROWAVE DEVICES, CIRCUITS AND THEIR INTERACTION • *Charles A. Lee and G. Conrad Dalman*

ADVANCES IN MICROSTRIP AND PRINTED ANTENNAS • *Kai-Fong Lee and Wei Chen (eds.)*

SPHEROIDAL WAVE FUNCTIONS IN ELECTROMAGNETIC THEORY • *Le-Wei Li, Xiao-Kang Kang, and Mook-Seng Leong*

OPTICAL FILTER DESIGN AND ANALYSIS: A SIGNAL PROCESSING APPROACH •

*Christi K. Madsen and Jian H. Zhao*

THEORY AND PRACTICE OF INFRARED TECHNOLOGY FOR NONDESTRUCTIVE TESTING •

*Xavier P. V. Maldague*

OPTOELECTRONIC PACKAGING • *A. R. Mickelson, N. R. Basavanhally, and Y. C. Lee (eds.)*

OPTICAL CHARACTER RECOGNITION • *Shunji Mori, Hirobumi Nishida, and Hiromitsu Yamada*

ANTENNAS FOR RADAR AND COMMUNICATIONS: A POLARIMETRIC APPROACH •

*Harold Mott*

INTEGRATED ACTIVE ANTENNAS AND SPATIAL POWER COMBINING • *Julio A. Navarro and Kai Chang*

ANALYSIS METHODS FOR RF, MICROWAVE, AND MILLIMETER-WAVE PLANAR TRANSMISSION LINE STRUCTURES • *Cam Nguyen*

FREQUENCY CONTROL OF SEMICONDUCTOR LASERS • *Motoichi Ohtsu (ed.)*

SOLAR CELLS AND THEIR APPLICATIONS • *Larry D. Partain (ed.)*

ANALYSIS OF MULTICONDUCTOR TRANSMISSION LINES • *Clayton R. Paul*

INTRODUCTION TO ELECTROMAGNETIC COMPATIBILITY • *Clayton R. Paul*

ELECTROMAGNETIC OPTIMIZATION BY GENETIC ALGORITHMS • *Yahya Rahmat-Samii and Eric Michielssen (eds.)*

INTRODUCTION TO HIGH-SPEED ELECTRONICS AND OPTOELECTRONICS •  
*Leonard M. Riazat*

NEW FRONTIERS IN MEDICAL DEVICE TECHNOLOGY • *Arye Rosen and Harel Rosen (eds.)*

ELECTROMAGNETIC PROPAGATION IN MULTI-MODE RANDOM MEDIA • *Harrison E. Rowe*

ELECTROMAGNETIC PROPAGATION IN ONE-DIMENSIONAL RANDOM MEDIA •  
*Harrison E. Rowe*

NONLINEAR OPTICS • *E. G. Sauter*

COPLANAR WAVEGUIDE CIRCUITS, COMPONENTS, AND SYSTEMS • *Rainee N. Simons*

ELECTROMAGNETIC FIELDS IN UNCONVENTIONAL MATERIALS AND STRUCTURES •  
*Onkar N. Singh and Akhlesh Lakhtakia (eds.)*

FUNDAMENTALS OF GLOBAL POSITIONING SYSTEM RECEIVERS: A SOFTWARE APPROACH • *James Bao-yen Tsui*

InP-BASED MATERIALS AND DEVICES: PHYSICS AND TECHNOLOGY • *Osamu Wada and Hideki Hasegawa (eds.)*

COMPACT AND BROADBAND MICROSTRIP ANTENNAS • *Kin-Lu Wong*

DESIGN OF NONPLANAR MICROSTRIP ANTENNAS AND TRANSMISSION LINES • *Kin-Lu Wong*

FREQUENCY SELECTIVE SURFACE AND GRID ARRAY • *T. K. Wu (ed.)*

ACTIVE AND QUASI-OPTICAL ARRAYS FOR SOLID-STATE POWER COMBINING •  
*Robert A. York and Zoya B. Popović (eds.)*

OPTICAL SIGNAL PROCESSING, COMPUTING AND NEURAL NETWORKS • *Francis T. S. Yu and Suganda Jutamulia*

SiGe, GaAs, AND InP HETEROJUNCTION BIPOLAR TRANSISTORS • *Jiann Yuan*

ELECTRODYNAMICS OF SOLIDS AND MICROWAVE SUPERCONDUCTIVITY • *Shu-Ang Zhou*

## CHAPTER ONE

---

# Introduction and Overview

---

### 1.1 INTRODUCTION

Conventional microstrip antennas in general have a conducting patch printed on a grounded microwave substrate, and have the attractive features of low profile, light weight, easy fabrication, and conformability to mounting hosts [1]. However, microstrip antennas inherently have a narrow bandwidth, and bandwidth enhancement is usually demanded for practical applications. In addition, applications in present-day mobile communication systems usually require smaller antenna size in order to meet the miniaturization requirements of mobile units. Thus, size reduction and bandwidth enhancement are becoming major design considerations for practical applications of microstrip antennas. For this reason, studies to achieve compact and broadband operations of microstrip antennas have greatly increased. Much significant progress in the design of compact microstrip antennas with broadband, dual-frequency, dual-polarized, circularly polarized, and gain-enhanced operations have been reported over the past several years. In addition, various novel broadband microstrip antenna designs with dual-frequency, dual-polarized, and circularly polarized operations have been published in the open literature. This book organizes and presents these recently reported novel designs for compact and broadband microstrip antennas.

### 1.2 COMPACT MICROSTRIP ANTENNAS

Many techniques have been reported to reduce the size of microstrip antennas at a fixed operating frequency. In general, microstrip antennas are half-wavelength structures and are operated at the fundamental resonant mode  $\text{TM}_{01}$  or  $\text{TM}_{10}$ , with a resonant frequency given by (valid for a rectangular microstrip antenna with a thin microwave substrate)

$$f \cong \frac{c}{2L\sqrt{\epsilon_r}}, \quad (1.1)$$

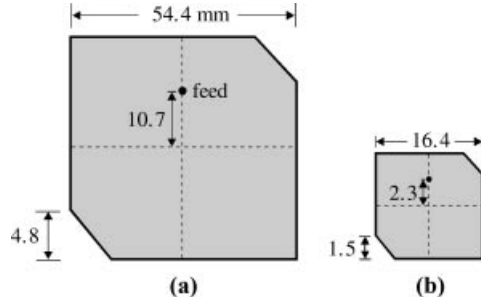


**FIGURE 1.1** Circularly polarized corner-truncated square microstrip antennas for GPS application at 1575 MHz. (a) Design with a microwave substrate ( $\epsilon_r = 3.0$ ,  $h = 1.524$  mm); (b) design with a ceramic substrate ( $\epsilon_r = 28.2$ ,  $h = 4.75$  mm). Dimensions are in millimeters and not to scale.

where  $c$  is the speed of light,  $L$  is the patch length of the rectangular microstrip antenna, and  $\epsilon_r$  is the relative permittivity of the grounded microwave substrate. From (1.1), it is found that the radiating patch of the microstrip antenna has a resonant length approximately proportional to  $1/\sqrt{\epsilon_r}$ , and the use of a microwave substrate with a larger permittivity thus can result in a smaller physical antenna length at a fixed operating frequency. Figure 1.1 shows a comparison of the required dimensions for two circularly polarized corner-truncated square microstrip antennas with different substrates for global positioning system (GPS) application. The first design uses a microwave substrate with relative permittivity  $\epsilon_r = 3.0$  and thickness  $h = 1.524$  mm; the second design uses a high-permittivity or ceramic substrate with  $\epsilon_r = 28.2$  and  $h = 4.75$  mm. The relatively larger substrate thickness for the second design is needed to obtain the required circular polarization (CP) bandwidth for GPS application. From the patch areas of the two designs, it can be seen that the second design has a patch size about 10% of that of the first design. This reduction in antenna size can be expected from (1.1), from which the antenna's fundamental resonant frequency of the design with  $\epsilon_r = 28.2$  is expected to be only about 0.326 times that of the design with  $\epsilon_r = 3.0$  for a fixed patch size. This result suggests that an antenna size reduction as large as about 90% can be obtained if the design with  $\epsilon_r = 28.2$  is used instead of the case with  $\epsilon_r = 3.0$  for a fixed operating frequency.

The use of an edge-shorted patch for size reduction is also well known [see the geometry in Figure 1.2(a)], and makes a microstrip antenna act as a quarter-wavelength structure and thus can reduce the antenna's physical length by half at a fixed operating frequency. When a shorting plate (also called a partial shorting wall) [see Figure 1.2(b)] or a shorting pin [Figure 1.2(c)] is used instead of a shorting wall, the antenna's fundamental resonant frequency can be further lowered and further size reduction can be obtained. In this case, the diameter of a shorting-pin-loaded circular microstrip patch [2] or the linear dimension of a shorting-pin-loaded rectangular microstrip patch [3] can be as small as one-third of that of the corresponding microstrip patch without a shorting pin at the same operating frequency. This suggests that an antenna size reduction of about 89% can be obtained. Moreover, by applying the

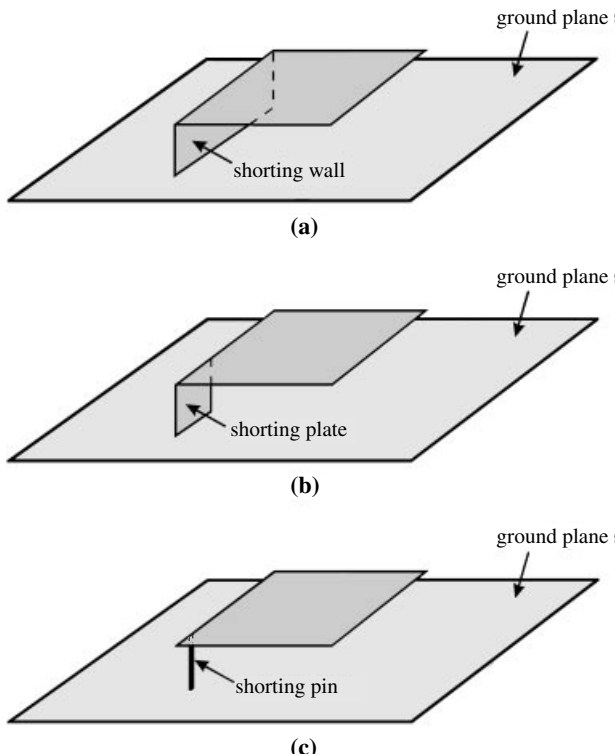


**FIGURE 1.2** Geometries of a rectangular patch antenna with (a) a shorting wall, (b) a shorting plate or partial shorting wall, and (c) a shorting pin. The feeds are not shown.

shorting-pin loading technique to an equilateral-triangular microstrip antenna, the size reduction can be made even greater, reaching as large as 94% [4]. This is largely because an equilateral-triangular microstrip antenna operates at its fundamental resonant mode, whose null-voltage point is at two-thirds of the distance from the triangle tip to the bottom side of the triangle; when a shorting pin is loaded at the triangle tip, a larger shifting of the null-voltage point compared to the cases of shorted rectangular and circular microstrip antennas occurs, leading to a greatly lowered antenna fundamental resonant frequency.

Meandering the excited patch surface current paths in the antenna's radiating patch is also an effective method for achieving a lowered fundamental resonant frequency for the microstrip antenna [3, 5–8]. For the case of a rectangular radiating patch, the meandering can be achieved by inserting several narrow slits at the patch's nonradiating edges. It can be seen in Figure 1.3(a) that the excited patch's surface currents are effectively meandered, leading to a greatly lengthened current path for a fixed patch linear dimension. This behavior results in a greatly lowered antenna fundamental resonant frequency, and thus a large antenna size reduction at a fixed operating frequency can be obtained. Figure 1.3(b) shows similar design, cutting a pair of triangular

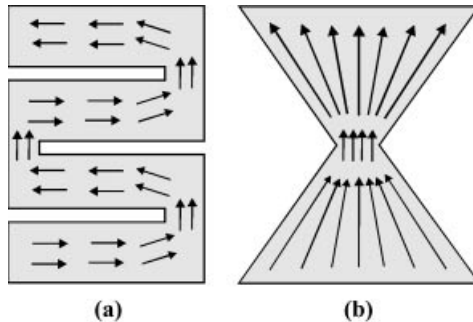


**FIGURE 1.3** Surface current distributions for meandered rectangular microstrip patches with (a) meandering slits and (b) a pair of triangular notches cut at the patch's nonradiating edges.

notches at the patch's nonradiating edges to lengthen the excited patch surface current path [8]. The resulting geometry is referred to as a bow-tie patch. Compared to a rectangular patch with the same linear dimension, a bow-tie patch will have a lower resonant frequency, and thus a size reduction can be obtained for bow-tie microstrip antennas at a given operating frequency.

The technique for lengthening the excited patch surface current path mentioned above is based on a coplanar or single-layer microstrip structure. Surface current lengthening for a fixed patch projection area can also be obtained by using an inverted U-shaped patch [Figure 1.4(a)], a folded patch [Figure 1.4(b)], or a double-folded patch [Figure 1.4(c)]. With these microstrip patches, the resonant frequency can be greatly lowered [9, 10] compared to a regular single-layer microstrip antenna with the same projection area. Note that the resonant frequency is greatly lowered due to the bending of the patch surface current paths along the antenna's resonant or excitation direction, and that no lateral current components are generated, in contrast to the case of the meandering technique shown in Figure 1.3. Probably for this reason, it has been observed that compact microstrip antennas using the bending technique described here have good cross-polarization levels for frequencies within the operating bandwidth.

By embedding suitable slots in the radiating patch, compact operation of microstrip antennas can be obtained. Figure 1.5 shows some slotted patches suitable for the design of compact microstrip antennas. In Figure 1.5(a), the embedded slot is a cross slot, whose two orthogonal arms can be of unequal [11] or equal [12–14] lengths. This kind of slotted patch causes meandering of the patch surface current path in two orthogonal directions and is suitable for achieving compact circularly polarized radiation [11, 12] or compact dual-frequency operation with orthogonal polarizations [13, 14]. Similarly, designs with a pair of bent slots [15] [Figure 1.5(b)], a group of four bent slots [16, 17] [Figure 1.5(c)], four 90°-spaced inserted slits [18] [Figure 1.5(d)], a perforated square patch or a square-ring patch with a cross strip [19] [Figure 1.5(e)], a circular slot [20] [Figure 1.5(f)], a square slot [21] [Figure 1.5(g)], an offset circular slot [22] [Figure 1.5(h)], and a perforated tip-truncated triangular patch [23] [Figure 1.5(i)] have been successfully applied to achieve compact circularly polarized or compact dual-frequency microstrip antennas.

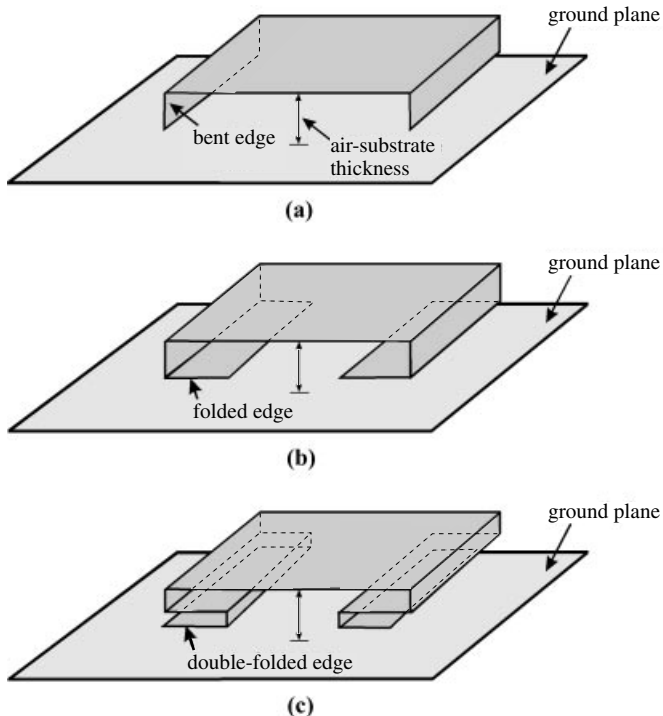


**FIGURE 1.4** Compact microstrip antennas with (a) an inverted U-shaped patch, (b) a folded patch, and (c) a double-folded patch for achieving lengthening of the excited patch surface current path at a fixed patch projection area. The feeds are not shown.

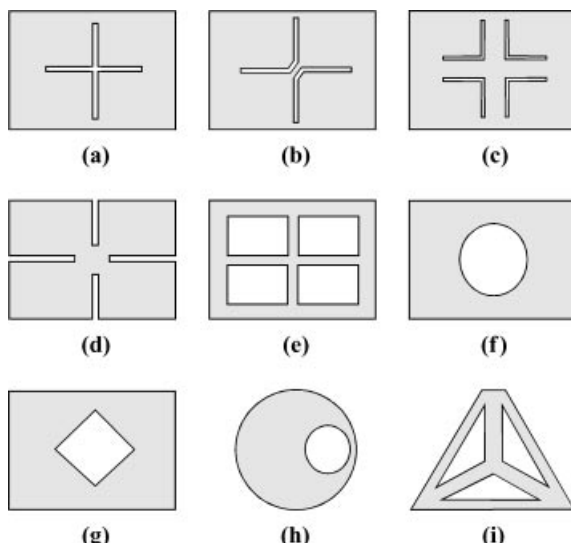


**FIGURE 1.5** Some reported slotted patches suitable for the design of compact microstrip antennas.

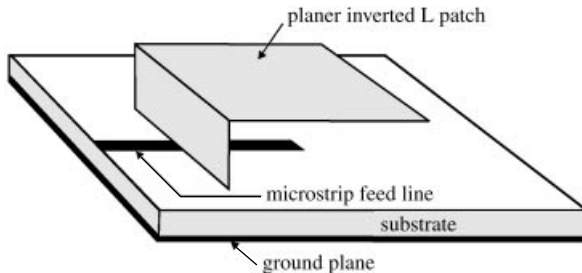


**FIGURE 1.6** Geometry of a microstrip-line-fed planar inverted-L patch antenna for compact operation.

The microstrip-line-fed planar inverted-L (PIL) patch antenna is a good candidate for compact operation. The antenna geometry is shown in Figure 1.6. When the antenna height is less than  $0.1\lambda_0$  ( $\lambda_0$  is the free-space wavelength of the center operating frequency), a PIL patch antenna can be used for broadside radiation with a resonant length of about  $0.25\lambda_0$  [24]; that is, the PIL patch antenna is a quarter-wavelength structure, and has the same broadside radiation characteristics as conventional half-wavelength microstrip antennas. This suggests that at a fixed operating frequency, the PIL patch antenna can have much reduced physical dimensions (by about 50%) compared to the conventional microstrip antenna.

Figure 1.7 shows another interesting compact design for a microstrip antenna. The antenna's ground plane is meandered by inserting several meandering slits at its edges. It has been experimentally observed [25] that similar meandering effects to those with the design with a meandering patch shown in Figure 1.3(a) can be obtained. Moreover, probably because the meandering slits in the antenna's ground plane can effectively reduce the quality factor of the microstrip structure, the obtained impedance bandwidth for a compact design with a meandered ground plane can be greater than that of the corresponding conventional microstrip antenna.

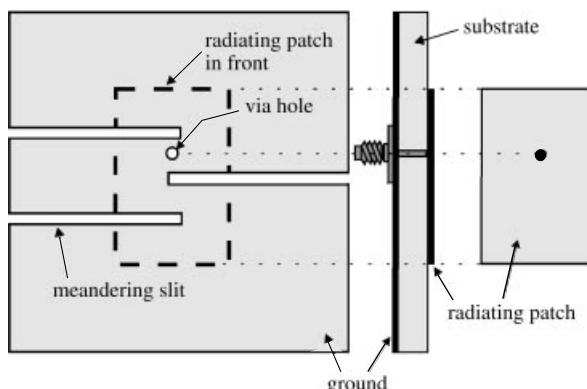


**FIGURE 1.7** Geometry of a probe-fed compact microstrip antenna with a meandered ground plane. (From Ref. 25, © 2001 John Wiley & Sons, Inc.)

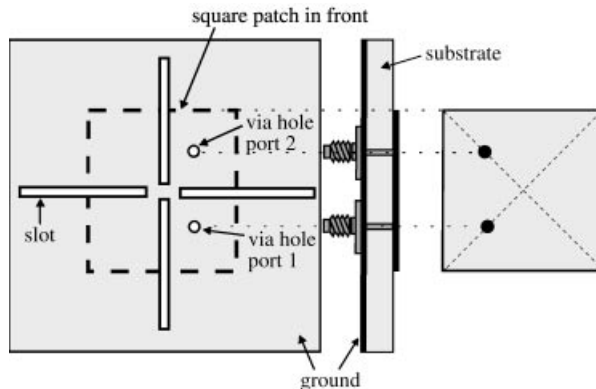


**FIGURE 1.8** Geometry of a probe-fed compact microstrip antenna with a slotted ground plane suitable for dual-polarized radiation.

### 1.3 COMPACT BROADBAND MICROSTRIP ANTENNAS

With a size reduction at a fixed operating frequency, the impedance bandwidth of a microstrip antenna is usually decreased. To obtain an enhanced impedance bandwidth, one can simply increase the antenna's substrate thickness to compensate for the decreased electrical thickness of the substrate due to the lowered operating frequency, or one can use a meandering ground plane (Figure 1.7) or a slotted ground plane (Figure 1.8). These design methods lower the quality factor of compact microstrip antennas and result in an enhanced impedance bandwidth.

By embedding suitable slots in a radiating patch, compact operation with an enhanced impedance bandwidth can be obtained. A typical design is shown in Figure 1.9. However, the obtained impedance bandwidth for such a design is usually about equal to or less than 2.0 times that of the corresponding conventional microstrip antenna. To achieve a much greater impedance bandwidth with a reduction in antenna size, one

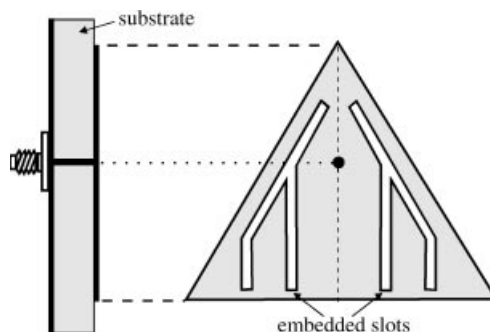


**FIGURE 1.9** Geometry of a probe-fed slotted triangular microstrip antenna for compact broadband operation.

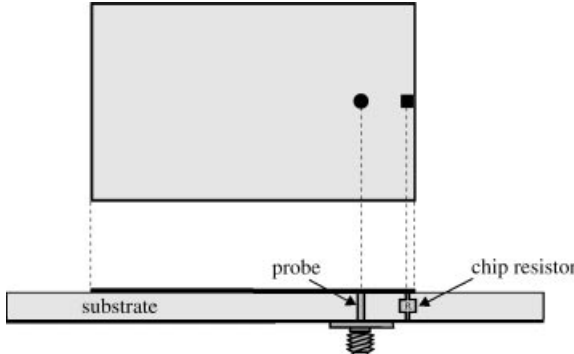


**FIGURE 1.10** Geometry of a compact broadband microstrip antenna with chip-resistor loading.

can use compact designs with chip-resistor loading [26, 27] (Figure 1.10) or stacked shorted patches [28–31] (Figure 1.11). The former design is achieved by replacing the shorting pin in a shorted patch antenna with a chip resistor of low resistance (generally  $1\ \Omega$ ). In this case, with the same antenna parameters, the obtained antenna size reduction can be greater than for the design using chip-resistor loading. Moreover, the obtained impedance bandwidth can be increased by a factor of six compared to a design using shorting-pin loading. For an FR4 substrate of thickness 1.6 mm and relative permittivity 4.4, the impedance bandwidth can reach 10% in L-band operation [26]. However, due to the introduced ohmic loss of the chip-resistor loading, the antenna gain is decreased, and is estimated to be about 2 dBi, compared to a shorted patch antenna with a shorting pin. For the latter design with stacked shorted patches, an impedance bandwidth of greater than 10% can be obtained. For this design, of course, the total antenna volume or height is increased.

#### 1.4 COMPACT DUAL-FREQUENCY MICROSTRIP ANTENNAS

Compact microstrip antennas with dual-frequency operation [32] have attracted much attention. The two operating frequencies can have the same polarization planes [7] or orthogonal polarization planes [33]. One of the reported compact dual-frequency designs with the same polarization planes uses the first two operating frequencies of shorted microstrip antennas with a shorting pin [34–36], and the obtained frequency ratios between the two operating frequencies have been reported to be about 2.0–3.2

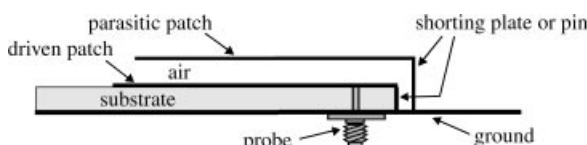


**FIGURE 1.11** Geometry of a stacked shorted patch antenna for compact broadband operation.

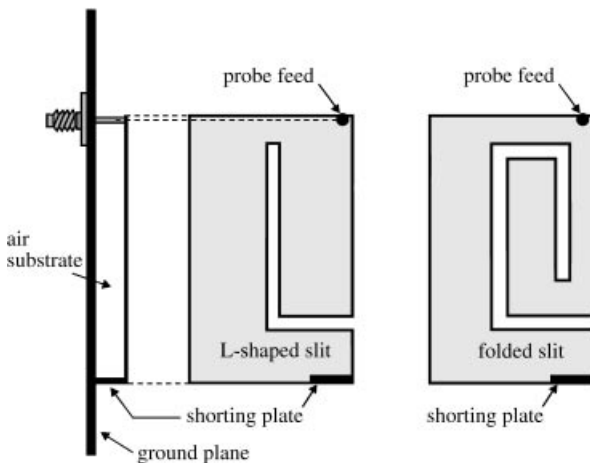


**FIGURE 1.12** Geometries of a shorted rectangular patch antenna with an L-shaped or a folded slit for dual-frequency operation.

[34], 2.55–3.83 [35], and 2.5–4.9 [36] for shorted rectangular, circular, and triangular patches, respectively.

Dual-frequency operation can be obtained using the compact design of a shorted rectangular patch antenna with an L-shaped or a folded slit (see Figure 1.12) [37, 38]. This antenna can be considered to consist of two connected resonators of different sizes. The smaller resonator is encircled by the slit and resonates at a higher resonant frequency; the larger resonator encircles the smaller one and resonates at a lower resonant frequency. This kind of compact dual-frequency design is very suitable for applications in handset antennas of mobile communication units. By loading a pair of narrow slots parallel and close to the radiating edges of a meandered rectangular or bow-tie patch (see Figure 1.13), dual-frequency operation with tunable

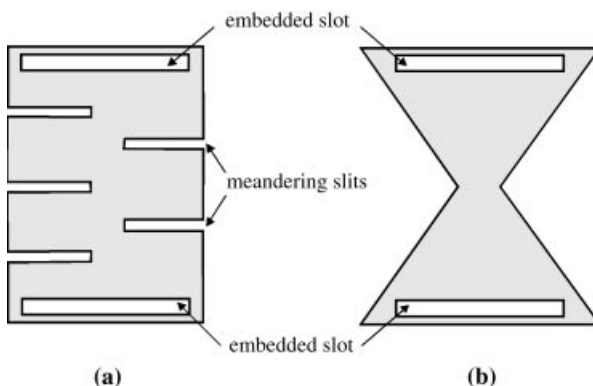


**FIGURE 1.13** Geometries of slot-loaded meandered (a) rectangular and (b) bow-tie microstrip patches for compact dual-frequency operation.

frequency-ratio ranges of about 1.8–2.4 [7] and 2.0–3.0 [39], respectively, have been reported. Many designs have been reported for compact dual-frequency operation with orthogonal polarization [13–15, 20–22]. These design methods mainly use the loading of suitable slots, such as a cross slot, a pair of bent slots, four inserted slits, a circular slot, a square slot, an offset circular slot, and so on in a rectangular or circular patch [see Figures 1.5(a), (b), (d), (f)–(g)].

## 1.5 COMPACT DUAL-POLARIZED MICROSTRIP ANTENNAS

Dual-polarized operation has been an important subject in microstrip antenna design and finds application in wireless communication systems that require frequency reuse or polarization diversity. Microstrip antennas capable of performing dual-polarized operation can combat multipath effects in wireless communications and enhance system performance. Designs of compact microstrip antennas for dual-polarized operation have been reported. Figure 1.14 shows a typical compact dual-polarized microstrip antenna fed by two probe feeds [17]. Antenna size reduction is achieved by having four bent slots embedded in a square patch. Results [17] show that, with the use of an FR4 substrate (thickness 1.6 mm and relative permittivity 4.4), good port decoupling ( $S_{21}$  less than  $-35$  dB) is obtained for the compact dual-polarized microstrip antenna shown in Figure 1.14 which is better than that of the corresponding conventional square microstrip antenna without embedded slots.

## 1.6 COMPACT CIRCULARLY POLARIZED MICROSTRIP ANTENNAS

Various novel designs have been reported recently to achieve compact circularly polarized radiation with microstrip antennas. In addition to the well-known technique of

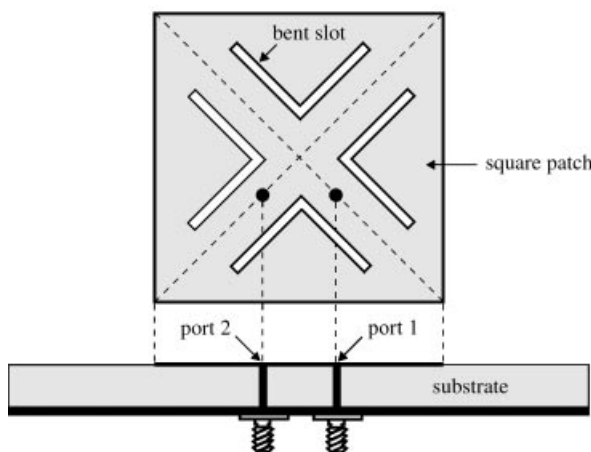


**FIGURE 1.14** Geometry of a probe-fed compact microstrip antenna with four bent slots for generating  $\pm 45^\circ$  slanted dual linear polarizations.

using a high-permittivity substrate as described in Figure 1.1, compact CP designs can be achieved by embedding suitable slots or slits in the radiating patch [11, 12, 16, 18, 40–47] or the antenna's ground plane. These designs mainly use a single probe feed or an edge-fed microstrip-line feed. By using a single inset microstrip-line feed, it is possible for microstrip antennas with a slotted patch to achieve compact CP radiation [48].

For a compact CP design using a tuning stub [12, 47] (Figure 1.15), the required length of the tuning stub increases as the CP center operating frequency is lowered. The increase in allowable tuning-stub length accompanying the reduction in antenna size for such compact CP designs allows a greatly relaxed manufacturing tolerance compared to the corresponding conventional circularly polarized microstrip antenna at the same operating frequency. This is a great advantage for practical applications,

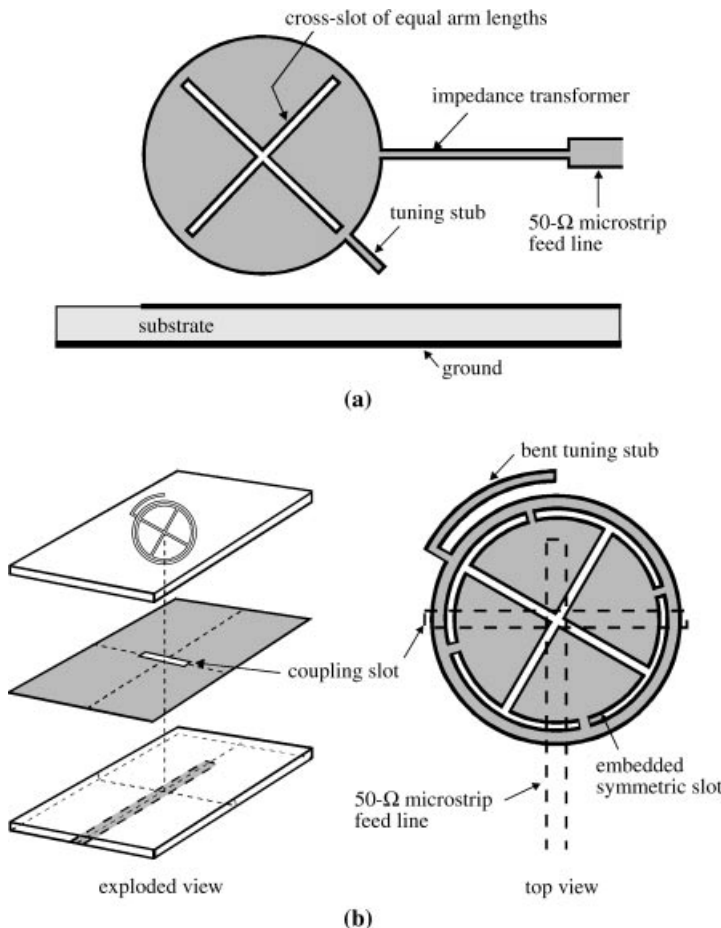


**FIGURE 1.15** Geometries of (a) a microstrip-line-fed compact circularly polarized microstrip antenna with a tuning stub and (b) an aperture-coupled compact circularly polarized microstrip antenna with a bent tuning stub.

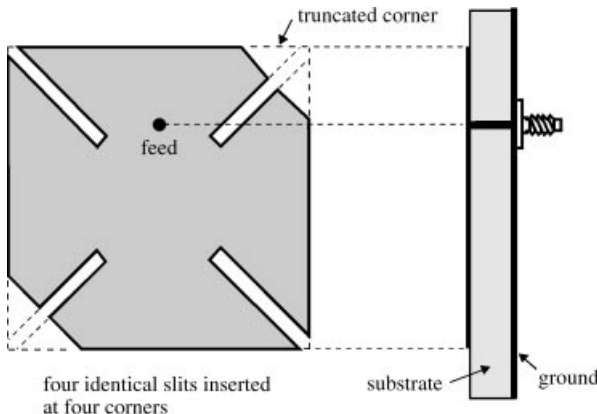


**FIGURE 1.16** Geometry of a probe-fed corner-truncated square microstrip antenna with four inserted slits for compact CP radiation.

especially when a large reduction in antenna size is required for circularly polarized microstrip antennas. The design for a probe-fed corner-truncated square microstrip antenna with four inserted slits for compact CP radiation (see Figure 1.16) shows similar behavior [43]. When the length of the inserted slits increases, leading to a lowering in the antenna's fundamental resonant frequency and thus a reduction in the antenna size at a fixed operating frequency, the required size of the truncated corners increases. Thus, there is a greatly relaxed manufacturing tolerance for a large antenna size reduction for this kind of circularly polarized microstrip antenna.

## 1.7 COMPACT MICROSTRIP ANTENNAS WITH ENHANCED GAIN

It is generally observed that when the antenna size is reduced at a fixed operating frequency, the antenna gain is also decreased. To obtain an enhanced antenna gain, methods involving the loading a high-permittivity dielectric superstrate [40, 49] or an amplifier-type active circuitry [50, 51] to a compact microstrip antenna have been demonstrated. For the former case, with the antenna's projection area unchanged or even smaller, the antenna gain can be enhanced by about 10 dBi [49]. For the latter case, the radiating patch is modified to incorporate active circuitry to provide an enhanced antenna gain, and an extra antenna gain of 8 dBi in L-band operation has been reported [50].

## 1.8 BROADBAND MICROSTRIP ANTENNAS

A narrow bandwidth is a major disadvantage of microstrip antennas in practical applications. For present-day wireless communication systems, the required operating bandwidths for antennas are about 7.6% for a global system for mobile communication

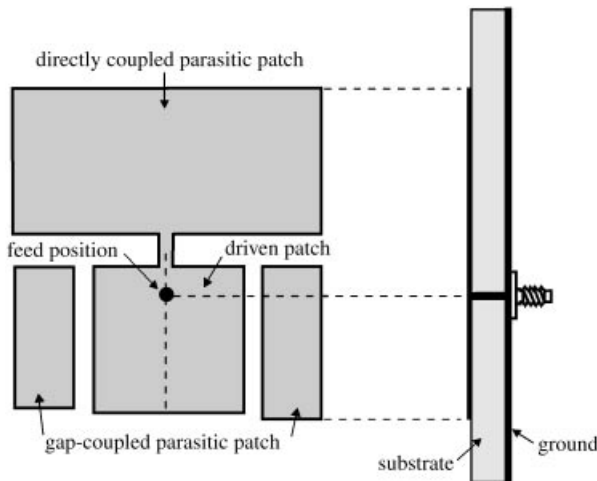


**FIGURE 1.17** Geometry of a broadband microstrip antenna with a directly coupled patch and two gap-coupled patches.

(GSM; 890–960 MHz), 9.5% for a digital communication system (DCS; 1710–1880 MHz), 7.5% for a personal communication system (PCS; 1850–1990 MHz), and 12.2% for a universal mobile telecommunication system (UMTS; 1920–2170 MHz). To meet these bandwidth requirements, many bandwidth-enhancement or broadband techniques for microstrip antennas have been reported recently. One bandwidth-enhancement technique uses coplanar directly coupled and gap-coupled parasitic patches [52]. A typical design is shown in Figure 1.17, which shows a rectangular microstrip antenna with a directly coupled patch and two gap-coupled patches. This antenna has a compact configuration such that the required realty space for implementing the antenna is minimized. Experimental results show that, with the use of an inexpensive FR4 substrate of thickness 1.6 mm and relative permittivity 4.4, such an antenna can have an impedance bandwidth of about 12.7% [52], which is about 6.35 times that of the antenna with a driven patch only (about 2%). The parasitic patches can be stacked on top of the microstrip antenna [53, 54] and significant bandwidth enhancement can be achieved.

Decreasing the quality factor of the microstrip antenna is also an effective way of increasing the antenna's impedance bandwidth. This kind of bandwidth-enhancement technique includes the use of a thick air or foam substrate [55–65] and the loading of a chip resistor on a microstrip antenna with a thin dielectric substrate [26, 66]. In the former case, for feeding using a probe feed, a large reactance owing to the long probe pin in the thick substrate layer is usually a problem in achieving good impedance matching over a wide frequency range. To overcome this problem associated with probe-fed microstrip antennas, designs have been reported that embed a U-shaped slot in the patch (U-slotted patch) [55, 56], use a three-dimensional (3D) microstrip transition feed [57], cut a pair of wide slits at one of the patch's radiating edges

(E-patch) [58], bend the patch into a 3D V-shaped patch [59] or the ground plane into an inverted V-shaped ground [60], and use modified probe configurations such as an L-strip feed [61], an L-probe feed [62], a gap-coupled probe feed [63], or a capacitively coupled feed [64, 65], among others. With the above-mentioned designs, the impedance bandwidth of a probe-fed microstrip antenna with a thick air substrate can easily be enhanced to greater than 25%. It has also been demonstrated that the use of a larger coupling slot for the case with an aperture-coupled feed can effectively lower the quality factor of a microstrip antenna, and impedance matching can be enhanced [67].

Another effective bandwidth-enhancement technique is to excite two or more resonant modes of similar radiating characteristics at adjacent frequencies to form a wide operating bandwidth. Such bandwidth-enhancement techniques include the loading of suitable slots in a radiating patch [68–75] or the integration of cascaded microstrip-line sections (microstrip reactive loading) into a radiating patch [76–80]. For both slot loading and integrated microstrip reactive loading, the low-profile advantage of the microstrip antenna is retained, and the impedance bandwidth can be about 2.0–3.5 times that of the corresponding conventional microstrip antenna. Through the design of an external optimal matching network for a microstrip antenna, bandwidth enhancement can also be obtained [81, 82]. This design technique increases the realty space of the microstrip antenna due to the external matching network, and it has been reported that the impedance matching can be increased by a factor of three if an optimal matching network is achieved [81].

Some novel designs for broadband microstrip antennas with reduced cross-polarization radiation have also been demonstrated. An effective method is to add an additional feed of equal amplitude and a 180° phase shift to the microstrip antenna; significant cross-polarization reduction of about 5–10 and 12–15 dB in the *E*-plane and *H*-plane patterns, respectively, has been achieved [83]. Details of the related antenna designs and experimental results are given in Chapter 7.

## 1.9 BROADBAND DUAL-FREQUENCY AND DUAL-POLARIZED MICROSTRIP ANTENNAS

Designs of dual-frequency microstrip antennas with impedance bandwidths of both their two operating frequencies greater than 10% have been reported [59, 84]. By using an L-probe feed for a two-element patch antenna [84], dual-frequency operation for a GSM/PCS dual-band base-station antenna has been demonstrated. It has also been shown that broadband dual-frequency operation can be obtained by using a three-dimensional V-shaped patch [59]. This design can be fed by an aperture-coupled feed or a probe feed (see Figure 1.18). For the case with an aperture-coupled feed, two separate operating bands with a 10-dB return-loss bandwidth greater than 10% can be obtained, and the frequency ratios between the two operating frequencies are about 1.28–1.31 [59].

Various broadband dual-polarized microstrip antennas have been reported recently [85–90]. High isolation between two feeding ports and low cross-polarization for two linear polarizations over a wide impedance bandwidth are the major design

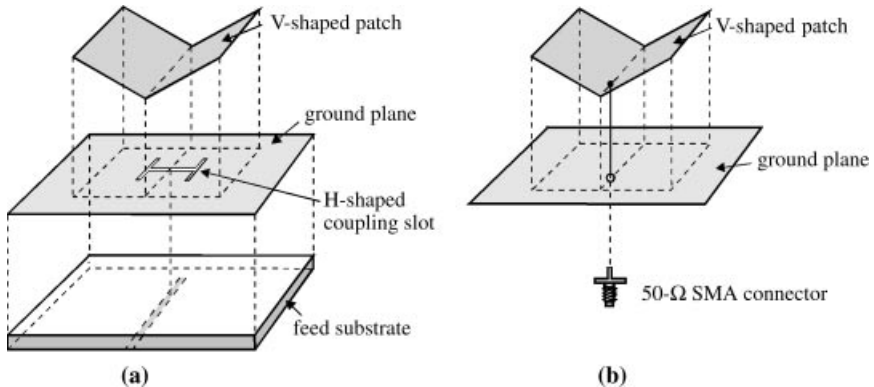


**FIGURE 1.18** Exploded views of a three-dimensional V-shaped patch with (a) an aperture-coupled feed and (b) a probe feed.

considerations. Very good port decoupling ( $S_{21} < -40$  dB) between two feeding ports for an aperture-coupled microstrip antenna across a wide impedance bandwidth has been obtained by carefully aligning the two coupling slots in the antenna's ground plane [86]. The use of hybrid feeds of a gap-coupled probe feed and an H-slot coupled feed has also been found to be a promising dual-polarized design for achieving high port decoupling [85]. Details of typical design examples are included in Chapter 8.

## 1.10 BROADBAND AND DUAL-BAND CIRCULARLY POLARIZED MICROSTRIP ANTENNAS

To achieve broadband, single-feed, circularly polarized microstrip antennas, a design with chip-resistor loading has been shown to be promising [91, 92]; the CP bandwidth can be enhanced by a factor of two. By using an aperture-coupled feed with a Y-Y-shaped coupling slot for a rectangular microstrip antenna [67], the CP bandwidth can also be enhanced to about 2.1 times that obtained using a simple inclined slot for CP operation. The obtained CP bandwidths for these broadband single-feed microstrip antennas with a thin dielectric substrate are generally less than 3%. As for the case of a single-feed microstrip antenna with a thick air substrate, it is not an easy task to achieve a CP bandwidth larger than 6%.

To achieve a much larger CP bandwidth, one should use a two-feed design incorporating a thick air substrate and an external phase shifter or power divider. It has been reported that, by using two gap-coupled or capacitively coupled feeds with a Wilkinson power divider to provide good equal-power splitting for the two feeds, the obtained 3-dB axial-ratio bandwidths can be as large as about 46% [93] and 34% [94], respectively. One can also use a branch-line coupler as the external phase shifter, and the obtained 3-dB axial-ratio bandwidth can reach 60% referenced to a center frequency at 2.2 GHz. A four-feed design with  $0^\circ$ - $90^\circ$ - $180^\circ$ - $270^\circ$  phase shifts for a

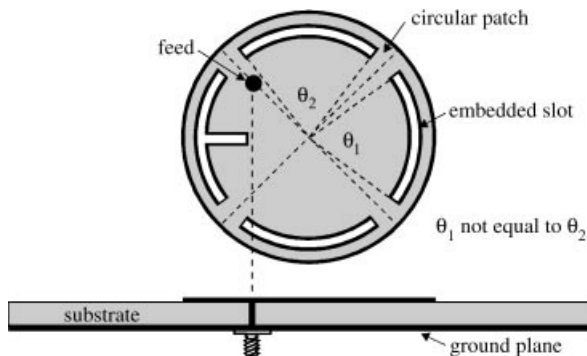


**FIGURE 1.19** Geometry of a dual-band circularly polarized microstrip antenna.

single-patch microstrip antenna has also been implemented, and very good CP quality has been obtained. The 2-dB axial-ratio bandwidth is 38%, and the 3-dB axial-ratio beamwidth for frequencies within the obtained CP bandwidth can be greater than  $100^\circ$ . Relatively very slow degradation of the axial ratio from the antenna's broadside direction to large angles can be obtained compared to a corresponding broadband circularly polarized microstrip antenna with two-feed design.

Several dual-band CP designs have been reported [95–98]. A typical design is shown in Figure 1.19. Dual-band CP operation is obtained by embedding two pairs of arc-shaped slots of proper lengths close to the boundary of a circular patch and protruding one of the arc-shaped slots with a narrow slot. The two separate CP bands are centered at 1561 and 2335 MHz, with CP bandwidths of about 1.3% and 1.1%, respectively [95]. Other methods include the use of a probe-fed square microstrip antenna with a center slot and inserted slits [96], a probe-fed stacked elliptic microstrip antenna [97], and an aperture-coupled stacked microstrip antenna [98]. Typical constructed prototypes are described in detail in Chapter 9.

## REFERENCES

1. K. L. Wong, *Design of Nonplanar Microstrip Antennas and Transmission Lines*, Wiley, New York, 1999.
2. R. Waterhouse, "Small microstrip patch antenna," *Electron. Lett.* **31**, 604–605, April 13, 1995.
3. S. Dey and R. Mittra, "Compact microstrip patch antenna," *Microwave Opt. Technol. Lett.* **13**, 12–14, Sept. 1996.
4. K. L. Wong and S. C. Pan, "Compact triangular microstrip antenna," *Electron. Lett.* **33**, 433–434, March 13, 1997.
5. K. L. Wong, C. L. Tang, and H. T. Chen, "A compact meandered circular microstrip antenna with a shorting pin," *Microwave Opt. Technol. Lett.* **15**, 147–149, June 20, 1997.
6. C. K. Wu, K. L. Wong, and W. S. Chen, "Slot-coupled meandered microstrip antenna for compact dual-frequency operation," *Electron. Lett.* **34**, 1047–1048, May 28, 1998.

7. J. H. Lu and K. L. Wong, "Slot-loaded, meandered rectangular microstrip antenna with compact dual-frequency operation," *Electron. Lett.* **34**, 1048–1050, May 28, 1998.
8. J. George, M. Deepukumar, C. K. Aanandan, P. Mohanan, and K. G. Nair, "New compact microstrip antenna," *Electron. Lett.* **32**, 508–509, March 14, 1996.
9. R. Chair, K. M. Luk, and K. F. Lee, "Small dual patch antenna," *Electron. Lett.* **35**, 762–764, May 13, 1999.
10. K. M. Luk, R. Chair, and K. F. Lee, "Small rectangular patch antenna," *Electron. Lett.* **34**, 2366–2367, Dec. 10, 1999.
11. H. Iwasaki, "A circularly polarized small-size microstrip antenna with a cross slot," *IEEE Trans. Antennas Propagat.* **44**, 1399–1401, Oct. 1996.
12. K. L. Wong and Y. F. Lin, "Circularly polarized microstrip antenna with a tuning stub," *Electron. Lett.* **34**, 831–832, April 30, 1998.
13. K. L. Wong and K. P. Yang, "Small dual-frequency microstrip antenna with cross slot," *Electron. Lett.* **33**, 1916–1917, Nov. 6, 1997.
14. K. P. Yang and K. L. Wong, "Inclined-slot-coupled compact dual-frequency microstrip antenna with cross-slot," *Electron. Lett.* **34**, 321–322, Feb. 19, 1998.
15. K. L. Wong and K. P. Yang, "Compact dual-frequency microstrip antenna with a pair of bent slots," *Electron. Lett.* **34**, 225–226, Feb. 5, 1998.
16. W. S. Chen, C. K. Wu, and K. L. Wong, "Compact circularly polarized microstrip antenna with bent slots," *Electron. Lett.* **34**, 1278–1279, June 25, 1998.
17. G. S. Row, S. H. Yeh, and K. L. Wong, "Compact dual-polarized microstrip antennas," *Microwave Opt. Technol. Lett.* **27**, 284–287, Nov. 20, 2000.
18. K. L. Wong and J. Y. Wu, "Single-feed small circularly polarized square microstrip antenna," *Electron. Lett.* **33**, 1833–1834, Oct. 23, 1997.
19. W. S. Chen, C. K. Wu, and K. L. Wong, "Square-ring microstrip antenna with a cross strip for compact circular polarization operation," *IEEE Trans. Antennas Propagat.* **47**, 1566–1568, Oct. 1999.
20. H. D. Chen, "A dual-frequency rectangular microstrip antenna with a circular slot," *Microwave Opt. Technol. Lett.* **18**, 130–132, June 5, 1998.
21. W. S. Chen, "Single-feed dual-frequency rectangular microstrip antenna with square slot," *Electron. Lett.* **34**, 231–232, Feb. 5, 1998.
22. J. H. Lu and K. L. Wong, "Compact dual-frequency circular microstrip antenna with an offset circular slot," *Microwave Opt. Technol. Lett.* **22**, 254–256, Aug. 20, 1999.
23. C. L. Tang and K. L. Wong, "A modified equilateral-triangular-ring microstrip antenna for circular polarization," *Microwave Opt. Technol. Lett.* **23**, 123–126, Oct. 20, 1999.
24. J. S. Kuo and K. L. Wong, "Dual-frequency operation of a planar inverted L antenna with tapered patch width," *Microwave Opt. Technol. Lett.* **28**, 126–127, Jan. 20, 2001.
25. J. S. Kuo and K. L. Wong, "A compact microstrip antenna with meandering slots in the ground plane," *Microwave Opt. Technol. Lett.* **29**, 95–97, April 20, 2001.
26. K. L. Wong and Y. F. Lin, "Small broadband rectangular microstrip antenna with chip-resistor loading," *Electron. Lett.* **33**, 1593–1594, Sept. 11, 1997.
27. K. L. Wong and Y. F. Lin, "Microstrip-line-fed compact broadband circular microstrip antenna with chip-resistor loading," *Microwave Opt. Technol. Lett.* **17**, 53–55, Jan. 1998.
28. R. B. Waterhouse, "Broadband stacked shorted patch," *Electron. Lett.* **35**, 98–100, Jan. 21, 1999.

29. J. Ollikainen, M. Fischer, and P. Vainikainen, "Thin dual-resonant stacked shorted patch antenna for mobile communications," *Electron. Lett.* **35**, 437–438, March 18, 1999.
30. L. Zaid, G. Kossiavas, J. Dauvignac, J. Cazajous, and A. Papiernik, "Dual-frequency and broad-band antennas with stacked quarter wavelength elements," *IEEE Trans. Antennas Propagat.* **47**, 654–660, April 1999.
31. R. Chair, K. M. Luk, and K. F. Lee, "Miniature multiplayer shorted patch antenna," *Electron. Lett.* **36**, 3–4, Jan. 6, 2000.
32. S. Maci and G. Biffi Gentili, "Dual-frequency patch antennas," *IEEE Antennas Propagat. Mag.* **39**, 13–20, Dec. 1997.
33. J. S. Chen and K. L. Wong, "A single-layer dual-frequency rectangular microstrip patch antenna using a single probe feed," *Microwave Opt. Technol. Lett.* **11**, 83–84, Feb. 5, 1996.
34. K. L. Wong and W. S. Chen, "Compact microstrip antenna with dual-frequency operation," *Electron. Lett.* **33**, 646–647, April 10, 1997.
35. C. L. Tang, H. T. Chen, and K. L. Wong, "Small circular microstrip antenna with dual-frequency operation," *Electron. Lett.* **33**, 1112–1113, June 19, 1997.
36. S. C. Pan and K. L. Wong, "Dual-frequency triangular microstrip antenna with a shorting pin," *IEEE Trans. Antennas Propagat.* **45**, 1889–1891, Dec. 1997.
37. Z. D. Liu, P. S. Hall, and D. Wake, "Dual-frequency planar inverted F antenna," *IEEE Trans. Antennas Propagat.* **45**, 1451–1458, Oct. 1997.
38. S. Tarvas and A. Isohatala, "An internal dual-band mobile phone antenna," in *2000 IEEE Antennas Propagat. Soc. Int. Symp. Dig.*, pp. 266–269.
39. K. L. Wong and W. S. Chen, "Slot-loaded bow-tie microstrip antenna for dual-frequency operation," *Electron. Lett.* **34**, 1713–1714, Sept. 3, 1998.
40. C. Y. Huang, J. Y. Wu, and K. L. Wong, "High-gain compact circularly polarized microstrip antenna," *Electron. Lett.* **34**, 712–713, April 16, 1998.
41. J. H. Lu, C. L. Tang, and K. L. Wong, "Single-feed slotted equilateral-triangular microstrip antenna for circular polarization," *IEEE Trans. Antennas Propagat.* **47**, 1174–1178, July 1999.
42. J. H. Lu and K. L. Wong, "Single-feed circularly-polarized equilateral-triangular microstrip antenna with a tuning stub," *IEEE Trans. Antennas Propagat.* **48**, 1869–1872, Dec. 2000.
43. W. S. Chen, C. K. Wu, and K. L. Wong, "Novel compact circularly polarized square microstrip antenna," *IEEE Trans. Antennas Propagat.* **49**, 340–342, March 2001.
44. K. P. Yang, K. L. Wong, and J. H. Lu, "Compact circularly-polarized equilateral-triangular microstrip antenna with Y-shaped slot," *Microwave Opt. Technol. Lett.* **20**, 31–34, Jan. 5, 1999.
45. W. S. Chen, C. K. Wu, and K. L. Wong, "Compact circularly polarized circular microstrip antenna with cross slot and peripheral cuts," *Electron. Lett.* **34**, 1040–1041, May 28, 1998.
46. W. S. Chen, C. K. Wu, and K. L. Wong, "Single-feed square-ring microstrip antenna with truncated corners for compact circular polarization operation," *Electron. Lett.* **34**, 1045–1047, May 28, 1998.
47. K. L. Wong and M. H. Chen, "Slot-coupled small circularly polarized microstrip antenna with modified cross-slot and bent tuning-stub," *Electron. Lett.* **34**, 1542–1543, Aug. 6, 1998.
48. W. S. Chen, K. L. Wong, and C. K. Wu, "Inset microstripline-fed circularly polarized microstrip antennas," *IEEE Trans. Antennas Propagat.* **48**, 1253–1254, Aug. 2000.

49. C. Y. Huang, J. Y. Wu, C. F. Yang, and K. L. Wong, "Gain-enhanced compact broadband microstrip antenna," *Electron. Lett.* **34**, 138–139, Jan. 22, 1998.
50. B. Robert, T. Razban, and A. Papiernik, "Compact amplifier integration in square patch antenna," *Electron. Lett.* **28**, 1808–1810, Sept. 10, 1992.
51. M. C. Pan and K. L. Wong, "A broadband active equilateral-triangular microstrip antenna," *Microwave Opt. Technol. Lett.* **22**, 387–389, Sept. 20, 1999.
52. C. K. Wu and K. L. Wong, "Broadband microstrip antenna with directly coupled and gap-coupled parasitic patches," *Microwave Opt. Technol. Lett.* **22**, 348–349, Sept. 5, 1999.
53. T. M. Au and K. M. Luk, "Effects of parasitic elements on the characteristics of microstrip antennas," *IEEE Trans. Antennas Propagat.* **39**, 1247–1251, Aug. 1991.
54. K. F. Tong, T. M. Au, K. M. Luk, and K. F. Lee, "Two-layer five-patch broadband microstrip antenna," *Electron. Lett.* **31**, 1621–1622, Sept. 14, 1995.
55. T. Huynh and K. F. Lee, "Single-layer single-patch wideband microstrip antenna," *Electron. Lett.* **31**, 1310–1311, Aug. 3, 1995.
56. K. L. Wong and W. H. Hsu, "Broadband triangular microstrip antenna with U-shaped slot," *Electron. Lett.* **33**, 2085–2087, Dec. 4, 1997.
57. N. Herscovici, "A wide-band single-layer patch antenna," *IEEE Trans. Antennas Propagat.* **46**, 471–473, April 1998.
58. K. L. Wong and W. H. Hsu, "A broadband rectangular patch antenna with a pair of wide slits," *IEEE Trans. Antennas Propagat.* **49**, 1345–1347, Sept. 2001.
59. C. L. Tang, C. W. Chiou, and K. L. Wong, "Broadband dual-frequency V-shape patch antenna," *Microwave Opt. Technol. Lett.* **25**, 121–123, April 20, 2000.
60. C. L. Tang, J. Y. Chiou, and K. L. Wong, "A broadband probe-fed patch antenna with a bent ground plane," in *Proceedings 2000 Asia Pacific Microwave Conference*, pp. 1356–1359.
61. C. L. Mak, K. M. Luk, and K. F. Lee, "Microstrip line-fed L-strip patch antenna," *IEE Proc. Microw. Antennas Propagat.* **146**, 282–284, Aug. 1999.
62. K. M. Luk, L. K. Au Yeung, C. L. Mak, and K. F. Lee, "Circular patch antenna with an L-shaped probe," *Microwave Opt. Technol. Lett.* **20**, 256–257, Feb. 20, 1999.
63. P. S. Hall, "Probe compensation in thick microstrip patches," *Electron. Lett.* **23**, 606–607, May 21, 1987.
64. G. A. E. Vandenbosch and A. R. Vande Capelle, "Study of the capacitively fed microstrip antenna element," *IEEE Trans. Antennas Propagat.* **42**, 1648–1652, Dec. 1994.
65. G. A. E. Vandenbosch, "Network model for capacitively fed microstrip antenna," *Electron. Lett.* **35**, 1597–1599, Sept. 16, 1999.
66. K. L. Wong and K. P. Yang, "Modified planar inverted F antenna," *Electron. Lett.* **34**, 6–7, Jan. 8, 1998.
67. C. Y. Huang, J. Y. Wu, and K. L. Wong, "Slot-coupled microstrip antenna for broadband circular polarization," *Electron. Lett.* **34**, 835–836, April 30, 1998.
68. S. Dey, C. K. Aanandan, P. Mohanan, and K. G. Nair, "A new broadband circular patch antenna," *Microwave Opt. Technol. Lett.* **7**, 604–605, Sept. 1994.
69. J. Y. Sze and K. L. Wong, "Broadband rectangular microstrip antenna with a pair of toothbrush-shaped slots," *Electron. Lett.* **34**, 2186–2187, Nov. 12, 1998.
70. J. Y. Sze and K. L. Wong, "Single-layer single-patch broadband rectangular microstrip antenna," *Microwave Opt. Technol. Lett.* **22**, 234–236, Aug. 20, 1999.

71. J. Y. Sze and K. L. Wong, "Slotted rectangular microstrip antenna for bandwidth enhancement," *IEEE Trans. Antennas Propagat.* **48**, 1149–1152, Aug. 2000.
72. J. Y. Jan and K. L. Wong, "A broadband circular microstrip antenna with two open-ring slots," *Microwave Opt. Technol. Lett.* **23**, 205–207, Nov. 20, 1999.
73. S. T. Fang, K. L. Wong, and T. W. Chiou, "Bandwidth enhancement of inset-microstrip line-fed equilateral-triangular microstrip antenna," *Electron. Lett.* **34**, 2184–2186, Nov. 12, 1998.
74. M. C. Pan and K. L. Wong, "A broadband slot-loaded trapezoid microstrip antenna," *Microwave Opt. Technol. Lett.* **24**, 16–19, Jan. 5, 2000.
75. J. H. Lu, C. L. Tang, and K. L. Wong, "Novel dual-frequency and broadband designs of single-feed slot-loaded equilateral-triangular microstrip antennas," *IEEE Trans. Antennas Propagat.* **48**, 1048–1054, July 2000.
76. K. L. Wong and J. Y. Jan, "Broadband circular microstrip antenna with embedded reactive loading," *Electron. Lett.* **34**, 1804–1805, Sept. 17, 1998.
77. J. Y. Jan and K. L. Wong, "Microstrip-line-fed broadband circular microstrip antenna with embedded reactive loading," *Microwave Opt. Technol. Lett.* **22**, 200–202, Aug. 5, 1999.
78. N. Fayyaz and S. Safavi-Naeini, "Bandwidth enhancement of a rectangular patch antenna by integrated reactive loading," in *1998 IEEE Antennas Propagat. Soc. Int. Symp. Dig.*, pp. 1100–1103.
79. K. L. Wong and J. S. Kuo, "Bandwidth enhancement of bow-tie microstrip antenna using integrated reactive loading," *Microwave Opt. Technol. Lett.* **22**, 69–71, July 5, 1999.
80. K. L. Wong, J. S. Kuo, S. T. Fang, and T. W. Chiou, "Broadband microstrip antennas with integrated reactive loading," in *Proceedings 1999 Asia Pacific Microwave Conference*, pp. 352–354.
81. H. F. Pues and A. Van de Capelle, "An impedance-matching technique for increasing the bandwidth of microstrip antennas," *IEEE Trans. Antennas Propagat.* **37**, 1345–1354, Nov. 1989.
82. K. W. Loi, S. Uysai, and M. S. Leong, "Design of a wideband microstrip bowtie patch antenna," *IEE Proc. Microw. Antennas Propagat.* **145**, 137–140, April 1998.
83. W. H. Hsu and K. L. Wong, "A dual-capacitively-fed broadband patch antenna with reduced cross-polarization radiation," *Microwave Opt. Technol. Lett.* **26**, 169–171, Aug. 5, 2000.
84. K. M. Luk, C. H. Lai, and K. F. Lee, "Wideband L-probe-fed patch antenna with dual-band operation for GSM/PCS base stations," *Electron. Lett.* **35**, 1123–1124, July 8, 1999.
85. T. W. Chiou, H. C. Tung, and K. L. Wong, "A dual-polarization wideband circular patch antenna with hybrid feeds," *Microwave Opt. Technol. Lett.* **26**, 37–39, July 5, 2000.
86. S. Hienonen, A. Lehto, and A. V. Raisanen, "Simple broadband dual-polarized aperture-coupled microstrip antenna," in *1999 IEEE Antennas Propagat. Soc. Int. Symp. Dig.*, pp. 1228–1231.
87. B. Lindmark, "A novel dual polarized aperture coupled patch element with a single layer feed network and high isolation," in *1997 IEEE Antennas Propagat. Soc. Int. Symp. Dig.*, pp. 2190–2193.
88. I. Nystrom and D. Karlsson, "Reduction of back radiation and cross-coupling in dual polarized aperture coupled patch antennas," in *1997 IEEE Antennas Propagat. Soc. Int. Symp. Dig.*, pp. 2222–2225.

89. P. Brachat and J. M. Baracco, "Printed radiating element with two highly decoupled input ports," *Electron. Lett.* **31**, 245–246, Feb. 16, 1995.
90. J.-F. Zuercher, Ph. Gay-Balmaz, R. C. Hall, and S. Kolb, "Dual polarized, single- and double-layer strip-slot-foam inverted patch (SSFIP) antennas," *Microwave Opt. Technol. Lett.* **7**, 406–410, 1994.
91. C. Y. Huang, J. Y. Wu, and K. L. Wong, "Broadband circularly polarized microstrip antenna using chip-resistor loading," *IEE Proc. Microw. Antennas Propagat.* **146**, 94–96, Feb. 1999.
92. K. L. Wong and K. B. Hsieh, "Broadband circularly polarized microstrip antenna with a chip-resistor loading," *Microwave Opt. Technol. Lett.* **19**, 34–36, Sept. 1998.
93. T. W. Chiou and K. L. Wong, "Single-layer wideband probe-fed circularly polarized microstrip antenna," *Microwave Opt. Technol. Lett.* **25**, 74–76, April 5, 2000.
94. K. L. Wong and T. W. Chiou, "A broadband single-patch circularly polarized microstrip antenna with dual capacitively-coupled feeds," *IEEE Trans. Antennas Propagat.* **49**, 41–44, Jan. 2001.
95. K. B. Hsieh, M. H. Chen, and K. L. Wong, "Single-feed dual-band circularly polarized microstrip antenna," *Electron. Lett.* **34**, 1170–1171, June 11, 1998.
96. K. P. Yang and K. L. Wong, "Dual-band circularly-polarized square microstrip antenna," *IEEE Trans. Antennas Propagat.* **49**, 377–382, March 2001.
97. J. Y. Jan and K. L. Wong, "A dual-band circularly polarized stacked elliptic microstrip antenna," *Microwave Opt. Technol. Lett.* **24**, 354–357, March 5, 2000.
98. D. M. Pozar and S. M. Duffy, "A dual-band circularly polarized aperture-coupled stacked microstrip antenna for global positioning satellite," *IEEE Trans. Antennas Propagat.* **45**, 1618–1625, Nov. 1997.

## CHAPTER TWO

---

# Compact Microstrip Antennas

---

### 2.1 INTRODUCTION

Compact microstrip antennas have recently received much attention due to the increasing demand of small antennas for personal communications equipment. For achieving microstrip antennas with a reduced size at a fixed operating frequency, the use of a high-permittivity substrate is an effective method; an example is described in Figure 1.1 in Chapter 1. Recently, it has been demonstrated that loading the microstrip patch with a shorting pin can also effectively reduce the required patch size for a fixed operating frequency [1–8]. Typical designs of this kind of compact microstrip antenna with a thin dielectric substrate are presented in this chapter, and compact designs combining a shorting-pin loading with the patch-meandering method [1, 6] are also described.

By applying the meandering method to the ground plane of a microstrip antenna, a similar significant lowering of the antenna's fundamental resonant frequency to the patch-meandering method can be achieved [9]. In addition, the impedance bandwidth and antenna gain can be enhanced, which is a great advantage of this kind of ground-meandering method over the patch-meandering one. Experimental results for a constructed prototype will be presented and discussed. A compact design using a planar inverted-L (PIL) patch has also been addressed [10, 11]. This kind of PIL patch antenna can be operated as a quarter-wavelength antenna, but with similar broadside radiation characteristics to the conventional half-wavelength microstrip antenna. Antenna size can be reduced by using a PIL patch antenna in place of the conventional microstrip antenna at a fixed operating frequency. Two design examples of a PIL patch antenna are given in this chapter. Finally, the use of an inverted U-shaped or folded patch to achieve a compact microstrip antenna is demonstrated. By using an inverted U-shaped patch, the excited patch surface current path of a microstrip antenna with a fixed projection area can be effectively lengthened, and thus the antenna's fundamental resonant frequency can be greatly lowered [12]. This behavior leads to a large antenna size reduction for a fixed operating frequency.

## 2.2 USE OF A SHORTED PATCH WITH A THIN DIELECTRIC SUBSTRATE

Figure 2.1 shows the configurations of shorted rectangular, circular, and triangular microstrip antennas with a shorting pin. For the case of a rectangular patch with a shorting pin absent, the rectangular microstrip antenna is usually operated as a half-wavelength antenna. Based on the cavity-model approximation, the fundamental or first resonant frequency of the rectangular patch in Figure 2.1(a) without a shorting pin is determined from

$$f_{10} = \frac{c}{2L\sqrt{\epsilon_r}}, \quad (2.1)$$

where  $f_{10}$  denotes the resonant frequency of the  $\text{TM}_{10}$  mode. When there is a shorting pin placed at  $x = -L/2$ ,  $y = 0$  (center of the patch edge) and the feed position is chosen on the centerline ( $x$  axis), the first resonant frequency occurs at about  $0.38f_{01}$  [2] (When there is more than one shorting pin at the edge or a shorting wall is used, the first resonant frequency occurs close to or at about  $0.5f_{01}$ . In this case, the shorted microstrip antenna is operated as a quarter-wavelength antenna.).

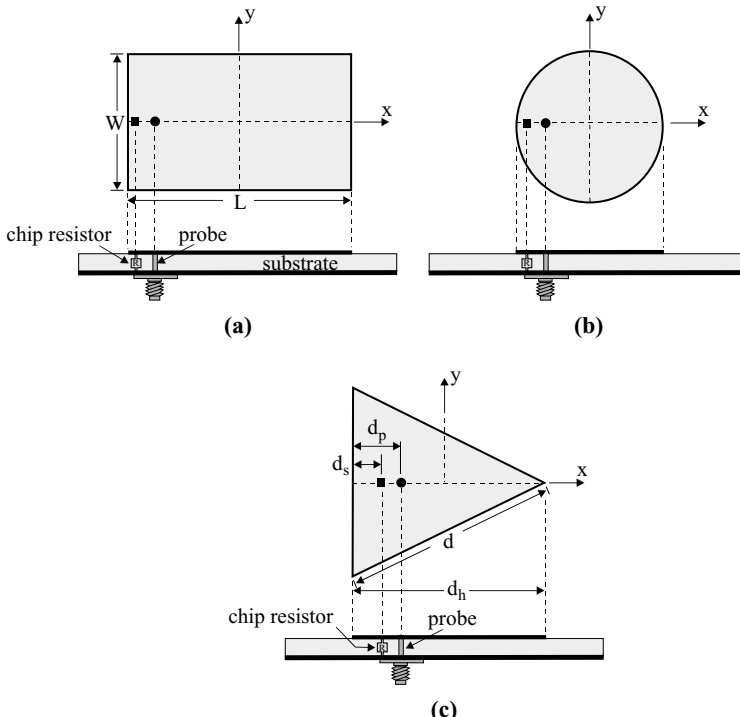


**FIGURE 2.1** Geometries of compact (a) rectangular, (b) circular, and (c) triangular microstrip antennas with shorting-pin loading.

This behavior suggests that the shorting-pin-loaded rectangular microstrip antenna is operated with a resonant length less than one quarter-wavelength, and a greater reduced antenna size than for the case with a shorting wall can be obtained.

With the shorting-pin-loading technique, the antenna size reduction is mainly due to the shifting of the null-voltage point at the center of the rectangular patch (excited at the  $\text{TM}_{01}$  mode) and the circular patch (operated at the  $\text{TM}_{11}$  mode) to their respective patch edges, which makes the shorted patches resonate at a much lower frequency. Thus, at a given operating frequency, the required patch dimensions can be significantly reduced, and the reduction in the patch size is limited by the distance between the null-voltage point in the patch and the patch edge. For this reason, compared to the case of shorting-pin-loaded rectangular and circular patches, it is expected that an equilateral-triangular microstrip patch excited at its fundamental mode ( $\text{TM}_{10}$  mode), where the null-voltage point is at two-thirds of the distance from the triangle tip to the bottom edge of the triangle, will have a much larger reduction in the resonant frequency when applying the shorting-pin loading technique.

An example of a shorting-pin-loaded equilateral-triangular microstrip antenna for compact operation is described in Figures 2.2–2.4. Consider the geometry shown in Figure 2.1(c) for  $\text{TM}_{10}$  mode excitation; the feed and shorting-pin positions are on the  $x$  axis at distances  $d_p$  and  $d_s$  away from the patch's bottom edge, respectively. Prototypes of shorting-pin-loaded triangular microstrip patches with various values of  $d_s$  were constructed. The radius  $r_s$  of the shorting pin was selected to be 0.13 mm, and the feed radius  $r_p$  was 0.3 mm. The measured lowest resonant frequency of the microstrip patch against the shorting-pin position is shown in Figure 2.2. It should be noted that, without shorting-pin loading, the triangular microstrip patch resonates at

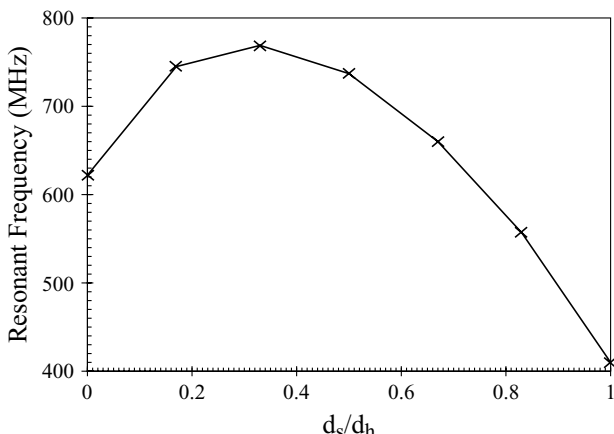


**FIGURE 2.2** Measured resonant frequency against shorting-pin position for the shorting-pin-loaded equilateral-triangular microstrip antenna shown in Figure 2.1(c);  $\epsilon_r = 3.0$ ,  $h = 0.762$  mm, and  $d = 59.9$  mm. (From Ref. 7, © 1997 IEE, reprinted with permission.)

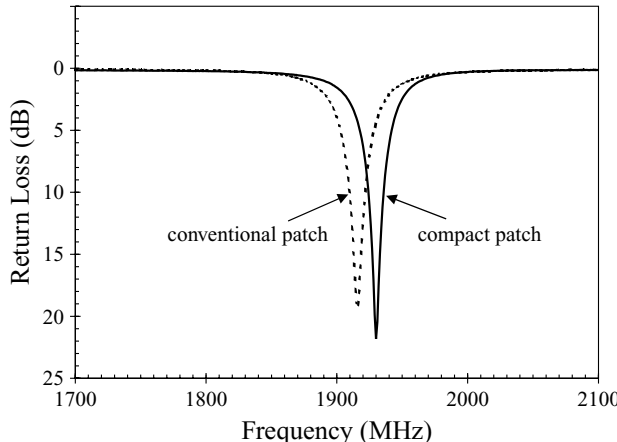


**FIGURE 2.3** Measured return loss of shorted and conventional triangular microstrip antennas. The solid line is for a shorted antenna with  $d = 15.3$  mm, and  $d_s = 13.25$  mm, and  $d_p = 12.75$  mm; the dashed line is for a conventional antenna with  $d = 59.9$  mm and  $d_p = 24.1$  mm. (From Ref. 7, © 1997 IEE, reprinted with permission.)

about 1.9 GHz, its lowest resonant frequency. It is clearly seen that, with shorting-pin loading, the resonant frequency of the triangular patch is significantly reduced and is much lower than 1.9 GHz. A significant dependence of the resonant frequency on the shorting-pin position is also observed. The resonant frequency has a maximum value at  $d_s/d_h = 0.33$ , where the null voltage occurs for  $\text{TM}_{10}$  mode excitation. At  $d_s/d_h = 1.0$  (the triangle tip), the resonant frequency has a minimum value. This agrees with our expectation because the shorting pin at the triangle tip results in a shifting of the null-voltage point from  $d_s/d_h = 0.33$  to 1.0, the largest shifting in this case. The measured resonant frequency is 410 MHz, which is about 22% of that of a conventional triangular microstrip patch without a shorting pin.

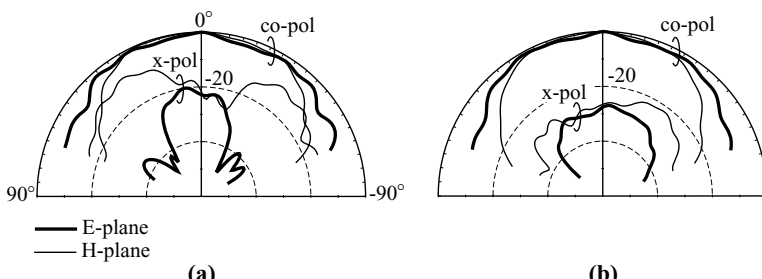


**FIGURE 2.4** Measured  $E$ - and  $H$ -plane radiation patterns at resonance of (a) shorted and (b) conventional triangular microstrip antennas with parameters given in Figure 2.3. (From Ref. 7, © 1997 IEE, reprinted with permission.)

Based on the results, a compact triangular microstrip antenna with a shorting pin loaded at the triangle tip was constructed. The center frequency is at about 1930 MHz, and the measured return loss is shown in Figure 2.3. The results for a conventional triangular microstrip antenna without a shorting pin operated at about the same frequency are presented for comparison. The side lengths of the compact (shorted) and conventional triangular microstrip antennas are 15.3 and 59.9 mm, respectively. This means a reduction of about 74% of the linear dimension of the antenna, or the size of the compact antenna is only about 7% of that of the conventional microstrip antenna. This reduction in the antenna size is greater than those reported for compact rectangular and circular microstrip antennas using the same technique. It is also noted that the 10-dB return-loss bandwidth is only slightly decreased compared to that of the conventional microstrip antenna. The measured radiation patterns for the compact and conventional microstrip antennas are plotted in Figure 2.4. It is observed that the component of cross-polarization radiation is increased due to the shorting-pin loading, especially for *H*-plane (*y*-*z* plane) radiation. However, for *E*-plane (*x*-*z* plane) radiation, the cross-polarization radiation is still below –20 dB. Note that, due to the antenna size reduction, a decrease in the antenna gain is expected.

### 2.3 USE OF A MEANDED PATCH

Compact operation of microstrip antennas can be obtained by meandering the radiating patch [1, 6]. This kind of patch-meandering technique is achieved mainly by loading several meandering slits at the nonradiating edges of a rectangular patch [1] or at the boundary of a circular patch [6]. In the following, a compact design combining the techniques of patch meandering and shorting-pin loading for a circular microstrip antenna is demonstrated. Figure 2.5 shows the geometry of a short-circuited, meandered circular microstrip antenna. The circular patch is short-circuited at the edge with a shorting pin, and three narrow slots of the same length  $\ell$  and width  $w$  are cut

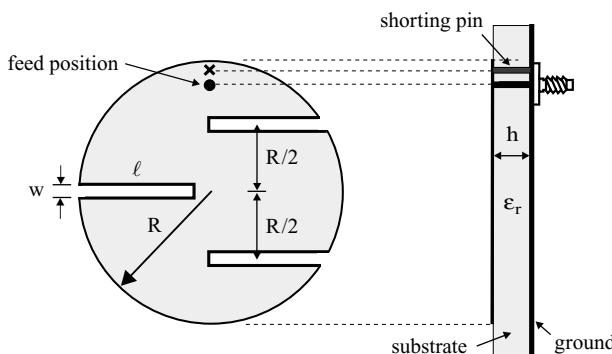


**FIGURE 2.5** Geometry of a meandered circular microstrip antenna with a shorting pin. (From Ref. 6, © 1997 John Wiley & Sons, Inc.)

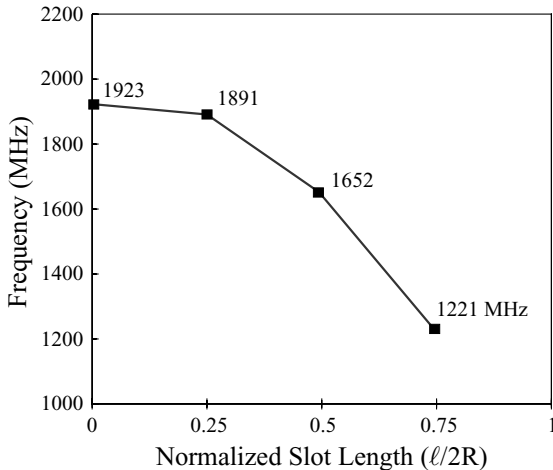


**FIGURE 2.6** Measured resonant frequency against slot length  $\ell$  in the circular patch in Figure 2.5;  $R = 7.5$  mm,  $d_s = 6.5$  mm. (From Ref. 6, © 1997 John Wiley & Sons, Inc.)

in the patch. The shorting pin makes the circular patch resonate at a much lower frequency compared with a conventional circular patch of the same size, and the narrow slots meander the patch, which increases the effective electrical length of the patch. These two factors effectively reduce the required disk size for an antenna operated at a given frequency.

Based on the above design concept, short-circuited circular microstrip antennas with different slot lengths were constructed. The circular patch has a radius  $R$  of 7.5 mm, and a shorting pin of radius  $r_s = 0.4$  mm is placed near the patch edge at  $d_s = 6.5$  mm. The patch substrate has a relative permittivity  $\epsilon_r = 4.4$  and thickness  $h = 1.6$  mm. Figure 2.6 shows the measured resonant frequency against the slot length in the short-circuited circular patch. Results clearly indicate that, with increasing slot length, the resonant frequency of the meandered patch decreases. It is also found that the slot width has relatively little effect on the resonant frequency. From the results for the case of  $\ell = R$ , a circular patch of radius 7.5 mm has a resonant frequency of 1652 MHz. For a conventional circular patch antenna (without a shorting pin and slots in the patch) to be operated at 1652 MHz, the radius of the circular patch needs to be about 25.2 mm (with the same substrate material). That is, the patch size is reduced to about 9% compared with the conventional circular patch of the same operating frequency. When the slot length increases, the resonant frequency of the patch can be reduced further, which can make the patch size reduction even greater at a given frequency.

The measured return loss for the case of  $\ell = R$  is presented in Figure 2.7. In order to obtain a good matching condition, the feed position is placed close to the shorting pin. When the feed position is away from the shorting pin, the resonant input resistance quickly increases. For good impedance matching, the feed position is chosen at  $d_p = 5.2$  mm, with the probe having a radius  $r_p$  of 0.65 mm. The impedance bandwidth

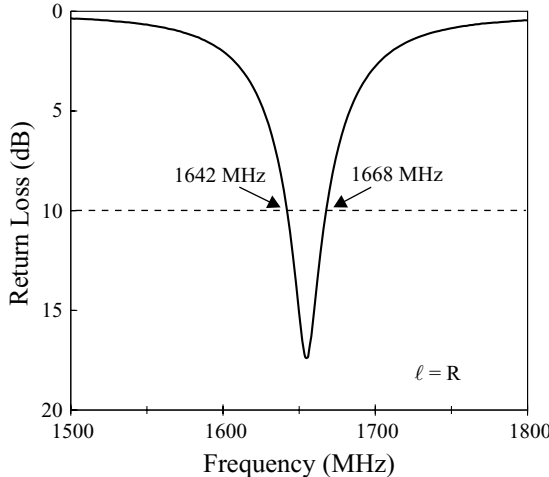


**FIGURE 2.7** Measured return loss against frequency for an antenna with  $\ell = R$ . Other antenna parameters are given in Figure 2.6. (From Ref. 6, © 1997 John Wiley & Sons, Inc.)

determined from a 10-dB return loss is found to be about 1.6%, which is less than that (1.9%) of a conventional circular microstrip antenna at the same operating frequency. This reduction in the antenna bandwidth is expected due to the reduced antenna size. However, it is interesting to find that, with slots in the patch, the reduction in the impedance bandwidth is smaller than for the case of the short-circuited circular patch without slots, where the impedance bandwidth is reduced by about 33% compared with the conventional microstrip antenna. This is probably because the slots in the patch introduce an additional capacitive reactance that compensates the inductive reactance contributed by the shorting pin and the probe, and thus a wider impedance bandwidth can be achieved.

Measured radiation patterns for a compact antenna with  $\ell = R$  are plotted in Figure 2.8. It is seen that the radiation patterns remain broadside. Figure 2.9 shows the case for an antenna without slots ( $\ell = 0$ ), where the patch resonates at about 1923 MHz. Similar broadside radiation is observed. However, probably owing to the increasing of the patch surface current component perpendicular to the main excitation direction, the cross-polarization radiation in the *H* plane is increased (compare Figures 2.8 and 2.9). The cross-polarization level in the *E* plane is seen to be about the same.

## 2.4 USE OF A MEANDED GROUND PLANE

The meandering technique for lengthening the excited patch surface current path to lower the antenna's fundamental resonant frequency can also be applied to the antenna's ground plane [9]. Figure 2.10 shows the geometry of a compact

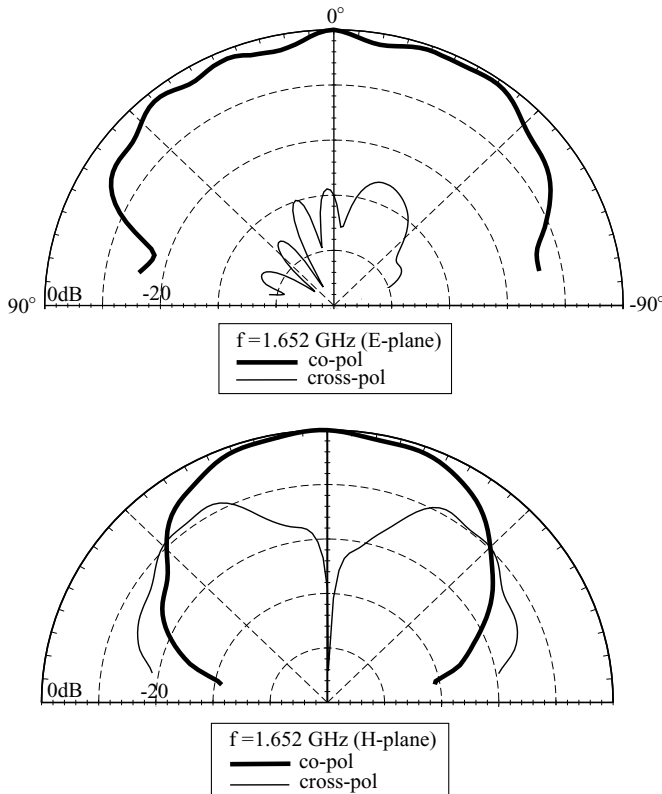


**FIGURE 2.8** Measured  $E$ - and  $H$ -plane radiation patterns at resonance for an antenna with  $\ell = R$ . Other antenna parameters are given in Figure 2.6. (From Ref. 6, © 1997 John Wiley & Sons, Inc.)

microstrip antenna with a meandered ground plane. The rectangular radiating patch has dimensions  $L \times W$  and is printed on a microwave substrate of thickness  $h$  and relative permittivity  $\epsilon_r$ . Three identical slots are embedded in the antenna's ground plane and aligned with an equal spacing of  $L/4$  and parallel to the patch's radiating edges, or the  $y$  axis. The embedded slots are narrow (1 mm in this design) and have a length of  $\ell_o + \ell_i$ , where  $\ell_o$  and  $\ell_i$  are, respectively, the slot lengths outside and inside the projection image of the radiating patch in the ground plane. A probe feed is placed along the patch's centerline ( $x$  axis) at a position  $d_p$  from the patch center. Prototypes (antennas 1–4) were constructed and experimentally studied. Figure 2.11 shows the measured return loss of the constructed prototypes. The corresponding measured data are given in Table 2.1 for comparison. In the study, inexpensive FR4 substrates ( $\epsilon_r = 4.4$ ,  $h = 1.6$  mm) were used. The dimensions of the rectangular radiating patch were chosen to be 30 mm  $\times$  20 mm ( $L \times W$ ). The slot length  $\ell_o$  for the prototypes was fixed to be 10 mm and the slot length  $\ell_i$  was varied from 8 to 14 mm.

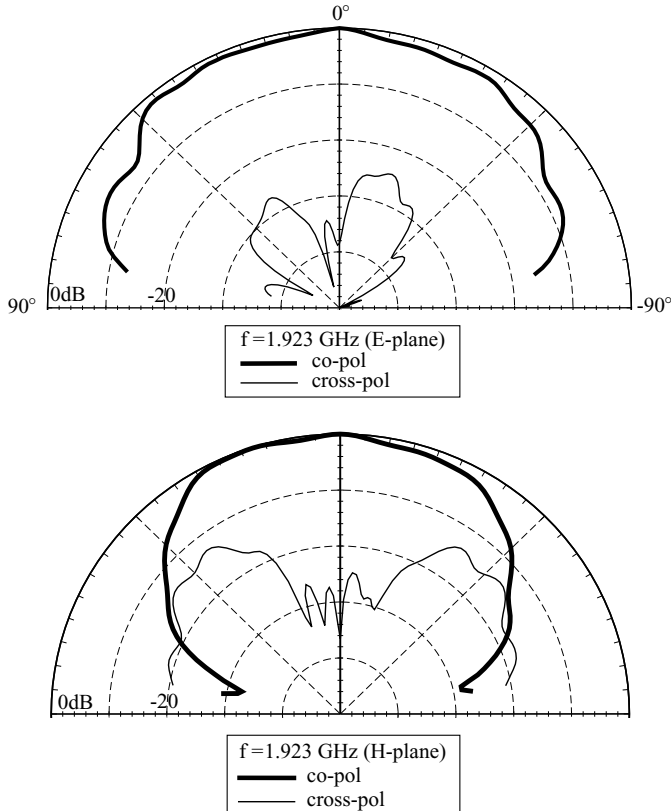


**FIGURE 2.9** Measured *E*- and *H*-plane radiation patterns at resonance for an antenna without slots ( $\ell = 0$ ). Other antenna parameters are given in Figure 2.6. (From Ref. 6, © 1997 John Wiley & Sons, Inc.)

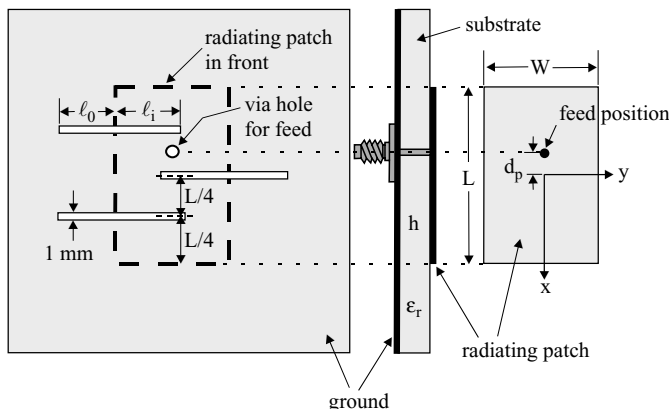


**FIGURE 2.10** Geometry of a compact microstrip antenna with a meandered ground plane. (From Ref. 9, © 2001 John Wiley & Sons, Inc.)

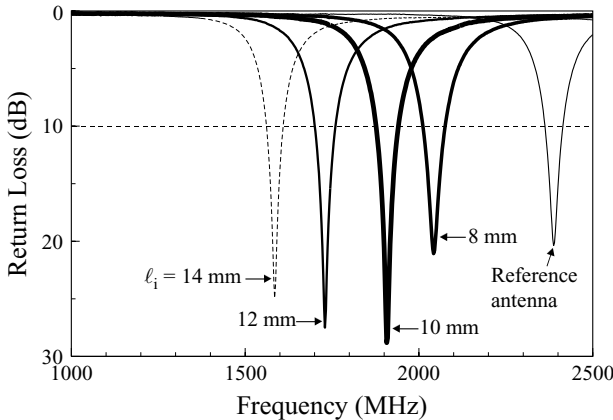


**FIGURE 2.11** Measured return loss against frequency; antenna parameters are given in Table 2.1. (From Ref. 9, © 2001 John Wiley & Sons, Inc.)

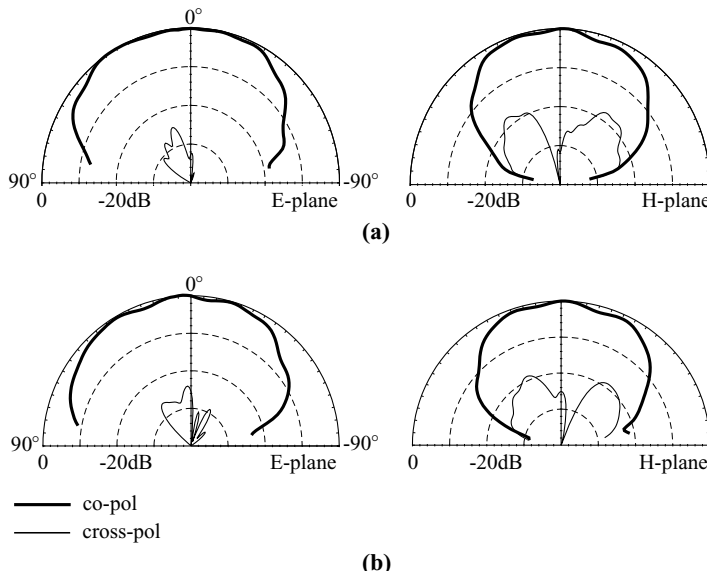
Results for a reference antenna ( $\ell_o = \ell_i = 0$ ) are shown for comparison. Note that the embedded slots in the ground plane have very small effects on the feed position  $d_p$  for achieving good impedance matching of the prototypes;  $d_p$  was chosen to be 5 mm.

For the reference antenna, the fundamental resonant mode is excited at 2387 MHz with a 10-dB return-loss bandwidth of 2.0%. For increasing slot length  $\ell_i$ , it is seen that the fundamental resonant frequency is quickly lowered. For antenna 4 ( $\ell_i = 14$  mm), the resonant frequency  $f_r$  is 1587 MHz, which is about 0.66 times that of the reference antenna. This suggests that an antenna size reduction as large as about 56% can be achieved for the proposed antenna operated at a fixed frequency. Moreover, it is clearly seen that the impedance bandwidths of the prototypes (antennas 1–4) are all greater than that of the reference antenna. This behavior is largely owing to the meandering slots embedded in the antenna's ground plane, which effectively lower the quality factor of the proposed antenna.

**TABLE 2.1 Performance of the Compact Microstrip Antenna with a Meandered Ground Plane Shown in Figure 2.10 [9]<sup>a</sup>**

	$\ell_o, \ell_i$ (mm)	$d_p$ (mm)	$f_r$ (MHz)	Bandwidth (MHz, %)	Gain at $f_r$ (dBi)	F/B (dB)
Antenna 1	10, 8	5	2043	64, 3.1	4.1	3.1
Antenna 2	10, 10	5	1907	67, 3.5	4.1	2.8
Antenna 3	10, 12	5	1723	64, 3.7	4.6	2.2
Antenna 4	10, 14	5	1587	50, 3.2	3.9	2.0
Reference	0, 0	5	2387	48, 2.0	3.0	9.3

<sup>a</sup> $h = 1.6$  mm,  $\epsilon_r = 4.4$ ,  $L = 30$  mm,  $W = 20$  mm,  $\ell_i = 10$  mm, and ground-plane size =  $50 \times 50$  mm<sup>2</sup>. F/B is the measured front-to-back ratio of the radiation intensity.



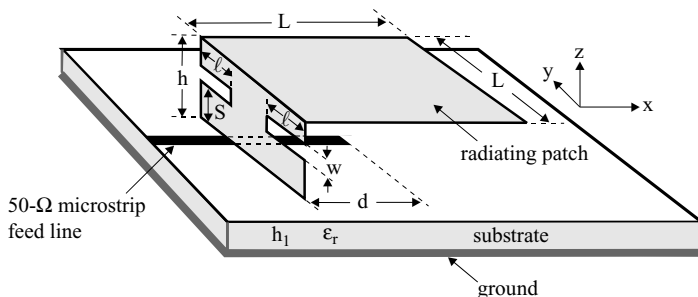
**FIGURE 2.12** Measured *E*-plane ( $x$ - $z$  plane) and *H*-plane ( $y$ - $z$  plane) radiation patterns for the compact microstrip antenna studied in Figure 2.11. (a) Antenna 3 ( $\ell_i = 12$  mm) at 1723 MHz, (b) antenna 4 ( $\ell_i = 14$  mm) at 1587 MHz. (From Ref. 9, © 2001 John Wiley & Sons, Inc.)

Figure 2.12 plots the measured *E*- and *H*-plane radiation patterns for antennas 3 and 4. Good broadside radiation patterns are observed. The measured antenna gain (see Table 2.1) is seen to be greater than that of the reference antenna. From IE3D™ simulation results, the radiation efficiency of the proposed antenna with an FR4 substrate is greater than 50%, which is much greater than that (about 30%) of the reference antenna with the same FR4 substrate. The increase in the radiation efficiency is probably associated with the embedded slots in the ground plane, which lower the quality factor of the proposed antenna, and may account for the observed antenna gain enhancement for the proposed antenna. The results also suggest that, for obtaining optimal bandwidth and gain enhancement, the slot length  $\ell_i$  should be slightly greater than half the patch width ( $W/2 = 10$  mm in this study) in the proposed design (see antenna 3 in Table 2.1). The front-to-back ratio (F/B) was also measured. From the measured results, the backward radiation of antenna 3 is increased by about 7 dBi compared to the reference antenna. This increase in the backward radiation is contributed to by the embedded slots in the ground plane and the decreased ground-plane size in wavelength. In summary, for the case using an FR4 substrate studied here, the impedance bandwidth of the constructed prototype is about 1.85 times that (3.7% vs. 2%) of a corresponding conventional microstrip antenna without embedded slots in the antenna's ground plane, and a gain enhancement of 1.6 dBi (4.6 vs. 3.0 dBi) is obtained.

## 2.5 USE OF A PLANAR INVERTED-L PATCH

The PIL patch is also a good candidate for achieving compact microstrip antennas. Two design examples of the PIL patch antenna with a microstrip-line feed [10, 11] are discussed here. Figure 2.13 shows the geometry of a microstrip-line-fed PIL patch antenna. In addition to compact operation, this proposed design is also suitable for dual-frequency operation. The PIL patch has a total length of  $L + h$ , and consists of a horizontal portion (length  $L$ ) and a vertical portion (length  $h$ ). The horizontal portion is selected to be a square patch having dimensions of  $L \times L$ , and is supported by plastic posts with a height of  $h$  above a grounded substrate. The grounded substrate has a thickness of  $h_1$  and relative permittivity  $\epsilon_r$ , on which a  $50\text{-}\Omega$  microstrip feed line is printed. The PIL patch is centered above the microstrip feed line, with the edge of the patch's vertical portion directly connected to the feed line. The portion of the feed line below the patch's horizontal portion has a length of  $d$ , which is used as a tuning stub for achieving good impedance matching for the PIL patch antenna. The optimal length  $d$  is found to be about 40% of the total length of the PIL patch [i.e.,  $d \approx 0.4(L + h)$ ].

With the proposed design, the antenna's first two resonant frequencies, which are, respectively, associated with resonant modes with the length of the PIL patch being about one quarter-wavelength and one half-wavelength, can be excited with good impedance matching, and single-feed dual-frequency operation can thus be obtained. In order to obtain various frequency ratios of the two resonant frequencies, two identical slits having dimensions of  $\ell \times w$  are inserted at the nonradiating edges of the PIL patch's vertical portion. The two inserted slits cause different meandering effects on the excited patch surface current paths of the two resonant frequencies, and thus various frequency ratios can be obtained with the selection of various slit dimensions. Prototypes of the present design have been constructed and studied. Figure 2.14 shows the measured return loss of the constructed prototypes, and Figure 2.15 presents the measured first two resonant frequencies  $f_1$  and  $f_2$  and their frequency



**FIGURE 2.13** Geometry of a planar inverted-L patch antenna for compact operation. (From Ref. 10, © 2000 John Wiley & Sons, Inc.)

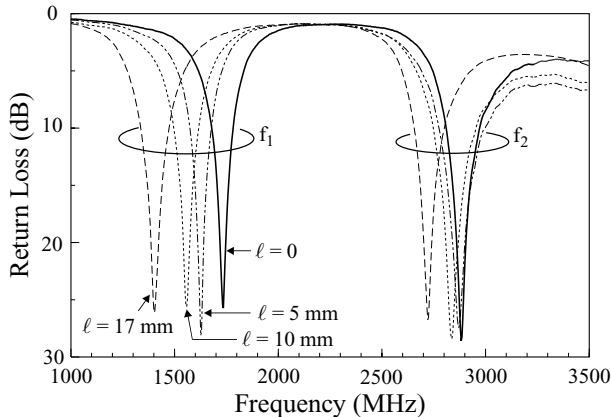


**FIGURE 2.14** Measured return loss against frequency for the PIL patch antenna shown in Figure 2.13;  $\epsilon_r = 4.4$ ,  $L = 35$  mm,  $h = 10$  mm,  $S = 4.5$  mm,  $w = 1.6$  mm,  $h_1 = 0.8$  mm,  $d = 18$  mm, and ground-plane size =  $110 \times 130$  mm $^2$ . (From Ref. 10, © 2000 John Wiley & Sons, Inc.)

ratio  $f_2/f_1$ . The corresponding measured data are listed in Table 2.2. The PIL patch has a total length of 45 mm ( $L = 35$  mm,  $h = 10$  mm). Note that, with the selection of the length  $h$  of about 30% of the length  $L$ , good broadside radiation characteristics for the antenna's first two resonant frequencies are obtained. Inexpensive FR4 substrates ( $\epsilon_r = 4.4$ ,  $h_1 = 0.8$  mm) with a ground plane size of  $110 \times 130$  mm $^2$  were used in the study.

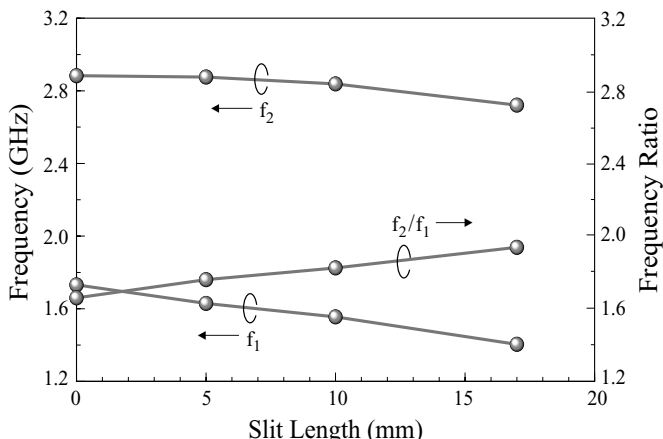


**FIGURE 2.15** Measured first two resonant frequencies  $f_1$  and  $f_2$  and their frequency ratio,  $f_2/f_1$ , for the PIL patch antenna studied in Figure 2.14. (From Ref. 10, © 2000 John Wiley & Sons, Inc.)

**TABLE 2.2 Dual-Frequency Performance of the PIL Patch Antenna Shown in Figure 2.13 [10]<sup>a</sup>**

	$\ell$ (mm)	$f_1$ (MHz), BW (%)	$f_2$ (MHz), BW (%)	$f_2/f_1$
Antenna 1	0	1731, 5.7	2883, 6.0	1.66
Antenna 2	5	1629, 6.4	2876, 7.8	1.76
Antenna 3	10	1555, 7.4	2838, 7.4	1.83
Antenna 4	17	1404, 9.7	2721, 5.4	1.94

<sup>a</sup>Antenna parameters are given in Figure 2.14.

When there are no inserted slits ( $\ell = 0$ ), the frequency  $f_1$  approximately corresponds to the length of the PIL patch being about one quarter-wavelength, that is,

$$f_1 = \frac{c}{4(L + h)}, \quad (2.2)$$

where  $c$  is the speed of light. On the other hand, the frequency  $f_2$  is associated with the length of the PIL patch being about one half-wavelength. However, mainly owing to the bending of the PIL patch, the null point of the excited patch surface current distributions is shifted from the patch center to the bent edge (see the simulated results in Figure 2.16, which are obtained from the simulation software IE3D™). This characteristic makes the excited patch surface current distribution on the patch's horizontal portion at the frequency  $f_2$  a uniform distribution and about the same as that at the frequency  $f_1$ . Similar broadside radiation characteristics for both  $f_1$  and  $f_2$  can thus be expected. Measured radiation patterns of  $f_1$  and  $f_2$  shown in Figure 2.17 confirm this prediction. Figure 2.18 shows the measured antenna gain against frequency for the two operating bands; about 6 dBi for  $f_1$  and 8 dBi for  $f_2$  are obtained.

When there are inserted slits, it is observed that, with increasing slit length, the frequency  $f_1$  is quickly decreased, whereas the frequency  $f_2$  is relatively insensitive

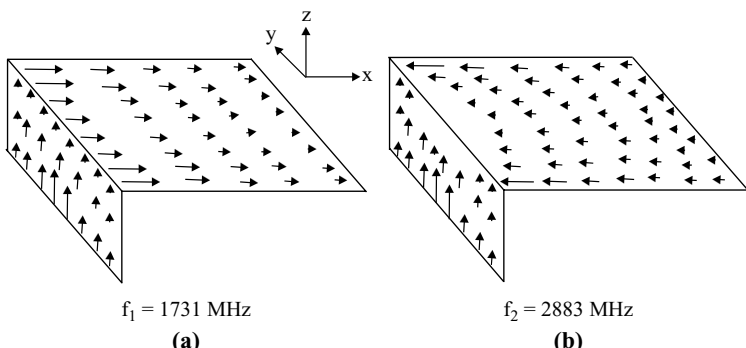


**FIGURE 2.16** Simulated patch surface current distribution for the PIL patch antenna studied in Figure 2.14 with  $\ell = 0$ . (a)  $f_1 = 1731$  MHz, (b)  $f_2 = 2883$  MHz. (From Ref. 10, © 2000 John Wiley & Sons, Inc.)

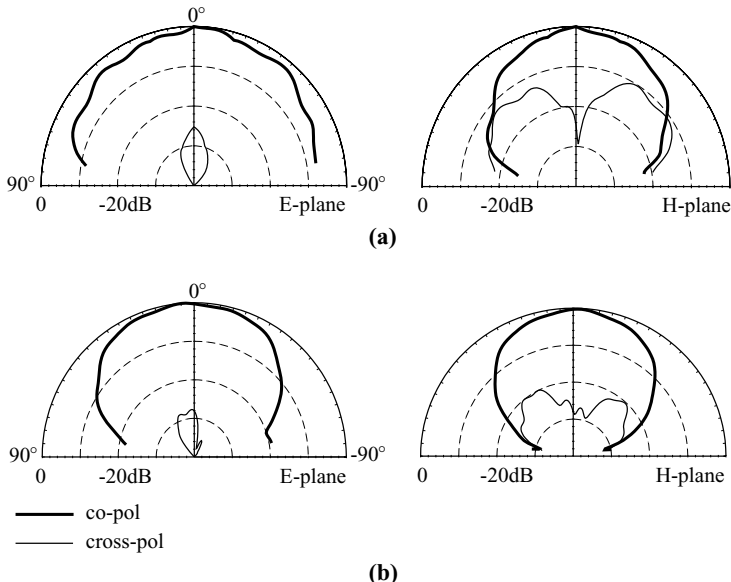


**FIGURE 2.17** Measured *E*-plane ( $x$ - $z$  plane) and *H*-plane ( $y$ - $z$  plane) radiation patterns for the PIL patch antenna studied in Figure 2.14 with  $\ell = 0$ . (a)  $f_1 = 1731$  MHz, (b)  $f_2 = 2883$  MHz. (From Ref. 10, © 2000 John Wiley & Sons, Inc.)

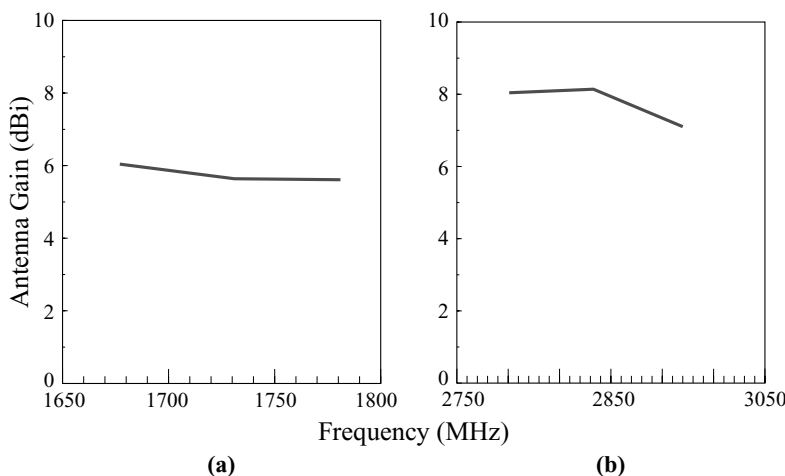


**FIGURE 2.18** Measured antenna gain against frequency for the PIL patch antenna studied in Figure 2.14 with  $\ell = 0$ . (a) The lower band, (b) the upper band. (From Ref. 10, © 2000 John Wiley & Sons, Inc.)

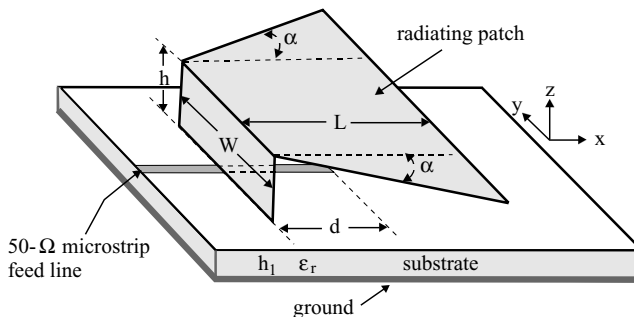


**FIGURE 2.19** Geometry of a planar inverted-L patch antenna with a tapered patch width for compact operation. (From Ref. 11, © 2001 John Wiley & Sons, Inc.)

to the inserted slits. This behavior results in a tunable frequency ratio in a range of about 1.66–1.94. The measured radiation characteristics are similar to those shown in Figures 2.17 and 2.18. For the impedance bandwidths, 5.7–9.7% for the frequency  $f_1$  and 5.4–7.8% for the frequency  $f_2$  have been obtained.

Figure 2.19 shows the geometry of another design for a PIL patch antenna for compact operation. This design is also suitable for dual-frequency operation. This antenna's vertical portion has a height of  $h$  and a width of  $W$ . The horizontal portion has a length of  $L$  and a tapering angle of  $\alpha$ . The antenna is directly fed by a 50- $\Omega$  microstrip line, which has a tuning stub of length  $d$  and is printed on a microwave substrate of thickness  $h_1$  and relative permittivity  $\epsilon_r$ . By varying the tapering angle  $\alpha$ , the first two resonant frequencies of the proposed antenna can have good impedance matching simply by adjusting the tuning-stub length  $d$ . However, for  $\alpha$  greater than 45°, it becomes difficult to obtain good impedance matching for the first two resonant frequencies of the proposed antenna.

Prototypes of this design have been successfully implemented. Table 2.3 lists the obtained dual-frequency performance for the constructed prototypes with  $\alpha$  varying

**TABLE 2.3** Dual-Frequency Performance of the PIL Patch Antenna Shown in Figure 2.19 [11]<sup>a</sup>

	$\alpha$ (deg)	$d$ (mm)	$f_1$ , BW (MHz, %)	$f_2$ , BW (MHz, %)	$f_2/f_1$
Antenna 1	0	17	1755, 7.6	2926, 4.7	1.67
Antenna 2	8	17	1671, 6.8	2844, 5.4	1.70
Antenna 3	16	17	1625, 7.1	2820, 5.5	1.74
Antenna 4	24	18	1532, 7.1	2765, 5.8	1.80
Antenna 5	30	18	1482, 6.8	2710, 5.9	1.83
Antenna 6	35	20	1437, 6.1	2638, 5.7	1.84
Antenna 7	40	23	1364, 5.1	2814, 12.0	2.06
Antenna 8	45	26	1268, 3.7	2902, 10.2	2.29

<sup>a</sup>Antenna parameters are given in Figure 2.20.

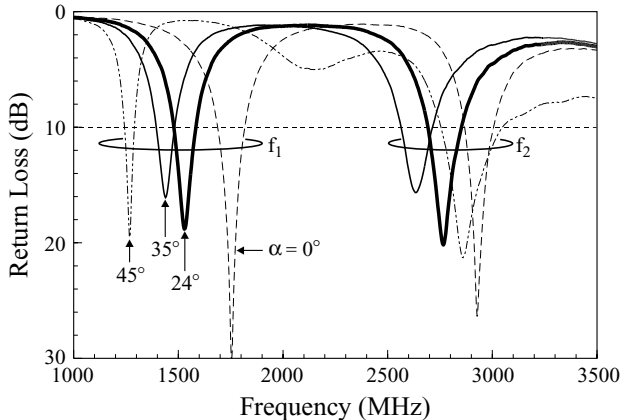


**FIGURE 2.20** Measured return loss against frequency for the PIL patch antenna shown in Figure 2.19;  $L = 35$  mm,  $W = 35$  mm,  $h = 8$  mm,  $\epsilon_r = 4.4$ ,  $h_1 = 0.8$  mm, and ground-plane size =  $110 \times 150$  mm $^2$ . (From Ref. 11, © 2001 John Wiley & Sons, Inc.)

from  $0^\circ$  to  $45^\circ$ . Figure 2.20 shows the measured return loss for  $\alpha = 0^\circ, 24^\circ, 35^\circ$ , and  $45^\circ$ , the measured first two resonant frequencies and their frequency ratio are presented in Figure 2.21. The lengths of the vertical and horizontal portions were chosen to be 8 mm ( $h$ ) and 35 mm ( $L$ ), respectively. The microstrip feed line was printed on an FR4 substrate of thickness 0.8 mm and relative permittivity 4.4. The results clearly show that the first resonant frequency  $f_1$  decreases with increasing angle  $\alpha$ . For the case with  $\alpha = 0^\circ$ ,  $f_1$  can be approximately determined from Equation (2.2);

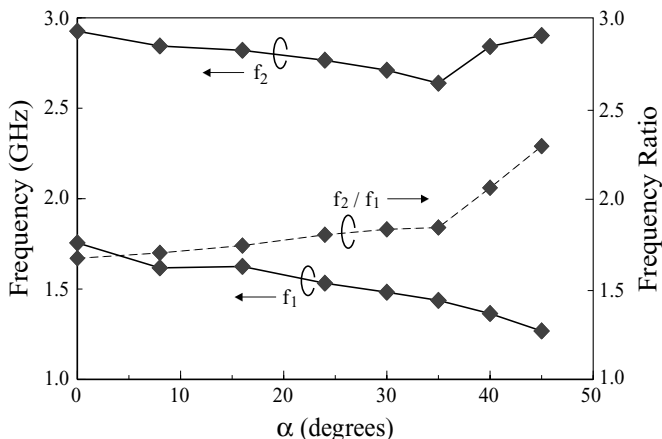


**FIGURE 2.21** Measured first two resonant frequencies  $f_1$  and  $f_2$  and their frequency ratio,  $f_2/f_1$ , for the PIL patch antenna studied in Figure 2.20. (From Ref. 11, © 2001 John Wiley & Sons, Inc.)

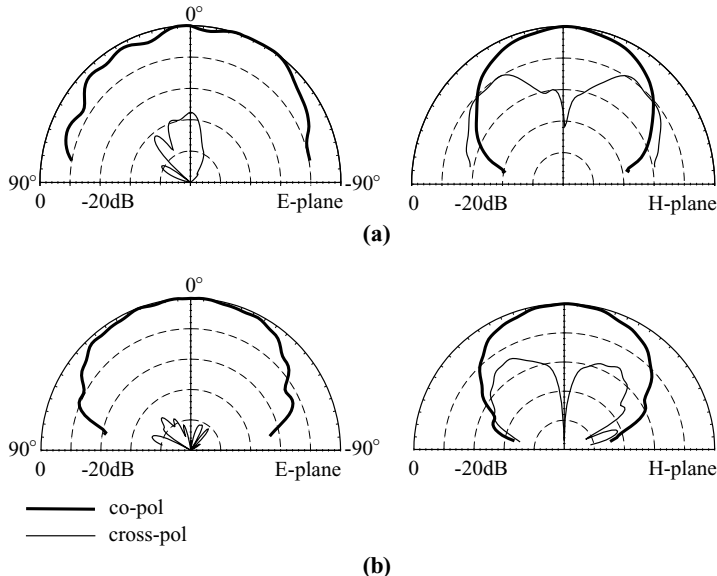


**FIGURE 2.22** Measured *E*-plane ( $x$ - $z$  plane) and *H*-plane ( $y$ - $z$  plane) radiation patterns for the PIL patch antenna studied in Figure 2.20 with  $\alpha = 24^\circ$ . (a)  $f_1 = 1532$  MHz; (b)  $f_2 = 2765$  MHz. (From Ref. 11, © 2001 John Wiley & Sons, Inc.)

that is, the first resonant frequency is associated with the length of the PIL patch antenna being about one quarter-wavelength. The second resonant frequency  $f_2$  also shows a decreasing trend when the angle of  $\alpha$  increases up to  $35^\circ$ . When  $\alpha$  is greater than  $35^\circ$ ,  $f_2$  is seen to increase with increasing angle  $\alpha$ . This characteristic makes the frequency ratio  $f_2/f_1$  of the two operating frequencies increase, and a wider frequency-ratio range (about 1.67–2.29) than that (about 1.66–1.94) obtained for the PIL patch antenna shown in Figure 2.13 is achieved.

Typical measured radiation patterns at the two operating frequencies for the prototype with  $\alpha = 24^\circ$  are plotted in Figure 2.22. The two operating frequencies are seen to have the same polarization planes, and good broadside radiation patterns are observed, although relatively larger cross-polarization for *H*-plane radiation is seen. Figure 2.23 shows the measured antenna gain for the lower and upper operating bands of a prototype with  $\alpha = 24^\circ$ . The two operating bands are seen to have about the same antenna gain level of about 6.5 dBi.

## 2.6 USE OF AN INVERTED U-SHAPED OR FOLDED PATCH

The lengthening of the excited patch surface current path for antenna size reduction can be achieved by using an inverted U-shaped or folded patch. Figure 2.24 shows a typical design example with an inverted U-shaped patch, which is obtained by adding

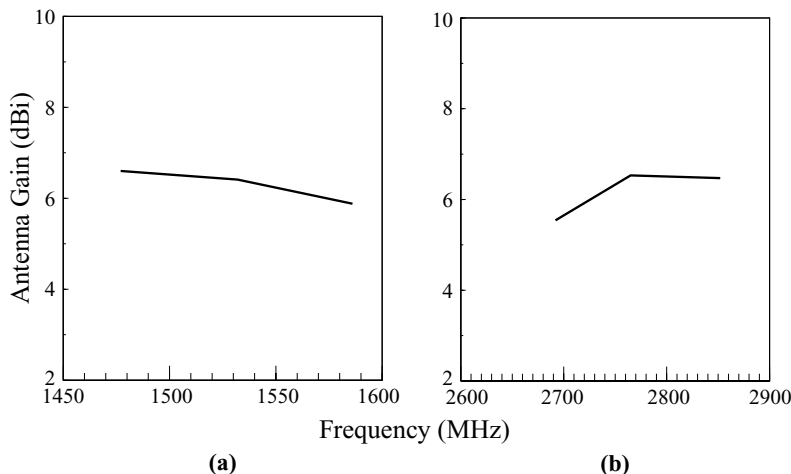


**FIGURE 2.23** Measured antenna gain against frequency for the PIL patch antenna studied in Figure 2.20 with  $\alpha = 24^\circ$ . (a) The lower band, (b) the upper band. (From Ref. 11, © 2001 John Wiley & Sons, Inc.)

two downward rims at the two radiating edges of a planar rectangular or square patch. [When the two downward rims are further bent toward the patch center, a folded patch can be obtained (see the configurations shown in Figure 1.4).] With the added rims, the effective resonant length of the inverted U-shaped patch will be greater than that of a conventional planar patch. This compact design is especially suitable for applications with air-substrate patch antennas, and although the maximum length of the downward rim is limited by the air-substrate thickness, a significant lowering of the resonant frequency of about 32% can be achieved for a patch antenna with

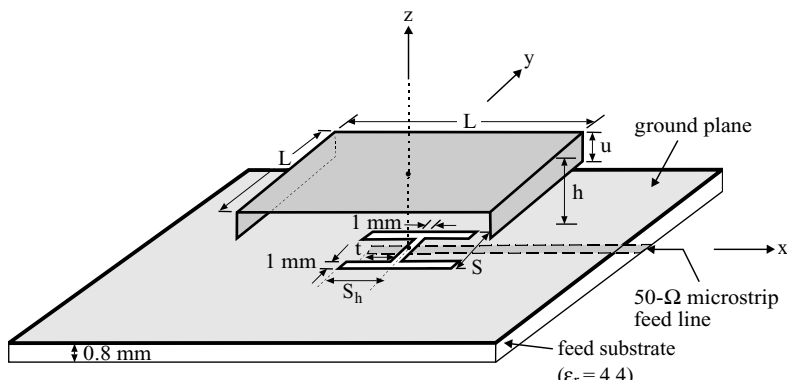


**FIGURE 2.24** Geometry of a compact design with an inverted U-shaped radiating patch. (From Ref. 12, © 2001 IEEE, reprinted with permission.)

an air-substrate thickness of about 5% of the wavelength of the center operating frequency. When the patch's aspect ratio and desired operating frequency are fixed, this lowering in resonant frequency corresponds to an antenna size reduction of about 54%. Since the lengthening of the effective patch's surface current paths is due to the additional downward paths in the added rims, which is different from that of the meandered designs [1, 6], a relatively very small perturbation on the excited surface current distribution in the radiating patch is expected. This implies that it is possible for the radiation characteristics of this compact design to be as good as those of a corresponding conventional patch antenna with a planar radiating patch.

Prototypes of this compact design have been successfully implemented [12]. The planar or top portion of the inverted U-shaped radiating patch is square and has a side length  $L$ . The two downward rims are identical and are added at the two radiating edges of the top patch. The downward rims have a length of  $u$ , which is smaller than the air-substrate thickness  $h$ . Centered below the inverted U-shaped patch is an H-shaped coupling slot cut in the ground plane of a microwave substrate of thickness 0.8 mm and relative permittivity 4.4. On the other side of the ground plane, a  $50\text{-}\Omega$  microstrip feed line for feeding the inverted U-shaped patch through the H-shaped coupling slot is printed. The H-shaped coupling slot has a central arm of dimensions  $1 \text{ mm} \times S$  and two side arms of dimensions  $1 \text{ mm} \times 2S_h$ . Compared to a conventional narrow rectangular coupling slot, the use of an H-shaped coupling slot can reduce the antenna's backward radiation. For the proposed design with various rim lengths, good impedance matching can be obtained by selecting proper values of  $S$ ,  $S_h$ , and the tuning-stub length  $t$  of the  $50\text{-}\Omega$  microstrip feed line.

Figure 2.25 shows the measured return loss for constructed prototypes (antennas 1–3) and a reference antenna (a design without downward rims). The top square patch had a side length of 46 mm, and the air-substrate thickness was chosen to be

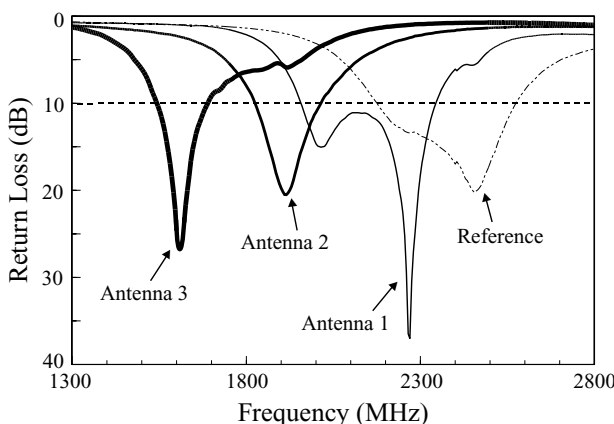


**FIGURE 2.25** Measured return loss for the reference antenna and the prototypes (antennas 1–3) of the compact design in Figure 2.24. Antenna parameters are given in Table 2.4. (From Ref. 12, © 2001 IEEE, reprinted with permission.)

**TABLE 2.4 Parameters and Performance of the Antenna Design Shown in Figure 2.24 [12]<sup>a</sup>**

	$u$ (mm)	$S, S_h, t$ (mm)	$f_c$ (MHz)	Bandwidth (MHz, %)
Reference	0	21, 3, 5	2375	400, 16.8
Antenna 1	4	21, 5, 10	2150	388, 18.0
Antenna 2	6	21, 10, 10	1920	190, 9.9
Antenna 3	9	17, 10, 7	1615	150, 9.3

<sup>a</sup> $L = 46$  mm,  $h = 9.6$  mm, and ground-plane size =  $100 \times 100$  mm<sup>2</sup>.

9.6 mm. The length of the downward rim was varied from 0 (reference antenna) to 4 mm (antenna 1), 6 mm (antenna 2), and 9 mm (antenna 3). The corresponding design parameters ( $S, S_h, t$ ) and obtained center operating frequency and impedance bandwidth are listed in Table 2.4. It is clearly seen that the center operating frequency  $f_c$  quickly decreases with increasing rim length. For antenna 3, the center frequency is lowered to 1615 MHz, which is about 0.68 times that (2375 MHz) of the reference antenna. The lowering ratio in the center operating frequency can also be approximately predicted from  $L/(L + 2u)$ , which gives a value of about 0.72 for antenna 3. This indicates that the lowering of the center operating frequency indeed results from

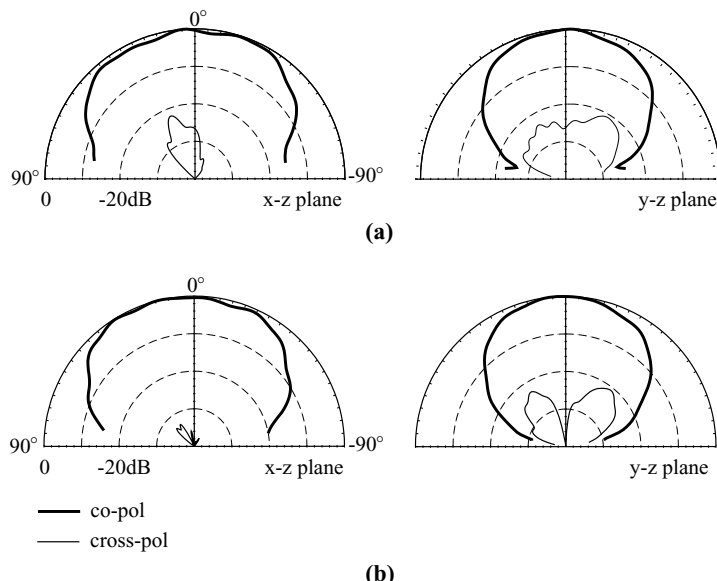


**FIGURE 2.26** Measured  $E$ -plane ( $x$ - $z$  plane) and  $H$ -plane ( $y$ - $z$  plane) radiation patterns for the compact antenna studied in Figure 2.25. (a) Antenna 2 at 1920 MHz, (b) antenna 3 at 1615 MHz. (From Ref. 12, © 2001 IEEE, reprinted with permission.)

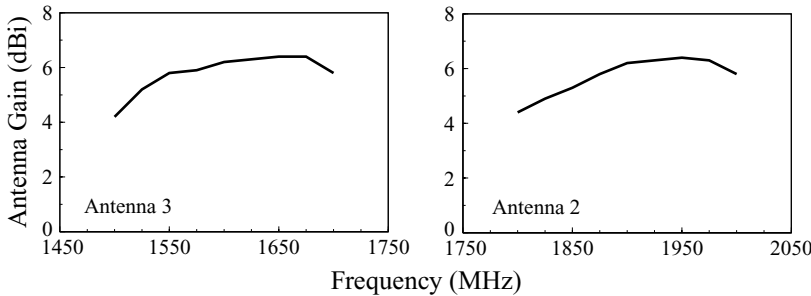


**FIGURE 2.27** Measured antenna gain in broadside direction against frequency for antennas 2 and 3 of the compact antenna studied in Figure 2.25. (From Ref. 12, © 2001 IEEE, reprinted with permission.)

adding the downward rims. Notice that, when considering the fixed patch aspect ratio and operating frequency, antenna 3 will have an antenna size about 46% of that of the reference antenna; that is, a 54% antenna size reduction is achieved.

Also note that the obtained impedance bandwidth decreases from 16.8% for the reference antenna to 9.3% for antenna 3. This is largely owing to the large decrease of the electrical thickness of the air substrate for antenna 3, whose air-substrate thickness corresponds to about  $0.05\lambda_0$  ( $\lambda_0$  is the free-space wavelength of the center operating frequency), smaller than that of the reference antenna (about  $0.076\lambda_0$ ). Measured radiation patterns at the center operating frequency for antennas 2 and 3 are plotted in Figure 2.26 and measured antenna gain is shown in Figure 2.27. Very good broadside radiation patterns are observed, and the cross-polarization radiation in the principal planes is seen to be less than  $-20$  dB. In the broadside direction of antenna 3, the cross-polarization radiation is even lower than  $-40$  dB. Peak antenna gain for antennas 2 and 3 is about 6.4 dBi, with gain variations less than about 2.0 dBi for operating frequencies within the impedance bandwidth. The results show that, with the present compact design, the required lowering in the antenna's fundamental resonant frequency can easily be controlled by the length of the downward rim of the inverted U-shaped patch. Although the antenna's resonant frequency is significantly lowered, very small perturbations on the surface current distribution in the planar or top portion of the inverted U-shaped patch can be expected, and good broadside radiation characteristics for this compact design can be obtained.

## REFERENCES

1. S. Dey and R. Mittra, "Compact microstrip patch antenna," *Microwave Opt. Technol. Lett.* **13**, 12–14, Sept. 1996.
2. K. L. Wong and W. S. Chen, "Compact microstrip antenna with dual-frequency operation," *Electron. Lett.* **33**, 646–647, April 10, 1997.
3. R. Waterhouse, "Small microstrip patch antenna," *Electron. Lett.* **31**, 604–605, April 13, 1995.

4. I. Park and R. Mittra, "Aperture-coupled small microstrip antenna," *Electron. Lett.* **32**, 1741–1742, Sept. 12, 1996.
5. C. L. Tang, H. T. Chen, and K. L. Wong, "Small circular microstrip antenna with dual-frequency operation," *Electron. Lett.* **33**, 1112–1113, June 19, 1997.
6. K. L. Wong, C. L. Tang, and H. T. Chen, "A compact meandered circular microstrip antenna with a shorting pin," *Microwave Opt. Technol. Lett.* **15**, 147–149, June 20, 1997.
7. K. L. Wong and S. C. Pan, "Compact triangular microstrip antenna," *Electron. Lett.* **33**, 433–434, March 13, 1997.
8. S. C. Pan and K. L. Wong, "Dual-frequency triangular microstrip antenna with a shorting pin," *IEEE Trans. Antennas Propagat.* **45**, 1889–1891, Dec. 1997.
9. J. S. Kuo and K. L. Wong, "A compact microstrip antenna with meandering slots in the ground plane," *Microwave Opt. Technol. Lett.* **29**, 95–97, April 20, 2001.
10. J. S. Kuo and K. L. Wong, "A dual-frequency L-shaped patch antenna," *Microwave Opt. Technol. Lett.* **27**, 177–179, Nov. 5, 2000.
11. J. S. Kuo and K. L. Wong, "Dual-frequency operation of a planar inverted L antenna with tapered patch width," *Microwave Opt. Technol. Lett.* **28**, 126–127, Jan. 20, 2001.
12. K. L. Wong and H. C. Tung, "A compact patch antenna with an inverted U-shaped radiating patch," in *2001 IEEE Antennas Propagat. Soc. Int. Symp. Dig.*, pp. 728–731.

## CHAPTER THREE

---

# Compact Broadband Microstrip Antennas

---

### 3.1 INTRODUCTION

The problem of achieving a wide impedance bandwidth (e.g., greater than or about 10% suitable for present-day cellular communication systems) for a compact microstrip antenna is becoming an important topic in microstrip antenna design. Recently, for a compact design using a shorted patch with a thick air substrate, the obtained impedance bandwidth (10-dB return loss) has been reported to be 10% or much greater. This kind of broadband shorted patch antenna is conventionally fed by using a probe feed [1–4], and is usually referred to as a planar inverted-F antenna (PIFA). Recently, various feed methods such as the use of an aperture-coupled feed [5], a microstrip-line feed [6], or a capacitively coupled [7] or an L-probe [8] feed for exciting shorted patch antennas for broadband operation have been demonstrated. Some typical design examples of reported broadband shorted patch antennas are given in this chapter.

Broadband operation has been achieved with the use of two stacked shorted patches [9–14]. It has been reported that, with a total thickness of 4 mm ( $0.024\lambda_0$  at 1800 MHz), a stacked shorted patch antenna can have a 10-dB return-loss bandwidth of 9.6%, meeting the requirement for GSM1800 [12]. Broadband techniques suitable for applications for compact microstrip antennas with a thin dielectric substrate are available in the open literature. One of these compact broadband techniques uses a chip resistor of low resistance (usually on the order of  $1\ \Omega$ ) connected between the antenna's radiating patch and ground plane [15–21]. In this case, with the chip-resistor loading technique, similar antenna size reduction to the compact design using shorting-pin loading can be obtained. Moreover, owing to the introduced small ohmic loss of the chip resistor, the quality factor of the microstrip antenna is greatly lowered. When an inexpensive FR4 substrate of thickness 1.6 mm and relative permittivity 4.4 is used, such a chip-resistor-loaded microstrip antenna can have an

impedance bandwidth of about 10% or greater. Design examples of the chip-resistor loading technique applied to rectangular, circular, and triangular microstrip antennas with various feed methods such as a probe feed, a microstrip-line feed, and an aperture-coupled feed are presented. The design of a meandered planar inverted-F antenna with a chip resistor is also discussed. Other compact broadband microstrip antenna designs such as embedding suitable slots in the antenna's radiating patch [22] or in the ground plane [23] are also described.

### 3.2 USE OF A SHORTED PATCH WITH A THICK AIR SUBSTRATE

#### 3.2.1 Probe-Fed Shorted Patch or Planar Inverted-F Antenna (PIFA)

Figure 3.1 shows a typical design example for a probe-fed shorted patch antenna operated at dual bands of 1.8 and 2.45 GHz. Between the rectangular radiating patch and the ground plane is an air substrate of thickness 9.6 mm. The rectangular patch has dimensions of  $36 \times 16$  mm<sup>2</sup>, an L-shaped slit of width 1 mm and total length 40 mm is cut in the rectangular patch for achieving an additional operating band at 2.45 GHz (the industrial, scientific, medical [ISM] band); the lower operating band at 1.8 GHz is mainly controlled by the dimensions of the rectangular patch. A shorting strip of width 2.5 mm is used for short-circuiting the rectangular patch to the ground plane. Measured return loss for this probe-fed shorted patch antenna is shown in Figure 3.2. The IE3D™ simulation results are shown in the figure for comparison. Reasonable agreement between the simulation results and measured data is seen. For the lower operating band, a wide impedance bandwidth of 302 MHz (1588–1890 MHz), or about 17.4% referenced to the center frequency (1739 MHz), is obtained, which covers the DCS band (1710–1880 MHz). For the higher operating band, the impedance

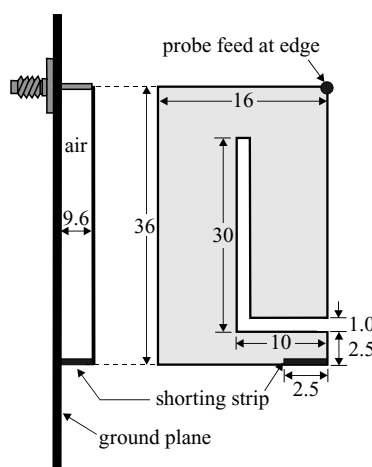


**FIGURE 3.1** Geometry of a probe-fed shorted patch antenna for broadband and dual-frequency operations. The dimensions given in the figure are in millimeters.

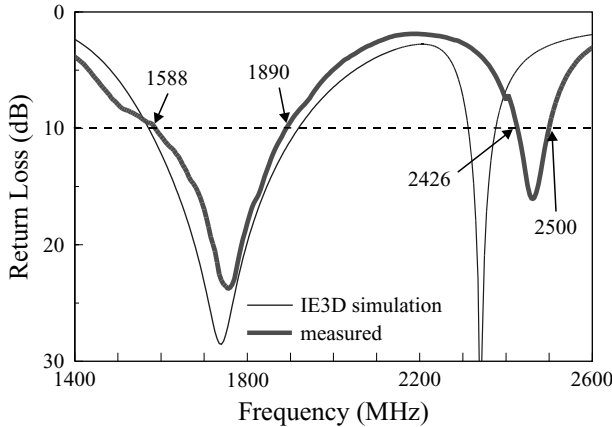


**FIGURE 3.2** Measured and simulated return loss of the probe-fed shorted patch antenna shown in Figure 3.1 with a ground-plane size of  $18 \times 80 \text{ mm}^2$ .

bandwidth obtained is 74 MHz (2426–2500 MHz), or about 3.0% referenced to the center frequency at 2463 MHz. The obtained impedance bandwidth of the higher operating band is close to the bandwidth requirement of the ISM band at 2.45 GHz. Radiation patterns at the center frequency of the lower and upper operating bands were also measured. Results are presented in Figure 3.3. Large cross-polarization is

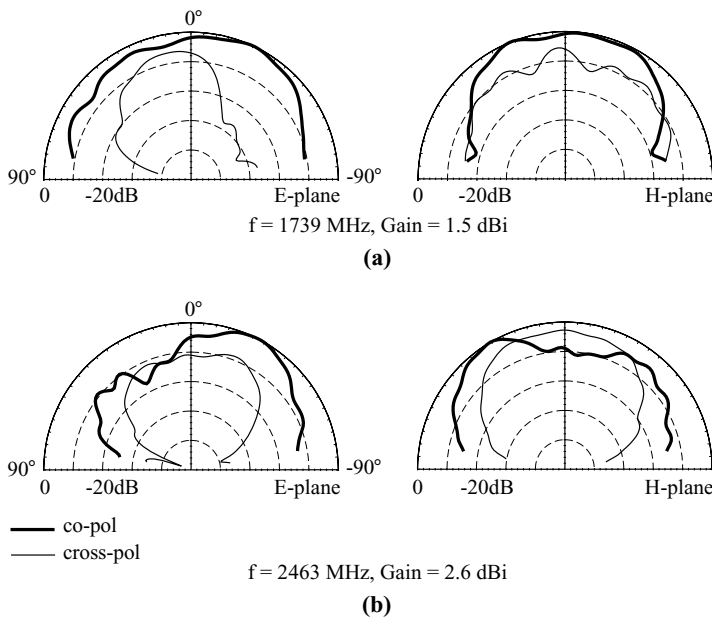


**FIGURE 3.3** Measured radiation patterns of the probe-fed shorted patch antenna shown in Figure 3.1. (a)  $f = 1739 \text{ MHz}$ , (b)  $f = 2463 \text{ MHz}$ .

observed for both operating frequencies. It should be noted that this characteristic can be an advantage for indoor wireless communication applications.

### 3.2.2 Aperture-Coupled Shorted Patch

A shorted patch antenna fed by an aperture-coupled feed is a promising design for achieving broadband operation. Figure 3.4 shows the geometry of a broadband aperture-coupled shorted patch antenna with an H-shaped coupling slot. A rectangular patch of length  $L$  and width  $W$  is short-circuited to the ground plane of a grounded FR4 substrate (thickness 0.8 mm and relative permittivity 4.4) by a conducting wall of dimensions  $W \times h$ . In this case, the shorted patch is considered to have an air substrate of thickness  $h$ . An H-shaped coupling slot is cut in the ground plane and centered below the shorted patch. The center arm of the H-shaped slot has a width of 2 mm and a length of  $W_s$ . The upper (closer to the shorting wall) and lower sections of the two side arms of the H-shaped slots have lengths  $S_1$  and  $S_2$ , respectively, and have the same width of 1 mm. Through the H-shaped coupling slot, the electromagnetic energy from the  $50\text{-}\Omega$  microstrip feed line printed on the other side of the grounded substrate can be efficiently coupled to the shorted patch. By tuning  $W_s$ ,  $S_1$ ,  $S_2$ , and the tuning-stub length  $t$  of the microstrip feed line, good impedance matching over a wide frequency range can be achieved for this antenna. To achieve proper values of the above parameters, the simulation software IE3D<sup>TM</sup> is helpful in the design process, and with the use of an H-shaped coupling slot, the backward radiation of the aperture-coupled patch antenna can be reduced [24] compared to the design with a conventional narrow coupling slot.

Figure 3.5 shows the measured return loss of a constructed prototype. The thickness  $h$  of the air substrate was chosen to be 12 mm, which corresponds to about 0.07 times that of the free-space wavelength of the center operating frequency. The dimensions of the shorted patch were chosen to be  $30 \times 40 \text{ mm}^2$ . Measured results show that two resonant modes are excited with good impedance matching. This characteristic is similar to that observed for broadband patch antennas with a thick air substrate [25–27]. In this case, the impedance bandwidth, defined by the 10-dB return loss, is 450 MHz,

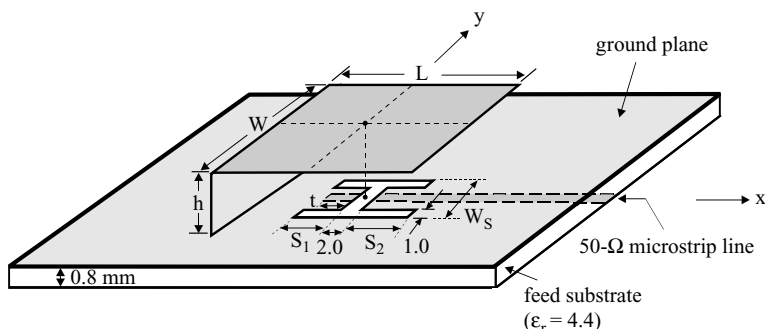


**FIGURE 3.4** Geometry of a broadband aperture-coupled shorted patch antenna with an H-shaped coupling slot. (From Ref. 5, © 2001 John Wiley & Sons, Inc.)

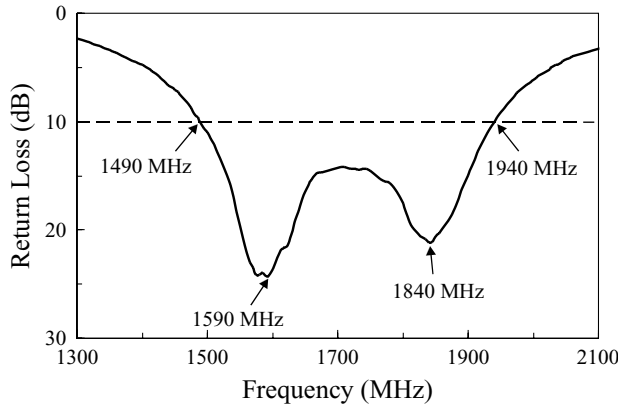


**FIGURE 3.5** Measured return loss for the aperture-coupled shorted patch antenna shown in Figure 3.4;  $L = 30$  mm,  $W = 40$  mm,  $h = 12$  mm,  $W_s = 18$  mm,  $S_1 = 11$  mm,  $S_2 = 13$  mm, and ground-plane size =  $100 \times 100$  mm $^2$ . (From Ref. 5, © 2001 John Wiley & Sons, Inc.)

or about 26.2% referenced to the center frequency at 1715 MHz. The impedance bandwidth obtained is also comparable to that of a conventional broadband probe-fed patch antenna with a U-slotted or E-shaped patch [25–27], although the patch size for the antenna studied is significantly smaller for a fixed operating frequency.

Radiation characteristics of the operating frequencies within the impedance bandwidth were also studied. Figure 3.6 plots the measured *E*-plane (*x*-*z* plane) and

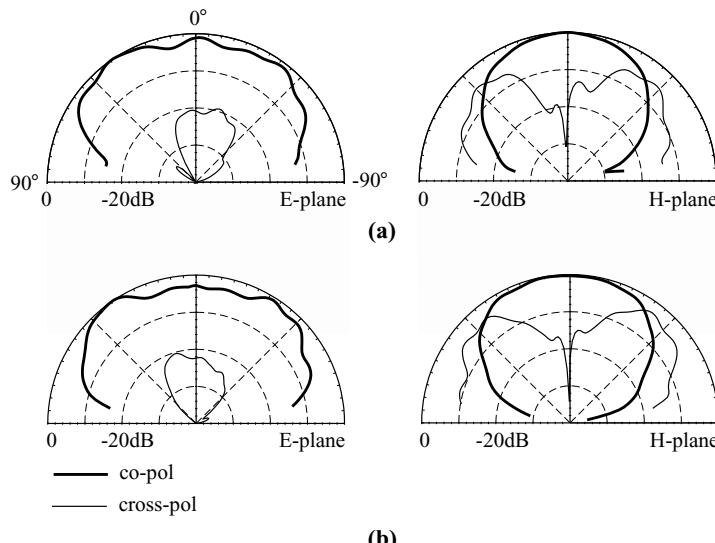


**FIGURE 3.6** Measured *E*- and *H*-plane radiation patterns for the antenna studied in Figure 3.5. (a)  $f = 1590$  MHz, (b)  $f = 1840$  MHz. (From Ref. 5, © 2001 John Wiley & Sons, Inc.)

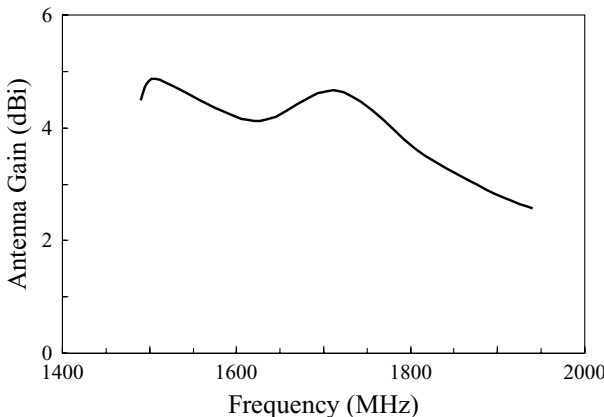


**FIGURE 3.7** Measured antenna gain in broadside direction for the antenna studied in Figure 3.5. (From Ref. 5, © 2001 John Wiley & Sons, Inc.)

*H*-plane (*y*–*z* plane) radiation patterns at the resonant frequencies of the two excited resonant modes. Good broadside radiation patterns are observed; however, relatively larger cross-polarization radiation is seen in the *H*-plane patterns, which is similar to what is observed for conventional probe-fed patch antennas with a thick air substrate [25–27]. The measured antenna gain for operating frequencies across the obtained wide impedance bandwidth is presented in Figure 3.7. The peak antenna gain measured is 4.9 dBi, and the gain variations within the bandwidth are less than 2.4 dBi.

### 3.2.3 Microstrip-Line-Fed Shorted Patch

A low-cost microstrip-line-fed shorted patch antenna suitable for base-station applications in DCS cellular communication systems has been studied. The geometry of the antenna is described in Figure 3.8. Both the shorted patch and the  $50\text{-}\Omega$  microstrip feed line have an air substrate, and the material cost is thus reduced to a

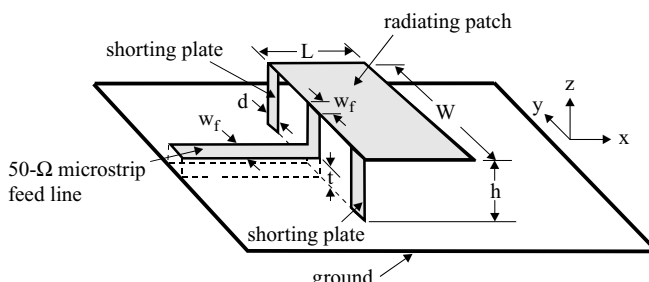


**FIGURE 3.8** Geometry of a broadband microstrip-line-fed shorted patch antenna. (From Ref. 6, © 2001 John Wiley & Sons, Inc.)

minimum. By using a pair of shorting plates of proper widths for short-circuiting the radiating patch to the antenna's ground plane, this antenna can be directly fed by the  $50\text{-}\Omega$  microstrip feed line, which greatly simplifies the antenna's impedance matching design.

The radiating patch has a length  $L$  and a width  $W$ , and is supported by plastic posts (not shown in the figure) above a ground plane. The distance of the radiating patch to the ground plane is  $h$ , and the radiating patch is short-circuited to the ground plane by using two identical shorting plates of width  $d$  placed at two ends of one of the patch's radiating edges. At the center of the patch edge with shorting plates, a  $50\text{-}\Omega$  microstrip feed line is used to directly feed the radiating patch. The signal strip of the microstrip feed line has a width  $w_f$  and is connected to the radiating patch, at the patch's shorted edge, by using a conducting strip of the same width  $w_f$ . Note that both the microstrip feed line and the shorted patch have an air substrate and have different heights of  $t$  and  $h$ , respectively, which provides more freedom in the antenna design. By selecting a suitable value of  $h$ , a wide impedance bandwidth suitable for applications in a DCS base station can be obtained, and good impedance matching of the proposed antenna is easily achieved by adjusting the width  $d$  of the two shorting plates.

For DCS base-station application, design parameters of this antenna were chosen to be  $L = 23.5$  mm,  $W = 58$  mm,  $h = 12.8$  mm,  $t = 3.2$  mm,  $d = 5.5$  mm, and  $w_f = 16$  mm. Figure 3.9 shows the measured return loss against frequency. It is clearly seen that an impedance bandwidth (1:1.5 voltage standing wave ratio [VSWR]) of larger than 10% covering the bandwidth requirement of the 1800-MHz band (1710–1880 MHz) is obtained. Typical measured radiation patterns at 1710, 1789, and 1880 MHz are presented in Figure 3.10. Good broadside radiation patterns are obtained. Again, relatively greater cross-polarization radiation is observed in the

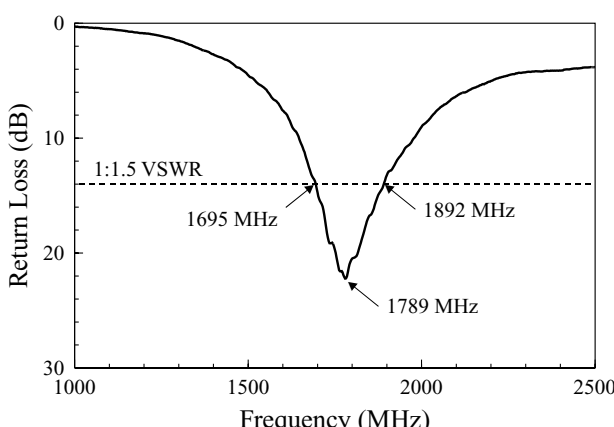


**FIGURE 3.9** Measured return loss for the microstrip-line-fed shorted patch antenna shown in Figure 3.8;  $L = 23.5$  mm,  $W = 58$  mm,  $h = 12.8$  mm,  $t = 3.2$  mm,  $w_f = 16$  mm,  $d = 5.5$  mm, and ground-plane size =  $100 \times 100$  mm $^2$ . (From Ref. 6, © 2001 John Wiley & Sons, Inc.)

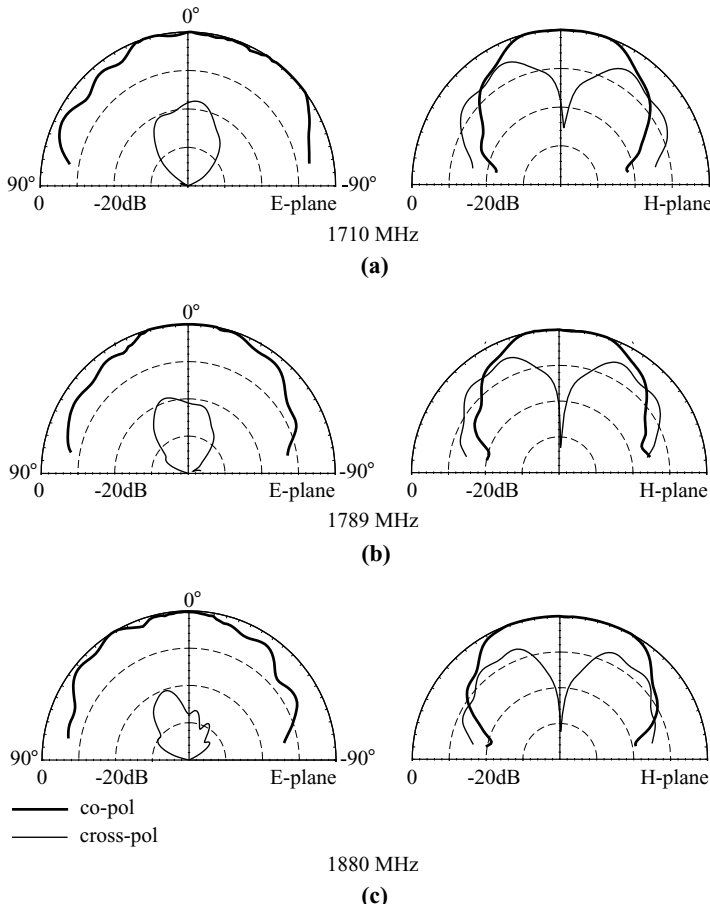


**FIGURE 3.10** Measured *E*- and *H*-plane radiation patterns for the antenna studied in Figure 3.9. (a)  $f = 1710$  MHz, (b)  $f = 1789$  MHz, (c)  $f = 1880$  MHz. (From Ref. 6, © 2001 John Wiley & Sons, Inc.)

*H*-plane patterns, which is similar to what is observed for conventional patch antennas with a thick air substrate. It is also possible that this greater cross-polarization radiation can be greatly reduced in practical base-station design with a  $1 \times N$  ( $N = 2, 4, 6, \dots$ ) array configuration in which two adjacent patches are fed out of phase using a simple microstrip T network having a half guided-wavelength difference in length between its two output feed lines. In this case, the cross-polarization radiation owing to the higher order modes of two adjacent antennas can be canceled [28, 29], and reduced cross-polarization radiation can be expected. Measured antenna gain against frequency is shown in Figure 3.11. A peak antenna gain of about 6.8 dBi is obtained, with a small gain variation of less than 0.6 dBi. The results show that the antenna studied has a low cost of construction and is suitable for applications in DCS base stations.

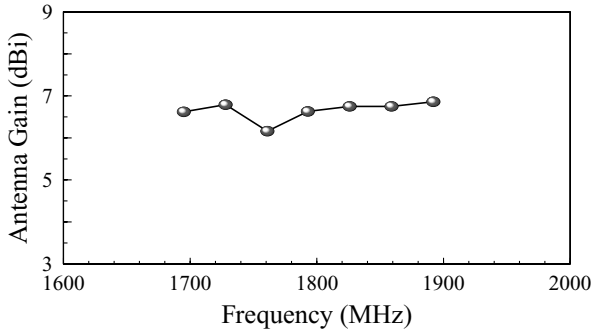


**FIGURE 3.11** Measured antenna gain in broadside direction for the antenna studied in Figure 3.9. (From Ref. 6, © 2001 John Wiley & Sons, Inc.)

### 3.2.4 Capacitively Coupled or L-Probe-Fed Shorted Patch

Broadband shorted patch antennas fed by using a capacitively coupled feed [7] or an L-probe feed [8] have been reported. Figure 3.12 shows typical geometries of this kind of shorted patch antenna. For the design shown in Figure 3.12(a), the capacitive feed can have a circular or a rectangular conducting plate to capacitively couple the electromagnetic energy from the source to the shorted radiating patch. By further

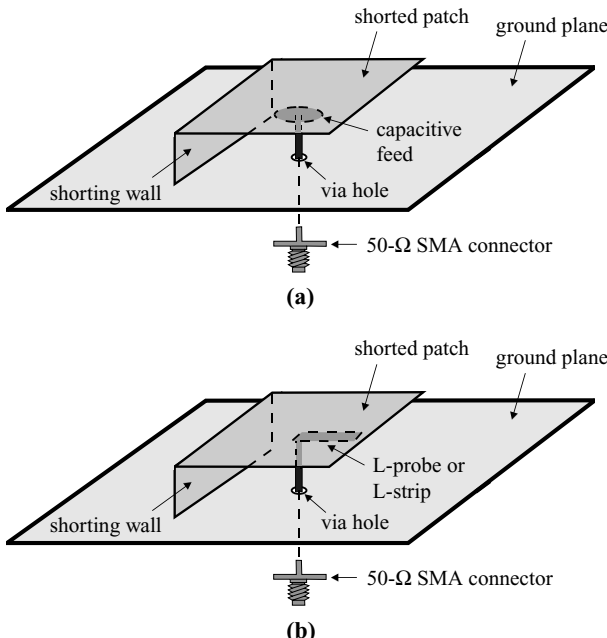


**FIGURE 3.12** Geometries of (a) a capacitively coupled shorted patch antenna and (b) an L-probe-fed or L-strip-fed shorted patch antenna for broadband operation.

incorporating a capacitive load to this shorted patch, it has been demonstrated that the overall length of a shorted patch antenna with an air substrate can be reduced from one-quarter wavelength to less than one-eighth wavelength [7]. Such a design with a volume of  $20 \times 8 \times 4 \text{ mm}^3$  has been constructed, and an impedance bandwidth of 178 MHz centered at 1.8 GHz has been obtained, which meets the bandwidth requirement of a DCS cellular communication system.

For the geometry shown in Figure 3.12(b), the capacitive coupling of the electromagnetic energy from the source to the shorted patch is achieved by using an L-probe [8] or an L-strip [29]. It has been reported that, with the use of a foam substrate of thickness about  $0.1\lambda_0$  ( $\lambda_0$  is the free-space wavelength of the center operating frequency), an impedance bandwidth of 39% can be obtained for an L-probe-fed shorted patch antenna [8]. In this design, the L-probe incorporated with the shorted patch introduces a capacitance compensating some of the large inductance introduced by the long probe pin in the thick foam substrate, which makes it possible to achieve good impedance matching over a wide frequency range. However, a beam squint of about  $15\text{--}60^\circ$  in the obtained *H*- and *E*-plane radiation patterns has been observed, which can probably be attributed to the asymmetric current distribution of the shorted patch due to the presence of the shorting wall and the L-probe [8].

### 3.3 USE OF STACKED SHORTED PATCHES

The impedance bandwidth of a patch antenna is in general proportional to the antenna volume measured in wavelengths. However, by using two stacked shorted patches and making both patches radiate as equally as possible and having a radiation quality factor as low as possible, one can obtain enhanced impedance bandwidth for a fixed antenna volume [12]. Figure 3.13 shows two typical geometries of stacked shorted patch antennas for broadband operation. In Figure 3.13(a), the two stacked shorted patches have different shorting walls. By selecting the proper distance between the two offset shorting walls, one can achieve a wide impedance bandwidth for the antenna. For the geometry shown in Figure 3.13(b), a common shorting wall is used for the two stacked shorted patches. In this case, impedance matching is achieved mainly by selecting the proper feed position and proper distance between the two shorted patches. It should also be noted that, for the two geometries in Figure 3.13, the upper shorted patch can be considered to be a parasitic element coupled to the lower shorted patch, the driven element. In the design, the two shorted patches are usually selected to have approximately the same, but unequal dimensions. The substrates between the two shorted patches and between the lower shorted patch and the ground plane can be air, foam, or dielectric materials. Also, a partial shorting wall or a shorting pin can be used in place of the offset shorting walls or the common shorting wall shown in Figure 3.13.

A design based on the geometry of Figure 3.13(b) has been constructed for DCS operation. With a total thickness of only 4 mm, which corresponds to about  $0.024\lambda_0$  at 1800 MHz, an impedance bandwidth of 9.6% centered at 1798 MHz has been obtained by using a stacked shorted patch antenna [12]. The impedance bandwidth obtained is almost double that for a conventional short-circuited single-patch antenna

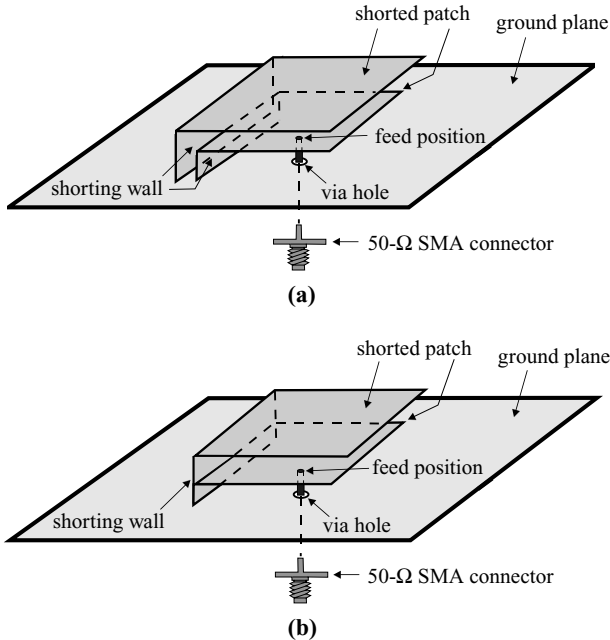


**FIGURE 3.13** Geometries of stacked shorted patch antennas with (a) offset shorting walls and (b) a common shorting wall.

with the same total thickness of 4 mm. It is also reported that, probably because the driven lower patch is shielded by the parasitic upper patch, the stacked shorted patch antenna is less sensitive to the hand of a cellular telephone user than the conventional short-circuited single patch antenna for handset antenna applications.

### 3.4 USE OF CHIP-RESISTOR AND CHIP-CAPACITOR LOADING TECHNIQUE

#### 3.4.1 Design with a Rectangular Patch

Microstrip antennas loaded with a shorting pin for compact operation are well known. Recently, it has been proposed that, by replacing the shorting pin with a chip resistor of low resistance, the required antenna size can be significantly reduced for operating at a fixed frequency; moreover, the antenna bandwidth can be greatly enhanced. To demonstrate the capability of such a chip-resistor loading technique, related designs for a rectangular microstrip antenna have been studied. Two different feed mechanisms using a probe feed and an inset microstrip-line feed (see Figure 3.14) have been implemented and analyzed.

The geometry of a probe-fed rectangular microstrip antenna with chip-resistor loading given in Figure 3.14(a) is studied first. The rectangular patch had dimensions  $L \times W$ , and the substrate had a relative permittivity  $\epsilon_r$  and a thickness  $h$ . A  $1.0-\Omega$

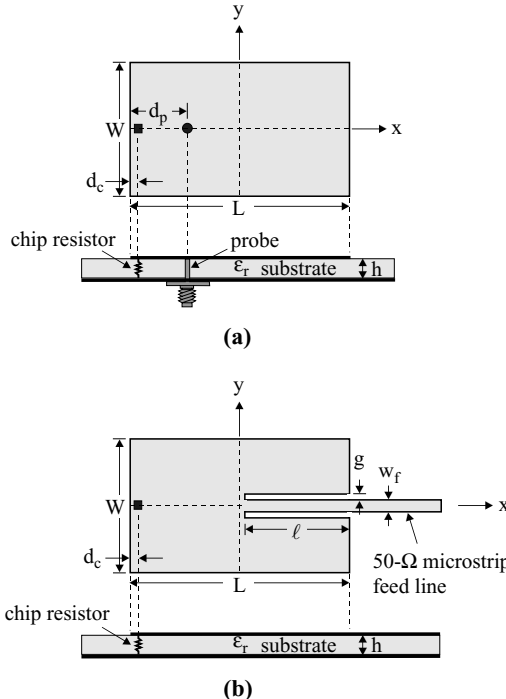


**FIGURE 3.14** Geometries of a chip-resistor-loaded rectangular microstrip antenna with (a) a probe feed and (b) an inset microstrip-line feed.

chip resistor was selected and placed at about the edge of the patch ( $d_c = 1.65$  mm or  $d_c/L = 0.044$ ) for maximum resonant frequency reduction. Variation of the measured resonant input resistance with the feed position is shown in Figure 3.15. The input resistance is seen to increase monotonically when the feed position is moved away from the loading position, and at  $d_p/L = 0.36$  or  $d_p = 13.5$  mm, the patch can be excited with a  $50\text{-}\Omega$  input resistance. The measured return loss is shown in Figure 3.16. The resonant frequency is 710 MHz, which is much lower than that (1900 MHz) of a regular patch and is also lower than that (722 MHz) of the patch with a shorting-pin loading; moreover, the 10-dB return-loss impedance bandwidth is 9.3%, about 4.9 times that (1.9%) of a conventional patch and 6.6 times that (1.4%) of the short-circuited patch.

A feed structure using a  $50\text{-}\Omega$  inset transmission line [see Figure 3.14(b)] has also been studied. Two different spacings  $g$  between the patch and the inset transmission line were studied. With an inset length  $\ell$  of 29.5 mm, a good matching condition was obtained and a wide impedance bandwidth was achieved. It can be seen from Figure 3.17 that, for  $g = 1$  mm, the patch resonates at 739 MHz and has a bandwidth of 9.3%, while for  $g = 2$  mm, the resonant frequency is 742 MHz and the bandwidth is 9.8%. Both cases have a higher resonant frequency than that (710 MHz) in Figure 3.16 for the probe-fed case. This is largely due to the notch cut in the rectangular patch

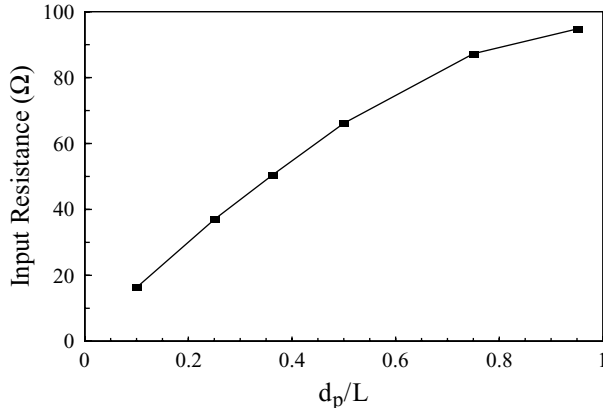


**FIGURE 3.15** Measured input resistance at resonance against the feed position of the antenna shown in Figure 3.14(a);  $\epsilon_r = 4.4$ ,  $h = 1.6$  mm,  $L = 37.3$  mm,  $W = 24.87$  mm, and  $d_c = 1.65$  mm. (From Ref. 15, © 1997 IEE, reprinted with permission.)

for the inset microstrip-line feed, which decreases the effective length of the excited patch surface current, and the effect is larger for a larger notch.

Figure 3.18 shows another case for operating in the 1500-MHz band. The patch size was selected to be  $21 \times 14$  mm $^2$  and the inset length of the 50- $\Omega$  transmission line was 16.9 mm ( $\ell/L \cong 0.80$ ). Again, a good matching condition was achieved and a large operating bandwidth of 7.8% was obtained. Note that, with a large notch cut in the patch for inset microstrip-line feed, the radiation pattern is still broadside. The results are shown in Figure 3.19. The cross-polarization radiation is seen to be higher in the  $H$  plane than in the  $E$  plane, similar to what is observed for a short-circuited rectangular patch [30]. In this case, the antenna gain reduction due to the ohmic loss

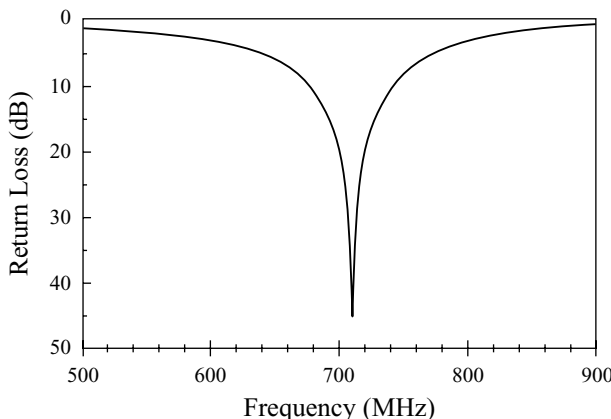


**FIGURE 3.16** Measured return loss against frequency for the antenna studied in Figure 3.15 with  $d_p = 13.5$  mm ( $d_p/L = 0.36$ ). (From Ref. 15, © 1997 IEE, reprinted with permission.)

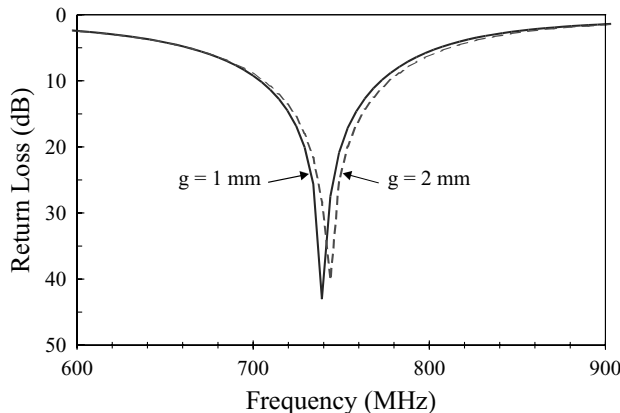


**FIGURE 3.17** Measured return loss against frequency for the antenna shown in Figure 3.14(b);  $\epsilon_r = 4.4$ ,  $h = 1.6\text{ mm}$ ,  $L = 37.3\text{ mm}$ ,  $W = 24.87\text{ mm}$ ,  $d_c = 1.65\text{ mm}$ ,  $w_f = 3.0\text{ mm}$ , and  $\ell = 29.5\text{ mm}$ . (From Ref. 15, © 1997 IEE, reprinted with permission.)

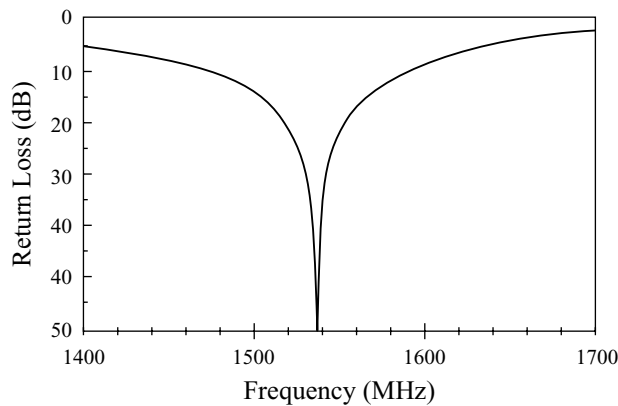


**FIGURE 3.18** Measured return loss against frequency for the antenna shown in Figure 3.14(b);  $\epsilon_r = 3.0$ ,  $h = 0.762\text{ mm}$ ,  $L = 21\text{ mm}$ ,  $W = 14\text{ mm}$ ,  $d_c = 1.65\text{ mm}$ ,  $w_f = 1.9\text{ mm}$ ,  $\ell = 16.9\text{ mm}$ , and  $g = 1\text{ mm}$ . (From Ref. 15, © 1997 IEE, reprinted with permission.)

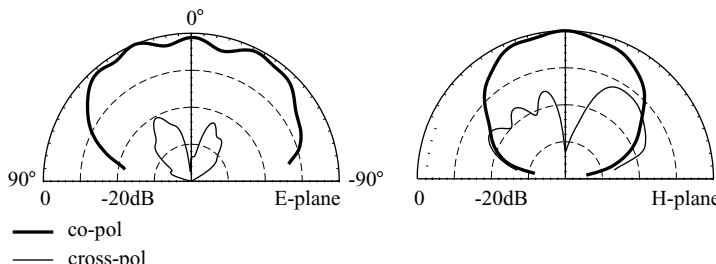


**FIGURE 3.19** Measured radiation patterns at resonance for the antenna studied in Figure 3.18. (From Ref. 15, © 1997 IEE, reprinted with permission.)

of the loaded  $1\text{-}\Omega$  chip resistor is estimated to be about 2 dBi, which needs to be considered in practical applications.

### 3.4.2 Design with a Circular Patch

**3.4.2.1 With a Microstrip-Line Feed** With chip-resistor loading, direct matching of the antenna using a  $50\text{-}\Omega$  microstrip-line feed has been described [16]. Figure 3.20 shows the geometry of a chip-resistor-loaded circular microstrip antenna with a  $50\text{-}\Omega$  microstrip-line feed. This design is achieved simply by loading a  $1\text{-}\Omega$  chip resistor near the edge of the circular patch, which significantly reduces the resonant frequency of the microstrip patch, broadens the operating bandwidth, and causes a wide variation in the input impedance along the patch edge. The last behavior makes direct matching of the antenna with a  $50\text{-}\Omega$  microstrip line possible.

As shown in Figure 3.20, the circular patch has a radius  $d$ , and the chip resistor is placed a distance  $r_c$  from the patch center. The angle between the feed line and the chip resistor is denoted  $\phi_c$ . The width  $w_f$  of the feed line is selected to have a  $50\text{-}\Omega$  characteristic impedance. A typical result showing the measured input resistance at resonance against the angle  $\phi_c$  is presented in Figure 3.21, where the circular patch has a radius of 21.97 mm and the chip resistor, having a rectangular cross section of  $2.07 \times 1.27 \text{ mm}^2$ , is placed at  $r_c = 20 \text{ mm}$ . An FR4 substrate of thickness  $h = 1.6 \text{ mm}$  and relative permittivity  $\epsilon_r = 4.4$  is used, and the resonant frequency occurs at about 553 MHz. From the results, it is seen that the resonant input resistance increases with increasing  $\phi_c$  and reaches a maximum when  $\phi_c$  is  $180^\circ$ . The optimal value of  $\phi_c$  for a  $50\text{-}\Omega$  input impedance is  $110^\circ$ . With this optimal angle, the measured return loss against frequency is shown in Figure 3.22. The impedance bandwidth, determined from the 10-dB return loss, is 10.9%, which is much greater than

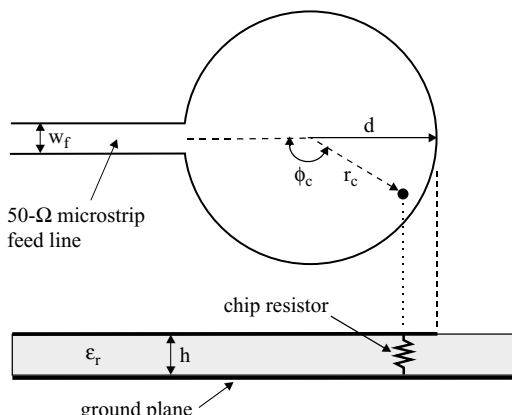


**FIGURE 3.20** Geometry of a chip-resistor-loaded circular microstrip antenna with a microstrip-line feed. (From Ref. 16, © 1998 John Wiley & Sons, Inc.)

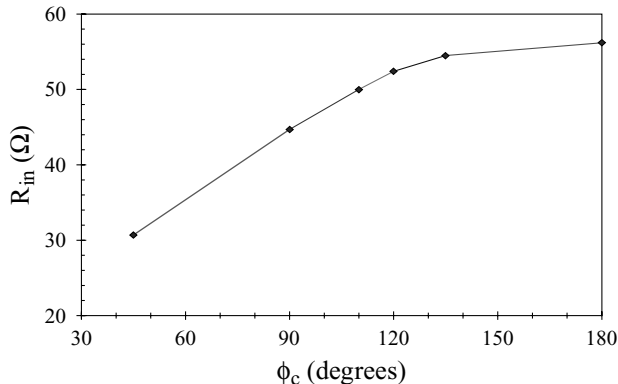


**FIGURE 3.21** Measured input resistance at resonance as a function of  $\phi_c$ , the angle between the microstrip line and the chip resistor, for the antenna shown in Figure 3.20;  $\epsilon_r = 4.4$ ,  $h = 1.6$  mm,  $d = 21.97$  mm, and  $r_c = 20$  mm. (From Ref. 16, © 1998 John Wiley & Sons, Inc.)

that (about 1.8%) of a conventional circular patch (radius about 74 mm) without chip-resistor loading operating at the same frequency of 553 MHz. In this case, the antenna size reduction is more than 91%. Note that the conventional circular patch is fed through a coax with the feed position selected within the patch because the input impedance along the circumference of the circular patch is usually much larger than 50  $\Omega$  and the direct use of a 50- $\Omega$  microstrip line is thus not feasible.

Two other typical results have been presented [16]. Figure 3.23(a) shows the measured return loss for a microstrip patch printed on a Duroid substrate ( $\epsilon_r = 3.0$ ,  $h = 1.524$  mm). The patch parameters are the same as in Figure 3.21. In this case the optimal  $\phi_c$  for a 50- $\Omega$  input resistance is about 60°. The resonant frequency is seen to be at 646 MHz, and the impedance bandwidth is about 9.3%, also much greater

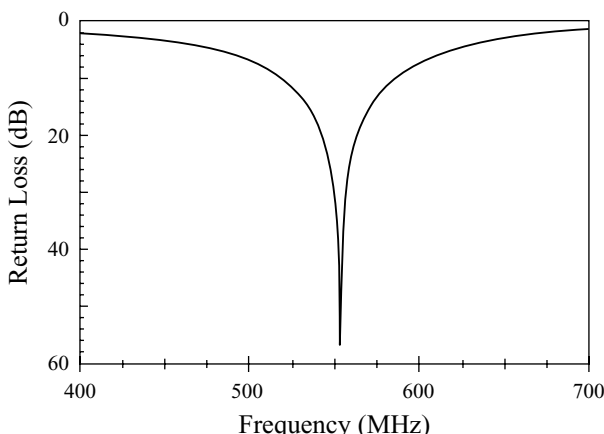


**FIGURE 3.22** Measured return loss against frequency for the antenna studied in Figure 3.21 with  $\phi_c = 110^\circ$ . (From Ref. 16, © 1998 John Wiley & Sons, Inc.)

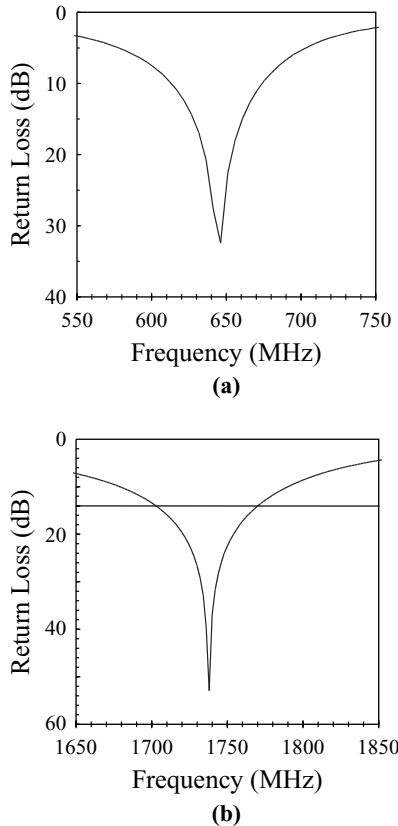


**FIGURE 3.23** Measured return loss against frequency for the antenna shown in Figure 3.20. (a)  $\epsilon_r = 3.0$ ,  $h = 1.524$  mm,  $d = 21.97$  mm,  $r_c = 20$  mm,  $w_f = 3.8$  mm, and  $\phi_c = 60^\circ$ ; (b)  $\epsilon_r = 4.4$ ,  $h = 1.6$  mm,  $d = 7.5$  mm,  $r_c = 6.5$  mm,  $w_f = 3.0$  mm, and  $\phi_c = 0^\circ$ . (From Ref. 16, © 1998 John Wiley & Sons, Inc.)

than that (about 1.7%) of a conventional circular microstrip antenna (radius about 77.7 mm) operated at 646 MHz.

Figure 3.23(b) shows the results for operation at higher frequencies. A smaller circular patch of radius 7.5 mm is printed on an FR4 substrate with the same parameters given in Figure 3.21. The resonant frequency is about 1738 MHz. In this case, the optimal  $\phi_c$  is about  $0^\circ$ . Note that, since the minimum resonant input resistance along the circumference of the circular patch occurs at  $\phi_c = 0^\circ$ , there exists a limitation for the direct matching of such a compact microstrip antenna with a  $50\text{-}\Omega$  microstrip line. It is found that when the patch size in Figure 3.23(b) becomes smaller, the minimum attainable resonant input resistance along the circumference of the circular patch is greater than  $50\ \Omega$ . This suggests that, in such a case, direct matching with a  $50\text{-}\Omega$  microstrip line becomes impractical. From the results in Figure 3.23(b), the impedance bandwidth is 6.4%, which is again much greater than that (about 2.1%) of a conventional circular microstrip antenna (radius 24 mm) operated at 1738 MHz. The measured radiation patterns have also been studied. The results are shown in

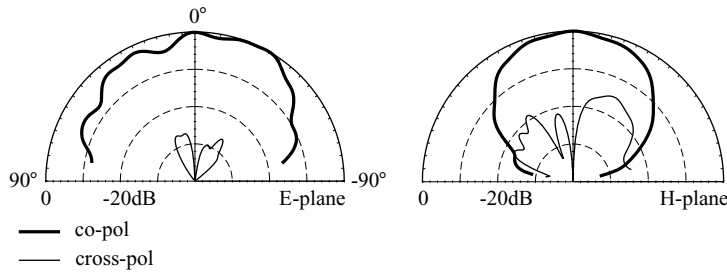


**FIGURE 3.24** Measured radiation patterns at 1738 MHz for the antenna studied in Figure 3.23(b). (From Ref. 16, © 1998 John Wiley & Sons, Inc.)

Figure 3.24. The cross-polarization component is seen to be higher in the *H*-plane case than in the *E*-plane case, and some asymmetry is also observed in the *E*-plane pattern. This behavior is due to the loading in the patch, which results in a high surface current density around the loading position and makes the excited patch surface currents asymmetric in the *E*-plane direction. Note that due to the significant antenna size reduction and the ohmic loss of the loaded  $1\text{-}\Omega$  chip resistor, the antenna gain is reduced. Compared to the shorting-pin loading case, which has a similar antenna size reduction to the chip-resistor loading case, the antenna gain is about 2 dBi lower for the antenna parameters given in Figure 3.23(b) at 1738 MHz.

**3.4.2.2 With a Probe Feed** The characteristics of loading a circular microstrip antenna with chip resistors and chip capacitors have also been studied [17]. The geometry is shown in Figure 3.25. Results show that, by incorporating the loading of a chip capacitor to a chip-resistor-loaded microstrip antenna, a much greater decrease in the antenna's fundamental resonant frequency can be obtained, which corresponds to an even larger antenna size reduction at a given operating frequency. In the following study, effects of the chip capacitor and chip resistor loadings on the probe-fed circular microstrip antenna are analyzed experimentally.

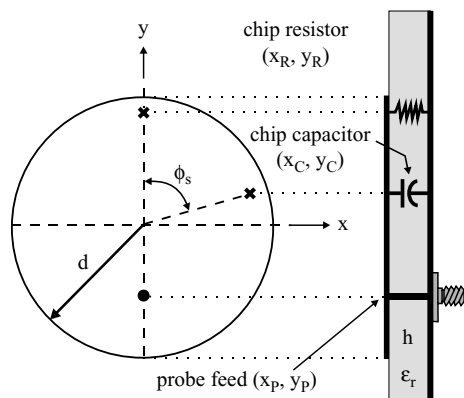


**FIGURE 3.25** Geometry of a probe-fed circular microstrip antenna with a chip resistor and a chip capacitor.

Consider the geometry in Figure 3.25; the circular patch has a radius  $d$  and is printed on a microwave substrate (thickness  $h$  and relative permittivity  $\epsilon_r$ ). The chip resistor has a cross section of  $2.07 \times 1.27 \text{ mm}^2$  and is soldered to the ground plane at  $(x_R, y_R)$ , where there is a circular hole drilled through the substrate large enough for the insertion of the chip resistor. The chip capacitor has a cross section of  $2.0 \times 1.28 \text{ mm}^2$  and is loaded at  $(x_c, y_c)$ . The probe feed is at  $(x_p, y_p)$  and has a circular cross section of radius 0.63 mm. The spacing angle between the chip resistor and the chip capacitor is denoted  $\phi_s$ . Since the excited electric field under the circular patch at the fundamental  $\text{TM}_{11}$  mode has a maximum value around the patch edge, both the chip resistor and chip capacitor are placed at the patch edge for maximum effects on the resonant-frequency lowering of the circular microstrip antenna.

The case with chip-capacitor loading only is first discussed. Figure 3.26(a) shows the measured return loss of the antenna loaded with various chip capacitors. Simulated

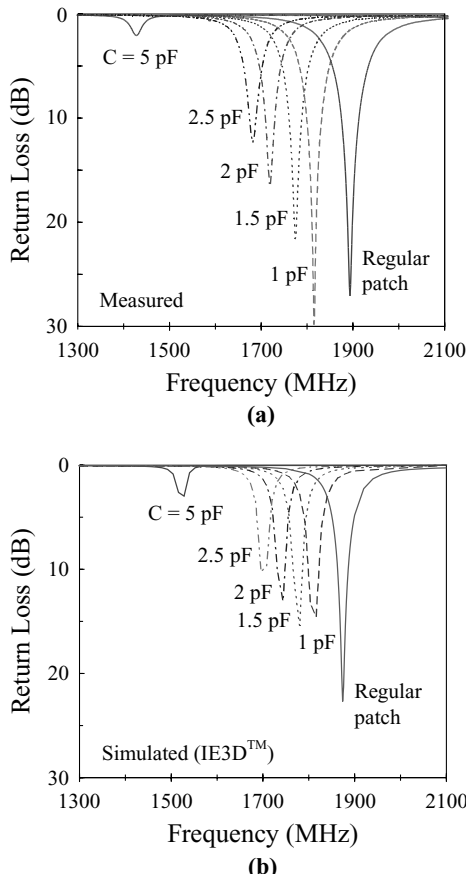


**FIGURE 3.26** (a) Measured and (b) simulated return loss against frequency for the antenna shown in Figure 3.25 with chip-capacitor loading only;  $\epsilon_r = 4.4$ ,  $h = 1.6 \text{ mm}$ ,  $d = 21.97 \text{ mm}$ ,  $(x_c, y_c) = (0, 21 \text{ mm})$ , and  $(x_p, y_p) = (0, 8.5 \text{ mm})$ .

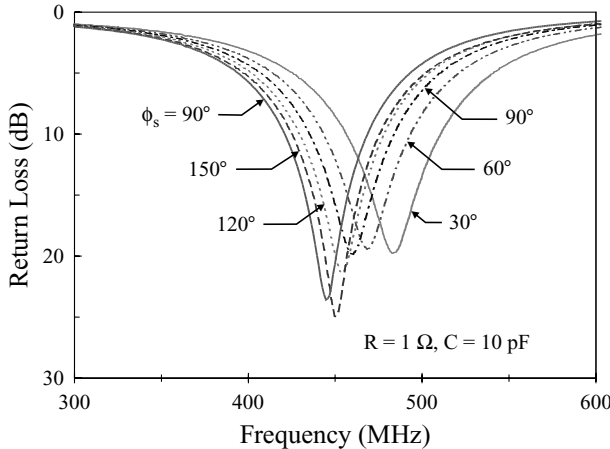


**FIGURE 3.27** Variations of the measured return loss with the spacing angle  $\phi_s$  between the loaded chip resistor and chip capacitor;  $\epsilon_r = 4.4$ ,  $h = 1.6$  mm,  $d = 21.97$  mm,  $R = 1 \Omega$ ,  $C = 10 \text{ pF}$ ,  $(x_R, y_R) = (0, 21 \text{ mm})$ ,  $(x_c, y_c) = (0, -21 \text{ mm})$ , and  $(x_p, y_p) = (0, -18 \text{ mm})$ .

results obtained with IE3D<sup>TM</sup> are shown in Figure 3.26(b) for comparison. Measured and simulated results are observed to have similar decreasing resonant frequency with increasing capacitance of the loading chip capacitor. Also note that the feed position in Figure 3.26 was fixed for various loading capacitances and selected such that good impedance matching was achieved for the case with a 1-pF chip-capacitor loading, in which an impedance bandwidth of about 1.7% is observed. The bandwidth is lower than that (about 1.9%) of a corresponding regular circular microstrip antenna with a center frequency at about 1.9 GHz. This suggests that, although chip-capacitor loading can result in a reduction in the antenna's fundamental resonant frequency, the impedance bandwidth is reduced, which is similar to the case of using the shorting-pin loading technique and also agrees with observations [7] for the case with a parallel-plate-capacitor load.

To investigate the combined effect of loading both a chip resistor and a chip capacitor, we first study the optimal loading positions for the two lumped loads. Figure 3.27 presents the measured return loss for various spacing angles between the two loading positions. The case shown in the figure is for  $R = 1 \Omega$  and  $C = 10 \text{ pF}$ . Notice that, for maximum resonant frequency reduction, the two loads are placed around the edge of the circular patch. The corresponding resonant frequency  $f_r$  and impedance bandwidth BW for different spacing angles are listed in Table 3.1. Again, the feed position is selected for optimal impedance matching for the case of  $\phi_s = 180^\circ$ ; that is, the chip resistor and chip capacitor are placed on opposite sides of the circular patch. However, it is noted that, by varying the spacing angle of  $\phi_s$ , good impedance matching is slightly affected and the impedance bandwidth is about the same. As for the resonant frequency, it is found that the case with  $\phi_s = 180^\circ$  has the lowest resonant frequency, 446 MHz, which is lowered by about 17.7% compared to that (542 MHz) for the case with chip-resistor loading only and is about 23.5% times that (1.9 GHz) of a

**TABLE 3.1 Measured Resonant Frequency and Impedance Bandwidth as a Function of Angle  $\phi_s$  between the Loading Chip Resistor and Chip Capacitor for the Case in Figure 3.27 [17]**

$\phi_s$ (deg)	180	150	120	90	60	30
$f_r$ (MHz)	446	451	455	461	470	485
BW (%)	10.9	10.9	10.6	10.4	10.6	10.9

regular circular microstrip antenna. A significant lowering of the resonant frequency of a microstrip patch is thus obtained by using chip-resistor and chip-capacitor loadings.

Results for a fixed loading resistance and various loading capacitances with  $\phi_s = 180^\circ$  are presented in Figure 3.28. The corresponding resonant frequency and impedance bandwidth are listed in Table 3.2. Again, the feed position was selected for achieving good impedance matching for the case with chip-resistor loading only and remained unchanged when the loading capacitance varied. From the results, it is seen that the resonant frequency decreases with increasing loading capacitance, similar to what is observed in Figure 3.26. However, the measured return loss varies slightly with increasing loading capacitance, which is in contrast to the results shown in Figure 3.26. The impedance bandwidth is about 11%, which is much greater than that observed in Figure 3.26 for the case with chip-capacitor loading only.

Another set of antenna parameters with a smaller disk radius has been studied. The results are shown in Figure 3.29 and Table 3.3. In this study, the loading capacitance is fixed to 1 pF and the loading resistance is varied. The resonant frequency in this case is slightly shifted to lower frequencies with increasing loading resistance. The optimal feed position also needs to be slightly moved farther from the probe feed when

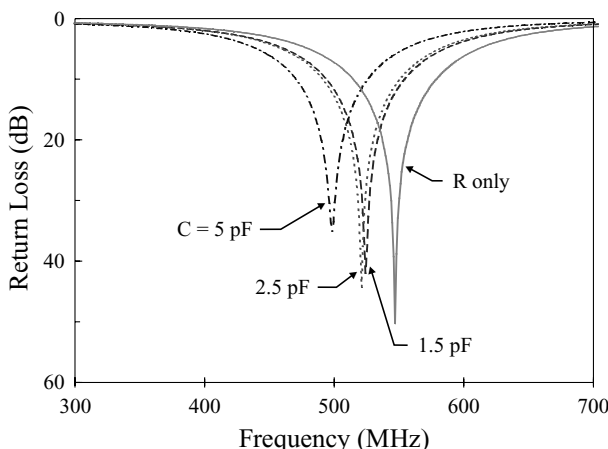


**FIGURE 3.28** Measured return loss for the antenna shown in Figure 3.25 with chip-resistor and chip-capacitor loading;  $\epsilon_r = 4.4$ ,  $h = 1.6$  mm,  $d = 21.97$  mm,  $R = 1 \Omega$ ,  $(x_R, y_R) = (0, 21$  mm),  $(x_c, y_c) = (0, -21$  mm),  $(x_p, y_p) = (0, -11.5$  mm), and  $\phi_s = 180^\circ$ .

**TABLE 3.2 Measured Resonant Frequency and Impedance Bandwidth as a Function of Loading Capacitance for the Case in Figure 3.28 [17]**

$C$ (pF)	0 ( $R$ only)	1.5	2.5	5.0
$f_r$ (MHz)	542	524	521	498
BW (%)	11.5	11.4	11.4	11.0

the loading resistance increases. For the impedance bandwidth, a significant increase with increasing loading resistance is seen. This behavior is reasonable because the quality factor of the microstrip patch is further decreased with the introduction of larger loading resistance. By comparing the results in Figures 3.28 and 3.29, the enhancement in the impedance bandwidth is seen to be more effective for the circular patch with a larger radius [i.e., a smaller resonant (operating) frequency] studied in Figure 3.28, where the loading of a 1- $\Omega$  chip resistor results in an impedance bandwidth larger than 11%.

Figure 3.30 plots the measured radiation patterns at resonance for the antenna studied in Figure 3.29 with  $R = 1 \Omega$  and  $C = 1 \text{ pF}$ . The cross-polarization radiation in the  $E$  plane is less than about  $-20 \text{ dB}$ , while in the  $H$  plane, the cross-polarization radiation is greater. In summary, the antenna studied has an impedance bandwidth of 11.5% with the loading of a 1- $\Omega$  chip resistor and is much larger than that (about 1.5%) of a short-circuited microstrip antenna. Also, by combining chip-resistor and chip-capacitor loadings, a significant effect in lowering the resonant frequency of the microstrip antenna with broadband characteristic can be obtained with only a very slight effect on the optimal feed position, which makes the present compact broadband microstrip antenna design very easy to implement.

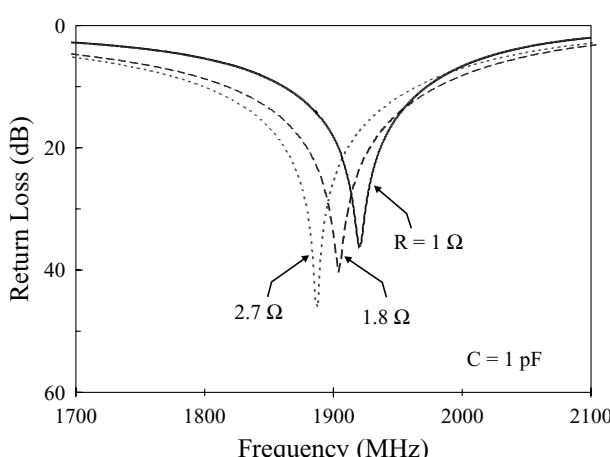


**FIGURE 3.29** Variation of the measured return loss with the loading resistance;  $\epsilon_r = 4.4$ ,  $h = 1.6 \text{ mm}$ ,  $d = 6.0 \text{ mm}$ ,  $C = 1 \text{ pF}$ ,  $(x_R, y_R) = (0, 5 \text{ mm})$ , and  $(x_c, y_c) = (0, -5 \text{ mm})$ .

**TABLE 3.3 Dependence of the Feed Position, Resonant Frequency, and Impedance Bandwidth on Loading Resistance for the Case in Figure 3.29 [17]**

$R$ ( $\Omega$ )	1.0	1.8	2.7	Regular patch
$f_r$ (MHz)	1920	1904	1887	6550
BW (%)	5.7	8.5	8.8	3.5
Feed ( $x_p, y_p$ ) (mm)	(0, 3.5)	(0, 3.0)	(0, 3.0)	(0, 1.5)

**3.4.2.3 With an Aperture-Coupled Feed** An aperture-coupled circular microstrip antenna loaded with a chip resistor and a chip capacitor (see Figure 3.31) has been investigated [18]. The aperture-coupled feed structure can provide the advantage of no probe penetration through the substrate layer and is more flexible in input-impedance matching through the control of coupling-slot size and tuning-stub length. In this study, the chip capacitor was placed in the opposite direction to the chip resistor at the boundary of the circular patch. The chip resistor and chip capacitor, respectively, were soldered to the ground plane at distances of  $d_s$  and  $d_c$  from the patch

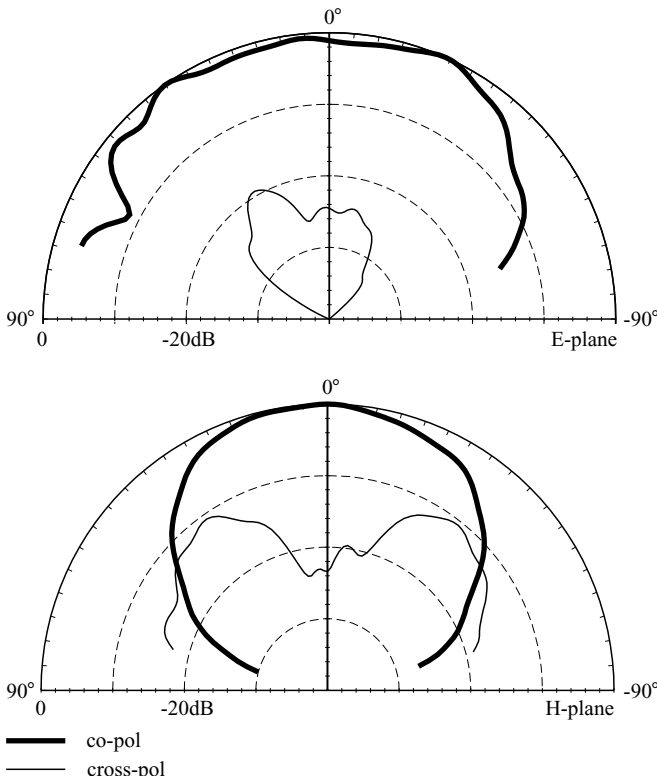


**FIGURE 3.30** Measured radiation patterns at resonance for the antenna studied in Figure 3.29 with  $R = 1 \Omega$  and  $C = 1 \text{ pF}$ .

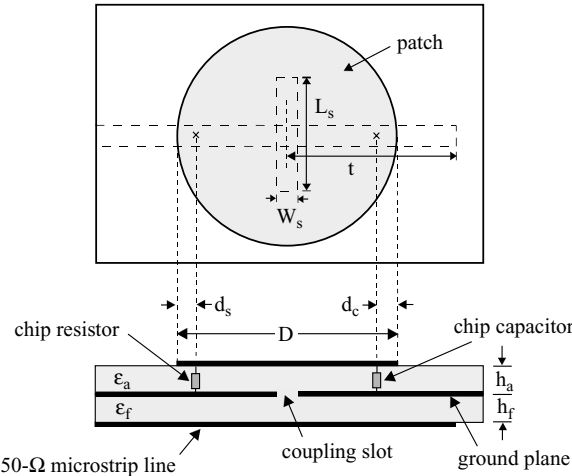


**FIGURE 3.31** Geometry of an aperture-coupled circular microstrip antenna loaded with a chip resistor and a chip capacitor. (From Ref. 18, © 1998 John Wiley & Sons, Inc.)

boundary. The circular patch had a diameter of  $D$ . The relative permittivity and thickness for the patch substrate were  $\epsilon_a$  and  $h_a$ , respectively, and the corresponding parameters for the feed substrate were  $\epsilon_f$  and  $h_f$ . The coupling slot had dimensions  $L_s \times W_s$ , and the feed line had a width  $w_f$  and a tuning-stub length  $t$ . The coupling slot was centered below the circular patch, and through the adjustment of the coupling-slot size and tuning-stub length, input-impedance matching could easily be achieved.

The chip-resistor loading case is studied first. In order to obtain maximum effects on the resonant-frequency lowering, the chip resistor was placed near the patch boundary ( $d_s$  was selected to be 1 mm). Typical results of the measured return loss for a circular patch of 32.5 mm diameter are shown in Figure 3.32. To match the input impedance to  $50\ \Omega$ , the optimal dimensions of the slot size and the tuning-stub length were as listed in Table 3.4. The corresponding fundamental resonant frequency and impedance bandwidth are given in Table 3.4. It is found that the fundamental resonant frequency for the shorting-pin ( $R = 0\ \Omega$ ) loading case is 818 MHz, which is about 0.314 times that (2605 MHz, see Table 3.4) of a regular circular patch without the loading. However, the impedance bandwidth is reduced from 4.8% at 2605 MHz to 1.7% at 818 MHz. For the cases with  $0.3\text{-}\Omega$  and  $1.0\text{-}\Omega$  chip resistors, the required slot size for impedance matching is increased with increasing loading resistance. From these results, it is observed that the resonant frequency decreases with increasing loading resistance. This behavior is probably caused by the increased slot size in the ground plane for impedance matching, which decreases the resonant frequency of the structure [31]. For the case of a  $1\text{-}\Omega$  chip resistor, the resonant frequency is 0.275 times that (2605 MHz) of the regular microstrip antenna. This corresponds to more than 90% antenna size reduction if such an antenna is used to replace a regular microstrip antenna at the same operating frequency. Furthermore, the impedance bandwidth for

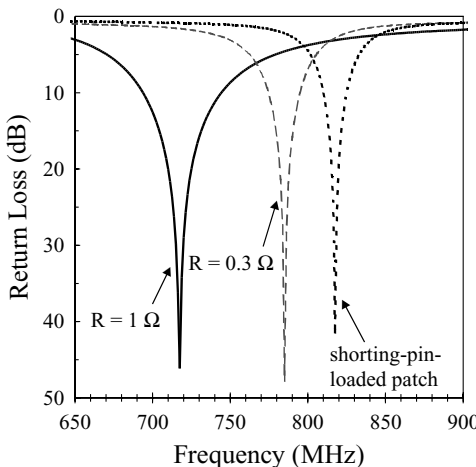


**FIGURE 3.32** Measured return loss for the antenna shown in Figure 3.31 with chip-resistor loading only; antenna parameters are given in Table 3.4. (From Ref. 18, © 1998 John Wiley & Sons, Inc.)

the case of a 1- $\Omega$  chip resistor increases to 6.8%, which is 4.0 times that (1.7%) of the shorting-pin case. Note that, when a chip resistor of larger resistance is used, a much greater slot size for impedance matching is required. The coupling slot may start to dominate the antenna radiation (that is, as a radiator rather than a coupling slot), and therefore a chip resistor of larger resistance was not tested.

To investigate the effect of incorporating chip-capacitor loading on a chip-resistor-loaded microstrip antenna, the characteristics of an antenna with various chip-capacitor loadings were studied. Figure 3.33 shows the measured return loss for an antenna with a 1- $\Omega$  chip resistor and a chip capacitor of various capacitances. The resonant frequency and impedance bandwidth for different loading capacitances are listed in Table 3.5. Results show that the resonant frequency decreases when the loading capacitance increases, and the required coupling-slot size for impedance matching also increases. For the case with  $C = 15 \text{ pF}$ , the resonant frequency is about 0.685 times that (536 MHz) of the case with  $C = 0 \text{ pF}$ . It is also observed that the impedance bandwidth is very slightly affected by the loading capacitance. The results

**TABLE 3.4 Comparison of the Antennas in Figure 3.32 [18]<sup>a</sup>**

	Slot Size ( $\text{mm}^2$ )	Tuning Stub (mm)	$f_r$ (MHz)	BW (%)
Regular patch	$14.2 \times 1.1$	11.8	2605	4.8
Shorting-pin-loaded patch	$23.2 \times 1.8$	43.8	818	1.7
$R = 0.3 \Omega$	$26.4 \times 1.8$	45.0	785	2.6
$R = 1.0 \Omega$	$33.6 \times 3.1$	45.0	718	6.8

<sup>a</sup>  $\epsilon_a = \epsilon_f = 4.4$ ,  $h_a = h_f = 1.6 \text{ mm}$ ,  $D = 32.5 \text{ mm}$ ,  $d_s = 1 \text{ mm}$ , and  $C = 0 \text{ pF}$  (no chip capacitor added).

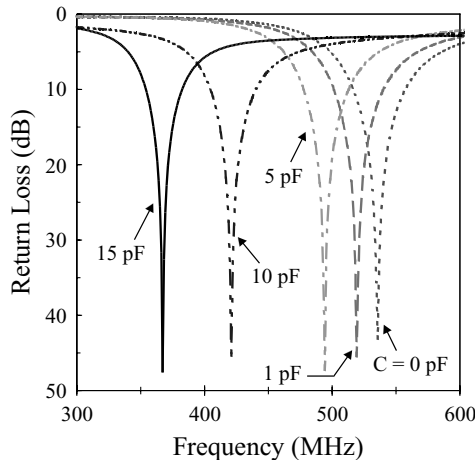


**FIGURE 3.33** Measured return loss for the antenna shown in Figure 3.31 with a  $1\text{-}\Omega$  chip resistor and a chip capacitor of various capacitances; antenna parameters are given in Table 3.5. (From Ref. 18, © 1998 John Wiley & Sons, Inc.)

indicate that significant antenna size reduction can be expected by using chip-resistor and chip-capacitor loadings.

### 3.4.3 Design with a Triangular Patch

**3.4.3.1 With an Inset Microstrip-Line Feed** An inset microstrip-line-fed triangular microstrip antenna with a chip resistor has been studied (Figure 3.34) [19]. The triangular patch considered here is equilateral with a side length  $d$ . The  $50\text{-}\Omega$  inset microstrip line has an inset length  $\ell$  and a width  $w_f$ . Measured return-loss results for typical cases using  $1.0\text{-, }1.2\text{-, and }1.5\text{-}\Omega$  chip resistors are shown in Figure 3.35. In this case, the patch's side length was selected to be 40 mm, and the fundamental resonant frequency of the regular patch (without a chip resistor) was about 2850 MHz. From the results obtained, it can be seen that the resonant frequency for a chip-resistor-loaded patch decreases to around 700 MHz, about 24.5% times that (2850 MHz) of a regular patch. This can result in a significant patch size reduction

**TABLE 3.5 Comparison of the Antennas in Figure 3.33 [18]<sup>a</sup>**

C (pF)	Slot Size ( $\text{mm}^2$ )	Tuning Stub (mm)	$f_r$ (MHz)	BW (%)
0	$43.9 \times 3.6$	67.7	536	7.5
1	$44.1 \times 3.6$	68.5	519	7.4
5	$44.5 \times 3.6$	72.0	494	7.1
10	$45.4 \times 3.6$	91.5	421	8.1
15	$46.9 \times 3.6$	105.2	367	7.3

<sup>a</sup>  $\epsilon_a = \epsilon_f = 4.4$ ,  $h_a = h_f = 1.6$  mm,  $D = 42$  mm,  $d_s = 1$  mm,  $d_c = 1$  mm, and  $R = 1\text{ }\Omega$ .

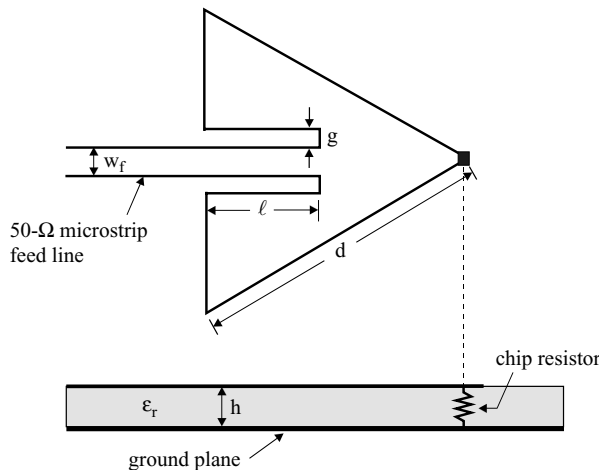


**FIGURE 3.34** Geometry of an inset microstrip-line-fed triangular microstrip antenna loaded with a chip resistor. (From Ref. 19, © 1998 John Wiley & Sons, Inc.)

for such a design at a given operating frequency. The corresponding inset lengths for impedance matching and the impedance bandwidths are given in Table 3.6 for comparison. It is seen that the required inset length decreases with increasing loading resistance. Also, the resonant frequency is decreased when the loading resistance increases. This is probably because the decreasing inset length in the patch causes an increased effective surface current path, which decreases the resonant frequency of the antenna. Furthermore, the impedance bandwidth is significantly increased with increasing loading resistance.

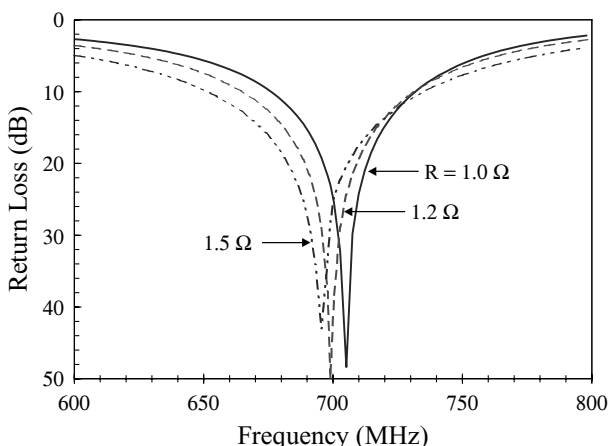


**FIGURE 3.35** Measured return loss against frequency for the antenna shown in Figure 3.34;  $\epsilon_r = 3.0$ ,  $h = 0.762$  mm,  $d = 40$  mm,  $g = 1$  mm, and  $w_f = 1.9$  mm. (From Ref. 19, © 1998 John Wiley & Sons, Inc.)

**TABLE 3.6 Comparison of the Triangular Microstrip Antennas in Figures 3.35 and 3.36 [19]<sup>a</sup>**

Resistance ( $\Omega$ )	Side Length $d$ (mm)	Inset Length $\ell$ (mm)	$f_r$ (MHz)	Bandwidth (%)
1.0	40	23.3	705	7.8
1.2	40	18.8	700	9.6
1.5	40	12.1	695	12.1
3.9	20	8.9	1593	19.0

<sup>a</sup>  $\epsilon_r = 3.0$ ,  $h = 0.762$  mm,  $g = 1$  mm, and  $w_f = 1.9$  mm.

A design for operating at a higher frequency band has been investigated in which the patch's side length was selected to be 20 mm and a large loading resistance of  $3.9\ \Omega$  was used. The measured return loss is presented in Figure 3.36 and the corresponding results are given in Table 3.6. The resonant frequency for the loaded patch is 1593 MHz. Since the required side length of a regular triangular patch operated at 1593 MHz is about 71.3 mm, the size of the loaded patch corresponds to about 7.9% times that of a regular patch. The impedance bandwidth of the loaded patch is about 19%, which is more than 10 times that (about 1.8%) of a regular patch. The measured  $E$ - and  $H$ -plane radiation patterns are plotted in Figure 3.37. An asymmetric pattern in the  $E$  plane is observed, which may be due to the high current density excited around the chip-resistor loading position. The  $H$ -plane pattern shows a greater cross-polarization radiation than the  $E$ -plane case.

**3.4.3.2 With an Aperture-Coupled Feed** Figure 3.38 shows the geometry of an aperture-coupled compact triangular microstrip antenna loaded with a shorting pin or

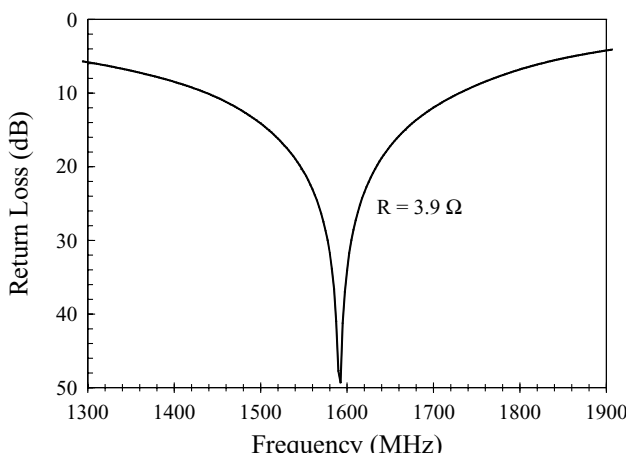


**FIGURE 3.36** Measured return loss against frequency for the antenna shown in Figure 3.34 with a  $3.9\text{-}\Omega$  chip resistor;  $\epsilon_r = 3.0$ ,  $h = 0.762$  mm,  $d = 20$  mm,  $g = 1$  mm, and  $w_f = 1.9$  m. (From Ref. 19, © 1998 John Wiley & Sons, Inc.)

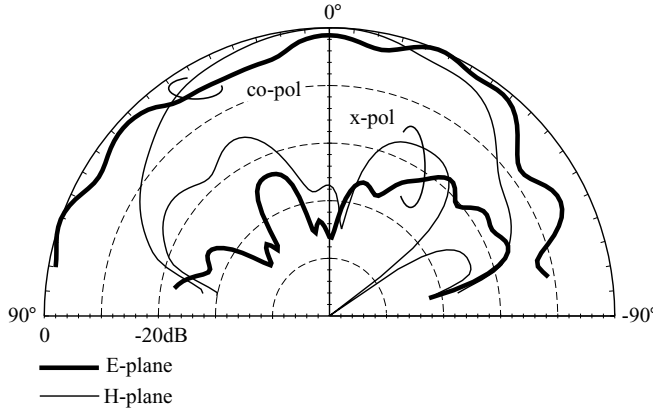


**FIGURE 3.37** Measured radiation patterns for the antenna studied in Figure 3.36 at 1593 MHz. (From Ref. 19, © 1998 John Wiley & Sons, Inc.)

chip resistor [20]. A coupling slot of dimensions  $L_s \times W_s$  is cut in the ground plane, and the slot center is fixed at the position where the excited field of the fundamental  $\text{TM}_{10}$  mode is null. This null-field point is at two-thirds of the distance from the tip to the bottom edge of the triangle. The triangular patch is assumed to be equilateral with a side length of  $d$ . The tuning-stub length is denoted  $t$ . In this study, a shorting pin of radius 0.63 mm and a chip resistor of cross section  $2.07 \times 1.27 \text{ mm}^2$  were loaded at the tip of the triangular patch.

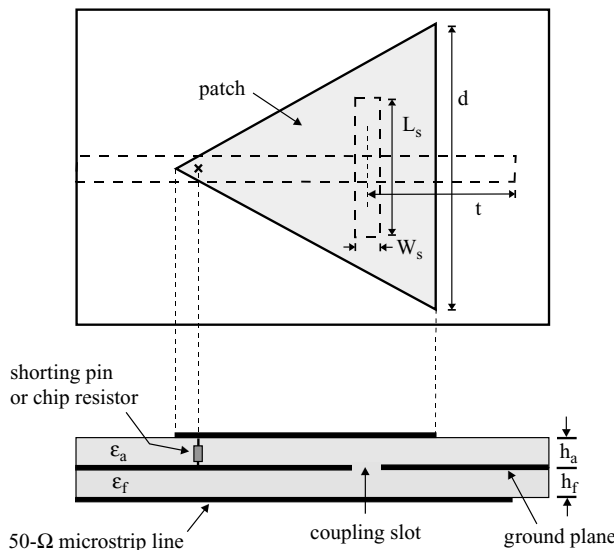


**FIGURE 3.38** Geometry of an aperture-coupled triangular microstrip antenna loaded with a shorting pin or chip resistor. (From Ref. 20, © 1997 John Wiley & Sons, Inc.)

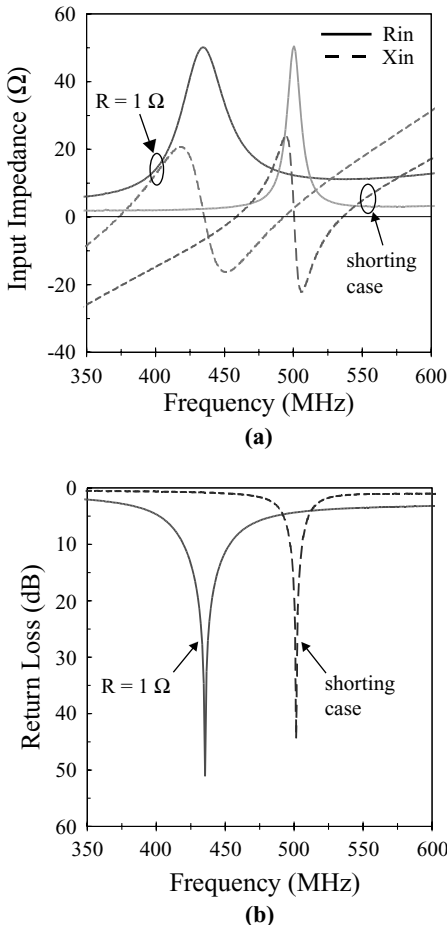


**FIGURE 3.39** Measured (a) input impedance and (b) return loss for a triangular microstrip antenna with a shorting-pin loading or a chip-resistor loading. Antenna parameters are given in Table 3.7. (From Ref. 20, © 1997 John Wiley & Sons, Inc.)

A regular triangular patch without a shorting pin or a chip resistor was first implemented. The measured center frequency is 1866 MHz and the impedance bandwidth is about 4.0%. Figure 3.39 shows the results for a shorted triangular patch and a chip-resistor-loaded triangular patch. Both cases show a significant resonant frequency reduction, especially for the chip-resistor-loading case. It is also noted that the impedance bandwidth is 7.6% for the chip-resistor loading, which is 4.7 times that of the shorted patch and is also greater than that of the regular patch. A comparison of the regular, shorted, and chip-resistor-loaded patches is given in Table 3.7. The case using a  $0.3\text{-}\Omega$  chip resistor is also shown. It is clearly seen that the required slot size increases with increasing loading resistance (the shorting pin can be considered as a  $0\text{-}\Omega$  chip resistor), and the resulting fundamental resonant frequency is

**TABLE 3.7 Results for the Antenna in Figure 3.38 [20]<sup>a</sup>**

	Slot Size ( $\text{mm}^2$ )	Tuning Stub (mm)	$f_r$ (MHz)	BW (%)
Regular patch	$17.4 \times 1.0$	18.4	1866	4.0
Shorting-pin-loaded patch	$32.8 \times 2.8$	75.3	501	1.6
$R = 0.3 \Omega$	$33.1 \times 3.3$	85.9	473	2.2
$R = 1.0 \Omega$	$45.0 \times 3.6$	87.4	435	7.6

<sup>a</sup> $d = 50$  mm,  $\epsilon_a = \epsilon_f = 4.4$ , and  $h_a = h_f = 1.6$  mm.

decreased with increasing loading resistance. It is also observed that the bandwidth enhancement using a  $0.3\text{-}\Omega$  chip resistor is much smaller than that using a  $1\text{-}\Omega$  chip resistor. For the case using a chip resistor of larger resistance ( $>1\text{ }\Omega$ ), the ohmic loss of the antenna quickly increases and the required slot length is much greater than the patch's linear dimension, which makes the antenna design impractical. Using a large-resistance chip resistor is therefore not recommended.

To estimate the antenna size reduction, different antenna parameters for operating in the 1.8-GHz band have been considered. The measured return loss for the shorted patch and the chip-resistor-loaded patch in the 1.8-GHz band are presented in Figure 3.40, and a comparison of two reduced-size microstrip antennas with a regular microstrip antenna is given in Table 3.8. The shorting pin and the chip resistor are loaded at the tip of the triangular patch, and the sizes of both the shorted patch and the chip-resistor-loaded patch are reduced to about 9% of that of the regular patch. The impedance bandwidth for the chip-resistor-loaded patch is much greater than those of the regular and shorted patches. The radiation patterns for these three different antennas have been measured. The results [20] show slightly

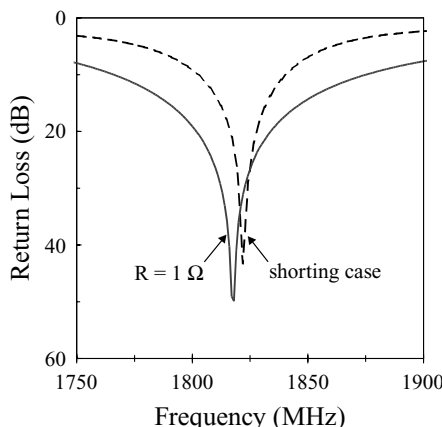


**FIGURE 3.40** Measured return loss for a shorted triangular patch with  $d = 15.2$  mm,  $L_s = 11.2$ ,  $W_s = 1.0$  mm, and  $t = 18.6$  mm and for a chip-resistor-loaded triangular patch with  $d = 15.0$  mm,  $L_s = 14.7$  mm,  $W_s = 1.3$  mm, and  $t = 18.7$  mm. Other parameters are in Table 3.8. (From Ref. 20, © 1997 John Wiley & Sons, Inc.)

**TABLE 3.8 Results for the Antenna in Figure 3.38 Operating in the 1.8-GHz Band [20]<sup>a</sup>**

	Side Length (mm)	Slot Size (mm <sup>2</sup> )	Tuning Stub (mm)	$f_r$ (MHz)	BW (%)
Regular patch	50	17.4 × 1.0	18.4	1866	4.0
Shorting-pin-loaded patch	15.2	11.2 × 1.0	18.6	1822	2.0
$R = 1.0 \Omega$	15.0	14.7 × 1.3	18.7	1818	6.0

<sup>a</sup>  $\epsilon_a = \epsilon_f = 4.4$  and  $h_a = h_f = 1.6$  mm.

asymmetric  $E$ -plane patterns for the shorted and chip-resistor-loaded patches, largely owing to the excited high current density around the shorting pin/chip resistor in the microstrip patch. The cross-polarization radiation in the  $H$ -plane patterns of the shorted and chip-resistor-loaded patches is increased, as reported for related studies.

### 3.4.4 Design with a Meandered PIFA

The design of a meandered planar inverted-F antenna (PIFA) with a more compact size (antenna length less than  $\lambda_0/8$  and antenna height less than  $0.01\lambda_0$ ) and a much wider impedance bandwidth (greater than 10 times that of a corresponding regular PIFA) has been demonstrated [21]. A reduction in antenna length is achieved by meandering the radiating patch, while an enhanced bandwidth with a low antenna height is obtained by using a chip-resistor load in place of the shorting pin. A typical design of a modified PIFA in the 800-MHz band has been implemented. The geometry is shown in Figure 3.41. The modified PIFA has a meandered rectangular patch of dimensions  $L \times W$  and a chip-resistor loaded at point A (center of the radiating edge). The PIFA has an air-filled substrate of thickness  $h$ , and three narrow slots of length  $\ell$  and width  $w$  ( $\ell \gg w$ ) are cut in the rectangular patch. This modified PIFA can be directly fed using a  $50\Omega$  coax with the feed position selected from within the line segment  $\overline{AB}$ , with point B at a position about  $(W - \ell)/2$  from the patch edge. The

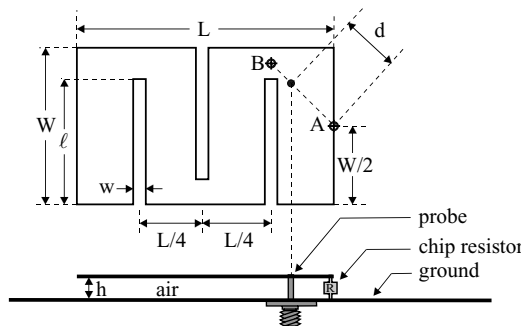


**FIGURE 3.41** Geometry of a meandered PIFA with a chip resistor. (From Ref. 21, © 1998 IEE, reprinted with permission.)

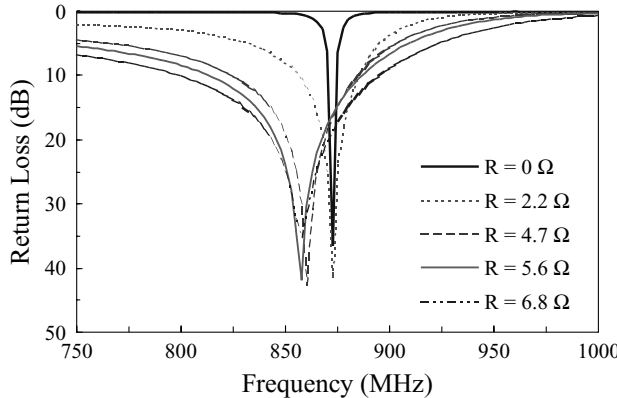


**FIGURE 3.42** Measured return loss for the antenna shown in Figure 3.38;  $h = 3.2$  mm,  $L = 40$  mm,  $W = 25$  mm,  $\ell = 20$  mm, and  $w = 2$  mm. (From Ref. 21, © 1998 IEE, reprinted with permission.)

distance  $d$  between point  $A$  and the feed position increases with increasing loading resistance.

In this experiment, the slot length was selected such that the required antenna length  $L$  for operating in the 800-MHz band was less than  $\lambda_0/8$ . The antenna height was chosen to be less than  $0.01\lambda_0$  for low profile. In this case, modified PIFA parameters were selected as  $L = 40$  mm (about  $0.115\lambda_0$ ;  $\lambda_0 = 34.88$  cm at 860 MHz),  $W = 25$  mm,  $\ell = 20$  mm,  $w = 2$  mm, and  $h = 3.2$  mm (about  $0.0092\lambda_0$ ). Figure 3.42 shows the measured return loss for the modified PIFA with various loading chip resistors. The case denoted  $R = 0\Omega$  is for the modified PIFA with a shorting pin. Table 3.9 lists the resonant frequency and impedance bandwidth for a modified PIFA with various loading resistances. The results for a regular PIFA (no slot in the patch and  $R = 0\Omega$ ) are shown for comparison. It is clearly seen that, by meandering the patch, the resonant frequency of the PIFA is reduced to 872 MHz, about 0.67 times that (1298 MHz) of a regular PIFA. However, due to the antenna size reduction, the impedance bandwidth is decreased from 0.9% to be 0.6% for the modified PIFA with  $R = 0\Omega$ . This smaller impedance bandwidth is due to the thin air-substrate thickness here. It is also observed that, with increasing loading resistance, the impedance bandwidth is significantly enhanced. For the case with  $R = 6.8\Omega$ , the impedance bandwidth is 11.2%, about 12.4 times that (0.9%) of a regular PIFA. It is also seen that the feed position for impedance

**TABLE 3.9 Characteristics of Modified PIFA with Various Loading Resistors [21]<sup>a</sup>**

$R(\Omega)$	0	2.2	3.3	4.7	5.6	6.8	Regular Patch
$D/\overline{AB}$	0.06	0.25	0.35	0.5	0.6	0.7	0.06
$f_r$ (MHz)	872	871	861	860	857	857	1298
BW (%)	0.6	3.4	4.7	6.8	8.6	11.2	0.9

<sup>a</sup>  $\overline{AB} = 14.1$  mm. Other parameters are given in Figure 3.42.

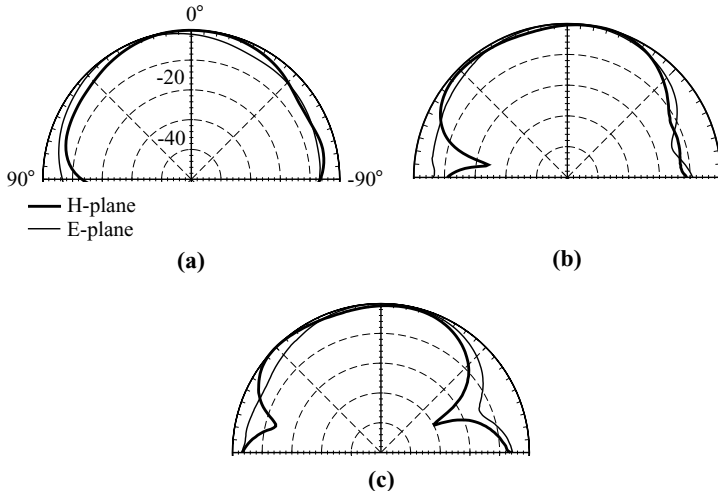


**FIGURE 3.43** Measured radiation patterns for (a) a simple PIFA at resonance ( $f = 1298$  MHz), (b) a meandered PIFA with a shorting pin ( $R = 0\ \Omega$ ) at resonance ( $f = 872$  MHz), and (c) a meandered PIFA with a  $5.6\text{-}\Omega$  chip resistor at resonance ( $f = 857$  MHz); other parameters are given in Figure 3.42. (From Ref. 21, © 1998 IEE, reprinted with permission.)

matching moves away from point A (i.e., the distance  $d$  increases) for the case with larger loading resistance. The resonant frequency is found to be slightly shifted to lower frequencies when the loading resistance increases.

The radiation patterns were also studied. Typical results for a regular PIFA and modified PIAs with  $R = 0\ \Omega$  and  $5.6\ \Omega$  are presented in Figure 3.43. All the patterns show broadside radiation, but the variation in the  $E$ -plane pattern is smoother than that in the  $H$ -plane pattern. The  $H$ -plane pattern is lobed near  $\theta = \pm 90^\circ$  (the plane with the finite ground plane) for modified PIAs, especially for the case with larger loading resistance. Finally, it should be noted that an enhanced impedance bandwidth for the modified PIFA occurs at some expense of antenna gain due to the ohmic loss of the loading resistance. It is estimated that the loss in antenna gain is about 6 dBi due to the ohmic loss of a  $5.6\text{-}\Omega$  chip-resistor loading, based on comparing the maximum receiving power of the modified PIAs in Figures 3.43(b) and 3.43(c).

### 3.5 USE OF A SLOT-LOADING TECHNIQUE

By embedding suitable slots in the radiating patch of a microstrip antenna, enhanced bandwidth with a reduced antenna size can be obtained. A typical design with a triangular patch is shown in Figure 3.44. It is found that, by embedding a pair of branchlike slots of proper dimensions, the first two broadside-radiation modes  $\text{TM}_{10}$  and  $\text{TM}_{20}$  of the triangular microstrip antenna can be perturbed such that their resonant frequencies are lowered and close to each other to form a wide impedance bandwidth [22].

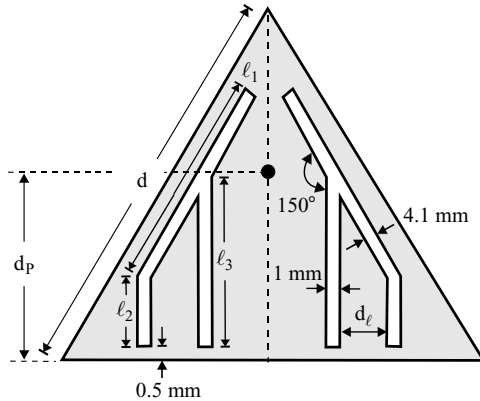


**FIGURE 3.44** Geometry of an equilateral-triangular microstrip patch with a pair of branchlike slots.

Three typical designs (antennas 1–3) have been implemented, and the measured return loss is shown in Figure 3.45. Two resonant modes are excited, and enhanced impedance bandwidth is obtained. For the three antennas, the obtained impedance bandwidths are 96 MHz (or about 5.2%) for antenna 1, 92 MHz (or about 5.2%) for antenna 2, and 90 MHz (or about 5.3%) for antenna 3. The three impedance bandwidths obtained are all about 3.0 times that of the corresponding regular triangular microstrip antenna. Also notice that the two resonant modes occur at decreasing resonant frequencies, which suggests that an antenna size reduction for the antenna studied can be obtained for a fixed operating frequency. The corresponding antenna size reduction for antenna 3 is about 25%. It should be noted that the optimal feed positions for antennas 1–3 are all along the centerline of the triangular patch at a distance of about  $0.46d$  from the bottom edge of the patch, which suggests that easy impedance matching can be obtained for the antenna studied. The radiation characteristics were also studied. Figure 3.46 shows the measured *E*- and *H*-plane radiation patterns for antenna 1 at resonance (1808 and 1868 MHz) of the two excited modes. Similar broadside radiation characteristics and the same polarization planes for the two resonant modes are observed, and good cross-polarization radiation is seen.

### 3.6 USE OF A SLOTTED GROUND PLANE

When the proper slots are embedded in the ground plane of a microstrip antenna, a lowering of the antenna's fundamental resonant frequency can be obtained [23]. Also, increased impedance bandwidth can be achieved by increasing the length of the embedded slots. A related design with a meandered ground plane was described in Section 2.4. In this section, another promising design is studied (Figure 3.47). In this design, a pair of narrow slots (length  $\ell$  and width 1 mm) are embedded in a finite ground plane ( $G \times G$ ) of a square microstrip antenna with a side length  $L$ . The two narrow slots are placed along the centerline of the ground plane

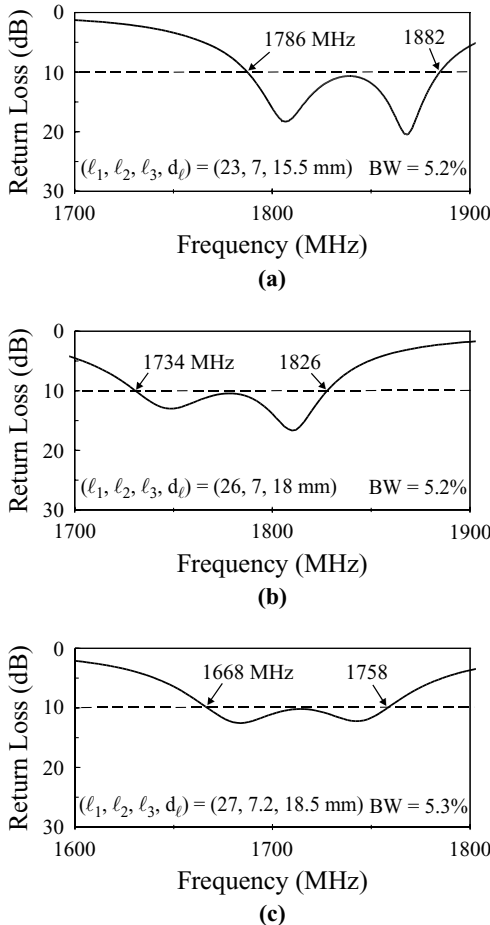


**FIGURE 3.45** Measured return loss against frequency for the antenna shown in Figure 3.41;  $\epsilon_r = 4.4$ ,  $h = 1.6$  mm,  $d = 50$  mm,  $d_p = 23$  mm, and ground-plane size =  $75 \times 75$  mm $^2$ . (a) Antenna 1, (b) antenna 2, (c) antenna 3.

perpendicular to the antenna's resonant direction ( $x$  axis in this study) to effectively meander the excited surface current paths in the ground plane. The distance of the narrow slots to the edge of the ground plane is  $S$ , which is fixed to be 2 mm in the study. A 50- $\Omega$  probe feed placed along the  $x$  axis and at a position  $d_p$  from the patch center is used to excite the antenna.

Several prototypes were constructed. The side lengths of the radiating patch and ground plane were chosen to be 30 and 50 mm, respectively. An inexpensive FR4 substrate ( $h = 1.6$  mm,  $\epsilon_r = 4.4$ , loss tangent = 0.0245) was used. Figure 3.48 shows the measured return loss against frequency for the cases with  $\ell = 0, 18$ , and  $20$  mm; the case with  $\ell = 0$  represents the corresponding regular microstrip antenna. The corresponding measured data are listed in Table 3.10 for comparison. The feed

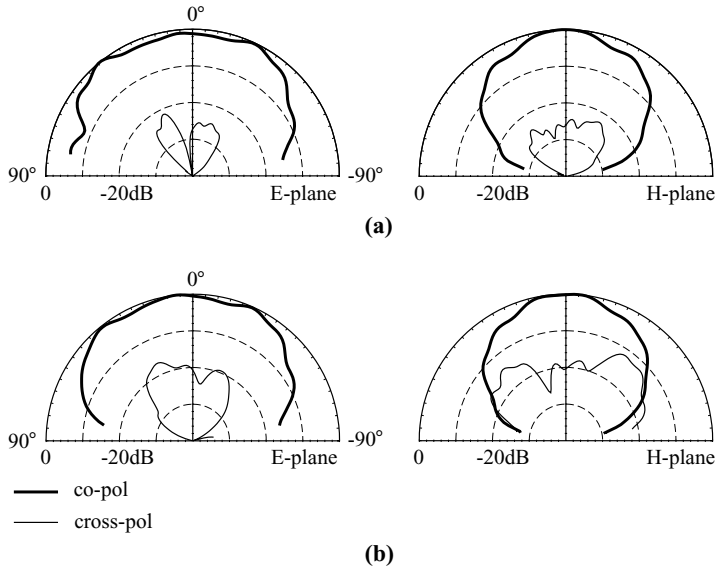


**FIGURE 3.46** Measured radiation patterns for antenna 1 studied in Figure 3.45. (a)  $f = 1808$  MHz, (b)  $f = 1868$  MHz.

positions for the three cases were all fixed at  $d_p = 7$  mm, and the antenna was excited at the fundamental mode ( $\text{TM}_{10}$  mode). It is clearly seen that the resonant frequency  $f_r$  is decreased with increasing slot length. For the case with  $\ell = 20$  mm, the resonant frequency is about 78% of that of the corresponding regular microstrip antenna (1835 vs. 2345 MHz). This corresponds to an antenna size reduction of about 39% for the antenna studied compared to the corresponding regular microstrip antenna at a fixed operating frequency. The impedance bandwidth (BW) for the case with  $\ell = 20$  mm is measured to be 3.1%, which is greater than that (2.7%) of the corresponding regular microstrip antenna. This behavior is largely owing to the embedded slots in the ground plane, which effectively lower the quality factor of the microstrip antenna.

Radiation characteristics of the constructed prototypes were also studied. Note that, owing to the limitation of the planar near-field antenna measurement system used, the measured data near the endfire direction have limited accuracy, and thus are not shown in the patterns. Figure 3.49 plots the radiation patterns of the antennas studied; the measured antenna gain is given in Table 3.10. Good broadside radiation characteristics are observed, and it is found that the antenna gain for the case with  $\ell = 20$  mm is 1.5 dBi greater than that of the corresponding regular microstrip antenna (4.5 vs. 3.0 dBi). By using the simulation software IE3D<sup>TM</sup>, simulated surface current distributions in the ground plane and radiating patch for the cases with  $\ell = 0$  and 20 mm were obtained and shown in Figure 3.50. It is clearly seen that the excited surface currents in the ground plane are strongly meandered by the two embedded slots, which in turn causes meandering of the surface currents on the radiating patch and results

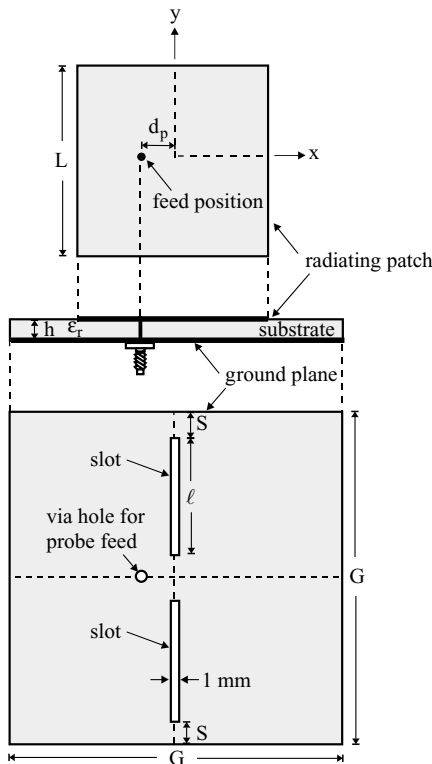


**FIGURE 3.47** Geometry of a compact microstrip antenna with a slotted ground plane. (From Ref. 23, © 2001 IEEE, reprinted with permission.)

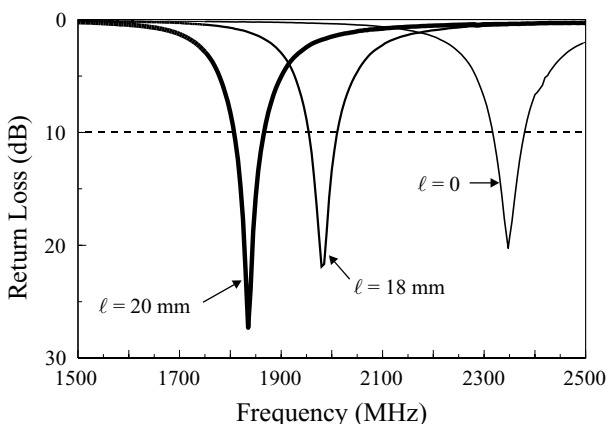


**FIGURE 3.48** Measured return loss against frequency for the antenna shown in Figure 3.46;  $L = 30$  mm,  $G = 50$  mm,  $S = 2$  mm,  $\epsilon_r = 4.4$ ,  $h = 1.6$  mm, and  $d_p = 7$  mm. (From Ref. 23, © 2001 IEEE, reprinted with permission.)

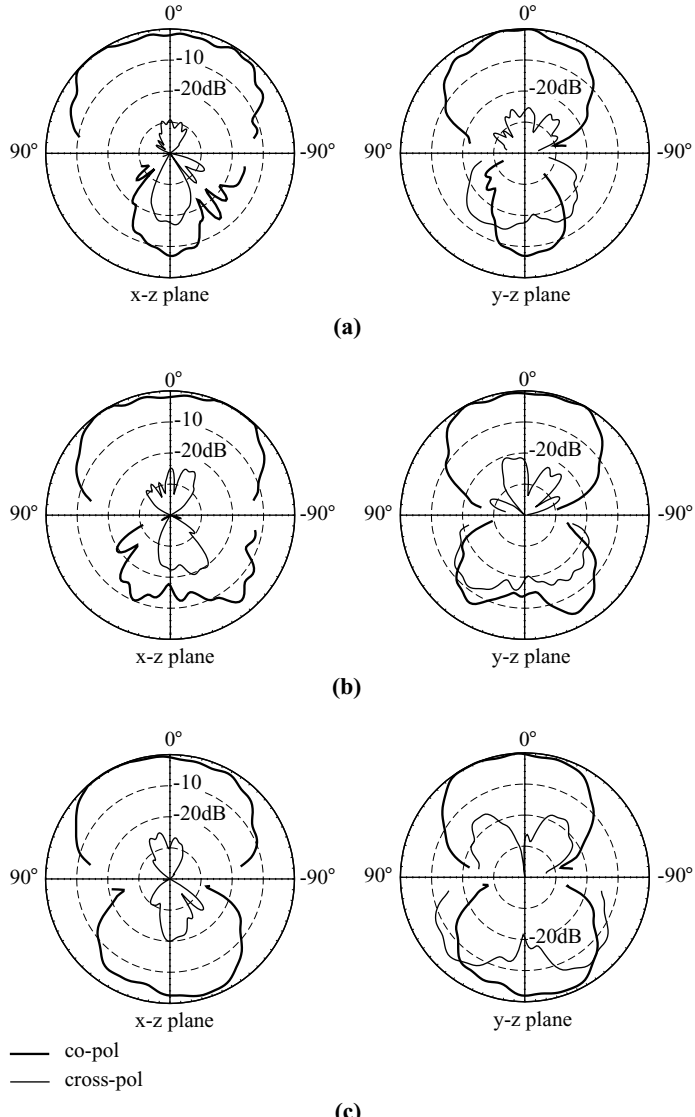


**FIGURE 3.49** Measured radiation patterns for the antenna studied in Figure 3.48. (a)  $\ell = 0$ ,  $f = 2345$  MHz; (b)  $\ell = 18$  mm,  $f = 1980$  MHz; (c)  $\ell = 20$  mm,  $f = 1835$  MHz. (From Ref. 23, © 2001 IEEE, reprinted with permission.)

in the lengthening of the equivalent surface current path. The antenna's fundamental resonant frequency is thus decreased, which agrees with the measured results.

Moreover, it is observed that the total excited patch surface currents are increased, and the excited surface current distribution in the central portion of the radiating patch is also greatly enhanced for the proposed design. The simulation radiation

**TABLE 3.10 Performance of the Antenna in Figure 3.48 [23]<sup>a</sup>**

$\ell$ (mm)	$f_r$ (MHz)	BW (%)	Gain (dBi)	F/B (dB)
0	2345	2.7	3.0	6.9
18	1980	2.8	3.7	4.3
20	1835	3.1	4.5	1.2

<sup>a</sup>F/B is the ratio of the front-to-back radiation intensity.

efficiency, obtained from IE3D™, of the proposed antenna is about 60%, which is much greater than that of a regular microstrip antenna with an FR4 substrate (usually about 30–40%). These characteristics may be the reason for the enhanced antenna gain obtained. Also note that, due to the embedded slots in the ground plane, backward radiation of the microstrip antenna could be increased. From experiments, the backward radiation for the case with  $\ell = 20$  mm studied here is increased by about 5.7 dBi compared to the case with  $\ell = 0$  (see Table 3.10). However, it should be noted that

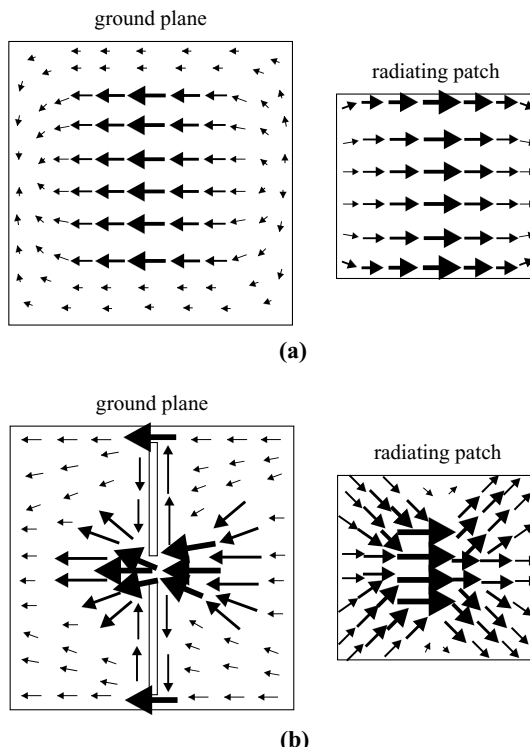


**FIGURE 3.50** Simulated surface current distributions in the ground plane and radiating patch of the antennas studied in Figure 3.48. (a) Design with an unslotted ground plane ( $\ell = 0$ ) at 2345 MHz; (b) design with a slotted ground plane ( $\ell = 20$  mm) at 1835 MHz. (From Ref. 23, © 2001 IEEE, reprinted with permission.)

the increase in the backward radiation arises from both the embedded slots in the ground plane and the decreased ground-plane size in wavelength units. In summary, in addition to the lowered resonant frequency, which leads to a possible antenna size reduction, the antenna studied also has widened impedance bandwidth and enhanced antenna gain, which are advantages over compact designs with a slotted radiating patch.

## REFERENCES

1. T. Taga, "Analysis of planar inverted-F antennas and antenna design for portable radio equipment," in K. Hirasawa and M. Haneishi, eds., *Analysis, Design and Measurement of Small and Low-Profile Antennas*, Artech House, Norwood, MA, 1992, pp. 161–180.
2. J.-Z. Zuercher, O. Staub, and K. Skrivervik, "SMILA: A compact and efficient antenna for mobile communications," *Microwave Opt. Technol. Lett.* **27**, pp. 155–157, Nov. 5, 2000.
3. S. Tarvas and A. Isohatala, "An internal dual-band mobile phone antenna," in *2000 IEEE Antennas Propagat. Soc. Int. Symp. Dig.*, pp. 266–269.
4. Z. D. Liu, P. S. Hall, and D. Wake, "Dual-frequency planar inverted F antenna," *IEEE Trans. Antennas Propagat.* **45**, 1451–1458, Oct. 1997.
5. W. H. Hsu and K. L. Wong, "Broadband aperture-coupled shorted patch antenna," *Microwave Opt. Technol. Lett.* **28**, 306–307, March 5, 2001.
6. J. S. Kuo and K. L. Wong, "A low-cost microstrip-line-fed shorted patch antenna for PCS base station," *Microwave Opt. Technol. Lett.* **29**, 146–148, May 5, 2001.
7. C. R. Rowell and R. D. Murch, "A capacitively loaded PIFA for compact mobile telephone handset," *IEEE Trans. Antennas Propagat.* **45**, 837–842, May 1997.
8. Y. X. Guo, K. M. Luk, and K. F. Lee, "L-probe proximity-fed short-circuited patch antenna," *Electron. Lett.* **35**, 2069–2070, Nov. 25, 1999.
9. R. Chair, K. M. Luk, and K. F. Lee, "Small dual patch antenna," *Electron. Lett.* **35**, 762–764, May 13, 1999.
10. K. M. Luk, R. Chair, and K. F. Lee, "Small rectangular patch antenna," *Electron. Lett.* **34**, 2366–2367, Dec. 10, 1999.
11. R. B. Waterhouse, "Broadband stacked shorted patch," *Electron. Lett.* **35**, 98–100, Jan. 21, 1999.
12. J. Ollikainen, M. Fischer, and P. Vainikainen, "Thin dual-resonant stacked shorted patch antenna for mobile communications," *Electron. Lett.* **35**, 437–438, March 18, 1999.
13. L. Zaid, G. Kossiavas, J. Dauvignac, J. Cazajous, and A. Papiernik, "Dual-frequency and broad-band antennas with stacked quarter wavelength elements," *IEEE Trans. Antennas Propagat.* **47**, 654–660, April 1999.
14. R. Chair, K. M. Luk, and K. F. Lee, "Miniature multiplayer shorted patch antenna," *Electron. Lett.* **36**, 3–4, Jan. 6, 2000.
15. K. L. Wong and Y. F. Lin, "Small broadband rectangular microstrip antenna with chip-resistor loading," *Electron. Lett.* **33**, 1593–1594, Sept. 11, 1997.
16. K. L. Wong and Y. F. Lin, "Microstrip-line-fed compact broadband circular microstrip antenna with chip-resistor loading," *Microwave Opt. Technol. Lett.* **17**, 53–55, Jan. 1998.
17. C. L. Tang, Studies of compact circular microstrip antennas, M.S. thesis, Department of Electrical Engineering, National Sun Yat-Sen University, Kaohsiung, Taiwan, 1998.

18. J. H. Lu, C. L. Tang, and K. L. Wong, "Slot-coupled compact broadband circular microstrip antenna with chip-resistor and chip-capacitor loadings," *Microwave Opt. Technol. Lett.* **18**, 345–349, Aug. 5, 1998.
19. Y. F. Lin and K. L. Wong, "Compact broadband triangular microstrip antennas with an inset microstrip-line feed," *Microwave Opt. Technol. Lett.* **17**, 169–170, Feb. 20, 1998.
20. J. H. Lu, C. L. Tang, and K. L. Wong, "Slot-coupled small triangular microstrip antenna," *Microwave Opt. Technol. Lett.* **16**, 371–374, Dec. 20, 1997.
21. K. L. Wong and K. P. Yang, "Modified planar inverted F antenna," *Electron. Lett.* **34**, 6–7, Jan. 8, 1998.
22. S. T. Fang, Analysis and design of triangular microstrip antennas, Ph.D. dissertation, Department of Electrical Engineering, National Sun Yat-Sen University, Kaohsiung, Taiwan, 1999.
23. T. W. Chiou and K. L. Wong, "Designs of compact microstrip antennas with a slotted ground plane," in *2001 IEEE Antennas Propagat. Soc. Int. Symp. Dig.* pp. 732–735.
24. M. El Yazidi, M. Himdi, and J. P. Daniel, "Transmission line analysis of nonlinear slot coupled microstrip antenna," *Electron. Lett.* **28**, 1406–1408, July 16, 1992.
25. K. F. Lee, K. M. Luk, K. F. Tong, S. M. Shum, T. Huynh, and R. Q. Lee, "Experimental and simulation studies of the coaxially fed U-slot rectangular patch antenna," *IEE Proc. Microwave Antennas Propagat.* **144**, 354–358, Oct. 1997.
26. F. Yang and Y. Rahmat-Samii, "Wideband dual parallel slot patch antenna (DPSPA) for wireless communications," in *2000 IEEE Antennas Propagat. Soc. Int. Symp. Dig.*, pp. 1650–1653.
27. K. L. Wong and W. H. Hsu, "A broadband rectangular patch antenna with a pair of wide slits," *IEEE Trans. Antennas Propagat.* **49**, 1345–1347, Sept. 2001.
28. J. Huang, "A technique for an array to generate circular polarization with linearly polarized elements," *IEEE Trans. Antennas Propagat.* **34**, 1113–1124, Sept. 1986.
29. W. H. Hsu and K. L. Wong, "A dual capacitively fed broadband patch antenna with reduced cross-polarization radiation," *Microwave Opt. Technol. Lett.* **26**, 169–171, Aug. 5, 2000.
30. K. L. Wong and W. S. Chen, "Compact microstrip antenna with dual-frequency operation," *Electron. Lett.* **33**, 646–647, April 10, 1997.
31. K. L. Wong and Y. C. Chen, "Resonant frequency of a slot-coupled cylindrical-rectangular microstrip structure," *Microwave Opt. Technol. Lett.* **7**, 566–570, Aug. 20, 1994.

## CHAPTER FOUR

---

# Compact Dual-Frequency and Dual-Polarized Microstrip Antennas

---

### 4.1 INTRODUCTION

Dual-frequency operation is an important subject in microstrip antenna design [1], and many such designs are known. These dual-frequency microstrip antennas include the use of multilayer stacked patches [2, 3], a rectangular patch with a pair of narrow slots placed close to the patch's radiating edges [4], a square patch with a rectangular notch [5], a rectangular patch loaded with shorting pins and slots [6], a rectangular patch fed by an inclined coupling slot [7], among others. Recently, many single-feed, single-layer, dual-frequency microstrip antenna designs have been demonstrated [8–15], and a new design for a dual-frequency feed network for feeding a microstrip array with dual-frequency radiating elements has been achieved [16]. These designs, however, are mainly applicable for regular-size microstrip antennas. To achieve dual-frequency operation in reduced-size or compact microstrip antennas, many promising designs have been reported [17–36]. Details of these compact dual-frequency designs and some recent advances in regular-size dual-frequency designs are presented in this chapter. Designs with a planar inverted-F antenna (PIFA) for dual-band or triple-band operation [37–39] are also addressed. Finally, recent advances in compact dual-polarized designs [40] are reviewed, and design examples of some promising compact dual-polarized microstrip antennas are given. Compact microstrip antennas capable of dual-polarized radiation are very suitable for applications in wireless communication systems that demand frequency reuse or polarization diversity.

## 4.2 SOME RECENT ADVANCES IN REGULAR-SIZE DUAL-FREQUENCY DESIGNS

In this section, design examples of some recent advances in regular-size microstrip antennas, mainly with a single-feed, single-layer microstrip structure, are presented. The dual-frequency designs presented are divided into two groups, depending on whether the two operating frequencies have the same polarization plane [16–26] or orthogonal polarization planes [27–36]. A simple method for obtaining a dual-frequency microstrip-line feed network [16] suitable for applications in dual-frequency microstrip array design is also described.

### 4.2.1 Dual-Frequency Operation with Same Polarization Planes

**4.2.1.1 Design with a Rectangular Patch** It has been demonstrated that, by loading a rectangular microstrip antenna with a pair of narrow slots placed close to the patch's radiating edges, dual-frequency operation can be obtained [1, 4]. In such dual-frequency designs, the two operating frequencies are associated with the  $\text{TM}_{10}$  and  $\text{TM}_{30}$  modes of the unslotted rectangular patch. In addition, the two operating frequencies have the same polarization planes and broadside radiation patterns, with a frequency ratio generally within the range of 1.6–2.0 for the single-probe-feed case [4]. Recently, it has been shown that, by placing the embedded slots close to the patch's nonradiating edges instead of the radiating edges as reported in Ref. 4, and replacing the narrow slots with properly bent slots (see Figure 4.1), a novel dual-frequency operation of the microstrip antenna can easily be achieved using a single probe feed [8]. The two operating frequencies of the antenna are found to have the same polarization planes and broadside radiation patterns; the frequency ratio of the

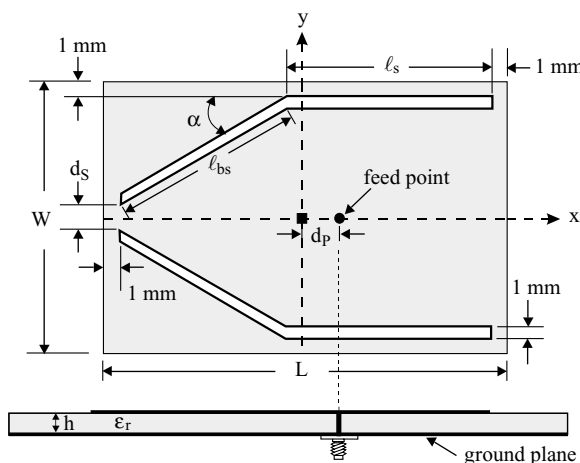


**FIGURE 4.1** Geometry of a dual-frequency rectangular microstrip antenna with a pair of bent slots placed close to the patch's nonradiating edges. (From Ref. 8, © 1998 IEE, reprinted with permission.)

two operating frequencies is found to range from about 1.29 to 1.60, different from that (1.6–2.0) of the conventional design [4].

Consider the geometry shown in Figure 4.1; the rectangular patch has dimensions  $L \times W$  and is printed on a substrate of thickness  $h$  and relative permittivity  $\varepsilon_r$ . Embedded slots, with a bend angle  $\alpha$ , are placed close to the patch's nonradiating edges and have a narrow width of 1 mm and a length of  $\ell_s + \ell_{bs}$ , where  $\ell_s$  is the length of the straight section of the slot parallel to the patch edge and  $\ell_{bs}$  is the length of the bent section, determined by  $(L - \ell_s - 2d_w)/\cos \alpha$  in the present design. The distances of the bent slots from the nonradiating and radiating patch edges are both set to 1 mm. For each bend angle  $\alpha$ , the distance between the bent-section ends of the two slots is given by  $d_s = W - 2(d_L + \ell_{bs} \sin \alpha)$ . Good impedance matching of the two operating frequencies can be obtained by using a single probe feed placed along the  $x$  axis at a distance  $d_p$  from the patch center.

It is found that, with the presence of the bent slots, the fundamental mode ( $TM_{10}$  mode) of the unslotted patch antenna is perturbed and its resonant frequency decreases with increasing bend angle. In addition, a new resonance mode, denoted here the  $TM_{\delta 0}$  mode with  $1 < \delta < 2$ , is excited between the  $TM_{10}$  and  $TM_{20}$  modes. When the bend angle of the slot is small, the IE3D<sup>TM</sup> simulation results show that this new mode has a null excited surface current density near the patch center, with the surface current density slightly increased toward the two radiating edges. In this condition, experimental results show that this new resonance mode has a low radiation efficiency and is not suitable for radiation applications. However, when the bend angle  $\alpha$  is within the range  $15^\circ$ – $30^\circ$ , the null-current point of this new  $TM_{\delta 0}$  mode moves close to the radiating edge at the slot's bent-section side and the current distribution in the central portion of the patch becomes uniformly distributed, which makes the radiation efficiency of the  $TM_{\delta 0}$  mode almost as good as that of the  $TM_{10}$  mode. Owing to their similar current distributions in the central portion of the patch, the modes  $TM_{10}$  and  $TM_{\delta 0}$  are expected to have the same polarization planes and similar radiation patterns, and both can be excited using a single probe feed with good impedance matching.

Figure 4.2 shows the measured return loss for the antenna studied. The resonant frequencies  $f_1$  and  $f_2$  of the two operating modes and their frequency ratio are plotted against the bent-slot angle in Figure 4.3. The obtained dual-frequency performance

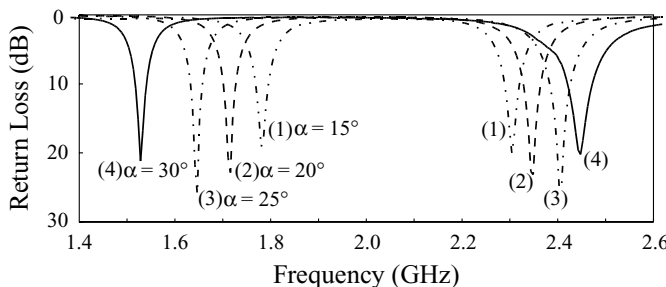


**FIGURE 4.2** Measured return loss for the antenna shown in Figure 4.1;  $\varepsilon_r = 4.4$ ,  $h = 1.6$  mm,  $L = 37.3$  mm,  $W = 24.87$  mm, and  $\ell_s = 19$  mm. (From Ref. 8, © 1998 IEE, reprinted with permission.)

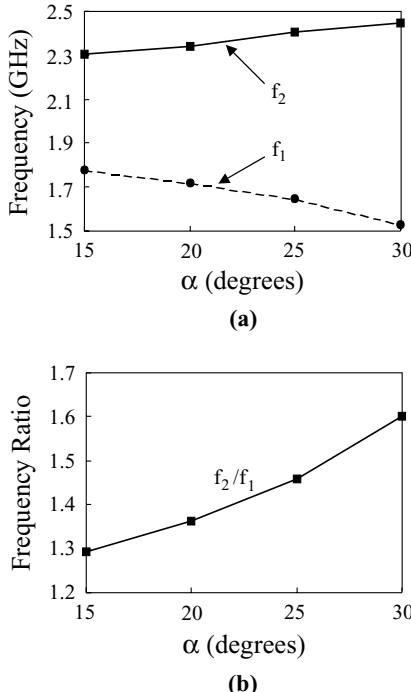


**FIGURE 4.3** (a) The two operating frequencies  $f_1$  and  $f_2$  and (b) the frequency ratio  $f_2/f_1$  against the bend angle of embedded slots; antenna parameters are given in Figure 4.2. (From Ref. 8, © 1998 IEE, reprinted with permission.)

is listed in Table 4.1 for comparison. It is clearly seen that, with decreasing bent-slot angle, the two frequencies are shifted closer to each other, which results in a lower frequency ratio. For the present study, the frequency ratio can be tuned from 1.29 to 1.60 by varying the bend angle. The measured radiation patterns of the antenna at the two operating frequencies are plotted in Figures 4.4 and 4.5 for  $\alpha = 15^\circ$  and  $30^\circ$ , respectively. It is seen that both operating modes have the same broadside radiation patterns and polarization planes, and cross-polarization radiation less than about  $-20$  dB is observed. The difference of the antenna gain in the broadside

**TABLE 4.1 Dual-Frequency Performance of the Antenna in Figure 4.1 [8]<sup>a</sup>**

$\alpha$ (deg)	$d_p$ (mm)	$f_1$ , BW (MHz, %)	$f_2$ , BW (MHz, %)	$f_2/f_1$
15	2.9	1780, 1.6	2304, 1.4	1.29
20	2.1	1716, 1.5	2340, 1.5	1.36
25	1.7	1646, 1.4	2403, 2.0	1.46
30	0.7	1528, 1.3	2448, 2.0	1.60

<sup>a</sup>Antenna parameters are given in Figure 4.2.

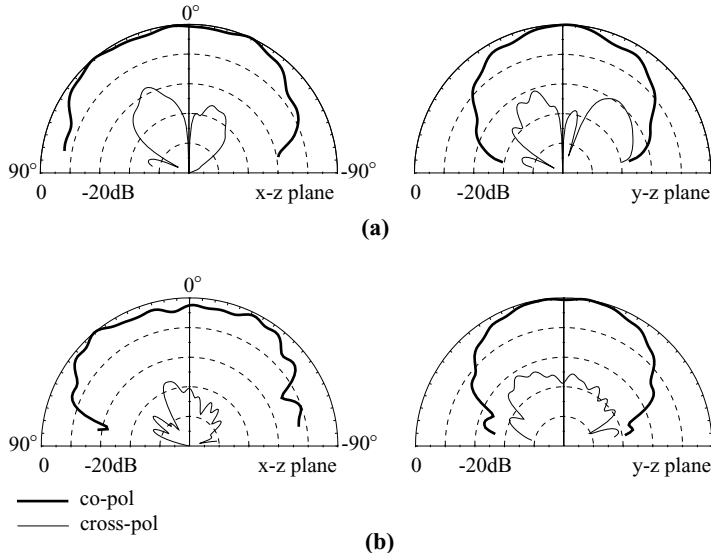


**FIGURE 4.4** Measured  $E$ -plane ( $x$ - $z$  plane) and  $H$ -plane ( $y$ - $z$  plane) radiation patterns for the antenna studied in Figure 4.2 with  $\alpha = 15^\circ$ . (a)  $f = 1780$  MHz, (b)  $f = 2304$  MHz. (From Ref. 8, © 1998 IEE, reprinted with permission.)

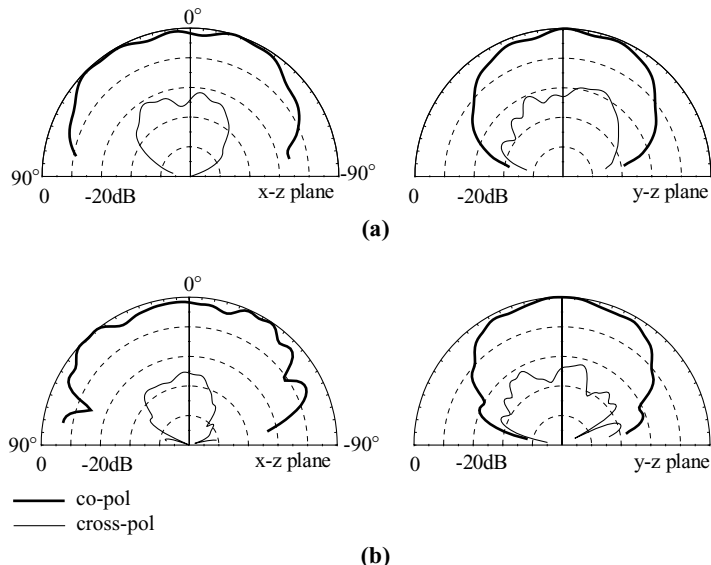


**FIGURE 4.5** Measured  $E$ -plane ( $x$ - $z$  plane) and  $H$ -plane ( $y$ - $z$  plane) radiation patterns for the antenna studied in Figure 4.2 with  $\alpha = 30^\circ$ . (a)  $f = 1528$  MHz, (b)  $f = 2448$  MHz. (From Ref. 8, © 1998 IEE, reprinted with permission.)

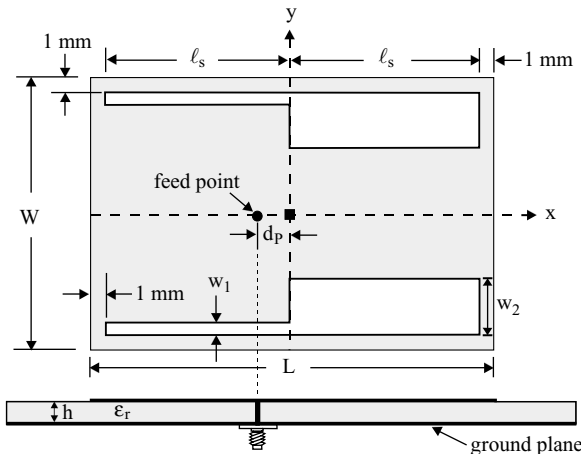


**FIGURE 4.6** Geometry of a dual-frequency rectangular microstrip antenna with a pair of step slots. (From Ref. 9, © 1999 IEE, reprinted with permission.)

direction of the two frequencies is estimated to vary within 0–3 dBi, depending on the bent-slot angle.

By using a pair of step slots in place of the bent slots used in Figure 4.1, dual-frequency operation of a rectangular microstrip antenna can be obtained [9]. The geometry is shown in Figure 4.6. The embedded step slots are placed close to the patch's nonradiating edges and have different widths  $w_1$  and  $w_2$ . The two sections of different widths are designed to have the same length  $\ell_s$ . The spacings of the step slots away from the nonradiating and radiating patch edges are set to be 1 mm. By varying the step ratio  $w_2/w_1$  of the step slots, the frequency ratio between the two operating frequencies can be varied, resulting in a tunable frequency ratio for the antenna. Typical measured return loss for the antenna is shown in Figure 4.7. In the experiments,

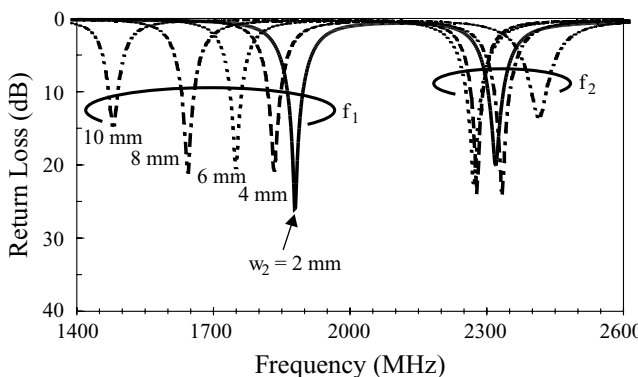


**FIGURE 4.7** Measured return loss for the antenna shown in Figure 4.6;  $\epsilon_r = 4.4$ ,  $h = 1.6$  mm,  $L = 38$  mm,  $W = 25$  mm,  $w_1 = 1$  mm,  $\ell_s = 18$  mm, and ground-plane size =  $75 \times 75$  mm $^2$ . (From Ref. 9, © 1999 IEE, reprinted with permission.)

**TABLE 4.2 Dual-Frequency Performance of the Antenna in Figure 4.6 [9]<sup>a</sup>**

Slot Widths $w_1, w_2$ (mm)	$d_p$ (mm)	$f_1$ , BW (MHz, %)	$f_2$ , BW (MHz, %)	$f_2/f_1$
1, 2	6.5	1878, 1.8	2320, 1.4	1.23
1, 4	4.2	1834, 1.5	2278, 1.2	1.24
1, 6	3.5	1750, 1.5	2272, 1.5	1.30
1, 8	3.1	1644, 1.7	2334, 1.4	1.42
1, 10	2.2	1480, 1.4	2414, 1.3	1.63

<sup>a</sup>Antenna parameters are given in Figure 4.7.

the width of the narrower section  $w_1$  is fixed and the width of the wider section  $w_2$  is varied, which results in different step ratios for the step slots embedded in the patch. The corresponding data for dual-frequency performance are listed in Table 4.2 for comparison. It is clearly seen that, with increasing step ratio, the lower operating frequency  $f_1$  (or the fundamental resonant frequency  $f_{10}$ ) is significantly decreased. On the other hand, the higher frequency  $f_2$  is slightly varied, which provides a tunable frequency ratio ranging from about 1.23 to 1.63, close to that of the antenna shown in Figure 4.1.

A design for a dual-frequency microstrip antenna with embedded spur lines and integrated reactive loading (see Figure 4.8) has been reported [10]. This antenna has a ratio of the two operating frequencies of about 1.1, a value lower than that of the designs shown in Figures 4.1 and 4.6. The embedded spur lines are at the patch's nonradiating edges, and the integrated reactive loading is formed by an inset microstrip-line section and inserted at one of the patch's radiating edges. In this

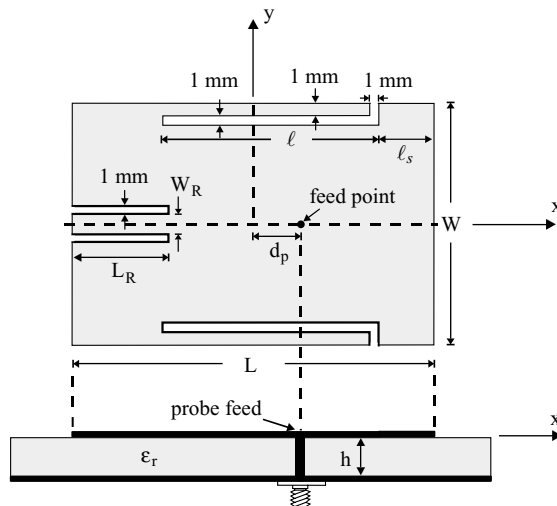


**FIGURE 4.8** Geometry of a dual-frequency rectangular microstrip antenna with a pair of spur lines and an integrated reactive loading. (From Ref. 10, © 1999 John Wiley & Sons, Inc.)

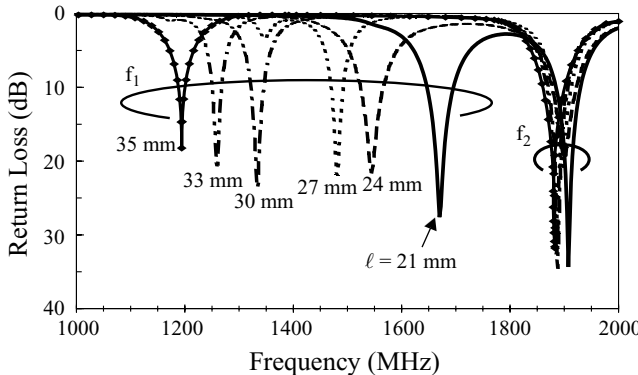


**FIGURE 4.9** Measured return loss for the antenna shown in Figure 4.8 with various spur-line lengths;  $\epsilon_r = 4.4$ ,  $h = 1.6$  mm,  $L = 38.5$  mm,  $W = 28$  mm,  $\ell_s = 2$  mm,  $L_R = 11.5$  mm, and  $W_R = 3$  mm. (From Ref. 10, © 1999 John Wiley & Sons, Inc.)

design, a new resonant mode with its resonant frequency lower than that of the  $\text{TM}_{10}$  mode can be excited. This characteristic is different from that observed for the designs with a pair of bent slots (Figure 4.1) or step slots (Figure 4.6), where the resonant frequency of the new excited mode is higher than that of the  $\text{TM}_{10}$  mode. This new resonant mode is denoted the  $\text{TM}_{\beta 0}$  mode ( $0 < \beta < 1$ ); it has the same polarization plane as the  $\text{TM}_{10}$  mode. The resonant frequency of the  $\text{TM}_{\beta 0}$  mode is found to be strongly dependent on the spur-line length. On the other hand, since the embedded spur lines are oriented mainly parallel to the patch edges, a very small effect on the performance of the  $\text{TM}_{10}$  mode is expected; that is, the resonant frequency  $f_{10}$  will be very slightly affected by the spur-line perturbation. The different effects of the embedded spur lines on the  $\text{TM}_{\beta 0}$  and  $\text{TM}_{10}$  modes make the frequency ratio of the two operating frequencies tunable and result in an even lower frequency ratio than that obtained in Refs. 8 and 9. However, without the inset microstrip-line section as an integrated reactive loading in this design, good impedance matching of the  $\text{TM}_{\beta 0}$  and  $\text{TM}_{10}$  modes using a single probe feed is difficult to obtain.

Prototypes of the antenna shown in Figure 4.8 have been implemented. Figure 4.9 shows the measured return loss for the two operating frequencies  $f_1$  ( $= f_{\beta 0}$ ) and  $f_2$  ( $= f_{10}$ ), which are the first two resonant frequencies of the antenna. Note that the dimensions of the inset 50- $\Omega$  microstrip-line section for providing proper reactive impedance to improve good impedance matching are fixed at  $L_R = 11.5$  mm (or about  $0.3L$ ) and  $W_R = 3$  mm for the various spur-line lengths. Also note that the antenna parameters studied here give a fundamental resonant frequency at about 1900 MHz for the case of a simple rectangular microstrip antenna. The corresponding dual-frequency performance is listed in Table 4.3. The results clearly show that, upon increasing the spur-line length, the lower frequency  $f_1$  is decreased and is lower than 1900 MHz. On the other hand, the higher frequency  $f_2$  is very slightly affected by the variation in the spur-line length and is about the same as the frequency  $f_{10}$  of a simple rectangular microstrip antenna. By varying the spur-line length, this design has a tunable

**TABLE 4.3 Dual-Frequency Performance of the Antenna in Figure 4.8 [10]<sup>a</sup>**

Spur-line Length $\ell$ (mm)	$d_p$ (mm)	$f_1$ , BW (MHz, %)	$f_2$ , BW (MHz, %)	$f_2/f_1$
21	9.0	1670, 2.4	1908, 2.9	1.14
24	9.0	1545, 2.4	1900, 2.8	1.23
27	8.8	1483, 1.8	1895, 1.4	1.28
30	8.8	1333, 1.9	1888, 1.8	1.42
33	8.8	1260, 2.0	1885, 1.4	1.50
35	8.8	1205, 2.0	1883, 1.3	1.56

<sup>a</sup>Antenna parameters are given in Figure 4.9.

frequency-ratio range of about 1.1–1.6. Also, from the results in Table 4.3, it is found that the optimal feed positions for the present design are almost about the same, which indicates that the feed position is insensitive to the variation in the spur-line length. Radiation patterns at the two operating frequencies for the cases with  $\ell = 24$  and 33 mm were also measured. The two operating frequencies have the same polarization planes and similar broadside radiation characteristics.

**4.2.1.2 Design with a Circular Patch** Single-feed dual-frequency circular microstrip antennas with a pair of arc-shaped slots [11], a single arc-shaped slot [12], or an open-ring slot [13] have been reported. We first discuss the case with a pair of arc-shaped slots. In the geometry shown in Figure 4.10, two arc-shaped slots, having a narrow width of 1 mm and subtended by an angle  $\theta$ , are placed close to the boundary of the circular patch at a distance of 1 mm. The two arc-shaped slots are centered with respect to the  $x$  axis. A single probe feed for dual-frequency operation

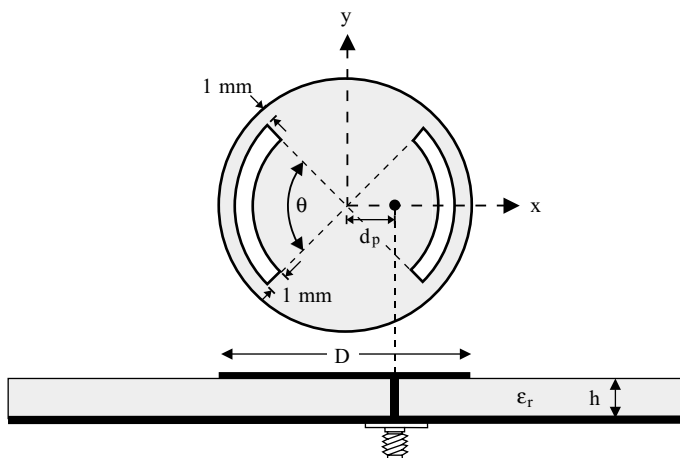


**FIGURE 4.10** Geometry of a dual-frequency circular microstrip antenna with a pair of arc-shaped slots. (From Ref. 11, © 1998 John Wiley & Sons, Inc.)

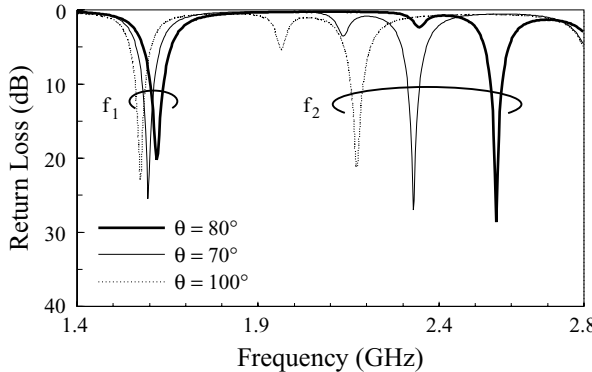


**FIGURE 4.11** Measured return loss for the antenna shown in Figure 4.10;  $\epsilon_r = 4.4$ ,  $h = 1.6$  mm, and  $D = 50$  mm. (From Ref. 11, © 1998 John Wiley & Sons, Inc.)

is placed along the  $x$  axis at a distance  $d$  from the patch center. With the presence of the slots, the fundamental mode  $\text{TM}_{11}$  of the circular microstrip antenna is slightly perturbed because the slots are located close to the patch boundary, where the excited patch surface current for the  $\text{TM}_{11}$  mode has a minimum value; that is, the resonant frequency  $f_{11}$  will be slightly varied by the introduced slots in the circular patch. The second resonant mode excited in the present design is the  $\text{TM}_{12}$  mode. Since the excited patch surface current for the  $\text{TM}_{12}$  mode is maximum close to the patch boundary, it is expected that the  $\text{TM}_{12}$  mode will be significantly perturbed due to the presence of the slots. From the simulated results using IE3D<sup>TM</sup>, it is found that the patch surface current path of the  $\text{TM}_{12}$  mode is lengthened and strongly modified such that the excited patch surface currents circulate around the two arc-shaped slots, and a resonant condition with nulls close to the edges of the two slots is obtained. This suggests that the resonant frequency  $f_{12}$  will be significantly decreased, and the current distribution of the perturbed  $\text{TM}_{12}$  mode will become similar to that of the  $\text{TM}_{11}$  mode; that is, the radiation pattern of the perturbed  $\text{TM}_{12}$  mode will become similar to that of the  $\text{TM}_{11}$  mode. Thus, from the results obtained, it is expected that dual-frequency operation of the same polarization planes and similar radiation characteristics for the present antenna can be obtained.

Experiments have been conducted on this design. Figure 4.11 shows the measured return loss for the cases with  $\theta = 80^\circ$ ,  $90^\circ$ , and  $100^\circ$ . The corresponding resonant frequencies and impedance bandwidths, determined from the 10-dB return loss, are listed in Table 4.4. The diameter of the circular patch was selected to be 50 mm and the microwave substrate used had a thickness  $h = 1.6$  mm and a relative permittivity  $\epsilon_r = 4.4$ . From the results obtained, it is found that there exists a range of subtending angles for the present design to have a single probe feed for achieving  $50\Omega$  impedance matching of the two operating frequencies. In this case, the subtending angles are within the range of about  $80^\circ$ – $100^\circ$ . The resonant frequencies  $f_{11}$  and  $f_{12}$  of the present design without slots are 1.65 and 4.77 GHz, respectively. From the results in Figure 4.11, it is seen that the first resonant frequency  $f_1$  is about

**TABLE 4.4 Dual-Frequency Performance of the Antenna in Figure 4.10 [11]<sup>a</sup>**

Subtending Angle $\theta$ (deg)	$d_p$ (mm)	$f_1$ , BW (MHz, %)	$f_2$ , BW (MHz, %)	$f_2/f_1$
80	12	1616, 2.2	2554, 1.3	1.58
84	12	1606, 2.2	2470, 1.3	1.54
90	12	1593, 2.0	2326, 1.5	1.46
96	12	1586, 2.0	2236, 1.5	1.41
100	12	1570, 1.8	2167, 1.6	1.38

<sup>a</sup>Antenna parameters are given in Figure 4.11.

1.6 GHz, very slightly affected by the variation in the subtending angle of various arc-shaped slots and also about the same as the resonant frequency of the  $\text{TM}_{11}$  mode of the case without slots. On the other hand, the second resonant frequency  $f_2$  is significantly decreased with increasing  $\theta$ , and is much lower than the resonant frequency of the unperturbed  $\text{TM}_{12}$  mode of the case without slots. The feed positions are insensitive to various arc-shaped slots introduced in the present design and fixed at  $d_p = 12$  mm from the patch center. The frequency ratio  $f_2/f_1$  of the two operating frequencies is within the range 1.38–1.58. Figure 4.12 plots the measured radiation patterns for the two operating frequencies for the case with  $\theta = 100^\circ$ . These two operating frequencies have the same polarization planes and similar radiation patterns. Good cross-polarization radiation is observed for the two operating frequencies.

Dual-frequency operation can be obtained with a single arc-shaped slot embedded in a circular patch [12]. In Figure 4.13, the dual-frequency design of an inset-microstrip-line-fed circular microstrip antenna with a single arc-shaped slot is presented. The arc-shaped slot is also centered with respect to the  $x$  axis and subtended by an angle  $\theta$ . The inset-microstrip line has a characteristic impedance of  $50 \Omega$ , and the length of the microstrip line inset into the circular patch is  $\ell$ . This design is very suitable for integration with coplanar microwave circuitry. The application of this

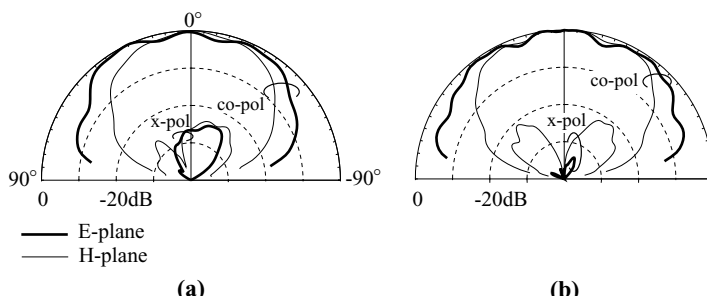


**FIGURE 4.12** Measured  $E$ -plane ( $x$ – $z$  plane) and  $H$ -plane ( $y$ – $z$  plane) radiation patterns for the antenna studied in Figure 4.11 with  $\theta = 100^\circ$ . (a)  $f = 1570$  MHz, (b)  $f = 2167$  MHz. (From Ref. 11, © 1998 John Wiley & Sons, Inc.)

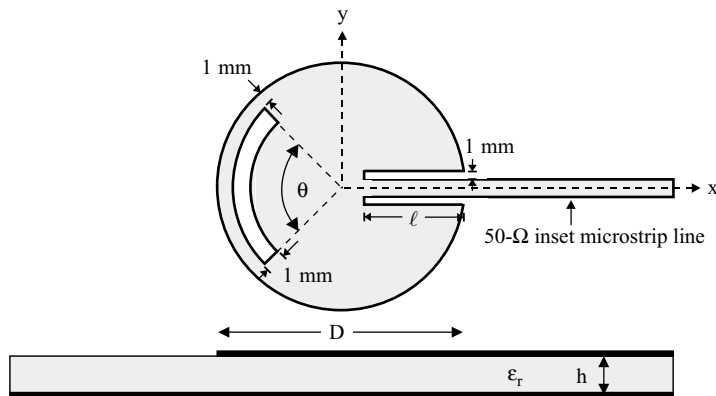


**FIGURE 4.13** Geometry of an inset microstrip-line-fed circular microstrip antenna with an arc-shaped slot for dual-frequency operation. (From Ref. 12, © 1999 IEE, reprinted with permission.)

design to a two-element dual-frequency microstrip array has been demonstrated. The two-element microstrip array can find applications in base-station antenna designs for wireless communications since it can have a narrower beamwidth radiation pattern in the elevation direction and a broadside radiation pattern with a wide beamwidth in the azimuthal direction.

Prototypes have been constructed based on the geometry shown in Figure 4.13. Figure 4.14 shows the measured return loss for the cases with  $\theta = 87^\circ$ ,  $93^\circ$ , and  $100^\circ$ . The corresponding dual-frequency performance is listed in Table 4.5. In the experiments, the circular patch was selected to have a diameter of 50 mm. The required inset length of the microstrip feed line is fixed at  $\ell = 37$  mm (about  $0.74D$ ) away from the patch boundary and is insensitive to various arc-shaped slots embedded in the circular patch. This optimal inset microstrip-line length is derived from numerous

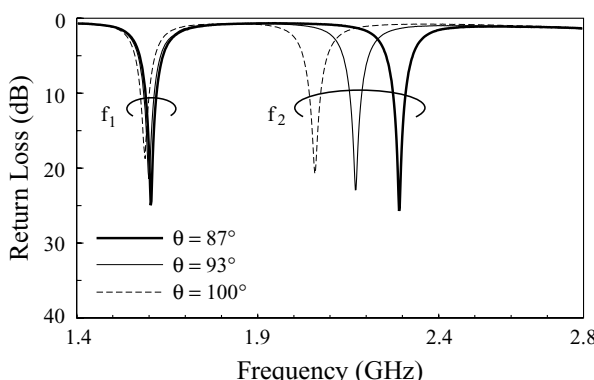


**FIGURE 4.14** Measured return loss for the antenna shown in Figure 4.13;  $\epsilon_r = 4.4$ ,  $h = 1.6$  mm,  $D = 50$  mm, and  $\ell = 37$  mm. (From Ref. 12, © 1999 IEE, reprinted with permission.)

**TABLE 4.5 Dual-Frequency Performance for the Antenna shown in Figure 4.13 [12]<sup>a</sup>**

Subtending Angle $\theta$ (deg)	Inset Length $\ell$ (mm)	$f_1$ , BW (MHz, %)	$f_2$ , BW (MHz, %)	$f_2/f_1$
87	37	1605, 1.9	2292, 1.5	1.43
90	37	1603, 1.9	2244, 1.5	1.40
93	37	1600, 1.8	2171, 1.5	1.36
96	37	1592, 1.8	2107, 1.6	1.32
100	37	1584, 1.7	2051, 1.6	1.29

<sup>a</sup> Antenna parameters are given in Figure 4.14.

experiments. In order to achieve good impedance matching and similar broadside radiation patterns for the two operating frequencies, there exists a limited range of subtending angles for the present design. In this study, the subtending angles can be varied from  $87^\circ$  to  $100^\circ$ . When the angle  $\theta$  is greater than about  $100^\circ$ , it is difficult to obtain good impedance matching for the two operating frequencies. On the other hand, when the angle  $\theta$  is smaller than about  $87^\circ$ , the radiation pattern of the second resonant frequency will become asymmetric with respect to the broadside direction. It is also noted that the first resonant frequency  $f_1$ , about 1.6 GHz, is very slightly affected by the variation in the subtending angle of the arc-shaped slot and is also about the same as the resonant frequency (about 1.65 GHz) of the TM<sub>11</sub> mode of the simple unslotted circular patch. On the other hand, the second resonant frequency  $f_2$  decreases rapidly with increasing  $\theta$ . The different effects of the arc-shaped slot on the first two resonant frequencies result in a tunable frequency ratio  $f_2/f_1$  between the two operating frequencies in the range of about 1.29–1.43 (see Table 4.5).

By using the simulation software IE3D™, the excited patch surface currents for the two operating frequencies of the antenna have been simulated and analyzed. The simulated current distributions of the two operating frequencies  $f_1$  and  $f_2$  for  $\theta = 100^\circ$  are plotted in Figure 4.15. For the case of  $f_1$  shown in Figure 4.15(a), the resonant mode is the perturbed TM<sub>11</sub> mode. It is seen that the excited current distribution is

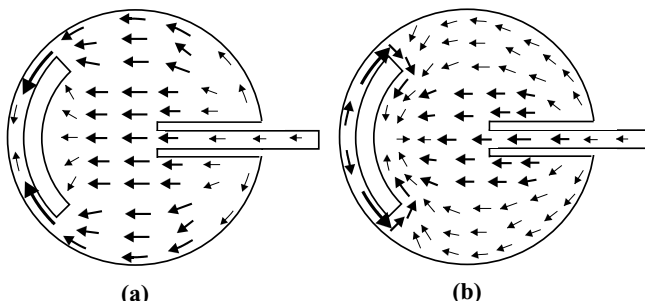


**FIGURE 4.15** Simulated current distributions for the antenna studied in Figure 4.14 with  $\theta = 100^\circ$ . (a)  $f_1 = 1584$  MHz, (b)  $f_2 = 2051$  MHz. (From Ref. 12, © 1999 IEE, reprinted with permission.)

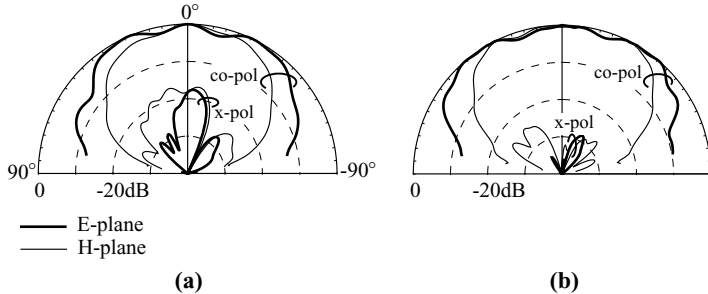


**FIGURE 4.16** Measured *E*-plane (*x*-*z* plane) and *H*-plane (*y*-*z* plane) radiation patterns for the antenna studied in Figure 4.14 with  $\theta = 100^\circ$ . (a)  $f_1 = 1584$  MHz, (b)  $f_2 = 2051$  MHz. (From Ref. 12, © 1999 IEE, reprinted with permission.)

very similar to that of the  $\text{TM}_{11}$  mode of the case without the slot, especially in the central portion of the circular patch. This is largely because the slot is embedded close to the patch boundary, where the excited patch surface current for the  $\text{TM}_{11}$  mode has a minimum value. This makes the resonant frequency of the perturbed  $\text{TM}_{11}$  mode slightly lower than that of the  $\text{TM}_{11}$  mode of the case without the slot. For the case of  $f_2$  shown in Figure 4.15(b), the resonant mode is the perturbed  $\text{TM}_{01}$  mode, in contrast to that (the perturbed  $\text{TM}_{12}$  mode) in the design with a pair of two arc-shaped slots [11]. Owing to the arc-shaped slot loading, the null of the current distribution, usually located in the center of the circular patch for the unperturbed  $\text{TM}_{01}$  mode of the case without a slot, is pulled close to the edge of the slot, such that the central portion of the current distribution becomes similar to that of the  $\text{TM}_{11}$  mode. Thus, for the present design, the two operating frequencies are expected to have the same polarization planes and similar radiation characteristics. The experimental results for the radiation patterns shown in Figure 4.16 agree with this hypothesis. Good cross-polarization radiation for the two operating frequencies is observed.

The on-axis antenna gain for  $f_1$  and  $f_2$  was also measured and found to be about 4.7 and 1.4 dBi, respectively. The smaller antenna gain for  $f_2$  is probably because the radiation efficiency of the  $\text{TM}_{01}$  mode is not as good as that of the  $\text{TM}_{11}$  mode. It should also be noted that, owing to the stronger perturbation effect of the arc-shaped slot on the  $\text{TM}_{01}$  mode, the frequency  $f_2$  (about 2.0–2.3 GHz) in the present design is much lower than that (about 3.33 GHz) of the unperturbed  $\text{TM}_{01}$  mode of the case without a slot. The excitation of different resonant modes ( $\text{TM}_{11}$  and  $\text{TM}_{01}$ ) for dual-frequency operation also makes the obtained tunable frequency-ratio range (1.29–1.43) different from that (1.38–1.58) of the design with a pair of arc-shaped slots in which the  $\text{TM}_{11}$  and  $\text{TM}_{12}$  modes are excited for dual-frequency radiation.

The present design has been applied to a two-element dual-frequency microstrip array. The geometry is shown in Figure 4.17. The two circular patches have the same structure as shown in Figure 4.13. The patch parameters are the same as given in Figure 4.14 for the case with  $\theta = 100^\circ$ . The feed network consists of one  $50\text{-}\Omega$  microstrip feed line and two  $100\text{-}\Omega$  inset-microstrip feed lines. By considering that the optimal array gain can be obtained when the spacing  $S$  between the centers of the patches is about  $(0.7\text{--}0.9)\lambda_0$  [41], one chooses the spacing between the two patch

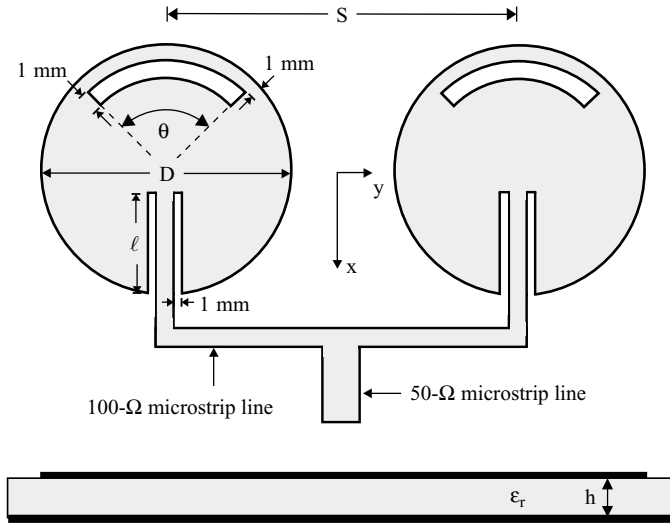


**FIGURE 4.17** Geometry of a two-element dual-frequency microstrip array using dual-frequency antenna elements shown in Figure 4.13. (From Ref. 12, © 1999 IEE, reprinted with permission.)

centers to be 132.5 mm, which is equivalent to about  $0.7\lambda_0$  at the lower frequency of 1.59 GHz and is about  $0.9\lambda_0$  at the higher frequency of 2.03 GHz. Measured return loss for the dual-frequency array is shown in Figure 4.18. The impedance bandwidths are about 34 MHz (2.1%) and 33 MHz (1.6%) for the 1.59- and 2.03-GHz bands, respectively. For the lower frequency band, the obtained bandwidth (2.1%) is also greater than that (1.7%) of the single-patch case largely owing to the effect of the feed network used in the present array design. Figure 4.19 plots the measured radiation patterns at 1.59 GHz. Good cross-polarization radiation (below

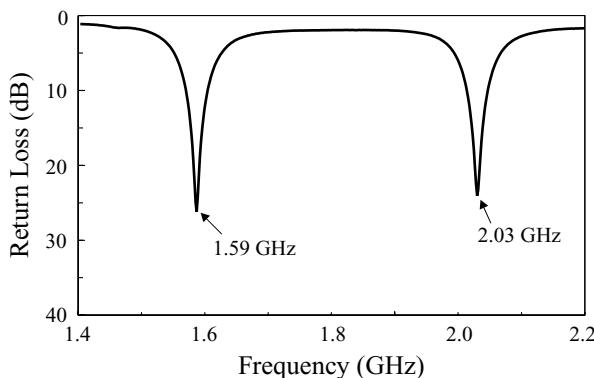


**FIGURE 4.18** Measured return loss of the two-element dual-frequency microstrip array shown in Figure 4.17;  $\epsilon_r = 4.4$ ,  $h = 1.6$  mm,  $D = 50$  mm,  $\ell = 42$  mm,  $S = 132.5$  mm, and  $\theta = 100^\circ$ . (From Ref. 12, © 1999 IEE, reprinted with permission.)

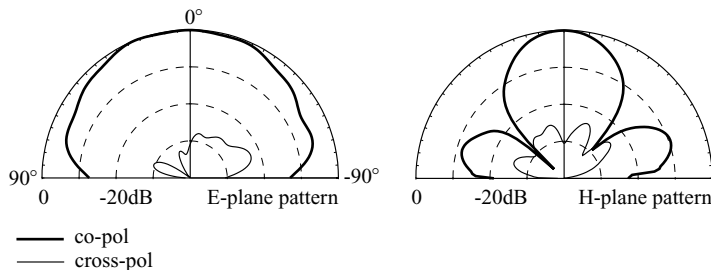


**FIGURE 4.19** Measured *E*-plane ( $x$ - $z$  plane) and *H*-plane ( $y$ - $z$  plane) radiation patterns for the dual-frequency microstrip array studied in Figure 4.18;  $f = 1.59$  GHz. (From Ref. 12, © 1999 IEE, reprinted with permission.)

–20 dB) is observed. Note that the *H*-plane pattern becomes narrower, owing to the array effect, while the *E*-plane pattern remains similar to that of a single-patch antenna, having a broadside radiation pattern with a wide beamwidth. The results for 2.03 GHz are presented in Figure 4.20. Similar results to those in Figure 4.19 are observed. Note that the on-axis antenna gain for the two operating frequencies increases by about 3.0 dBi compared to that of the single-patch, dual-frequency design shown in Figure 4.13.

A design with an open-ring slot embedded in a circular patch (see Figure 4.21) has been demonstrated [13]. In this case, the two operating frequencies are associated with the fundamental resonant mode  $\text{TM}_{11}$  of the circular microstrip antenna. For this reason, the two operating frequencies are expected to have about the same excited patch surface current distribution, leading to a dual-frequency operation with the two frequencies having very similar radiation characteristics. In the geometry shown in Figure 4.21, a circular patch having a radius  $R_2$  is printed on a microwave substrate of thickness  $h$  and relative permittivity  $\epsilon_r$ . An open-ring slot of width  $W$  is embedded close to the boundary of the circular patch at a small distance 1 mm from the patch boundary. The gap spacing  $S$  between the two open ends of the open-ring slot is selected to be small (2 mm in this study). For the present design, the portion of the patch enclosed by the open-ring slot can be considered as a circular patch with a radius  $R_1$ ,

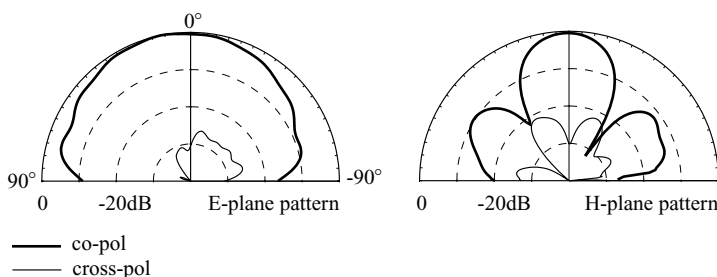


**FIGURE 4.20** Measured *E*-plane ( $x$ - $z$  plane) and *H*-plane ( $y$ - $z$  plane) radiation patterns for the dual-frequency microstrip array studied in Figure 4.18;  $f = 2.03$  GHz. (From Ref. 12, © 1999 IEE, reprinted with permission.)

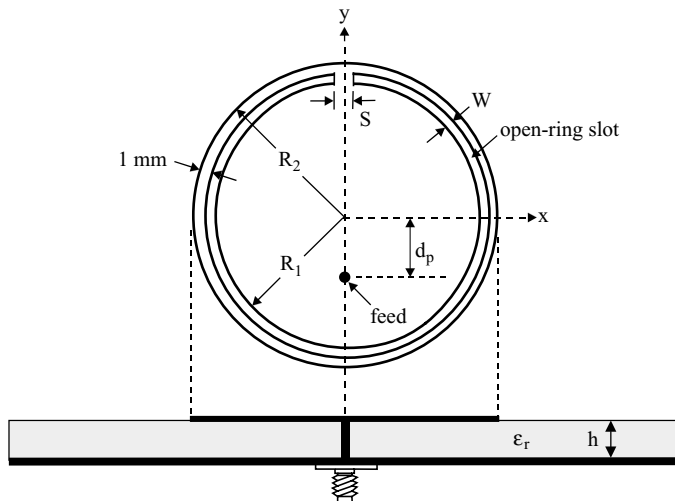


**FIGURE 4.21** Geometry of a dual-frequency circular microstrip antenna with an open-ring slot. (From Ref. 13, © 1999 John Wiley & Sons, Inc.)

and we have the relation of  $R_1 + W + 1 \text{ mm} = R_2$ . That is, in the present design, there exist two circular patches of different radii  $R_1$  and  $R_2$ . It is then expected that, with a suitably chosen feed position (see Figure 4.21, at a distance  $d_p$  from the disk center), two resonant frequencies associated with the  $\text{TM}_{11}$  mode of a circular microstrip antenna can be excited; thus, dual-frequency operation with the two frequencies having very similar radiation characteristics is possible.

The antenna described in Figure 4.21 has been experimentally studied [13]. Figure 4.22 shows measured return loss for constructed prototypes with various slot

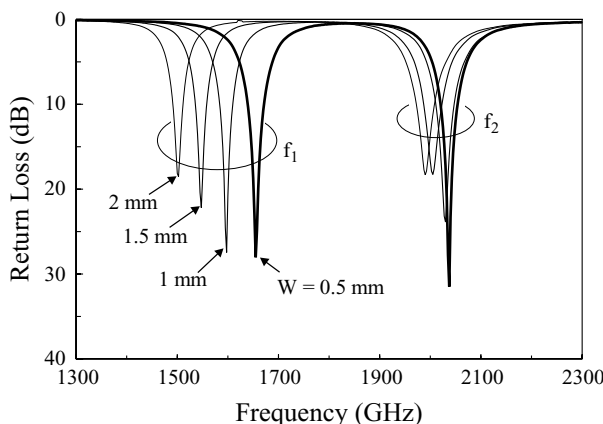


**FIGURE 4.22** Measured return loss against frequency for the antenna shown in Figure 4.21;  $\epsilon_r = 4.4$ ,  $h = 1.6 \text{ mm}$ ,  $R_1 = 21.86 \text{ mm}$ ,  $R_2 = 22.86 \text{ mm} + W$ ,  $S = 2 \text{ mm}$ , and ground-plane size =  $75 \times 75 \text{ mm}^2$ . (From Ref. 13, © 1999 John Wiley & Sons, Inc.)

**TABLE 4.6 Dual-Frequency Performance of the Antenna in Figure 4.21 [13]<sup>a</sup>**

Slot Width W (mm)	$d_p$ (mm)	$f_1$ , BW (MHz, %)	$f_2$ , BW (MHz, %)	$f_2/f_1$
0.5	11.6	1660, 2.0	2041, 1.7	1.23
1.0	11.2	1601, 1.6	2033, 1.8	1.27
1.5	11.0	1549, 1.5	2006, 1.8	1.30
2.0	11.0	1503, 1.5	1990, 1.8	1.32

<sup>a</sup>Antenna parameters are given in Figure 4.22.

widths. The corresponding dual-frequency performance is listed in Table 4.6. In this study, the radius  $R_1$  is fixed to 21.86 mm and the radius  $R_2$  ( $= 22.86 \text{ mm} + W$ ) is varied with various slot widths. It is first noted that, for a conventional unslotted circular microstrip antenna with a radius of 21.86 mm, the fundamental resonant frequency  $f_{11}$  is about 1.9 GHz. For the present design, in the vicinity of 1.9 GHz, two resonant modes instead of a single  $\text{TM}_{11}$  mode for a conventional circular microstrip antenna are excited. The lower mode has a resonant frequency  $f_1$  less than 1.9 GHz, while the higher mode has a resonant frequency  $f_2$  greater than 1.9 GHz. These two resonant modes are associated with the  $\text{TM}_{11}$  mode of a conventional circular microstrip antenna according to IE3D™ simulation results for their corresponding excited patch surface current distributions. It is seen that, with increasing slot width, the lower frequency  $f_1$  is decreased faster than the higher frequency  $f_2$ . This is because the lower frequency  $f_1$  is mainly dependent on the radius  $R_2$ , which increases as the slot width increases, and the higher frequency  $f_2$  is largely a function of  $R_1$ , which is fixed to 21.86 mm and is independent of the slot width. Thus, owing to the different effects of the open-ring slot on the lower and higher frequencies, the present design has dual-frequency operation with the tunable frequency ratio in the range of about 1.23–1.32 (see Table 4.6). Only the results for the slot width up to 2.0 mm are shown; when the slot width is greater than 2.0 mm, the single feed position for good impedance matching of the two resonant modes becomes difficult to locate in this particular case.

Measured radiation patterns at the two operating frequencies for the case with  $W = 0.5$  mm are plotted in Figure 4.23. It is observed that the operating frequencies have the same polarization planes and similar broadside radiation characteristics. Good cross-polarized radiation, below  $-20$  dB, in the  $H$  and  $E$  planes is also observed. The antenna gain for the frequencies within the two operating bandwidths has also been measured, and results indicate that the two operating frequencies have about the same antenna gain level.

#### 4.2.2 Dual-Frequency Operation with Orthogonal Polarization Planes

**4.2.2.1 Design with a Simple Rectangular Patch** In this section, we present a simple design for a single-layer, single-feed rectangular microstrip antenna to achieve dual-frequency operation with orthogonal polarization [14]. In this design, the two operating frequencies are mainly determined from the rectangular patch dimensions

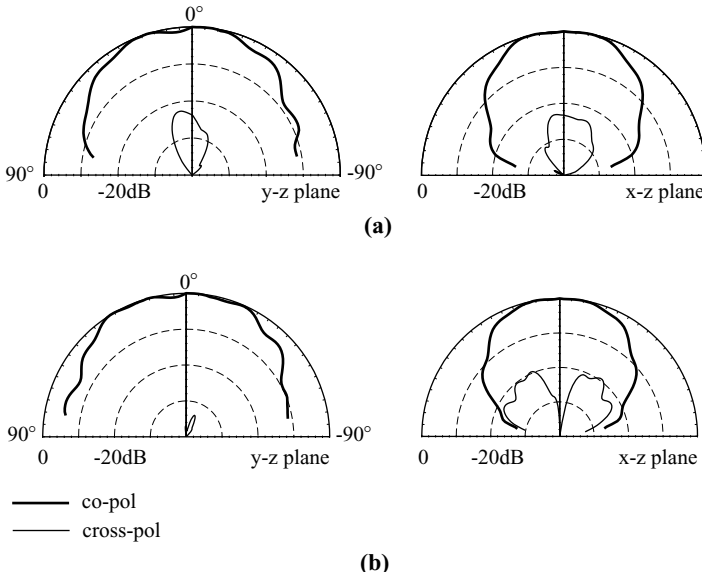


**FIGURE 4.23** Measured *E*-plane (*y*-*z* plane) and *H*-plane (*x*-*z* plane) radiation patterns for the antenna studied in Figure 4.22 with  $W = 0.5$  mm. (a)  $f_1 = 1660$  MHz, (b)  $f_2 = 2041$  MHz. (From Ref. 13, © 1999 John Wiley & Sons, Inc.)

and the substrate permittivity, and the feed position is selected such that the  $\text{TM}_{01}$  and  $\text{TM}_{10}$  modes are excited, respectively, at the first and second resonant frequencies. Figure 4.24 shows the geometry of a rectangular microstrip antenna. The rectangular patch has length  $L$  and width  $W$ . The substrate has thickness  $h$  and relative permittivity  $\varepsilon_r$ . Based on the cavity-model approximation, we can express the resonant frequencies for the  $\text{TM}_{mn}$  mode as

$$f_{mn} = \frac{c}{2\sqrt{\varepsilon_r}} \sqrt{\left(\frac{m}{L}\right)^2 + \left(\frac{n}{W}\right)^2}, \quad (4.1)$$

where  $c$  is the speed of light in air. The resonant frequencies  $f_{01}$  and  $f_{10}$  depend on  $W$  and  $L$ , respectively. By choosing the feed position (point *A*) along the *y* axis, we can excite the patch in the  $\text{TM}_{01}$  mode only. In this case, the excitation of the  $\text{TM}_{m0}$  mode,  $m = 1, 3, 5, \dots$ , is eliminated. On the other hand, when we select the feed position (point *B*) along the *x* axis, the  $\text{TM}_{10}$  mode can be excited without the excitation of the  $\text{TM}_{0n}$  mode,  $n = 1, 3, 5, \dots$ . By first adjusting so that the input impedances seen by the probe at feed positions *A* ( $0, y_A$ ) for the  $\text{TM}_{01}$  mode and *B* ( $x_B, 0$ ) for the  $\text{TM}_{10}$  mode are  $50 \Omega$ , dual-frequency operation ( $f_{01}$  and  $f_{10}$ ) can be obtained when the patch is excited at  $(x_B, y_A)$  (point *C*).

An antenna with dual-frequency operation at about 1.42 and 1.54 GHz was designed and constructed. The antenna was fabricated using a copper-clad microwave substrate of thickness 0.762 mm and relative permittivity 3.0. For operating at 1.42

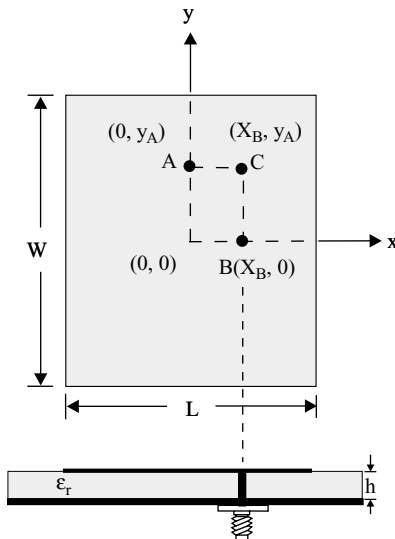


**FIGURE 4.24** Selection of the feed position for dual-frequency operation: point  $A$  at  $(0, y_A)$  for  $TM_{01}$  mode excitation only, point  $B$  at  $(x_B, 0)$  for  $TM_{10}$  mode excitation only, and point  $C$  at  $(x_B, y_A)$  for dual-frequency operation. (From Ref. 14, © 1996 John Wiley & Sons, Inc.)

and 1.54 GHz, the patch dimensions were chosen to be  $60.6 \times 55.5$  mm $^2$ . By moving the feed position along the  $x$  axis, one can find a 50- $\Omega$  input impedance at  $(9.6$  mm,  $0)$  (point  $B$ ) for the excitation of the  $TM_{10}$  mode; by selecting a feed position at  $(0, 9.5$  mm) (point  $A$ ), a 50- $\Omega$  input impedance is obtained for the  $TM_{01}$  mode. Measured return loss is shown in Figure 4.25. It is clear that only one resonant mode is excited in the frequency band of interest for both feed positions. By changing the feed position to  $(9.6$  mm,  $9.5$  mm) (point  $C$ ), two resonant modes are excited at about 1.42 and 1.54 GHz with a good matching condition (see Figure 4.26). Theoretical results calculated using a cavity-model analysis [42] are also shown in the figure, and good agreement between the theory and measurement is obtained. For the radiation pattern of the antenna at the two operating frequencies, no significant variations are to be expected because no modifications of the patch shape are made in this design.

**4.2.2.2 Design with a Notched Square Patch** By using a notched square patch, dual-frequency operations with orthogonal polarization planes have been shown [5, 15]. Figure 4.27 shows the geometries of two dual-frequency square microstrip patches with a (a) single rectangular notch and (b) double notches. For the case with a single notch, the excitation of the antenna's first two resonant frequencies using a probe feed placed along the patch's diagonal line has been achieved [5]. It has been observed that, with increasing notch depth [ $d$  in Figure 4.27(a)], a larger frequency ratio (about 1.4) between the two operating frequencies can be obtained.

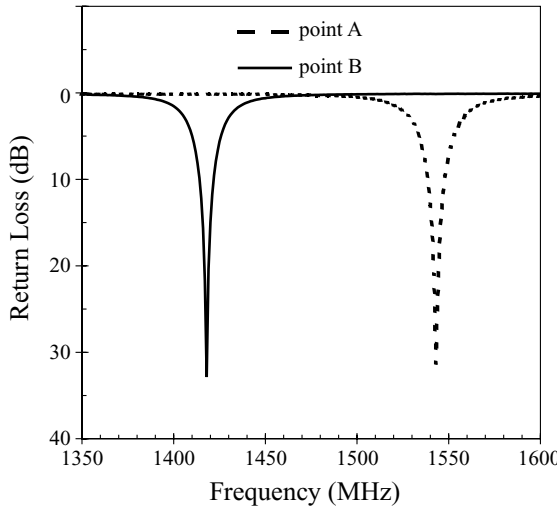


**FIGURE 4.25** Measured return loss for the feed positions at  $(0, y_A)$  (point A) and  $(x_B, 0)$  (point B);  $\epsilon_r = 3.0$ ,  $h = 0.762$  mm,  $L = 60.6$  mm,  $W = 55.5$  mm,  $y_A = 9.5$  mm, and  $x_B = 9.6$  mm. (From Ref. 14, © 1996 John Wiley & Sons, Inc.)

The polarization planes of the two frequencies are found to be perpendicular to each other. For the case with double notches, dual-frequency operation using an aperture-coupled feed with a coupling cross-slot has been achieved [15]. The antenna's first two resonant frequencies  $f_{10}$  and  $f_{01}$  have been successfully excited, and dual operating frequencies with orthogonal polarization planes have been obtained.

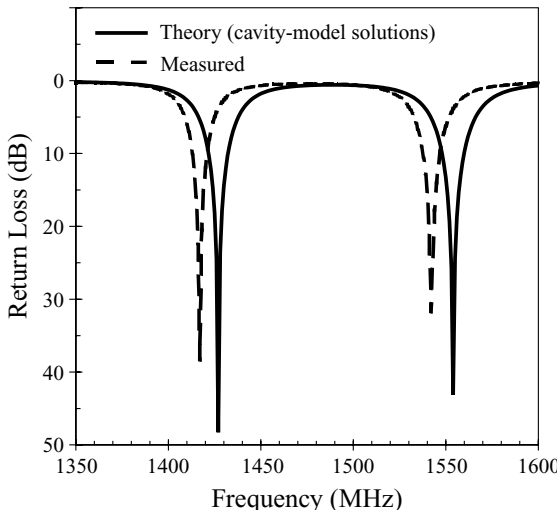


**FIGURE 4.26** Measured and calculated return loss for the feed position at  $(x_B, y_A)$  (point C); antenna parameters are the same as in Figure 4.25. (From Ref. 14, © 1996 John Wiley & Sons, Inc.)

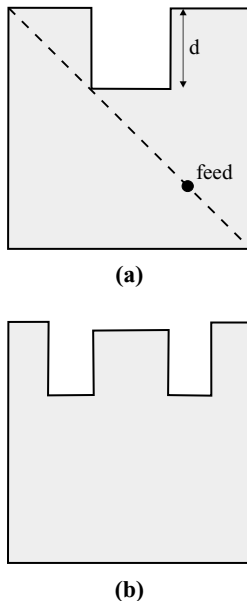


**FIGURE 4.27** Geometries of dual-frequency square microstrip patches with (a) a rectangular notch and (b) double notches.

#### 4.2.3 Dual-Frequency Feed Network Designs

Dual-frequency designs that have been reported focus mainly on the geometry of the radiating elements. Relatively very few studies on the dual-frequency feed network have been reported. This is probably because the required feed network can be relatively complicated when good impedance matching at two separate operating frequencies is required, especially for applications in dual-frequency array design. Some related studies use two individual feed networks in different layers to excite separate radiating elements [43–45]. These designs require a multilayer structure for implementing dual-frequency arrays and are very well suited for dual-frequency operation with a large frequency ratio.

In this section, a simple dual-frequency network design suitable for applications in dual-frequency microstrip arrays with dual-frequency radiating patches is presented. This dual-frequency feed network (see Figure 4.28 for the  $2 \times 2$  subarray case) is a corporate H-shaped microstrip-line network and consists of several quarter-wavelength impedance transformers and  $50\text{-}\Omega/100\text{-}\Omega$  microstrip-line segments. It is found that, by first designing the H-shape feed network to obtain impedance matching for either of the two desired operating frequencies and then selecting an optimal length of the  $50\text{-}\Omega$  microstrip-line segments ( $\overline{cf}$  and  $\overline{jk}$ ; see Figure 4.28) in the H-shaped network, good impedance matching for the other desired operating frequencies can be achieved using the same feed network; that is, with the use of a single feed network, impedance matching at two separate operating frequencies can be obtained. By further incorporating

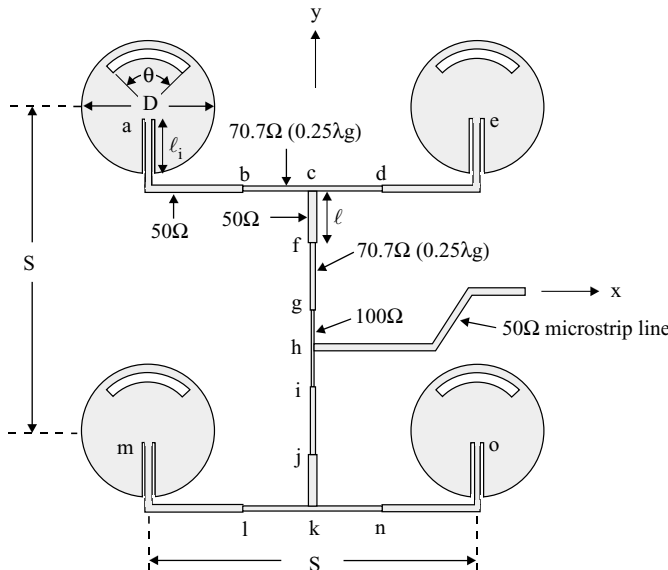


**FIGURE 4.28** Geometry of a  $2 \times 2$  dual-frequency microstrip subarray with dual-frequency feed network and slotted circular patches. The slotted circular patches have the same geometry as given in Figure 4.13.

dual-frequency radiating patches that have been reported in the literature, one can obtain dual-frequency microstrip arrays fed by using the proposed dual-frequency feed network. The proposed dual-frequency feed network has no constraints on the frequency ratio between the two desired operating frequencies if the frequency dependence of the linewidths of the microstrip-line segments in the feed network is very slight and can be ignored. However, since the two operating frequencies use the same radiating patch and good array gain can be obtained when the interelement spacing between the patches in the array is within 0.6–0.9 free-space wavelengths [41], the proposed feed network is limited to applications of feeding a dual-frequency microstrip array with a frequency ratio between its two operating frequencies less than 1.5.

Given the geometry in Figure 4.28, the radiating elements used are circular patches with an arc-shaped slot (see Section 4.2.1). The radius of the circular patch is  $D$  and the arc-shaped slot is subtended by an angle  $\theta$ . By varying the length of the arc-shaped slot in the circular patch, dual-frequency operation with a tunable frequency ratio of about 1.29–1.43 between the two frequencies can be obtained. The spacings between the slotted circular patches in both  $x$  and  $y$  directions are denoted  $S$ , and all the patches are uniformly excited. The slotted circular patches can be excited with good impedance matching at two desired frequencies using  $50\Omega$  inset-microstrip lines with an inset length  $\ell_i$ . The problem is that, at the array's feed position (point  $h$  in the figure), the subarray should also be excited with good impedance matching at

the two desired frequencies. This can be accomplished by the present dual-frequency feed network, which is a corporate H-shaped microstrip-line network consisting of 70.7- $\Omega$  microstrip-line sections as quarter-wavelength impedance transformers and 50- $\Omega$ /100- $\Omega$  microstrip-line segments.

For the design of the dual-frequency feed network, we first consider the lower operating frequency  $f_1$  of the desired dual-frequency operation. The impedance transformer segments  $\overline{bc}$ ,  $\overline{cd}$ ,  $\overline{kl}$ , and  $\overline{kn}$  are designed to transform the 50- $\Omega$  microstrip-line segments of  $\overline{ab}$ ,  $\overline{de}$ ,  $\overline{lm}$ , and  $\overline{no}$  into 100  $\Omega$  at the frequency  $f_1$ . In this case, the impedance looking into the patches at points  $c$  and  $k$  is 50  $\Omega$ . By again designing additional 70.7- $\Omega$  impedance transformer segments  $\overline{fg}$  and  $\overline{ij}$ , the impedance looking into the patches at point  $h$  will be 50  $\Omega$ , and good impedance matching for the subarray studied can be obtained at the frequency  $f_1$ . Then it is found that the impedance looking into patches at point  $h$  at the higher frequency  $f_2$  is a strong function of the length  $\ell$  of the 50- $\Omega$  microstrip-line segments  $\overline{cf}$  and  $\overline{jk}$  in the H-shaped network. We use the expressions (considering all microstrip-line segments to be lossless)

$$Z_{in} = \frac{1}{2} \times (100 \Omega) \times \frac{Z_g + j(100 \Omega) \tan \beta_{gh} \ell_{gh}}{(100 \Omega) + j Z_g \tan \beta_{gh} \ell_{gh}}, \quad (4.2)$$

with

$$Z_g = (70.7 \Omega) \times \frac{Z_f + j(70.7 \Omega) \tan \beta_{fg} \ell_{fg}}{(70.7 \Omega) + j Z_f \tan \beta_{fg} \ell_{fg}}, \quad (4.3)$$

$$Z_f = (50 \Omega) \times \frac{Z_c + j(50 \Omega) \tan \beta_{cf} \ell_{cf}}{(50 \Omega) + j Z_c \tan \beta_{cf} \ell_{cf}}, \quad (4.4)$$

$$Z_c = \frac{1}{2} \times (70.7 \Omega) \times \frac{Z_b + j(70.7 \Omega) \tan \beta_{bc} \ell_{bc}}{(70.7 \Omega) + j Z_b \tan \beta_{bc} \ell_{bc}}, \quad (4.5)$$

to calculate the impedance seen at point  $h$ . In the above expressions,  $Z_{in}$ ,  $Z_g$ ,  $Z_f$ ,  $Z_c$ , and  $Z_b$  are, respectively, the impedance looking into patches at points  $h$ ,  $g$ ,  $f$ ,  $c$ , and  $b$ . The parameters  $\ell_{gh}$  and  $\beta_{gh}$  are, respectively, the length and propagation constant of the microstrip-line segment  $\overline{gh}$ ;  $\ell_{fg}$ ,  $\ell_{cf}$  ( $= \ell$ ),  $\ell_{bc}$ ,  $\beta_{fg}$ ,  $\beta_{cf}$ , and  $\beta_{bc}$  have similar meanings. Then, by ignoring the inductance of the probe feed in the substrate layer, one can calculate the return loss (RL) seen by the 50- $\Omega$  probe from

$$RL = -20 \log \left| \frac{Z_{in} - 50 \Omega}{Z_{in} + 50 \Omega} \right| \quad (\text{dB}). \quad (4.6)$$

From the results calculated from (4.6), it is found that an optimal return loss, usually larger than 20 dB, for the frequency  $f_2$  can be obtained using an optimal length  $\ell$ . At the same time the return loss seen at point  $h$  for the frequency  $f_1$  is not affected by varying the length  $\ell$ . Thus, by following the design procedure described above (denoted design

**TABLE 4.7 Dual-Frequency Performance of the  $2 \times 2$  Subarray in Figure 4.28<sup>a</sup>**

$\theta$ (deg)	$S$ (mm)	$\ell$ (mm)	$f_1$ , BW (MHz, %)	$f_2$ , BW (MHz, %)	$f_2/f_1$
88	122	8.0	1582, 1.8	2223, 2.0	1.405
92	123	28.0	1585, 2.1	2190, 2.3	1.382
100	134	30.6	1567, 1.9	2010, 2.3	1.283

<sup>a</sup>Substrate thickness 1.6 mm and relative permittivity 4.4 [16];  $D = 50$  mm,  $\ell_i = 37$  mm.

procedure 1), the present feed network can have good impedance matching for both frequencies  $f_1$  and  $f_2$ ; that is, a dual-frequency feed network is obtained.

We can also consider the higher frequency  $f_2$  of the desired dual-frequency operation and design the impedance transformer for the frequency  $f_2$ . Then, by applying (4.2)–(4.6) to obtain an optimal length  $\ell$  of the  $50\text{-}\Omega$  microstrip-line segments  $cf$  and  $jk$  for the frequency  $f_1$ , we can also obtain a dual-frequency feed network for both  $f_1$  and  $f_2$ . This design procedure is denoted design procedure 2; the obtained parameters for the proposed dual-frequency feed network using design procedures 1 and 2 are different. However, both solutions are good for implementing a dual-frequency feed network.

Based on the above theoretical analysis, the dual-frequency microstrip array shown in Figure 4.28 has been studied experimentally. The measured results for the design using design procedure 1 are shown in Table 4.7. Cases using dual-frequency circular patches (geometry given in Figure 4.13) with  $D = 50$  mm and  $\theta = 88^\circ$ ,  $92^\circ$ , and  $100^\circ$  were studied. Good dual-frequency performance is obtained, and the optimal length  $\ell$  in the dual-frequency feed network is 8 mm for  $\theta = 88^\circ$ , 28 mm for  $\theta = 92^\circ$ , and 30.6 mm for  $\theta = 100^\circ$ . By using the  $2 \times 2$  dual-frequency subarray shown in Figure 4.28 as a basic building block, larger dual-frequency arrays can easily be implemented.

### 4.3 COMPACT DUAL-FREQUENCY OPERATION WITH SAME POLARIZATION PLANES

Some novel dual-frequency designs of compact microstrip antennas are presented in this section. In these designs, the two operating frequencies have the same polarization planes. In Section 4.3.1, the technique of embedding a pair of narrow slots to a meandered rectangular patch [17] and a bow-tie patch [18] is described. Results show that with increasing slit length in the rectangular patch or flare angle of the bow-tie patch, the antenna's first two resonant frequencies are both quickly lowered. This behavior suggests that an antenna size reduction can be achieved for this kind of antenna in fixed dual-frequency operation. Recently, it has been demonstrated that compact dual-frequency operation for short-circuited microstrip antennas can be achieved. Experimental results for designs with a rectangular patch [19], a circular

patch [20], a triangular patch [21], and a bow-tie patch [22] are discussed in Section 4.3.2. Finally, in Section 4.3.3, some novel dual-frequency designs applicable to triangular microstrip antennas [23–26] are shown. Triangular microstrip antennas are a good substitute for regular rectangular microstrip antenna due to their similar radiation properties and smaller patch dimensions.

#### 4.3.1 Design with a Pair of Narrow Slots

**4.3.1.1 With a Meandered Rectangular Patch** Figure 4.29 shows the geometry of a dual-frequency meandered rectangular microstrip antenna loaded with a pair of narrow slots close to the patch's radiating edges. In this design, the radiation characteristics of the antenna operated in the  $\text{TM}_{01}$  and  $\text{TM}_{30}$  modes are similar and have the same polarization planes. These two modes can be excited with good impedance matching using a single probe feed, and owing to the meandering of the rectangular patch with slits inserted at the patch's nonradiating edges, the resonant frequencies  $f_{10}$  and  $f_{30}$  of the two operating modes can be significantly lowered, with the radiation characteristics only slightly affected. This indicates that a large antenna size reduction can be obtained by using the present design compared to the slot-loaded patch without slits for fixed dual-frequency operation. Prototypes of the present design have been constructed and measured [17]. The obtained dual-frequency performance is given in Table 4.8, in which the impedance bandwidth is determined from the 10-dB return loss, and  $d_p$  is the distance between the optimal feed position and the patch center. It can be seen that the optimal feed point is within a variation of 2 mm and thus is not sensitive to the slit length. However,

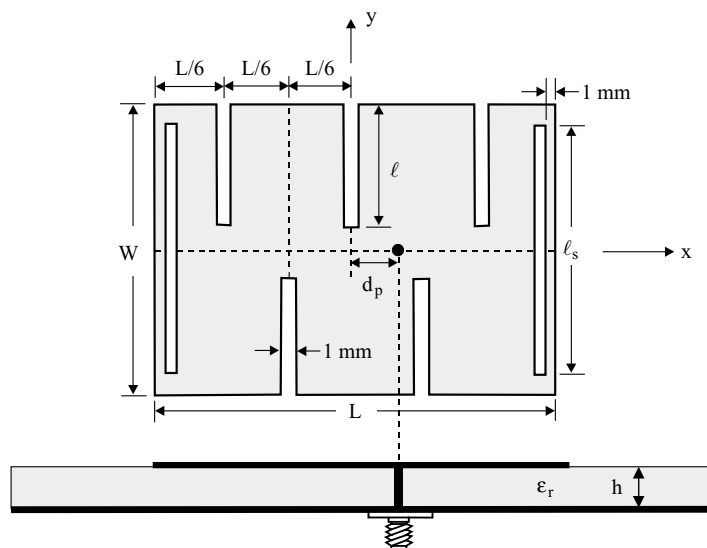


**FIGURE 4.29** Geometry of a slot-loaded, meandered rectangular microstrip antenna with compact dual-frequency operation. (From Ref. 17, © 1998 IEE, reprinted with permission.)

**TABLE 4.8 Dual-Frequency Performance of the Antenna in Figure 4.29 [17]<sup>a</sup>**

Slit Length $\ell$ (mm)	$d_p$ (mm)	$f_1$ , BW (MHz, %)	$f_2$ , BW (MHz, %)	$f_2/f_1$
0	6.7	1915, 1.8	3620, 1.2	1.89
4	6.3	1811, 1.6	3620, 1.2	2.00
6	5.9	1698, 1.5	3531, 1.1	2.08
8	5.0	1553, 1.5	3318, 1.1	2.14
10	5.0	1389, 1.4	3062, 1.1	2.21
12	5.0	1196, 1.3	2730, 1.2	2.28
13	5.0	1096, 1.5	2590, 1.2	2.36

<sup>a</sup> $\epsilon_r = 4.4$ ,  $h = 1.6$  mm,  $L = 36$  mm,  $W = 24$  mm, and  $\ell_s = 22$  mm.

when the slit length is greater than 13 mm (about 0.54W) in this design, the feed point for exciting the two frequencies with good matching conditions becomes difficult to locate. This suggests that there exists a limit for the present dual-frequency design using a single probe feed. Radiation patterns at two operating frequencies were also measured, and results indicate that the two operating frequencies have the same polarization planes and similar broadside radiation characteristics.

**4.3.1.2 With a Bow-Tie Patch** Based on its compact antenna size for a fixed operating frequency and its similar radiation characteristics to those of a regular rectangular microstrip antenna, the bow-tie microstrip antenna has been proposed and studied [18]. In this section, a dual-frequency design of bow-tie microstrip antennas in which a pair of narrow slots is embedded close to the radiating edges of the bow-tie patch is presented. Figure 4.30 shows the geometry. The bow-tie patch has a flare angle  $\alpha$  and a patch width  $W$ . The linear dimension of the bow-tie patch in the resonant

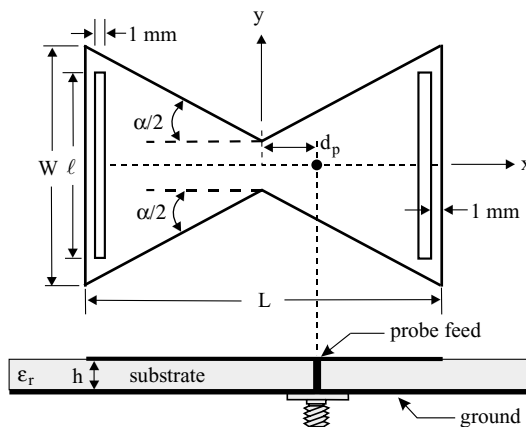


**FIGURE 4.30** Geometry of a dual-frequency bow-tie microstrip antenna with a pair of narrow slots. (From Ref. 18, © 1998 IEE, reprinted with permission.)

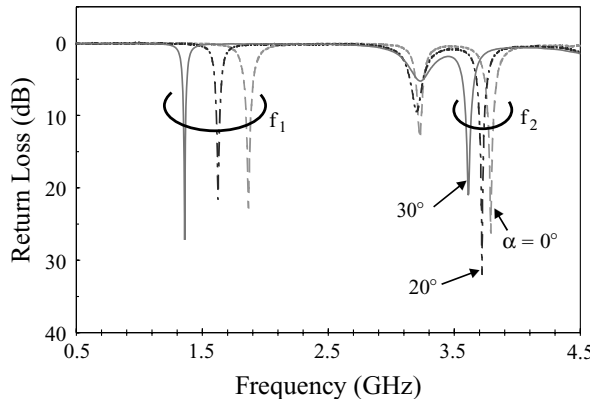


**FIGURE 4.31** Measured return loss for the antenna shown in Figure 4.30;  $\epsilon_r = 4.4$ ,  $h = 1.6$  mm,  $L = 37.5$  mm,  $W = 25.2$  mm,  $\ell = 20.7$  mm, and  $d_p = 2.7$  mm. (From Ref. 18, © 1998 IEE, reprinted with permission.)

direction is fixed to be  $L$ . A pair of narrow slots having dimensions  $1\text{ mm} \times \ell$  are embedded in the bow-tie patch and placed close to the radiating edges at a distance of 1 mm. A single probe feed is located along the centerline of the bow-tie patch at a distance of  $d_p$  from the patch center. It is found that both the  $\text{TM}_{10}$  and  $\text{TM}_{30}$  modes are strongly perturbed, with their respective resonant frequencies decreased with increasing flare angle of the bow-tie patch. In addition, there exists a feed position for good impedance matching of the two operating frequencies.

Many prototypes of the proposed antenna with various flare angles have been constructed and investigated. Figure 4.31 shows measured return loss for the cases with  $\alpha = 0^\circ$ ,  $20^\circ$ , and  $30^\circ$ . The perturbed  $\text{TM}_{10}$  and  $\text{TM}_{30}$  modes are excited with good impedance matching, and the small dips between these two modes are the  $\text{TM}_{20}$  mode. Measured resonant frequencies  $f_1 (= f_{10})$  and  $f_2 (= f_{30})$  and the frequency ratio  $f_2/f_1$  are listed in Table 4.9. It is seen that  $f_1$  is more sensitive to the flare-angle variation than is  $f_2$ ; the obtained frequency ratio for the present design varies in the

**TABLE 4.9 Dual-Frequency Performance of the Antenna in Figure 4.30 [18]<sup>a</sup>**

Flare Angle $\alpha$ (deg)	$d_p$ (mm)	$f_1$ , BW (MHz, %)	$f_2$ , BW (MHz, %)	$f_2/f_1$
0	7.3	1865, 2.1	3785, 1.2	2.02
5	6.3	1825, 1.7	3770, 1.2	2.07
10	6.1	1775, 1.8	3765, 1.2	2.12
15	5.8	1700, 1.8	3730, 1.2	2.19
20	4.8	1625, 1.6	3720, 1.1	2.29
30	3.0	1360, 1.3	3615, 1.2	2.66
35	2.7	1215, 1.2	3560, 1.1	2.93

<sup>a</sup>Antenna parameters are given in Figure 4.31.

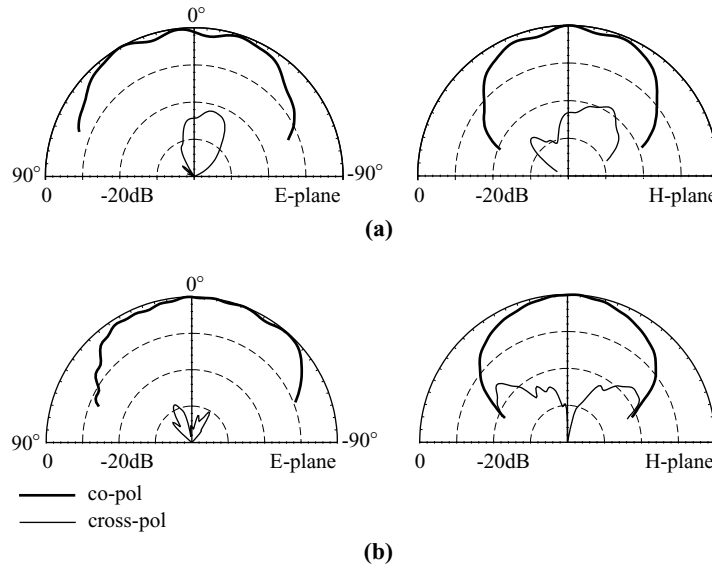


**FIGURE 4.32** Measured  $E$ -plane ( $x-z$  plane) and  $H$ -plane ( $y-z$  plane) radiation patterns for the antenna studied in Figure 4.31 with  $\alpha = 30^\circ$ . (a)  $f = 1360$  MHz, (b)  $f = 3615$  MHz. (From Ref. 18, © 1998 IEE, reprinted with permission.)

range 2.0–3.0 and increases monotonically with increasing flare angle. The radiation patterns were also measured. Figure 4.32 plots the typical patterns at the two operating frequencies for the case with  $\alpha = 30^\circ$ . It is seen that the two operating frequencies have the same polarization planes, and good cross-polarization radiation is observed, especially for the  $E$ -plane radiation.

#### 4.3.2 Design with a Shorted Microstrip Antenna

**4.3.2.1 With a Rectangular Patch** By incorporating a shorting pin in the centerline of a rectangular microstrip patch and exciting the patch through a suitable feed position chosen from the centerline, a good matching condition for the first two resonant frequencies of the microstrip antenna can be obtained, which makes possible the dual-frequency operation of such a compact microstrip antenna through a single coax feed. To demonstrate the results, an experimental study of the single-feed dual-frequency compact microstrip antenna has been presented [19]. Figure 4.33 shows the antenna geometry. The rectangular patch, printed on a substrate of thickness  $h$  and relative permittivity  $\epsilon_r$ , has a length  $L$  and a width  $W$ . When the shorting pin is absent, the rectangular patch antenna is usually operated as a half-wavelength antenna. When there is a shorting pin placed at  $x = -L/2$ ,  $y = 0$  (center of the patch edge) and the feed position is chosen from the centerline, a condition for eliminating the excitation of the  $TM_{0m}$  mode,  $m = 1, 3, 5, \dots$ , the first two resonant frequencies of the rectangular patch are dominated by the patch length (i.e., with the same polarization plane, the  $x-z$

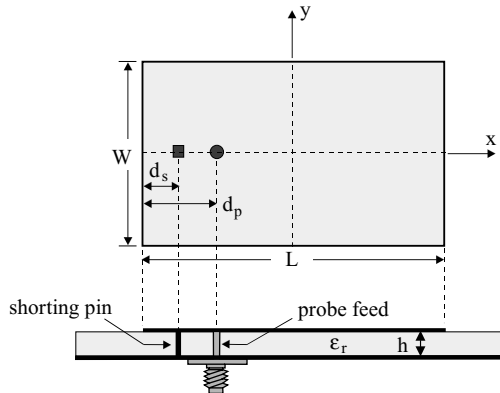


**FIGURE 4.33** Geometry of a shorted rectangular microstrip antenna for compact dual-frequency operation. (From Ref. 19, © 1997 IEE, reprinted with permission.)

plane) and can be approximately expressed as  $p_1 \times 0.5f_{10}$  and  $p_2 \times 1.5f_{10}$ , where  $p_1$  and  $p_2$  are constants of about 0.7–0.9, depending on the microstrip patch parameters.

Typical measured results can be seen in Figure 4.34, where the resonant frequencies are shown as a function of the shorting-pin position. The fundamental resonant frequency of the conventional patch (without a shorting pin) is designed at 1.9 GHz ( $f_{10}$ ). It can be seen that, when the shorting pin is placed almost at the patch edge ( $d_s = 1$  mm in this case), the first resonant frequency  $f_1$  occurs at about 722 MHz ( $p_1 \approx 0.76$ ) and the second resonant frequency ( $f_2$ ) is about 2310 MHz ( $p_2 \approx 0.81$ ). In this case, the frequency ratio  $f_2/f_1$  is about 3.2. However, when the shorting pin moves toward the patch center,  $f_1$  increases and  $f_2$  decreases, which decreases the

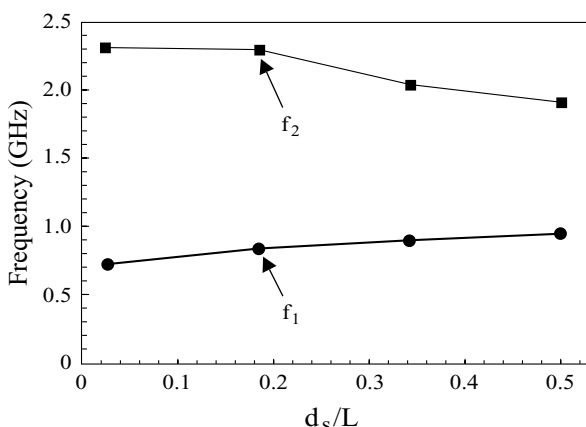


**FIGURE 4.34** Dependence of the first two resonant frequencies on the shorting-pin position for the antenna shown in Figure 4.33;  $\epsilon_r = 4.4$ ,  $h = 1.6$  mm,  $L = 37.3$  mm,  $W = 24.87$  mm,  $r_s = 0.32$  mm, and  $r_p = 0.63$  mm. (From Ref. 19, © 1997 IEE, reprinted with permission.)

frequency ratio. At  $d_s/L = 0.5$  (the patch center), the frequency ratio is 2.0, with  $f_1$  and  $f_2$  about 950 and 1900 MHz, respectively. The results suggest that the frequency ratio of the present antenna is tunable from 2.0 to about 3.2. It should also be noted that, in the case of shorting the patch at the center ( $x = 0$ ,  $y = 0$ ), the resonant frequency of the  $\text{TM}_{10}$  mode is not affected ( $f_2 = f_{10}$ ) and a new resonant frequency at  $0.5f_{10}$  ( $= f_1$ ) occurs. In this case, the modified microstrip patch can be operated as either a half-wavelength or a quarter-wavelength antenna.

From many experiments, it is found that there exists a feed position at the centerline for the shorting-pin-loaded microstrip antenna to operate at two resonant frequencies with a good matching condition. This optimal feed position is usually close to the shorting-pin position within about 1 mm to several millimeters. Based on this characteristic, one can easily design a dual-frequency operation with a tunable frequency ratio between 2.0 and 3.2. With proper selection of the microstrip patch parameters and the shorting-pin position,  $f_1$  and  $f_2$  can be controlled. Then, a feed position is selected near the shorting pin to obtain a good matching condition for operation at  $f_1$  and  $f_2$ . Figure 4.35 shows a typical result of dual-frequency operation. The shorting pin is placed near the patch edge ( $d_s = 1$  mm), and in this case, two resonant frequencies at about 722 and 2310 MHz are excited with a good matching condition. The ratio of these two frequencies is about 3.2. The impedance bandwidths determined from the 10-dB return loss are about 1.4% for the 722-MHz band and 1.8% for the 2310-MHz band. By comparing with the results (about 1.9% and 2.4% for the first two resonant frequencies) for a conventional rectangular microstrip antenna using the same substrate material, it can be seen that the impedance bandwidth of the present compact dual-frequency microstrip antenna is reduced. From the results shown in Section 2.2, the radiation patterns of the present compact antenna at the fundamental resonant frequency remain broadside radiation. However, the cross-polarization radiation, owing to the presence of the shorting pin, increases. Figure 4.36 shows the measured results for operation at the second resonant frequency (2310 MHz). Broadside radiation is

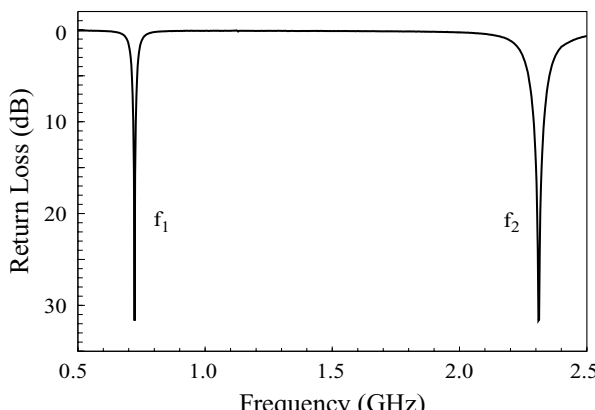


**FIGURE 4.35** Measured return loss against frequency for the antenna studied in Figure 4.34 with  $d_s = 1$  mm and  $d_p = 2.72$  mm. (From Ref. 19, © 1997 IEE, reprinted with permission.)

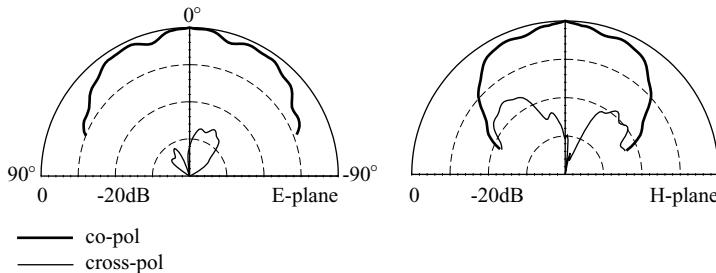


**FIGURE 4.36** Measured *E*-plane ( $x$ - $z$  plane) and *H*-plane ( $y$ - $z$  plane) radiation patterns at 2310 MHz for the antenna studied in Figure 4.34 with  $d_s = 1$  mm and  $d_p = 2.72$  mm. (From Ref. 19, © 1997 IEE, reprinted with permission.)

also observed, and the cross-polarization radiation is greater in the *H* plane than in the *E* plane.

**4.3.2.2 With a Circular Patch** By applying the shorting-pin loading technique to a circular microstrip antenna, dual-frequency operation has been obtained [20]. In addition to a much reduced antenna size, it is reported that a tunable frequency ratio of about 2.55–3.83 for the two operating frequencies can be obtained. This frequency-ratio range is different from that of the shorted rectangular microstrip antenna. This is largely because, when loaded with a shorting pin, the resonance behavior of the microstrip antenna against the shorting-pin position will not be the same for different patch shapes.

Figure 4.37 shows the geometry of a shorted circular microstrip antenna for dual-frequency operation. For comparison with the dual-frequency compact rectangular microstrip antenna studied in Section 4.3.2.1, the same substrate material ( $\epsilon_r = 4.4$ ,

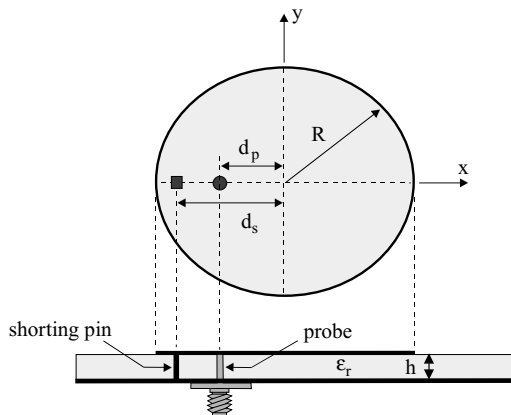


**FIGURE 4.37** Geometry of a shorted circular microstrip antenna for compact dual-frequency operation. (From Ref. 20, © 1997 IEE, reprinted with permission.)

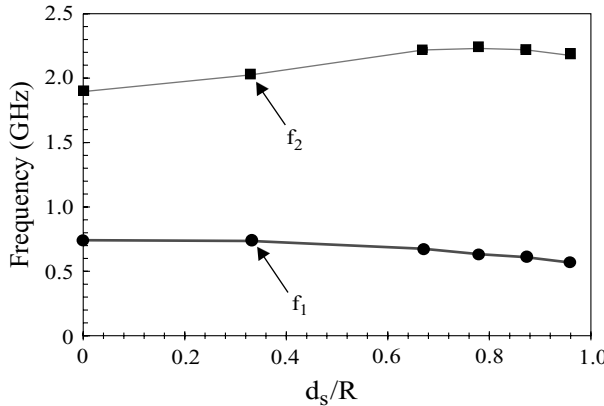


**FIGURE 4.38** Dependence of the resonant frequencies on the shorting-pin position for the antenna shown in Figure 4.37;  $\epsilon_r = 4.4$ ,  $h = 1.6$  mm,  $R = 21.86$  cm, and  $r_s = 0.32$  mm. (From Ref. 20, © 1997 IEE, reprinted with permission.)

$h = 1.6$  mm) is used and the resonant frequency of the conventional disk (without a shorting pin) at the fundamental mode ( $\text{TM}_{11}$  mode) is designed as 1.9 GHz, which requires a disk radius of 21.86 mm. By placing a shorting pin of radius  $r_s = 0.32$  mm along the disk radius from the patch center to any point at the patch edge, it is observed that the fundamental resonant frequency of the circular patch is strongly dependent on the shorting-pin position and decreases monotonically when the shorting pin is moved close to the patch edge. The results are presented in Figure 4.38. With the shorting pin placed at about the edge, the circular patch has a lowest resonant frequency of about 568 MHz, which is smaller than the result for the corresponding case (722 MHz) of a shorted rectangular patch. This is probably because, in the edge-shorting case, both the rectangular and circular microstrip patches act as nearly quarter-wavelength antennas and the circular patch has a larger linear dimension ( $2R = 43.72$  mm) than that (37.3 mm) of the rectangular one. For this reason, the second resonant frequency of the circular patch is smaller than that of the rectangular patch, and in this case both patches can roughly be treated as three-quarter-wavelength antennas. The second resonant frequency in general decreases when the shorting pin is moved from the patch edge to the patch center, except near the patch edge, where there is a slightly resonant peak value. From these two resonant frequencies, it suggests that the tunable frequency ratio of the dual-frequency operation of a shorted circular patch is about 2.55–3.83. This range is different from that (2.0–3.2) of a shorted rectangular patch and has a higher tunable frequency ratio. Radiation patterns at the two operating frequencies have been measured. The two frequencies are observed to have the same polarization planes and similar broadside radiation characteristics. However, the cross-polarization radiation is much higher in the  $H$  plane than in the  $E$  plane.

**4.3.2.3 With a Triangular Patch** A shorted triangular microstrip antenna with dual-frequency operation has been studied [21]. This design provides a large frequency

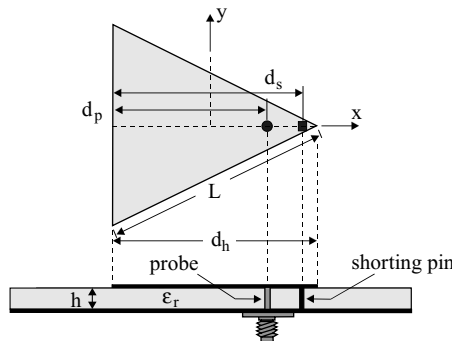


**FIGURE 4.39** Geometry of a shorted triangular microstrip antenna for compact dual-frequency operation. (From Ref. 21, © 1997 IEEE, reprinted with permission.)

ratio of about 2.5–4.9 for the two operating frequencies. The antenna geometry is shown in Figure 4.39. The triangular patch was designed to resonate at 1.9 GHz, which gives a side length of 50 mm. A shorting pin of radius  $r_s$  ( $= 0.32$  mm) and a probe feed of radius  $r_p$  ( $= 0.63$  mm) are placed along the line segment between the triangle tip and the bottom side of the patch, as shown in Figure 4.39. By varying the shorting-pin position  $d_s$ , a strong dependence of the first two resonant frequencies on  $d_s$  is observed. The results are shown in Figure 4.40. It can be seen that, at  $d_s/d_h = 0.33$  (the null-voltage point for the  $\text{TM}_{10}$  mode), the first resonant frequency  $f_1$  has a maximum value and the second resonant frequency  $f_2$  has a minimum value. In this case, the frequency ratio  $f_2/f_1$  has a minimum value of about 2.5. Away from this point, the frequency ratio increases. At the triangle tip, there is a maximum frequency ratio of about 4.9. The results suggest that, by properly selecting the shorting-pin

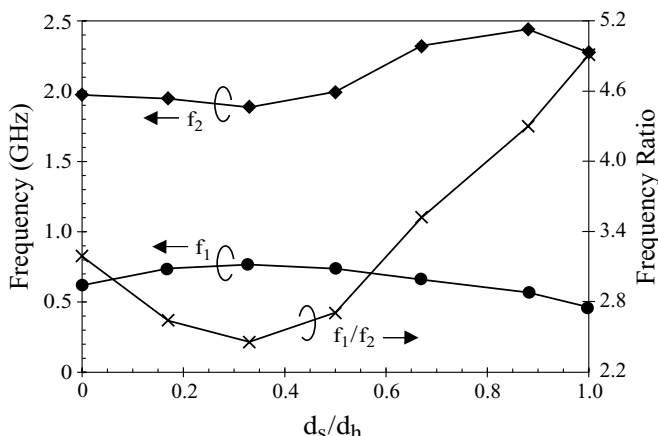


**FIGURE 4.40** The first two resonant frequencies against shorting-pin position for the antenna shown in Figure 4.39;  $\epsilon_r = 4.4$ ,  $h = 1.6$  mm,  $L = 50$  mm, and  $r_s = 0.32$  mm. (From Ref. 21, © 1997 IEEE, reprinted with permission.)

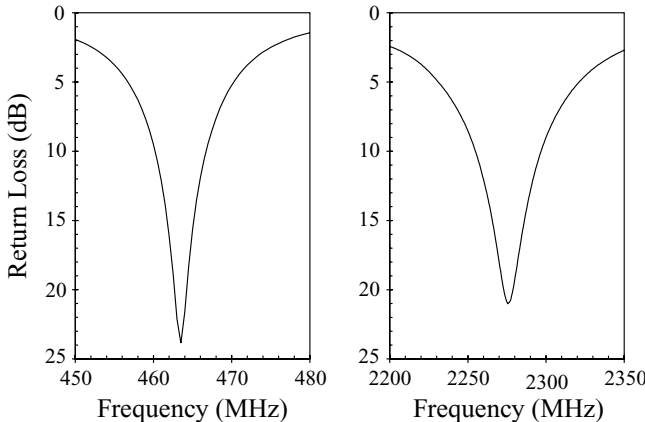


**FIGURE 4.41** Measured return loss for the antenna studied in Figure 4.40. (From Ref. 21, © 1997 IEEE, reprinted with permission.)

position, dual-frequency operation with a frequency ratio in the range 2.5–4.9 can be achieved.

Another important factor to be considered is the impedance matching of both operating frequencies. The optimal feed position for impedance matching is usually close to the shorting-pin position, within several millimeters. For the case of  $d_s/d_h = 1.0$ , the optimal feed position is about 2.5 mm from the shorting pin. (This distance between the feed position and shorting pin also approximately holds for other values of  $d_s/d_h$ ; i.e., the two other operating frequencies. By slightly adjusting this distance, a good matching condition for the two operating frequencies for a specific value of  $d_s/d_h$  can be obtained.) Figure 4.41 shows the measured return loss for this case. Two frequencies at 464 and 2276 MHz are excited. The impedance bandwidths are about 1.4% and 1.8% for the 464- and 2276-MHz bands, respectively. It should also be noted that these two operating bands have the same polarization plane and similar radiation characteristics as described for shorted rectangular and circular microstrip antennas in Sections 4.3.2.1 and 4.3.2.2.

**4.3.2.4 With a Bow-Tie Patch** The case of a shorted bow-tie microstrip antenna for compact dual-frequency operation has been studied [22]. In this design (see Figure 4.42), with proper selection of the feed position along the patch's centerline, the antenna's first two resonant frequencies are found to have the same polarization planes and can both be excited with good impedance matching. By varying the patch's aspect ratio ( $L/W$  in the figure) or the flare angle  $\alpha$ , it is possible to obtain a frequency ratio of about 5.0.

### 4.3.3 Design with a Triangular Microstrip Antenna

**4.3.3.1 With a Pair of Narrow Slots** Dual-frequency operation can be obtained by embedding a pair of narrow slots in a triangular microstrip antenna [23]. The

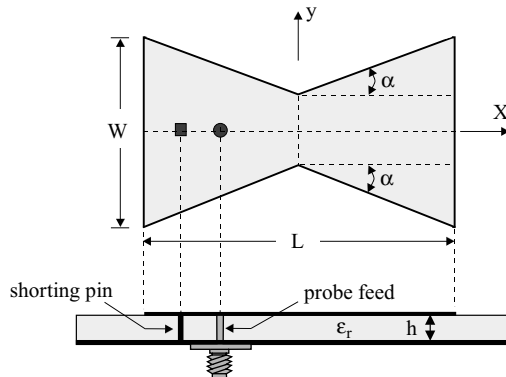


**FIGURE 4.42** Geometry of a short-circuited bow-tie microstrip antenna for compact dual-frequency operation.

antenna geometry is shown in Figure 4.43. The triangular patch is equilateral and has a side length  $L$ . Two narrow slots of length  $\ell$  and width 1 mm are placed symmetrically with respect to the centerline ( $x$  axis) of the triangular patch. The two slots are also a distance 1 mm from the bottom edge of the triangular patch and have a spacing  $S$ . With the present design, the first two broadside-radiation modes,  $\text{TM}_{10}$  and  $\text{TM}_{20}$ , of the triangular microstrip antenna are perturbed and their corresponding patch surface current paths are both lengthened. However, since the two slots are placed parallel to

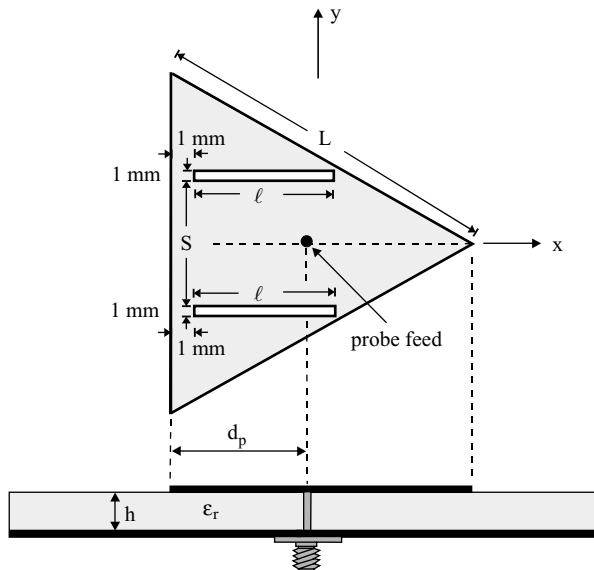


**FIGURE 4.43** Geometry of a dual-frequency equilateral-triangular microstrip antenna with a pair of narrow slots. (From Ref. 23, © 1999 John Wiley & Sons, Inc.)

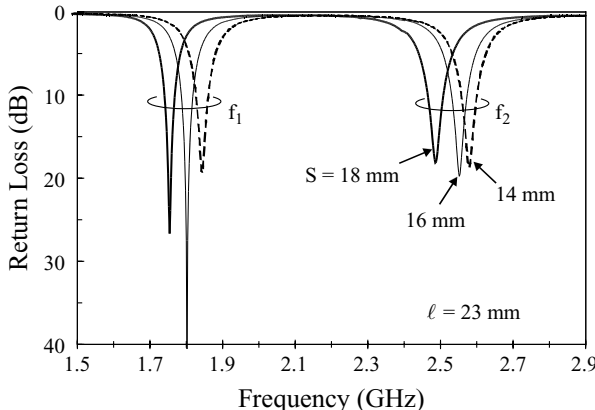


**FIGURE 4.44** Measured return loss for various spacings between two embedded slots for the antenna shown in Figure 4.43;  $\epsilon_r = 4.4$ ,  $h = 1.6$  mm,  $L = 50$  mm, and ground-plane size =  $75 \times 75$  mm $^2$ . (From Ref. 23, © 1999 John Wiley & Sons, Inc.)

the centerline of the patch, the perturbation effects on the  $\text{TM}_{10}$  mode are relatively much smaller than those on the  $\text{TM}_{20}$  mode, which leads to a slight lowering in the resonant frequency  $f_{10}$  of the  $\text{TM}_{10}$  mode and a significant lowering in the resonant frequency  $f_{20}$  of the  $\text{TM}_{20}$  mode. This behavior makes possible a lower frequency ratio for the present dual-frequency design.

The present antenna with various parameters of the two slots has been implemented and studied. Figure 4.44 shows the measured return loss for various spacings between the two slots. In this case, the side length of the patch is selected to be 50 mm, and the length  $\ell$  of the two slots is fixed to be 23 mm. Note that, from the excited patch surface current densities obtained from IE3D<sup>TM</sup> simulation, the first two resonant modes are identified as associated with the  $\text{TM}_{10}$  and  $\text{TM}_{20}$  modes of the simple triangular microstrip antenna without slots; that is, the two operating modes in the present design can be treated as perturbed  $\text{TM}_{10}$  and  $\text{TM}_{20}$  modes. The resonant frequencies of these two modes are here denoted  $f_1$  and  $f_2$ . The corresponding dual-frequency performance of the antenna is given in Table 4.10. It is seen that  $f_1$  is slightly lowered than  $f_{10}$  (about 1870 MHz) of the simple triangular microstrip antenna. Conversely,  $f_2$  is significantly decreased compared to  $f_{20}$  (about 3730 MHz) of the simple triangular microstrip antenna. This behavior agrees with the prediction mentioned earlier, and a low frequency ratio  $f_2/f_1$  of about 1.4 is obtained for the case shown in Figure 4.44.

Figure 4.45 shows the measured return loss for various slot lengths with a fixed spacing between the two slots ( $S = 18$  mm). The corresponding results are listed in Table 4.10. In this case, the frequency ratio is varied from about 1.4 to 1.45, and this implies that the frequency ratio is more sensitive to the variation in the spacing between the two slots than to the variation in the slot length. In addition to the cases studied in Figures 4.44 and 4.45, other cases with different slot lengths and spacings have also been constructed and measured. The results are shown in Table 4.10. In general, by controlling the length of the slots and the spacing between the two slots, the

**TABLE 4.10 Dual-Frequency Performance of the Antenna in Figure 4.43 [23]<sup>a</sup>**

$\ell$ (mm)	$S$ (mm)	$d_p$ (mm)	$f_1$ , BW (MHz, %)	$f_2$ , BW (MHz, %)	$f_2/f_1$
17	22	20.4	1838, 1.4	2743, 1.3	1.492
19	18	19.6	1836, 1.5	2674, 1.3	1.456
21	18	18.7	1800, 1.6	2572, 1.4	1.429
23	18	18.0	1754, 1.7	2486, 1.5	1.417
23	16	19.0	1802, 1.8	2552, 1.7	1.416
23	14	19.8	1844, 1.8	2580, 1.7	1.399
30	10	21.2	1740, 1.9	2365, 1.7	1.359

<sup>a</sup>Antenna parameters are given in Figure 4.44.

present antenna can have a tunable frequency-ratio range of about 1.35–1.5. Radiation patterns of the antenna were also measured. Similar broadside radiation characteristics and same-polarization planes for the two operating frequencies are observed.

**4.3.3.2 With a Pair of Spur Lines** Dual-frequency operation of a single-feed equilateral-triangular microstrip antenna with a pair of spur lines has been demonstrated [25]. The two operating frequencies have the same polarization planes and, by varying the spur-line length, the frequency ratio of the two operating frequencies is tunable in the range of about 1.2–2.1. Figure 4.46 depicts the antenna geometry. The equilateral-triangular patch has a side length of  $L$ . Two spur lines of narrow width 1 mm and length  $\ell$  are embedded in the patch at a small distance 1 mm from the patch edge and the bottom side of the triangular patch. It is found that, when the spur-line length is greater than about one-half of the patch's side length, this antenna can have

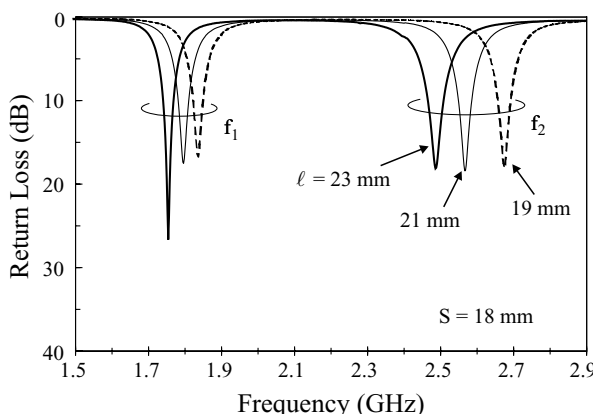


**FIGURE 4.45** Measured return loss for various lengths of the embedded slots for the antenna shown in Figure 4.43;  $\epsilon_r = 4.4$ ,  $h = 1.6$  mm,  $L = 50$  mm, and ground-plane size =  $75 \times 75$  mm<sup>2</sup>. (From Ref. 23, © 1999 John Wiley & Sons, Inc.)

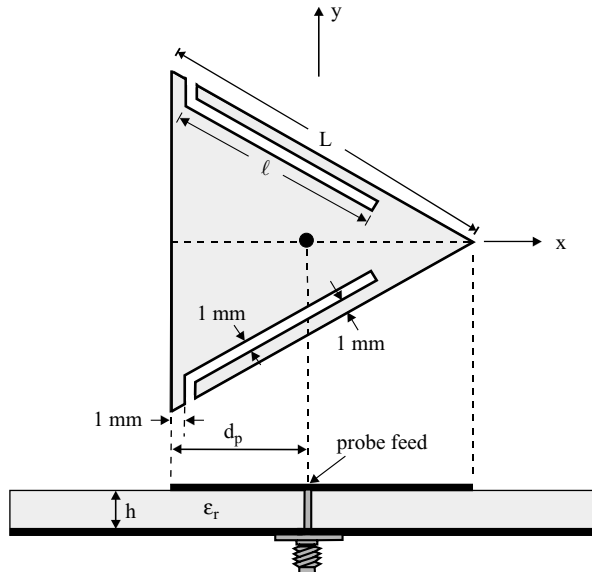


**FIGURE 4.46** Geometry of a dual-frequency equilateral-triangular microstrip antenna with a pair of spur lines. (From Ref. 25, © 1998 IEE, reprinted with permission.)

a new resonant mode at a frequency less than the fundamental resonant frequency  $f_{10}$  of the simple triangular microstrip antenna. Furthermore, this new resonant mode and the  $\text{TM}_{10}$  mode can both be excited with good impedance matching using a single probe feed located along the centerline ( $x$  axis) at a distance  $d_p$  from the bottom of the triangular patch.

Based on the above-described antenna design, prototypes of the antenna with various spur-line lengths were constructed and measured. The obtained dual-frequency performance is listed in Table 4.11. It is first noted that the antenna parameters studied here give a fundamental resonant frequency at about 1900 MHz for the case without spur lines. The results clearly show that, by increasing the spur-line length, the lower

**TABLE 4.11 Dual-Frequency Performance of the Antenna in Figure 4.46 [25]<sup>a</sup>**

Spur-Line Length $\ell$ (mm)	$d_p$ (mm)	$f_1$ , BW (MHz, %)	$f_2$ , BW (MHz, %)	$f_2/f_1$
24	2.7	1624, 2.0	1883, 1.3	1.16
28	2.7	1428, 1.7	1878, 1.7	1.32
32	2.7	1242, 1.6	1878, 1.7	1.51
36	2.8	1037, 1.7	1878, 1.7	1.81
40	2.8	949, 1.5	1878, 1.7	1.98
42	2.8	890, 1.7	1878, 1.7	2.11

<sup>a</sup> $\epsilon_r = 4.4$ ,  $h = 1.6$  mm,  $L = 50$  mm.

frequency  $f_1$  is decreased and is lower than 1900 MHz. On the other hand, the higher frequency  $f_2$  is very slightly affected by the variation in the spur-line length and is about the same as the frequency  $f_{10}$  of the simple triangular microstrip antenna. This is because the embedded spur lines are parallel to the excited patch surface current path of the  $\text{TM}_{10}$  mode, and thus a very small perturbation in the  $\text{TM}_{10}$  mode can be expected. Such different effects of the spur-line length on  $f_1$  and  $f_2$  provide the present design with a tunable frequency-ratio range of about 1.2–2.1. It can be seen that the optimal feed positions in this design are almost about the same, which indicates that the feed position is insensitive to the variation in the spur-line length. Radiation patterns at the two operating frequencies were also measured. It is observed that the two operating frequencies have the same polarization planes ( $x$ - $z$  plane) and similar broadside radiation characteristics. In addition, probably owing to the spur-line perturbation, the radiation pattern of the lower operating frequency has a relatively larger cross-polarization component than that of the higher operating frequency.

**4.3.3.3 With a V-Shaped Slot** Dual-frequency operation of a slotted triangular microstrip antenna incorporating the use of a thick foam substrate has been presented [26]. Figure 4.47 shows the proposed geometry with a V-shaped slot embedded in the triangular patch. The triangular patch is equilateral with side length  $L$ . The V-shaped slot has dimensions  $\ell_1$ ,  $\ell_2$ ,  $w_1$ , and  $w_2$ , where  $\ell_1$  and  $\ell_2$  are, respectively, the lengths of the outer and inner edges of the V-shaped slot and  $w_1$  and  $w_2$  are, respectively, the distances of the outer and inner edges of the V-shaped slot away from the patch edge. The V-shaped slot is centered in the triangular patch, with the slot tip facing the

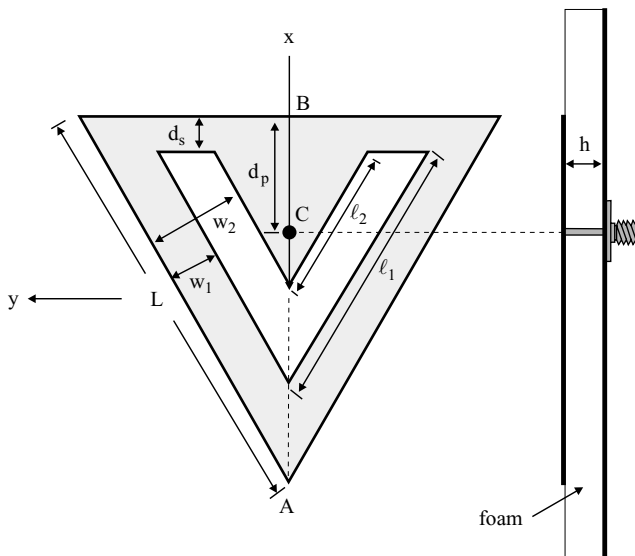


**FIGURE 4.47** Geometry of a dual-frequency triangular microstrip antenna with a V-shaped slot. (From Ref. 26, © 1999 John Wiley & Sons, Inc.)

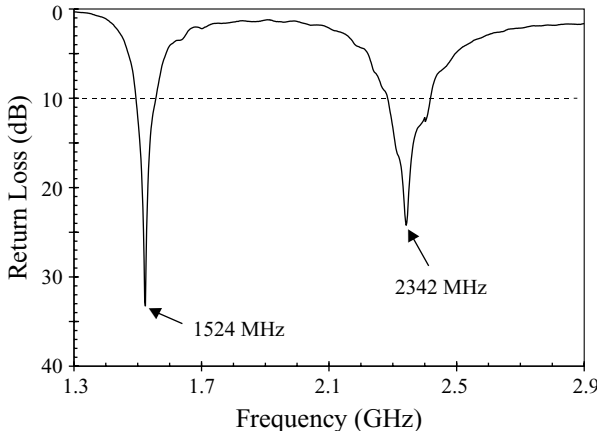


**FIGURE 4.48** Measured return loss for the antenna shown in Figure 4.47;  $h = 13.5$  mm,  $L = 91$  mm,  $d_s = 7$  mm,  $d_p = 26.2$  mm,  $\ell_1 = 52.5$  mm,  $\ell_2 = 37$  mm,  $w_1 = 13$  mm, and  $w_2 = 20$  mm. (From Ref. 26, © 1999 John Wiley & Sons, Inc.)

triangle tip, and the upper edge of the V-shaped slot is  $d_s$  from the patch edge. A probe feed is placed at point  $C$  for the proposed dual-frequency operation, where point  $C$  is the null-voltage point along the centerline  $\overline{AB}$  for the fundamental  $TM_{10}$  mode of the unslotted triangular microstrip antenna. The frequency ratio of the two operating frequencies is controlled by the dimensions of the V-shaped slot and the position of the slot relative to the edge of the triangular patch. The lower and higher operating frequencies occur, respectively, at a frequency below and above the fundamental resonant frequency  $f_{10}$  of the unslotted triangular microstrip antenna.

A number of prototypes have been constructed. Figure 4.48 shows the measured return loss for a design in which the V-shaped slot was chosen to be of dimensions  $(\ell_1, \ell_2, w_1, w_2) = (52.5, 36, 13, 20)$  mm and placed away from the patch edge at a distance  $d_s = 7$  mm. When there is no slot present, the fundamental resonant frequency of the antenna parameters ( $L = 91$  mm,  $h = 13.5$  mm) studied here is about 1800 MHz. From the results obtained, it is seen that the two operating frequencies at 1524 and 2342 MHz are excited with good matching conditions, which gives a frequency ratio of about 1.537. The impedance bandwidths are found to be about 4.1% and 5.6% for the two operating bands centered at 1524 and 2342 MHz, respectively. Radiation patterns at the two operating frequencies were also measured, and the  $E$ -plane ( $x-z$  plane) and  $H$ -plane ( $y-z$  plane) patterns are plotted in Figure 4.49. Similar radiation characteristics for the two operating frequencies can be seen, both having the same polarization planes ( $y-z$  plane) and showing relatively larger cross-polarization radiation in the  $H$  plane than in the  $E$  plane. The antenna gain in the broadside direction for the two operating frequencies is also about the same, and is measured to be about 7.0 dBi.

By varying the dimensions of the V-shaped slot embedded in the triangular patch, different dual-frequency operations can be obtained. Table 4.12 lists the

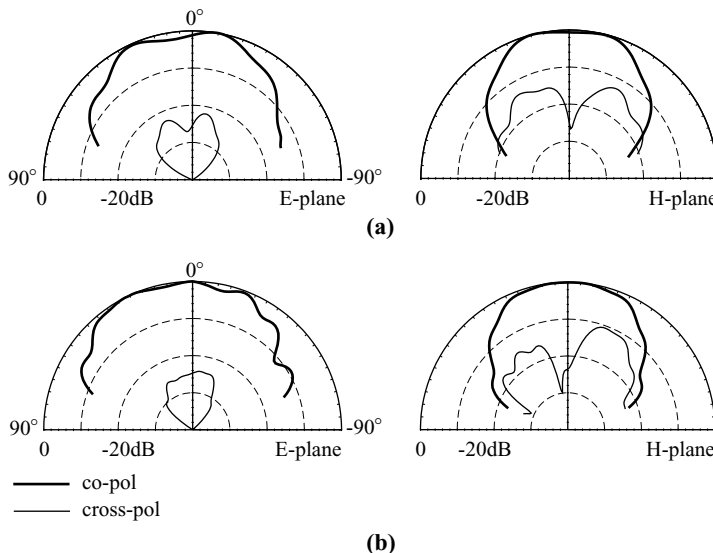


**FIGURE 4.49** Measured radiation patterns for the antenna studied in Figure 4.48. (a)  $f = 1524$  MHz, (b)  $f = 2342$  MHz. (From Ref. 26, © 1999 John Wiley & Sons, Inc.)

dual-frequency performance of the antenna with various slot dimensions. From the results, it is observed that, although all the dimensions of the V-shaped slot can affect the dual-frequency performance, the higher operating frequency  $f_2$  is most sensitive to a variation in the distance  $d_s$  between the slot's upper edge and the patch edge. On the other hand, the lower resonant frequency  $f_1$  is relatively insensitive to variations in the slot dimensions. By varying  $d_s$  from 5 to 16 mm in the present design, dual-frequency operation with a frequency ratio in the range 1.488–1.834 is obtained. For a fixed value of  $d_s$ , one can fine tune the dual-frequency operation by adjusting the dimensions  $(\ell_1, \ell_2, w_1, w_2)$  of the V-shaped slot.

**TABLE 4.12 Dual-Frequency Performance of the Antenna in Figure 4.47 [26]<sup>a</sup>**

$d_s$ (mm)	$\ell_1$ (mm)	$w_1$ (mm)	$f_1$ , BW (MHz, %)	$f_2$ , BW (MHz, %)	$f_2/f_1$
5	49	15	1530, 3.1	2276, 5.1	1.488
5	54	13	1498, 3.7	2270, 5.4	1.515
5	56	12	1484, 3.8	2262, 5.6	1.524
7	48	15	1568, 3.1	2356, 5.4	1.503
7	53	13	1524, 4.1	2342, 5.5	1.537
7	54	12	1496, 3.5	2334, 5.4	1.560
7	49	15	1560, 3.3	2312, 6.0	1.482
10	52	11	1538, 3.8	2452, 5.8	1.594
16	54	8	1498, 2.8	2748, 5.2	1.834

<sup>a</sup>Antenna parameters are given in Figure 4.48.

## 4.4 COMPACT DUAL-FREQUENCY OPERATION WITH ORTHOGONAL POLARIZATION PLANES

In this section, rectangular microstrip antennas with embedded slots or inserted slits for achieving compact dual-frequency operation [27–33] are described. The embedded slots or inserted slits that have been studied include a cross slot, a pair of bent slots, four inserted slits, four T-shaped slots, a square slot, a circular slot, and meandering slits, among others. The first two resonant frequencies for these designs are found to have orthogonal polarization planes, and are both greatly lowered with increasing dimensions of the slots or slits. Dual-frequency operation of microstrip antennas with a compact size is thus obtained. For circular and triangular microstrip antennas, similar compact dual-frequency operations have been obtained [34–36]. Typical design examples, such as a circular patch with four inserted slits or an offset slot and a triangular patch with a slit, are presented.

### 4.4.1 Design with a Rectangular Microstrip Antenna

**4.4.1.1 With a Cross Slot** Figure 4.50 shows the antenna geometry. The rectangular patch has dimensions  $L \times W$ , and the cross slot has equal slot lengths  $\ell$  and is centered at point  $B$  in the rectangular patch. Point  $A$  in the patch is the feed position for dual-frequency operation for the case without a cross slot, which is determined from the optimal feed positions of the  $\text{TM}_{01}$  and  $\text{TM}_{10}$  mode excitations. By choosing an equal-length cross slot, the optimal feed position for dual-frequency operation can easily be chosen between points  $A$  and  $B$ , as shown in the figure. Another reason for choosing an equal-length cross slot instead of using an unequal-length cross slot is that the frequency ratio of the two excited frequencies are mainly determined by the aspect ratio of the rectangular patch, which makes the dual-frequency design much simpler. In addition, by increasing the cross-slot length, both excited frequencies can be lowered with the frequency ratio almost unchanged.

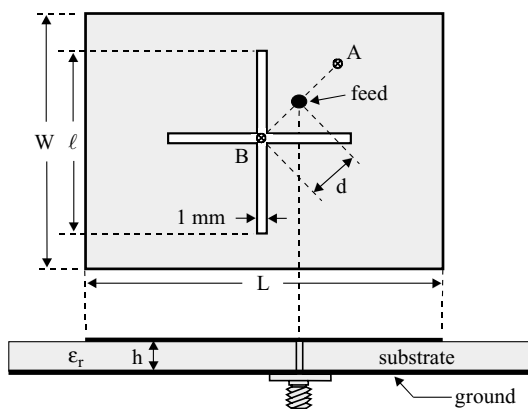


**FIGURE 4.50** Geometry of a compact dual-frequency rectangular microstrip antenna with a cross slot. (From Ref. 27, © 1997 IEE, reprinted with permission.)

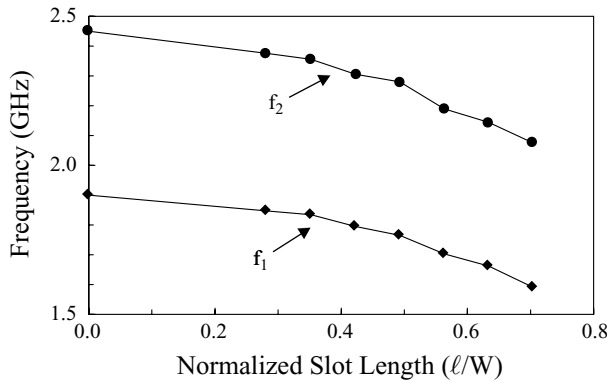


**FIGURE 4.51** The first two resonant frequencies against normalized cross-slot length for the antenna shown in Figure 4.50;  $\epsilon_r = 4.4$ ,  $h = 1.6$  mm,  $L = 37.7$  mm, and  $W = 28.4$  mm. (From Ref. 27, © 1997 IEE, reprinted with permission.)

The present design concept has been implemented [27]. Typical results for the first two resonant frequencies as a function of the cross-slot length are presented in Figure 4.51. The corresponding characteristics of the two excited frequencies are listed in Table 4.13. From these results, it is observed that the first two resonant frequencies decrease with increasing slot length with almost the same frequency ratio (about 1.29). This frequency ratio is slightly lower than the aspect ratio (1.327) of the rectangular patch, probably due to substrate effects. The optimal feed position for the two different frequency excitations is closer to the patch center (point *B*) when the cross-slot length increases. For smaller slot length, however, the optimal feed position is about the same as that (point *A*) for the simple patch case. When the cross-slot length is greater than 18 mm ( $0.634W$ ), there exist no proper feed positions in the rectangular patch for the two different frequency excitations. In this case, other feeding mechanisms such as an aperture-coupled feed can be used, which will be described later. However, for the case with  $\ell = 18$  mm, both resonant frequencies (1662 and 2144 MHz) are lowered by about 12% compared to those (1900 and 2446 MHz) of the simple rectangular patch.

**TABLE 4.13 Dual-Frequency Performance of the Antenna in Figure 4.50 [27]<sup>a</sup>**

$\ell$ (mm)	$d / \overline{AB}$	$f_1$ , BW (MHz, %)	$f_2$ , BW (MHz, %)	$f_2/f_1$
0	1.0	1900, 1.8	2446, 2.4	1.287
8	1.0	1848, 1.8	2376, 2.4	1.286
12	0.94	1795, 1.8	2306, 2.3	1.285
14	0.87	1764, 1.7	2280, 2.2	1.292
16	0.59	1703, 1.5	2187, 2.0	1.284
18	0.20	1662, 1.4	2144, 1.8	1.290

<sup>a</sup>Antenna parameters are given in Figure 4.51.

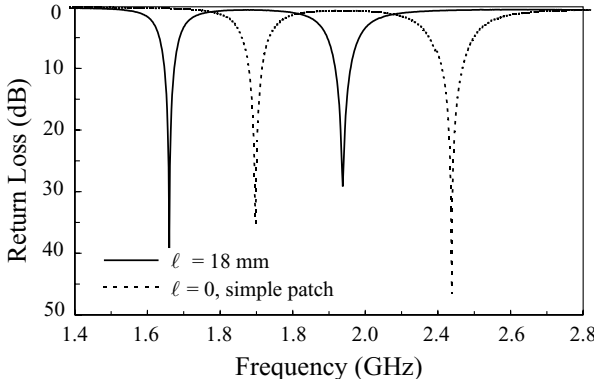


**FIGURE 4.52** Measured return loss against frequency for the antenna studied in Figure 4.51 with a cross slot of 18 mm and for the case without a cross slot ( $\ell = 0$ ). (From Ref. 27, © 1997 IEE, reprinted with permission.)

without a cross slot. The results for the measured return loss for these two cases are shown in Figure 4.52. This reduction in the two excited frequencies results in a patch size reduction of about 23% for a given dual-frequency design. For the impedance bandwidth, determined from the 10-dB return loss, it is found that both bandwidths for the two operating frequencies decrease with increasing cross-slot length, probably due to the antenna-size reduction. The radiation characteristics for the two excited frequencies have been studied. Good cross-polarization levels (better than 20 dB) for both operating frequencies are obtained for the *E*- and *H*-plane radiation, and no special distinction compared to those of the dual-frequency rectangular microstrip antenna without a cross slot is observed.

A design with an aperture-coupled feed has been investigated [28]. The antenna geometry is shown in Figure 4.53. The rectangular patch has dimensions  $L \times W$ , and the aspect ratio  $L/W$  controls the frequency ratio of the two operating frequencies; the cross slot is of equal length  $\ell$  in both directions, which effectively lowers the two excited frequencies with the frequency ratio very slightly affected and remaining mainly controlled by the aspect ratio of the rectangular patch. Typical results for cross-slot effects on the occurrence of the first two resonant frequencies are presented in Figure 4.54. It is noted that, to effectively excite the two frequencies, the coupling slot in the ground plane of the microstrip line is centered below the patch with an inclination angle given by (with respect to the microstrip line)

$$\alpha = \tan^{-1}(W/L). \quad (4.7)$$

For good impedance matching, the coupling-slot length is increased with increasing cross-slot length. The tuning-stub length  $\ell_t$  is first chosen to be about the average of the guided wavelength in the microstrip line for the two frequencies and then fine tuned to achieve a good matching condition for the two frequencies. Details of the experimental results are listed in Table 4.14. The results for the return loss for the patch with a large cross slot [ $\ell = 26$  cm ( $= 0.915W$ )] and a simple patch without

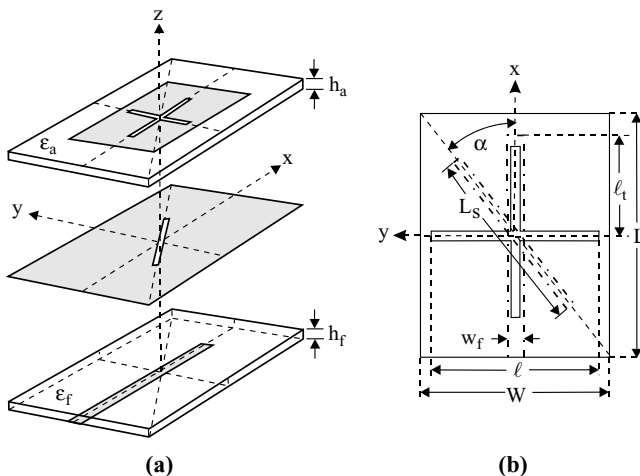


**FIGURE 4.53** (a) Exploded view and (b) top view of an inclined-aperture-coupled rectangular microstrip antenna with a cross slot for compact dual-frequency operation. (From Ref. 28, © 1998 IEE, reprinted with permission.)

a cross slot ( $\ell = 0$ ) are shown in Figure 4.55 for comparison. From the results, it is seen that the frequency ratio is nearly independent of the cross-slot length and is slightly less than the aspect ratio (1.327) of the rectangular patch. This difference is mainly due to substrate effects. For the case  $\ell = 26$  cm, both frequencies are lowered to about 78% times those of the simple patch case, which implies that the antenna size can be reduced to about 60% that of the design using a simple patch. Note that this antenna size reduction is 40%, which is nearly twice the attainable antenna size reduction (about 23%) using the coax feed shown in Figure 4.50. This

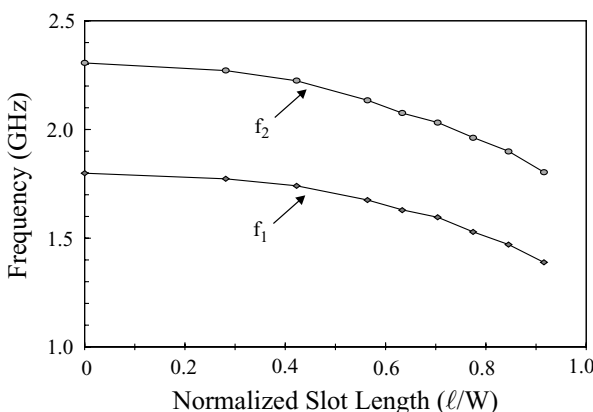


**FIGURE 4.54** The first two resonant frequencies  $f_1$  and  $f_2$  against normalized cross-slot length for the antenna shown in Figure 4.53;  $h = t = 1.6$  mm,  $\epsilon_a = \epsilon_f = 4.4$ ,  $L = 37.7$  mm,  $W = 28.4$  mm,  $w_f = 3.0$  mm,  $\alpha = 37^\circ$ . (From Ref. 28, © 1998 IEE, reprinted with permission.)

**TABLE 4.14 Dual-Frequency Performance of the Antenna in Figure 4.53 [28]<sup>a</sup>**

$\ell$ (mm)	Coupling-Slot Size (mm <sup>2</sup> )	Tuning-Stub Length (mm)	$f_1$ , BW (MHz, %)	$f_2$ , BW (MHz, %)	$f_2/f_1$
0	1.2 × 18.5	18.3	1799, 2.1	2306, 2.4	1.282
8	1.2 × 19.0	18.3	1773, 2.0	2271, 2.3	1.281
12	1.2 × 20.0	20.8	1741, 1.8	2224, 2.3	1.277
16	1.2 × 21.0	21.9	1676, 1.9	2135, 2.2	1.274
20	1.2 × 22.0	23.2	1596, 1.6	2062, 1.8	1.292
22	1.2 × 23.5	24.1	1529, 1.6	1963, 1.7	1.284
24	1.2 × 24.5	25.3	1471, 1.6	1900, 1.6	1.292
26	1.2 × 25.5	26.2	1389, 1.5	1804, 1.6	1.299

<sup>a</sup>Antenna parameters are given in Figure 4.54.

is mainly because the aperture-coupled feed method has more freedom to control the input impedance for impedance matching than does the probe-feed case. Results show that the impedance bandwidth decreases with decreasing resonant frequency (see Table 4.14). This is largely owing to the decrease in the electrical thickness of the substrate when the resonant frequency decreases. The radiation patterns of the dual-frequency patch antenna with a cross slot have been measured, and good broadside radiation characteristics for both operating frequencies have been observed.

**4.4.1.2 With a Pair of Bent Slots** With the loading of a pair of bent slots, compact dual-frequency operation for a rectangular microstrip antenna has been reported [29]. Figure 4.56 shows the antenna geometry studied. A pair of bent slots of length  $\ell$  and width 1 mm is cut in the patch center, with a small spacing  $S$  between the two bent slots. The feed position for the excitation of the two operating frequencies for various bent-slot sizes is obtained between points *A* and *B* (see Figure 4.56), which is quite

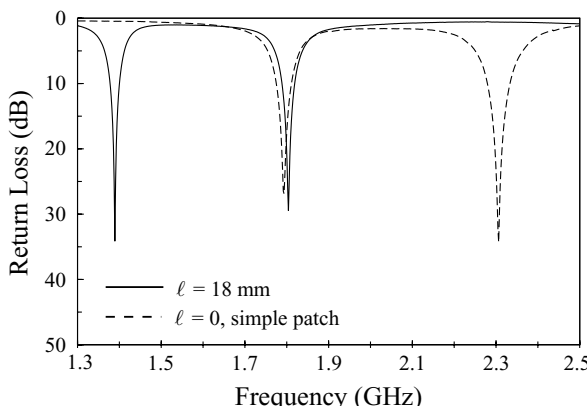


**FIGURE 4.55** Measured return loss against frequency for a simple patch antenna ( $\ell = 0$ ) and a patch antenna with a cross slot of 26 mm; antenna parameters are given in Figure 4.54. (From Ref. 28, © 1998 IEE, reprinted with permission.)

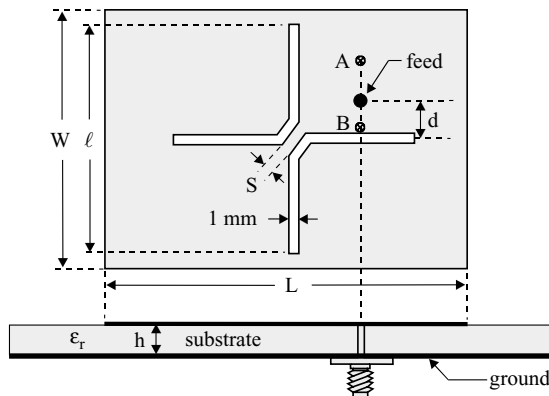


**FIGURE 4.56** Geometry of a compact dual-frequency rectangular microstrip antenna with a pair of bent slots. (From Ref. 29, © 1998 IEE, reprinted with permission.)

different from that obtained for the case with a cross slot (see Section 4.4.1.1). The difference in the feed positions is due to the different surface current paths of the first two dominant modes for the patch with different slot cuts. Point *A* is the optimal ( $50\Omega$ ) feed position for impedance matching of two operating frequencies for the case without bent slots, while point *B* is at the boundary of the bent slots. The location of point *A* can be determined from the optimal feed positions of the  $\text{TM}_{01}$  and  $\text{TM}_{10}$  mode excitations.

Prototypes of designs with various sizes of bent slots were constructed and measured. Figure 4.57 shows the first two operating resonant frequencies as a function of the bent-slot length. The corresponding impedance bandwidth, optimal feed position, and frequency ratio are listed in Table 4.15. Measured return loss for  $\ell = 0, 22$ , and

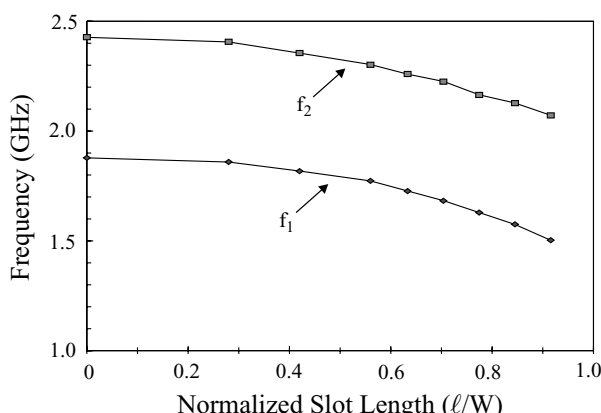


**FIGURE 4.57** The first two resonant frequencies  $f_1$  and  $f_2$  against normalized bent-slot length for the antenna shown in Figure 4.56;  $\epsilon_r = 4.4$ ,  $h = 1.6$  mm,  $L = 37.7$  mm,  $W = 28.4$  mm, and  $S = 1.4$  mm. (From Ref. 29, © 1998 IEE, reprinted with permission.)

**TABLE 4.15 Dual-Frequency Performance of the Antenna in Figure 4.56 [29]<sup>a</sup>**

$\ell$ (mm)	$d$ (mm)	$f_1$ , BW (MHz, %)	$f_2$ , BW (MHz, %)	$f_2/f_1$
0	6.5	1878, 1.9	2427, 2.8	1.292
8	7.0	1859, 1.8	2406, 2.6	1.294
12	6.5	1818, 1.9	2355, 2.4	1.295
16	5.5	1773, 1.7	2303, 2.2	1.298
18	5.0	1727, 1.7	2259, 2.0	1.308
20	3.5	1683, 1.6	2226, 2.0	1.322
22	3.0	1629, 1.5	2165, 1.9	1.329
24	2.5	1575, 1.5	2128, 2.1	1.351
26	2.0	1503, 1.5	2072, 1.8	1.378

<sup>a</sup> Antenna parameters are given in Figure 4.57.

26 mm is presented in Figure 4.58. It can be seen that, for  $\ell = 26$  mm ( $= 0.915W$ ), the two operating frequencies are lowered by about 20% and 15%, respectively, compared to those of the simple patch case ( $\ell = 0$ ). This implies that, for fixed dual-frequency operation, the required antenna size is only about 68% that of the design using a simple patch without bent slots. This corresponds to a 32% antenna size reduction. The results in Table 4.15 show that the lowering of the first resonant frequency is more significant than that in the second resonant frequency, which leads to a small increase in the ratio of the two frequencies with increasing bent-slot size. In general, the frequency ratio is still mainly controlled by the aspect ratio of the rectangular patch. The measured radiation patterns of the two operating frequencies were also measured. Although the excited patch surface current paths are significantly altered to lower the desired resonant frequencies, no special distortion of the radiation patterns is observed and the cross-polarization radiation is at an acceptable level.

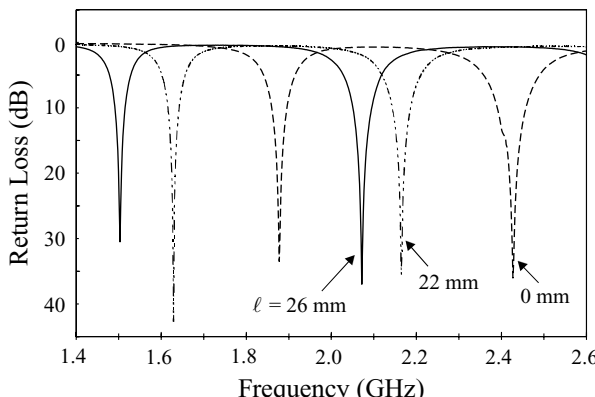


**FIGURE 4.58** Measured return loss against frequency for  $\ell = 0$  (a simple patch) and  $\ell = 22, 26$  mm; antenna parameters are given in Figure 4.57. (From Ref. 29, © 1998 IEE, reprinted with permission.)

**4.4.1.3 With Four Inserted Slits** The use of four inserted slits at the patch edges of a rectangular patch [30] has been shown to be a promising compact dual-frequency design. The antenna design is shown in Figure 4.59. The four inserted slits are of equal length  $\ell$  and narrow width 1 mm. When the slit length increases, the resonant frequencies of the first two resonant modes are lowered, similar to the cases with a cross slot or a pair of bent slots. Point A in the patch is again the feed position for dual-frequency operation for a simple rectangular patch without slots, which is determined from the optimal feed positions of the  $\text{TM}_{01}$  and  $\text{TM}_{10}$  mode excitations. With the presence of slits, it is found that the optimal feed position for the excitation of the first two resonant modes can be approximately obtained by moving horizontally toward point B (see Figure 4.59). When the slot length increases, the 50- $\Omega$  feed position for the two modes moves closer to point B.

Several prototypes have been constructed. Figure 4.60 shows measured results for the first two resonant frequencies as a function of the normalized slit length. It is clearly seen that the two resonant frequencies decrease with increasing slit length, with the frequency ratio of the two frequencies very slightly affected by the slit-length variation and mainly controlled by the aspect ratio of the rectangular patch. The dual-frequency performance for various slit lengths is given in Table 4.16. The measured return loss for  $\ell = 0$ , 11, and 12 mm is shown in Figure 4.61. The results give a frequency ratio of about 1.30, which is slightly less than the aspect ratio (1.327) of the rectangular patch. This difference is mainly due to the substrate effect. It should also be noted that, for slit length greater than 12 mm, a single probe feed for obtaining a good 50- $\Omega$  matching condition of the two modes becomes difficult to locate. From the results for  $\ell = 12$  mm ( $= 0.423W$ ), both frequencies are lowered by about 25% as compared to those of a simple patch without slots. This suggests that, for fixed dual-frequency operation, the antenna size of the present design can be reduced to

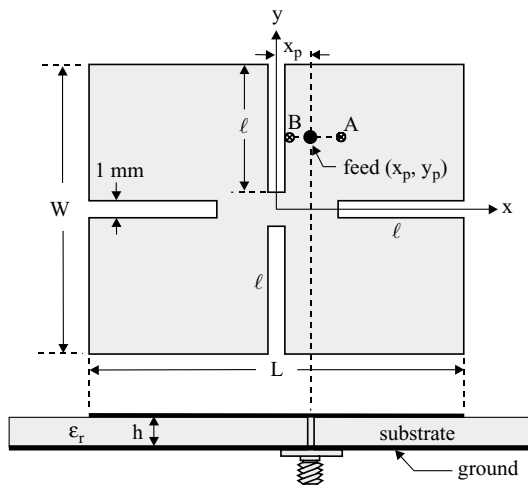


**FIGURE 4.59** Geometry of a compact dual-frequency rectangular microstrip antenna with four narrow inserted slits.

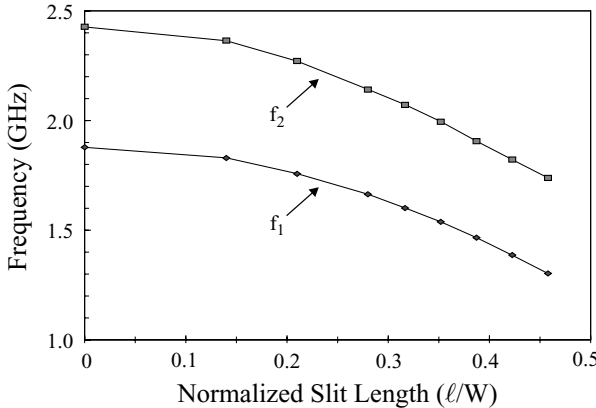


**FIGURE 4.60** The first two resonant frequencies against normalized slit length for the antenna shown in Figure 4.59;  $\epsilon_r = 4.4$ ,  $h = 1.6$  mm,  $L = 37.7$  mm, and  $W = 28.4$  mm.

56% of that using the regular-size dual-frequency design studied in Section 4.4.2. Figure 4.62 presents the measured *E*- and *H*-plane radiation patterns for the two operating frequencies of the design with  $\ell = 11$  and 12 mm. The results show good broadside radiation and acceptable cross-polarization levels for the two operating frequencies in the present design.

**4.4.1.4 With Four T-Shaped Slots** The case with four T-shaped slots has been studied, and the design is shown in Figure 4.63. In this design, four T-shaped slots are aligned to face the four edges of the rectangular patch, leaving a spacing of 1.4 mm in the patch center. The length  $\ell$  of the T-shaped slot is fixed to 12 mm ( $= 0.423W$ ) and the width  $t$  of the T-shaped slot is varied from 0 to 24 mm. Other antenna parameters are the same as used in Sections 4.4.1.1–4.4.1.3. Figure 4.64 presents the measured return loss against frequency for the present design with different slot sizes. The corresponding design parameters and antenna performance are listed in Table 4.17. It

**TABLE 4.16 Dual-Frequency Performance of the Antenna in Figure 4.59 [30]<sup>a</sup>**

Slit Length $\ell$ (mm)	$x_p$ (mm)	$f_1$ , BW (MHz, %)	$f_2$ , BW (MHz, %)	$f_2/f_1$
0	6.5	1878, 1.9	2427, 2.4	1.292
4	6.5	1830, 1.9	2364, 2.1	1.291
6	6.0	1758, 1.8	2271, 2.0	1.292
8	5.5	1664, 1.7	2142, 1.9	1.287
9	4.7	1601, 1.6	2072, 1.7	1.294
10	4.0	1538, 1.6	1995, 1.7	1.297
11	3.5	1466, 1.6	1906, 1.6	1.300
12	2.0	1386, 1.4	1822, 1.5	1.315

<sup>a</sup>Antenna parameters are given in Figure 4.60.

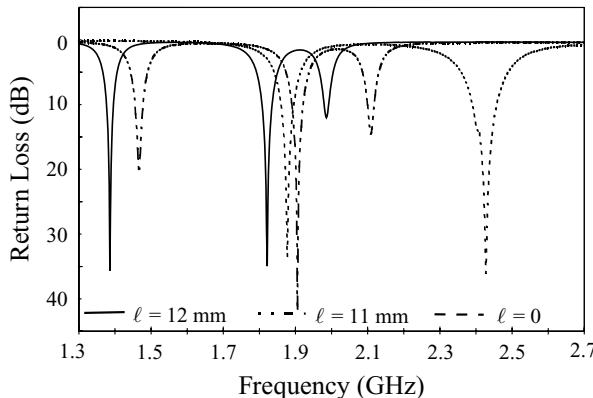


**FIGURE 4.61** Measured return loss against frequency for the simple patch case ( $\ell = 0$ ) and the cases with  $\ell = 11$  and  $12 \text{ mm}$ ; antenna parameters are given in Figure 4.60.

is observed that the first two resonant frequencies decrease with increasing slot size. The loci of the  $50\text{-}\Omega$  feed position for various slot sizes are found to be roughly on the diagonal of the rectangular patch, which is similar to the feed-position loci of the designs with a cross slot (Section 4.4.1.1) and a square slot (Section 4.4.1.5), but quite different from the feed-position loci of the design with a pair of bent slots (Section 4.4.1.2) or four inserted slits (Section 4.4.1.3). This is largely owing to the different excited patch surface current paths for the rectangular patch with different slot

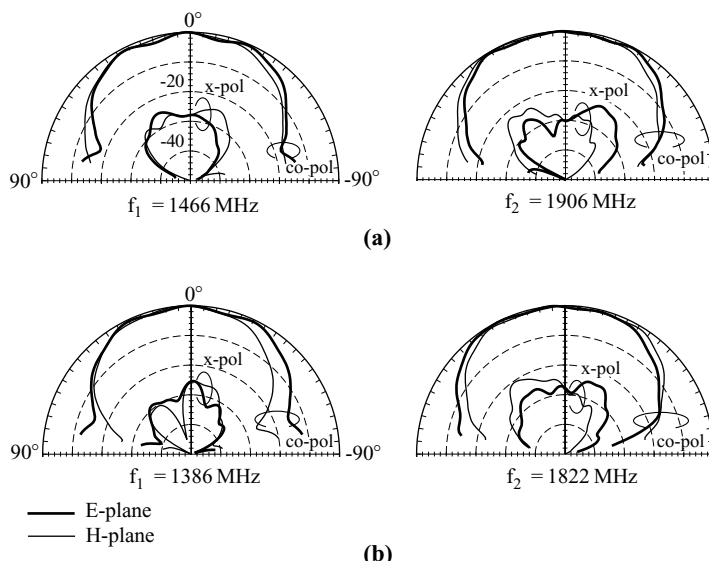


**FIGURE 4.62** Measured radiation patterns at the two operating frequencies for the antenna studied in Figure 4.60. (a)  $\ell = 11 \text{ mm}$ ; (b)  $\ell = 12 \text{ mm}$ .

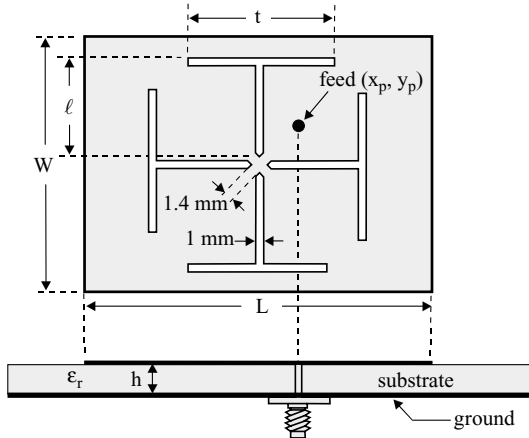


**FIGURE 4.63** Geometry of a compact dual-frequency rectangular microstrip antenna with four T-shaped slits.

perturbations. The results show that, for the case with a T-shaped slot of dimensions  $12 \text{ mm} \times 24 \text{ mm}$  ( $\ell \times t$ ), the first two resonant frequencies are lowered by about 24% and 19%, respectively, compared to the case without a slot. This lowering of the resonant frequencies corresponds to an antenna size reduction of about 38% using the present design. The measured radiation patterns were measured, and good radiation characteristics were observed.

**4.4.1.5 With a Square or Circular Slot** Figure 4.65 shows a compact dual-frequency design with a square slot [31] or a circular slot [32]. The dual-frequency performance is shown in Table 4.18 for the design with a square slot. The two operating frequencies decrease with increasing square-slot dimensions, and dual-frequency

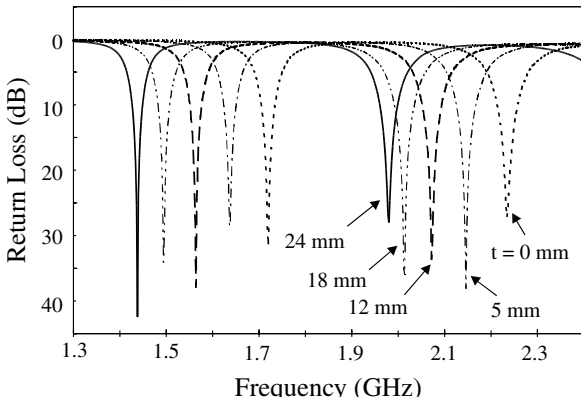


**FIGURE 4.64** Measured return loss against frequency for the antenna shown in Figure 4.63;  $\epsilon_r = 4.4$ ,  $h = 1.6 \text{ mm}$ ,  $L = 37.7 \text{ mm}$ ,  $W = 28.4 \text{ mm}$ ,  $\ell = 12 \text{ mm}$ .

**TABLE 4.17 Dual-Frequency Performance of the Antenna in Figure 4.63 [30]<sup>a</sup>**

T-Slot Size $\ell, t$ (mm)	$x_p, y_p$ (mm)	$f_1$ , BW (MHz, %)	$f_2$ , BW (MHz, %)	$f_2/f_1$
0, 0	6.5, 6.0	1878, 1.9	2427, 2.4	1.292
12, 0	5.0, 5.0	1720, 1.8	2238, 2.2	1.301
12, 5	4.0, 4.0	1636, 1.8	2148, 2.2	1.313
12, 12	4.0, 4.0	1562, 1.7	2070, 2.2	1.325
12, 18	4.0, 4.5	1496, 1.9	2014, 2.3	1.346
12, 24	5.0, 3.0	1438, 1.6	1978, 2.1	1.375

<sup>a</sup>Antenna parameters are given in Figure 4.64.

operation with a reduced antenna size can be obtained. For the design with a circular slot, similar results have been observed, and a 20% antenna size reduction has been demonstrated [32] by comparing the design with the regular-size dual-frequency rectangular microstrip antenna without a slot.

**4.4.1.6 With Meandering Slits** By using a meandered patch and an aperture-coupled feed, compact dual-frequency operation of microstrip antennas has been achieved [33]. In this design (see the geometry shown in Figure 4.66), the two operating frequencies are mainly controlled by the patch dimensions and the length of the meandering slits. Experiments have been conducted, and the obtained dual-frequency performance is given in Table 4.19. The patch and coupling-slot dimensions are, respectively,  $27 \times 18 \text{ mm}^2$  ( $L \times W$ ) and  $10 \times 2 \text{ mm}^2$  ( $L_s \times W_s$ ), and the rectangular patch is arranged such that the direction of the patch length is inclined to the microstrip feed line with an inclination angle of  $\alpha$ . The coupling slot center is placed right below point  $C$  in the rectangular patch; point  $C$  is positioned a distance  $L/8$  from the patch center (or at the center between the first and second slits) along the patch's centerline. Such an arrangement incorporating the selection of a suitable tuning-stub length  $\ell_t$  is found to be most effective in achieving impedance matching for the two different operating frequencies in the present design. A large frequency ratio ( $>2.5$ ) of the two operating frequencies can be obtained. For fixed dual-frequency operation, an antenna size reduction of about 50% has been obtained using the present design compared to the case using a regular rectangular patch without slits.

#### 4.4.2 Design with a Circular Microstrip Antenna

**4.4.2.1 With Four Inserted Slits** Figure 4.67 shows a circular microstrip antenna with four inserted slits for compact dual-frequency operation [34]. The patch-size reduction is achieved by cutting four equally spaced slits at the boundary of the circular patch. The circular patch has a radius of  $R$ . The two slits on the  $x$  axis have the same length  $\ell_x$ , and the two slits on the  $y$  axis have an equal length  $\ell_y$ . When  $\ell_x = \ell_y$ , dual-frequency excitation cannot be obtained. In this design, we select  $\ell_y$  to be fixed at a length slightly less than the disk radius, which can significantly lengthen the

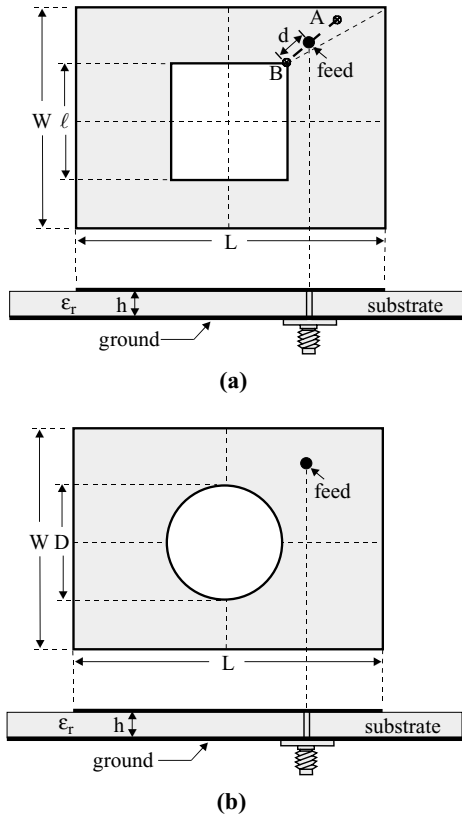


**FIGURE 4.65** Geometries of a compact dual-frequency rectangular microstrip antenna with (a) a square slot and (b) a circular slot.

equivalent surface current path in the  $x$  direction and lower the fundamental resonant frequency of the circular patch. Then, by varying  $\ell_x$  ( $0 < \ell_x < \ell_y$ ), it is expected that the equivalent surface current path in the  $y$  direction can be lengthened compared to that of the  $\text{TM}_{11}$  mode of a simple circular patch; however, this lengthening is less than that in the  $x$ -direction excitation. This behavior results in two different resonant

**TABLE 4.18 Dual-Frequency Performance of the Antenna in Figure 4.65(a) [31]<sup>a</sup>**

$\ell$ (mm)	$d_p$ (mm)	$f_1$ , BW (MHz, %)	$f_2$ , BW (MHz, %)	$f_2/f_1$
0	6	2115, 1.9	2698, 2.2	1.276
2.5	5	2094, 1.9	2675, 2.1	1.277
7.5	2	2034, 1.8	2587, 2.1	1.272
9.0	0	1932, 1.8	2475, 2.0	1.281

<sup>a</sup>  $\epsilon_r = 4.4$ ,  $h = 1.6$  mm,  $L = 25.5$  mm, and  $W = 33.2$  mm.

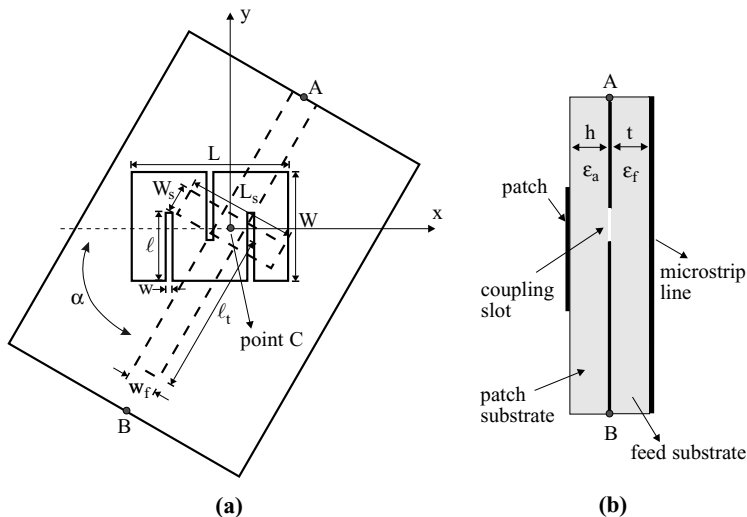


**FIGURE 4.66** (a) Top view and (b) cross-sectional view of a slot-coupled, meandered rectangular microstrip antenna for compact dual-frequency operation. (From Ref. 33, © 1998 IEE, reprinted with permission.)

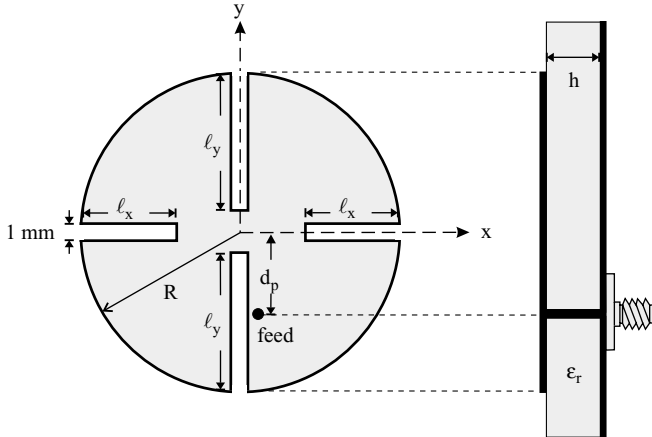
lengths in orthogonal directions; that is, dual-frequency operation with orthogonal polarization planes is obtained. It is also found that, owing to the unequal lengths of the slits in the  $x$  and  $y$  directions, the optimal feed position for the excitation of the two different frequencies with a good matching condition is along the edge of the longer slit as shown in Figure 4.67.

Figure 4.68(a) presents typical measured results for the first two resonant frequencies as a function of the slit ratio  $\ell_x/\ell_y$ . It is seen that the lowest resonant frequency  $f_1$  is independent of the slit ratio and occurs at about 1643 MHz, which is about 0.63 times that (2586 MHz) for a simple patch without slits. This corresponds to an antenna size reduction of about 60%. On the other hand, the second resonant frequency  $f_2$  decreases with increasing  $\ell_x$ . The frequency ratio of  $f_1$  and  $f_2$  is shown in

**TABLE 4.19 Dual-Frequency Performance of the Antenna in Figure 4.66 [33]<sup>a</sup>**

$\ell$ (mm)	$\alpha$ (deg)	Tuning-Stub Length (mm)	$f_1$ , BW (MHz, %)	$f_2$ , BW (MHz, %)	$f_2/f_1$
0	43	11.5	2592, 1.7	3728, 2.7	1.438
6	31	30.3	1968, 1.5	3790, 2.7	1.926
11	38	30.3	1400, 1.5	3667, 2.0	2.619
6	34	28.3	1991, 1.5	3763, 2.8	1.890
11	53	28.3	1394, 1.6	3616, 2.1	2.594

<sup>a</sup> $\epsilon_a = \epsilon_f = 4.4$ ,  $h_a = h_f = 1.6$  mm,  $L \times W = 27 \times 18$  mm<sup>2</sup>, and  $L_s \times W_s = 10 \times 2$  mm<sup>2</sup>.



**FIGURE 4.67** Geometry of a circular microstrip antenna with four inserted slits for compact dual-frequency operation. (From Ref. 34, © 1998 John Wiley & Sons, Inc.)

Figure 4.68(b). From the experimental results, an approximate equation for determining  $f_2/f_1$  is derived as follows (applicable for  $\ell_x/\ell_y \approx 0.28\text{--}0.85$ ):

$$df_{\text{ratio}} \approx (d + \ell_y)/(d + 0.8\ell_x). \quad (4.8)$$

The calculated results from (4.8) are shown in the figure for comparison. From this approximate equation, the frequency ratio of the dual-frequency operation can

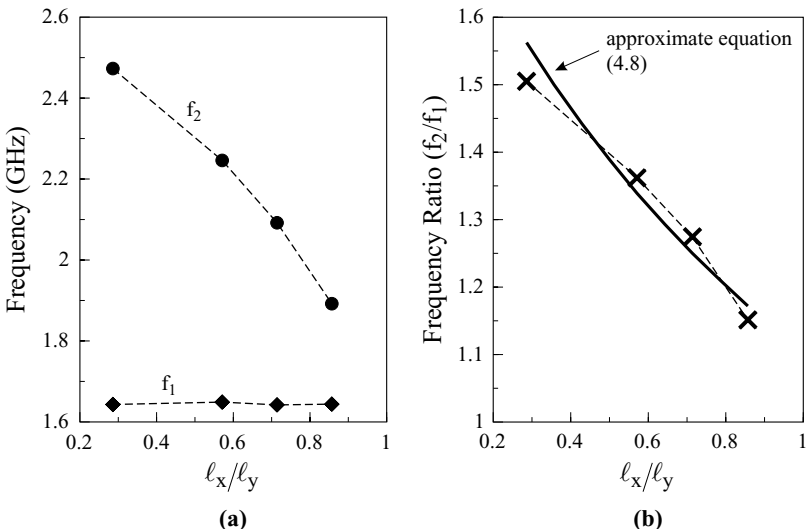


**FIGURE 4.68** (a) The first two resonant frequencies  $f_1$  and  $f_2$  and (b) frequency ratio  $f_2/f_1$  against the slit ratio  $\ell_x/\ell_y$ ;  $\epsilon_r = 4.4$ ,  $h = 1.6$  mm,  $R = 16$  mm, and  $\ell_y = 14$  mm ( $= 0.875R$ ). (From Ref. 34, © 1998 John Wiley & Sons, Inc.)

**TABLE 4.20 Dual-Frequency Performance of the Antenna in Figure 4.67 [34]<sup>a</sup>**

$\ell_x, \ell_y$ (mm)	$d_p$ (mm)	$f_1, \text{BW}$ (MHz, %)	$f_2, \text{BW}$ (MHz, %)	$f_2/f_1$
4, 14	5.2	1643, 1.2	2473, 2.2	1.505
8, 14	4.5	1644, 1.4	2246, 1.8	1.366
10, 14	4.1	1642, 1.5	2092, 1.6	1.274
12, 14	3.7	1644, 1.3	1892, 1.6	1.151

<sup>a</sup>Antenna parameters are given in Figure 4.68.

be controlled. Also, from the results shown in Figure 4.68(b), the tunable range of the frequency ratio is about 1.15–1.5. When  $\ell_x$  is small or about the same as  $\ell_y$  (in this case, the frequency ratio can be larger than 1.5 or less than 1.15), a single feed for exciting the two frequencies with a good matching condition cannot be obtained in the present design. The corresponding resonant frequency and impedance bandwidth for the cases studied are listed in Table 4.20, and typical measured return loss for  $\ell_x = 12$  and 10 mm is presented in Figure 4.69. It is observed that the difference in the impedance bandwidth for the two frequencies increases with increasing frequency ratio. This is largely because the impedance bandwidth strongly depends on the electrical thickness of the substrate and is larger for an electrically thicker substrate. For the radiation patterns measured, good broadside radiation with cross-polarization less than –20 dB is observed for the present design.

**4.4.2.2 With an Offset Circular Slot** Compact dual-frequency operation has been obtained by embedding an offset circular slot close to the boundary of a circular patch [35]. The antenna geometry is shown in Figure 4.70. It is found that, when

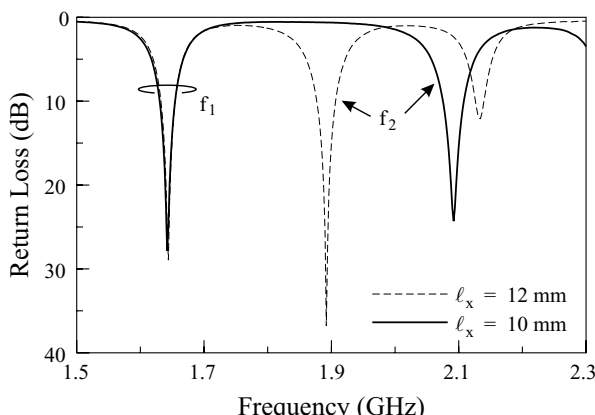


**FIGURE 4.69** Measured return loss for dual-frequency operation; antenna parameters are given in Figure 4.68. (From Ref. 34, © 1998 John Wiley & Sons, Inc.)

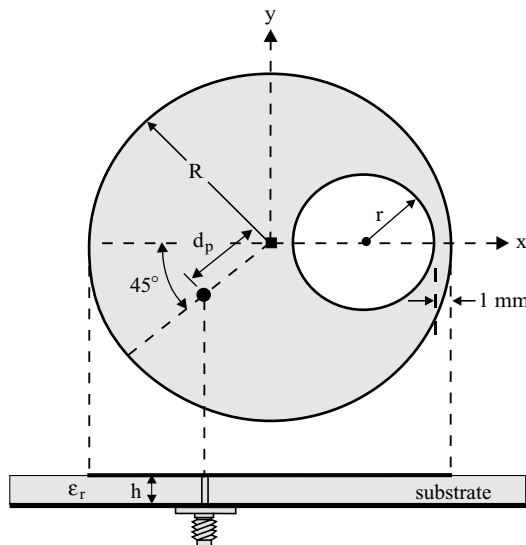


**FIGURE 4.70** Geometry of a circular microstrip antenna with an offset circular slot for compact dual-frequency operation. (From Ref. 35, © 1999 John Wiley & Sons, Inc.)

the radius of the offset slots is about 0.38–0.62 times the radius of the circular patch, the antenna's first two resonant frequencies can be easily excited using a single probe feed. The two resonant frequencies have orthogonal polarization planes and have a low frequency ratio of about 1.15–1.18. The two frequencies can also be much lower than the fundamental resonant frequency of the corresponding simple circular microstrip antenna without an offset slot. Compact dual-frequency operation can thus be obtained for the present design.

An experimental study has been conducted in which the circular slot is offset close to the patch boundary, with a small distance of 1 mm between the slot edge and the patch boundary. It is found that, for a specific range of the slot radius, a single probe feed (point  $A$  in the figure at a distance  $d_p$  from the patch center) placed  $45^\circ$  from the centerline ( $x$  axis or  $y$  axis) of the circular patch can excite two resonant modes with good impedance matching. Measured results for the obtained dual-frequency performance are listed in Table 4.21. Note that, when the slot radius is less than  $8\text{ mm}$  (about  $0.38D$ ), no good excitation of two separate resonant modes in the vicinity of the fundamental resonant mode ( $\text{TM}_{11}$ ) of the corresponding unslotted circular microstrip antenna can be observed; that is, no dual-frequency operation can be achieved. On the other hand, when the slot radius is within the range  $8$ – $13\text{ mm}$  (about  $0.62D$ ), good excitation of two separate resonant modes can easily be achieved by using a single probe feed. Depending on the slot radius, the obtained frequency ratio is within the range of about 1.15–1.18. The optimal feed position is shifted toward the patch center as the slot radius increases. This behavior leads to the fact that, when the slot radius is greater than  $13\text{ mm}$ , there are no proper feed positions in the circular patch for good impedance matching of the two operating frequencies. This suggests that single-feed,

**TABLE 4.21 Dual-Frequency Performance of the Antenna in Figure 4.70 [35]<sup>a</sup>**

Slot Radius <i>r</i> (mm)	<i>d<sub>p</sub></i> (mm)	<i>f<sub>1</sub></i> , BW (MHz, %)	<i>f<sub>2</sub></i> , BW (MHz, %)	<i>f<sub>2</sub>/f<sub>1</sub></i>
8	12.9	1742, 1.8	2009, 1.9	1.153
9	12.5	1733, 1.9	2003, 2.2	1.156
10	11.9	1619, 1.7	1919, 2.0	1.185
11	11.8	1564, 1.7	1860, 2.0	1.182
12	11.4	1533, 1.6	1802, 1.8	1.175
13	10.5	1490, 1.6	1733, 1.8	1.163

<sup>a</sup>Antenna parameters are given in Figure 4.71.

dual-frequency operation of the proposed antenna can only be obtained when the slot radius is within a specific range of about 0.38–0.62 times the disk radius.

The results for the measured return loss for designs with various slot radii are shown in Figure 4.71. It can be seen that, for the case with a slot radius  $r = 13$  mm, the resonant frequencies (1490 and 1733 MHz) are lowered by about 25% and 13%, respectively, compared to the fundamental resonant frequency  $f_{11}$  (about 2.0 GHz) of the corresponding simple circular microstrip antenna without a circular slot. This suggests that the proposed antenna can have a size about 44% or 25% lower than that of a simple circular patch antenna operated at the lower or higher frequency of the dual-frequency operation. For the measured radiation patterns for the present design, good broadside radiation characteristics have been observed.

#### 4.4.3 Design with a Triangular Microstrip Antenna

The design of a triangular microstrip antenna with an inserted slit (see the geometry shown in Figure 4.72) for dual-frequency operation has been reported [36]. This antenna design with a frequency ratio of the two operating frequencies ranging from 1.201 to 1.563 has been implemented and analyzed. It is found that, for a fixed

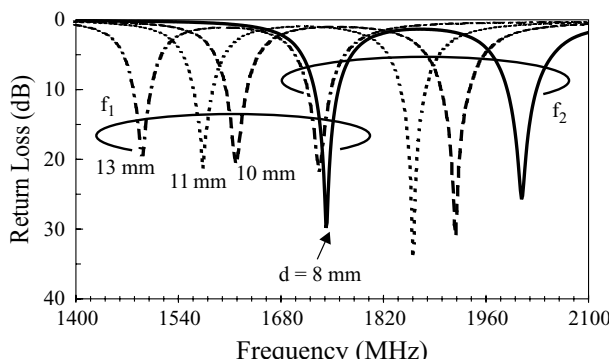


**FIGURE 4.71** Measured return loss for the antenna shown in Figure 4.70;  $\epsilon_r = 4.4$ ,  $h = 1.6$  mm, and  $R = 21$  mm. (From Ref. 35, © 1999 John Wiley & Sons, Inc.)

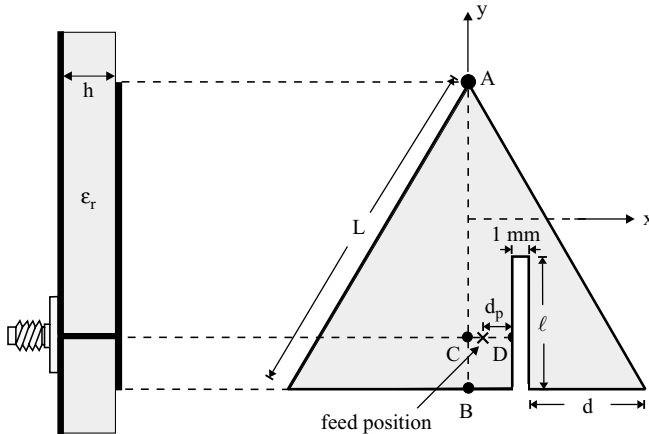


**FIGURE 4.72** Geometry of a dual-frequency equilateral-triangular microstrip antenna with a slit. (From Ref. 36, © 1998 John Wiley & Sons, Inc.)

dual-frequency operation, this antenna can have a much smaller patch size (less than 50%) than that required by the design using a regular rectangular microstrip antenna.

In this design, a narrow slit of length  $\ell$  and width 1 mm is inserted at the edge of the patch and aligned parallel to the centerline ( $\overline{AB}$ ) of the triangular patch. In this case, the perturbation effect of the slit on the excited patch surface current path of the  $TM_{10}$  mode (the fundamental mode) in the  $y$  direction is very small; that is, the resonant frequency  $f_{10}$  remains almost unchanged. However, the inserted slit lengthens the equivalent current path in the  $x$  direction of the patch; a resonant mode with resonant frequency less than  $f_{10}$  can be created. By selecting the proper feed position, these two orthogonal modes can both be excited with good impedance matching. The experiments show that the optimal feed position for dual-frequency operation is approximately located on the line segment  $CD$  parallel to the bottom side of the patch, where point  $C$  is on the  $y$  axis and is the  $50\text{-}\Omega$  feed position of the  $TM_{10}$  mode for the patch without a slit, and point  $D$  is at the edge of the slit. When the slit length increases, the feed position should move away from point  $C$  toward point  $D$ . By varying the slit position  $d$  and slit length  $\ell$ , the frequency ratio of the two excited resonant frequencies can be controlled. In the experiments, a frequency ratio of up to about 1.56 has been obtained, with a good impedance matching condition for the two operating modes. Figure 4.73 presents the measured return loss for a design with various slit lengths. The corresponding dual-frequency performance is listed in Table 4.22. Two cases of the slit position,  $d = 18$  and  $16$  mm, are shown. Note that, to obtain the dual-frequency operation at 1258 and 1966 MHz ( $f_2/f_1 = 1.563$ ) shown in Table 4.22, the present design requires a patch size of about  $998 \text{ mm}^2$ , which is about 49% times that (about  $2024 \text{ mm}^2$ ) for a regular rectangular microstrip patch (see Section 4.2.2.1).

The results show that the higher frequency  $f_2$  is almost unchanged for various slit positions and slit lengths, whereas the lower frequency  $f_1$  significantly decreases with increasing slit length. There exists a limiting slit length for each slit in order to have a  $50\text{-}\Omega$  feed position for the excitation of both operating modes. For  $d = 18$

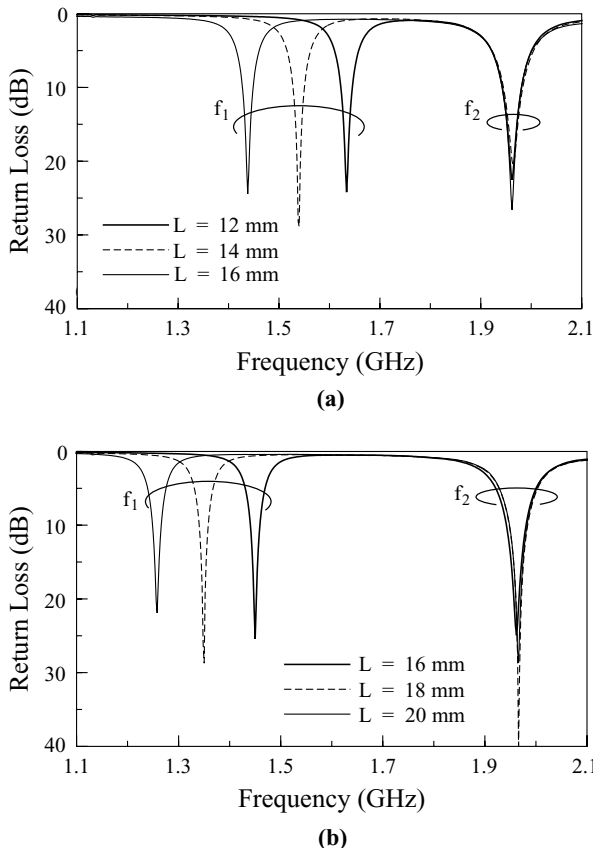


**FIGURE 4.73** Measured return loss against frequency for the antenna shown in Figure 4.72;  $\epsilon_r = 4.4$ ,  $h = 1.6$  mm,  $L = 48$  mm, and  $\overline{BC} = 2.6$  mm. (a)  $d = 18$  mm, (b)  $d = 16$  mm. (From Ref. 36, © 1998 John Wiley & Sons, Inc.)

**TABLE 4.22 Dual-Frequency Performance of the Antenna in Figure 4.72 [36]<sup>a</sup>**

$d, \ell$ (mm)	$d_p$ (mm)	$f_1$ , BW (MHz, %)	$f_2$ , BW (MHz, %)	$f_2/f_1$
18, 12	6.8	1634, 1.7	1962, 2.3	1.201
18, 14	4.3	1538, 1.7	1964, 2.2	1.277
18, 16	1.1	1438, 1.7	1962, 2.1	1.364
16, 16	6.0	1450, 1.4	1962, 2.1	1.353
16, 18	2.7	1350, 1.6	1962, 2.0	1.456
16, 20	1.3	1258, 1.6	1962, 1.9	1.563

<sup>a</sup>Antenna parameters are given in Figure 4.73.

and 16 mm, the limiting slit lengths are about 16 and 20 mm, respectively, where the  $50\text{-}\Omega$  feed position is almost at point  $D$ . When the slit length increases further, it becomes difficult for the present design to achieve a good matching condition for the two operating frequencies using a single probe feed.

## 4.5 DUAL-BAND OR TRIPLE-BAND PIFA

Owing to their compactness and possible wide bandwidth, planar inverted-F antennas (PIFAs) have been employed as internal dual-band antennas for cellular telephone handsets for GSM900/1800 systems. The basic design concept and an example for achieving dual-band operation are described in Section 3.2.1. Other interesting PIFA designs for dual-band operation have been discussed [37, 38]. Recently, a meandered planar inverted-F antenna with a single probe feed for achieving triple-frequency operation has been reported [39]. This triple-band planar inverted-F antenna is achieved by inserting two linear slits of different dimensions at opposite edges of the radiating patch and using two shorting strips for short-circuiting the radiating patch. By controlling the dimensions of the two inserted slits and using an antenna volume of  $40 \times 38 \times 9 \text{ mm}^3$  (air-filled substrate), it is reported that three operating frequencies at 900, 1900, and 2450 MHz can be obtained, although the obtained impedance bandwidth (10-dB return loss) is only about 4% for the three frequencies [39].

## 4.6 COMPACT DUAL-POLARIZED DESIGNS

This section describes the dual linearly polarized operation of a compact square microstrip antenna with a slotted radiating patch. It is demonstrated that such a slotted microstrip antenna with a group of four symmetrical bent slots can give excellent dual-polarized radiation [40], while the antenna size is significantly reduced for operating at a fixed frequency. Obtaining compact dual-polarized radiation by embedding suitable slots in the ground plane of a microstrip antenna is also discussed, and experimental results for a constructed prototype are presented. Finally, dual-polarized radiation for a triangular microstrip antenna excited by two probe feeds is shown. Experimental results obtained from a constructed prototype with an inexpensive FR4 substrate show that high isolation between the two feeding ports (less than  $-30 \text{ dB}$ ) can be obtained, and good dual linear polarization is achieved.

### 4.6.1 Design with a Slotted Square Patch

Geometries of compact dual-polarized square microstrip antennas with four bent slots parallel to the patch's central lines (denoted design A) and the patch's diagonals (design B) are shown, respectively, in Figures 4.74(a) and 4.74(b). The square patch has a side length  $L$ , and the four bent slots are of the same dimensions and have a narrow width of 1 mm. The two arms of each bent slot have the same length  $\ell$  and are perpendicular to each other. The spacing between two adjacent bent slots is

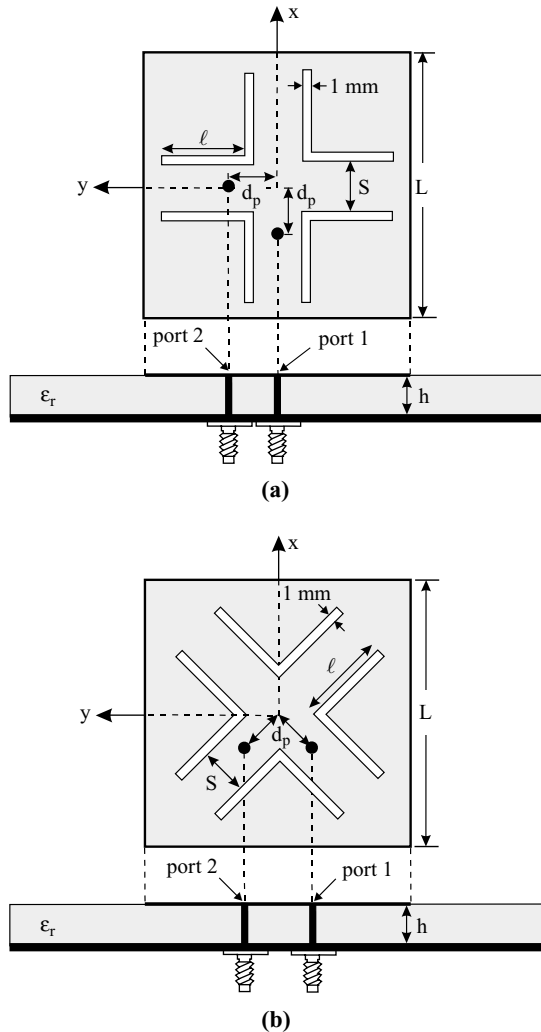


**FIGURE 4.74** Geometries of compact dual-polarized square microstrip antennas. (a) Design with bent slots in parallel with the patch's central line (design A), (b) design with bent slots in parallel with the patch's diagonals (design B). (From Ref. 40, © 2000 John Wiley & Sons, Inc.)

denoted  $S$ . The two probe feeds for the two feeding ports are located a distance of  $d_p$  from the patch center; the feed arrangement in design A excites  $0^\circ$  ( $\hat{x}$ -directed) and  $90^\circ$  ( $\hat{y}$ -directed) linearly polarized waves, whereas the feed arrangement in design B radiates  $\pm 45^\circ$  slanted linearly polarized waves.

For design A, three prototypes, antennas A1–A3, and a corresponding antenna without bent slots (reference A) were constructed and experimentally studied. Figure 4.75 presents the measured  $S_{11}$  and  $S_{21}$  against frequency. The side length of the square radiating patch was chosen to be 28.5 mm, and inexpensive FR4 microwave

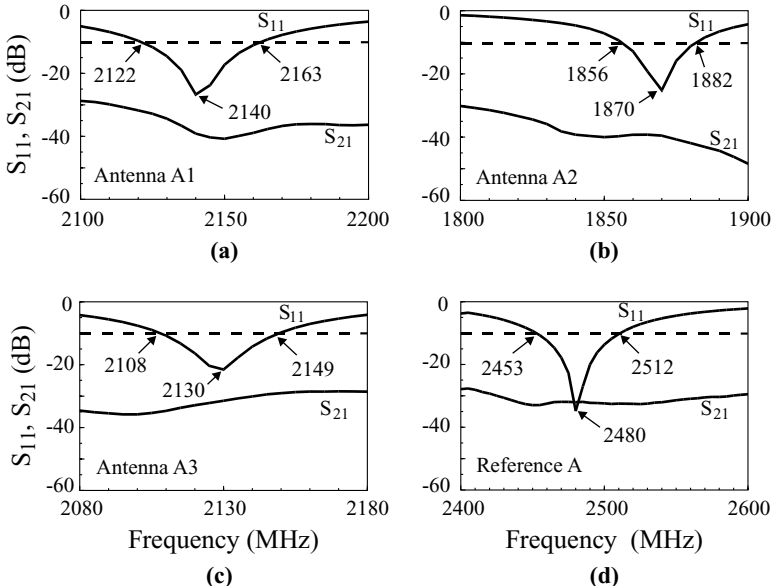


**FIGURE 4.75** Measured  $S_{11}$  and  $S_{21}$  against frequency for prototypes of design A shown in Figure 4.74;  $\epsilon_r = 4.4$ ,  $h = 1.6$  mm,  $L = 28.5$  mm,  $d_p = 5.8$  mm, and ground-plane size =  $60 \times 60$  mm<sup>2</sup>. (a) Antenna A1:  $\ell = 7.5$  mm,  $S = 5$  mm; (b) antenna A2:  $\ell = 10$  mm,  $S = 5$  mm; (c) antenna A3:  $\ell = 7.5$  mm,  $S = 3$  mm; (d) reference A:  $\ell = 0$ . (From Ref. 40, © 2000 John Wiley & Sons, Inc.)

substrates of thickness 1.6 mm and relative permittivity 4.4 were used. The parameters of the bent slots and obtained dual-polarized performance are given in Table 4.23. Note that the feed positions of antennas A1–A3 are all the same as that of reference A, and the obtained return loss  $S_{11}$  at the resonant frequency  $f_r$ , defined as the frequency with minimum  $S_{11}$  in the impedance bandwidth, is below  $-20$  dB. This suggests that the optimal feed position for achieving good impedance matching for the proposed compact dual-polarized microstrip antenna is insensitive to the bent slots introduced in the square patch. By comparing the resonant frequencies of antennas A1 and A2 to that of reference A, it is clearly seen that the obtained resonant frequencies are

**TABLE 4.23 Dual-Frequency Performance of the Antenna in Figure 4.74(a) [40]<sup>a</sup>**

	$\ell$ (mm)	$d_p$ (mm)	$S$ (mm)	$f_r$ (MHz)	BW (%)	$S_{21,\max}$ (dB)
Antenna A1	7.5	5.8	5.0	2140	1.9	-32.3
Antenna A2	10	5.8	5.0	1870	1.4	-39.2
Antenna A3	7.5	5.8	3.0	2130	1.9	-29.5
Reference A	0	5.8	—	2480	2.4	-31.9

<sup>a</sup>Antenna parameters are given in Figure 4.75.

greatly lowered with increasing length of the bent slots. For antenna A2, the resonant frequency (1870 MHz) is lowered by about 25% compared to that (2480 MHz) of reference A. This lowering in the resonant frequency corresponds to an antenna size reduction of about 44%. Furthermore, antenna A2 has an input isolation  $S_{21}$  less than  $-39.2$  dB across the obtained impedance bandwidth, which is better than that ( $-31.9$  dB) of reference A. This behavior suggests that improved input isolation can be obtained while resonant frequencies are significantly lowered for achieving compact operation.

Figure 4.76 shows the measured radiation patterns of antenna A2 and reference A for port 1 excitation at their corresponding resonant frequencies. The cross-polarization levels (XPLs) of antenna A2 in the  $E$  and  $H$  planes are both better than 20 dB, and the XPL in the broadside direction is about 23 dB, which is roughly as good as that of reference A. Comparison of antenna A3 to antenna A1 shows that the variation in the spacing between two adjacent bent slots has a small effect on the lowering of the resonant frequency; however, the obtained input isolation within the impedance bandwidth for antenna A3 is not as good as that of antenna A1 (maximum  $S_{21}$ :  $-29.5$  vs.  $-32.3$  dB).

Prototypes (antennas B1–B3) of design B were also constructed and studied. In this study, effects of small variations of the feed position on the obtained dual-polarized performance were investigated. The side lengths of the square radiating patch and

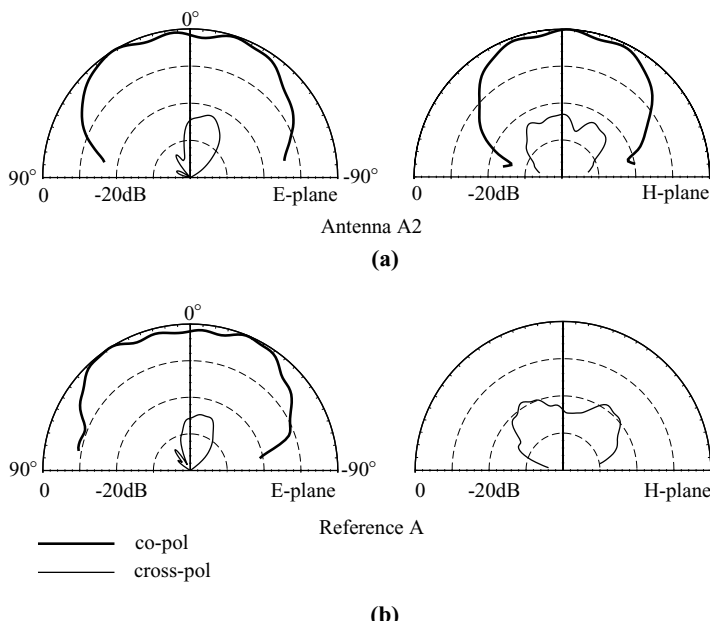


**FIGURE 4.76** Measured radiation patterns for port 1 excitation of antenna A2 and reference A studied in Figure 4.75. (a) Antenna A2 at 1870 MHz, (b) reference A at 2480 MHz. (From Ref. 40, © 2000 John Wiley & Sons, Inc.)

**TABLE 4.24 Dual-Frequency Performance of the Antenna in Figure 4.74(b) [40]<sup>a</sup>**

	$\ell$ (mm)	$d_p$ (mm)	$S$ (mm)	$f_r$ (MHz)	BW (%)	$S_{21,\max}$ (dB)
Antenna B1	10	5.6	7.0	2060	1.8	-26.7
Antenna B2	10	5.8	7.0	2075	1.8	-36.0
Antenna B3	10	6.0	7.0	2090	1.9	-25.7
Reference B	0	5.8	—	2480	2.5	-27.5

<sup>a</sup>Antenna parameters are given in Figure 4.77.

microwave substrate used were the same as those in the study of design A. The lengths of the bent slots and their spacings were fixed to be 10 and 7.0 mm, respectively. The experimental results are given in Table 4.24, and the measured  $S_{11}$  and  $S_{21}$  against frequency are presented in Figure 4.77. Results for the case without bent slots (reference B) are shown for comparison. It is observed that the variations of  $S_{11}$  are not sensitive to the movement of the feed position from  $d_p = 5.6$  mm (antenna B1) to 6.0 mm (antenna B3), and the resonant frequencies of antennas B1–B3 are about the same and are greatly reduced by about 16% compared to that (2480 MHz) of reference B. This lowering in the resonant frequency corresponds to about 30% reduction in

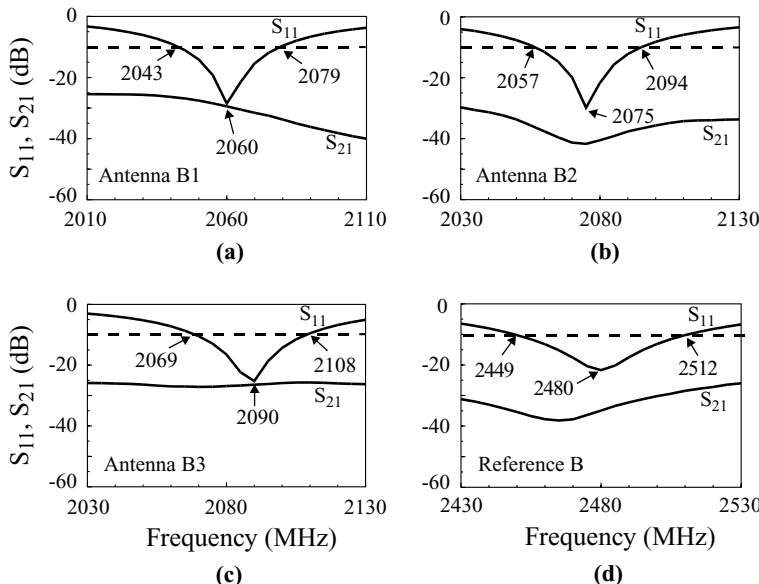


**FIGURE 4.77** Measured  $S_{11}$  and  $S_{21}$  against frequency for prototypes of design B shown in Figure 4.74;  $\epsilon_r = 4.4$ ,  $h = 1.6$  mm,  $L = 28.5$  mm, and ground-plane size =  $60 \times 60$  mm<sup>2</sup>. (a) Antenna B1:  $\ell = 10$  mm,  $S = 7$  mm,  $d_p = 5.6$  mm; (b) Antenna B2:  $\ell = 10$  mm,  $S = 7$  mm,  $d_p = 5.8$  mm; (c) antenna B3:  $\ell = 10$  mm,  $S = 7$  mm,  $d_p = 6.0$  mm; (d) reference B:  $\ell = 0$ ,  $d_p = 5.8$  mm. (From Ref. 40, © 2000 John Wiley & Sons, Inc.)

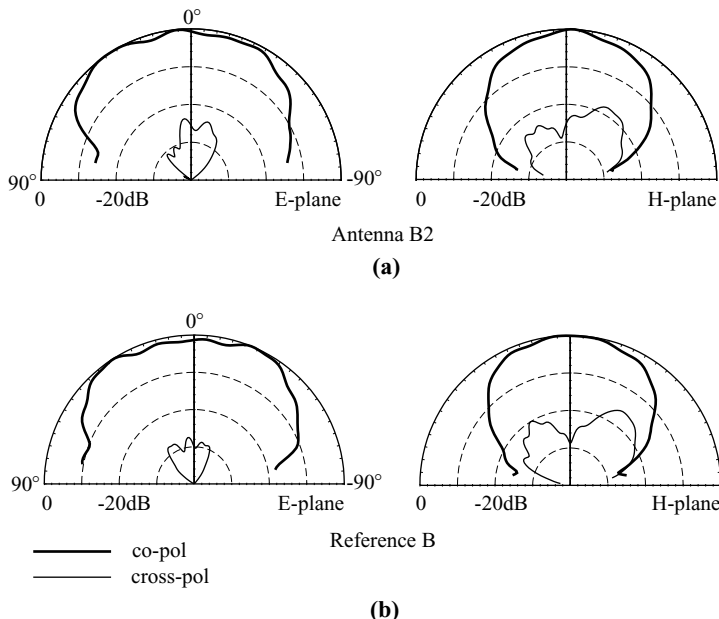


**FIGURE 4.78** Measured radiation patterns for port 1 excitation of antenna B2 and reference B studied in Figure 4.77. (a) Antenna B2 at 2075 MHz, (b) reference B at 2480 MHz. (From Ref. 40, © 2000 John Wiley & Sons, Inc.)

antenna size for the proposed antenna compared to the design with a corresponding unslotted antenna for fixed dual-polarized operation.

The trace of input isolation against frequency changes greatly with a small variation in the feed position. An improvement of 8.5 dB in the maximum  $S_{21}$  is seen for antenna B2 compared to that of reference B ( $-36.0$  vs.  $-27.5$  dB). This input isolation improvement is similar to that observed for the study of design A. This suggests that accurate determination of the feed position is important in achieving optimal input isolation for the proposed compact dual-polarized microstrip antenna. Figure 4.78 presents the radiation patterns of antenna B2 and reference B for port 1 excitation at their corresponding resonant frequencies. The results are similar to those observed for design A. Owing to the antenna size reduction, the antenna gain of the present compact dual-polarized antenna will be decreased compared to that of the corresponding unslotted microstrip antenna (references A and B). Comparing antenna A1 to reference A shows a lowering of antenna gain level by about 1.5 dBi.

#### 4.6.2 Design with a Slotted Ground Plane

The design shown in Figure 4.79 has been studied for achieving dual-polarized radiation for a microstrip antenna with a slotted ground plane [46]. In the design, two pairs of narrow slots of equal lengths are embedded in the ground plane of a regular

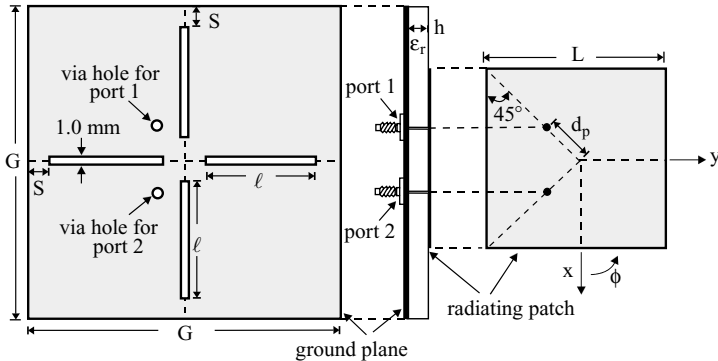


**FIGURE 4.79** Geometry of a compact dual-polarized microstrip antenna with a slotted ground plane. (From Ref. 46, © 2001 IEEE, reprinted with permission.)

microstrip antenna. The two pairs of narrow slots are placed along two centerlines ( $x$  axis and  $y$  axis in the figure) of the ground plane. Two probe feeds (ports 1 and 2) are placed along the diagonals of the radiating patch and are at a position  $d_p$  from the patch center. The present antenna radiates  $\pm 45^\circ$  slanted polarizations. A prototype of the antenna shown in Figure 4.79 with  $\ell = 20$  mm was constructed. The feed position was at  $d_p = 5.7$  mm. Measured  $S_{11}$  and  $S_{21}$  against frequency are presented in Figure 4.80. Note that the obtained impedance bandwidth is 70 MHz, or about 3.8% referenced to the resonant frequency at 1838 MHz. The resonant frequency is about the same as that obtained for the antenna with  $\ell = 20$  mm studied in Section 3.6 (1838 vs. 1835 MHz). This suggests that an antenna size reduction of about 39% for the present compact dual polarized microstrip antenna can be obtained compared to the regular dual-polarized microstrip antenna (no embedded slots in

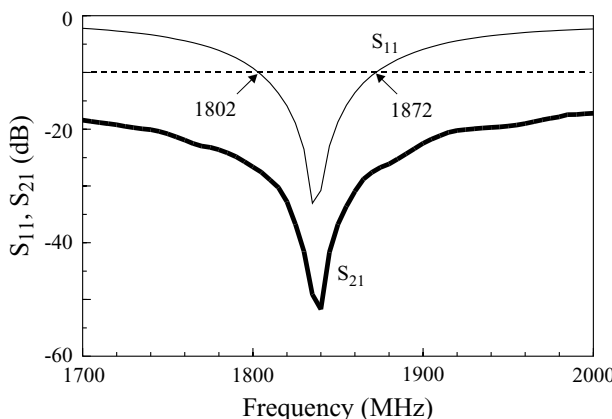


**FIGURE 4.80** Measured  $S_{11}$  and  $S_{21}$  against frequency for the antenna shown in Figure 4.79;  $\epsilon_r = 4.4$ ,  $h = 1.6$  mm,  $L = 30$  mm,  $G = 50$  mm,  $S = 2$  mm,  $\ell = 20$  mm, and  $d_p = 5.7$  mm. (From Ref. 46, © 2001 IEEE, reprinted with permission.)

the antenna's ground plane) at a fixed operating frequency. The obtained impedance bandwidth is greater than that studied in Section 3.6 (3.8% vs. 3.1%). This is probably because more slots are embedded in the ground plane, which results in a lower quality factor of the microstrip antenna. For the isolation ( $S_{21}$ ) between the two feeding ports, the measured isolation across the entire impedance bandwidth is less than  $-27$  dB, with the isolation at the resonant frequency only about  $-50$  dB. Good radiation characteristics for the present design have been observed, and the measured antenna gain is about  $4.5$  dBi, the same as for the antenna with  $\ell = 20$  mm studied in Section 3.6.

#### 4.6.3 Design with a Triangular Patch

To achieve dual-polarized radiation of a triangular microstrip antenna with highly decoupled feeding ports and low cross-polarization, the two feed positions for the dual linear polarizations need to be carefully determined. The selection of proper feed positions is described here. Figure 4.81 shows the antenna geometry. The triangular patch is equilateral and has a side length  $L$ . The feed position  $(x_1, y_1) = (0, y_1)$  of port 1 is placed along the centerline ( $y$  axis) of the patch for the excitation of the fundamental mode of  $\text{TM}_{10}$ , which has a polarization plane along the  $y-z$  plane in the figure. In order to excite a linearly polarized wave with its polarization plane orthogonal to the  $y-z$  plane and have good port decoupling, the possible feed position  $(x_2, y_2)$  of port 2 is between points  $A$  and  $B$  along the null-voltage locus for port 1 excitation. Points  $A$  and  $B$  are, respectively, the intersections of the null-voltage locus with the loci  $\ell_1$  and  $\ell_2$ , which represent the loci with  $50\text{-}\Omega$  input impedance for the excitation of a linearly polarized wave with its polarization plane  $-30^\circ$  and  $\pm 30^\circ$  slanted to the  $x-z$  plane, respectively. Note that, when high port decoupling is not considered, the optimal feed position should be at point  $C$ , the intersection of loci  $\ell_1$

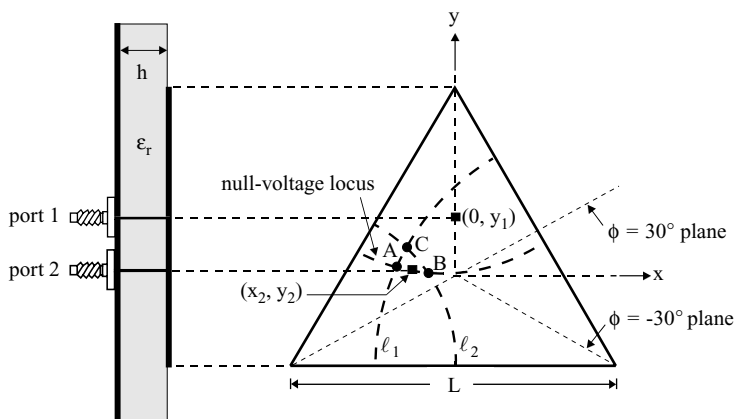


**FIGURE 4.81** Geometry of a dual-polarized equilateral-triangular microstrip antenna.

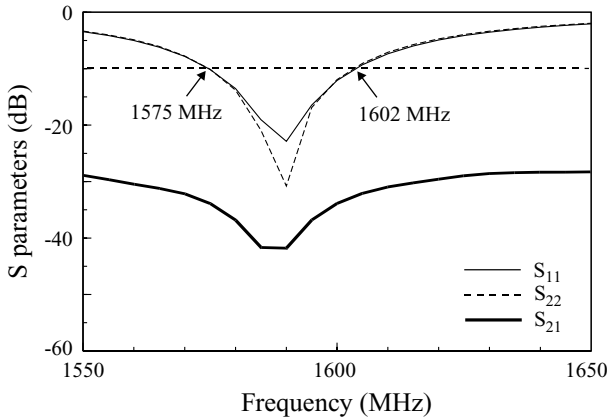


**FIGURE 4.82** Measured  $S$  parameters for the antenna shown in Figure 4.81;  $\epsilon_r = 4.4$ ,  $h = 1.6$  mm,  $L = 60$  mm,  $(x_1, y_1) = (0, 8.7$  mm),  $(x_2, y_2) = (-20.0, 1.5$  mm), and ground-plane size =  $75 \times 75$  mm $^2$ .

and  $\ell_2$ . In this case, good excitation of the resulting linearly polarized wave with its polarization plane along the  $x-z$  plane can be obtained. However, in dual-polarized radiation, high port decoupling is of major concern. For this consideration, the feed position for port 2 excitation is selected from the null-voltage locus between points  $A$  and  $B$ . It is experimentally found that, by moving the feed position along the null-voltage locus between points  $A$  and  $B$ , high port decoupling is obtained and there also exists a feed position with good impedance matching and capable of exciting a linearly polarized wave with its polarization plane along the  $x-z$  plane. In this case, two orthogonal linearly polarized waves with good radiation characteristics can be excited for the proposed antenna, and, moreover, highly decoupled feeding ports can be obtained.

Several prototypes of the dual-polarized design have been constructed. Figures 4.82 and 4.83 present, respectively, the measured  $S$  parameters and radiation patterns for the constructed prototype with  $L = 60$  mm. It is seen that both feeding ports have about the same impedance bandwidth (determined from 10-dB return loss), about 27 MHz, or 1.7% referenced to the resonant frequency at 1590 MHz. Also, across the impedance bandwidth, the measured isolation ( $S_{21}$ ) is below  $-32$  dB, with the isolation at the resonant frequency only about  $-43.5$  dB. Good radiation characteristics of the two orthogonal linearly polarized waves are obtained. The cross-polarization radiation in the principal planes of the two linear polarizations is less than  $-20$  dB. The antenna gain at the resonant frequency, 1590 MHz, is measured to be about 3.0 and 3.2 dBi, respectively, for the two linear polarizations; the gain variations across the respective impedance bandwidth are all less than 0.3 dBi. Results for prototype with  $L = 50$  mm are presented in Figure 4.84. The resonant frequency is about 1900 MHz, and the impedance bandwidths are about 37 MHz, or 1.9%, for both port 1 and port 2 excitation. The isolation across the respective impedance bandwidths of ports 1 and 2 is measured to be better than  $-31$  dB and the isolation

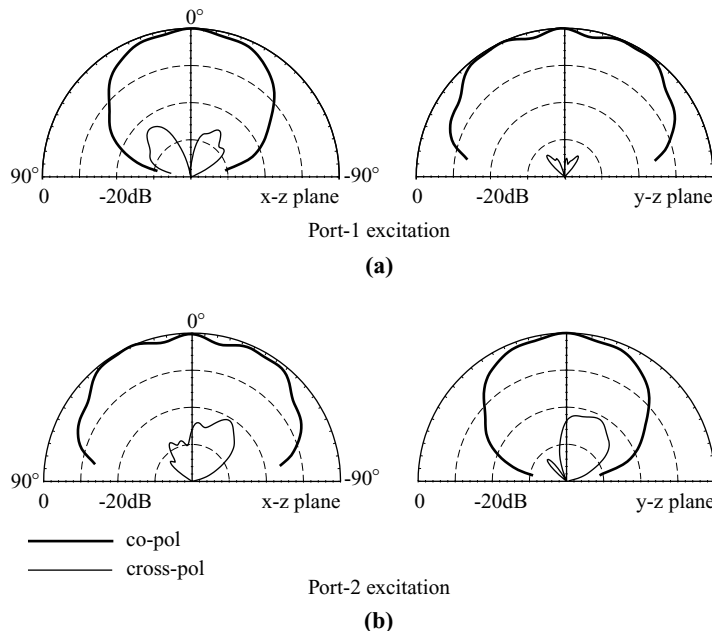


**FIGURE 4.83** Measured radiation patterns for the antenna studied in Figure 4.82;  $f = 1590$  MHz. (a) Port 1 excitation, (b) port 2 excitation.

at 1900 MHz is about  $-43$  dB. The cross-polarization radiation in the principal planes of the two linear polarizations is less than  $-20$  dB. The antenna gain for port 1 and port 2 excitation is measured to be about  $3.0$  dBi, and has small variations, less than about  $0.3$  dBi, for operating frequencies within the respective impedance bandwidth.

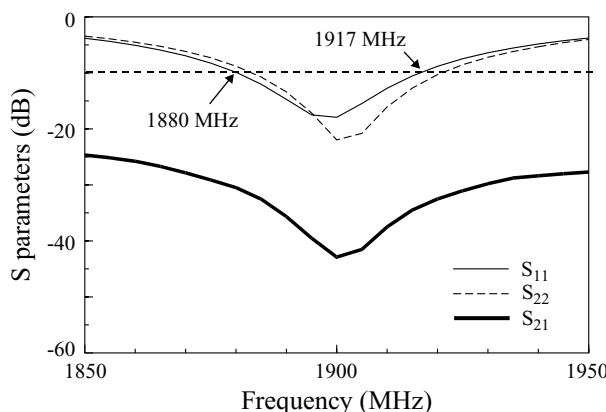


**FIGURE 4.84** Measured  $S$  parameters for the antenna shown in Figure 4.81;  $\epsilon_r = 4.4$ ,  $h = 1.6$  mm,  $L = 50$  mm,  $(x_1, y_1) = (0, 7.2$  mm),  $(x_2, y_2) = (-16.7, 1.2$  mm), and ground-plane size =  $75 \times 75$  mm $^2$ .

## REFERENCES

1. S. Maci and G. Biffi Gentili, "Dual-frequency patch antennas," *IEEE Antennas Propagat. Mag.* **39**, 13–20, Dec. 1997.
2. J. S. Dahele, K. F. Lee, and D. P. Wong, "Dual-frequency stacked annular-ring microstrip antennas," *IEEE Trans. Antennas Propagat.* **35**, 1281–1285, Nov. 1987.
3. S. A. Long and M. D. Walton, "A dual-frequency stacked circular-disk antenna," *IEEE Trans. Antennas Propagat.* **27**, 270–273, March 1979.
4. S. Maci, G. Biffi Gentili, P. Piazzesi, and C. Salvador, "Dual-band slot-loaded patch antenna," *IEE Proc. Microw. Antennas Propagat.* **142**, 225–232, June 1995.
5. H. Nakano and K. Vichien, "Dual-frequency square patch antenna with rectangular notch," *Electron. Lett.* **25**, 1067–1068, Aug. 3, 1989.
6. B. F. Wang and Y. T. Lo, "Microstrip antennas for dual-frequency operation," *IEEE Trans. Antennas Propagat.* **32**, 938–943, Sept. 1984.
7. Y. M. M. Antar, A. I. Ittipiboon, and A. K. Bhattacharyya, "A dual-frequency antenna using a single patch and an inclined slot," *Microwave Opt. Technol. Lett.* **8**, 309–311, April 20, 1995.
8. K. L. Wong and J. Y. Sze, "Dual-frequency slotted rectangular microstrip antenna," *Electron. Lett.* **34**, 1368–1370, July 9, 1998.
9. J. H. Lu, "Single-feed dual-frequency rectangular microstrip antenna with pair of step-slots," *Electron. Lett.* **35**, 354–355, March 4, 1999.
10. J. H. Lu and K. L. Wong, "Dual-frequency rectangular microstrip antenna with embedded spur lines and integrated reactive loading," *Microwave Opt. Technol. Lett.* **21**, 272–275, May 20, 1999.
11. K. L. Wong and K. B. Hsieh, "Dual-frequency circular microstrip antenna with a pair of arc-shaped slots," *Microwave Opt. Technol. Lett.* **19**, 410–412, Dec. 20, 1998.
12. K. B. Hsieh and K. L. Wong, "Inset-microstrip-line-fed dual-frequency circular microstrip antenna and its application to a two-element dual-frequency microstrip array," *IEE Proc. Microw. Antennas Propagat.* **147**, 359–361, Oct. 1999.
13. J. Y. Jan and K. L. Wong, "Single-feed dual-frequency circular microstrip antenna with an open-ring slot," *Microwave Opt. Technol. Lett.* **22**, 157–160, Aug. 5, 1999.
14. J. S. Chen and K. L. Wong, "A single-layer dual-frequency rectangular microstrip patch antenna using a single probe feed," *Microwave Opt. Technol. Lett.* **11**, 83–84, Feb. 5, 1996.
15. K. S. Kim, T. Kim, and J. Choi, "Dual-frequency aperture-coupled square patch antenna with double notches," *Microwave Opt. Technol. Lett.* **24**, 370–374, March 20, 2000.
16. C. C. Huang, Dual-frequency microstrip arrays with a dual-frequency feed network, M.S. thesis, Department of Electrical Engineering, National Sun Yat-Sen University, Kaohsiung, Taiwan, 2000.
17. J. H. Lu and K. L. Wong, "Slot-loaded, meandered rectangular microstrip antenna with compact dual-frequency operation," *Electron. Lett.* **34**, 1048–1050, May 28, 1998.
18. K. L. Wong and W. S. Chen, "Slot-loaded bow-tie microstrip antenna for dual-frequency operation," *Electron. Lett.* **34**, 1713–1714, Sept. 3, 1998.
19. K. L. Wong and W. S. Chen, "Compact microstrip antenna with dual-frequency operation," *Electron. Lett.* **33**, 646–647, April 10, 1997.
20. C. L. Tang, H. T. Chen, and K. L. Wong, "Small circular microstrip antenna with dual-frequency operation," *Electron. Lett.* **33**, 1112–1113, June 19, 1997.

21. S. C. Pan and K. L. Wong, "Dual-frequency triangular microstrip antenna with a shorting pin," *IEEE Trans. Antennas Propagat.* **45**, 1889–1891, Dec. 1997.
22. J. George, K. Vasudevan, P. Mohanan, and K. G. Nair, "Dual frequency miniature microstrip antenna," *Electron. Lett.* **34**, 1168–1170, June 11, 1998.
23. S. T. Fang and K. L. Wong, "A dual-frequency equilateral-triangular microstrip antenna with a pair of narrow slots," *Microwave Opt. Technol. Lett.* **23**, 82–84, Oct. 20, 1999.
24. J. H. Lu, C. L. Tang, and K. L. Wong, "Novel dual-frequency and broadband designs of single-feed slot-loaded equilateral-triangular microstrip antennas," *IEEE Trans. Antennas Propagat.* **48**, 1048–1054, July 2000.
25. J. H. Lu and K. L. Wong, "Dual-frequency equilateral-triangular microstrip antenna with a pair of spur lines," *Electron. Lett.* **34**, 1171–1173, June 11, 1998.
26. K. L. Wong, M. C. Pan, and W. H. Hsu, "Single-feed dual-frequency triangular microstrip antenna with a V-shaped slot," *Microwave Optical Technol. Lett.* **20**, 133–134, Jan. 20, 1999.
27. K. L. Wong and K. P. Yang, "Small dual-frequency microstrip antenna with cross slot," *Electron. Lett.* **33**, 1916–1917, Nov. 6, 1997.
28. K. P. Yang and K. L. Wong, "Inclined-slot-coupled compact dual-frequency microstrip antenna with cross-slot," *Electron. Lett.* **34**, 321–322, Feb. 19, 1998.
29. K. L. Wong and K. P. Yang, "Compact dual-frequency microstrip antenna with a pair of bent slots," *Electron. Lett.* **34**, 225–226, Feb. 5, 1998.
30. K. P. Yang, Studies of compact dual-frequency microstrip antennas, Ph.D. dissertation, Department of Electrical Engineering, National Sun Yat-Sen University, Kaohsiung, Taiwan, 1999.
31. W. S. Chen, "Single-feed dual-frequency rectangular microstrip antenna with square slot," *Electron. Lett.* **34**, 231–232, Feb. 5, 1998.
32. H. D. Chen, "A dual-frequency rectangular microstrip antenna with a circular slot," *Microwave Opt. Technol. Lett.* **18**, 130–132, June 5, 1998.
33. C. K. Wu, K. L. Wong, and W. S. Chen, "Slot-coupled meandered microstrip antenna for compact dual-frequency operation," *Electron. Lett.* **34**, 1047–1048, May 28, 1998.
34. K. L. Wong and S. T. Fang, "Reduced-size circular microstrip antenna with dual-frequency operation," *Microwave Opt. Technol. Lett.* **18**, 54–56, May 1998.
35. J. H. Lu and K. L. Wong, "Compact dual-frequency circular microstrip antenna with an offset circular slot," *Microwave Opt. Technol. Lett.* **22**, 254–256, Aug. 20, 1999.
36. K. L. Wong, S. T. Fang, and J. H. Lu, "Dual-frequency equilateral-triangular microstrip antenna with a slit," *Microwave Opt. Technol. Lett.* **19**, 348–350, Dec. 5, 1998.
37. Z. D. Liu, P. S. Hall, and D. Wake, "Dual-frequency planar inverted-F antenna," *IEEE Trans. Antennas Propagat.* **45**, 1451–1458, Oct. 1997.
38. C. R. Rowell and R. D. Murch, "A compact PIFA suitable for dual-frequency 900/1800-MHz operation," *IEEE Trans. Antennas Propagat.* **46**, 596–598, April 1998.
39. W. P. Dou and Y. W. M. Chia, "Novel meandered planar inverted-F antenna for triple-frequency operation," *Microwave Opt. Technol. Lett.* **27**, 58–60, Oct. 5, 2000.
40. G. S. Row, S. H. Yeh, and K. L. Wong, "Compact dual-polarized microstrip antennas," *Microwave Opt. Technol. Lett.* **27**, 284–287, Nov. 20, 2000.
41. E. Levine, G. Malamud, S. Shtrikman, and D. Treves, "A study of microstrip array antennas with the feed network," *IEEE Trans. Antennas Propagat.* **37**, 426–434, April 1989.

42. J. S. Chen, Studies of probe-fed and slot-coupled cylindrical microstrip antennas using cavity model theory, Ph.D. dissertation, Department of Electrical Engineering, National Sun Yat-Sen University, Kaohsiung, Taiwan, 1996.
43. J. R. James and G. Andrasic, "Superimposed dichroic microstrip antenna arrays," *IEE Proc. H* **135**, 304–312, Oct. 1988.
44. R. Pokuls, J. Uher, and D. M. Pozar, "Dual-frequency and dual-polarization microstrip antennas for SAR applications," *IEEE Trans. Antennas Propagat.* **46**, 1289–1296, Sept. 1998.
45. S. D. Targonski and D. M. Pozar, "Dual-band dual polarized printed antenna element," *Electron. Lett.* **34**, 2193–2194, Nov. 12, 1998.
46. T. W. Chiou and K. L. Wong, "Designs of compact microstrip antennas with a slotted ground plane," in *2001 IEEE Antennas Propagat. Soc. Int. Symp. Dig.*, pp. 732–735.

## CHAPTER FIVE

---

# Compact Circularly Polarized Microstrip Antennas

---

### 5.1 INTRODUCTION

The major advantage of single-feed, circularly polarized microstrip antennas is their simple structure, which does not require an external polarizer. They can, therefore, be realized more compactly by using less board space than do dual-feed, circularly polarized microstrip antennas. Many designs of single-feed, circularly polarized microstrip antennas with square or circular patches are known [1]. Recently, various CP designs with a compact patch size at a fixed operating frequency have been reported. In these designs, the compact CP techniques used include embedding a cross-slot of unequal arm lengths [2, 3], embedding a Y-shaped slot of unequal arm lengths [4], inserting slits or spur lines at the patch boundary [5–13], truncating patch corners or tips [14–17], introducing small peripheral cuts at the boundary of a circular patch [18], adding a tuning stub [19–21] or a bent tuning stub [22], among others. For feeding these compact CP designs, a probe feed or an edge-fed microstrip-line feed can be used. Prototypes of these designs are presented and discussed in this chapter. A compact CP design using a  $50\text{-}\Omega$  inset microstrip-line feed is also discussed. In this case, the main problem to be solved arises from the perturbation effects caused by the inset microstrip line on the excited patch surface currents, which makes it difficult for the excitation of two orthogonal near-degenerate resonant modes for CP radiation. Several possible designs for solving this problem have been reported [23], and details of the designs applied to a corner-truncated square microstrip antenna are presented.

### 5.2 DESIGNS WITH A CROSS-SLOT OF UNEQUAL ARM LENGTHS

Figure 5.1 shows the geometry of a compact circularly polarized microstrip antenna with a cross-slot of unequal arm lengths. By incorporating a probe feed at  $45^\circ$  to

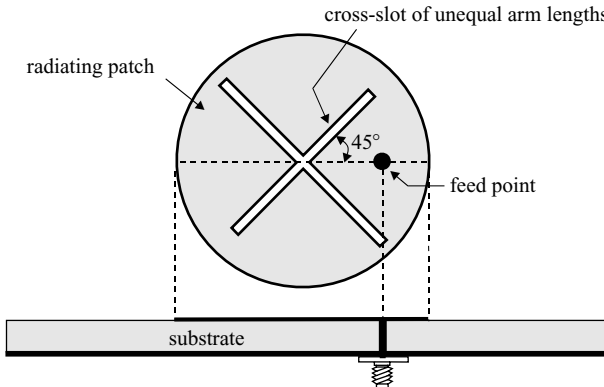


**FIGURE 5.1** Geometry of a compact circularly polarized circular microstrip antenna with a cross-slot of unequal arm lengths.

the two arms of the cross-slot as shown in the figure or using a proximity coupled feed [2], it has been found that CP radiation can be obtained at frequencies much lower than the fundamental resonant frequency of the antenna without a cross-slot. That is, for a fixed operating frequency, the antenna shown in Figure 5.1 can be used for CP radiation with a smaller antenna size than a regular microstrip antenna without a cross-slot.

This compact CP design technique has been successfully applied to triangular microstrip antennas [3]. Since the triangular microstrip antenna has the advantage of being smaller at a fixed operating frequency than square or circular microstrip antennas [24], the present study using a triangular patch is of interest for achieving a more compact circularly polarized microstrip antenna. For comparison, both regular-size and compact CP operations of triangular microstrip antennas are studied in this section. Compact CP operation is defined here as the circularly polarized radiation of a reduced-size or compact triangular microstrip antenna. Conversely, regular-size CP operation refers to the circularly polarized radiation of triangular microstrip antennas without a reduction of antenna size at a fixed operating frequency. Figure 5.2(a) shows a promising regular-size CP design for a triangular microstrip antenna with an embedded narrow horizontal slot. By using a cross-slot of unequal arm lengths [see Figure 5.2(b)] in place of the embedded horizontal slot, the circularly polarized radiation of the slotted triangular microstrip antenna occurs at a lower operating frequency. This implies that an even smaller antenna size for a fixed CP operation can be achieved if one uses the present compact circularly polarized triangular microstrip antenna with a cross-slot in place of conventional CP designs of square or circular microstrip antennas [1].

For the regular-size CP designs in Figure 5.2(a), a narrow slot of dimensions  $\ell \times 1$  mm is embedded in the patch, with the slot oriented parallel to the bottom of the triangular patch and the slot center at the null-voltage point of the fundamental  $TM_{10}$  mode of the simple triangular microstrip antenna without a slot. It is then expected that, due to the slot perturbation, the equivalent excited patch surface current path of the

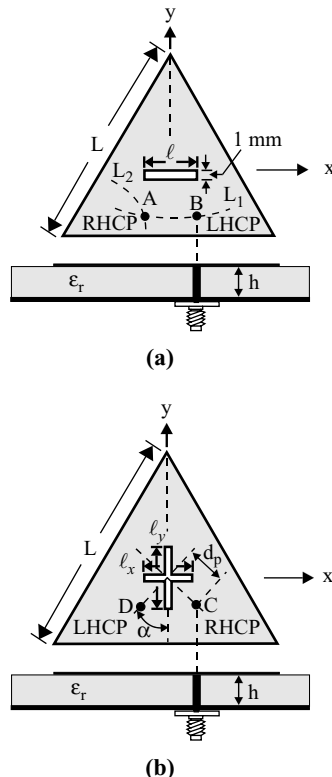


**FIGURE 5.2** Geometries of circularly polarized triangular microstrip antennas with (a) a horizontal narrow slot and (b) a cross-slot of unequal arm lengths. (From Ref. 3, © 1999 IEEE, reprinted with permission.)

TM<sub>10</sub> mode along the direction perpendicular to the narrow slot is lengthened while the one parallel to the slot orientation is only slightly affected. This behavior results in the splitting of the TM<sub>10</sub> mode into two near-degenerate orthogonal resonant modes. By further selecting the proper slot length and feeding the patch at a suitable position, the two near-degenerate orthogonal resonant modes can have equal amplitudes and a 90° phase difference, and CP operation can thus be obtained. Referring to the geometry in Figure 5.2(b), the feed position can be determined from the 50- $\Omega$  feed-location loci  $L_1$  and  $L_2$  of the two orthogonal modes, which are determined experimentally in this study. For the feed position at point A, which is the intersection of loci  $L_1$  and  $L_2$  and is usually located in the left half of the triangular patch, right-hand CP operation with a good matching condition is obtained. Left-hand CP operation is obtained by feeding the patch at point B (the mirror image of point A with respect to the centerline of the triangular patch).

The antenna shown in Figure 5.2(b) is designed for compact CP operation. A cross-slot of unequal arm lengths is embedded in the triangular patch and centered at the

null-voltage position for the  $\text{TM}_{10}$  mode of the simple triangular microstrip antenna. It is found that, due to the additional slot perturbation for the horizontal patch surface current path compared to the design in Figure 5.2(a), the surface current paths of the two orthogonal resonant modes are lengthened, which lowers their corresponding resonant frequencies. By adjusting the cross-slot to have unequal arm lengths  $\ell_x$  and  $\ell_y$  and feeding the patch at a position along the lines inclined to the  $y$  axis with an angle of  $\alpha = \tan^{-1}(\ell_x/\ell_y)$  [see Figure 5.2(b)], the two orthogonal resonant modes have equal amplitudes and a  $90^\circ$  phase difference, and compact CP operation is achieved. The feed position at point  $C$  shown in the figure (with  $\ell_y > \ell_x$ ) is for right-hand CP operation and point  $D$  is for left-hand CP operation. The distance between the feed position and the slot center is denoted  $d_p$ .

Several prototypes of the CP designs shown in Figure 5.2 have been implemented. Experimental results for a typical case with right-hand CP operation are presented in Figure 5.3, where the measured input impedance is shown. Note that, without the presence of a slot, the fundamental resonant frequency  $f_{10}$  of the triangular microstrip antenna studied here is about 1.9 GHz. The results show a dip in the impedance locus near 1.9 GHz, which indicates that two resonant modes are excited at very close frequencies (if the two modes are excited at frequencies far apart, a loop instead of a dip will be observed in the impedance locus; and if only one resonant mode is excited, there will be no dip in the impedance locus). This suggests that the fundamental  $\text{TM}_{10}$  mode in the present design is split into two near-degenerate resonant modes. It is also found that, when the slot length is adjusted to be about 0.25 times the side length of the triangular patch (11.9 mm for the antenna with a side length of 48 mm studied here), these two resonant modes can be excited

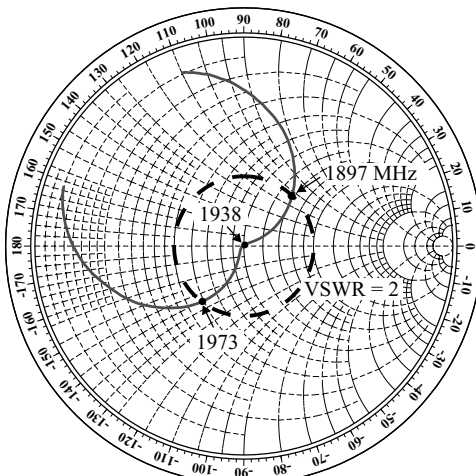


**FIGURE 5.3** Measured input impedance for the antenna shown in Figure 5.2(a) with feed at point  $A$ ;  $\varepsilon_r = 4.4$ ,  $h = 1.6$  mm,  $L = 48$  mm,  $\ell = 11.9$  mm, and  $(x_p, y_p) = (-6.0, -8.5$  mm). (From Ref. 3, © 1999 IEEE, reprinted with permission.)

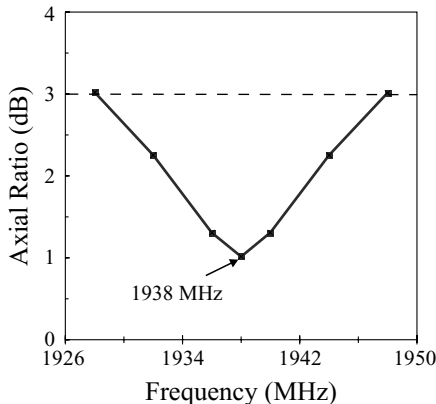


**FIGURE 5.4** Measured axial ratio in the broadside direction for the antenna studied in Figure 5.3. (From Ref. 3, © 1999 IEEE, reprinted with permission.)

with equal amplitudes and a  $90^\circ$  phase difference, resulting in CP radiation. The measured axial ratio in the broadside direction is presented in Figure 5.4. It is observed that the CP bandwidth, determined from the 3-dB axial ratio, is 18 MHz, or about 0.93% with respect to the center frequency (1938 MHz), defined here to be the frequency with minimum axial ratio in the impedance bandwidth. The measured radiation patterns of the present design in two orthogonal planes at the center frequency are plotted in Figure 5.5, and good right-hand CP radiation is observed.

A compact CP design with a cross-slot of various slot lengths was implemented and studied. The feed position is selected at point *C* for achieving right-hand CP operation. Figure 5.6 shows the measured input impedance of an antenna with different cross-slot sizes. The antenna parameters are the same as used in Figure 5.3, and antennas 1–3 shown denote designs with different cross-slot sizes. It is found that, by properly adjusting the slot lengths, two near-degenerate orthogonal resonant modes with equal amplitudes and a  $90^\circ$  phase difference for CP operation are excited. The measured

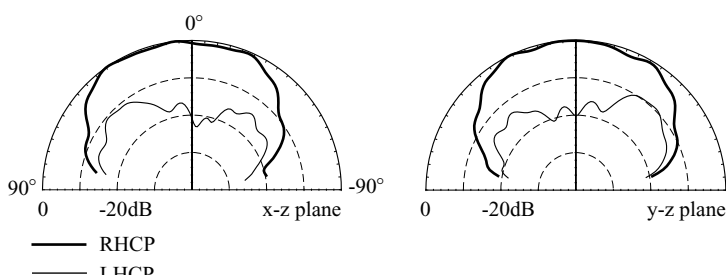


**FIGURE 5.5** Measured radiation patterns at 1938 MHz for the antenna studied in Figure 5.3. (From Ref. 3, © 1999 IEEE, reprinted with permission.)

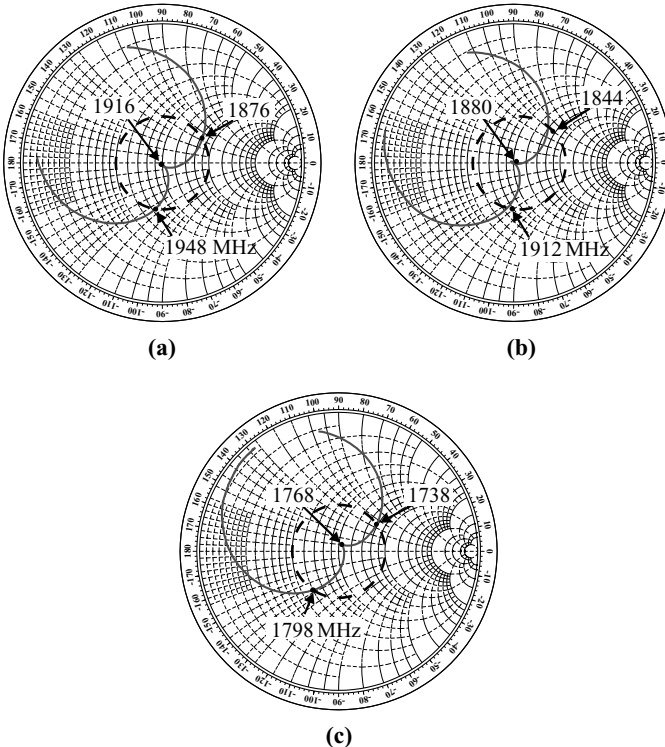


**FIGURE 5.6** Measured input impedance for the antenna shown in Figure 5.2(b) with different cross-slot sizes;  $\epsilon_r = 4.4$ ,  $h = 1.6$  mm,  $L = 48$  mm, and feed at point  $C$ . (a) Antenna 1:  $(\ell_x, \ell_y) = (6.5, 10.4$  mm),  $d_p = 9$  mm; (b) antenna 2:  $(\ell_x, \ell_y) = (11, 14$  mm),  $d_p = 7.5$  mm; (c) antenna 3:  $(\ell_x, \ell_y) = (17.8, 18$  mm),  $d_p = 1.5$  mm. (From Ref. 3, © 1999 IEEE, reprinted with permission.)

axial ratio in the broadside direction is presented in Figure 5.7, and the corresponding CP performance is listed in Table 5.1. The results show that the center frequency for CP operation decreases with increasing cross-slot size, which is as expected. For antenna 3, the center frequency  $f_c$  is decreased to 1768 MHz, which is about 0.91 times that (1938 MHz) of the regular-size CP design. This lowering of the center operating frequency corresponds to an antenna size reduction of about 17%. Note that, with increasing cross-slot size, the feed position needs to be moved closer to the slot center. This limits the use of a larger cross slot for achieving an even greater antenna size reduction using a probe feed.

The CP bandwidth of antenna 3 is about the same as that obtained for the regular-size CP design in Figure 5.4, although the electrical thickness of the substrate of antenna 3 is smaller, due to the lowering of the center operating frequency. For antennas 1 and 2, the CP bandwidths are even greater than that of the regular-size CP design. This is probably because in this particular case, the use of a cross slot more easily generates two orthogonal polarizations than the case with a single narrow slot;

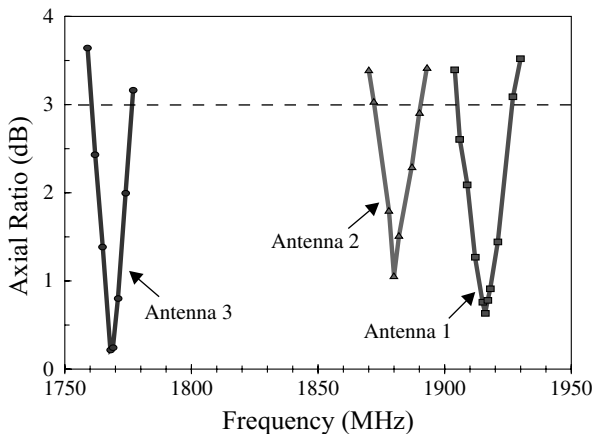


**FIGURE 5.7** Measured axial ratio in the broadside direction for the antennas studied in Figure 5.6. (From Ref. 3, © 1999 IEEE, reprinted with permission.)

thus, wider CP bandwidths for antennas 1 and 2 result. Figure 5.8 shows measured radiation patterns of compact CP designs in two orthogonal planes; good right-hand CP operation is seen.

### 5.3 DESIGNS WITH A Y-SHAPED SLOT OF UNEQUAL ARM LENGTHS

A new design for compact triangular microstrip antennas with a Y-shaped slot for CP radiation has been reported [4]. The Y-shaped slot is centered in the triangular patch, with its upper two arms facing either the triangle tip or the bottom of the triangular patch [see Figures 5.9(a) and 5.9(b)]. It is expected that, due to the presence of the Y-shaped slot in the patch, the excited patch surface current path is lengthened and thus the resonant frequency of the microstrip patch is reduced. Furthermore, it is found that, by selecting a proper size of the Y-shaped slot, two near-degenerate orthogonal modes with equal amplitudes and a  $90^\circ$  phase difference for CP operation can be excited using a single probe feed; that is, compact CP operation of triangular microstrip antennas can be obtained.

**TABLE 5.1** CP Performance of the Compact Circularly Polarized Equilateral-Triangular Microstrip Antenna in Figure 5.2(b) [3]<sup>a</sup>

	$\ell_x, \ell_y,$ (mm)	$d_p$ (mm)	$f_c$ (MHz)	3-dB Axial-Ratio CP Bandwidth (MHz, %)
Antenna 1	6.5, 10.4	9.0	1916	22, 1.2
Antenna 2	11, 14	7.5	1880	19, 1.0
Antenna 3	17.8, 18	1.5	1768	16, 0.9

<sup>a</sup>Antenna parameters are given in Figure 5.6.

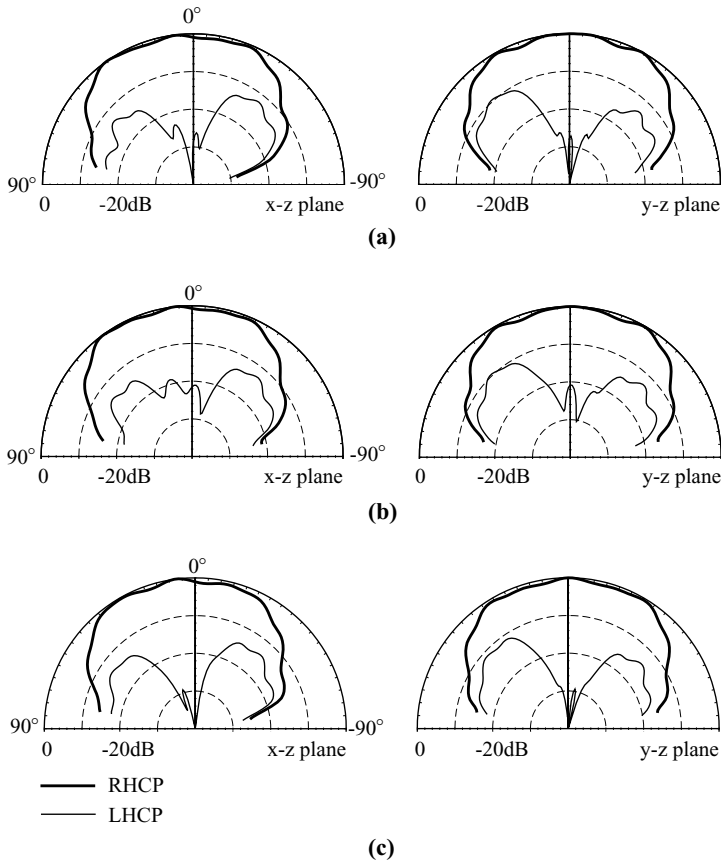


**FIGURE 5.8** Measured radiation patterns for the antennas studied in Figure 5.6. (a) Antenna 1 at 1916 MHz, (b) antenna 2 at 1880 MHz, (c) antenna 3 at 1768 MHz. (From Ref. 3, © 1999 IEEE, reprinted with permission.)

As shown in Figure 5.9, the upper two arms of the Y-shaped slot are of equal length  $y_a$  and its lower arm has a smaller length  $y_b$  ( $y_a > y_b$ ). By choosing proper arm lengths ( $y_a, y_b$ ) of the Y-shaped slot and placing a single probe feed at the edge of its lower arm, compact CP operation of the triangular microstrip antenna can be obtained. The feed positions at points *A* and *B* in the figure, both a distance  $y_p$  from the patch center, are for right-hand and left-hand CP operations, respectively. The case with right-hand CP operation is studied here; that is, the probe feed is placed at point *A*. Figures 5.10(a) and 5.10(b) show, respectively, the measured input impedance for the designs of Figure 5.9(a) (antenna 1) and Figure 5.9(b) (antenna 2); the measured axial ratio is presented in Figures 5.11(a) and 5.11(b). The corresponding results are listed in Table 5.2. For the design of antenna 1 with  $y_a = 8.4$  mm and  $y_b = 7.6$  mm, a single probe feed with  $y_p = 4.3$  mm along the edge of the lower arm of the Y-shaped slot splits the fundamental resonant mode of the slotted triangular patch into two near-degenerate

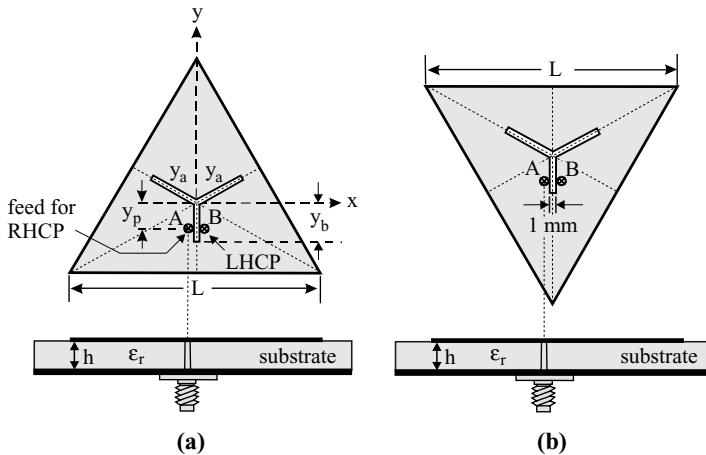


**FIGURE 5.9** Geometries of compact circularly polarized quilateral-triangular microstrip antennas. (a) The Y-shaped slot facing the triangle tip (antenna 1), (b) the Y-shaped slot facing the bottom side of the triangular patch (antenna 2). (From Ref. 4, © 1999 John Wiley & Sons, Inc.)

orthogonal modes for CP operation at a center frequency  $f_c$  of 2108 MHz, which is about 10% lower than that (2347 MHz) of the design using a regular-size circularly polarized triangular microstrip antenna [6]. This suggests that the present design can have an antenna size reduction of about 19% compared to that of the regular-size CP design at a fixed operating frequency. The 3-dB axial-ratio CP bandwidth is also seen to decrease from 1.1% to 0.9% due to the antenna size reduction.

For the design of antenna 2, the center frequency is lowered to 2174 MHz (about 92.7% times that of the regular-size CP design [6]). In this case, an antenna size

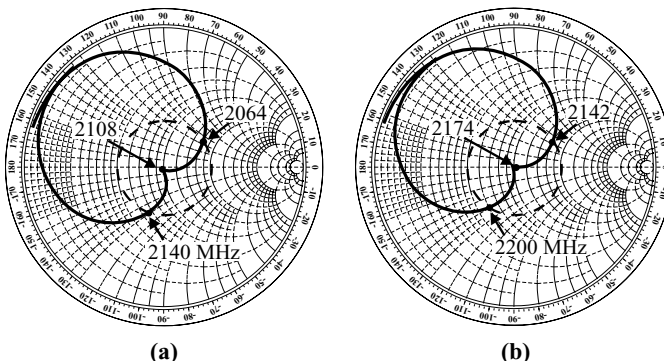


**FIGURE 5.10** Measured input impedance for the antennas shown in Figure 5.9;  $\epsilon_r = 4.4$ ,  $h = 1.6$  mm,  $L = 40$  mm, and feed at point A. (a) Antenna 1:  $y_a = 8.4$  mm,  $y_b = 7.6$  mm,  $y_p = 4.3$  mm; (b) antenna 2:  $y_a = 9.4$  mm,  $y_b = 7.6$  mm,  $y_p = 4.0$  mm. (From Ref. 4, © 1999 John Wiley & Sons, Inc.)

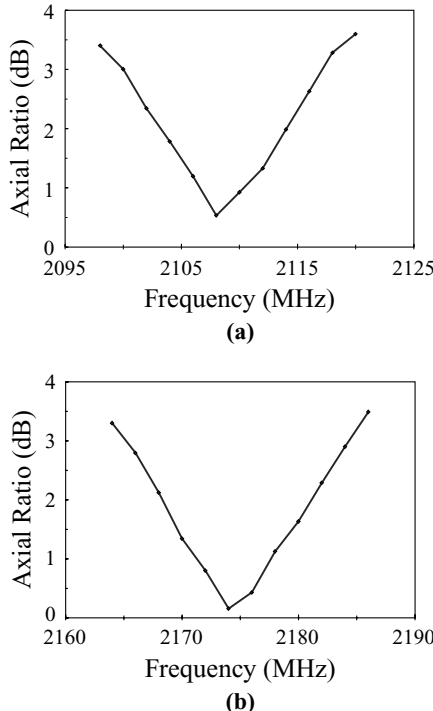


**FIGURE 5.11** Measured axial ratio in the broadside direction for the antennas studied in Figure 5.10. (a) Antenna 1, (b) antenna 2. (From Ref. 4, © 1999 John Wiley & Sons, Inc.)

reduction of about 14% for the present design at a fixed operating frequency is obtained. The CP bandwidth is also smaller (0.8% vs. 1.1%) due to the antenna size reduction. Typical measured radiation patterns in two orthogonal planes for antennas 1 and 2 are plotted in Figures 5.12(a) and 5.12(b), respectively. It can be seen that good right-hand CP radiation is obtained.

**TABLE 5.2 CP Performance of the Antennas in Figures 5.9(a) and 5.9(b) [4]<sup>a</sup>**

	Slot Size $y_a, y_b$ (mm)	$y_p$ (mm)	$f_c$ (MHz)	3-dB Axial-Ratio CP Bandwidth (%)
Antenna 1	8.4, 7.6	4.3	2108	0.9
Antenna 2	9.4, 7.6	4.0	2174	0.8
Reference	—	—	2347	1.1

<sup>a</sup>Antenna parameters are given in Figure 5.10. The reference antenna is constructed based on the regular-size CP design of a triangular microstrip antenna with a slit (see Section 5.4.1.2).

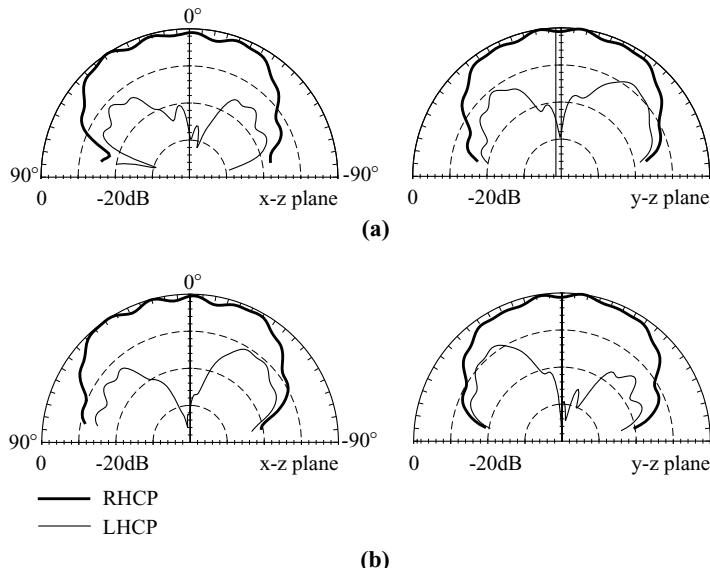


**FIGURE 5.12** Measured radiation patterns for the antennas studied in Figure 5.10. (a) Antenna 1 at 2108 MHz, (b) antenna 2 at 2174 MHz. (From Ref. 4, © 1999 John Wiley & Sons, Inc.)

## 5.4 DESIGNS WITH SLITS

By inserting a single slit to the boundary of a microstrip patch and placing a single feed along an axis  $45^\circ$  to the one containing the slit, CP radiation of microstrip antennas can be achieved [5, 6]. Applications of this CP design technique to square and circular microstrip antennas are discussed in Section 5.4.1. This CP design technique has also been successfully applied to a triangular microstrip antenna [6], and details of the results are also described here. Related CP design techniques using a pair of slits [7] or four inserted slits [8–11] for compact CP radiation are discussed in Sections 5.4.2 and 5.4.3, respectively. For the case of a pair of slits, CP radiation of an annular-ring microstrip antenna operated at the  $\text{TM}_{11}$  mode has been achieved. Good CP performance is obtained and the required antenna size at a fixed operating frequency is much less than that of a regular circularly polarized circular microstrip antenna operated in the  $\text{TM}_{11}$  mode. In the case of four inserted slits, design examples of microstrip antennas with a square patch [8], a circular patch [9], a corner-truncated square patch [10], and a chip-resistor-loaded square patch [11] have been demonstrated.

### 5.4.1 With a Slit

**5.4.1.1 With a Square or Circular Patch** Figure 5.13 shows the geometries of square and circular microstrip antennas with a slit for CP radiation. A narrow slit of length  $\ell$  and width 1 mm is inserted at the boundary of the microstrip patch. The square patch has a side length  $L$  and the diameter of the circular patch is  $d$ . For both the square and circular patches, the feed at point  $C$  along the diagonal/diameter  $\overline{AB}$

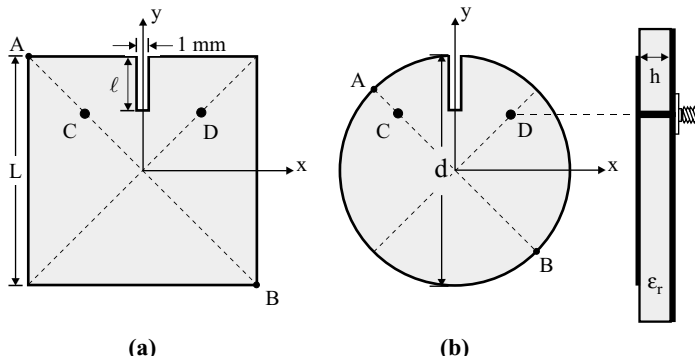


**FIGURE 5.13** Geometries of microstrip antennas with a slit for CP radiation; the feed at point *C* is for right-hand CP and the feed at point *D* is for left-hand CP. (a) Square patch case, (b) circular patch case. (From Ref. 5, © 1998 John Wiley & Sons, Inc.)

is for right-hand CP operation, while point *D* is for left-hand CP operation. Due to the slit perturbation, the excited  $\hat{x}$ -directed (orthogonal to the slit orientation) patch surface current path is lengthened, with the one in the  $y$  direction (parallel to the slit orientation) slightly affected, which splits the dominant resonant mode of the microstrip patch into two orthogonal near-degenerate modes. Then, given a proper slit length (about 0.15 times the side length  $L$  of the square patch or about 0.18 times the diameter  $d$  of the circular patch for the experiments conducted here), these two orthogonal modes can have a  $90^\circ$  phase difference, resulting in CP radiation.

Several prototypes have been constructed. Figure 5.14 shows the measured input impedance for a square microstrip antenna with a slit. The case with right-hand

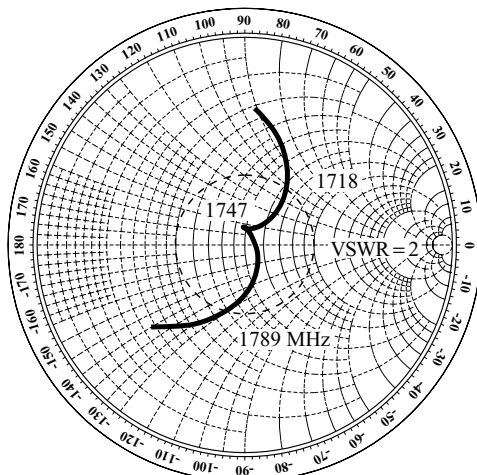


**FIGURE 5.14** Measured input impedance for a square microstrip antenna with a slit [Figure 5.13(a)] for right-hand CP operation;  $\epsilon_r = 4.4$ ,  $h = 1.6$  mm,  $L = 39.7$  mm,  $\ell = 6$  mm, and  $AC = 17$  mm ( $\cong 0.30\overline{AB}$ ). (From Ref. 5, © 1998 John Wiley & Sons, Inc.)

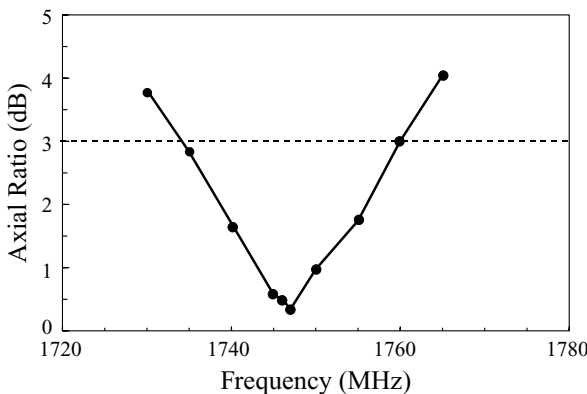


**FIGURE 5.15** Measured axial ratio for the square microstrip antenna studied in Figure 5.14. (From Ref. 5, © 1998 John Wiley & Sons, Inc.)

CP operation (i.e., the feed at point *C*) is shown. To achieve CP radiation, the slit length is adjusted to be 6 mm (about  $0.15L$ ) and the feed (point *C*) is at a position about  $0.3\overline{AB}$  from the patch corner. The measured axial ratio is presented in Figure 5.15. The results give the CP bandwidth, determined from the 3-dB axial ratio, as 25 MHz (or about 1.4% with respect to the center frequency, the frequency with a minimum axial ratio). The measured radiation patterns in the *x*-*z* and *y*-*z* planes at the center frequency (1747 MHz) are plotted in Figure 5.16. Good right-hand CP radiation is observed. The results for a circular microstrip antenna with a slit are shown in Figures 5.17 and 5.18. For right-hand CP radiation, by adjusting the slit length to be 7.7 mm (about  $0.18d$ ) and the feed at about  $0.25\overline{AB}$  from the boundary of the circular patch, CP radiation with good impedance matching is obtained. From the measured axial ratio shown in Figure 5.17, a 32 MHz (about 1.7%) CP bandwidth is obtained. The measured radiation patterns in two orthogonal planes plotted in Figure 5.18 at the center frequency (1875 MHz) show good right-hand CP radiation.

**5.4.1.2 With a Triangular Patch** The present CP design has been applied to a triangular microstrip antenna [6]. The antenna geometry is shown in Figure 5.19. In

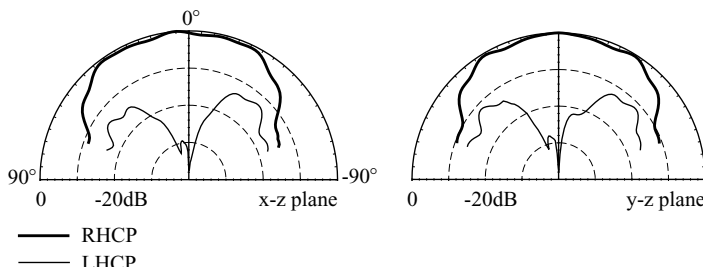


**FIGURE 5.16** Measured radiation patterns for the antenna studied in Figure 5.14 at 1747 MHz. (From Ref. 5, © 1998 John Wiley & Sons, Inc.)

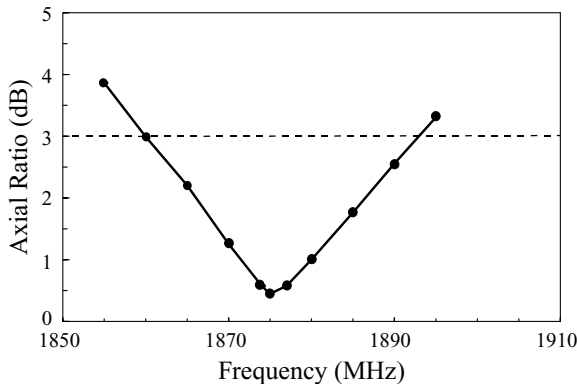


**FIGURE 5.17** Measured axial ratio for a circular microstrip antenna with a slit [Figure 5.13(b)] for right-hand CP operation;  $\epsilon_r = 4.4$ ,  $h = 1.6$  mm,  $d = 43$  mm,  $\ell = 7.75$  mm, and  $AC = 10.64$  mm ( $\cong 0.25AB$ ). (From Ref. 5, © 1998 John Wiley & Sons, Inc.)

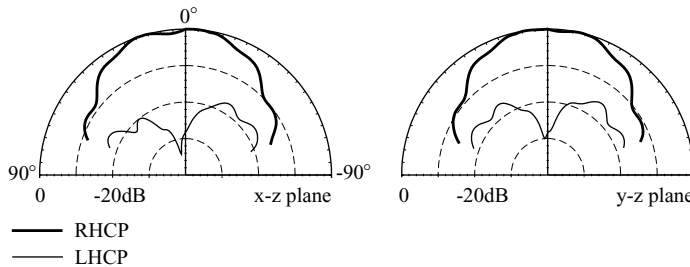


**FIGURE 5.18** Measured radiation patterns for the antenna studied in Figure 5.17 at 1875 MHz. (From Ref. 5, © 1998 John Wiley & Sons, Inc.)

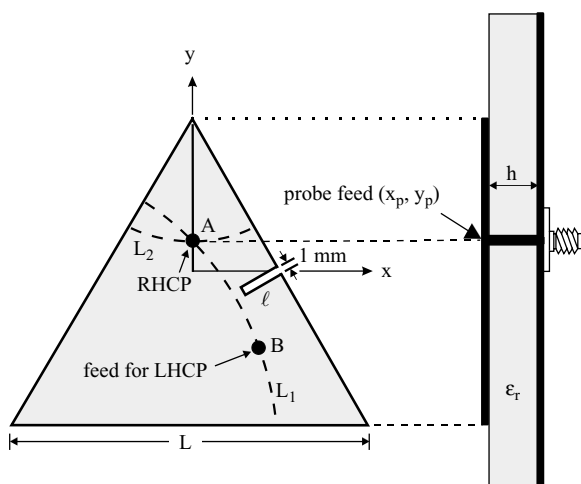


**FIGURE 5.19** Geometry of a single-feed triangular microstrip antenna with a single slit for CP radiation. (From Ref. 6, © 1998 IEE, reprinted with permission.)

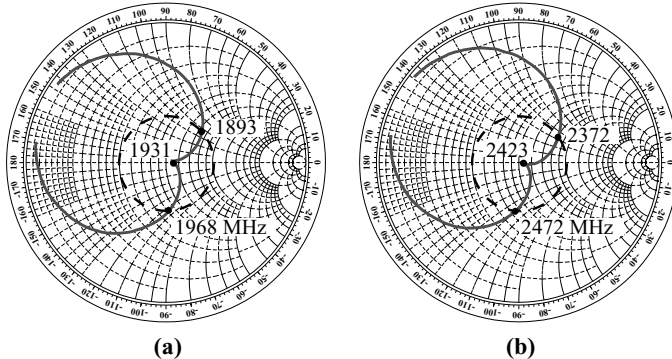


**FIGURE 5.20** Measured input impedance for the antenna shown in Figure 5.19;  $\epsilon_r = 4.4$ ,  $h = 1.6$  mm, and feed at point  $C$ . (a) Antenna 1:  $L = 48.2$  mm,  $l = 4.5$  mm; (b) antenna 2:  $L = 38.5$  mm,  $l = 3.8$  mm. (From Ref. 6, © 1998 IEE, reprinted with permission.)

the figure,  $L_1$  and  $L_2$  represent, respectively, the 50- $\Omega$  feed-location loci of the two orthogonal modes, which are determined experimentally in the study. For the probe feed at point  $A$ , which is the intersection of loci  $L_1$  and  $L_2$  and is usually located in the upper half of the triangular patch, right-hand CP radiation with a good matching condition can be obtained. Conversely, left-hand CP radiation can be obtained by feeding the patch at point  $B$  (the mirror image of point  $A$  with respect to the inserted slit). Figure 5.20 shows the measured input impedance of constructed prototypes. Two designs of different triangular patch sizes operated at 1931 and 2423 MHz have been studied, and the case for right-hand CP radiation is shown. The measured axial ratio is presented in Figure 5.21. The corresponding CP performance is given in Table 5.3. It is found that, by increasing the slit length, the effective excited patch surface current path in the  $y$  direction is slightly lengthened with respect to that in the  $x$  direction,

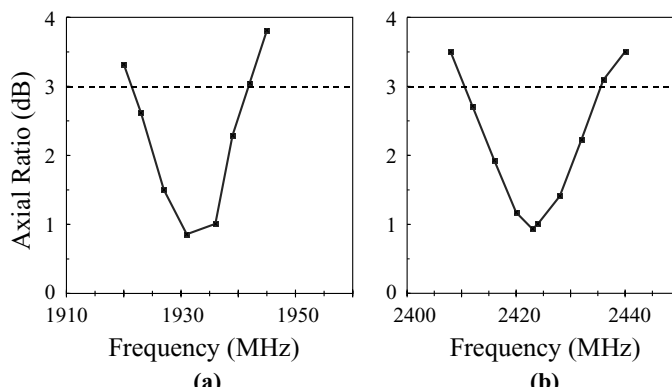


**FIGURE 5.21** Measured axial ratio for (a) antenna 1 and (b) antenna 2 studied in Figure 5.20. (From Ref. 6, © 1998 IEE, reprinted with permission.)

**TABLE 5.3 CP Performance of the Antennas in Figure 5.19 [6]<sup>a</sup>**

	Side Length <i>L</i> (mm)	Slit Length <i>ℓ</i> (mm)	<i>f<sub>c</sub></i> (MHz)	3-dB Axial-Ratio CP Bandwidth (MHz, %)
Antenna 1	48.2	4.5	1931	19, 1.0
Antenna 2	38.5	3.8	2423	25, 1.0

<sup>a</sup>Antenna parameters are given in Figure 5.20.

which means that the  $\hat{y}$ -directed resonant mode has a resonant frequency slightly lower than that of the  $\hat{x}$ -directed resonant mode. When the slit length is adjusted to be about 0.1 times the side length of the triangular patch (4.5 mm for antenna 1 and 3.8 mm for antenna 2), these two resonant modes can be excited with equal amplitudes and a  $90^\circ$  phase difference, resulting in CP radiation. The measured radiation patterns at the center frequency of antennas 1 and 2 were measured, and good right-hand CP operation was observed.

#### 5.4.2 With a Pair of Slits

CP operation of an annular-ring microstrip antenna with a pair of inserted slits at its fundamental  $TM_{11}$  mode has been studied [7]. Two examples of the antenna fed using a microstrip line at the inner and outer patch boundaries were studied with the geometries shown in Figures 5.22 and 5.23. Results show that such an antenna can have good CP performance, and, moreover, the required antenna size at fixed CP operation can be much less than that of a regular circularly polarized circular microstrip antenna operated in the  $TM_{11}$  mode. For the two designs shown, a pair of narrow slits of length  $\ell_s$  and width 1 mm is inserted at the annular ring's inner boundary

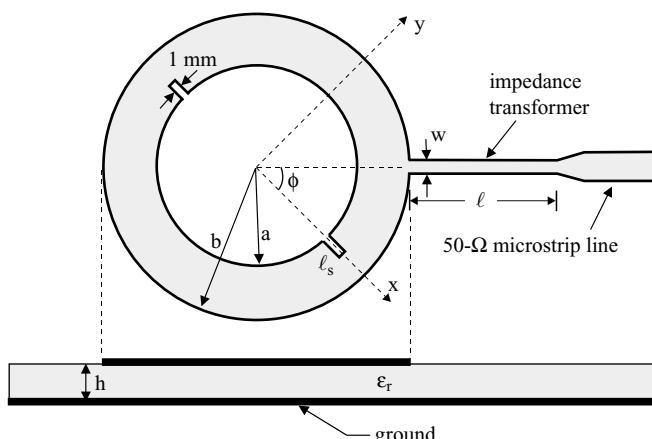


**FIGURE 5.22** Geometry of a circularly polarized annular-ring microstrip antenna with a pair of inserted slits (design A). The microstrip feed line is at the outer boundary of the patch. (From Ref. 7, © 1999 IEEE, reprinted with permission.)

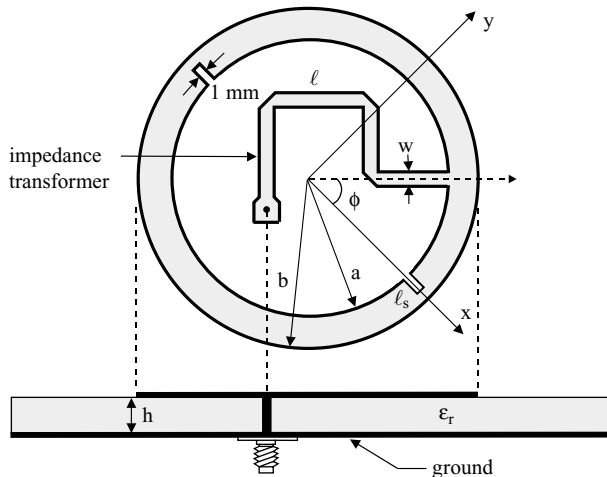


**FIGURE 5.23** Geometry of a circularly polarized annular-ring microstrip antenna with a pair of inserted slits (design B). The microstrip feed line is at the inner boundary of the patch. (From Ref. 7, © 1999 IEEE, reprinted with permission.)

in the  $x$  direction. In such an arrangement, the fundamental  $\text{TM}_{11}$  mode can be split into two near-degenerate resonant modes, and the resonant mode in the  $x$  direction can have a slightly larger resonant frequency than the resonant mode in the  $y$  direction. Also, upon increasing the inner radius, the two orthogonal modes will both have larger excited patch surface current paths, which causes the resulting CP operation to occur at a lower frequency. This corresponds to a smaller antenna size when the present antenna is used in place of the regular-size circular microstrip antenna.

For both feed arrangements in Figures 5.22 and 5.23, right-hand CP operation can be obtained when the microstrip feed line is placed in the  $\phi = 45^\circ$  plane. When the microstrip line is placed in the  $\phi = 135^\circ$  plane, left-hand CP operation can be achieved. The transmission-line section of length  $\ell$  and width  $w$  between the  $50\text{-}\Omega$  microstrip feed line and the outer/inner patch boundary for impedance transformation is determined by

$$50 = Z_T [(Z_A + j Z_L \tan \beta \ell)/(Z_T + j Z_A \tan \beta \ell)] \quad (\Omega), \quad (5.1)$$

where  $Z_A$  is the impedance at the outer or inner patch boundary and  $Z_T$  and  $\beta$  are, respectively, the characteristic impedance and wavenumber of the transmission-line section. By directly solving (5.1), we can select a proper transmission-line section to transform  $Z_A$ , usually a complex impedance, to  $50\ \Omega$ . The determination of the impedance transformer based on (5.1), instead of using a quarter-wavelength impedance transformer, gives the present design a much better impedance matching. In the design shown in Figure 5.23 for the inner-boundary-fed case, the impedance transformer is connected through a via hole to a  $50\text{-}\Omega$  probe feed. This design is especially suited for a compact active microstrip antenna in which the associated

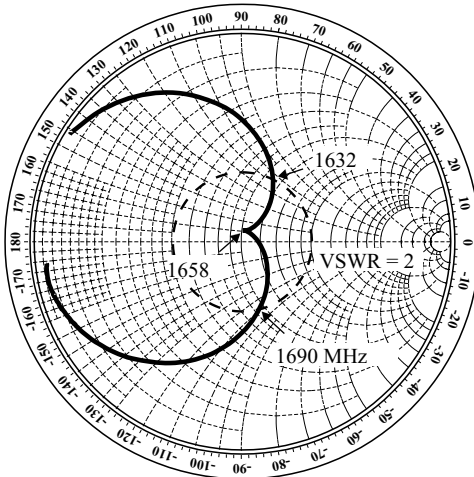


**FIGURE 5.24** Measured input impedance of the antenna shown in Figure 5.22;  $\epsilon_r = 4.4$ ,  $h = 1.6$  mm,  $a = 10$  mm,  $b = 20$  mm,  $\ell_s = 2.34$  mm,  $\phi = 45^\circ$ ,  $\ell = 32$  mm, and  $w = 0.8$  mm. (From Ref. 7, © 1999 IEEE, reprinted with permission.)

active circuitry can be integrated inside the annular-ring patch and placed between the impedance transformer and the via hole.

Consider the geometry shown in Figure 5.22 (denoted as design A); the case with right-hand CP operation is studied. The annular-ring patch is selected to have an outer radius of 20 mm and an inner radius of 10 mm. By adjusting the inserted slit length to be 2.34 mm, CP operation can be obtained. For good impedance matching, the impedance transformer is selected to have a width of 0.8 mm and a length of 32 mm. Figure 5.24 shows the measured input impedance on a Smith chart. It is clearly seen that two near-degenerate resonant modes are excited with good impedance matching. The measured axial ratio versus frequency in the broadside direction is presented in Figure 5.25. The center frequency, defined as the frequency with a minimum axial ratio, is 1658 MHz, and the CP bandwidth is about 14 MHz or 0.8%. For comparison, the results are listed in Table 5.4 along with those for a reference antenna having the same size as the proposed antenna (design A) and constructed using a regular-size circular microstrip antenna with a tuning stub [19]. We can see that the center frequency (1658 MHz) of design A is about 0.83 times that (2008 MHz) of the reference antenna. This indicates that design A can have a 32% antenna size reduction compared to the reference antenna at a fixed CP operation. The radiation patterns in two orthogonal planes were also measured. Figure 5.26 plots the radiation patterns of design A at 1658 MHz; good right-hand CP operation is observed.

In the CP design shown in Figure 5.23 (denoted design B), the outer radius of the circular patch and the substrate parameters are the same as for design A shown in Figure 5.24, but the inner radius is chosen to be 13 mm, larger than that of design A. The impedance transformer has a length of 31 mm and a width of 0.68 mm, and the inserted

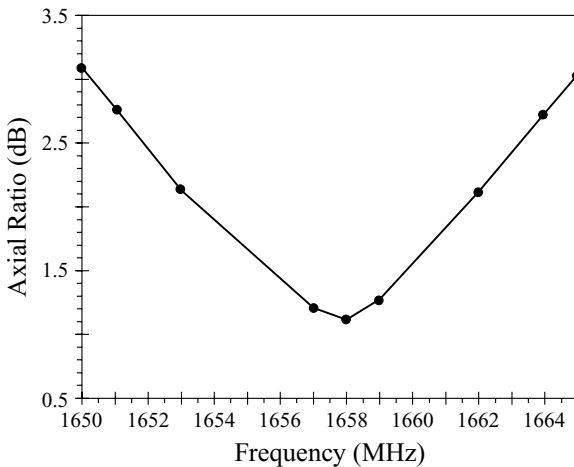


**FIGURE 5.25** Measured axial ratio in the broadside direction of the antenna studied in Figure 5.24. (From Ref. 7, © 1999 IEEE, reprinted with permission.)

slit has a length of 2.0 mm and a width of 1.0 mm. Right-hand CP operation has been demonstrated; that is, the transmission-line section for the impedance transformer is placed in the  $\phi = 45^\circ$  plane. The measured input impedance of design B is shown in Figure 5.27, and the measured axial ratio in the broadside direction is presented in Figure 5.28. The results show that the center operating frequency is significantly lowered from 2008 MHz (the reference antenna) to 1526 MHz, a 24% reduction in the center frequency, corresponding to a 42% antenna size reduction compared to the design of a regular-size circular patch antenna. The results are listed in Table 5.4. The CP bandwidth is 12 MHz, or about 0.8%, about the same as that of design A, and is smaller than that of the reference antenna due to the antenna size reduction. Finally, the measured radiation patterns in two orthogonal planes of design B at the center frequency are plotted in Figure 5.29. Good right-hand CP radiation is observed.

**TABLE 5.4** CP Performance [7] of the Antennas in Figures 5.22<sup>a</sup> and Figure 5.23<sup>b</sup> and a Reference Antenna<sup>c</sup>

	$f_c$ (MHz)	Impedance Bandwidth (MHz, %)	3-dB Axial-Ratio CP Bandwidth (MHz, %)	Maximum Received Power (dBm)
Design A	1658	58, 3.5	14, 0.8	-49.0
Design B	1526	49, 3.2	12, 0.8	-49.2
Reference	2008	98, 4.9	24, 1.2	-48.8

<sup>a</sup>Design A with parameters given in Figure 5.24.

<sup>b</sup>Design B with parameters given in Figure 5.27.

<sup>c</sup>Constructed based on the regular-size CP design of a triangular microstrip antenna with a tuning stub (see Section 5.8.1).

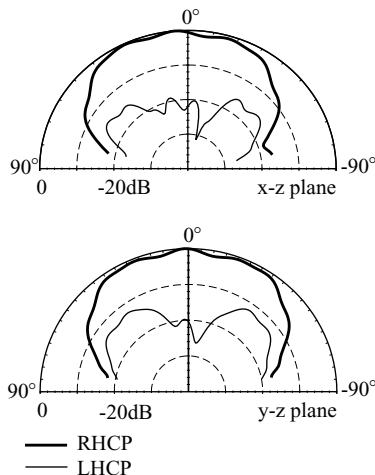


**FIGURE 5.26** Measured radiation patterns of the antenna studied in Figure 5.24;  $f = 1658$  MHz. (From Ref. 7, © 1999 IEEE, reprinted with permission.)

### 5.4.3 With Four Inserted Slits

**5.4.3.1 With a Square Patch** Figure 5.30 shows a square microstrip antenna with four inserted slits for compact CP operation. Two pairs of slits are cut in the  $x$  and  $y$  directions in the square patch. Each pair of slits has equal lengths, but the total lengths of the two pairs of slits  $\ell_x$  and  $\ell_y$  are unequal, which splits the resonant mode of

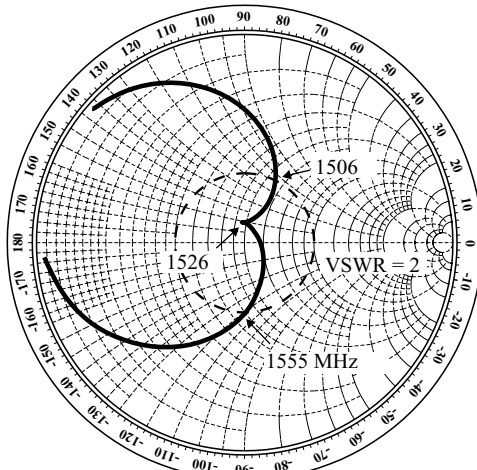


**FIGURE 5.27** Measured input impedance of the antenna shown in Figure 5.23;  $\epsilon_r = 4.4$ ,  $h = 1.6$  mm,  $a = 13$  mm,  $b = 20$  mm,  $\ell_s = 2.0$  mm,  $\phi = 45^\circ$ ,  $\ell = 31$  mm, and  $w = 0.68$  mm. (From Ref. 7, © 1999 IEEE, reprinted with permission.)

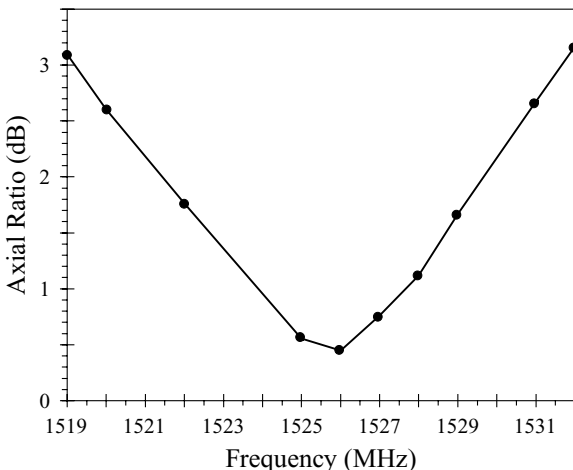


**FIGURE 5.28** Measured axial ratio in the broadside direction of the antenna studied in Figure 5.27. (From Ref. 7, © 1999 IEEE, reprinted with permission.)

interest into two orthogonal near-degenerate modes for CP radiation. When  $\ell_x > \ell_y$ , the feed position at point *C* along the diagonal  $\overline{AB}$  excites right-hand CP radiation, whereas point *D* is for left-hand CP operation. Results for right-hand CP operation are presented here. Figure 5.31 shows the measured input impedance for several constructed prototypes. The square patch has a side length  $L = 30$  mm and is printed on a substrate of thickness  $h = 1.6$  mm and relative permittivity  $\epsilon_r = 4.4$ . When there are no slits, the square patch has a fundamental resonant frequency at 2318 MHz. It

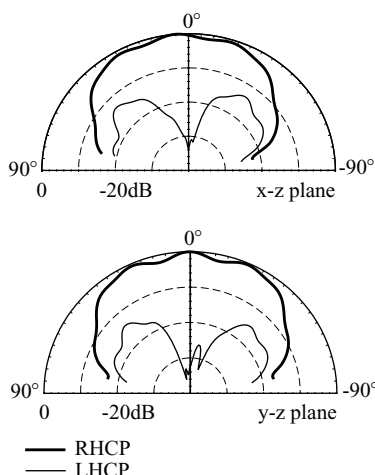


**FIGURE 5.29** Measured radiation patterns of the antenna studied in Figure 5.27;  $f = 1526$  MHz. (From Ref. 7, © 1999 IEEE, reprinted with permission.)

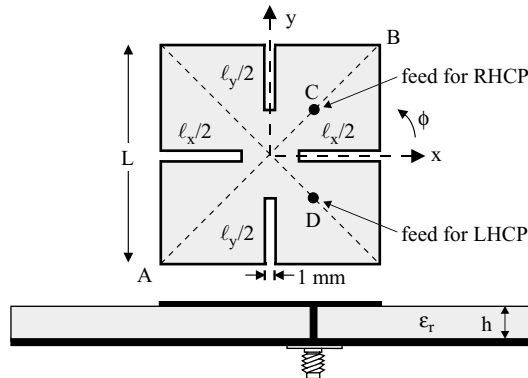


**FIGURE 5.30** Geometry of a compact square microstrip antenna with four inserted slits for CP radiation. (From Ref. 8, © 1997 IEE, reprinted with permission.)

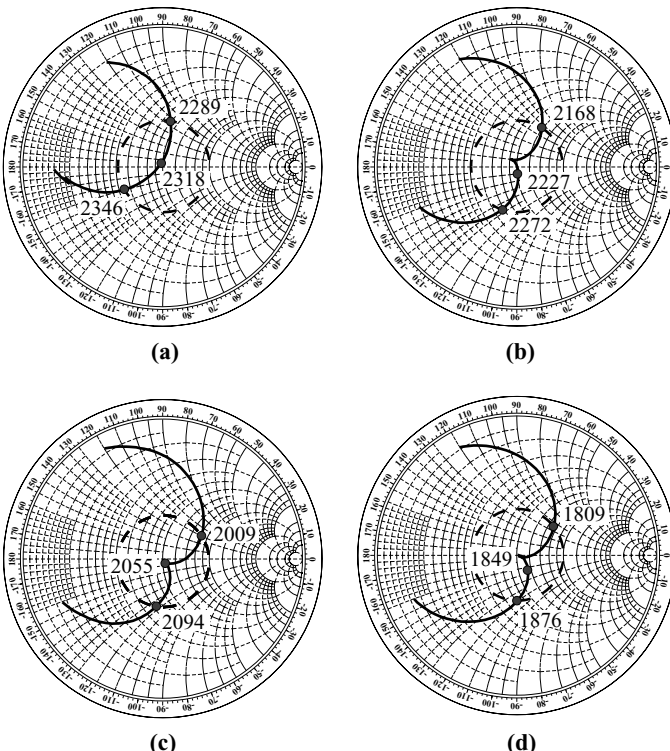


**FIGURE 5.31** Measured input impedance for the antenna with slits of different lengths;  $\epsilon_r = 4.4$ ,  $h = 1.6$  mm,  $L = 30$  mm, and feed at point C. (a)  $\ell_x = \ell_y = 0$ ; (b)  $\ell_x = 10$  mm,  $\ell_y = 6.4$  mm; (c)  $\ell_x = 15$  mm,  $\ell_y = 13.1$  mm; (d)  $\ell_x = 20$  mm,  $\ell_y = 18.4$  mm. (From Ref. 8, © 1997 IEE, reprinted with permission.)

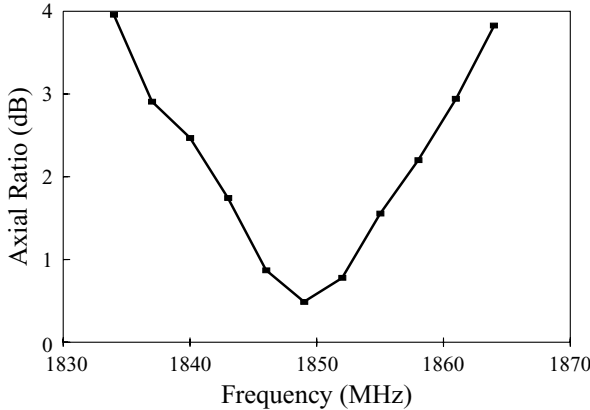


**FIGURE 5.32** Measured axial ratio for an antenna with  $\ell_x = 20$  mm and  $\ell_y = 18.4$  mm; other parameters are given in Figure 5.31. (From Ref. 8, © 1997 IEE, reprinted with permission.)

can be seen that, with four narrow slits cut in the patch, the fundamental resonant frequency is split into two near-degenerate resonant frequencies, which decrease with increasing slit length. For the case of  $\ell_x = 20$  mm and  $\ell_y = 18.4$  mm, the CP center frequency (see Figure 5.32) decreases to about 1849 MHz [about 0.8 times that (2318 MHz) of the case without slits]. This corresponds to a patch size reduction of about 36% compared to the case using the conventional single-feed CP design [1]. The measured radiation patterns in two orthogonal planes are plotted in Figure 5.33. No special distinction compared to the results obtained for conventional CP designs [1] is observed. Data for the cases in Figure 5.31 are listed in Table 5.5. It is seen that, for the case with a smaller slit length, the CP bandwidth is larger and the slit ratio is 1.553 for the case of  $\ell_x = 10$  mm and  $\ell_y = 6.4$  mm. This relaxes the fabrication tolerances compared to the case using conventional CP designs [1], where the aspect ratio of a design with a nearly square patch or with a patch with truncated corners is usually about or less than 1.05. Also note that the feed position  $d_p$  ( $= \overline{AC}/\overline{AB}$ ) for the

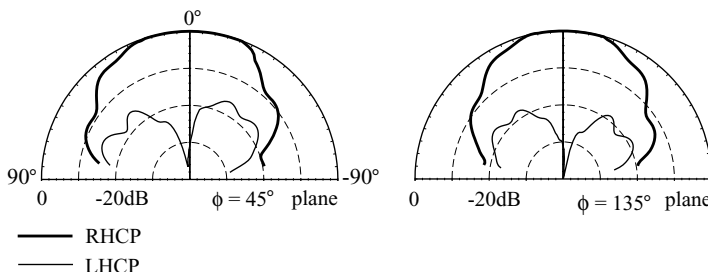


**FIGURE 5.33** Measured radiation patterns for an antenna with  $\ell_x = 20$  mm and  $\ell_y = 18.4$  mm;  $f = 1849$  MHz. Other parameters are given in Figure 5.31. (From Ref. 8, © 1997 IEE, reprinted with permission.)

**TABLE 5.5 CP Performance of the Antenna in Figure 5.30 [8]<sup>a</sup>**

Slit Lengths $\ell_x, \ell_y$ (mm)	Slit Ratio $\ell_x, \ell_y$	Feed Position $d_p = \overline{AC}/\overline{AB}$	$f_c$ (MHz)	3-dB Axial-Ratio CP Bandwidth (%)
0, 0	—	0.36	2318	—
10, 6.4	1.563	0.32	2227	1.6
15, 13.1	1.145	0.32	2055	1.5
20, 18.4	1.087	0.34	1849	1.3

<sup>a</sup>Antenna parameters are given in Figure 5.31.

present design is insensitive to the slit-length variation and is about (0.32–0.34)  $\overline{AB}$  from the patch corner.

**5.4.3.2 With a Circular Patch** Figure 5.34 shows the geometry of a compact circularly polarized circular microstrip antenna. The circular patch has a radius  $D$ , and four narrow slits equally spaced and inserted at the boundary of the circular patch lower the resonant frequency of the dominant  $TM_{11}$  mode. Several designs have been implemented. Figure 5.35 shows the measured input impedance for a right-hand circularly polarized circular microstrip antenna using the present compact CP design. Four designs (antennas 1–4 with parameters given in Table 5.6) with different slit ratio  $\ell_x/\ell_y$  are shown. The corresponding measured results are presented in Figure 5.36. Detailed results of the CP performance for the four designs are listed in Table 5.6. From the results obtained, the optimal feed positions for various slit lengths are seen to be at about one-third the diameter away from the boundary of the circular patch and are closer to the patch center for the case with a larger slit length. With increasing slit length, the CP center frequency decreases with increasing slit length. For antenna 4, the

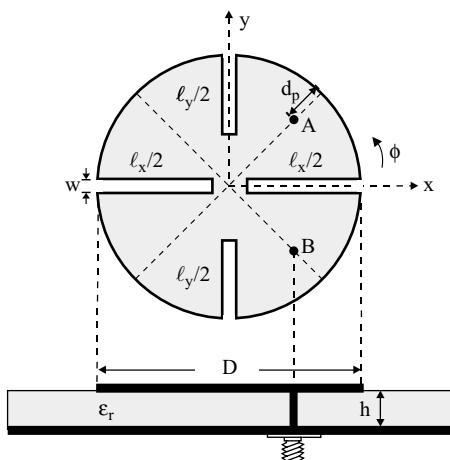


**FIGURE 5.34** Geometry of a compact circular microstrip antenna with slits for CP radiation. (From Ref. 9, © 1998 John Wiley & Sons, Inc.)

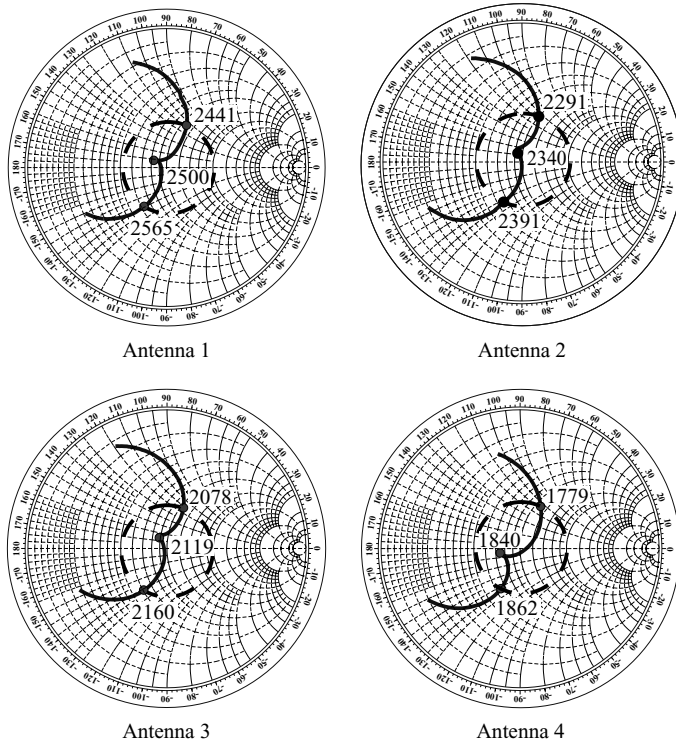


**FIGURE 5.35** Measured input impedance for the antenna shown in Figure 5.34; parameters of antennas 1–4 are given in Table 5.6. (From Ref. 9, © 1998 John Wiley & Sons, Inc.)

center frequency decreases to only about 71% times that (2576 MHz) of the dominant resonant frequency for the simple circular patch without slits. This suggests that the present compact CP design can achieve a 50% antenna size reduction compared to conventional regular-size CP designs at a fixed operating frequency. Note that, to achieve CP radiation, the slit ratio quickly decreases with increasing slit length, and the CP bandwidth also decreases with increasing slit length. Radiation patterns in two orthogonal planes for antenna 4 were also measured, and good right-hand CP radiation was observed.

**TABLE 5.6** CP Performance of the Antenna in Figure 5.34 [9]

	Slit Lengths $\ell_x, \ell_y$ (mm)	Slit Ratio $\ell_x/\ell_y$	Feed Position $d_p/D$	$f_c$ (MHz)	3-dB Axial-Ratio CP Bandwidth (%)
Antenna 1	10, 5	2.00	0.28	2500	1.4
Antenna 2	15, 13	1.15	0.30	2340	1.2
Antenna 3	20, 18.75	1.07	0.33	2119	1.1
Antenna 4	25, 24.5	1.02	0.37	1840	1.0

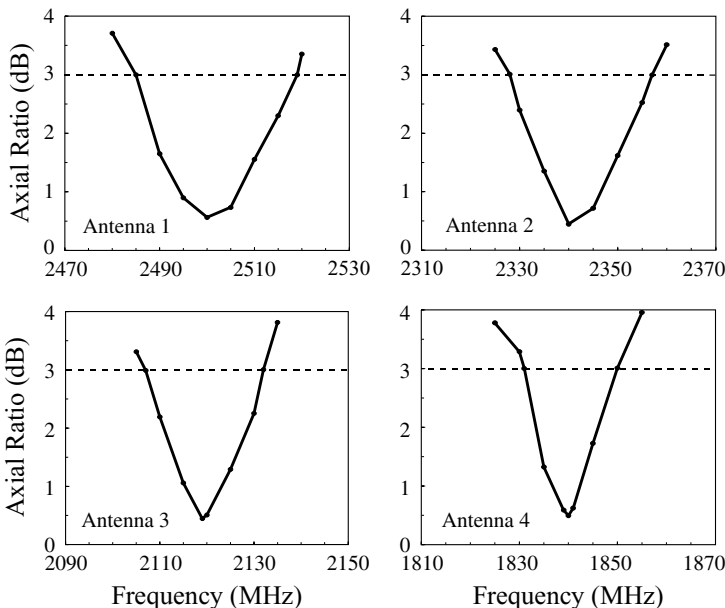


**FIGURE 5.36** Measured axial ratio for the antenna shown in Figure 5.34; parameters of antennas 1–4 are given in Table 5.6. (From Ref. 9, © 1998 John Wiley & Sons, Inc.)

**5.4.3.3 With a Corner-Truncated Square Patch** The method of producing single-feed CP operation of a square microstrip antenna by truncating a pair of patch corners has been widely used. Here we demonstrate that such a method can also be applied to a modified square microstrip patch with four inserted slits of equal lengths to achieve compact CP operation with relaxed manufacturing tolerances. The compactness of the proposed CP design is achieved due to the inserted slits at the patch corners of the square patch. These inserted slits result in meandering of the excited fundamental-mode patch surface current path, which effectively lowers the resonant frequency of the modified square patch, similar to the design using four inserted slits of different lengths at the boundary of a square patch (see Section 5.4.3.1). Instead of using different slit lengths for CP excitation, which usually requires a very small slit-length difference for a large reduction in antenna size, the present design uses the perturbation of truncating a pair of patch corners, with the inserted slits of equal lengths. Experimental results show that the required size of the truncated corners for CP operation increases with increasing reduction in antenna size. This behavior gives the present design a relaxed manufacturing tolerance for achieving a compact circularly polarized microstrip antenna.

The proposed antenna geometry is shown in Figure 5.37. The square microstrip patch has a side length of  $L$ . The four slits have an equal length of  $\ell$  and a width of 1 mm and are inserted at the four patch corners along the directions of  $\phi = \pm 45^\circ$ . The truncated corners are of equal side length  $\Delta L$ . The single probe feed is placed at point  $A$  on the  $y$  axis to achieve right-hand CP radiation. When the feed position

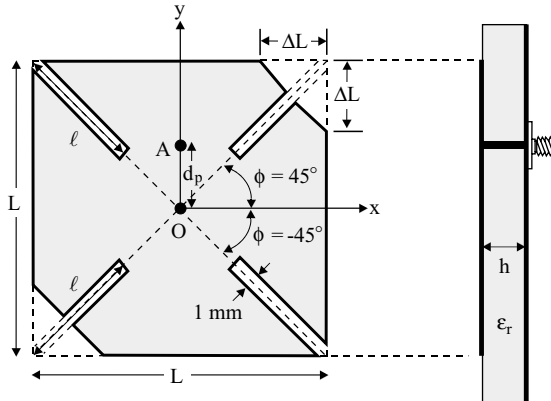


**FIGURE 5.37** Geometry of a compact circularly polarized square microstrip antenna with four slits and a pair of truncated corners. (From Ref. 10, © 2001 IEEE, reprinted with permission.)

is on the  $x$  axis, left-hand CP radiation is obtained. Figure 5.38 shows the measured return loss of constructed prototypes with  $\ell = 16$  mm (denoted antenna 1), 14 mm (antenna 2), and 12 mm (antenna 3), with the side length of the square patch fixed to 28 mm. The measured axial ratio in the broadside direction is shown in Figure 5.39. The corresponding CP performance is listed in Table 5.7. The CP center frequency  $f_c$  is 1970 MHz for antenna 1, 2101 MHz for antenna 2, 2262 MHz for antenna 3, and 2480 MHz for the reference antenna. In comparison to the reference antenna, the center frequency of antenna 1 is lowered by about 20%. The lowering in the center frequency corresponds to an antenna size reduction of about 36% by using the present design in place of the conventional CP design (reference antenna) at a fixed operating frequency. The required perturbation size of the truncated corners also increases

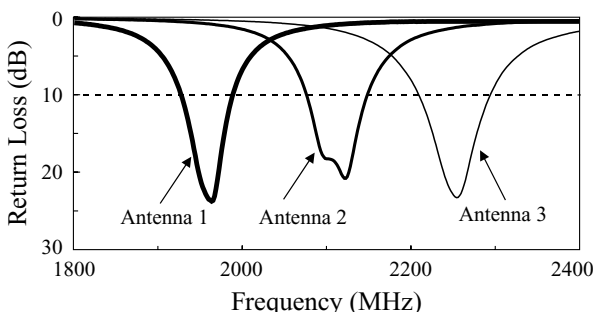


**FIGURE 5.38** Measured return loss for the antenna shown in Figure 5.37 with various slit lengths;  $\epsilon_r = 4.4$ ,  $h = 1.6$  mm,  $L = 28$  mm, and feed at point A. Antenna 1:  $\ell = 16$  mm,  $\Delta L = 6.3$  mm; antenna 2:  $\ell = 14$  mm,  $\Delta L = 4.5$  mm; antenna 3:  $\ell = 12$  mm,  $\Delta L = 2.9$  mm. (From Ref. 10, © 2001 IEEE, reprinted with permission.)

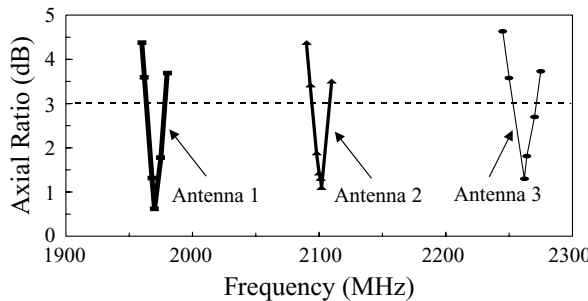


**FIGURE 5.39** Measured axial ratio in the broadside direction for the antennas studied in Figure 5.38. (From Ref. 10, © 2001 IEEE, reprinted with permission.)

with lowered center frequency. For the case of antenna 1 ( $\ell = 16$  mm), the required area of the truncated corners is about four times that of the reference antenna. This suggests that, compared to the design using a square patch with slits of unequal lengths (Section 5.4.3.1) or a simple corner-truncated square patch [1], the present compact CP design has a very relaxed manufacturing tolerance for CP operation. Measured radiation patterns of the present design are plotted in Figure 5.40. Good right-hand CP radiation is observed for the present study with the feed position at point *A*.

**5.4.3.4 With a Chip-Resistor-Loaded Square Patch** Figure 5.41 shows the antenna geometry studied here. The square patch has a side length of  $L$ . A single probe feed at point *C* gives right-hand CP radiation, and point *D* gives left-hand CP radiation. A narrow slit of length  $\ell/2$  and width 1 mm is inserted at the center of each patch edge. Note that the four inserted slits have equal lengths, and the total slit lengths in the  $x$  and  $y$  directions are the same,  $\ell$ . A chip resistor of resistance  $R$  is loaded along the positive  $y$  axis a distance  $S$  from the patch center. In this case, the resonant frequency of the  $\hat{y}$ -directed mode will be slightly larger than that of the  $\hat{x}$ -directed mode. By adjusting the distance  $S$ , these two orthogonal resonant modes can be excited with equal amplitudes, but with a  $90^\circ$  phase difference. With the present arrangement, compact CP operation with enhanced bandwidth can be obtained.

**TABLE 5.7 CP Performance of the Antenna in Figure 5.37 [10]<sup>a</sup>**

	$\ell$ (mm)	$\Delta L$ (mm)	$d_p$ (mm)	$f_c$ (MHz)	3-dB Axial-Ratio CP Bandwidth (%)	Antenna Gain (dBi)
Antenna 1	16	6.3	4.4	1970	0.80	1.4
Antenna 2	14	4.1	5.5	2101	0.81	2.0
Antenna 3	12	3.3	6.7	2262	0.84	2.8
Reference	0	3.2	7.8	2480	1.45	3.5

<sup>a</sup> Antenna parameters are given in Figure 5.38. The reference antenna is constructed based on the design using a regular corner-truncated square patch [1].

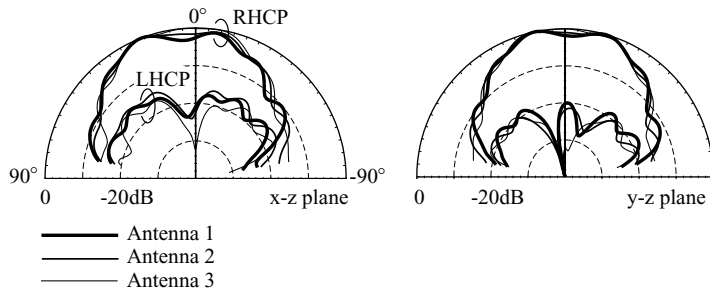


**FIGURE 5.40** Measured radiation patterns for the antennas studied in Figure 5.38; antenna 1 at 1970 MHz, antenna 2 at 2101 MHz, and antenna 3 at 2262 MHz. (From Ref. 10, © 2001 IEEE, reprinted with permission.)

Figure 5.42 shows the measured return loss for a constructed prototype of the present design with  $R = 4.7 \Omega$  and  $\ell = 19$  mm. Two near-degenerate resonant modes are clearly seen to be excited. When there is no chip resistor present, only the lower resonant mode, at about 1855 MHz, is excited. The higher resonant mode, at about 1880 MHz, is excited owing to the loading of the  $4.7\text{-}\Omega$  chip resistor. Figure 5.43 presents the axial ratio measurements. The corresponding CP performance is listed in Table 5.8. The results for the CP design using four slits of unequal lengths (Ref. 8 or Section 5.4.3.1) are shown in Table 5.8 as a reference. Note that a corresponding simple square patch antenna without chip-resistor loading and inserted slits has a fundamental resonant frequency of 2355 MHz. Since the antenna studied has a center frequency of 1867 MHz, a 20.7% lowering in the operating frequency compared to the conventional CP design using a simple square patch is thus obtained. This lowering in the center frequency is similar to the CP design with four inserted slits of unequal

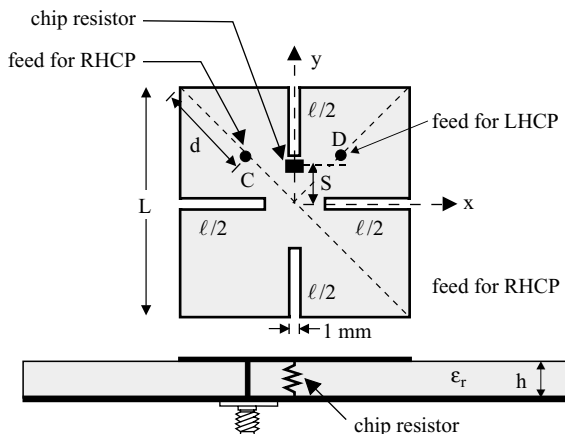


**FIGURE 5.41** Geometry of a compact circularly polarized square microstrip antenna with slits and a chip resistor. (From Ref. 11, © 1999 John Wiley & Sons, Inc.)

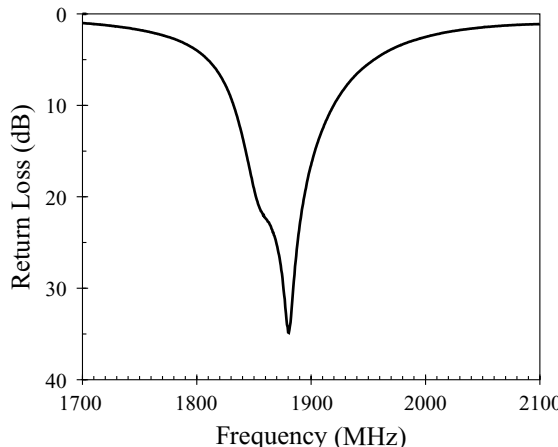


**FIGURE 5.42** Measured return loss for the antenna shown in Figure 5.41 with right-hand CP operation (feed at point C);  $\epsilon_r = 4.4$ ,  $h = 1.6$  mm,  $L = 30$  mm,  $\ell = 19$  mm,  $S = 4$  mm,  $d = 14$  mm, and  $R = 4.7 \Omega$ . (From Ref. 11, © 1999 John Wiley & Sons, Inc.)

lengths and corresponds to an antenna size reduction of about 37% by using the present antenna in place of the conventional regular-size CP design [1] for a fixed operating frequency. Also note that the CP operation of the reference antenna is very sensitive to the length difference between the inserted slits, and a small length difference of 1.6 mm (see Table 5.8) for the inserted slits is required for the reference antenna to achieve compact CP operation. An even smaller length difference is required if a much larger reduction in antenna size is desired. This may cause strict manufacturing tolerances for the reference antenna. However, this problem is avoided in the present antenna, which uses inserted slits of equal lengths.

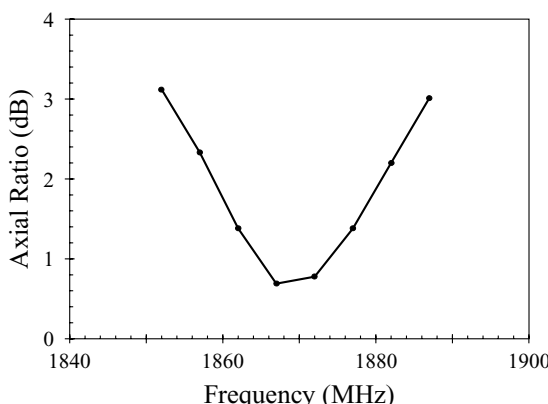


**FIGURE 5.43** Measured axial ratio for the antenna studied in Figure 5.42. (From Ref. 11, © 1999 John Wiley & Sons, Inc.)

**TABLE 5.8 CP Performance of the Antenna in Figure 5.41 [11]<sup>a</sup>**

	Slit Lengths on x, y Axes (mm)	$f_c$ (MHz)	3-dB Axial-Ratio CP Bandwidth (MHz, %)	Maximum Received Power (dBm)
This study	19, 19	1867	35, 1.9	-52.5
Ref. 8	20, 18.4	1849	24, 1.3	-51.3

<sup>a</sup>Antenna parameters are given in Figure 5.42.

Results show that the CP bandwidth is about 50% larger than that of the reference antenna shown in Table 5.8 (1.9% vs. 1.3%). This broadband characteristic is mainly due to the  $4.7\text{-}\Omega$  chip-resistor loading, and a much greater CP bandwidth can be obtained if a chip resistor of larger resistance is used for the present design. However, it should be noted that the increase in CP bandwidth is at some expense of the antenna gain. The maximum relative received power of the proposed antenna is 1.2 dBm less than that of the reference antenna. Finally, from the measured radiation patterns, good right-hand CP radiation is observed for the present proposed antenna.

## 5.5 DESIGNS WITH SPUR LINES

Recently, it has been reported that, by embedding a pair of spur lines in the triangular patch, a new resonant mode with a lower resonant frequency than that of the fundamental  $\text{TM}_{10}$  mode can be excited [25]. Based on such an interesting result, a compact CP design for triangular microstrip antennas with three inserted spur lines (see Figure 5.44) has been demonstrated. The spur lines are inserted at the center of each patch edge. It is found that, by properly adjusting the three spur lines to be of slightly different lengths, two near-degenerate orthogonal modes for CP operation can be excited. Furthermore, due to the presence of the spur lines, the excited patch

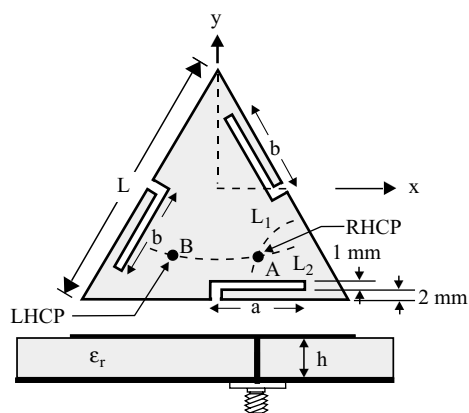


**FIGURE 5.44** Geometry of a compact circularly polarized triangular microstrip antenna with spur lines. (From Ref. 12, © 1998 IEE, reprinted with permission.)

**TABLE 5.9 CP Performance of the Antenna in Figure 5.44 [12]<sup>a</sup>**

	Spur-Line Size $a, b$ (mm)	Length Ratio $b/a$	Feed Position ( $x_p, y_p$ ) (mm)	$f_c$ (MHz)	3-dB Axial-Ratio CP Bandwidth (%)
Antenna 1	12, 11.5	0.958	(6.0, -17)	1664	0.9
Antenna 2	15.4, 14.8	0.961	(6.5, -17)	1605	0.9
Antenna 3	18.2, 17.5	0.961	(9.0, -17)	1504	0.7
Reference	0, 0	—	(5.5, -17.5)	1931	1.0

<sup>a</sup> $\epsilon_r = 4.4$ ,  $h = 1.6$  mm, and  $L = 50$  mm. Reference antenna is constructed based on the regular-size CP design of a triangular microstrip antenna with a slit (Ref. 6 or Section 5.4.1.2).

surface current path is lengthened and thus the resonant frequency of the triangular patch is lowered, and compact CP operation is obtained.

As shown in the geometry of Figure 5.44, the longer arms of the inserted spur lines are parallel to the patch edge and all are 2 mm from the patch edge. Two of the spur lines have the same longer-arm length  $a$ , and the third one has a slightly smaller longer-arm length  $b$ . The spur lines are also assumed to be narrow and have an equal width of 1 mm. It is found that, by choosing the length ratio, defined as  $b/a$  here, of the spur lines to be slightly less than one, two near-degenerate orthogonal modes with equal amplitudes and a 90° phase difference can be excited, which results in compact CP radiation.  $L_1$  and  $L_2$  in the patch represent, respectively, the 50-Ω feed-location loci of the two orthogonal modes, which are determined experimentally in this study. For the probe feed at point  $A$ , which is the intersection of loci  $L_1$  and  $L_2$  and is usually located in the right-hand half of the triangular patch, right-hand CP radiation with a good matching condition can be obtained. By feeding the patch at point  $B$ , a mirror image of point  $C$  with respect to the centerline ( $y$  axis) of the triangular patch, left-hand CP radiation can be obtained.

Several prototypes have been constructed. Three cases (denoted antennas 1–3) of the proposed design with different spur-line sizes have been studied. The feed position is chosen at point  $A$  for achieving right-hand CP radiation. The obtained CP performance is given in Table 5.9. It is found that, when the length ratio of the spur lines is about 0.96, CP operation of the present design is obtained. For the case of antenna 3 ( $a = 18.2$  mm,  $b = 17.5$  mm), the CP center frequency is lowered to about 78% that of a regular-size circularly polarized triangular microstrip antenna with a slit [6]. This lowering in center frequency suggests that, for a given operating frequency, the present CP design can have an antenna size reduction of about 40% compared to the case using a regular-size CP design.

## 5.6 DESIGNS WITH TRUNCATED CORNERS

The technique of truncating the patch corners of a simple square microstrip patch to obtain single-feed CP operation of microstrip antennas has been widely used in practical designs. In this section, we demonstrate that such a technique can also be applied to single-feed microstrip antennas with a triangular patch [14], a square-ring

patch [15], a triangular-ring patch [16], and a slotted square patch [17]. It is found that the required antenna size of these designs is smaller than that of the conventional design using a simple square patch at a fixed CP operation, and compact CP operation can be obtained. Experimental results of constructed prototypes of the designs [14–17] are described in the following.

### 5.6.1 With a Triangular Patch

Figure 5.45 shows the CP design of a single-feed, equilateral-triangular microstrip antenna with a truncated corner or tip. Experimental results for constructed prototypes of the present CP design are shown in Figures 5.46 and 5.47. Three different triangular patch dimensions were studied, with the feed at point A for right-hand CP radiation. The corresponding CP performance is given in Table 5.10. It is found that, when the side length of the truncated tip is adjusted to be about 0.09 times that of the triangular patch, the dominant mode of the triangular patch is split into two near-degenerate orthogonal modes of equal amplitudes and a  $90^\circ$  phase difference, which results in CP radiation. Results show that the obtained CP bandwidths are about 1.0–1.4%, which are largely dependent on the electrical thickness of the substrate, for the antenna parameters studied here. Radiation patterns at resonance of the prototypes were measured, and good right-hand CP radiation was observed.

### 5.6.2 With a Square-Ring Patch

Compact CP operation of a square-ring microstrip antenna with truncated corners has been shown [15]. The antenna geometry studied is shown in Figure 5.48. The

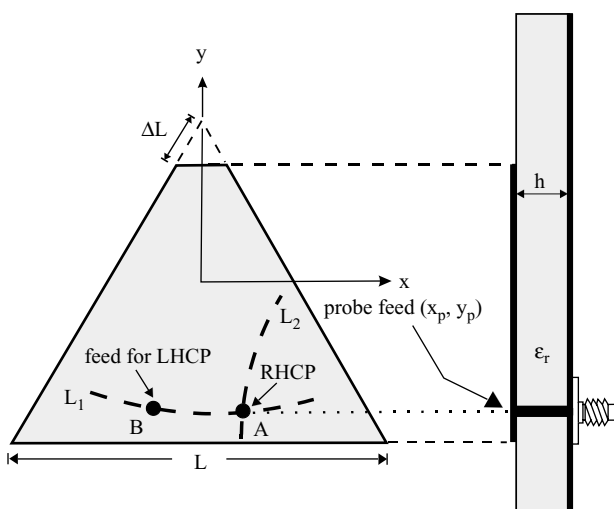


**FIGURE 5.45** Geometry of a single-feed equilateral-triangular microstrip antenna with a truncated tip for CP operation. (From Ref. 14, © 1998 IEE, reprinted with permission.)

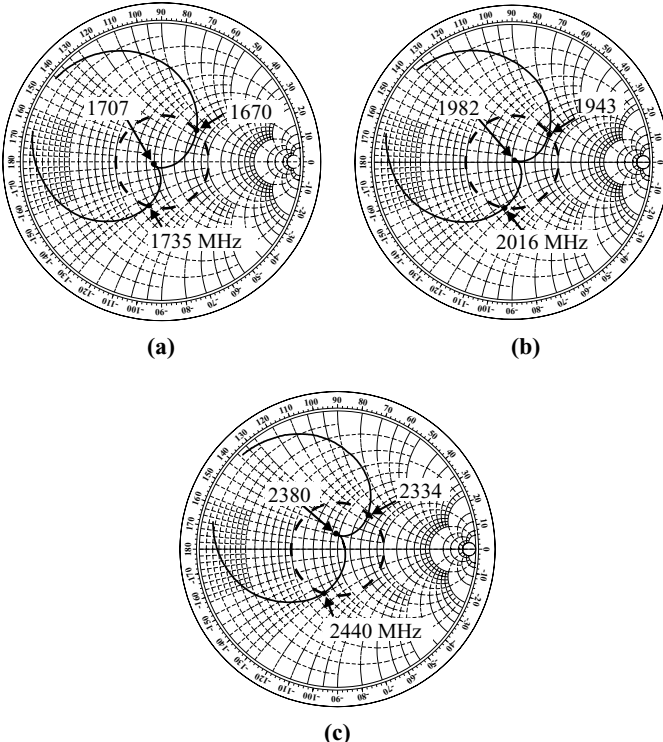


**FIGURE 5.46** Measured input impedance for the antenna shown in Figure 5.45;  $\epsilon_r = 4.4$ ,  $h = 1.6$  mm, and feed at point A. (a) Antenna 1, (b) antenna 2, (c) antenna 3; parameters are given in Table 5.10. (From Ref. 14, © 1998 IEE, reprinted with permission.)

square-ring microstrip patch has an outer side length  $L_1$  and an inner side length  $L_2$ . The truncated corners have equal side length  $\Delta L$ . The feed position at point A along the  $y$  axis shown in the figure is for right-hand CP operation, and the distance of the probe feed from the patch center (point O) is denoted  $d_p$ . By moving the feed position from point A to a point on the  $x$  axis, left-hand CP radiation can be obtained.

Experiments have been conducted, and Figure 5.49 shows the measured input impedance for two cases,  $L_2 = 8$  mm (antenna 1) and 10 mm (antenna 2), with the outer side length  $L_1$  of the square-ring patch being 28 mm. The results clearly show that two near-degenerate resonant modes are excited. The measured axial ratio in the broadside direction is shown in Figure 5.50. The corresponding CP performance is listed in Table 5.11, where a reference antenna using a corner-truncated square patch is shown for comparison. The CP center frequency  $f_c$  is 2330 MHz for antenna 1, 2247 MHz for antenna 2, and 2480 MHz for the reference antenna. In comparison with the reference antenna, the center frequency of antenna 2 is lowered by about 10%. The lowering in the center frequency corresponds to an antenna size reduction of about 19% by using the present design in place of the conventional CP design (reference antenna) for a fixed operating frequency. In the present design, the required size of the

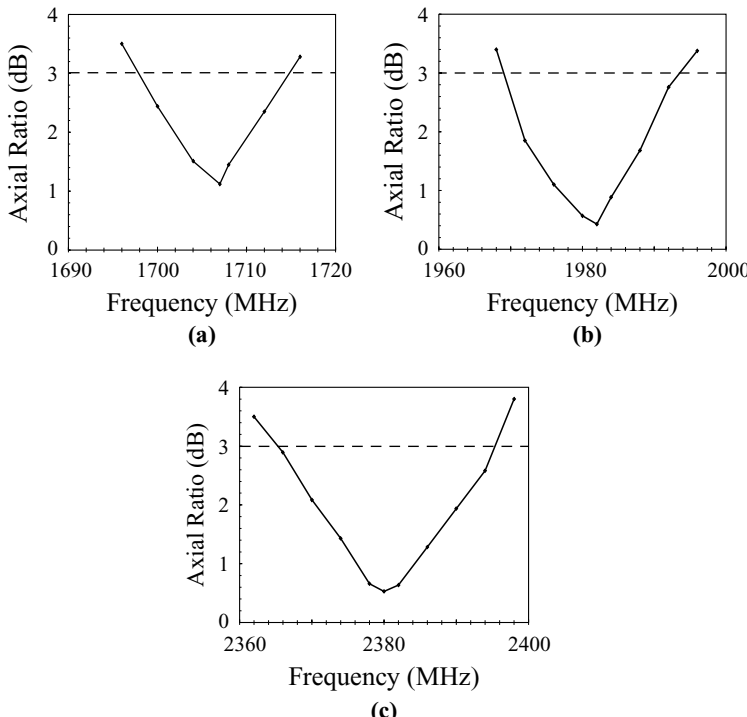


**FIGURE 5.47** Measured axial ratio for the antennas studied in Figure 5.46. (From Ref. 14, © 1998 IEE, reprinted with permission.)

truncated corners is larger, especially for the case with a larger value of  $L_2$ , compared to the conventional design using a square patch. This suggests that the present CP design has a relaxed manufacturing tolerance.

Owing to the lowering of the resonant frequency, which results in a decrease of the electrical thickness of the substrate, the CP bandwidth slightly decreases with increasing  $L_2$ . Since the feed position needs to be moved closer to the patch center for achieving  $50\text{-}\Omega$  impedance matching for the case with a larger inner side length, there exists a limit in  $L_2$  for the present design using a single probe-feed excitation; for example, in the typical case studied here, when  $L_2$  is larger than 10 mm, the

**TABLE 5.10** CP Performance of the Antenna in Figure 5.45 [14]<sup>a</sup>

	$L$ (mm)	$\Delta L$ (mm)	Feed Position ( $x_p, y_p$ ) (mm)	$f_c$ (MHz)	3-dB Axial-Ratio CP Bandwidth (MHz, %)
Antenna 1	56	5.0	(7.3, -16.8)	1707	17, 1.0
Antenna 2	48	4.2	(7.2, -13.6)	1982	28, 1.4
Antenna 3	40	3.6	(3.8, -12.2)	2380	30, 1.3

<sup>a</sup>  $\epsilon_r = 4.4$ ,  $h = 1.6$  mm, and feed at point A.

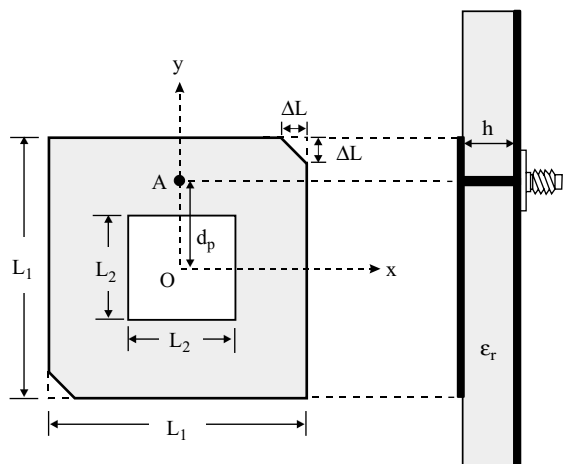


**FIGURE 5.48** Geometry of a square-ring microstrip antenna with truncated corners for compact CP operation. (From Ref. 15, © 1998 IEE, reprinted with permission.)

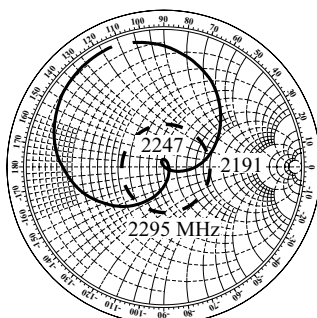
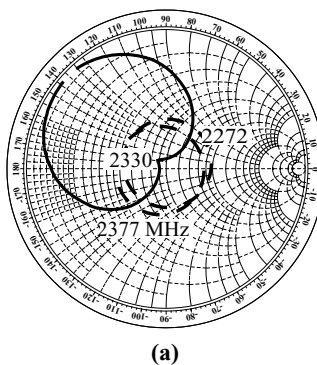


**FIGURE 5.49** Measured input impedance for the antenna shown in Figure 5.48;  $\epsilon_r = 4.4$ ,  $h = 1.6$  mm, and  $L_1 = 28$  mm. (a) Antenna 1:  $L_2 = 8$  mm,  $\Delta L = 4.2$  mm; (b) antenna 2:  $L_2 = 10$  mm,  $\Delta L = 4.8$  mm. (From Ref. 15, © 1998 IEE, reprinted with permission.)

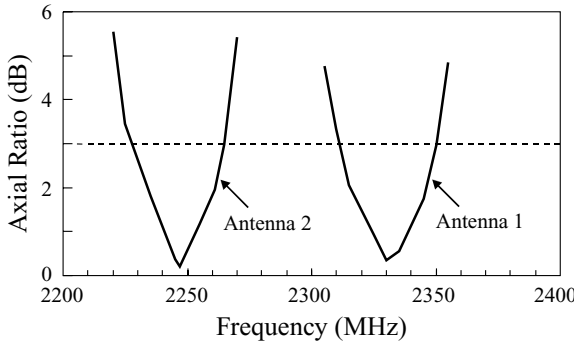


**FIGURE 5.50** Measured axial ratio in the broadside direction for antennas 1 and 2 studied in Figure 5.49. (From Ref. 15, © 1998 IEE, reprinted with permission.)

50- $\Omega$  feed position can no longer be located in the square-ring patch. The measured radiation patterns of the present design show that good right-hand CP radiation is observed.

### 5.6.3 With a Triangular-Ring Patch

Figure 5.51 shows a CP design for a modified equilateral-triangular-ring (ETR) microstrip antenna with a truncated tip and a Y-shaped conducting strip. The present antenna has a symmetric structure with respect to the centerline of the patch, and the splitting of the antenna's fundamental resonant mode into two near-degenerate modes is mainly controlled by the truncated tip size. Inside the Y-shaped conducting strip, there exists an optimal feed position for achieving right-hand or left-hand CP radiation. Compared to regular-size CP designs for equilateral-triangular microstrip antennas (see Sections 5.6.1 and Section 5.4.1.2), the ETR microstrip antenna can be used for CP radiation with a reduced antenna size at fixed CP operation.

In this design, the ETR patch has a side length  $L$  and a ring width  $W$ . A triangle tip of side length  $\Delta L$  is truncated in the patch. A Y-shaped conducting strip (facing the bottom edge of the ETR patch) of equal arm lengths is centered on the patch center (point C in the figure) and connected to the three tips of the patch. The three arms of the Y-shaped strip have an equal width  $W_y$ . From experiments, when  $W_y$  is chosen

**TABLE 5.11** CP Performance of the Antenna in Figure 5.48 [15]<sup>a</sup>

	$L_2$ (mm)	$\Delta L$ (mm)	$d_p$ (mm)	$f_c$ (MHz)	3-dB Axial-Ratio CP Bandwidth (%)
Antenna 1	8	4.2	5.3	2330	1.4
Antenna 2	10	4.8	5.0	2247	1.3
Reference	0	3.2	3.2	2480	1.5

<sup>a</sup>  $\epsilon_r = 4.4$ ,  $h = 1.6$  mm, and  $L_1 = 48$  mm.

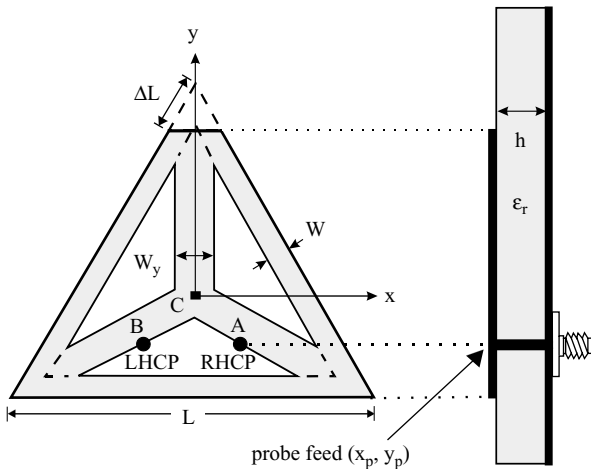


**FIGURE 5.51** Geometry of a circularly polarized equilateral-triangular-ring microstrip antenna with a truncated tip and a Y-shaped conducting strip. (From Ref. 16, © 1999 John Wiley & Sons, Inc.)

to be about 0.13–0.15 times the patch's side length  $L$ , an optimal feed position for CP radiation is located at about the edge center of the arms of the Y-shaped strip (see point  $A$  or  $B$  in the figure; point  $A$  is for right-hand CP radiation and point  $B$  is for left-hand CP radiation). For the required truncated tip for the splitting of the fundamental resonant mode of the ETR patch antenna into two near-degenerate orthogonal modes for CP radiation, its optimal side length is about 0.1 times the patch's side length (that is,  $\Delta L \cong 0.1L$ ) and is smaller for increasing ring width. By following empirical rules for the determination of the truncated tip's side length, the width of the Y-shaped strip, and the feed position, CP radiation of a modified ETR microstrip antenna with various ring widths can easily be implemented.

Figure 5.52 shows the measured input impedance of an antenna with  $L = 48$  mm. Two different ring widths, 5.1 mm (antenna 1) and 1.4 mm (antenna 2), are presented, and the width of the Y-shaped strip for both cases is fixed to be  $W_y = 7.2$  mm ( $\cong 0.15L$ ). The feed position is chosen at point  $A$ , and right-hand CP radiation is studied. The obtained axial ratio of CP radiation in the broadside direction is presented in Figure 5.53. The corresponding results are listed in Table 5.12. The results for a reference antenna constructed using a tip-truncated equilateral-triangular microstrip antenna (Section 5.6.1) with the same side length of 48 mm are shown for comparison. It can be seen that the center frequency decreases with decreasing ring width of the ETR patch, and is smaller than that of the reference antenna. This suggests that the required patch size of the antenna studied is smaller than that of a regular-size circularly polarized equilateral-triangular microstrip antenna. When antenna 2 is used in place of the reference antenna for operating at a fixed frequency, its required patch size of is about 24% less than that of the reference antenna.

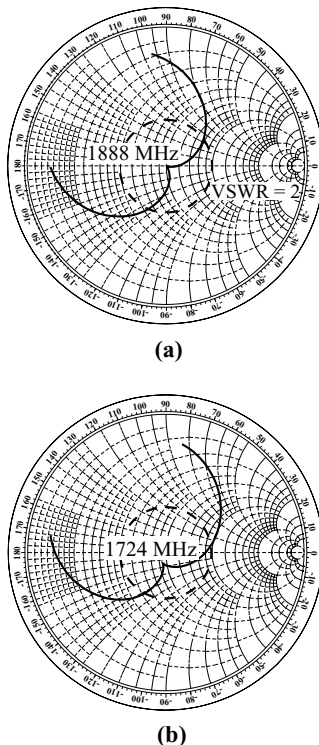


**FIGURE 5.52** Measured input impedance for the antenna shown in Figure 5.51;  $\epsilon_r = 4.4$ ,  $h = 1.6$  mm,  $L = 48$  mm,  $W_y = 7.2$  mm ( $\cong 0.15L$ ), and feed at point A. (a) Antenna 1:  $W = 5.1$  mm,  $\Delta L = 4.7$  mm, and  $(x_p, y_p) = (5.8, -6.6$  mm); (b) antenna 2:  $W = 1.4$  mm,  $\Delta L = 5.0$  mm, and  $(x_p, y_p) = (5.5, -6.5$  mm). (From Ref. 16, © 1999 John Wiley & Sons, Inc.)

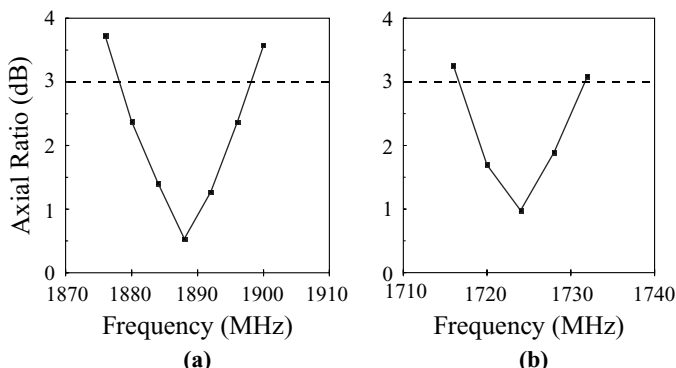


**FIGURE 5.53** Measured axial ratio in the broadside direction for the antennas studied in Figure 5.52. (a) Antenna 1, (b) antenna 2. (From Ref. 16, © 1999 John Wiley & Sons, Inc.)

**TABLE 5.12 CP Performance of the Antenna in Figure 5.51 [16]<sup>a</sup>**

	$W$ (mm)	$\Delta L$ (mm)	$f_c$ (MHz)	3-dB Axial-Ratio CP Bandwidth (%)
Antenna 1	5.1	4.7	1888	1.1
Antenna 2	1.4	5.0	1724	0.9
Reference	—	4.2	1982	1.4

<sup>a</sup> Antenna parameters are given in Figure 5.52.

### 5.6.4 With a Slotted Square Patch

By embedding a group of four bent slots in a corner-truncated square microstrip patch, a single-feed, compact circularly polarized microstrip antenna can easily be obtained. Results show that, for a given CP operation, the present antenna can have an antenna size reduction of more than 50% compared to the conventional CP design using a corner-truncated square patch without slots. Figure 5.54 shows the geometry of the antenna studied. The square microstrip patch has a side length  $L$ , and the four bent slots are of equal arm length  $\ell$  and narrow width 1 mm. The two arms of each bent slot are aligned parallel to the centerlines of the square patch. By increasing the arm length of the bent slots, the fundamental resonant frequency of the slotted square patch is significantly decreased. By further truncating a suitable size of the patch corners, which are of equal side length  $\Delta L$ , the present antenna can be used for CP operation. A single probe feed placed at point A (see Figure 5.54) on the  $y$  axis achieves right-hand CP radiation and when placed on the  $x$  axis gives left-hand CP radiation.

Several prototypes have been constructed and studied. Figure 5.55 shows the measured return loss for the cases of  $\ell = 12$  mm (antenna 1), 10 mm (antenna 2), and 8 mm (antenna 3), with the side length of the square patch being 28 mm. The measured

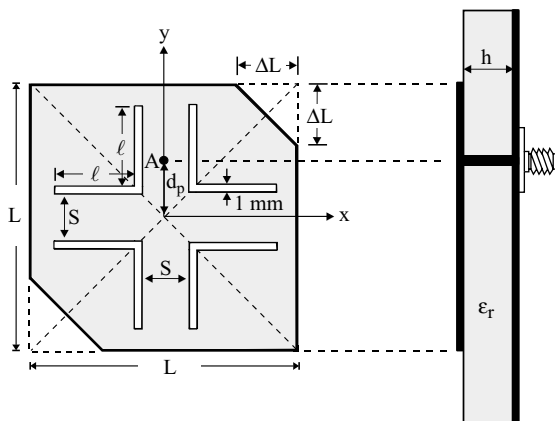


**FIGURE 5.54** Geometry of a compact circularly polarized corner-truncated square microstrip antenna with four bent slots. (From Ref. 17, © 1998 IEE, reprinted with permission.)

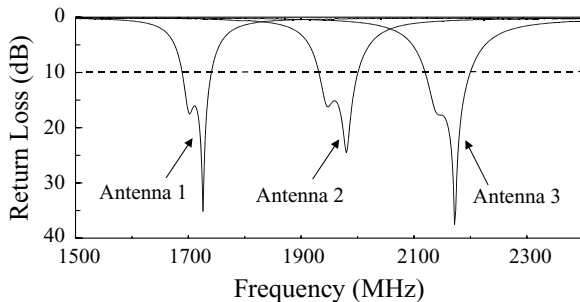


**FIGURE 5.55** Measured return loss for the antenna shown in Figure 5.54;  $\epsilon_r = 4.4$ ,  $h = 1.6$  mm,  $L = 28$  mm,  $S = 2$  mm,  $\Delta L = 3.2$  mm, and  $d_p = 6.7$  mm. Antenna 1:  $\ell = 12$  mm; antenna 2:  $\ell = 10$  mm; antenna 3:  $\ell = 8$  mm. (From Ref. 17, © 1998 IEE, reprinted with permission.)

axial ratio in the broadside direction is shown in Figure 5.56. The corresponding CP performance is listed in Table 5.13. Note that the CP center frequency  $f_c$  is 1711 MHz for antenna 1, 1960 MHz for antenna 2, 2153 MHz for antenna 3, and 2480 MHz for the reference antenna. In comparison with the reference antenna, the center frequency of antenna 1 is lowered by 31%. This lowering of the center frequency corresponds to an antenna size reduction of about 52% by using the present design in place of the conventional CP design (reference antenna) for a fixed CP operation. The results show that the prototypes (antennas 1–3) and the reference antenna have the same required perturbation area of the truncated corners for achieving CP operation. The 50- $\Omega$  feed positions for antennas 1–3 are the same and are slightly different from that of the reference antenna. This suggests that the bent slots introduced in the patch have very small or negligible effects on the required perturbation for achieving CP operation. This behavior makes the present antenna easy to design and construct.

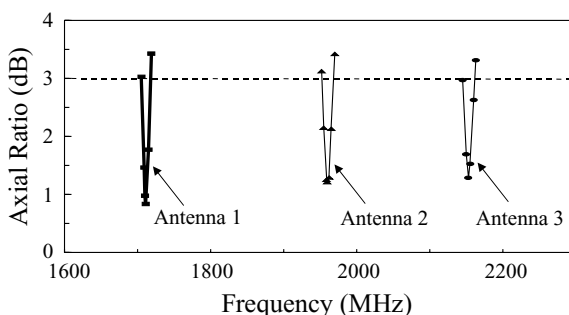


**FIGURE 5.56** Measured axial ratio for the antennas studied in Figure 5.55. (From Ref. 17, © 1998 IEE, reprinted with permission.)

**TABLE 5.13 CP Performance of the Antenna in Figure 5.54 [17]<sup>a</sup>**

	$\ell$ (mm)	$\Delta L$ (mm)	$d_p$ (mm)	$f_c$ (MHz)	3-dB Axial-Ratio CP Bandwidth (%)
Antenna 1	12	3.2	6.7	1711	0.80
Antenna 2	10	3.2	6.7	1960	0.86
Antenna 3	8	3.2	6.7	2153	0.86
Reference	0	3.2	7.8	2480	1.4

<sup>a</sup>Antenna parameters are given in Figure 5.55.

## 5.7 DESIGNS WITH PERIPHERAL CUTS

Compact CP operation of a circular microstrip antenna with a cross slot in the patch center and a pair of peripheral cuts at opposite sides of the patch boundary has been proposed and experimentally studied [18]. Figure 5.57 shows the antenna geometry. The circular patch has a radius  $R$ , and the cross slot has equal arm lengths  $\ell$  and narrow width 1 mm and is embedded in the circular patch with its two arms in line with the  $x$  and  $y$  axes, respectively. Peripheral cuts of depth  $\Delta R$  are at opposite sides of the patch boundary and centered with respect to the  $x$  axis as shown in the figure. A single probe feed placed at point A on the  $\phi = 45^\circ$  line achieves right-hand CP operation, while the feed at the mirror image of point A with respect to the  $x$  axis results in left-hand CP operation. The distance of the feed position from the patch center is denoted as  $d_p$ .

Figure 5.58 shows the measured input impedance for the cases with  $\ell = 0$  and 8 mm, which are denoted the regular-size and compact antennas, respectively. The circular patch has a radius of 16.5 mm. The results show clearly that two near-degenerate

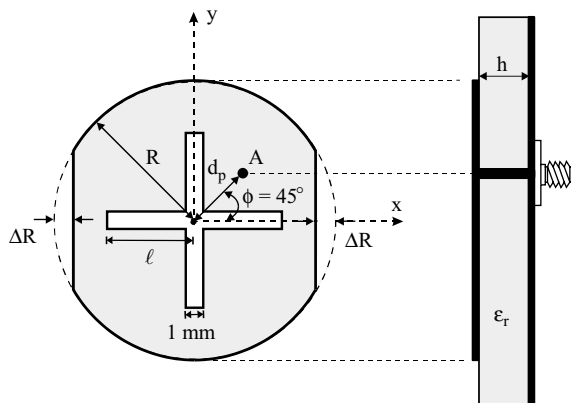


**FIGURE 5.57** Geometry of a circular microstrip antenna with a cross slot and peripheral cuts for compact CP operation. (From Ref. 18, © 1998 IEE, reprinted with permission.)

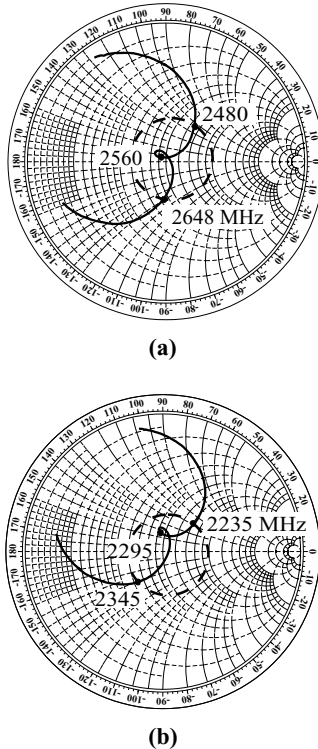


**FIGURE 5.58** Measured input impedance for the antenna shown in Figure 5.57;  $\epsilon_r = 4.4$ ,  $h = 1.6$  mm, and  $R = 16.5$  mm. (a) Regular-size antenna:  $\ell = 0$  mm,  $\Delta R = 1.2$  mm; (b) compact antenna:  $\ell = 8$  mm,  $\Delta R = 0.9$  mm. (From Ref. 18, © 1998 IEE, reprinted with permission.)

modes are excited by incorporating a pair of small peripheral cuts of depth  $\Delta R = 1.2$  and 0.9 mm, respectively, for the regular-size and compact antennas. The measured axial ratio in the broadside direction is shown in Figure 5.59. The corresponding CP performance is listed in Table 5.14. The CP center frequency  $f_c$  is 2560 and 2295 MHz for the regular-size and compact antennas, respectively. The compact antenna thus has a center frequency about 10.4% lower than that of the regular-size antenna. This lowering of the center frequency corresponds to an antenna size reduction of about 20% by using the compact design in place of the regular-size design at a fixed operating frequency. Also note that the feed position needs to be moved closer to the patch center for the compact antenna. This behavior makes it difficult to locate the  $50\text{-}\Omega$  feed position inside the circular patch when a larger cross slot than that studied here is introduced in the patch. In cases with a larger cross slot, other feed methods such as those using an aperture-coupled feed or proximity-coupled feed can be applied, and a much larger antenna size reduction than that obtained here can be expected.

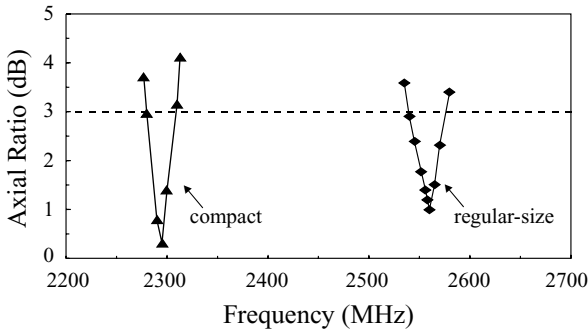


**FIGURE 5.59** Measured axial ratio for the antennas studied in Figure 5.58. (From Ref. 18, © 1998 IEE, reprinted with permission.)

## 5.8 DESIGNS WITH A TUNING STUB

The use of a tuning stub has been shown to be effective for the resonant frequency adjustment of microstrip antennas [26]. Due to the frequency tuning capability of the tuning stub, it is expected that, with a proper stub length, the resonant mode in the direction parallel to the stub can have a slightly lower resonant frequency than that in the direction perpendicular to the stub orientation. In this case, two near-degenerate orthogonal modes can be excited using a single probe feed, which makes CP operation possible. This design concept has been successfully applied to a circular patch [19], a square-ring patch [20], and a triangular patch [21]. Details of the experimental results for these studies are presented in the following.

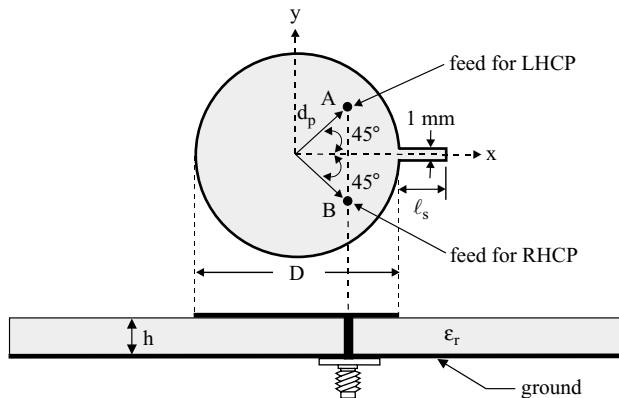
### 5.8.1 With a Circular Patch

Figure 5.60 shows a CP design with a tuning stub for a circularly polarized simple circular microstrip antenna. A tuning stub of length  $\ell_s$  and width 1 mm is placed at the disk boundary in the  $x$  direction. In this case, the  $\hat{x}$ -directed resonant mode will have a slightly lower resonant frequency than the  $\hat{y}$ -directed resonant mode. By choosing the proper stub length and exciting the patch at point *A* or *B*, CP radiation can be obtained. Figure 5.61 presents the measured input impedance and boresight-direction

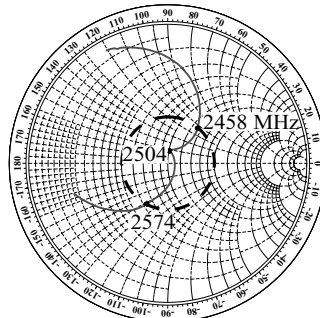
**TABLE 5.14 CP Performance of the Antenna in Figure 5.57 [18]<sup>a</sup>**

	$\ell$ (mm)	$\Delta R$ (mm)	$d_p$ (mm)	$f_c$ (MHz)	3-dB Axial-Ratio CP Bandwidth (%)
Regular-size	0	1.2	8.7	2560	1.6
Compact	8	0.9	1.6	2295	1.3

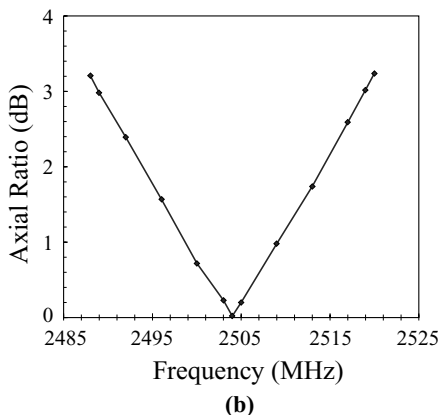
<sup>a</sup>Antenna parameters are given in Figure 5.58.



**FIGURE 5.60** Geometry of a circularly polarized circular microstrip antenna with a tuning stub. (From Ref. 19, © 1998 IEE, reprinted with permission.)



(a)



(b)

**FIGURE 5.61** Measured (a) input impedance and (b) axial ratio of the antenna shown in Figure 5.60;  $\epsilon_r = 4.4$ ,  $h = 1.6$  mm,  $D = 32$  mm,  $\ell_s = 6.9$  mm, and  $d_p = 8.6$  mm. (From Ref. 19, © 1998 IEE, reprinted with permission.)

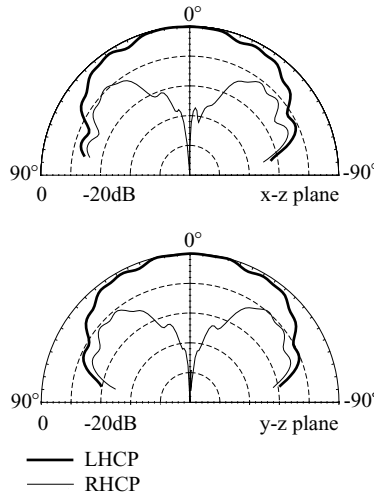


**FIGURE 5.62** Measured radiation patterns for the antenna studied in Figure 5.61 with  $f = 2504$  MHz. (From Ref. 19, © 1998 IEE, reprinted with permission.)

axial ratio of a typical design with left-hand CP operation (feed at point A). The center frequency is at 2504 MHz. The obtained CP bandwidth is 30 MHz, or 1.2%. The measured radiation patterns in two orthogonal planes at 2504 MHz are plotted in Figure 5.62, and good left-hand CP radiation is observed.

The present CP design has been applied to a circular microstrip patch with a cross slot of equal slot lengths. The antenna geometry is depicted in Figure 5.63. The cross slot has a length  $\ell$ , and the slot width is chosen to be 1 mm, the same as that of the tuning stub. Also, unlike the feed method shown in Figure 5.60 using a coax for a simple circular patch, a 50- $\Omega$  microstrip feed line with a quarter-wavelength impedance transformer is used as the feed for CP excitation. This feed method is

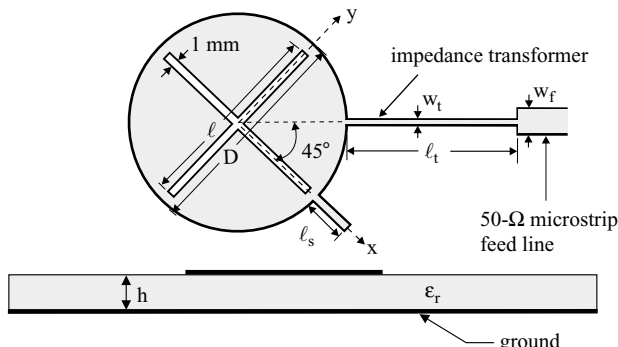


**FIGURE 5.63** Geometry of a compact circularly polarized circular microstrip antenna with a tuning stub for left-hand CP operation. (From Ref. 19, © 1998 IEE, reprinted with permission.)

a good alternative to the proximity-coupled method used in Ref. 2 and is useful for integration applications with coplanar microwave integrated circuits. These feed methods are used rather than a probe feed because, for such a design, no  $50\text{-}\Omega$  feed position exists in the microstrip patch when a large cross slot is introduced in the patch, and thus the probe feed method is not feasible for achieving CP radiation with a good impedance matching condition. Based on the design in Figure 5.63, a typical case with  $\ell = 30 \text{ mm}$  (about  $0.94D$ ) was implemented. The measured input impedance and axial ratio are presented in Figure 5.64. It is seen that the CP center frequency is decreased to 1587 MHz, which is about 63.4% that of the simple patch case. This decrease in the operating frequency corresponds to a 60% antenna size reduction. The 3-dB axial ratio bandwidth is found to be 14 MHz (or about 0.9%), which is less than that (1.2%) of the simple patch case, largely due to the decrease in

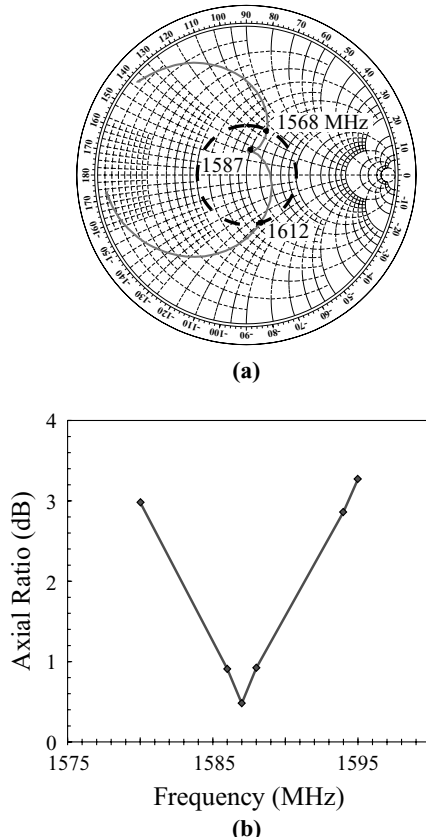


**FIGURE 5.64** Measured (a) input impedance and (b) axial ratio of the antenna shown in Figure 5.63;  $\epsilon_r = 4.4$ ,  $h = 1.6 \text{ mm}$ ,  $D = 32 \text{ mm}$ ,  $\ell = 30 \text{ mm}$ ,  $\ell_s = 8.5 \text{ mm}$ ,  $\ell_t = 27 \text{ mm}$ ,  $w_t = 0.8 \text{ mm}$ , and  $w_f = 3.0 \text{ mm}$ . (From Ref. 19, © 1998 IEE, reprinted with permission.)

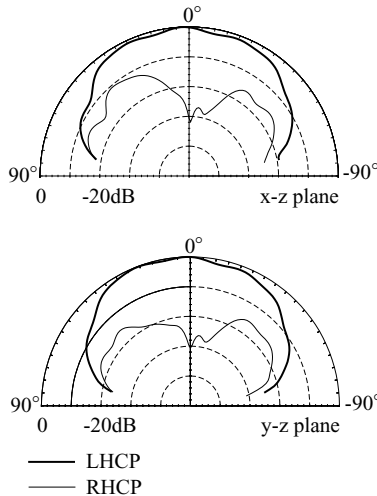


**FIGURE 5.65** Measured radiation patterns for the antenna studied in Figure 5.64 with  $f = 1587$  MHz. (From Ref. 19, © 1998 IEE, reprinted with permission.)

the electrical thickness of the substrate. The tuning stub in this design has a length of 8.5 mm (about  $0.26D$ ), which is slightly larger than that (6.9 mm) in the simple patch design, although the operating frequency is significantly decreased. Compared to the very small slot-length difference (0.5 mm, or about 0.0075 times the disk diameter) required in the design with a cross slot of unequal slot lengths [2], the present compact CP design with a tuning stub can have much relaxed manufacturing tolerances. The measured radiation patterns in two orthogonal planes at the center frequency are plotted in Figure 5.65. Good left-hand CP radiation is observed.

### 5.8.2 With a Square-Ring Patch

Figure 5.66 shows two antenna geometries of CP design with a tuning stub applied to a square-ring patch. The square-ring microstrip patch has an outer side length  $L_1$  and an inner side length  $L_2$ . The two arms of the cross strip are of equal width  $w_c$ . A small, narrow tuning stub of length  $\ell$  and width 1 mm is protruded at the patch corner for the case with a centerline cross strip [see Figure 5.66(a)] or at the center of the patch edge for the case with a diagonal cross strip [see Figure 5.67(b)]. With a tuning stub of proper length and a single probe feed at a position in the two arms of the cross strip [see Figures 5.66(a) and 5.66(b); point *A* for right-hand CP operation and point *B* for left-hand CP operation], the present design can be used for CP radiation with a compact antenna size compared to conventional CP designs [1].

Figure 5.67 shows the measured axial ratio of the constructed prototypes (antennas 1 and 2) of the design shown in Figure 5.66(a). The feed position is at point *A* for

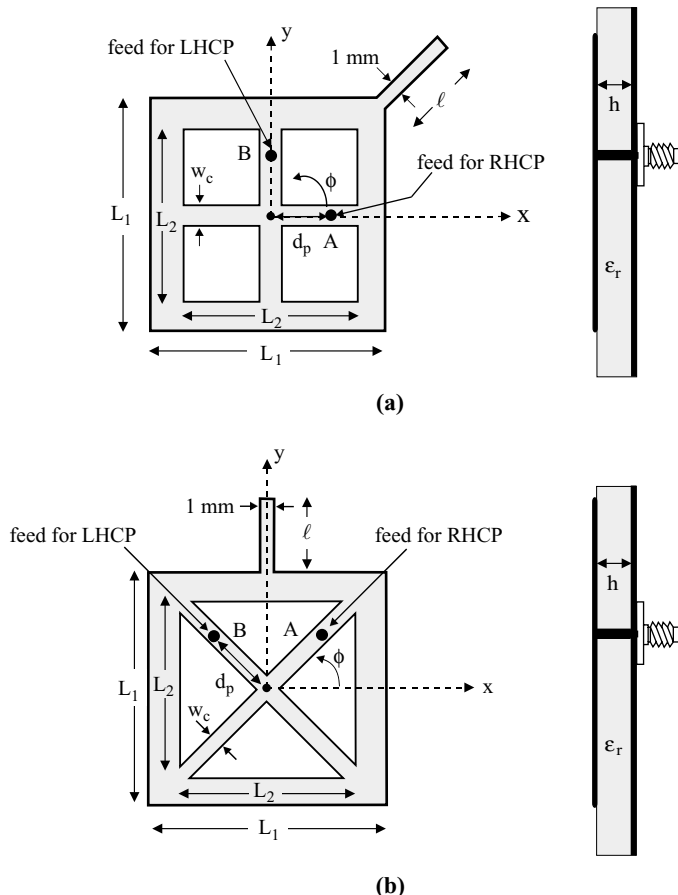


**FIGURE 5.66** Geometries of square-ring microstrip antennas with a cross strip for compact CP operation. (a) The case with a centerline cross strip, (b) the case with a diagonal cross strip. (From Ref. 20, © 1999 IEEE, reprinted with permission.)

right-hand CP radiation. The corresponding CP performance is listed in Table 5.15. The obtained CP center frequency is 1725 and 1695 MHz for antennas 1 and 2, respectively. Compared to the reference antenna (see Table 5.15), the center frequency of antenna 2 is lowered by about 18%. This lowering in center frequency corresponds to an antenna size reduction of about 33% by using the present design in place of the conventional CP design at a fixed frequency. From measured radiation patterns for antennas 1 and 2 at their respective center frequency, good right-hand CP radiation for both cases is observed.

The case with a diagonal cross strip has also been studied. The measured axial ratio for two constructed prototypes (antennas 3 and 4) is presented in Figure 5.68. Obtained CP performance is listed in Table 5.15. The center frequency is 1692 and

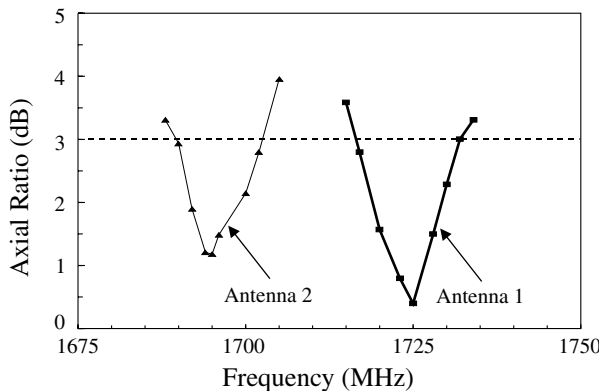


**FIGURE 5.67** Measured axial ratio for the case with a centerline cross strip shown in Figure 5.66(a);  $\epsilon_r = 4.4$ ,  $h = 1.6$  mm,  $L_1 = 34$  mm,  $w_c = 2$  mm, and feed at point A. Antenna 1:  $L_2 = 29$  mm,  $\ell = 5.5$  mm,  $d_p = 8$  mm; antenna 2:  $L_2 = 31.5$  mm,  $\ell = 4$  mm,  $d_p = 7.0$  mm. (From Ref. 20, © 1999 IEEE, reprinted with permission.)

1614 MHz, respectively, for antennas 3 and 4. For antenna 4, the center frequency is lowered by about 22% compared to that of the reference antenna. This suggests that an antenna size reduction of about 40% can be obtained by using the present design at a fixed frequency. Good radiation patterns of antennas 3 and 4 have been observed.

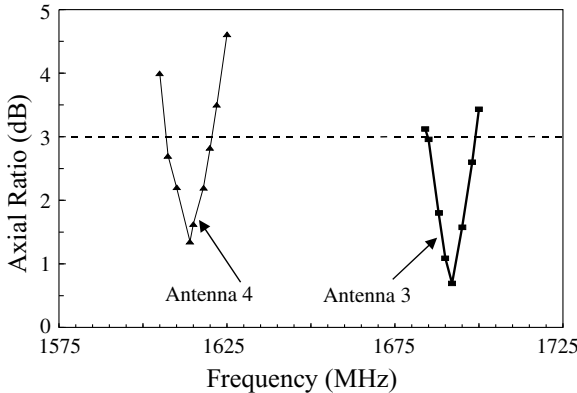
### 5.8.3 With a Triangular Patch

Figure 5.69 shows three promising CP designs with a tuning stub for triangular microstrip antennas. By simply loading a tuning stub of proper length at the triangular tip or at the center of the bottom edge of the triangular patch [see Figures 5.69(a) and 5.69(b)], two orthogonal near-degenerate resonant modes can easily be excited for

**TABLE 5.15 CP Performance of the Antennas in Figure 5.66 with a Centerline Cross Strip (Antennas 1 and 2) and with a Diagonal Cross Strip (antennas 3 and 4) [20]**

	$L_2$ (mm)	$\ell$ (mm)	$d_p$ (mm)	$f_c$ (MHz)	3-dB Axial-Ratio CP Bandwidth (%)	Maximum Received Power (dBm)
Antenna 1	29.0	5.5	8.0	1725	0.9	-51.8
Antenna 2	31.5	4.0	7.0	1695	0.9	-51.9
Antenna 3	29.0	8.3	7.5	1692	1.0	-51.9
Antenna 4	31.5	6.7	7.0	1614	1.8	-52.3
Reference <sup>a</sup>	—	—	—	2070	1.4	-50.0

<sup>a</sup>The reference antenna is based on a design using a conventional nearly square microstrip antenna of patch dimensions  $34 \times 33.14$  mm<sup>2</sup>.



**FIGURE 5.68** Measured axial ratio for the case with a diagonal cross strip shown in Figure 5.66(b);  $\epsilon_r = 4.4$ ,  $h = 1.6$  mm,  $L_1 = 34$  mm,  $w_c = 2$  mm, and feed at point *A*. Antenna 3:  $L_2 = 29$  mm,  $\ell = 8.3$  mm,  $d_p = 7.5$  mm; antenna 4:  $L_2 = 31.5$  mm,  $\ell = 6.7$  mm,  $d_p = 7.0$  mm. (From Ref. 20, © 1999 IEEE, reprinted with permission.)

CP operation. In addition, the present design can be applied to a compact triangular microstrip antenna with a cross-slot of equal slot lengths [see Figure 5.69(c)]. In this case, compact CP operation can be obtained.

**5.8.3.1 Design with a Tuning Stub Loaded at the Triangle Tip [Figure 5.69(a)]**  
For this design, three different patch side lengths (denoted antennas A1–A3) were studied; the CP performance is given in Table 5.16. Right-hand CP radiation is studied (feed at point *A* in the figure). Measured results indicate that good CP radiation is achieved, and the optimal tuning-stub length is about 0.09 times the side length of the triangular patch.

**5.8.3.2 Design with a Tuning Stub Loaded at the Bottom Edge [Figure 5.69(b)]**  
Three cases were studied (antennas B1–B3) and the results are listed in Table 5.17. The feed position is chosen at point *A* for right-hand CP radiation. It is seen that, when the tuning stub is at the bottom edge, the required tuning-stub length (about 0.3 times the patch's side length) for CP radiation is much larger than that in the design with the tuning stub at the triangle tip. This suggests that the effect of the tuning-stub loading is more prominent at the triangle tip than at the bottom edge.

**5.8.3.3 Design with a Tuning Stub and a Cross-Slot of Equal Slot Lengths [Figure 5.69(c)]**  
Compact CP design with three different cross-slot sizes (antennas C1–C3) has been studied. The obtained CP performance is listed in Table 5.18. It is observed that the CP center frequency decreases with increasing cross-slot length. For antenna C3, the center frequency is lowered to 1708 MHz, which is about 88% times that (1937 MHz) of the regular-size CP design (antenna A2). This lowering of the center frequency corresponds to an antenna size reduction of about 22% using

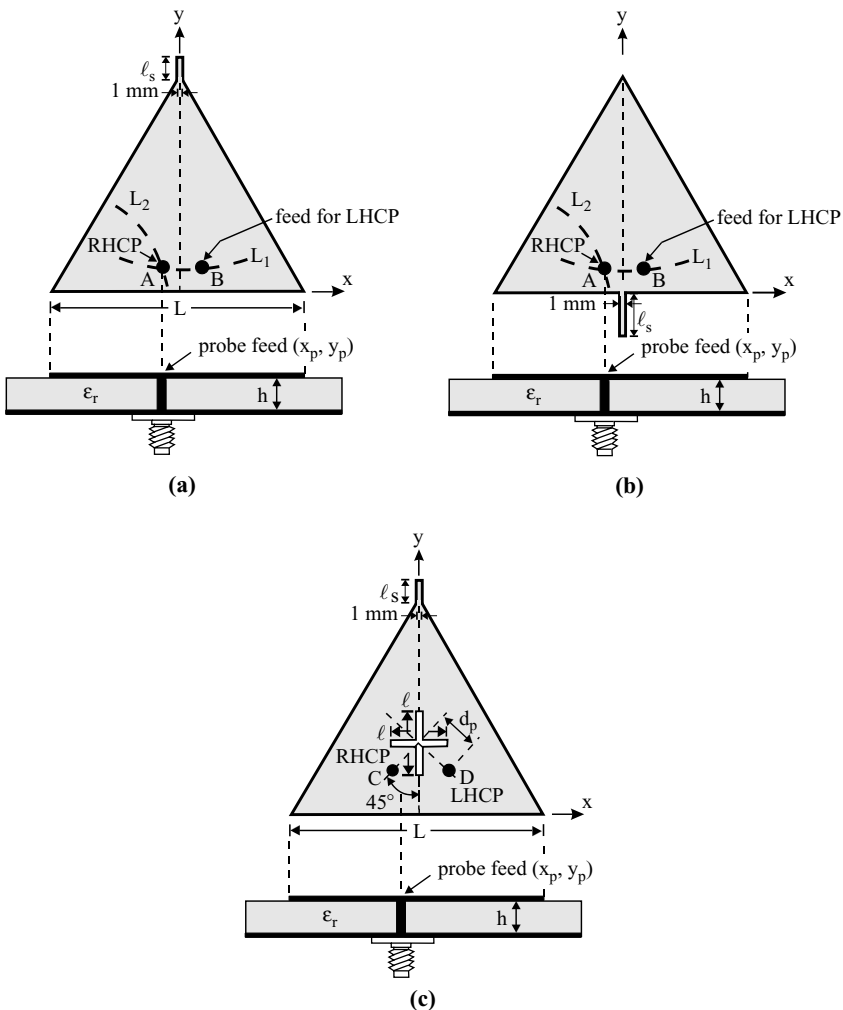


**FIGURE 5.69** Geometries of single-feed circularly polarized equilateral-triangular microstrip antennas. (a) With a tuning stub at the triangle tip, (b) with a tuning stub at the bottom edge of the triangular patch, and (c) with a tuning stub at the triangle tip and a cross slot at the patch center. (From Ref. 21, © 2000 IEEE, reprinted with permission.)

the present compact CP design in place of the CP design of Figure 5.69(a). Good measured right-hand CP radiation patterns have been obtained.

## 5.9 DESIGNS WITH A BENT TUNING STUB

A compact CP design with a symmetric cross-slot embedded in the patch center is shown in Section 5.8.1, in which CP operation is achieved by using a straight

**TABLE 5.16 CP Performance of the Antenna in Figure 5.69(a) [21]<sup>a</sup>**

	$L$ (mm)	$\ell_s$ (mm)	$f_c$ (MHz)	$(x_p, y_p)$ (mm)	3-dB Axial-Ratio CP Bandwidth (%)
Antenna A1	60	5.6	1564	(−8.0, 4.5)	1.15
Antenna A2	48	4.4	1937	(−5.2, 5.5)	1.14
Antenna A3	40	3.5	2325	(−3.5, 4.0)	1.16

<sup>a</sup> $\epsilon_r = 4.4$ ,  $h = 1.6$  mm, and feed at point  $A$ .

tuning stub loaded at the patch boundary, and the required tuning-stub length for CP operation for large antenna size reduction is about 26% of the patch's linear dimension; this significantly eases the stringent fabrication tolerances required in Ref. 2. In this section, another promising compact CP design with relaxed fabrication tolerances is described. This design uses a new symmetric slot embedded in the patch, and the CP operation is adjusted by using a bent tuning stub aligned along the patch boundary to make the antenna more compact in total size. The proposed patch geometry is shown in Figure 5.70. Excitation of the antenna is through a properly oriented coupling slot in the ground plane of the microstrip feed line; the feed arrangement is shown in Figure 1.15(b) in Chapter 1.

An experimental study has been conducted [22]. The required bent tuning stub has a length of 16.2 mm (or about  $0.65D$ ). This lengthening of the tuning stub yields a greatly relaxed fabrication tolerance for the proposed antenna, and the large tuning stub is bent to be aligned along the patch boundary in order to retain the compactness of the antenna. Since there exists no  $50\text{-}\Omega$  feed position inside the microstrip patch due to the large cross slot cut in the patch, the aperture-coupled feed method is used. It is found that, due to the bending of the tuning stub, the optimal relative position of the coupling slot and the modified cross slot in the microstrip patch for achieving good CP operation no longer has an angle  $\alpha$  of  $45^\circ$ . In the present design, the optimal angle is found to be  $2^\circ$ , which is significantly different from the case with a straight tuning stub. In this case, good right-hand CP operation is obtained. Figures 5.71 and 5.72 show the measured return loss and axial ratio, respectively. Good CP operation centered at 1470 MHz is obtained. Since this center frequency is about 0.44 times that (3300 MHz) of the design using an unslotted circular microstrip patch, a large

**TABLE 5.17 CP Performance of the Antenna in Figure 5.69(b) [21]<sup>a</sup>**

	$L$ (mm)	$\ell_s$ (mm)	$f_c$ (MHz)	$(x_p, y_p)$ (mm)	3-dB Axial-Ratio CP Bandwidth (%)
Antenna B1	60	18.5	1559	(−7.7, 4.7)	1.14
Antenna B2	48	14.7	1925	(−5.6, 3.8)	1.09
Antenna B3	40	12.2	2300	(−4.5, 3.2)	1.13

<sup>a</sup> $\epsilon_r = 4.4$ ,  $h = 1.6$  mm, and feed at point  $A$ .

**TABLE 5.18 CP Performance of the Antenna in Figure 5.69(c) [21]<sup>a</sup>**

	$\ell$ (mm)	$\ell_s$ (mm)	$f_c$ (MHz)	$d_p$ (mm)	3-dB Axial-Ratio CP Bandwidth (%)
Antenna C1	7.2	4.4	1915	8.8	1.09
Antenna C2	11.0	4.5	1860	7.0	1.02
Antenna C3	19.2	4.7	1708	2.5	0.88

<sup>a</sup> $\epsilon_r = 4.4$ ,  $h = 1.6$  mm,  $L = 48$  mm, and feed at point  $C$ .

antenna size reduction of about 80% can be expected for fixed CP operation. By choosing the angle  $\alpha$  to be  $178^\circ$ , left-hand CP operation is obtained for the present design.

## 5.10 COMPACT CP DESIGNS WITH AN INSET MICROSTRIP-LINE FEED

A CP design for exciting a circularly polarized microstrip antenna using a  $50\Omega$  inset microstrip-line feed has been reported [23]. The proposed designs are shown in Figure 5.73. Figure 5.73(a) shows the case with a narrow slit (denoted design A), Figure 5.73(b) is for the case with two pairs of slits (design B), and the design in Figure 5.73(c) is with three pairs of inserted slits (design C). The  $50\Omega$  inset microstrip line has a width  $w_c$  and an inset length  $\ell_t$ . All the inserted slits are of length  $\ell_s$  and width 1 mm, and the pairs of slits in Figures 5.73(b) and 5.73(c) are a distance  $d$  apart. The square patch has a side length  $L$  and a pair of truncated corners of dimensions

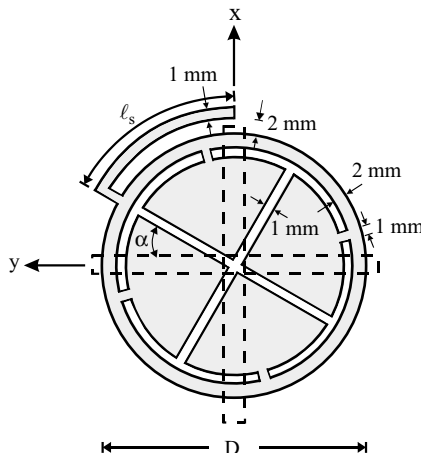


**FIGURE 5.70** Geometry of a circular microstrip patch with a modified cross slot and a bent tuning stub for compact CP operation. (From Ref. 22, © 1998 IEE, reprinted with permission.)

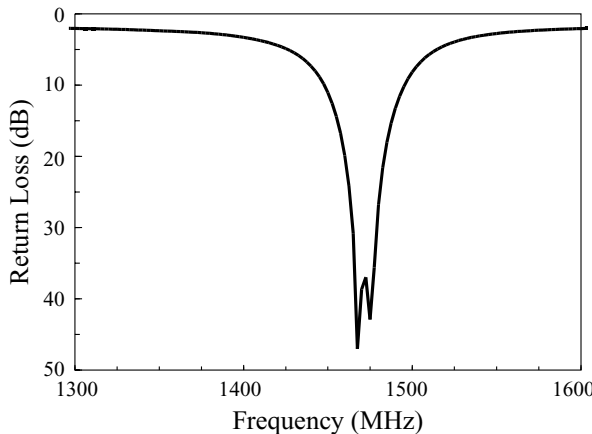


**FIGURE 5.71** Measured return loss for the antenna shown in Figure 5.70;  $\epsilon_1 = \epsilon_2 = 4.4$ ,  $h_1 = h_2 = 1.6$  mm,  $D = 25$  mm,  $\alpha = 2^\circ$ ,  $\ell_s = 16.2$  mm,  $L \times W = 26 \times 1.6$  mm $^2$ , and  $\ell_{ts} = 21$  mm. (From Ref. 22, © 1998 IEE, reprinted with permission.)

$\Delta L \times \Delta L$ . Because of the combined effects of the inset microstrip line and the slits, two orthogonal near-degenerate modes for CP radiation can easily be excited. Also, the excited patch surface currents are meandered in the present designs, and the obtained CP operating frequency is greatly lowered; thus, compact CP radiation can be achieved for the present designs.

A conventional probe-fed, circularly polarized, corner-truncated square microstrip antenna was first constructed as a reference antenna. The dimensions of truncated corners, the CP bandwidth, and the CP center frequency  $f_c$  are shown in Table 5.19. Figure 5.74 presents the measured input impedance and axial ratio of design A; the

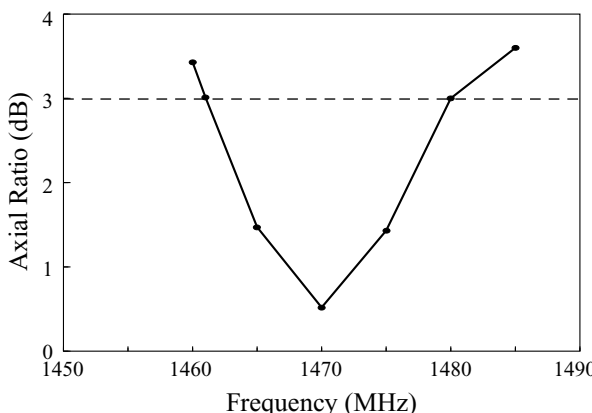


**FIGURE 5.72** Measured axial ratio for the antenna studied in Figure 5.71. (From Ref. 22, © 1998 IEE, reprinted with permission.)

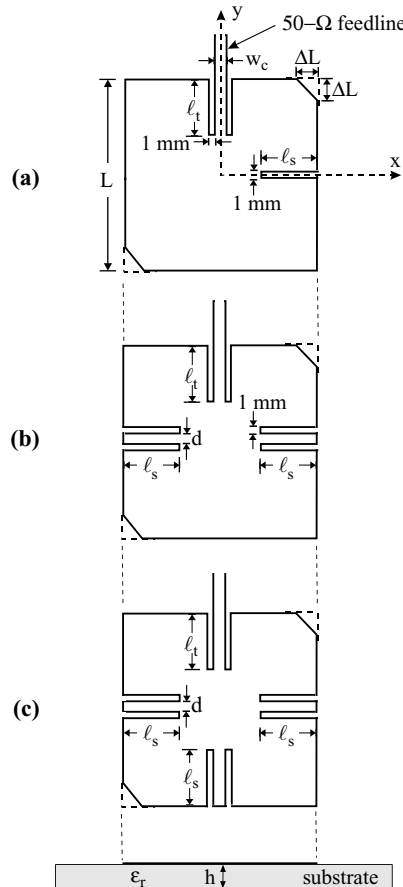


**FIGURE 5.73** Geometries of inset microstrip-line-fed microstrip antennas for compact CP operation. (a) Design A: corner-truncated square patch with a slit; (b) design B: corner-truncated square patch with two pairs of slits; (c) design C: corner-truncated square patch with three pairs of slits. Designs A–C are all with right-hand CP radiation. (From Ref. 23, © 1999 IEEE, reprinted with permission.)

**TABLE 5.19** CP Performance of the Antenna in Figure 5.73 [23]<sup>a</sup>

	$\ell_s$ (mm)	$d$ (mm)	$\ell_t$ (mm)	$\Delta L$ (mm)	$f_c$ (MHz)	3-dB Axial-Ratio CP Bandwidth (%)
Design A	9.7	—	7.4	3.3	2183	0.8
Design B	9.8	3.0	10.8	3.6	1775	0.8
Design C	10.8	3.0	10.8	3.9	1653	0.7
Reference	—	—	—	3.2	2480	1.4

<sup>a</sup> $\epsilon_r = 4.4$ ,  $h = 1.6$  mm,  $L = 28$  mm, and  $w_c = 3.0$  mm. Reference antenna is based on a simple corner-truncated square microstrip antenna with a probe feed.

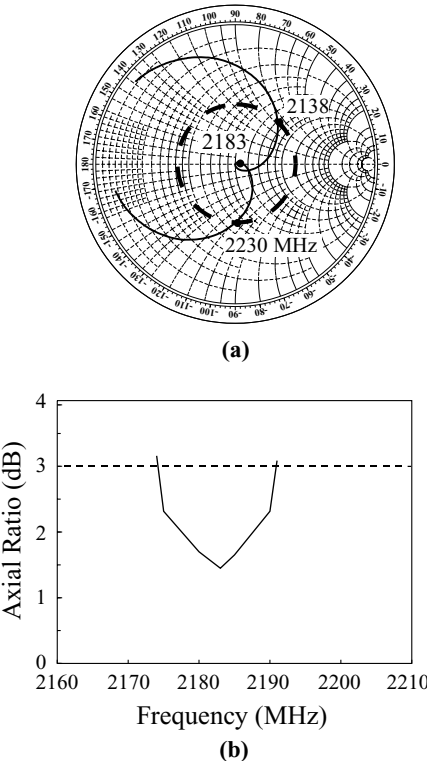


**FIGURE 5.74** Measured (a) input impedance and (b) axial ratio of the antenna shown in Figure 5.73(a) (design A);  $\epsilon_r = 4.4$ ,  $h = 1.6$  mm,  $L = 28$  mm,  $\Delta L = 3.3$  mm,  $\ell_s = 9.7$  mm,  $\ell_t = 7.4$  mm,  $w_c = 3.0$  mm, and ground-plane size =  $60 \times 60$  mm<sup>2</sup>. (From Ref. 23, © 1998 IEEE, reprinted with permission.)

corresponding results are given in Table 5.19. It is observed that two near-degenerate resonant modes with good impedance matching are excited [see Figure 5.74(a)], and the CP bandwidth [see Figure 5.74(b)] is 17 MHz, or about 0.8% with respect to the center frequency at 2183 MHz. Note that the center frequency is lowered by about 12% compared to that (2480 MHz) of the reference antenna. This corresponds to an antenna size reduction of about 23% for design A in place of the reference antenna at a fixed frequency. Measured radiation patterns are plotted in Figure 5.75, and good right-hand CP radiation is obtained. For designs B and C, parameters are given in Table 5.19. The CP center frequencies of designs B and C occur, respectively, at 1775 and 1653 MHz, which are lowered by about 28% and 33% compared to that of the reference antenna. That is, an antenna size reduction about 49% or 55% can be expected at a fixed frequency by replacing the reference antenna with design B or C, respectively. Measured radiation patterns of designs B and C indicate that good CP radiation is observed.

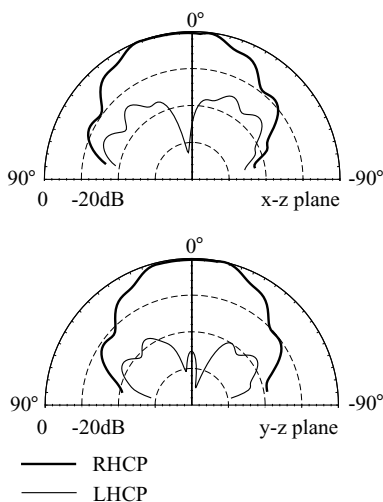


**FIGURE 5.75** Measured radiation patterns for the antenna studied in Figure 5.74 with  $f = 2183$  MHz. (From Ref. 23, © 1998 IEEE, reprinted with permission.)

## REFERENCES

1. J. R. James and P. S. Hall, *Handbook of Microstrip Antennas*, Peter Peregrinus, London, 1989.
2. H. Iwasaki, “A circularly polarized small-size microstrip antenna with a cross slot,” *IEEE Trans. Antennas Propagat.* **44**, 1399–1401, Oct. 1996.
3. J. H. Lu, C. L. Tang, and K. L. Wong, “Single-feed slotted equilateral-triangular microstrip antenna for circular polarization,” *IEEE Trans. Antennas Propagat.* **47**, 1174–1178, July 1999.
4. K. P. Yang, K. L. Wong, and J. H. Lu, “Compact circularly-polarized equilateral-triangular microstrip antenna with Y-shaped slot,” *Microwave Opt. Technol. Lett.* **20**, 31–34, Jan. 5, 1999.
5. K. L. Wong, W. H. Hsu, and C. K. Wu, “Single-feed circularly polarized microstrip antenna with a slit,” *Microwave Opt. Technol. Lett.* **18**, 306–308, July 1998.
6. J. H. Lu, C. L. Tang, and K. L. Wong, “Circular polarization design of a single-feed equilateral-triangular microstrip antenna,” *Electron. Lett.* **34**, 319–321, Feb. 19, 1998.
7. H. M. Chen and K. L. Wong, “On circular polarization design of annular-ring microstrip antennas,” *IEEE Trans. Antennas Propagat.* **47**, 1289–1292, Aug. 1999.
8. K. L. Wong and J. Y. Wu, “Single-feed small circularly polarized square microstrip antenna,” *Electron. Lett.* **33**, 1833–1834, Oct. 23, 1997.
9. K. L. Wong and M. H. Chen, “Single-feed small circular microstrip antenna with circular polarization,” *Microwave Opt. Technol. Lett.* **18**, 394–397, Aug. 20, 1998.
10. W. S. Chen, C. K. Wu, and K. L. Wong, “Novel compact circularly polarized square microstrip antenna,” *IEEE Trans. Antennas Propagat.* **49**, 340–342, March 2001.

11. J. Y. Wu, C. Y. Huang, and K. L. Wong, "Compact broadband circularly polarized square microstrip antenna," *Microwave Optical Technol. Lett.* **21**, 423–425, June 20, 1999.
12. J. H. Lu, H. C. Yu, and K. L. Wong, "Compact circular polarization design for equilateral-triangular microstrip antenna with spur lines," *Electron. Lett.* **34**, 1989–1990, Oct. 15, 1998.
13. S. A. Bokhari, J. F. Zuercher, J. R. Mosig, and F. E. Gardiol, "A small microstrip patch antenna with a convenient tuning option," *IEEE Trans. Antennas Propagat.* **44**, 1521–1528, Nov. 1996.
14. C. L. Tang, J. H. Lu, and K. L. Wong, "Circularly polarized equilateral-triangular microstrip antenna with truncated tip," *Electron. Lett.* **34**, 1277–1278, June 25, 1998.
15. W. S. Chen, C. K. Wu, and K. L. Wong, "Single-feed square-ring microstrip antenna with truncated corners for compact circular polarization operation," *Electron. Lett.* **34**, 1045–1047, May 28, 1998.
16. C. L. Tang and K. L. Wong, "A modified equilateral-triangular-ring microstrip antenna for circular polarization," *Microwave Opt. Technol. Lett.* **23**, 123–126, Oct. 20, 1999.
17. W. S. Chen, C. K. Wu, and K. L. Wong, "Compact circularly polarized microstrip antenna with bent slots," *Electron. Lett.* **34**, 1278–1279, June 25, 1998.
18. W. S. Chen, C. K. Wu, and K. L. Wong, "Compact circularly polarized circular microstrip antenna with cross slot and peripheral cuts," *Electron. Lett.* **34**, 1040–1041, May 28, 1998.
19. K. L. Wong and Y. F. Lin, "Circularly polarized microstrip antenna with a tuning stub," *Electron. Lett.* **34**, 831–832, April 30, 1998.
20. W. S. Chen, C. K. Wu, and K. L. Wong, "Square-ring microstrip antenna with a cross strip for compact circular polarization operation," *IEEE Trans. Antennas Propagat.* **47**, 1566–1568, Oct. 1999.
21. J. H. Lu and K. L. Wong, "Single-feed circularly-polarized equilateral-triangular microstrip antenna with a tuning stub," *IEEE Trans. Antennas Propagat.* **48**, 1869–1872, Dec. 2000.
22. K. L. Wong and M. H. Chen, "Slot-coupled small circularly polarized microstrip antenna with modified cross-slot and bent tuning-stub," *Electron. Lett.* **34**, 1542–1543, Aug. 6, 1998.
23. W. S. Chen, K. L. Wong, and C. K. Wu, "Inset microstripline-fed circularly polarized microstrip antennas," *IEEE Trans. Antennas Propagat.* **48**, 1253–1254, Aug. 2000.
24. Y. Suzuki, N. Miyano, and T. Chiba, "Circularly polarized radiation from singly fed equilateral-triangular microstrip antenna," *IEE Proc. Microw. Antennas Propagat.* **134**, 194–198, April 1987.
25. J. H. Lu and K. L. Wong, "Single-feed dual-frequency equilateral-triangular microstrip antenna with a pair of spur lines," *Electron. Lett.* **34**, 1171–1173, June 11, 1998.
26. M. D. Plessis and J. Cloete, "Tuning stubs for microstrip-patch antennas," *IEEE Antennas Propagat. Mag.* **36**, 52–56, Dec. 1994.

## CHAPTER SIX

---

# Compact Microstrip Antennas with Enhanced Gain

---

### 6.1 INTRODUCTION

Most compact microstrip antenna designs show decreased antenna gain owing to the antenna size reduction. To overcome this disadvantage and obtain an enhanced antenna gain, several designs for gain-enhanced compact microstrip antennas with the loading of a high-permittivity dielectric superstrate [1–3] or the inclusion of an amplifier-type active circuitry [4, 5] have been demonstrated. Use of a high-permittivity superstrate loading technique [6–8] gives an increase in antenna gain of about 10 dBi [1] with a smaller radiating patch. In Ref. 4, the radiating patch is modified to incorporate active circuitry to provide an enhanced antenna gain; an extra antenna gain of 8 dBi in L-band operation has been obtained. An amplifier-type active microstrip antenna as a transmitting antenna with enhanced gain and bandwidth has also been implemented [5]. Some design examples of these gain-enhanced compact microstrip antennas are presented.

### 6.2 COMPACT MICROSTRIP ANTENNAS WITH HIGH-PERMITTIVITY SUPERSTRATE

#### 6.2.1 Gain-Enhanced Compact Broadband Microstrip Antenna

Figure 6.1 shows the geometry of a gain-enhanced compact broadband rectangular microstrip antenna. It has been demonstrated that, by adding a high-permittivity superstrate layer, the antenna gain of a chip-resistor-loaded microstrip antenna can be increased to about the same level as that a conventional microstrip antenna [1]. The radiating patch has a  $1\text{-}\Omega$  chip resistor loaded at one of the patch edges. For operating at 1.84 GHz, a microwave substrate of  $\epsilon_r = 3.0$  and  $h_1 = 1.524$  mm is covered with a high-permittivity ceramic superstrate of  $\epsilon_r = 79$  and  $h_2 = 3.05$  mm. The superstrate thickness is determined by trying various thicknesses to optimize the enhanced

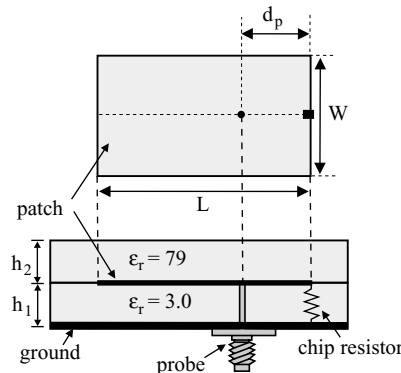


**FIGURE 6.1** Geometry of a gain-enhanced compact broadband rectangular microstrip antenna. (From Ref. 1, © 1998 IEE, reprinted with permission.)

gain with acceptable radiation patterns. Conventional and chip-resistor-loaded rectangular microstrip antennas were fabricated and measured for comparison. It was found that, at the fixed frequency  $f = 1.84$  GHz, the patch size of the resistor and superstrate-loaded microstrip antenna can be reduced to 6.05% times that of a conventional microstrip antenna. The dimensions of the three fabricated antennas are listed in Table 6.1.

Figure 6.2 shows the measured return loss for the three antennas in Table 6.1. The measured input impedance bandwidths (10-dB return-loss bandwidth) are 19.6 MHz (1.07%) for the conventional antenna, 145.6 MHz (7.91%) for the resistor-loaded antenna, and 120 MHz (6.52%) for the proposed resistor- and superstrate-loaded antenna. Figure 6.3 shows the  $E$ -plane radiation patterns of the three antennas. The maximum relative received power for the proposed antenna is  $-46.9$  dBm; that is, the proposed antenna has a net power increment of 10.4 dB compared with the resistor-loaded antenna ( $-57.3$  dBm) and about 1.3 dB lower than that of the conventional antenna ( $-45.6$  dBm). The measured  $H$ -plane radiation patterns are plotted in Figure 6.4. The maximum relative received power for the proposed antenna is  $-47.7$  dBm, a net power increment of 10.8 dB compared with the resistor-loaded antenna ( $-58.5$  dBm) and about 1.9 dB lower than that of the conventional antenna ( $-45.8$  dBm). The performance of the proposed antenna constructed here can be optimized by choosing different superstrate permittivities and thicknesses.

**TABLE 6.1 Dimensions of Three Rectangular Microstrip Antennas in Figure 6.2 Operated at 1.84 GHz [1]**

Antenna	$L$ (mm)	$W$ (mm)	$h_1$ (mm)	$h_2$ (mm)	$d_p$ (mm)
Conventional	46.7	30.0	1.524	—	18.3
1- $\Omega$ resistor loading	11.5	8.0	1.524	—	1.0
Resistor and superstrate loading	10.6	8.0	1.524	3.05	0.8

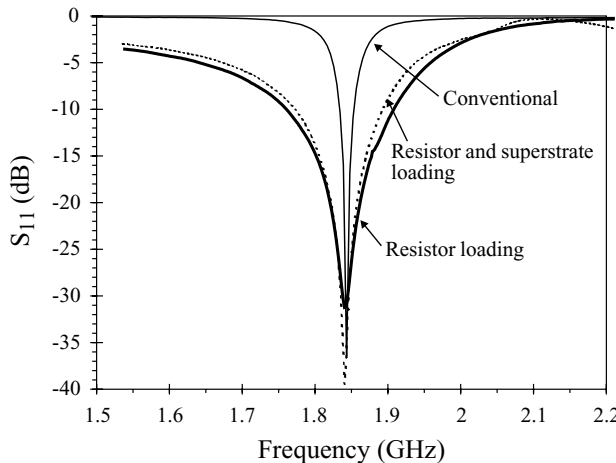


**FIGURE 6.2** Measured return loss of three fabricated microstrip antennas; parameters are given in Table 6.1. (From Ref. 1, © 1998 IEE, reprinted with permission.)

### 6.2.2 Gain-Enhanced Compact Circularly Polarized Microstrip Antenna

The design of a high-gain, compact microstrip antenna with CP radiation has been reported [2]. The small size of the microstrip antenna results from both the high-permittivity superstrate loading and slits cut in the patch. In addition, the antenna gain is enhanced by choosing the superstrate thickness to be about one-quarter wavelength in the superstrate layer. A typical design with 30% lower antenna size (projection area) and 5.2 dB higher antenna gain compared to the conventional CP design has

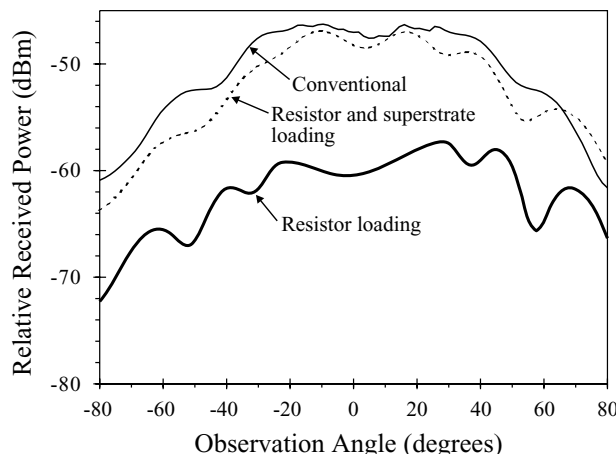


**FIGURE 6.3** Measured  $E$ -plane radiation patterns of three fabricated microstrip antennas; parameters are given in Table 6.1. (From Ref. 1, © 1998 IEE, reprinted with permission.)

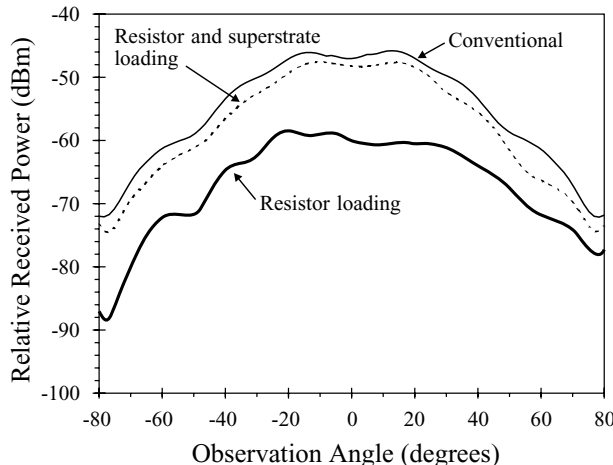


**FIGURE 6.4** Measured *H*-plane radiation patterns of three fabricated microstrip antennas; parameters are given in Table 6.1. (From Ref. 1, © 1998 IEE, reprinted with permission.)

been obtained. Figure 6.5 shows a proposed compact circularly polarized microstrip antenna with an enhanced gain. Two pairs of unequal slit lengths  $\ell_x$  and  $\ell_y$  ( $\ell_x > \ell_y$ ) are cut in the patch to split the fundamental resonant mode into two orthogonal near-degenerate modes for CP operation. The case with  $\ell_x > \ell_y$  and feed position at point *C* is for right-hand CP operation. When superstrates of various thicknesses are loaded onto the microstrip antenna, its resonant frequency is decreased, and the required slit lengths and 50- $\Omega$  feed position need to be adjusted to achieve good CP operation.

High-permittivity ( $\epsilon_{r2} = 79$ ) ceramic superstrates of various thicknesses were loaded onto a compact circularly polarized microstrip antenna. The antenna parameters and performance are listed in Table 6.2. When no slits and superstrate

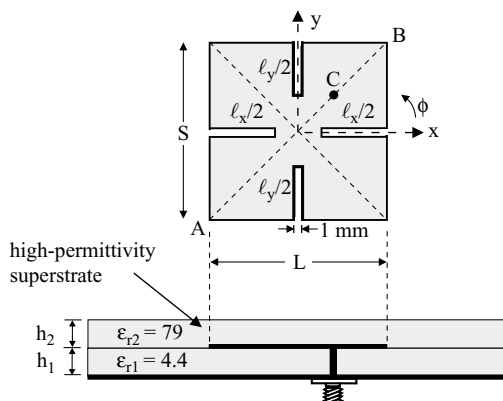


**FIGURE 6.5** Geometry of a gain-enhanced compact microstrip antenna with right-hand CP radiation. (From Ref. 2, © 1998 IEE, reprinted with permission.)

**TABLE 6.2 Comparison of Circularly Polarized Microstrip Antennas Covered with High-Permittivity Superstrates of Various Thicknesses [2]<sup>a</sup>**

	Patch Size $L \times S$ (mm $^2$ )	Slit Length $\ell_x, \ell_y$ (mm)	Superstrate Thickness $h_2$ (mm)	Feed Position $\overline{BC}$ (mm)	$f_c$ (MHz)	Maximum Received Power (dBm)
Antenna 1	$26.2 \times 26.2$	—	—	13.3	2697	-55.58
Antenna 2	$26.2 \times 26.2$	10.0, 9.0	2.18 (0.159 $\lambda_s$ )	12.7	2467	-52.56
Antenna 3	$26.2 \times 26.2$	10.5, 9.0	2.59 (0.186 $\lambda_s$ )	13.0	2422	-52.43
Antenna 4	$26.2 \times 26.2$	9.8, 9.0	3.20 (0.226 $\lambda_s$ )	12.8	2389	-51.70
Antenna 5	$26.2 \times 26.2$	9.7, 9.0	3.92 (0.264 $\lambda_s$ )	12.5	2272	-50.34
Antenna 6	$26.2 \times 26.2$	10.2, 9.0	4.34 (0.281 $\lambda_s$ )	12.1	2187	-52.22
Antenna 7	$31.1 \times 31.8$	—	—	15.8	2272	-55.55

<sup>a</sup> $\varepsilon_{r1} = 4.4$ ,  $\varepsilon_{r2} = 79$ ,  $h_1 = 1.6$  mm, and  $\lambda_s$  = wavelength in the superstrate.

are present, a square patch with dimensions  $26.2 \times 26.2$  mm $^2$  has a fundamental resonant frequency of 2697 MHz. For antennas with various superstrate loadings, the slit length  $\ell_y$  is fixed and  $\ell_x$  is adjusted to achieve CP operation. For good impedance matching, point  $C$  is slightly varied along the diagonal  $\overline{AB}$ . For the cases studied here, the optimal position for point  $C$  lies at about 12.1–13.3 mm [(0.326–0.354) $\overline{AB}$ ] from the patch corner. The results show that the microstrip antenna has a maximum relative received power when the superstrate thickness is about one-quarter of the wavelength of the wave propagating in the superstrate layer (see antenna 5 in Table 6.2). Compared to a conventional CP design (antenna 7 in Table 6.2) using a nearly square patch without slits and superstrate loading at the same operating frequency (2272 MHz), the proposed antenna (antenna 5) has a 30% smaller patch size and a 5.21 dB greater antenna gain. This gives the proposed antenna a gain nearly equivalent to that of a  $2 \times 2$  array with the conventional design (antenna 7) for the array elements. The measured input impedances for antennas 5 and 7 are shown in Figure 6.6. The measured axial ratio for antenna 5 is presented in Figure 6.7. The CP bandwidth determined from the 3-dB axial ratio is about 32 MHz, or 1.4%, which is much larger than that obtained for antenna 7 (0.65%; not shown). Typical measured radiation patterns for the proposed and conventional antennas are plotted in Figure 6.8. The proposed antenna is clearly seen to have a much higher antenna gain than the conventional antenna.

### 6.3 COMPACT MICROSTRIP ANTENNAS WITH ACTIVE CIRCUITRY

An amplifier-type active microstrip antenna integrates a two-port amplifier circuitry into a passive microstrip antenna and can work as a transmitting or receiving antenna [4, 5, 9]. In this section, the configuration of an amplifier-type active microstrip antenna for enhanced antenna gain and wider impedance bandwidth is presented. The active microstrip antenna studied here consists of a passive microstrip antenna and amplifier circuitry with a DC bias feedback resistor. With the selection of a possible maximum feedback resistance in the active circuitry for biasing the amplifier into

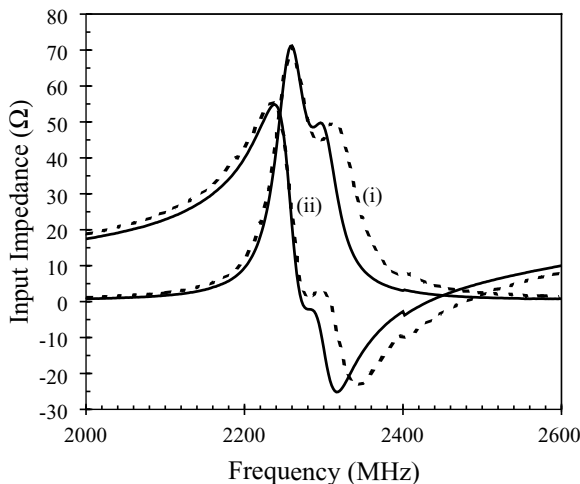


**FIGURE 6.6** Measured input impedance for the antenna shown in Figure 6.5. Curve (i) is for an antenna with a high-permittivity superstrate and slits in the patch, and curve (ii) is for an antenna with a nearly square patch. Parameters and performance of antennas (i) and (ii) are given, respectively, by antennas 5 and 7 in Table 6.2. (From Ref. 2, © 1998 IEE, reprinted with permission.)

the active region of performance, the impedance bandwidth of the active microstrip antenna can be greatly enhanced for a given extra output gain.

Figure 6.9 shows the antenna geometry studied. The antenna works as a transmitting antenna, and an equilateral-triangular radiating patch was used to give a smaller size compared to square or circular patches at a fixed operating frequency. When ports 1 and 2 are interchanged, the resulting active microstrip antenna functions as a receiving antenna. The passive microstrip antenna shown in the figure is an

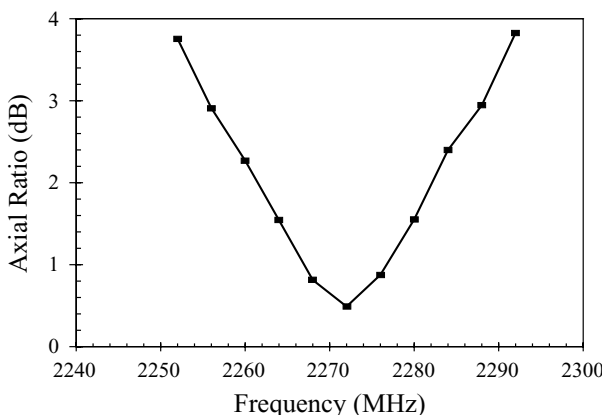


**FIGURE 6.7** Measured axial ratio for antenna 5 shown in Table 6.2. (From Ref. 2, © 1998 IEE, reprinted with permission.)

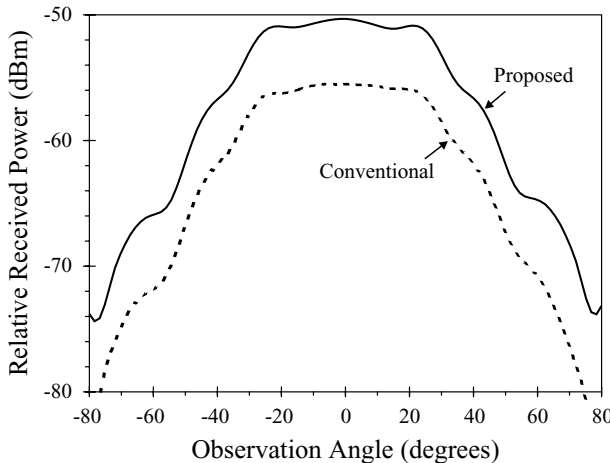


**FIGURE 6.8** Measured radiation patterns in the  $\phi = 135^\circ$  plane at 2272 MHz for the proposed antenna (antenna 5 in Table 6.2) and for a conventional nearly square microstrip antenna (antenna 7 in Table 6.2). (From Ref. 2, © 1998 IEE, reprinted with permission.)

inset-microstrip-line-fed equilateral-triangular microstrip antenna with a pair of bent slots of bend angle  $150^\circ$  [10]. This passive microstrip antenna can have a wide impedance bandwidth about 3.0 times that of a corresponding unslotted triangular microstrip antenna. The use of such a broadband passive antenna gives the resulting active antenna a wider impedance bandwidth than that obtained in Ref. 10 in addition to the extra output gains achieved.

The active circuitry is shown in Figure 6.9(b). This active circuitry is directly connected to the passive microstrip antenna through a  $50\Omega$  inset microstrip feed line, which eliminates the need for a quarter-wavelength transmission line for impedance matching. The active antenna can thus be implemented in a more compact configuration. In this study, a Hewlett Packard low-noise AT-41511 bipolar transistor is used, which is biased through a collector resistor  $R_C$  and a feedback resistor  $R_F$ . Here  $C_1$  and  $C_2$  are DC blocking capacitors and  $L_C$  and  $C_C$  are RF chokes, which prevent the RF signal from feeding back to the DC source. The two L-network filters  $L_S$ ,  $C_S$  and  $C_L$ ,  $L_L$  function as impedance matching networks for both input and output ports of the active circuitry. Owing to the presence of the feedback resistor  $R_F$ , which is usually much larger than  $R_C$ , the quality factor of the resulting active antenna will be lowered with an increase in  $R_F$ . This suggests that, by selecting a possible maximum value of  $R_F$  to bias the transistor into the active region of performance, the impedance bandwidth of the resulting active antenna can be greatly increased.

The active microstrip antenna is implemented using an inexpensive FR4 substrate (relative permittivity 4.4, thickness 1.6 mm). Figure 6.10 shows the measured return loss for three different values of  $R_F$ : 33.3, 42.7, and  $50.7\text{ k}\Omega$ . (Note that for the transistor to be in the active region, the value of  $R_F$  in this study should be less than about  $60\text{ k}\Omega$  and greater than about  $12\text{ k}\Omega$ .) The results show that the impedance bandwidth increases with increasing  $R_F$ . It is also observed that two resonant modes are excited owing to the broadband characteristics of the passive slotted triangular

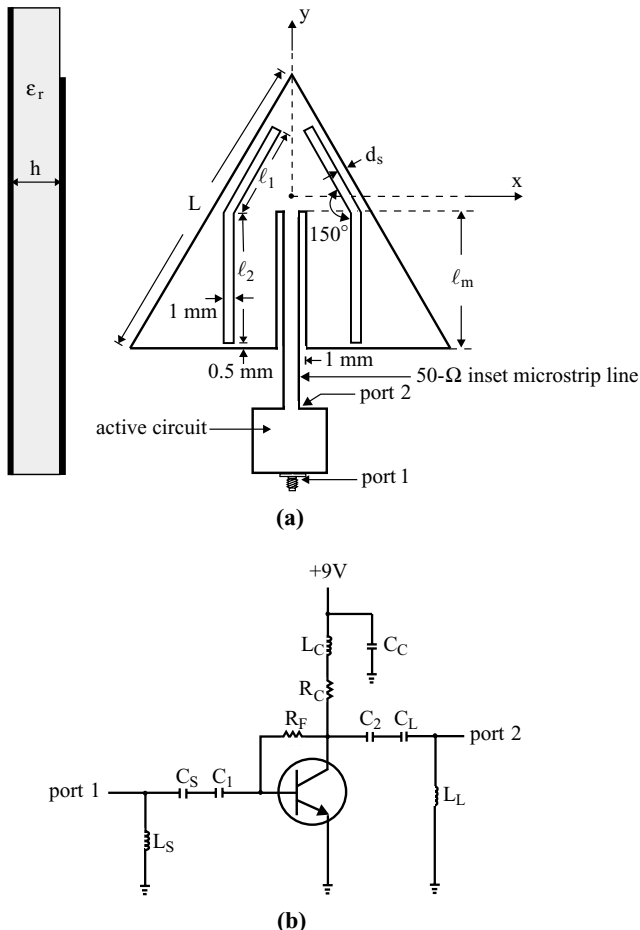


**FIGURE 6.9** (a) Geometry of an active equilateral-triangular microstrip antenna with enhanced gain and bandwidth and (b) layout of the active circuitry. (From Ref. 5, © 1999 John Wiley & Sons, Inc.)

microstrip antenna [10]. The impedance bandwidth, determined from the 10-dB return loss, for the case with  $R_F = 50.7\text{ k}\Omega$  is 164 MHz, or about 9.3% referenced to the center frequency at 1760 MHz. This impedance bandwidth is about 2.0 times that of the passive slotted antenna studied here (about 4.7% [10]) or 6.0 times that of the passive simple triangular microstrip antenna without slots (about 1.6%). The obtained impedance bandwidths for  $R_F = 33.3$  and  $42.7\text{ k}\Omega$  are also larger than that of the passive slotted antenna and are 125 MHz (about 7.1%) and 135 MHz (about 7.6%), respectively.

The radiation characteristics and antenna gain have been studied. Figure 6.11 shows typical measured  $E$ -plane ( $y$ - $z$  plane) and  $H$ -plane ( $x$ - $z$  plane) radiation patterns at the two resonant modes of the active antenna with  $R_F = 50.7\text{ k}\Omega$ . The results show

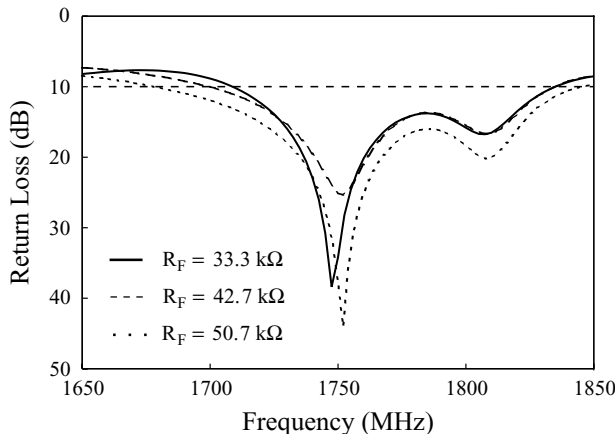


**FIGURE 6.10** Measured return loss for the active antenna shown in Figure 6.9;  $\epsilon_r = 4.4$ ,  $h = 1.6 \text{ mm}$ ,  $L = 50 \text{ mm}$ ,  $\ell_m = 26.2 \text{ mm}$ ,  $\ell_1 = 26.0 \text{ mm}$ ,  $\ell_2 = 11.5 \text{ mm}$ ,  $d_S = 2.3 \text{ mm}$ , ground-plane size =  $100 \times 100 \text{ mm}^2$ ,  $L_S = 4.44 \text{ nH}$ ,  $C_S = 2.4 \text{ pF}$ ,  $C_1 = 680 \text{ pF}$ ,  $C_2 = 6800 \text{ pF}$ ,  $C_L = 47 \text{ pF}$ ,  $L_L = 8.86 \text{ nH}$ ,  $L_C = 8.2 \mu\text{H}$ ,  $C_C = 6800 \text{ pF}$ , and  $R_C = 808 \Omega$ . (From Ref. 5, © 1999 John Wiley & Sons, Inc.)

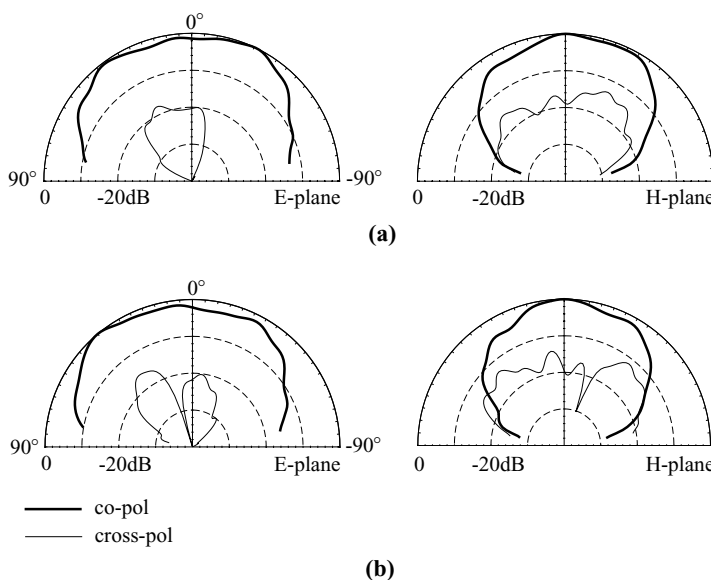


**FIGURE 6.11** Measured  $E$ -plane ( $y$ - $z$  plane) and  $H$ -plane ( $x$ - $z$  plane) radiation patterns of the active antenna studied in Figure 6.10 with  $R_F = 50.7 \text{ k}\Omega$ . (a)  $f = 1752 \text{ MHz}$ , (b)  $f = 1808 \text{ MHz}$ . (From Ref. 5, © 1999 John Wiley & Sons, Inc.)

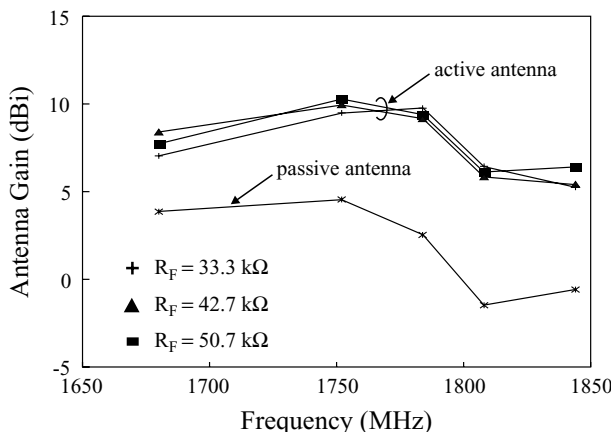


**FIGURE 6.12** Measured antenna gain in the broadside direction for the antennas studied in Figure 6.10. (From Ref. 5, © 1999 John Wiley & Sons, Inc.)

good radiation characteristics. Figure 6.12 presents the measured antenna gain in the broadside direction for the active antennas studied in Figure 6.10. The results clearly indicate that the antenna gain of active antennas with various bias feedback resistances is about the same, and about 6 dBi greater than that of the passive slotted triangular microstrip antenna. A relatively more uniform antenna gain as a function of frequency is observed for the active antennas compared to the passive slotted triangular microstrip antenna shown in the figure.

## REFERENCES

1. C. Y. Huang, J. Y. Wu, C. F. Yang, and K. L. Wong, "Gain-enhanced compact broadband microstrip antenna," *Electron. Lett.* **34**, 138–139, Jan. 22, 1998.
2. C. Y. Huang, J. Y. Wu, and K. L. Wong, "High-gain compact circularly polarized microstrip antenna," *Electron. Lett.* **34**, 712–713, April 16, 1998.
3. Y. Huang, Y. P. Zhang, G. X. Zheng, and T. K. C. Lo, "Planar inverted F antenna loaded with high permittivity material," *Electron. Lett.* **31**, 1710–1712, Sept. 28, 1995.
4. B. Robert, T. Razban, and A. Papiernik, "Compact amplifier integration in square patch antenna," *Electron. Lett.* **28**, 1808–1810, Sept. 10, 1992.
5. M. C. Pan and K. L. Wong, "A broadband active equilateral-triangular microstrip antenna," *Microwave Opt. Technol. Lett.* **22**, 387–389, Sept. 20, 1999.
6. H. Y. Yang and N. G. Alexopoulos, "Gain enhancement methods for printed circuit antennas through multiple superstrates," *IEEE Trans. Antennas Propagat.* **35**, 860–863, July 1987.
7. Y. P. Zhang, Y. Hwang, and G. X. Zheng, "A gain-enhanced probe-fed microstrip patch antenna of very high permittivity," *Microwave Opt. Technol. Lett.* **15**, 89–91, June 5, 1997.

8. T. K. Lo, C. O. Ho, Y. Hwang, E. K. W. Lam, and B. Lee, "Miniature aperture-coupled microstrip antenna of very high permittivity," *Electron. Lett.* **33**, 9–10, Jan. 2, 1997.
9. J. Lin and T. Itoh, "Active integrated antennas," *IEEE Trans. Microwave Theory Tech.* **42**, 2186–2194, Dec. 1994.
10. S. T. Fang, K. L. Wong, and T. W. Chiou, "Bandwidth enhancement of inset-microstrip-line-fed equilateral-triangular microstrip antenna," *Electron. Lett.* **34**, 2184–2186, Nov. 12, 1998.

## CHAPTER SEVEN

---

# Broadband Microstrip Antennas

---

### 7.1 INTRODUCTION

In this chapter, some recently reported broadband or bandwidth-enhancement techniques are presented. By applying the well-known method of using additional microstrip resonators [1, 2], a broadband design using both directly coupled and gap-coupled coplanar microstrip resonators for achieving an impedance bandwidth larger than 10% (with a thin dielectric substrate) [3] is presented in Section 7.2. In Section 7.3, some typical broadband designs with a thick air or foam substrate are demonstrated. These designs include the use of modified probe feeds [4–11] or modified radiating patches [12–20] for overcoming the problem of large probe reactance owing to the long probe pin in the thick substrate layer. The large probe reactance usually makes impedance matching over a wide bandwidth difficult to achieve, and the obtained impedance bandwidth is in general less than 10%. With the proposed designs [4–20], achieving an impedance bandwidth larger than 25% becomes easy. For modified probe feeds, designs with gap-coupled probe feed [4, 5], capacitively coupled feed [6, 7], L-probe/L-strip coupled feed [8–10], and three-dimensional microstrip transition feed [11] have been reported. For modified radiating patches, it has been shown that, by embedding a U-shaped slot in the radiating patch (U-slotted patch) [12–14], cutting a pair of wide slits (E-patch) at the boundary of the patch [15–18], or using a three-dimensional V-shaped patch [19] or a wedge-shaped patch [20], good impedance matching over a wide bandwidth can be obtained. Experimental results for prototypes of these designs are presented and discussed.

Promising methods of embedding suitable slots [21–24] and integrating microstrip reactive loading [25–28] in an antenna's radiating patch are discussed in Sections 7.4 and 7.5, respectively. These two methods are mainly applicable for microstrip antennas with thin substrates, and in this case, the low-profile advantage of microstrip antennas is retained. Finally, a typical design for a broadband microstrip antenna with

the use of two out-of-phase feeds to reduce the cross-polarization radiation [10] is shown in Section 7.6.

## 7.2 USE OF ADDITIONAL MICROSTRIP RESONATORS

By using additional microstrip patches directly coupled to the radiating or nonradiating edges of a rectangular microstrip antenna, a broadband microstrip antenna can be achieved. For such a design, a rectangular microstrip antenna with two additional patches directly coupled to its radiating edges, the impedance bandwidth can be five times that of a single rectangular microstrip antenna. However, the resulting broadband microstrip antenna also has a much increased antenna size compared to a single rectangular microstrip antenna. In this section, a compact configuration for a broadband rectangular microstrip antenna with a directly coupled patch and two gap-coupled parasitic patches (see Figure 7.1) for achieving broadband operation is demonstrated. The two parasitic patches are gap-coupled to the nonradiating edges of the rectangular microstrip antenna, while the directly coupled patch is connected to the radiating edge of the rectangular microstrip antenna through a narrow conducting strip. The present antenna has a more compact configuration than a rectangular microstrip antenna with two directly coupled patches [1]. In addition, by selecting the four patches in the present antenna to have slightly different resonant lengths, four resonant modes can be excited at frequencies close to each other; thus, an operating bandwidth greater than that of the design with two directly coupled patches [1], which usually shows three excited resonant modes in the operating bandwidth, can be expected.

As shown in Figure 7.1, a rectangular microstrip antenna having dimensions  $L_1 \times W_1$  (patch 1 in the figure) has additional resonators of a directly coupled patch of

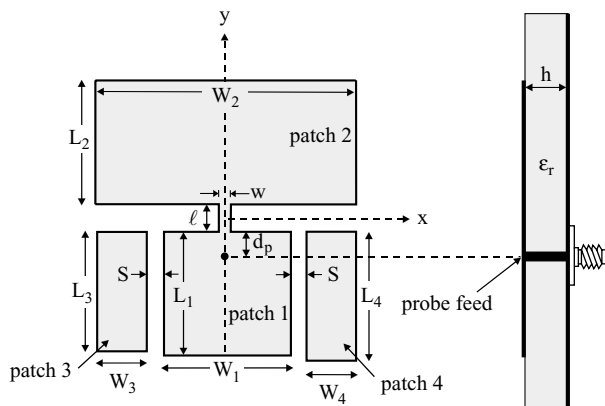


**FIGURE 7.1** Geometry of a proposed broadband microstrip antenna with directly coupled and parasitic patches. (From Ref. 3, © 1999 John Wiley & Sons, Inc.)

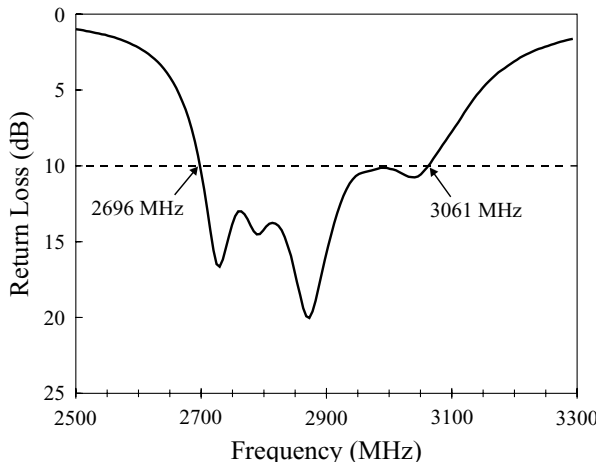


**FIGURE 7.2** Measured return loss against frequency for the antenna shown in Figure 7.1;  $\epsilon_r = 4.4$ ,  $h = 1.6$  mm,  $L_1 = 26.6$  mm,  $L_2 = 24.4$  mm,  $L_3 = 26.47$  mm,  $L_4 = 27$  mm,  $W_1 = 16$  mm,  $W_2 = 40$  mm,  $W_3 = W_4 = 10$  mm,  $S = 2$  mm,  $\ell = 2$  mm,  $w = 0.2$  mm, and  $d_p = 1.2$  mm. (From Ref. 3, © 1999 John Wiley & Sons, Inc.)

dimensions  $L_2 \times W_2$  (patch 2) and two gap-coupled parasitic patches of dimensions  $L_3 \times W_3$  (patch 3) and  $L_4 \times W_4$  (patch 4), respectively. Patch 2 is connected to the radiating edge of patch 1 through a narrow conducting strip of length  $\ell$  and width  $w$ . Patches 3 and 4 are gap-coupled, with a gap spacing of  $S$ , to the nonradiating edges of patch 1. The lengths  $L_2$ ,  $L_3$ , and  $L_4$  of patches 2–4 in the excitation direction are selected to be slightly different from that ( $L_1$ ) of the excited patch (patch 1), which can result in three additional resonant modes closely excited at frequencies near the fundamental resonant frequency of the excited patch. A wide impedance bandwidth can thus be obtained. Also, good impedance matching for the excited resonant modes can be achieved by placing a probe feed at a position along the centerline ( $y$  axis) of patch 1 a distance  $d_p$  from the connecting strip.

A prototype of the proposed design has been constructed and studied [3]. Figure 7.2 shows the measured return loss. It is clearly seen that there are four resonances in the measured return-loss curve. The impedance bandwidth, determined from the 10-dB return loss, is 365 MHz, which is about 12.7% of the center frequency at 2879 MHz [the center frequency is defined here to be  $(f_L + f_H)/2$ , where  $f_L$  and  $f_H$  are respectively the lower and higher frequencies with 10-dB return loss in the bandwidth]. Since the impedance bandwidth is 54 MHz, or about 2% with respect to the center frequency at 2710 MHz, for the rectangular microstrip antenna (patch 1) without directly coupled and parasitic patches, the impedance bandwidth for the constructed prototype is about 6.35 times that of the antenna with patch 1 only (12.7% vs. 2%). The radiation characteristics of the operating frequencies within the impedance bandwidth were studied. Figure 7.3 shows the measured radiation patterns at the four resonances

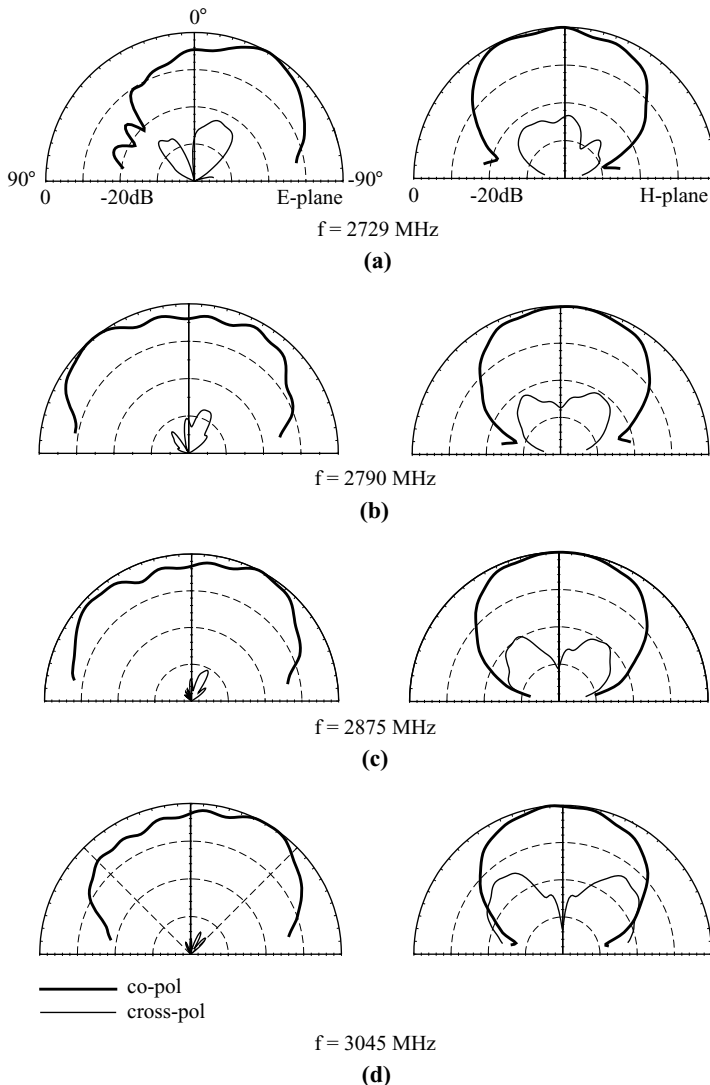


**FIGURE 7.3** Measured *E*-plane ( $y$ - $z$  plane) and *H*-plane ( $x$ - $z$  plane) radiation patterns for the antenna studied in Figure 7.2. (a)  $f = 2729$  MHz, (b)  $f = 2790$  MHz, (c)  $f = 2875$  MHz, (d)  $f = 3045$  MHz. (From Ref. 3, © 1999 John Wiley & Sons, Inc.)

in the impedance bandwidth. Good *H*-plane patterns are observed. However, some distortions in the *E*-plane patterns are seen. The measured maximum received power in the broadside direction of the antenna for frequencies within the impedance bandwidth is shown in Figure 7.4. The results suggest that the antenna gain variation for the operating frequencies within the impedance bandwidth is less than 2.5 dBi.

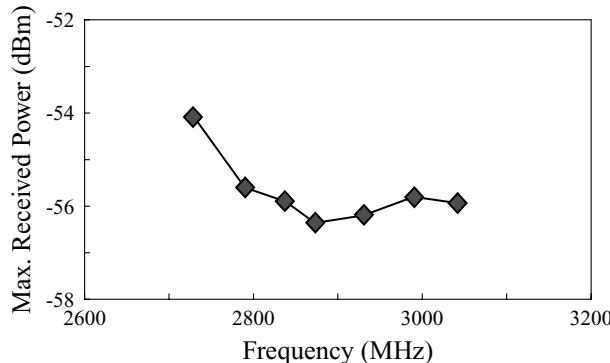


**FIGURE 7.4** Measured maximum received power in the broadside direction for the antenna studied in Figure 7.2. (From Ref. 3, © 1999 John Wiley & Sons, Inc.)

## 7.3 MICROSTRIP ANTENNAS WITH AN AIR SUBSTRATE

### 7.3.1 Design with a Modified Probe Feed

For conventional probe-fed microstrip antennas with a thick substrate, the major problem associated with impedance matching is the large probe reactance owing to the required long probe pin in the thick substrate layer. To solve this problem, a variety of designs with modified probe feeds have been reported. One design method is to cut an annular ring slot [4] or a narrow rectangular ring slot [5] around the feed point in the radiating patch. By choosing suitable dimensions of the ring slot, the large probe reactance can be compensated, and good impedance matching over a wide bandwidth can be obtained. By using a capacitively coupled feed [6, 7] or an L-probe/L-strip coupled feed [8–10], similar probe reactance compensation can be obtained. Typical design examples are shown in Section 8.3.

Another interesting design, using a three-dimensional microstrip transition feed, has been reported [11]. The antenna geometry is shown in Figure 7.5. In this case, although the antenna has a thick air substrate, a short probe pin can be used, which is connected to a rectangular patch as a feed transition to the antenna's radiating patch.

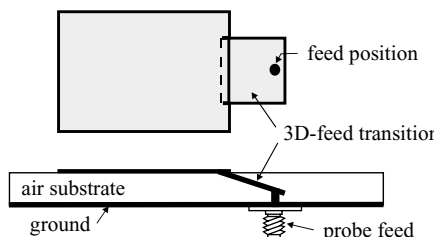


**FIGURE 7.5** Geometry of a broadband microstrip antenna with a three-dimensional microstrip transition feed.

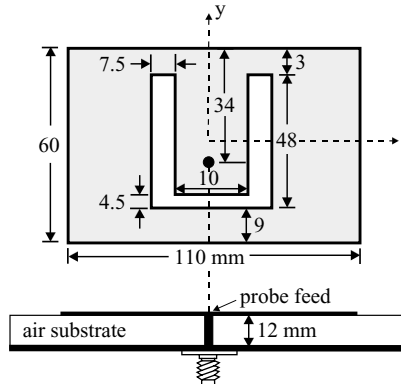


**FIGURE 7.6** Geometry of a broadband probe-fed rectangular microstrip antenna with a U-shaped slot.

The radiating patch can be very high above the ground plane for this design and a long probe pin is not required. This behavior makes good impedance matching over a wide bandwidth easy to achieve, and it has been shown that the typical operating bandwidth of this antenna is about 40% [11].

### 7.3.2 Design with a U-Slotted Patch

Embedding a suitable U-shaped slot in the antenna's radiating patch [12] is a very effective method for achieving a wide bandwidth for a probe-fed microstrip antenna with a thick air substrate. Figure 7.6 shows the geometry of a broadband probe-fed rectangular microstrip antenna with a U-shaped slot. A thick air substrate of 12 mm is used and the radiating patch has dimensions  $60 \times 110 \text{ mm}^2$ . The measured return loss is shown in Figure 7.7, and an impedance bandwidth (10-dB return loss) of 500 MHz, or about 27.5% referenced to the center frequency at 1815 MHz, is obtained. Figure 7.8

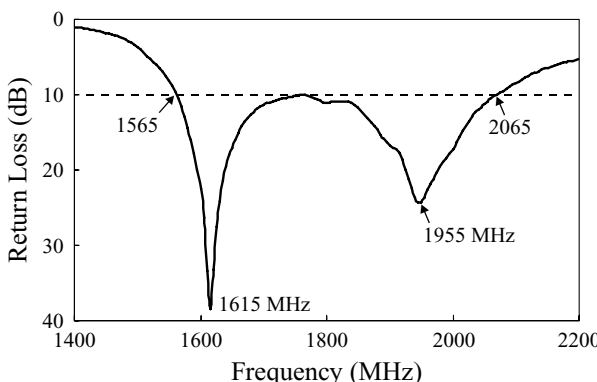


**FIGURE 7.7** Measured return loss for the antenna shown in Figure 7.6.

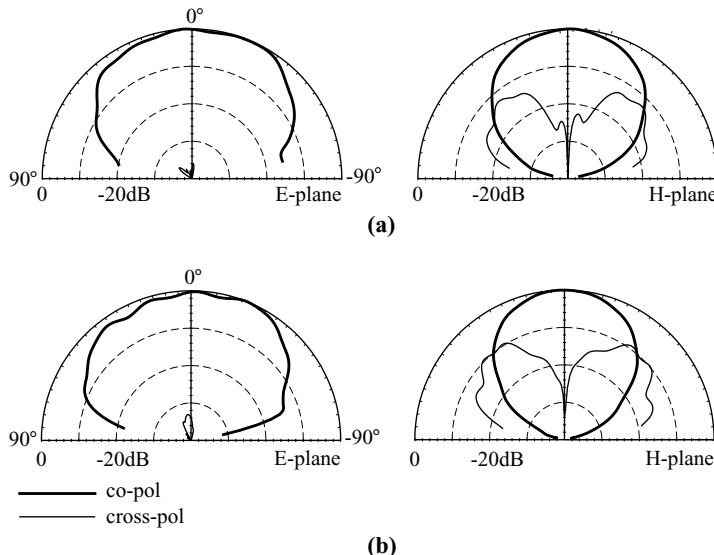


**FIGURE 7.8** Measured radiation patterns for the antenna shown in Figure 7.6. (a)  $f = 1615$  MHz; (b)  $f = 1955$  MHz.

shows the measured radiation patterns for the antenna at two resonant frequencies in the impedance bandwidth. Good broadside radiation patterns are observed. However, relatively large cross-polarization radiation in the  $H$ -plane pattern is also seen, which is a common characteristic of this kind of probe-fed microstrip antenna with a thick air substrate. To reduce the cross-polarization radiation, two out-of-phase feeds can be used, as discussed in Section 7.6. The antenna gain was also measured, and the results are presented in Figure 7.9. The peak antenna gain is about 9.0 dBi, and the gain variations within the bandwidth are less than about 1.0 dBi.

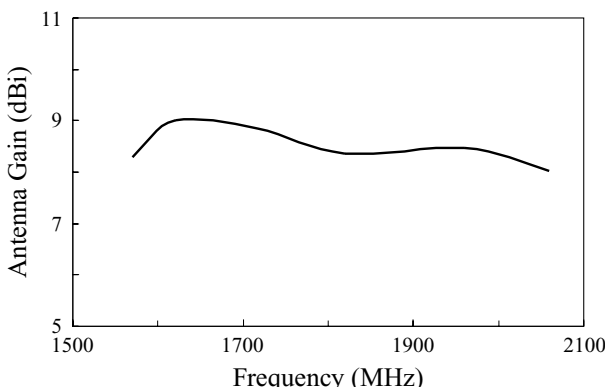


**FIGURE 7.9** Measured antenna gain for the antenna shown in Figure 7.6.

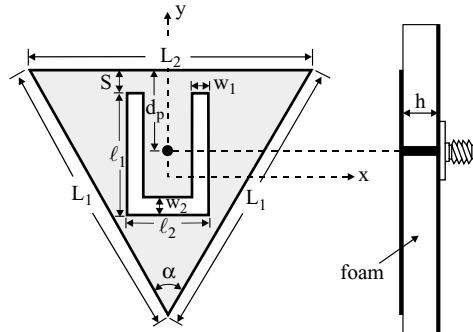


**FIGURE 7.10** Geometry of a broadband probe-fed triangular microstrip antenna with a U-shaped slot. (From Ref. 14, © 1997 IEE, reprinted with permission.)

The present design method has also been applied to a triangular microstrip antenna with a thick air substrate [14]. Figure 7.10 shows the antenna geometry. The U-shaped slot in the patch consists of a pair of parallel slots with dimensions  $\ell_1 \times w_1$  and a horizontal slot with dimensions  $\ell_2 \times w_2$  connecting the two parallel slots. This U-shaped slot is oriented with its horizontal slot facing the triangle tip or the bottom of the triangular patch. In the present study, the former arrangement is studied. The case of an equilateral triangular patch antenna is first investigated. Figure 7.11 shows the measured return loss for a constructed prototype. The slotted triangular patch is mounted on a foam substrate of thickness 14.3 mm (about  $0.08\lambda_0$ ), and the feed position is selected to be close to the null-voltage point for the  $\text{TM}_{10}$  mode (the fundamental mode) of the patch without the slot. It is clearly seen that two adjacent resonant modes at 1563 and 1746 MHz are excited, both in the vicinity

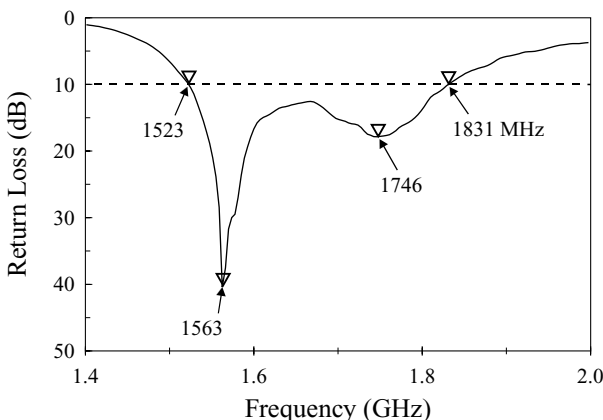


**FIGURE 7.11** Measured return loss for the antenna shown in Figure 7.10;  $h = 14.3$  mm,  $S = 3.2$  mm,  $L_1 = L_2 = 91$  mm,  $\alpha = 60^\circ$ ,  $d_p = 26.2$  mm,  $\ell_1 = 46.2$  mm,  $\ell_2 = 24$  mm,  $w_1 = 6$  mm, and  $w_2 = 2.5$  mm. (From Ref. 14, © 1997 IEE, reprinted with permission.)

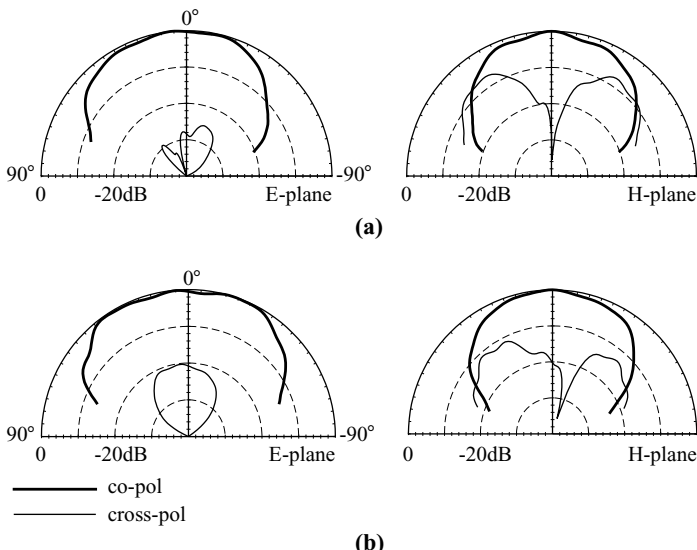


**FIGURE 7.12** Measured *E*-plane (*y*-*z* plane) and *H*-plane (*x*-*z* plane) radiation patterns for the antenna studied in Figure 7.11. (a)  $f = 1563$  MHz; (b)  $f = 1746$  MHz. (From Ref. 14, © 1997 IEE, reprinted with permission.)

of the fundamental resonant frequency  $f_{10}$  (about 1800 MHz) of the triangular patch without a slot. These two modes together give an impedance bandwidth of 308 MHz, or about 18.3% with respect to the center frequency at about 1677 MHz. This bandwidth is much greater than that (about 10%) of a corresponding simple triangular patch antenna. It is also observed that, although all the dimensions ( $\ell_1$ ,  $\ell_2$ ,  $w_1$ ,  $w_2$ ) of the U slot affect the broadband performance, the higher resonant mode is most sensitive to the length ( $\ell_2$ ) variation of the horizontal slot, while the lower resonant mode strongly depends on the perimeter of the U-shaped slot. Measured radiation patterns at resonance of the two resonant modes are plotted in Figure 7.12. These two resonant modes have the same polarization planes, and good cross-polarization radiation is observed for the *E*-plane patterns. However, the *H*-plane patterns show relatively large cross-polarization radiation, similar to the result shown in Figure 7.8.

A similar design using an isosceles triangular patch was constructed. Figure 7.13 shows the measured return loss. Owing to the smaller flare angle ( $\alpha = 53.9^\circ$ ) compared to the case ( $\alpha = 60^\circ$ ) in Figure 7.11, the length  $\ell_2$  of the horizontal slot needs to be reduced, and the width  $w_1$  of the parallel slot is thus decreased to adjust for the occurrence of the two adjacent resonant modes for broadband operation. The measured impedance bandwidth in this case is 304 MHz, or about 17.8% with respect to the center frequency (about 1709 MHz) of the impedance bandwidth. The radiation patterns for the two resonant modes in the impedance bandwidth were measured, and similar radiation characteristics as observed in Figure 7.12 were seen.

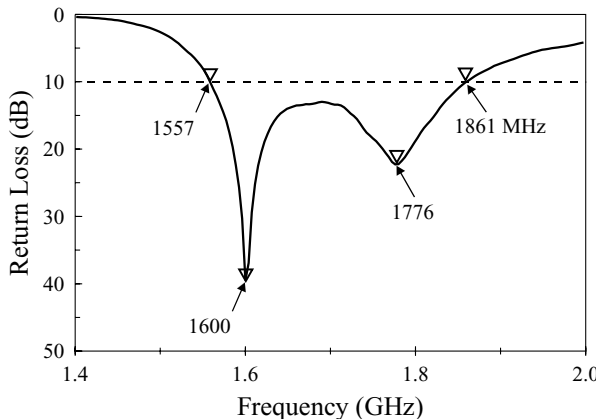


**FIGURE 7.13** Measured return loss for the antenna shown in Figure 7.10;  $h = 14.3$  mm,  $S = 3.2$  mm,  $L_1 = 88.7$ ,  $L_2 = 80.4$  mm,  $\alpha = 53.9^\circ$ ,  $d_p = 26.2$  mm,  $\ell_1 = 46.2$  mm,  $\ell_2 = 20$  mm,  $w_1 = 3.7$  mm, and  $w_2 = 2.5$  mm. (From Ref. 14, © 1997 IEE, reprinted with permission.)

### 7.3.3 Design with an E-Shaped Patch

By using an E-shaped patch instead of a U-slotted patch, similar broadband operation as described in Section 7.3.2 can be obtained. The E-shaped patch is formed by inserting a pair of wide slits at the boundary of a microstrip patch [13–15]. The present design can be applied to the antennas with rectangular, circular, or triangular patches.

**7.3.3.1 With a Rectangular Patch** Figure 7.14 shows a proposed design with a rectangular patch. The rectangular patch has dimensions  $L \times W$  and is supported by

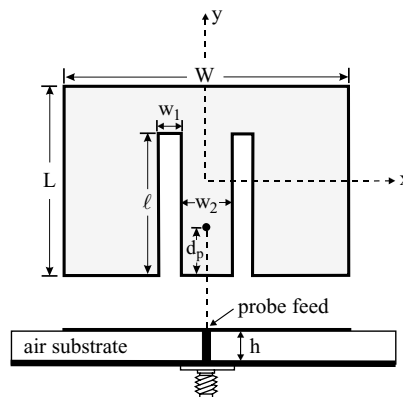


**FIGURE 7.14** Geometry of a broadband E-shaped microstrip antenna. (From Ref. 15, © 2001 IEEE, reprinted with permission.)

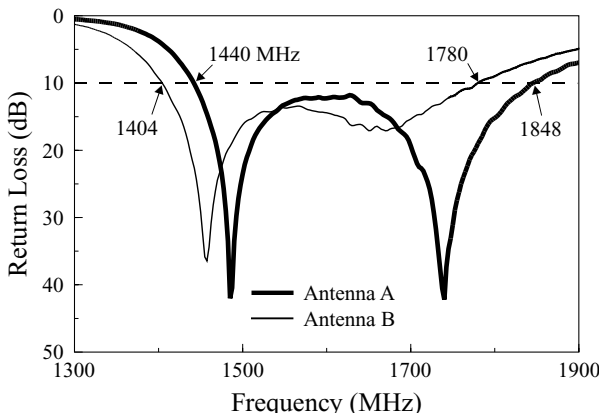


**FIGURE 7.15** Measured return loss for the antenna shown in Figure 7.14;  $L = 65$  mm,  $W = 105$  mm, and ground-plane size =  $150 \times 150$  mm $^2$ . Antenna A:  $h = 14.3$  mm,  $\ell = 47$  mm,  $w_1 = 6.3$  mm,  $w_2 = 15.3$  mm, and  $d_p = 10$  mm. Antenna B:  $h = 15.7$  mm,  $\ell = 53$  mm,  $w_1 = 10$  mm,  $w_2 = 8$  mm, and  $d_p = 13$  mm. (From Ref. 15, © 2001 IEEE, reprinted with permission.)

nonconducting posts of height  $h$  (not shown in the figure) from the ground plane. The two wide slits have the same length  $\ell$  and the same width  $w_1$  and are inserted at the bottom edge of the patch. The separation of the two wide slits is  $w_2$  and the two slits are placed symmetrically with respect to the patch's centerline ( $y$  axis). There are thus only three parameters ( $\ell$ ,  $w_1$ ,  $w_2$ ) for the wide slits used here. Along the patch's centerline, a probe feed at a distance  $d_p$  from the patch's bottom edge can be located for good excitation of the proposed antenna over a wide bandwidth.

Figure 7.15 shows the measured return loss for two constructed prototypes (antennas A and B). Note that, for achieving good impedance matching over a wide bandwidth, the slit length  $\ell$  is about  $(0.7\text{--}0.85)L$ , and the spacing between outer edges of the two slits ( $2w_1 + w_2$ ) is about  $0.27W$ . From the results, it is seen that two adjacent resonant modes are excited, which leads to a wide bandwidth. This characteristic is similar to that obtained for the U-slotted patch antenna (Section 7.3.2). For antenna A, the impedance bandwidth is 408 MHz, or about 24.8% with respect to the center frequency at 1644 MHz. For antenna B, the obtained bandwidth is 376 MHz, or about 23.6% referenced to the center frequency at 1592 MHz. Radiation characteristics of the antenna were also studied. Figure 7.16 plots the measured radiation patterns at three different operating frequencies for antenna A, which are all with the same polarization planes and similar radiation patterns. The cross-polarization radiation in the  $E$ -plane patterns is less than  $-20$  dB. The  $H$ -plane patterns, however, show relatively larger cross-polarization radiation. This behavior is similar to that reported for the U-slotted patch, and is largely due to the thick substrate thickness (about 0.08 times the wavelength of the center frequency in this study) and long probe pin in the substrate layer. Measured radiation patterns for antenna B show similar results. Measured antenna gain for frequencies within the impedance bandwidth is presented in Figure 7.17. For both antennas A and B, the antenna gain variation is less than 0.8 dBi, with the peak antenna gain at about 7.2 dBi.

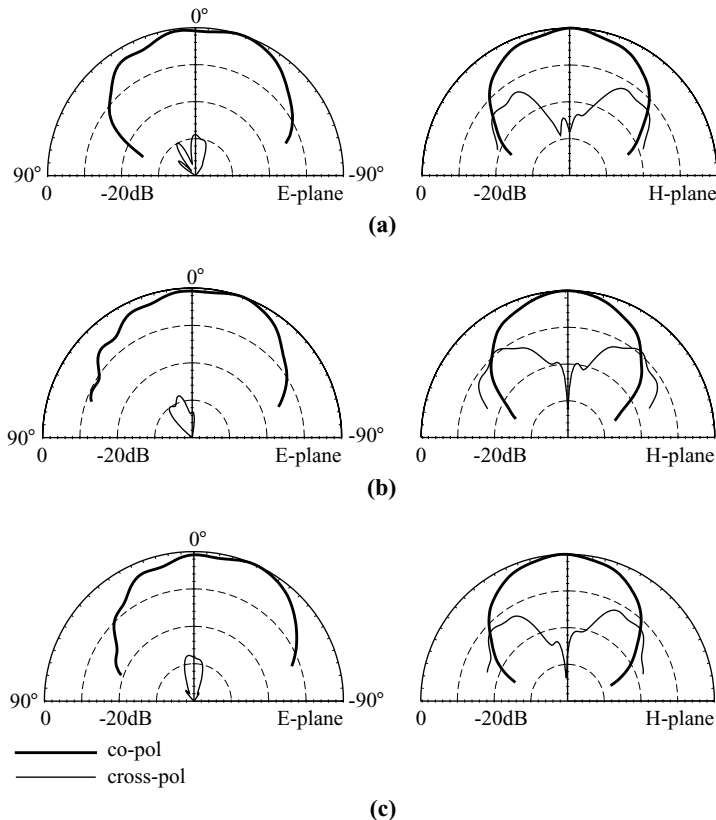


**FIGURE 7.16** Measured *E*-plane ( $y$ - $z$  plane) and *H*-plane ( $x$ - $z$  plane) radiation patterns for antenna A studied in Figure 7.15. (a)  $f = 1485$  MHz, (b)  $f = 1644$  MHz, (c)  $f = 1740$  MHz. (From Ref. 15, © 2001 IEEE, reprinted with permission.)

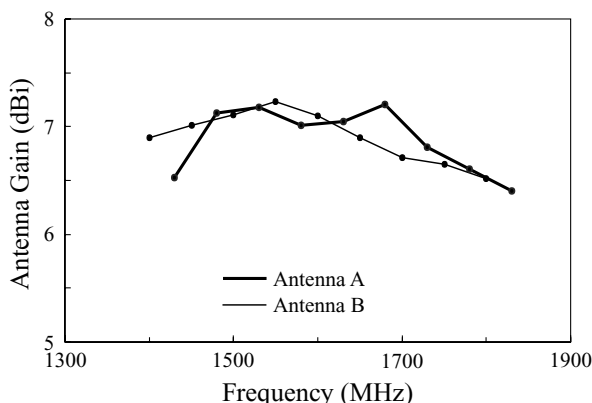


**FIGURE 7.17** Measured antenna gain in the broadside direction for antennas A and B studied in Figure 7.15. (From Ref. 15, © 2001 IEEE, reprinted with permission.)

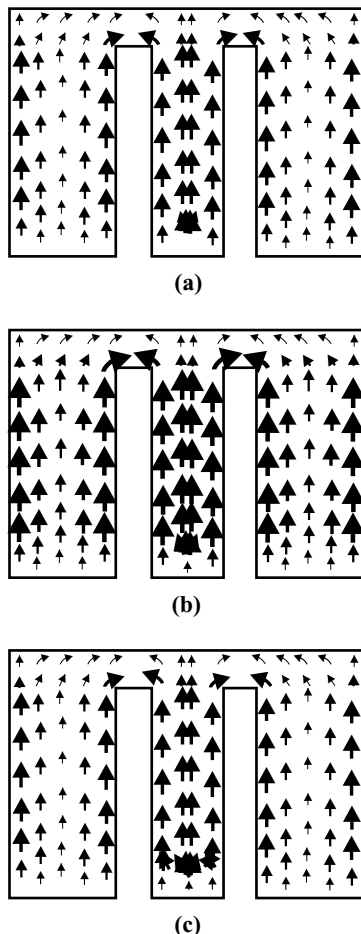


**FIGURE 7.18** Simulated current distributions on the E-shaped patch of antenna A studied in Figure 7.15. (a)  $f = 1485$  MHz, (b)  $f = 1644$  MHz, (c)  $f = 1740$  MHz. (From Ref. 15, © 2001 IEEE, reprinted with permission.)

The excited patch's surface current distribution for the proposed antenna was studied by using IE3D<sup>TM</sup> simulation. Figure 7.18 shows the simulated patch surface current distribution for antenna A for three typical frequencies, 1485, 1644, and 1740 MHz. It is seen that all three frequencies have similar surface current distributions in the rectangular patch. This characteristic agrees with the result that similar radiation patterns for the three frequencies are measured (see Figure 7.16).

**7.3.3.2 With a Circular Patch** Figure 7.19 shows the geometry of a broadband probe-fed circular-E microstrip antenna. It has been shown that, with an air-substrate thickness of about  $0.07\lambda_0$ , the proposed antenna has an impedance bandwidth of about 26% [17]. The measured return loss of a design example is presented in Figure 7.20.

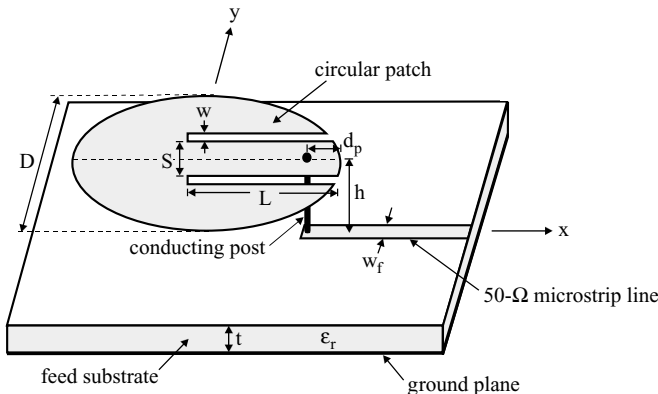


**FIGURE 7.19** Geometry of a broadband probe-fed circular-E microstrip antenna. (From Ref. 17, © 2000 John Wiley & Sons, Inc.)

The circular patch has a diameter of 76 mm and an air-substrate thickness of 12 mm (about  $0.07\lambda_0$ ). The optimal length  $L$  of the pair of slits is 47.8 mm (about 63% of the patch's diameter) and the optimal width of the slits is 5 mm (about 10% of their length). The optimal feed position is at  $d_p = 16.8$  mm. The obtained impedance bandwidth is 460 MHz, or about 26% referenced to the center operating frequency at 1768 MHz. Figure 7.21 plots the radiation patterns in the  $E$  plane ( $x-z$  plane) and  $H$  plane ( $y-z$  plane) for two typical operating frequencies; measured results of the antenna gain in the broadside direction are shown in Figure 7.22. Good broadside radiation patterns are observed, and the cross-polarization radiation in the  $E$  plane is seen to be less than  $-20$  dB. The antenna gain shows a peak value of about 8.3 dBi, with gain variations less than 1.5 dBi within the impedance bandwidth.

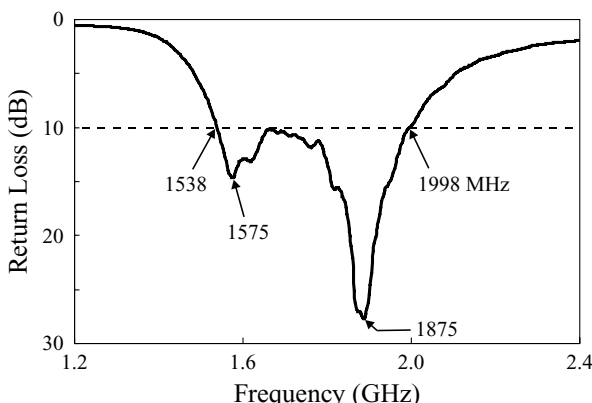


**FIGURE 7.20** Measured return loss for the antenna shown in Figure 7.19;  $h = 12$  mm,  $t = 0.8$  mm,  $D = 76$  mm,  $L = 47.8$  mm,  $w = 5$  mm,  $d_p = 16.8$  mm, and ground-plane size =  $150 \times 150$  mm $^2$ . (From Ref. 17, © 2000 John Wiley & Sons, Inc.)

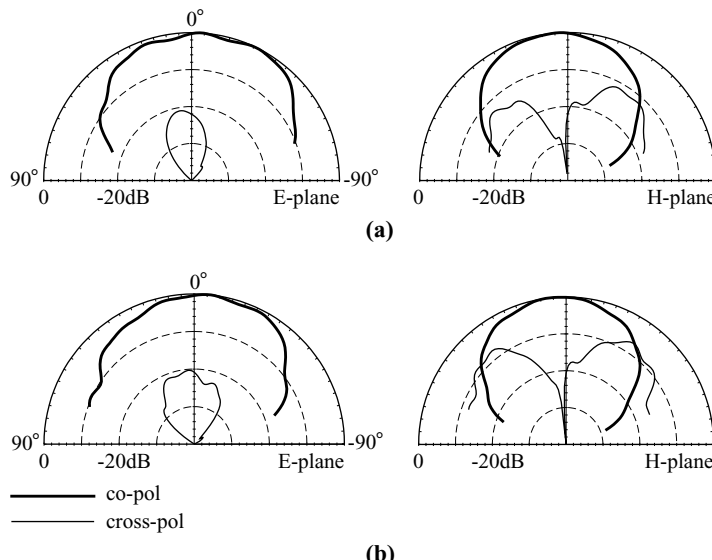


**FIGURE 7.21** Measured *E*-plane ( $x-z$  plane) and *H*-plane ( $y-z$  plane) radiation patterns for the antenna studied in Figure 7.20. (a)  $f = 1575$  MHz, (b)  $f = 1875$  MHz. (From Ref. 17, © 2000 John Wiley & Sons, Inc.)

A design with a capacitively coupled feed has also been studied. Figure 7.23 shows the antenna geometry. The capacitive feed is placed below the circular-E patch at a distance of  $g$  and along the patch's centerline ( $x$  axis). It is experimentally found that, to achieve good impedance matching over a wide bandwidth, the capacitive feed should be placed close to the opposite side of the patch's boundary where

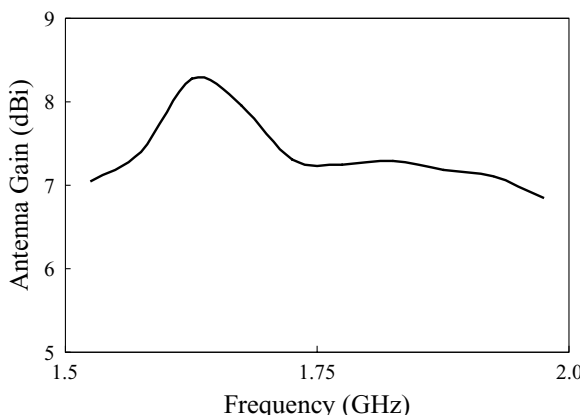


**FIGURE 7.22** Measured antenna gain in the broadside direction of the antenna studied in Figure 7.20. (From Ref. 17, © 2000 John Wiley & Sons, Inc.)

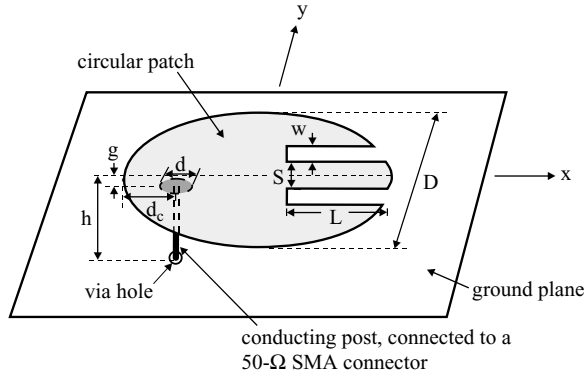


**FIGURE 7.23** Geometry of a broadband capacitively fed circular-E microstrip antenna. (From Ref. 18, © 2000 John Wiley & Sons, Inc.)

wide slits are inserted. That is, the optimal feed position  $d_c$  shown in Figure 7.23 is usually less than 0.5 times the patch's diameter. In this case, a group of three adjacent resonant modes for the proposed antenna can be excited with good impedance matching, and a wide impedance bandwidth is formed by the three adjacent resonant modes. A constructed prototype of the proposed antenna with designed center frequency at about 1.8 GHz shows a wide operating bandwidth of 35.6% [18]. Experimental results for the constructed prototype are presented in Figures 7.24 and 7.25. The diameter of the circular-E patch was chosen to be 70 mm, and the distance between the patch and ground plane was 16.8 mm. The capacitive feed had a small metallic disk of diameter 5 mm and was placed 2 mm below the circular-E patch. The two inserted wide slits had a length of 25 mm, a width of 5.2 mm, and a separation of 10 mm. From the measured return loss shown in Figure 7.24, it is

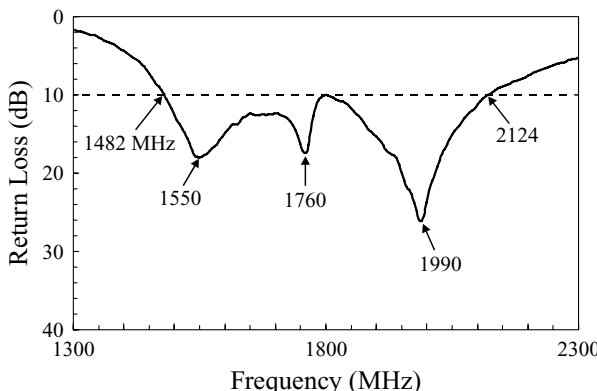


**FIGURE 7.24** Measured return loss for the antenna shown in Figure 7.23;  $h = 16.8$  mm,  $D = 70$  mm,  $L = 25$  mm,  $W = 5.2$  mm,  $S = 10$  mm,  $d_c = 17$  mm,  $d = 5$  mm,  $g = 2$  mm, and ground-plane size =  $150 \times 150$  mm $^2$ . (From Ref. 18, © 2000 John Wiley & Sons, Inc.)

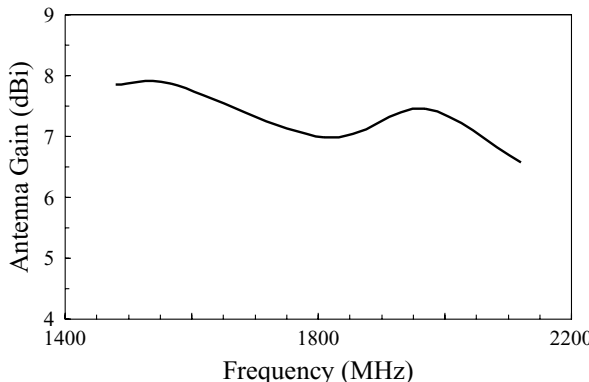


**FIGURE 7.25** Measured antenna gain in the broadside direction of the antenna studied in Figure 7.24. (From Ref. 18, © 2000 John Wiley & Sons, Inc.)

clearly seen that three adjacent resonant modes are excited with good impedance matching, and the impedance bandwidth is 642 MHz, or about 35.6% with respect to the center frequency at 1803 MHz. Figure 7.25 shows a peak measured antenna gain of about 7.9 dBi, with a gain variation within the bandwidth of less than 1.4 dBi.

**7.3.3.3 With a Triangular Patch** A probe-fed triangular-E (triangular patch with a pair of wide slits) microstrip antenna has been studied. The geometry is shown in Figure 7.26. Two wide slits are inserted at the bottom edge of the triangular patch. A prototype with a patch side length of 79 mm and an air-substrate thickness of 16 mm (about  $0.093\lambda_0$ ) has been constructed and studied. Experimental results on the return loss and antenna gain are shown in Figure 7.27. An impedance bandwidth of 350 MHz, or about 20% centered at 1737 MHz, is obtained. The peak antenna gain is about 8.0 dBi, and the gain variations within the impedance bandwidth are less

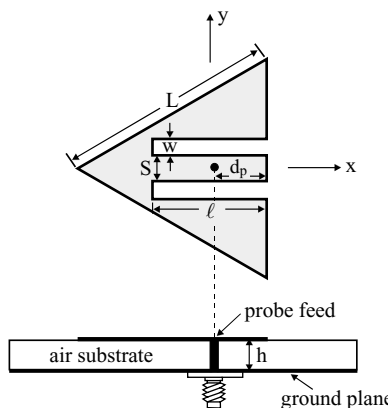


**FIGURE 7.26** Geometry of a broadband probe-fed triangular-E microstrip antenna.

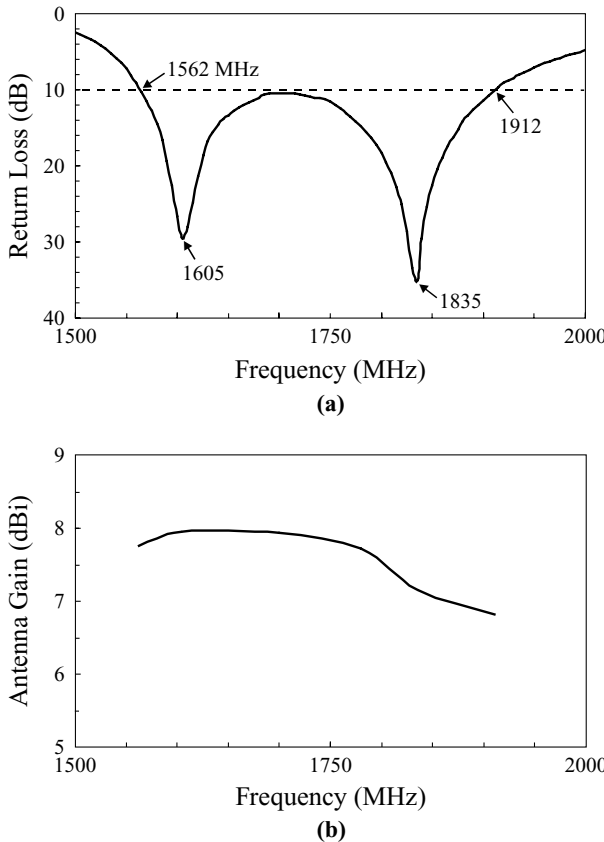


**FIGURE 7.27** (a) Measured return loss and (b) antenna gain for the antenna shown in Figure 7.26;  $h = 16$  mm,  $L = 79$  mm,  $w = 6$  mm,  $d_p = 15$  mm,  $\ell = 41$  mm, and ground-plane size =  $150 \times 150$  mm $^2$ .

than 1.5 dBi. For the measured radiation patterns, similar characteristics as seen for the U-slotted microstrip antennas are observed.

### 7.3.4 Design with a Three-Dimensional V-Shaped Patch

By using a three-dimensional V-shaped patch [19], a long probe pin for a thick air substrate is no longer required. In this case, the large probe reactance associated with a thick substrate layer is avoided, and good impedance matching over a wide frequency range can be obtained. Figure 7.28 shows the geometry of a broadband probe-fed microstrip antenna with a V-shaped patch. Experimental results for a constructed prototype are presented in Figures 7.29 and 7.30. The V-shaped patch has dimensions  $60 \times 90$  mm $^2$  ( $L \times W$ ), and the distance  $h_1$ , from the ground plane to the patch is chosen to be 2 mm (about  $0.015\lambda_0$ ). With such a small length, the effect of the inductive reactance of the probe pin in the air substrate on the impedance matching is small. The distance  $h_2$  is chosen to be 21 mm, and thus the effective thickness of

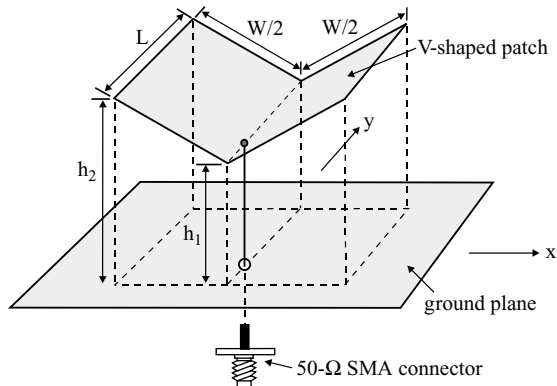


**FIGURE 7.28** Geometry of a broadband probe-fed microstrip antenna with a V-shaped patch.

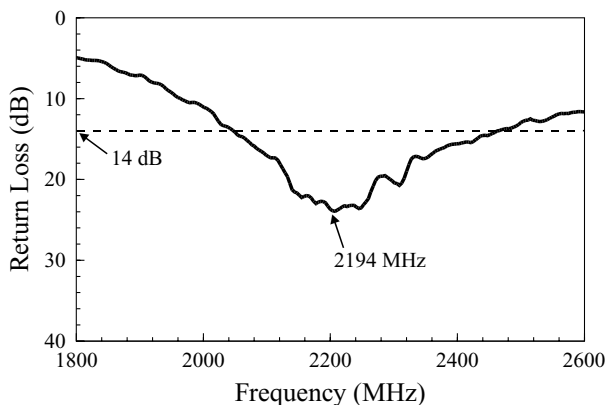


**FIGURE 7.29** Measured return loss for the antenna shown in Figure 7.28;  $L = 60$  mm,  $W = 90$  mm,  $h_1 = 2$  mm,  $h_2 = 21$  mm, and ground-plane size =  $180 \times 120$  mm $^2$ .

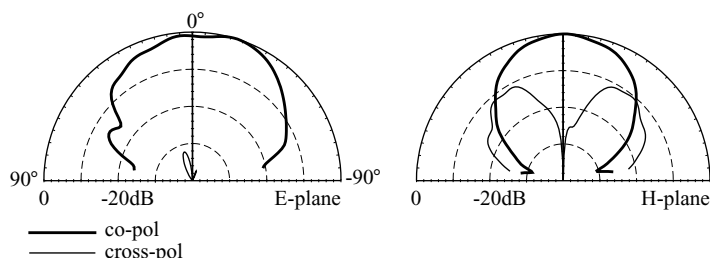


**FIGURE 7.30** Measured radiation patterns at 2194 MHz for the antenna studied in Figure 7.29.

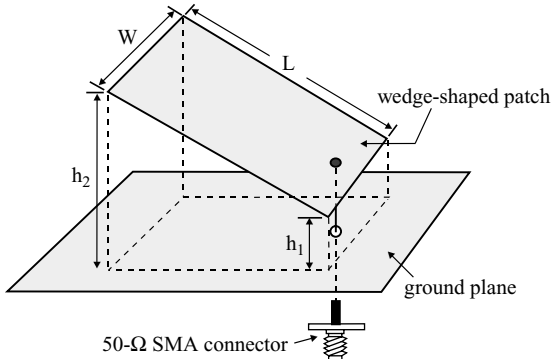


**FIGURE 7.31** Geometry of a broadband probe-fed wedge-shaped microstrip antenna.

the substrate is increased, which makes possible broadband operation of the antenna. Figure 7.29 gives the measured return loss. The obtained impedance bandwidth is greater than 18% (1:1.5 VSWR or 14-dB return loss), with a peak antenna gain of about 8.3 dBi. Figure 7.30 plots the measured radiation patterns at the center frequency 2194 MHz; good broadside radiation patterns are observed.

A similar design with a wedge-shaped patch has been demonstrated [20], with a typical geometry as shown in Figure 7.31. In this case, a short probe pin can be used for an antenna with a large effective air-substrate thickness. For a prototype constructed to be operated at 10.5 GHz [20], it has been shown that the wedge-shaped air-substrate microstrip antenna has double the bandwidth of a conventional microstrip antenna with a uniform substrate layer.

## 7.4 BROADBAND SLOT-LOADED MICROSTRIP ANTENNAS

This section presents experimental results for recent broadband designs with the loading of suitable slots such as a pair of toothbrush-shaped slots [21], a pair of double-bend slots [22], and a pair of right-angle slots and a modified U-shaped slot [23] for rectangular microstrip antennas and two open-ring slots [24] for circular microstrip antennas. Such slot-loading techniques for broadband operation are mainly applicable for microstrip antennas with thin dielectric substrates, and the obtained impedance bandwidth is usually about 2.0–3.0 times that of a conventional microstrip antenna without slots.

### 7.4.1 Design with a Rectangular Patch

**7.4.1.1 With a Pair of Toothbrush-Shaped Slots** Figure 7.32 shows the geometry of a broadband rectangular microstrip antenna with a pair of toothbrush-shaped slots. The rectangular patch has dimensions  $L \times W$ , and the embedded slots consist of a pair of bent slots with a bend angle  $\alpha = 15^\circ$  and two sets of three closely spaced slots protruding from the straight sections of the bent slots. The design considerations

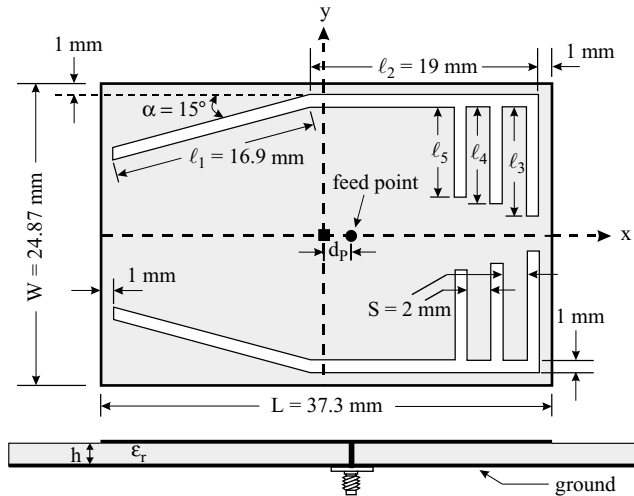


**FIGURE 7.32** Geometry of a broadband rectangular microstrip antenna with a pair of toothbrush-shaped slots. (From Ref. 21, © 1998 IEE, reprinted with permission.)

of the bent slots are the same as given in Section 4.2.1.1; the parameters ( $\ell_1$ ,  $\ell_2$ ,  $\alpha$ ) for the present design are shown in Figure 7.32. The three protruding slots are equally spaced ( $S = 2 \text{ mm}$ ), with their respective lengths given by  $\ell_3$ ,  $\ell_4$ , and  $\ell_5$ . All sections of the embedded slots have equal widths (selected to be 1 mm here). When protruding slots are not present (i.e.,  $\ell_3 = \ell_4 = \ell_5 = 0$ ), the two resonant modes of  $\text{TM}_{10}$  and  $\text{TM}_{80}$  cannot be excited at frequencies that are close enough to form a wide operating bandwidth (see Section 4.2.1.1). However, when the lengths  $\ell_3$ ,  $\ell_4$ , and  $\ell_5$  are properly chosen, the excited patch surface current densities of the  $\text{TM}_{10}$  and  $\text{TM}_{80}$  modes can be suitably perturbed such that these two modes are excited at adjacent frequencies with the ratio of the two resonant frequencies less than about 1.03, which results in a wide operating bandwidth.

The proposed design has been successfully implemented. Figure 7.33 shows the measured return loss of a typical design. In this case, the lengths  $\ell_3$ ,  $\ell_4$ , and  $\ell_5$  are

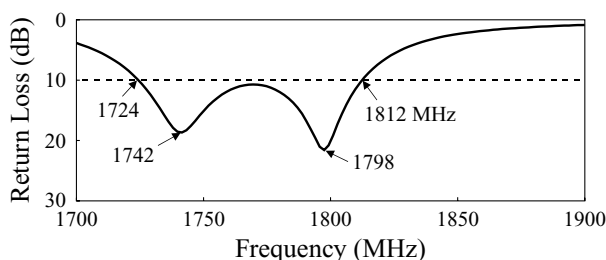


**FIGURE 7.33** Measured return loss for the antenna shown in Figure 7.32;  $\epsilon_r = 4.4$ ,  $h = 1.6 \text{ mm}$ ,  $\ell_3 = 9 \text{ mm}$ ,  $\ell_4 = 9 \text{ mm}$ ,  $\ell_5 = 7.5 \text{ mm}$ , and ground-plane size =  $60 \times 50 \text{ mm}^2$ ; other parameters are given in Figure 7.32. (From Ref. 21, © 1998 IEE, reprinted with permission.)

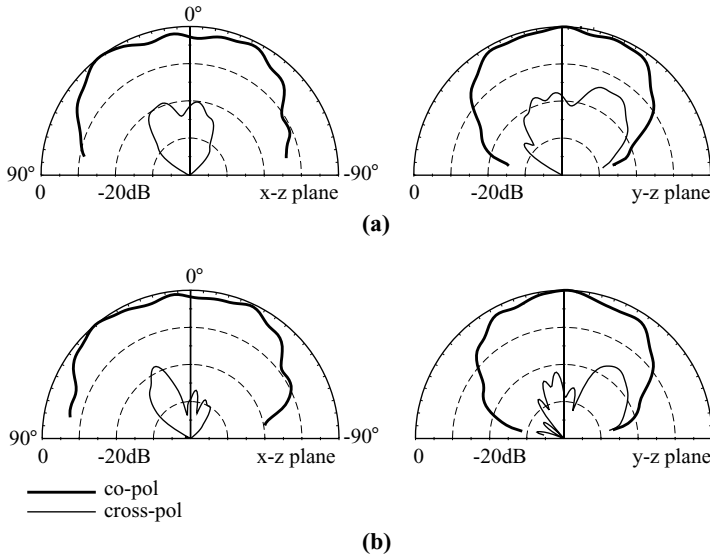


**FIGURE 7.34** Measured  $E$ -plane ( $x$ - $z$  plane) and  $H$ -plane ( $y$ - $z$  plane) radiation patterns for the antenna studied in Figure 7.33. (a)  $f = 1742$  MHz, (b)  $f = 1798$  MHz. (From Ref. 21, © 1998 IEE, reprinted with permission.)

chosen to be 9, 9, and 7.5 mm, respectively. Note that two adjacent resonant modes are excited at frequencies slightly lower than the fundamental resonant frequency (about 1.9 GHz) of the unslotted rectangular microstrip antenna with the same parameters. From simulation results using IE3D<sup>TM</sup>, the two resonant modes are identified to be the  $TM_{10}$  and  $TM_{80}$  modes, the same as the two modes studied in Section 4.2.1.1. This lowering of the two resonant frequencies is mainly due to the effect of meandering of the embedded slots on the excited patch surface current densities of the  $TM_{10}$  and  $TM_{80}$  modes. An impedance bandwidth of 88 MHz or about 5.0% is obtained, which is about 2.6 times that (about 1.9%) of the conventional unslotted rectangular microstrip antenna with the same parameters in the  $TM_{10}$  mode. The radiation characteristics have also been studied. Figure 7.34 plots the measured radiation patterns at the resonant frequencies of the two excited modes. Results show that the two frequencies have the same polarization planes and similar broadside radiation patterns. Good cross-polarization radiation is observed. The antenna gain in the broadside direction of the frequencies within the impedance bandwidth is measured to be within a variation of less than 2.5 dBi, and the antenna gain at the two resonant frequencies is about the same as that of a conventional unslotted rectangular microstrip antenna operated in the  $TM_{10}$  mode.

A design with  $\ell_3$ ,  $\ell_4$ , and  $\ell_5$  chosen to be 9, 8.5, and 8 mm, respectively, was studied. The measured return loss is shown in Figure 7.35. Again, a large impedance bandwidth of 85 MHz (or about 4.7%) is obtained, which is about 2.5 times that of the corresponding unslotted rectangular microstrip antenna. Measured radiation

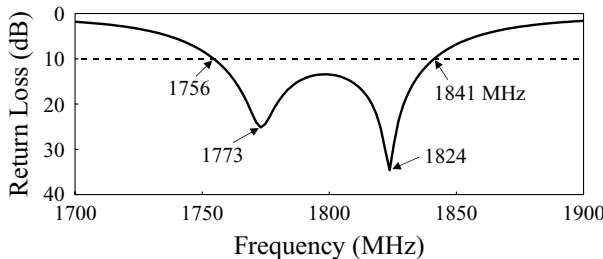


**FIGURE 7.35** Measured return loss for the antenna shown in Figure 7.32;  $\epsilon_r = 4.4$ ,  $h = 1.6$  mm,  $\ell_3 = 9$  mm,  $\ell_4 = 8.5$  mm,  $\ell_5 = 8$  mm, and ground-plane size =  $60 \times 50$  mm $^2$ ; other parameters are given in Figure 7.32. (From Ref. [21], © 1998 IEE, reprinted with permission.)

patterns at the resonant frequencies of the two excited modes show similar radiation characteristics to those observed in Figure 7.34.

**7.4.1.2 With a Pair of Double-Bend Slots** By using a pair of double-bend slots, similar broadband operation as shown in Section 7.4.1.1 can be obtained [22]. The antenna geometry is shown in Figure 7.36. The straight sections of the double-bend slots are placed close to the nonradiating edges at a distance of 1 mm. One end of the double-bend slots has a bend angle of  $15^\circ$ ; this bent section has a length of 16.9 mm and is a small distance (1 mm) from the radiating edge. The other end has a bend angle of  $75^\circ$ ; this bent section is 1.0 and 0.7 mm from the patch centerline ( $x$  axis) and the radiating edge, respectively. With the double-bend slots of specific bend angles  $15^\circ$  and  $75^\circ$  proposed here, the first two resonant modes  $\text{TM}_{10}$  and  $\text{TM}_{\delta 0}$  can be excited

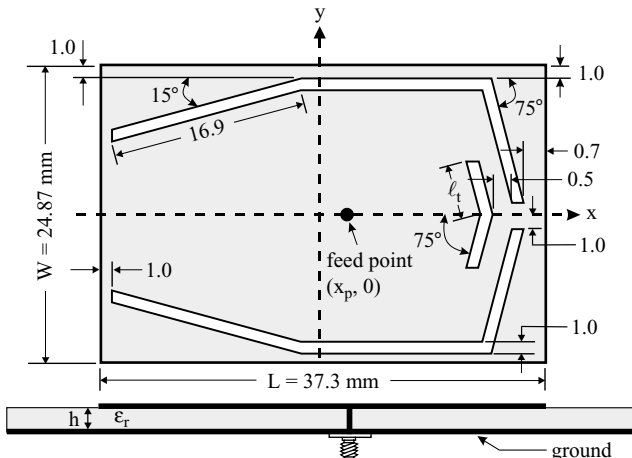


**FIGURE 7.36** Geometry of a broadband slotted rectangular microstrip antenna. The dimensions given in the figure are in millimeters and not to scale. (From Ref. 22, © 1999 John Wiley & Sons, Inc.)

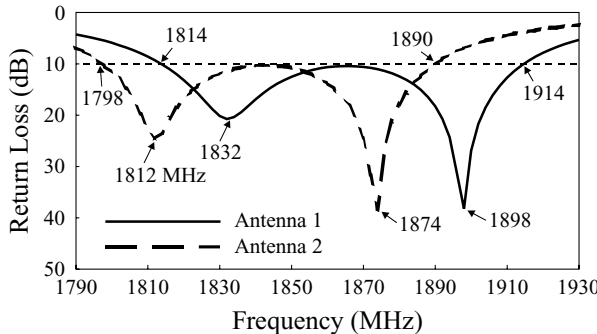


**FIGURE 7.37** Measured return loss for the antenna shown in Figure 7.36;  $\varepsilon_r = 4.4$ ,  $h = 1.6$  mm, and ground-plane size =  $60 \times 50$  mm $^2$ . Antenna 1:  $\ell_t = 4.6$  mm,  $x_p = 2.3$  mm; antenna 2:  $\ell_t = 5.0$  mm,  $x_p = -0.2$  mm. Other parameters are given in Figure 7.36. (From Ref. 22, © 1999 John Wiley & Sons, Inc.)

at frequencies with a frequency ratio  $f_{80}/f_{10}$  of about 1.07, where  $f_{80}$  and  $f_{10}$  are the resonant frequencies of the  $\text{TM}_{80}$  and  $\text{TM}_{10}$  modes, respectively. It is further found that, by incorporating an additional bent slot of bend angle  $150^\circ$  and arm length  $\ell_t$  as shown in Figure 7.36, the frequency ratio  $f_{80}/f_{10}$  can be decreased to about 1.03, making it possible to obtain a wide operating bandwidth formed by the resonant modes of  $\text{TM}_{10}$  and  $\text{TM}_{80}$ .

With the design parameters shown in Figure 7.36 and by tuning the arm length  $\ell_t$  of the bent slot at the patch's centerline, broadband operations have been achieved. Figure 7.37 shows the measured return loss for two different lengths  $\ell_t$ , 4.6 mm ( $\cong 0.123L$ ) and 5.0 mm ( $\cong 0.134L$ ). It is clearly seen that two resonant modes have been excited at close frequencies and with good impedance matching. From the results, the impedance bandwidth for antenna 1 ( $\ell_t = 4.6$  mm) is 100 MHz, or about 5.4% with respect to the center frequency at 1864 MHz. For antenna 2 ( $\ell_t = 5.0$  mm), the impedance bandwidth is 92 MHz, or about 5.0% referenced to the center frequency at 1844 MHz. The impedance bandwidths are about 2.6–2.8 times that (about 1.9%) of the corresponding conventional unslotted rectangular microstrip antenna. From the measured radiation patterns, the  $\text{TM}_{10}$  and  $\text{TM}_{80}$  modes have the same polarization planes and similar radiation characteristics. The measured maximum received powers in the broadside direction are presented in Figure 7.38. The results suggest that the antenna gain for operating frequencies within the obtained wide bandwidth is within a variation of less than 3 dBi.

**7.4.1.3 With a Pair of Right-Angle Slots and a Modified U-Shaped Slot** Figure 7.39 shows promising slot-loading design for achieving bandwidth enhancement of a rectangular microstrip antenna. As shown in the figure, the two right-angle slots have a width of  $w_s$  and are placed close to the nonradiating edges, 1 mm away. The rectangular patch has dimensions of  $37.3 \times 24.87$  mm $^2$  ( $L \times W$ ). In the design, the longer arm of the right-angle slots is parallel to the nonradiating edges and its arm

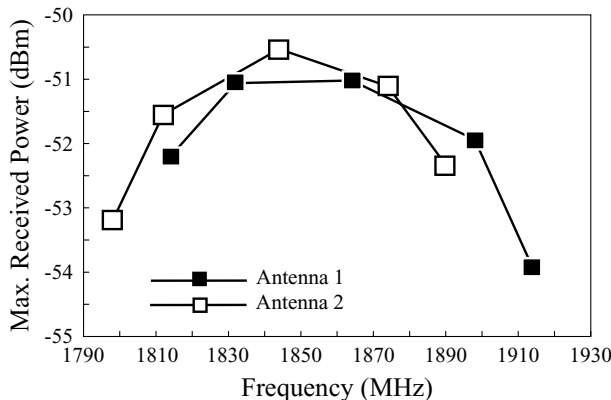


**FIGURE 7.38** Measured maximum received power in the broadside direction for antennas 1 and 2 studied in Figure 7.37. (From Ref. 22, © 1999 John Wiley & Sons, Inc.)

length  $\ell_2$  is about 90% of the patch length. The shorter arm is perpendicular to the nonradiating edges and its arm length  $\ell_1$  is greater than 40% of the patch width. The dimensions  $\ell_1$  and  $\ell_2$  of the right-angle slots are obtained from experiments. When only right-angle slots are present, the two modes  $\text{TM}_{80}$  and  $\text{TM}_{10}$  can be excited at frequencies with a ratio  $f_{80}/f_{10}$  of about 1.07. Although this frequency ratio is much lower than that (1.29) in Section 4.2.1.1, it is still not low enough to form a single wide operating bandwidth. Also, good impedance matching of the two resonant modes is difficult to achieve. However, it is found that, by further embedding a modified U-shaped slot along the centerline of the patch in the resonant direction, the resonant

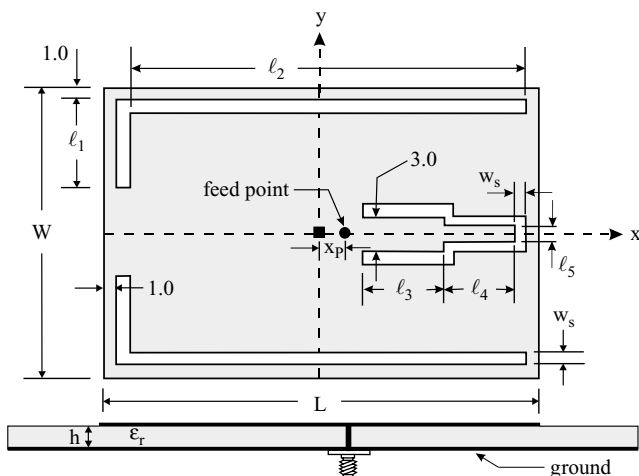


**FIGURE 7.39** Geometry of a broadband rectangular microstrip antenna with a pair of right-angle slots and a modified U-shaped slot. The dimensions given in the figure are in millimeters. (From Ref. 23, © 2000 IEEE, reprinted with permission.)

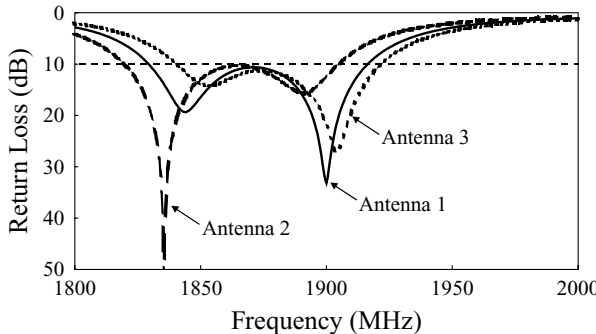


**FIGURE 7.40** Measured return loss for the antenna shown in Figure 7.39 with an FR4 substrate. Parameters for antennas 1–3 are given in Table 7.1. (From Ref. 23, © 2000 IEEE, reprinted with permission.)

frequency  $f_{\delta 0}$  can be lowered while the frequency  $f_{10}$  is only very slightly affected, which leads to a lower frequency ratio of about 1.03 and makes a wide impedance bandwidth possible. The modified U-shaped slot is of width  $w_s$ , its lower section is of length  $\ell_4$  and width  $\ell_5$ , and its upper section is of length  $\ell_3$  and width 3 mm. This modified U-shaped slot is designed to mainly perturb the excited patch surface current path of the  $\text{TM}_{\delta 0}$  mode to further decrease the frequency ratio  $f_{\delta 0}/f_{10}$ . Most important, with the presence of a modified U-shaped slot, good impedance matching of both the  $\text{TM}_{\delta 0}$  and  $\text{TM}_{10}$  modes is obtained easily by using a probe feed at a position  $x_p$  from the patch center.

Prototypes of the proposed design have been successfully implemented. The proper dimensions of the modified U-shaped slot in the constructed prototypes are obtained from experiment. Figure 7.40 shows the measured return loss for prototypes with different parameters (denoted antennas 1–3). The corresponding results are given in Table 7.1. From the IE3D™ simulation results, the lower and higher resonant modes are, respectively, the  $\text{TM}_{10}$  and  $\text{TM}_{\delta 0}$  modes, the same as those studied in Section 4.2.1.1. Note that the fundamental resonant frequency of the unslotted rectangular patch antenna is about 1.9 GHz, with an operating bandwidth of 1.9%. Since the obtained impedance bandwidths are 4.3–4.6% referenced to the center frequency  $f_c$ , the prototypes show a much greater bandwidth, more than 2.2 times that of an

**TABLE 7.1 Performance of Constructed Prototypes of the Antenna in Figure 7.39 [23]<sup>a</sup>**

	$\ell_1$ (mm)	$\ell_2$ (mm)	$x_p$ (mm)	$f_{10}$ (MHz)	$f_c$ (MHz)	$f_{\delta 0}$ (MHz)	Bandwidth (MHz, %)
Antenna 1	10.4	33.5	2.85	1844	1873	1900	86, 4.6
Antenna 2	10.4	33.9	2.85	1836	1864	1891	85, 4.6
Antenna 3	10.4	33.5	3.05	1854	1882	1905	81, 4.3

<sup>a</sup> $\varepsilon_r = 4.4$ ,  $h = 1.6$  mm,  $\ell_3 = 11.5$  mm,  $\ell_4 = 6.0$  mm,  $\ell_5 = 0.5$  mm,  $w_s = 1$  mm, and patch size =  $37.3 \times 24.87$  mm<sup>2</sup>.

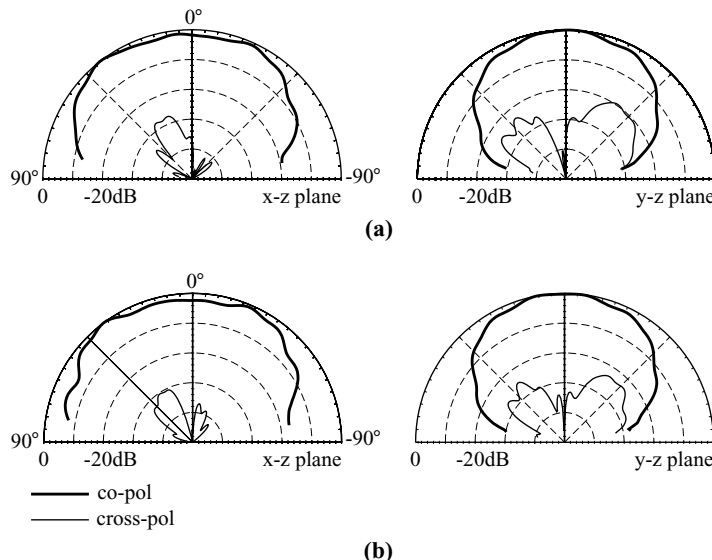


**FIGURE 7.41** Measured  $x$ - $z$  plane ( $E$ -plane) and  $y$ - $z$  plane ( $H$ -plane) radiation patterns for antenna 1 studied in Figure 7.40. (a)  $f = 1844$  MHz, (b)  $f = 1900$  MHz. (From Ref. 23, © 2000 IEEE, reprinted with permission.)

unslotted rectangular patch antenna. Typical radiation patterns in two orthogonal planes of antenna 1 are shown in Figure 7.41, in which the two resonant modes are seen to have the same polarization planes and similar radiation patterns. Figure 7.42 presents the measured peak antenna gain for antennas 1–3. The results indicate that the prototypes have gain variations less than 2.3 dBi (antenna 1) or 2.9 dBi (antennas 2 and 3) for frequencies within the impedance bandwidth, and the peak antenna gain is about 2.2–2.7 dBi. The lower antenna gain is mainly due to the large loss tangent (typically 0.025) associated with the FR4 substrates used. By comparing antenna 2

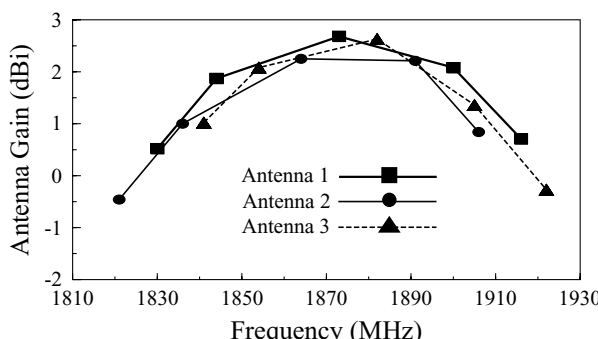


**FIGURE 7.42** Measured peak antenna gain for antennas 1–3 studied in Figure 7.40. (From Ref. 23, © 2000 IEEE, reprinted with permission.)

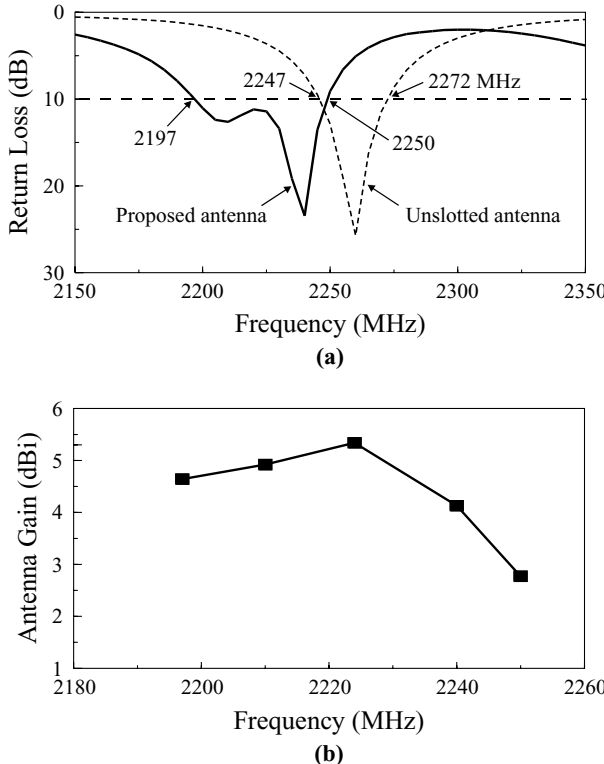


**FIGURE 7.43** (a) Measured return loss and (b) peak antenna gain against frequency for the antenna shown in Figure 7.39 with a Rogers RO3003™ substrate;  $\epsilon_r = 3.0$ ,  $h = 1.524$  mm,  $\ell_3 = 11$  mm,  $\ell_4 = 7$  mm,  $\ell_5 = 8$  mm,  $w_s = 0.5$  mm, and  $x_p = -9.4$  mm. Other parameters are the same as for antenna 2 in Table 7.1. (From Ref. 23, © 2000 IEEE, reprinted with permission.)

to antenna 1, it is also found that, when the length  $\ell_2$  is increased by about 1% with other parameters unchanged, good bandwidth-enhancement performance is observed with the center frequency slightly decreased. By comparing antenna 3 to antenna 1, it is seen that good bandwidth-enhancement characteristics are obtained for a small variation of the feed position. These results suggest that a small manufacturing error can be tolerated for the proposed design, which is important for practical applications.

A design with a Rogers RO3003™ microwave substrate ( $\epsilon_r = 3.0$ ,  $h = 1.524$  mm) has been studied with patch dimensions  $37.3 \times 24.87$  mm<sup>2</sup> ( $L \times W$ ). The modified U-shaped slot has a width  $w_s$  of 0.5 mm and upper and lower sections of lengths  $\ell_3 = 11$  mm and  $\ell_4 = 7$  mm, respectively; the width of the lower section is  $\ell_5 = 8$  mm. Note that, in contrast to antennas 1–3, the lower section in this case has a larger width than that (3 mm) of the upper section of the modified U-shaped slot. The dimensions of the right-angle slots are the same as those of antenna 2. Figures 7.43(a) and 7.43(b) show, respectively, the measured return loss and peak antenna gain. Similar bandwidth-enhancement results as obtained for antennas 1–3 are observed, and the

impedance bandwidth is 53 MHz (2197–2250 MHz), or about 2.4% referenced to the center frequency at 2224 MHz, which is about 2.2 times that (about 1.1%) of the corresponding unslotted microstrip antenna with the same substrate [see the dashed curve in Figure 7.43(a)]. The peak antenna gain is about 5.3 dBi, which is greater than those of antennas 1–3 and is mainly because the RO3003<sup>TM</sup> substrate has a lower loss tangent (typically 0.0013). The lower loss tangent also results in a smaller bandwidth in comparison to those of antennas 1–3 with an FR4 substrate. The measured radiation patterns over the obtained impedance bandwidth are similar to those shown in Figure 7.41.

### 7.4.2 Design with a Circular Patch

Bandwidth enhancement of circular microstrip antennas loaded with two open-ring slots has been reported [24]. The proposed antenna is shown in Figure 7.44. The circular patch in this study has a disk radius of 23.36 mm, and the outer open-ring slot is a small distance, 1 mm, from the patch boundary. The two open-ring slots have the same narrow width of 0.5 mm, and the distance between the two slots is set to be 1 mm. The slots are placed symmetrically with respect to the  $y$  axis, on which an optimal probe feed for good impedance matching is located. The distance between the probe feed and disk center is denoted  $d_p$ . The inner open-ring slot has a small opening and is fixed to be 2 mm. The outer open-ring slot has a relatively large opening and has an angle of  $\phi$ . In the present design, by choosing a suitable angle  $\phi$ , two resonant modes can be closely excited at frequencies in the vicinity of the fundamental resonant frequency  $f_{11}$  of the corresponding simple circular microstrip antenna without slots, leading to the enhancement of the impedance bandwidth of the proposed antenna.

Figure 7.45 presents the measured return loss for a constructed prototype. The angle  $\phi$  is selected to be  $32^\circ$  and the feed position is at  $d_p = 13$  mm. Note that, when

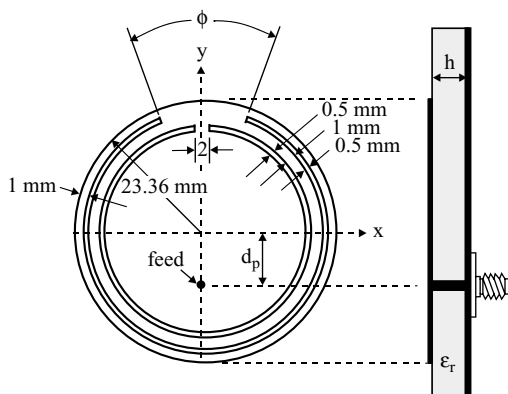


**FIGURE 7.44** Geometry of a broadband circular microstrip antenna with two open-ring slots. The dimensions shown in the figure are not to scale. (From Ref. 24, © 1999 John Wiley & Sons, Inc.)

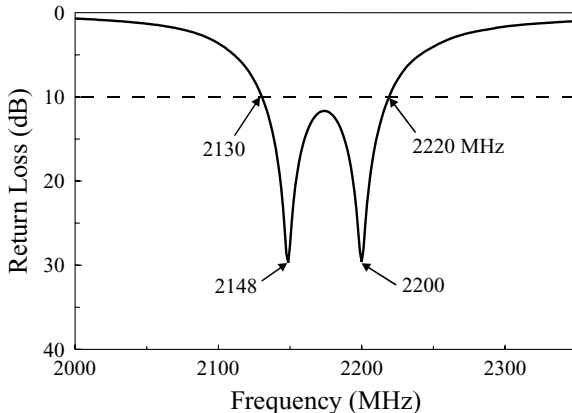


**FIGURE 7.45** Measured return loss for the antenna shown in Figure 7.44;  $\epsilon_r = 4.4$ ,  $h = 1.6$  mm,  $d_p = 13$  mm,  $\phi = 32^\circ$ , and ground-plane size =  $75 \times 75$  mm $^2$ . Other parameters are given in Figure 7.44. (From Ref. 24, © 1999 John Wiley & Sons, Inc.)

there are no open-ring slots, the fundamental resonant frequency  $f_{11}$  of the circular microstrip antenna with a radius of 23.36 mm is about 2 GHz. It is also clearly seen that the prototype antenna has two adjacent resonant modes excited at frequencies near 2 GHz: one at 2148 MHz and the other at 2200 MHz. The impedance bandwidth is 90 MHz, or about 4.1% with respect to the center frequency at 2175 MHz. This impedance bandwidth is about 2.1 times that (about 2%) of the corresponding simple circular microstrip antenna without slots.

The radiation characteristics of the antenna have also been studied. Figure 7.46 shows the measured radiation patterns at the two resonant frequencies of 2148 and 2200 MHz. Similar broadside radiation patterns have been observed for the two resonant modes, and good cross-polarized radiation (less than  $-20$  dB) is seen. Figure 7.47 shows the measured antenna gain in the broadside direction. The results show that the gain variation within the impedance bandwidth of the antenna is within a variation of less than 2.6 dB. It should also be noted that, mainly owing to the FR4 substrate used in this study, which has a large loss tangent (about 0.04), the antenna gain level is lower than about 3.5 dBi.

## 7.5 BROADBAND MICROSTRIP ANTENNAS WITH AN INTEGRATED REACTIVE LOADING

### 7.5.1 Design with a Rectangular Patch

By inserting a microstrip-line section at one of the radiating edges of a rectangular patch, dual-frequency operation of microstrip antennas has been reported [29]. In such a design, the inserted microstrip-line section provides an integrated reactive loading to the microstrip antenna. By varying the dimensions of the inserted microstrip-line section, which can affect the resonance condition of the microstrip

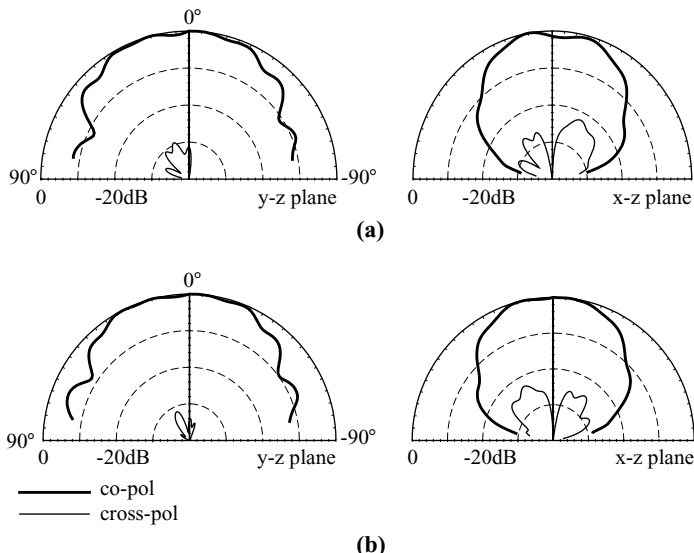


**FIGURE 7.46** Measured  $y-z$  plane ( $E$ -plane) and  $x-z$  plane ( $H$ -plane) radiation patterns for the antenna studied in Figure 7.45. (a)  $f = 2148$  MHz, (b)  $f = 2200$  MHz. (From Ref. 24, © 1999 John Wiley & Sons, Inc.)

antenna, two resonant modes near the fundamental mode of the original unloaded microstrip antenna can be excited, making dual-frequency operation possible. Recently, it has also been reported that, by applying this inserted-loading technique and modifying the inserted microstrip-line section to be an inserted microstrip structure of cascaded transmission-line sections [25], the two resonant modes can be designed to be excited at frequencies very close to each other to form a wide operating bandwidth. This enhancement in the impedance bandwidth greatly relieves the narrow-bandwidth

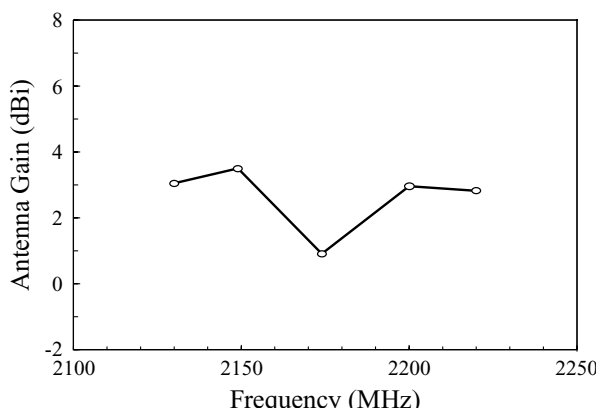


**FIGURE 7.47** Measured antenna gain in the broadside direction for the antenna studied in Figure 7.45. (From Ref. 24, © 1999 John Wiley & Sons, Inc.)

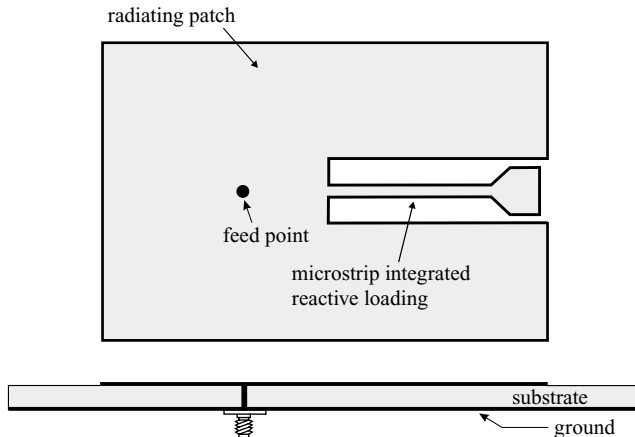


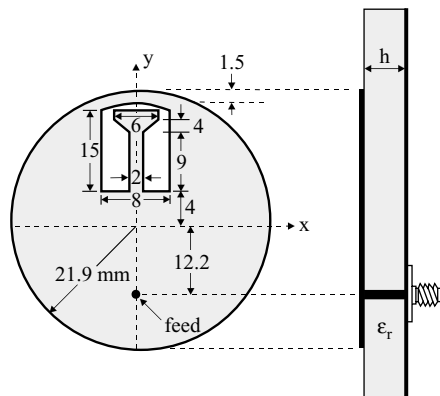
**FIGURE 7.48** Geometry of a broadband rectangular microstrip antenna with an inserted integrated reactive loading.

disadvantage of microstrip antennas. A typical geometry of such a design applied to a probe-fed rectangular microstrip antenna is shown in Figure 7.48, in which an integrated reactive loading is inserted at one of the patch's radiating edges for bandwidth enhancement. Results show that, with such a bandwidth-enhancement design, the antenna's impedance bandwidth can be almost three times larger than that of a corresponding regular microstrip antenna [25].

### 7.5.2 Design with a Circular Patch

The integrated reactive loading technique is also applicable for circular microstrip antennas. However, experimental studies show that broadband operation is very sensitive to small variations in the dimensions of the inserted microstrip structure providing the reactive loading, especially when applying the inserted-loading technique to a circular microstrip antenna. In this section, we demonstrate that, by modifying the inserted microstrip structure embedded within the circular microstrip patch (see Figure 7.49), a good impedance condition for broadband operation is easily achieved and good antenna performance within the impedance bandwidth is obtained [26].

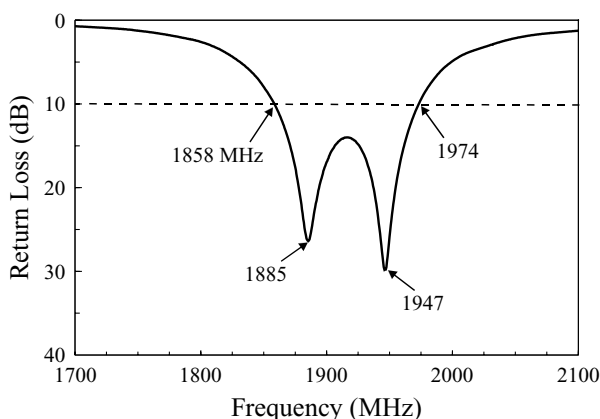
To provide the reactive loading, a microstrip structure consisting of a straight microstrip-line section and a tab microstrip-line section is embedded inside a near-rectangular slot cut in the circular patch. Both the microstrip structure and the near-rectangular slot are symmetric to the  $y$  axis; their dimensions are given in Figure 7.49. The straight microstrip-line section of the embedded microstrip structure is connected to the circular patch at the bottom edge of the slot, which is at a position about 0.2 times the disk radius away from the disk center. For the present design with  $h = 1.6$  mm,  $\epsilon_r = 4.4$ , and a ground-plane size of  $75 \times 75$  mm $^2$ , a single probe feed located at a position about 0.55 times the disk radius away from the disk center can excite two resonant modes close to each other, in the vicinity of the fundamental resonant mode ( $\text{TM}_{11}$ ) of the unloaded patch, to achieve a wide operating bandwidth.



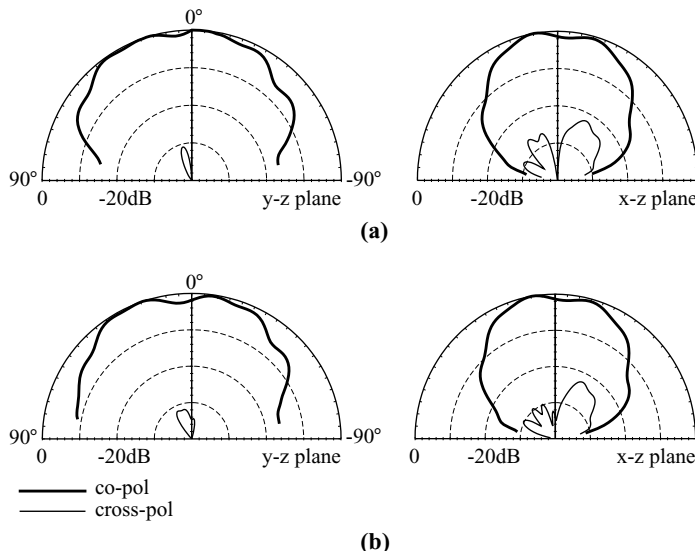
**FIGURE 7.49** Geometry of a broadband circular microstrip antenna with an embedded reactive loading. The dimensions shown in the figure are not to scale. (From Ref. 26, © 1998 IEE, reprinted with permission.)

Figure 7.50 shows the measured return loss for the proposed design. It is observed that two resonant modes are excited at frequencies close to 1.9 GHz, which is the fundamental resonant frequency of the unloaded circular patch antenna. The occurrence of the two resonant modes is mainly due to the embedded reactive loading, which provides a capacitive load at the lower resonant frequency and an inductive load at the higher resonant frequency. These two modes are also excited with a good impedance condition, and the measured return loss at the two resonant frequencies is greater than 25 dB. The obtained bandwidth is 116 MHz, or about 6.05%, which is about 3.2 times that (about 1.9%) of the corresponding unloaded circular microstrip antenna.

The radiation characteristics of the operating frequencies within the impedance bandwidth have been investigated. Typical patterns in two orthogonal planes at the



**FIGURE 7.50** Measured return loss for the antenna shown in Figure 7.49;  $\epsilon_r = 4.4$ ,  $h = 1.6$  mm, and ground-plane size =  $75 \times 75$  mm $^2$ . Patch dimensions are given in Figure 7.49. (From Ref. 26, © 1998 IEE, reprinted with permission.)



**FIGURE 7.51** Measured  $y$ - $z$  plane ( $E$ -plane) and  $x$ - $z$  plane ( $H$ -plane) radiation patterns for the antenna studied in Figure 7.50. (a)  $f = 1885$  MHz; (b)  $f = 1947$  MHz. (From Ref. 26, © 1998 IEE, reprinted with permission.)

two resonant frequencies are presented in Figure 7.51. It is seen that good broadside radiation characteristics with the same polarization planes are obtained, and the cross-polarization radiation is well below  $-20$  dB. The measured antenna gain in the broadside direction is shown in Figure 7.52. In general, the operating frequencies in the lower resonant mode have a relatively larger antenna gain than those within the higher resonant mode, and the variations of the antenna gain in the entire impedance bandwidth are within a range of less than  $2.5$  dBi.

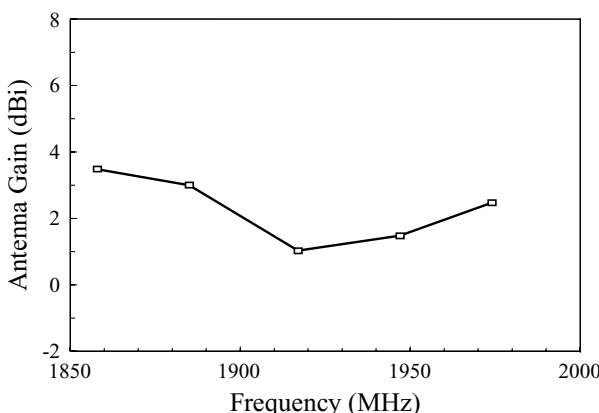


**FIGURE 7.52** Measured antenna gain in the broadside direction for the antenna studied in Figure 7.50. (From Ref. 26, © 1998 IEE, reprinted with permission.)

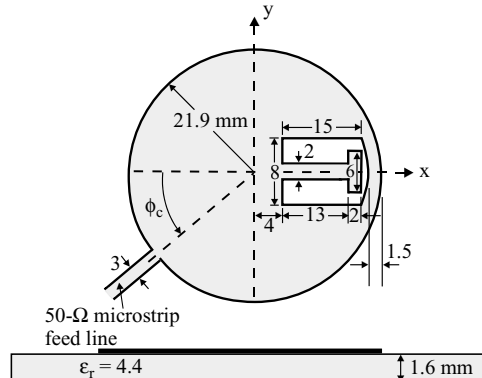


**FIGURE 7.53** Geometry of a microstrip-line-fed broadband circular microstrip antenna with embedded reactive loading. The dimensions (in millimeters) in the figure are not to scale. (From Ref. 27, © 1999 John Wiley & Sons, Inc.)

The present embedded integrated reactive loading technique can also be applied to a circular microstrip antenna directly fed by a 50- $\Omega$  microstrip line [27]. Figure 7.53 shows the geometry of a typical design. This design is made possible because the symmetry of the proposed circular microstrip antenna no longer holds, which causes a wide variation in the input impedance seen along the circumference of the circular patch. By choosing a suitable angle between the microstrip feed line and the embedded reactive loading, good impedance matching of the proposed broadband circular patch antenna can be obtained.

Figure 7.54 shows the measured return loss for an antenna with various angles  $\phi_c$ . The cases studied here all have a ground-plane size of  $75 \times 75 \text{ mm}^2$ . It is seen that for a smaller angle of  $\phi_c = 20^\circ$ , only a single resonant mode is excited with good impedance matching. For  $\phi_c = 40^\circ$  and  $60^\circ$ , however, two resonant modes are

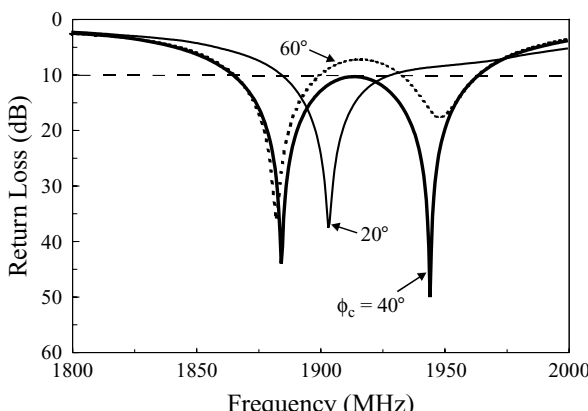


**FIGURE 7.54** Measured return loss for the antenna shown in Figure 7.53 with various angles  $\phi_c$ ;  $\epsilon_r = 4.4$ ,  $h = 1.6 \text{ mm}$ ,  $d = 21.9 \text{ mm}$ , and ground-plane size =  $75 \times 75 \text{ mm}^2$ . (From Ref. 27, © 1999 John Wiley & Sons, Inc.)

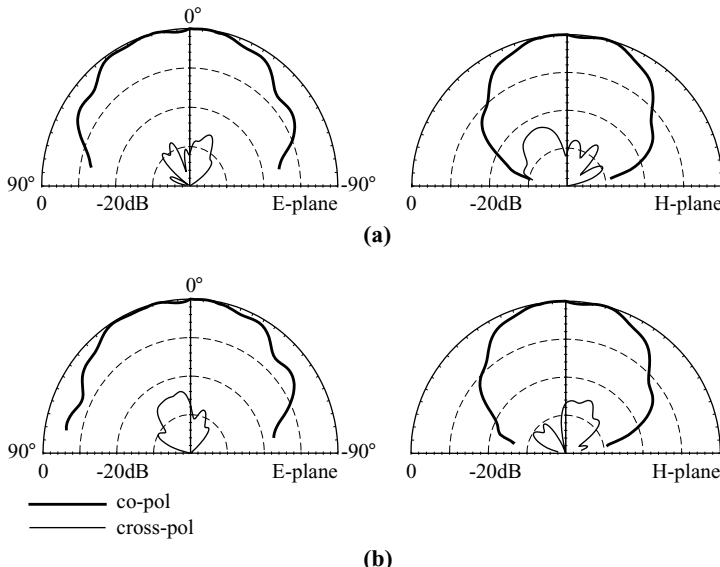


**FIGURE 7.55** Measured *E*- and *H*-plane radiation patterns for the antenna studied in Figure 7.54 with  $\phi_c = 40^\circ$ . (a)  $f = 1885$  MHz, (b)  $f = 1945$  MHz. (From Ref. 27, © 1999 John Wiley & Sons, Inc.)

excited. These two modes are seen to be excited at frequencies in the vicinity of the fundamental resonant frequency (about 1.9 GHz) of the unloaded patch. For the impedance bandwidth defined by 10-dB return loss, the case  $\phi_c = 40^\circ$  provides an impedance bandwidth of 100 MHz, or about 5.2%, which is about 2.7 times that (36 MHz, or about 1.9%) of the corresponding unloaded circular microstrip antenna with a probe feed.

Figure 7.55 shows the measured radiation patterns at resonance of the two resonant modes in the impedance bandwidth. Similar radiation characteristics have been observed for the two resonant modes, and cross-polarized radiation is seen below  $-20$  dB. Figure 7.56 shows the measured antenna gain in the broadside direction. The antenna-gain variation in the impedance bandwidth is within 3 dBi, and a lower antenna gain is observed near the center frequency or at frequencies between the two resonant modes. It is expected that, by exciting the two resonant modes at frequencies closer to each other, the antenna gain near the center frequency can be enhanced, and the antenna-gain variation within the impedance bandwidth can be further reduced.

### 7.5.3 Design with a Bow-Tie Patch

Figure 7.57 shows the geometry of a probe-fed bow-tie microstrip antenna with an inserted integrated reactive loading for bandwidth enhancement [28]. The dimensions of the bow-tie patch with integrated reactive loading are given in the figure. The bow-tie patch has a flare angle  $\alpha$  and a width 24.9 mm, and the length between its two radiating edges is fixed to be 37.3 mm. To integrate the cascaded microstrip-line sections to provide reactive loading, a rectangular notch of dimensions

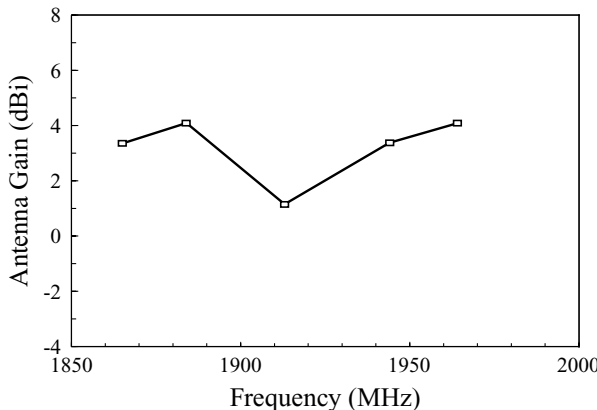


**FIGURE 7.56** Measured antenna gain in the broadside direction for the antenna studied in Figure 7.54 with  $\phi_c = 40^\circ$ . (From Ref. 27, © 1999 John Wiley & Sons, Inc.)

$16.2 \times 7.8 \text{ mm}^2$  is cut at one of the patch's radiating edges. The cascaded microstrip-line sections consist of three sections of different dimensions. The innermost section has a length of 7.3 mm and a width of 0.8 mm, and is connected to the notched bow-tie patch. The middle section has dimensions  $2.4 \times 4.0 \text{ mm}^2$ , and the outermost section has a width of 6.8 mm and a variable length  $d$ . For the proposed bow-tie patch antenna with a specific flare angle, there exists an optimal value of  $d$  for the integrated reactive loading to be resonant at the fundamental resonant frequency  $f_{10}$  of the bow-tie patch. In this case, the fundamental resonant modes can be split into two near-degenerate resonant modes, which makes bandwidth enhancement of the bow-tie patch antenna possible.

Experiments on the proposed antenna with various flare angles were conducted. The results are shown in Table 7.2. Measured return loss for the cases of  $\alpha = 0^\circ$  and  $30^\circ$  is shown in Figure 7.58. It is seen that two near-degenerate resonant modes are

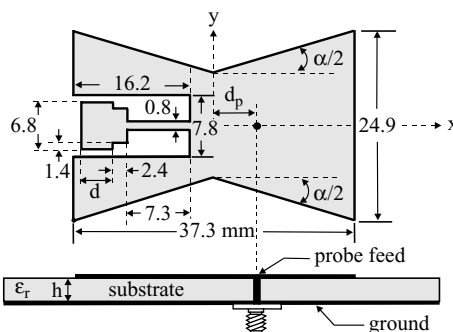


**FIGURE 7.57** Geometry of a broadband bow-tie microstrip antenna with integrated reactive loading. The patch dimensions are in millimeters and not to scale;  $\epsilon_r = 4.4$ ,  $h = 1.6 \text{ mm}$ , and ground-plane size =  $77 \times 55 \text{ mm}^2$ . (From Ref. 28, © 1999 John Wiley & Sons, Inc.)

**TABLE 7.2 Performance of Constructed Prototypes of the Antenna in Figure 7.57 [28]<sup>a</sup>**

Flare Angle $\alpha$ (deg)	$d_p$ (mm)	$d$ (mm)	$d_{RL}/\lambda_S$	$f_c$ (MHz)	Bandwidth (MHz, %)
0	9.6	2.8	0.170	1952	90, 4.6
10	10.6	3.1	0.168	1880	82, 4.4
20	10.4	3.9	0.173	1829	81, 4.4
30	9.0	4.2	0.169	1744	73, 4.2
40	8.7	4.9	0.168	1645	76, 4.6

<sup>a</sup> $\lambda_S (= \lambda_c / \sqrt{\epsilon_r})$  is the wavelength of the center frequency  $f_c$  in the substrate layer, and  $d_{RL} (= 7.3 \text{ mm} + 2.4 \text{ mm} + d)$  is the total length of the integrated reactive loading.

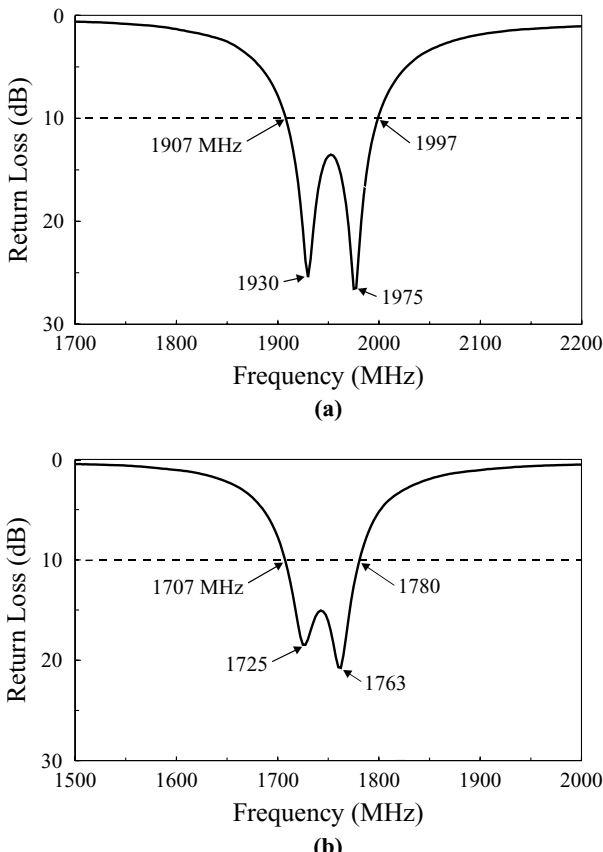


**FIGURE 7.58** Measured return loss for the antenna shown in Figure 7.57. (a)  $\alpha = 0^\circ$ , (b)  $\alpha = 30^\circ$ . (From Ref. 28, © 1999 John Wiley & Sons, Inc.)

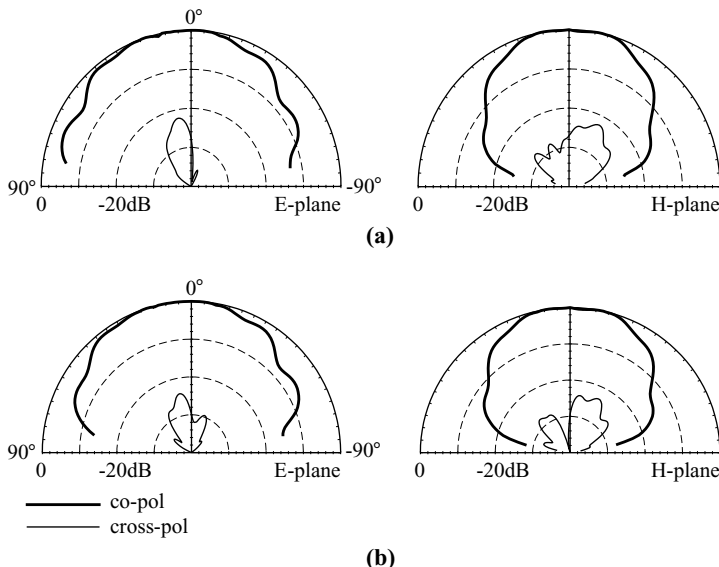


**FIGURE 7.59** Measured *E*-plane ( $x-z$  plane) and *H*-plane ( $y-z$  plane) radiation patterns for the antenna shown in Figure 7.57 with  $\alpha = 30^\circ$ . (a)  $f = 1725$  MHz, (b)  $f = 1763$  MHz. (From Ref. 28, © 1999 John Wiley & Sons, Inc.)

excited at decreasing frequencies with increasing flare angles, and large impedance bandwidths in the range of 4.2–4.6% (see Table 7.2) are obtained. For the case of  $\alpha = 40^\circ$ , the center frequency is about 15% lower than that of  $\alpha = 0^\circ$  (rectangular patch case), which suggests that the present design has a patch dimension 15% smaller than the case using a rectangular patch at a fixed operating frequency. Furthermore, since the impedance bandwidth of a conventional rectangular microstrip antenna with the same substrate parameters as used here is measured to be about 1.5% for operation at 1645 MHz, the present design with  $\alpha = 40^\circ$  shows an impedance bandwidth two times larger.

It is found that the total length of the cascaded microstrip-line sections for reactive loading is nearly independent of the flare angle and is about 17% of the operating wavelength in the substrate layer (see Table 7.2), which makes the present design with various flare angles easy to implement. Radiation characteristics were also studied, and results for the case of  $\alpha = 30^\circ$  are plotted in Figure 7.59. The two resonant modes in the impedance bandwidth are seen to have the same polarization planes and similar radiation performance. From the measured maximum received power in the broadside direction shown in Figure 7.60, the proposed design shows an antenna-gain variation of less than 3 dBi for frequencies within the impedance bandwidth.

#### 7.5.4 Design with a Triangular Patch

The integrated reactive loading technique has been applied to a probe-fed triangular microstrip antenna [30]. The antenna geometry is shown in Figure 7.61, and the

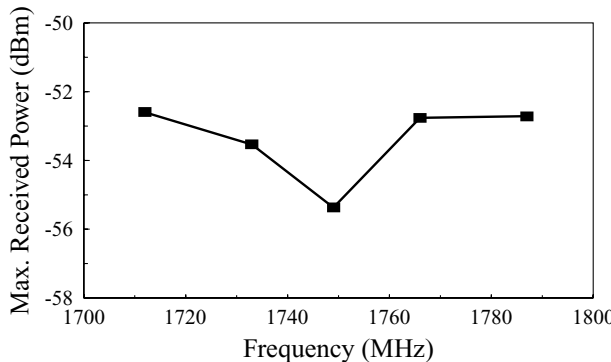


**FIGURE 7.60** Measured maximum received power in the broadside direction for the antenna shown in Figure 7.57 with  $\alpha = 30^\circ$ . (From Ref. 28, © 1999 John Wiley & Sons, Inc.)

reactive loading is with a narrow microstrip-line section of length  $\ell_m$  terminated with a second microstrip-line section of dimensions  $\ell_1 \times w_1$ . In order to integrate the proposed microstrip structure for reactive loading into the triangular patch, a rectangular slot of dimensions  $\ell_2 \times w_2$  is cut at the bottom edge of the triangular patch. The length  $\ell_2$  is selected to be greater than  $\ell_1 + \ell_m$  and the width  $w_2$  is greater than  $w_1$ . By using a probe feed at a position located about half-way from the tip to the bottom of the triangular patch, it is found that two near-degenerate resonant modes of similar radiation characteristics can be excited at frequencies near the fundamental resonant frequency of the unloaded patch antenna. These two resonant modes are utilized to form a wider impedance bandwidth for the proposed antenna.

The measured return loss of a constructed prototype is shown in Figure 7.62. Note that the fundamental resonant frequency  $f_{10}$  of the triangular microstrip antenna without reactive loading is about 1870 MHz, and it is clearly seen that two resonant modes, one with a lower resonant frequency (1854 MHz) than  $f_{10}$  and the other with

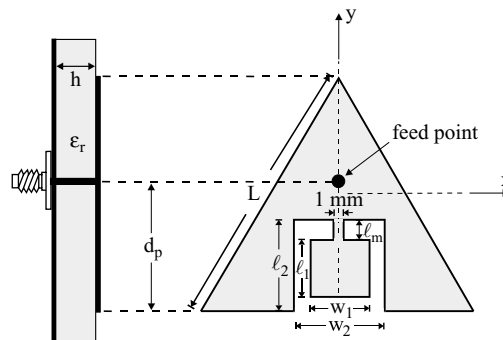


**FIGURE 7.61** Geometry of a broadband equilateral-triangular microstrip antenna with integrated reactive loading.

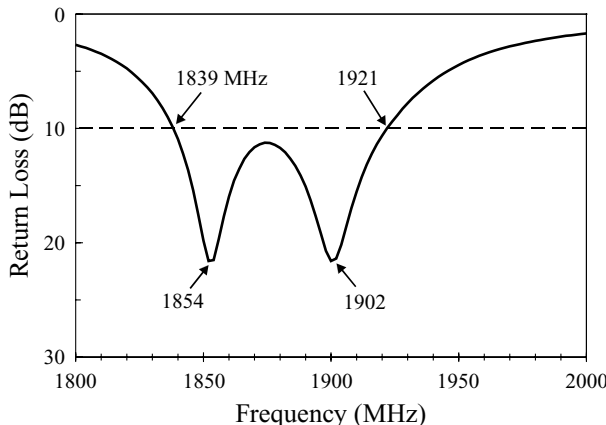


**FIGURE 7.62** Measured return loss for the antenna shown in Figure 7.61;  $\epsilon_r = 4.4$ ,  $h = 1.6$  mm,  $L = 50$  mm,  $d_p = 22.3$  mm,  $\ell_m = 3.5$  mm,  $\ell_1 = 9.2$  mm,  $w_1 = 7.3$  mm,  $\ell_2 = 14.1$  mm, and  $w_2 = 9.3$  mm.

a higher resonant frequency ( $1902$  MHz) than  $f_{10}$ , are excited with good impedance matching. The impedance bandwidth is  $82$  MHz, or about  $4.4\%$ , which is  $2.4$  times that ( $34$  MHz, or about  $1.8\%$ ) of the corresponding triangular microstrip antenna without reactive loading. In Figure 7.63, the measured on-axis ( $\theta = 0^\circ$ ) maximum received power for operating frequencies within the impedance bandwidth is presented, and the results show that the antenna gain variation within the impedance bandwidth is less than  $3$  dBi. Similar radiation patterns with the same polarization planes are observed for the two resonant frequencies within the impedance bandwidth, and good cross-polarization radiation is seen.

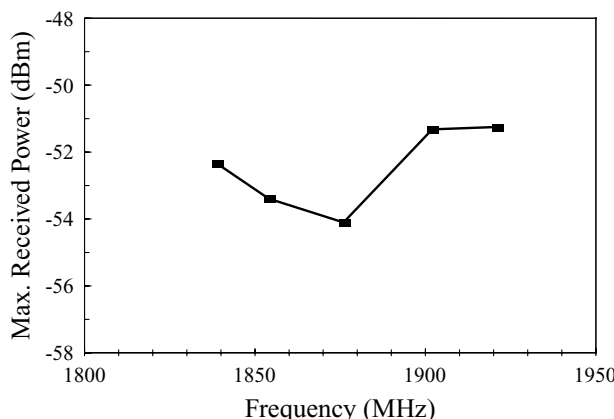
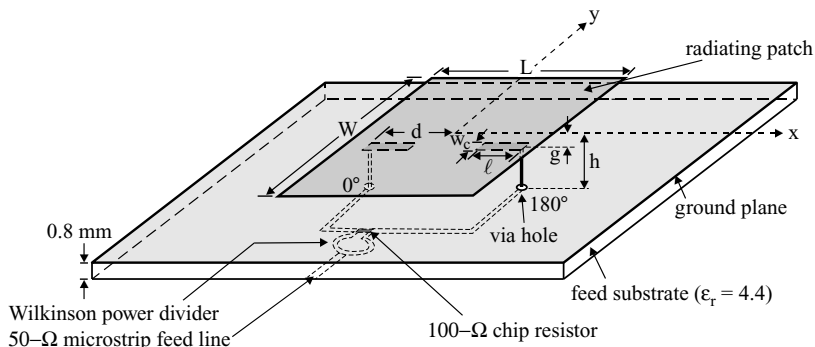


**FIGURE 7.63** Measured on-axis maximum received power for the antenna studied in Figure 7.62.

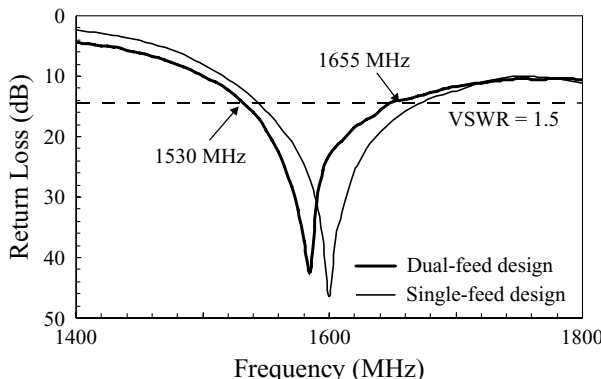
## 7.6 BROADBAND MICROSTRIP ANTENNAS WITH REDUCED CROSS-POLARIZATION RADIATION

As shown in the designs of Section 7.3, operating frequencies over a wide impedance bandwidth usually have relatively large cross-polarization radiation, especially in the *H*-plane pattern. This characteristic is related to the problem that some of the unwanted higher order modes that contribute to the polarization impurity are excited [31]. To ease the problem, it has been suggested that, by adding an additional feed of equal amplitude and a  $180^\circ$  phase shift, the microstrip antenna can be excited with some of the unwanted modes suppressed, and improved polarization purity can be obtained. Based on this technique, a dual capacitively fed broadband microstrip antenna with reduced cross-polarization radiation has been demonstrated. Several prototypes of the proposed antenna were constructed and studied. The experimental results show that the cross-polarization levels in both the *E*- and *H*-plane patterns can greatly be improved by, respectively, about 5–10 and 12–15 dB compared to the single-capacitive-feed design for operating frequencies over a bandwidth (1:1.5 VSWR) of about 7–8% suitable for practical applications in wireless communications systems.

Figure 7.64 shows the geometry of a proposed dual, capacitively fed broadband microstrip patch antenna. The radiating patch has a rectangular shape of dimensions  $L \times W$ . The radiating rectangular patch is supported by plastic supports (not shown in the figure) above the ground plane of an inexpensive FR4 substrate (denoted the feed substrate). The distance between the radiating patch and the ground plane is  $h$ . The dual capacitive feeds have the same dimensions, and have a narrow conducting strip of length  $\ell$  and width  $w_c$ , which is oriented along the excitation direction of the antenna and supported at one end by a conducting post above the ground plane. The conducting strip has a spacing of  $g$  below the radiating patch, and the supporting post is a distance  $d$  from the centerline (*y* axis) of the patch. Input powers with equal amplitudes and a  $180^\circ$  phase shift for dual capacitive feeds are provided by a Wilkinson power divider having a half-guided-wavelength difference in length between its two output feed lines.



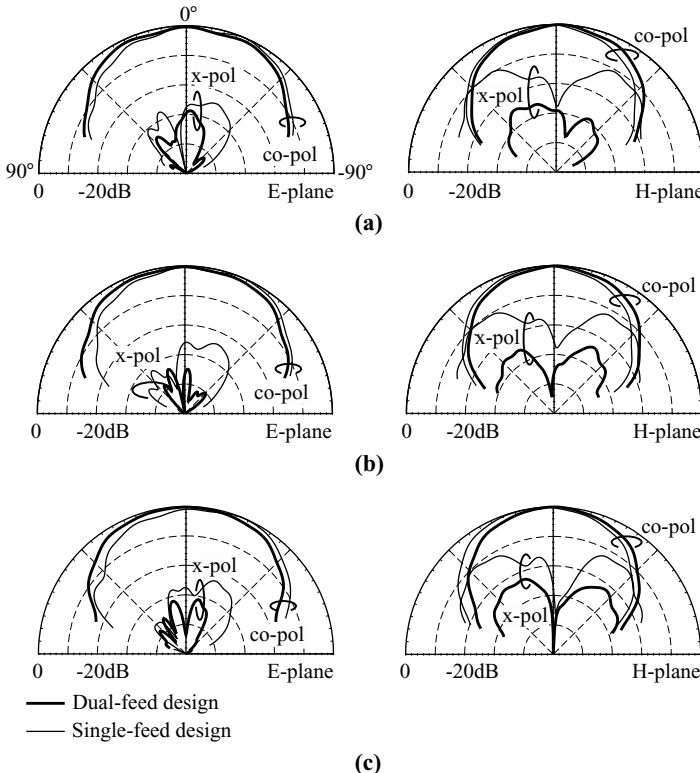
**FIGURE 7.64** Geometry of a broadband dual capacitively fed microstrip antenna with reduced cross-polarization radiation. (From Ref. 10, © 2000 John Wiley & Sons, Inc.)



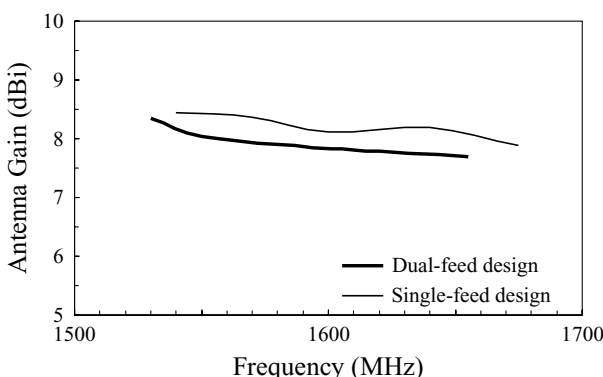
**FIGURE 7.65** Measured return loss for the antenna shown in Figure 7.64;  $h = 15$  mm,  $L = 60$  mm,  $W = 90$  mm,  $\ell = 13.5$  mm,  $g = 1.8$  mm,  $d = 16.8$  mm,  $w_c = 1.0$  mm, and ground-plane size =  $150 \times 150$  mm $^2$ . (From Ref. 10, © 2000 John Wiley & Sons, Inc.)

Figure 7.65 shows the measured return loss of a prototype with designed center frequency at 1.6 GHz. In this case, the patch dimensions were chosen to be  $60 \times 90$  mm $^2$ , and the distance between the radiating patch and the ground plane or the air-substrate thickness was chosen to be 15 mm, which corresponds to about 8% of the free-space wavelength of the center frequency. With proper dimensions for the capacitive feeds, good impedance matching is obtained for both the proposed dual-feed design and the single-feed design. The single-feed case corresponds to the antenna design shown in Figure 7.64 with one capacitive feed only. The obtained impedance bandwidth (1:1.5 VSWR) for the proposed design is 125 MHz, or about 7.8% with respect to the designed center frequency at 1.6 GHz, which is about the same as that of the single-feed design. Typical measured radiation patterns for frequencies across the impedance bandwidths are shown in Figure 7.66. It can be seen that, for the proposed antenna, the obtained cross-polarization levels (ratio of the maximum co-polarized radiation to the maximum cross-polarized radiation) are about 28–34 dB for the *E*-plane patterns and about 22–25 dB for the *H*-plane patterns. Compared to the single-feed design, the proposed antenna has larger cross-polarization levels of about 5–10 dB in the *E*-plane patterns. For the *H*-plane patterns, the proposed antenna has an even larger improvement, about 12–15 dB, in the cross-polarization level compared to those of the single-feed design. Figure 7.67 plots the measured antenna gain in the broadside direction. Probably due to the relatively more complicated feed network associated with the two-feed design, its antenna gain is about 0.2–0.5 dBi less than that of the single-feed design.

A prototype of the proposed antenna with a designed center frequency at 1.8 GHz was constructed. The patch dimensions were selected to be  $48 \times 72$  mm $^2$ . The air-substrate thickness was 17.2 mm, which is about 10% of the free-space wavelength of the center frequency. The measured return loss is presented in Figure 7.68. The obtained impedance bandwidth is 132 MHz (1748–1880 MHz), or about 7.3% referenced to the designed center frequency. Measured radiation patterns for frequencies



**FIGURE 7.66** Measured *E*-plane ( $x$ - $z$  plane) and *H*-plane ( $y$ - $z$  plane) radiation patterns for the antenna studied in Figure 7.65. (a)  $f = 1530$  MHz, (b)  $f = 1600$  MHz, (c)  $f = 1655$  MHz. (From Ref. 10, © 2000 John Wiley & Sons, Inc.)



**FIGURE 7.67** Measured on-axis antenna gain for the antenna studied in Figure 7.65. (From Ref. 10, © 2000 John Wiley & Sons, Inc.)

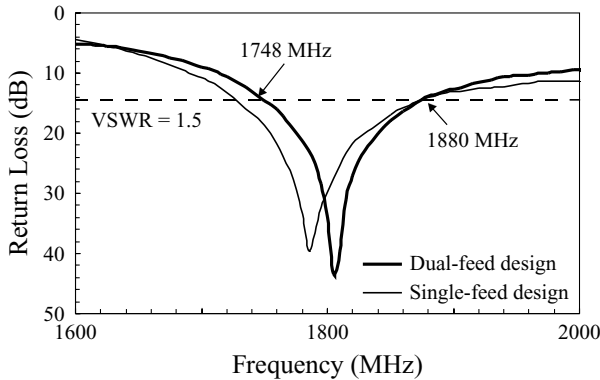


**FIGURE 7.68** Measured return loss for the antenna shown in Figure 7.64;  $h = 17.2$  mm,  $L = 48$  mm,  $W = 72$  mm,  $\ell = 14.8$  mm,  $g = 3.2$  mm,  $d = 19$  mm,  $w_c = 1.0$  mm, and ground-plane size =  $150 \times 150$  mm $^2$ . (From Ref. 10, © 2000 John Wiley & Sons, Inc.)

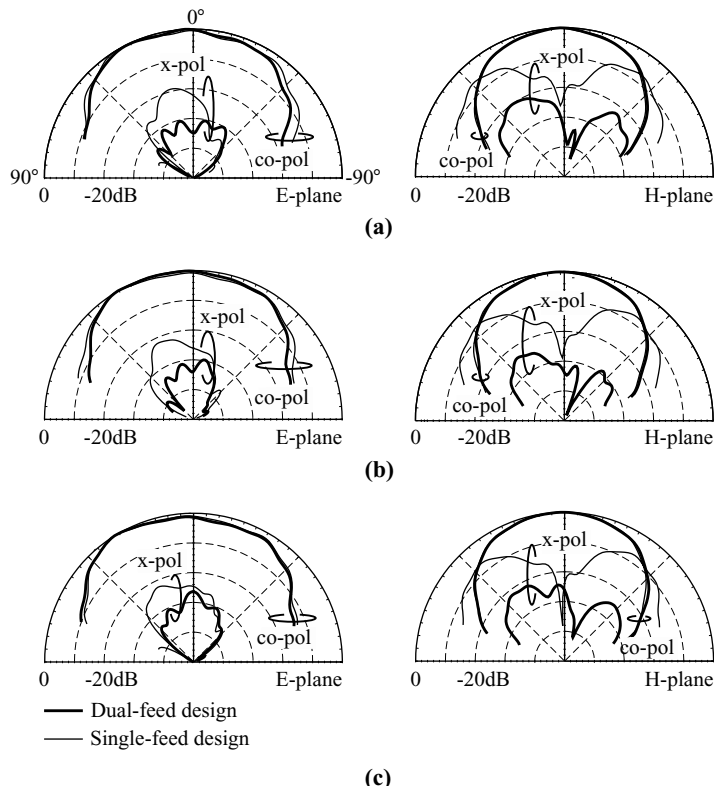


**FIGURE 7.69** Measured  $E$ -plane ( $x-z$  plane) and  $H$ -plane ( $y-z$  plane) radiation patterns for the antenna studied in Figure 7.68. (a)  $f = 1748$  MHz, (b)  $f = 1800$  MHz, (c)  $f = 1880$  MHz. (From Ref. 10, © 2000 John Wiley & Sons, Inc.)

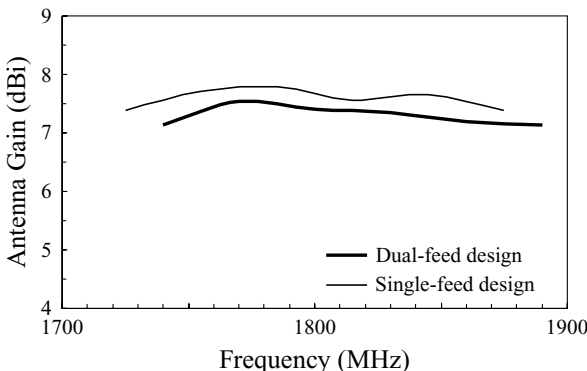


**FIGURE 7.70** Measured on-axis antenna gain for the antenna studied in Figure 7.68. (From Ref. 10, © 2000 John Wiley & Sons, Inc.)

across the impedance bandwidth are plotted in Figure 7.69, and the measured antenna gain is given in Figure 7.70. Similar improvements in the cross-polarization level to those observed in Figure 7.66 for the proposed two-feed design compared to the single-feed design are obtained.

## REFERENCES

1. G. Kumar and K. C. Gupta, "Directly coupled multiple resonator wide-band microstrip antennas," *IEEE Trans. Antennas Propagat.* **33**, 588–593, June 1985.
2. G. Kumar and K. C. Gupta, "Nonradiating edges and four edges gap-coupled multiple resonator broad-band microstrip antenna," *IEEE Trans. Antennas Propagat.* **33**, 173–178, Feb. 1985.
3. C. K. Wu and K. L. Wong, "Broadband microstrip antenna with directly coupled and gap-coupled parasitic patches," *Microwave Opt. Technol. Lett.* **22**, 348–349, Sept. 5, 1999.
4. P. S. Hall, "Probe compensation in thick microstrip patches," *Electron. Lett.* **23**, 606–607, May 21, 1987.
5. T. W. Chiou, H. C. Tung, and K. L. Wong, "A dual-polarization wideband circular patch antenna with hybrid feeds," *Microwave Opt. Technol. Lett.* **26**, 37–39, July 5, 2000.
6. G. A. E. Vandenbosch and A. R. Vande Capelle, "Study of the capacitively fed microstrip antenna element," *IEEE Trans. Antennas Propagat.* **42**, 1648–1652, Dec. 1994.
7. G. A. E. Vandenbosch, "Network model for capacitively fed microstrip antenna," *Electron. Lett.* **35**, 1597–1599, Sept. 16, 1999.
8. K. M. Luk, L. K. Au Yeung, C. L. Mak, and K. F. Lee, "Circular patch antenna with an L-shaped probe," *Microwave Opt. Technol. Lett.* **20**, 256–257, Feb. 20, 1999.
9. C. L. Mak, K. M. Luk, and K. F. Lee, "Microstrip line-fed L-strip patch antenna," *IEE Proc. Microw. Antennas Propagat.* **146**, 282–284, Aug. 1999.
10. W. H. Hsu and K. L. Wong, "A dual capacitively fed broadband patch antenna with reduced cross-polarization radiation," *Microwave Opt. Technol. Lett.* **26**, 169–171, Aug. 5, 2000.

11. N. Herscovici, "A wide-band single-layer patch antenna," *IEEE Trans. Antennas Propagat.* **46**, 471–473, April 1998.
12. T. Huynh and K. F. Lee, "Single-layer single-patch wideband microstrip antenna," *Electron. Lett.* **31**, 1310–1311, Aug. 3, 1995.
13. W. H. Hsu, Studies of broadband patch antennas with an air substrate, Ph.D. dissertation, Department of Electrical Engineering, National Sun Yat-Sen University, Kaohsiung, Taiwan, 2001.
14. K. L. Wong and W. H. Hsu, "Broadband triangular microstrip antenna with U-shaped slot," *Electron. Lett.* **33**, 2085–2087, Dec. 4, 1997.
15. K. L. Wong and W. H. Hsu, "A broadband rectangular patch antenna with a pair of wide slits," *IEEE Trans. Antennas Propagat.* **49**, 1345–1347, Sept. 2001.
16. B. L. Ooi and Q. Shen, "A novel E-shaped broadband microstrip patch antenna," *Microwave Opt. Technol. Lett.* **27**, 234–252, Dec. 5, 2000.
17. W. H. Hsu and K. L. Wong, "A wideband circular patch antenna," *Microwave Opt. Technol. Lett.* **25**, 327–328, June 5, 2000.
18. W. H. Hsu, G. Y. Lee, and K. L. Wong, "A wideband capacitively fed circular-E patch antenna," *Microwave Opt. Technol. Lett.* **27**, 134–135, Oct. 20, 2000.
19. C. L. Tang, Studies of three-dimensional patch antennas, Ph.D. dissertation, Department of Electrical Engineering, National Sun Yat-Sen University, Kaohsiung, Taiwan, 2001.
20. Y. M. Jo, "Broadband patch antennas using a wedge-shaped air dielectric substrate," in *1999 IEEE Antennas Propagat. Soc. Int. Symp. Dig.*, pp. 932–935.
21. J. Y. Sze and K. L. Wong, "Broadband rectangular microstrip antenna with a pair of toothbrush-shaped slots," *Electron. Lett.* **34**, 2186–2187, Nov. 12, 1998.
22. J. Y. Sze and K. L. Wong, "Single-layer single-patch broadband rectangular microstrip antenna," *Microwave Opt. Technol. Lett.* **22**, 234–236, Aug. 20, 1999.
23. J. Y. Sze and K. L. Wong, "Slotted rectangular microstrip antenna for bandwidth enhancement," *IEEE Trans. Antennas Propagat.* **48**, 1149–1152, Aug. 2000.
24. J. Y. Jan and K. L. Wong, "A broadband circular microstrip antenna with two open-ring slots," *Microwave Opt. Technol. Lett.* **23**, 205–207, Nov. 20, 1999.
25. N. Fayyaz and S. Safavi-Naeini, "Bandwidth enhancement of a rectangular patch antenna by integrated reactive loading," in *1998 IEEE Antennas Propagat. Soc. Int. Symp. Dig.*, pp. 1100–1103.
26. K. L. Wong and J. Y. Jan, "Broadband circular microstrip antenna with embedded reactive loading," *Electron. Lett.* **34**, 1804–1805, Sept. 17, 1998.
27. J. Y. Jan and K. L. Wong, "Microstrip-line-fed broadband circular microstrip antenna with embedded reactive loading," *Microwave Opt. Technol. Lett.* **22**, 200–202, Aug. 5, 1999.
28. K. L. Wong and J. S. Kuo, "Bandwidth enhancement of bow-tie microstrip antenna using integrated reactive loading," *Microwave Opt. Technol. Lett.* **22**, 69–71, July 5, 1999.
29. S. E. Davidson, S. A. Long, and W. F. Richards, "Dual-band microstrip antennas with monolithic reactive loading," *Electron. Lett.* **21**, 936–937, Sept. 26, 1985.
30. S. T. Fang, Analysis and design of triangular microstrip antennas, Ph.D. dissertation, Department of Electrical Engineering, National Sun Yat-Sen University, Kaohsiung, Taiwan, 1999.
31. J. Huang, "A technique for an array to generate circular polarization with linearly polarized elements," *IEEE Trans. Antennas Propagat.* **34**, 1113–1124, Sept. 1986.

## CHAPTER EIGHT

---

# Broadband Dual-Frequency and Dual-Polarized Microstrip Antennas

---

### 8.1 INTRODUCTION

Development of designs to achieve broadband operation at two separate frequencies for microstrip patch antennas has received much attention in recent years. This kind of broadband dual-frequency microstrip patch antenna can be implemented using the planar inverted-F antenna (PIFA) structure (see Section 3.2.1), which is compact and is suitable for handset antenna applications for cellular communications systems. Typical designs have been reported in Refs. 1–3. In this chapter, two other interesting designs for broadband dual-frequency operation are described: one with a two-element radiating patch [4] and one using a three-dimensional V-shaped radiating patch [5]. These designs are suitable for base station antennas for wireless communications systems. Experimental results for design examples are shown in Section 8.2. Section 8.3 presents some recently reported broadband dual-polarized microstrip patch antennas. Three designs based on the use of (a) two aperture-coupled feeds, (b) a gap-coupled probe feed and an H-slot coupled feed [6], and (c) an L-strip coupled feed and an H-slot coupled feed are demonstrated. These broadband dual-polarized microstrip patch antennas can have high isolation ( $<-30$  dB) between the two feeding ports for a wide impedance bandwidth larger than 10%. Good cross-polarization levels for the two polarizations are obtained.

### 8.2 BROADBAND DUAL-FREQUENCY MICROSTRIP ANTENNAS

#### 8.2.1 A Two-Element Microstrip Antenna

A broadband dual-frequency microstrip patch antenna consisting of two radiating patches and two L-probes has been proposed [4]. A design example for a base station

antenna for both GSM (890–960 MHz) and DCS (1710–1880 MHz) has been shown. This dual-band antenna has two rectangular patches of different sizes, which are excited at the fundamental mode  $\text{TM}_{10}$ . Two L-probes are connected to form a feed structure for the antenna. The impedance bandwidth of the lower and upper bands meet the bandwidth requirements of GSM and DCS mobile communications systems, and the maximum gain in the upper band of the proposed antenna is 8.5 dBi.

### 8.2.2 A Three-Dimensional V-Shaped Microstrip Antenna

Broadband dual-frequency operation has been demonstrated with the use of a V-shaped radiating patch [5]. Figure 8.1 shows the geometry of a broadband dual-frequency V-shaped microstrip patch antenna. The V-shaped patch is supported by nonconducting posts (not shown in the figure) and placed above the ground plane of the microstrip feed line. The V-shaped patch has dimensions  $L \times W$ , and the patch's centerline ( $\overline{AB}$ ) and nonradiating edges are, respectively, distances  $h_1$  and  $h_2$  from the ground plane;  $h_1$  is usually selected to be small, about  $0.02\lambda_0$  in this study ( $\lambda_0$  is the free-space operating wavelength), such that a smaller coupling slot can be used for achieving efficient coupling of the electromagnetic energy from the microstrip line to the radiating V-shaped patch. The distance  $h_2$  is chosen to be much greater than  $h_1$ , which effectively increases the antenna's average substrate thickness and makes possible the excitation of broadband resonant modes. An H-shaped coupling slot is cut

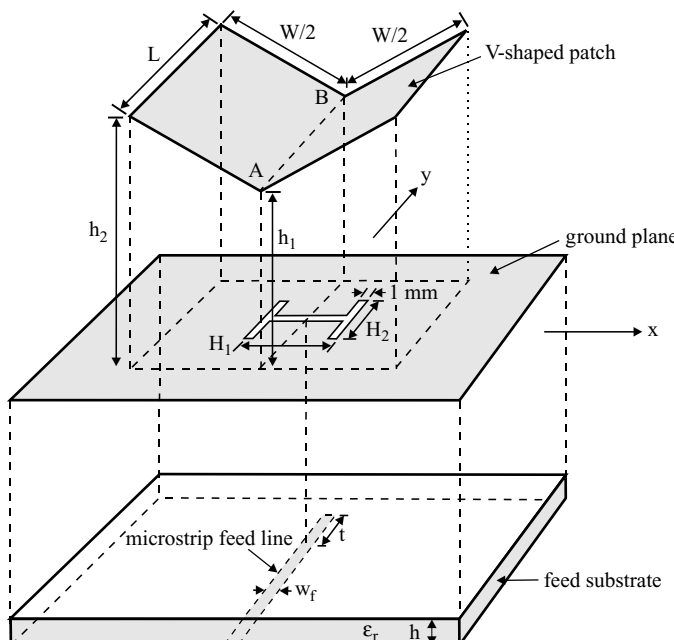


**FIGURE 8.1** Geometry of a broadband dual-frequency V-shaped microstrip patch antenna. (From Ref. 5, © 2000 John Wiley & Sons, Inc.)

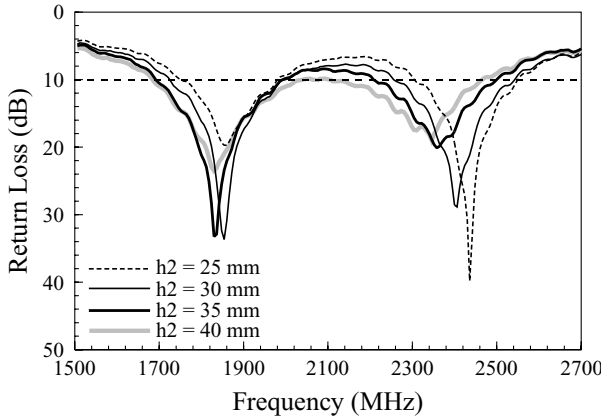


**FIGURE 8.2** Measured return loss for the antenna shown in Figure 8.1;  $\epsilon_r = 4.4$ ,  $h = 1.6$  mm,  $L = 60$  mm,  $W = 105$  mm,  $h_1 = 3$  mm,  $H_1 = 37$  mm,  $H_2 = 23$  mm,  $t = 25$  mm, and ground-plane size =  $180 \times 120$  mm<sup>2</sup>. (From Ref. 5, © 2000 John Wiley & Sons, Inc.)

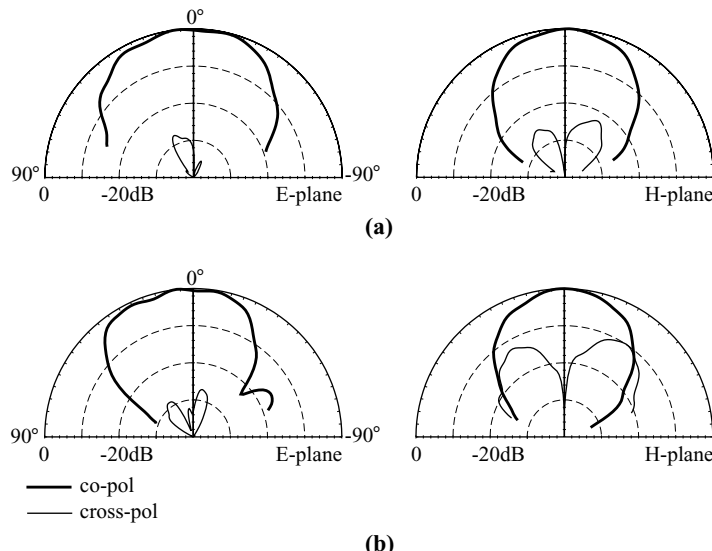
in the ground plane of the microstrip line and centered below the V-shaped patch. The use of an H-shaped slot allows a smaller slot size for efficient electromagnetic energy coupling and thus a reduction in the backradiation of the slot. The H-shaped slot is narrow, 1 mm wide. The lengths of the slot's central arm and two side arms are  $H_1$  and  $H_2$ , respectively; both are both much greater than 1 mm. The microstrip line has a width  $w_f$  and a tuning-stub length  $t$ , and is designed to have a  $50\text{-}\Omega$  characteristic impedance.

Figure 8.2 shows the measured return loss for constructed prototypes of the antenna. The V-shaped patch has dimensions  $60 \times 105$  mm<sup>2</sup> ( $L \times W$ ). The patch's centerline is fixed to 3 mm ( $h_1$ ) above the ground plane of the  $50\text{-}\Omega$  microstrip feed line. Experiments show that when the patch's two side edges are about 25–40 mm ( $h_2$ ) above the ground plane [i.e., about  $(0.15\text{--}0.25)\lambda_0$  referenced to  $f_1$  and about  $(0.20\text{--}0.32)\lambda_0$  referenced to  $f_2$ ], the first two resonant modes of the proposed antenna can both be excited with good impedance matching over a wide range of frequencies. The measured results of the dual-frequency operation are listed in Table 8.1. It can be seen that, when  $h_2$  is 40 mm, the 10-dB return-loss impedance bandwidths for lower ( $f_1$ ) and upper ( $f_2$ ) operating frequencies are 20% and 15.6%, respectively. The impedance bandwidths for  $f_1$  and  $f_2$  increase with increasing distance  $h_2$ . However,

**TABLE 8.1 Characteristics of the Antenna in Figure 8.1 [5]<sup>a</sup>**

$h_2$ (mm)	$f_1$ , BW (MHz, %)	$f_2$ , BW (MHz, %)	$f_2/f_1$
25	1860, 12.6	2436, 10.1	1.31
30	1854, 14.6	1406, 11.9	1.30
35	1830, 16.4	2358, 12.5	1.29
40	1830, 20.0	2346, 15.6	1.28

<sup>a</sup>Antenna parameters are given in Figure 8.2.



**FIGURE 8.3** Measured *E*-plane (*y*-*z* plane) and *H*-plane (*x*-*z* plane) radiation patterns for the antenna studied in Figure 8.2 with  $h_2 = 35$  mm. (a)  $f = 1830$  MHz, (b)  $f = 2358$  MHz. (From Ref. 5, © 2000 John Wiley & Sons, Inc.)

when  $h_2$  is less than 25 mm or greater than 40 mm, good impedance matching for both  $f_1$  and  $f_2$  cannot be achieved. For the prototypes, it is also seen that the frequency ratio between the two operating frequencies is slightly affected by the variation in  $h_2$  and is within the small range 1.28–1.31. From many experimental studies, it is found that dual-frequency operation with a frequency ratio up to about 1.45 can be obtained by varying the dimensions of the V-shaped patch.

Figures 8.3 and 8.4 show the measured radiation patterns at  $f_1$  and  $f_2$  for prototypes with  $h_2 = 35$  and 40 mm, respectively. Both  $f_1$  and  $f_2$  are seen to have the same polarization planes, and the cross-polarization radiation is less than  $-20$  dB, except for the *H*-plane (*x*-*z* plane) pattern at the upper frequency  $f_2$ . Good broadside radiation patterns for both  $f_1$  and  $f_2$  are observed, although there is a small dip in the direction about  $45^\circ$  from the broadside direction in the *E*-plane (*y*-*z* plane) pattern of  $f_2$ . Figure 8.5 shows the measured antenna gain for the lower and upper operating bands of the prototype with  $h_2 = 40$  mm. The lower band shows a peak antenna gain of about 8.1 dBi, while that for the upper band is about 6.4 dBi.

## 8.3 BROADBAND DUAL-POLARIZED MICROSTRIP ANTENNAS

### 8.3.1 Use of Two Aperture-Coupled Feeds

Aperture-coupled microstrip patch antennas have the advantage of easy fabrication, especially in the array designs, and a variety of aperture-coupled microstrip patch

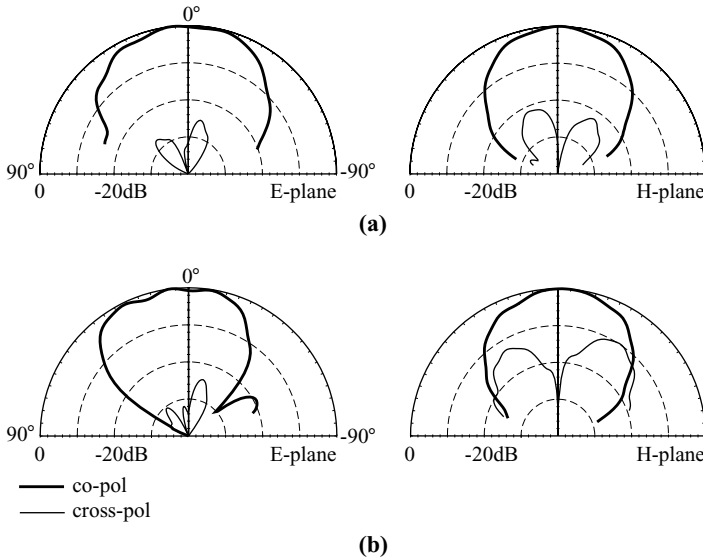


**FIGURE 8.4** Measured *E*-plane ( $y$ - $z$  plane) and *H*-plane ( $x$ - $z$  plane) radiation patterns for the antenna studied in Figure 8.2 with  $h_2 = 40$  mm. (a)  $f = 1830$  MHz, (b)  $f = 2346$  MHz. (From Ref. 5, © 2000 John Wiley & Sons, Inc.)

antennas for achieving dual-polarized radiation over a wide operating bandwidth have been reported [6–12]. The coupling slots used in these designs are often a cross slot or a pair of offset linear slots, among others. Since a thick air or foam substrate is usually used for such designs to have a wide operating bandwidth, the coupling slot size needs to be increased to obtain sufficient electromagnetic energy coupling from the microstrip feed line to the radiating patch. This condition results in a significant increase in the backward radiation of the patch antenna, which is a severe problem in practical applications in which a reflecting plate is required to be added behind the antenna's ground plane [9, 11]. This is because the reflecting plate and the ground plane form a waveguide where the backward radiation can propagate and decrease the decoupling between the two feeding ports.

The problem of backward radiation can be alleviated when an H-shaped coupling slot [13] is used. This is because the required length of the central arm (the two side arms mainly affect the reactive part of the input impedance) of the H-shaped slot for achieving sufficient electromagnetic energy coupling can be much smaller than that of a linear slot, and the backward radiation can thus be reduced. In this section, characteristics of a dual-polarized aperture-coupled microstrip patch antenna with H-shaped coupling slots are experimentally studied. Figure 8.6 shows the antenna geometry and four promising arrangements of the H-shaped coupling slots in the antenna's ground plane (denoted antennas 1–4). With these promising designs, high isolation between the two feeding ports can be obtained.

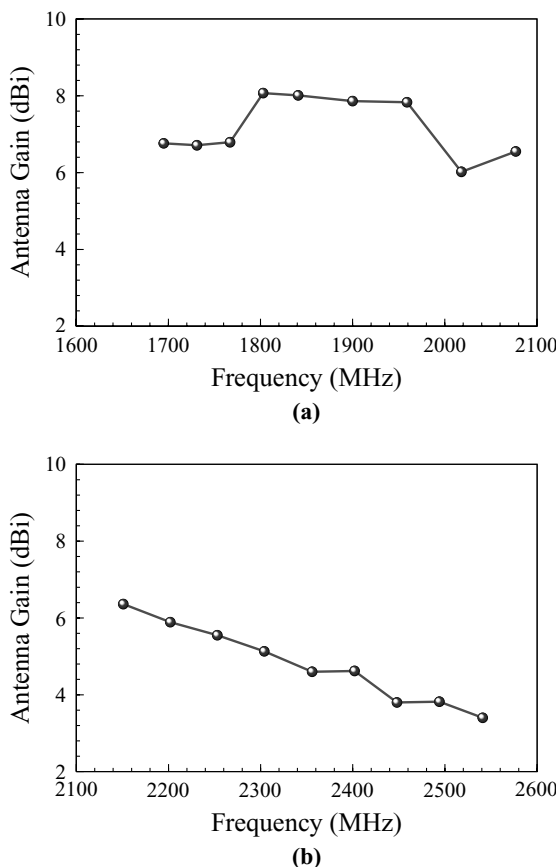


**FIGURE 8.5** Measured antenna gain in the broadside direction for the antenna studied in Figure 8.2 with  $h_2 = 40$  mm. (a) The lower band, (b) the upper band. (From Ref. 5, © 2000 John Wiley & Sons, Inc.)

The design of antenna 1 shown in Figure 8.6 is studied first. Figures 8.7(a) and 8.7(b) show the measured return loss for port 1 and port 2 excitation of antenna 1, respectively. The measured isolation  $S_{21}$  between ports 1 and 2 for antenna 1 is given in Figure 8.7(c). Both linear polarizations are designed to operate in the 1800-MHz band. The side length of the square patch is 60 mm, and the air-substrate thickness is 12.8 mm, which corresponds to about 7.7% of the free-space wavelength at 1800 MHz. The H-shaped coupling slots for ports 1 and 2 are identical and have dimensions  $H_1 = 19$  mm and  $H_2 = 21$  mm. The tuning-stub lengths are fixed to be 4 mm for ports 1 and 2. The impedance bandwidth for port 1 excitation of antenna 1 is found to be 152 MHz, or 8.4% referenced to 1800 MHz. For port 2, the measured impedance bandwidth is 300 MHz, or about 16.7%. The larger bandwidth is probably because the H-shaped coupling slot for port 2 is placed at the patch center and thus has better electromagnetic energy coupling, resulting in good impedance matching over a wider frequency range.

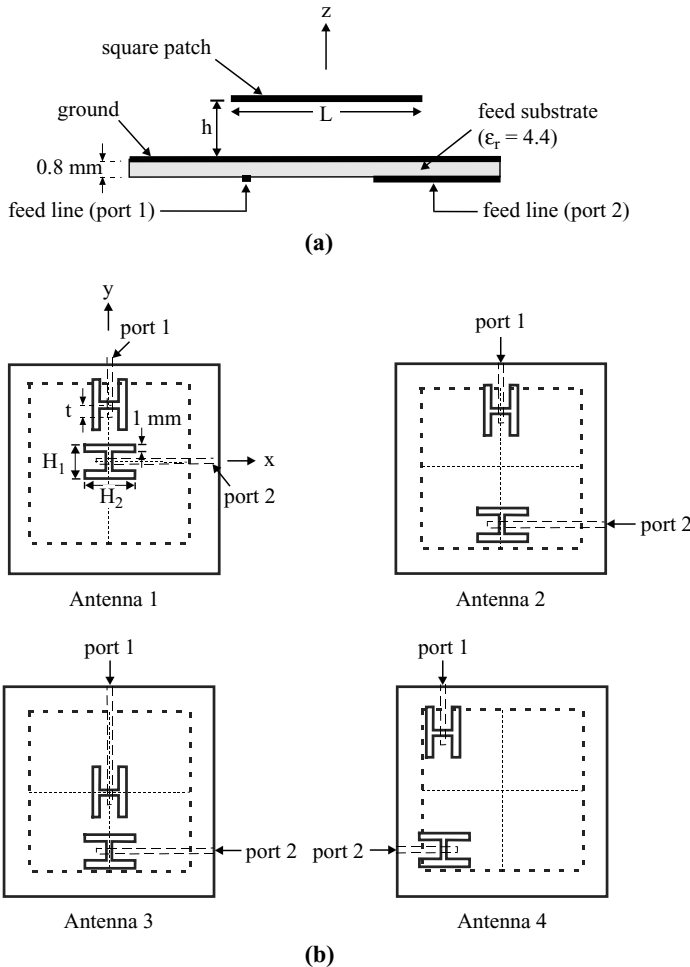


**FIGURE 8.6** Geometry of a dual-polarized aperture-coupled microstrip patch antenna with H-shaped coupling slot. (a) Side view of the antenna, (b) coupling slots in the ground plane for four different designs (antennas 1–4).

From the measured isolation  $S_{21}$  in Figure 8.7(c), it is seen that, within the impedance bandwidths of ports 1 and 2, the isolation between the two feeding ports is better than  $-40$  dB. This good isolation behavior is probably because the central arm of one H-shaped slot is aligned in the direction of the microstrip feed line of the other H-shaped slot, as shown in Figure 8.6. In this case, the H-shaped slot does not couple energy from the microstrip feed line of the other port, and thus good decoupling between the two feeding ports can be obtained. For the experimental studies conducted for antennas 2–4 (see Figure 8.6) with a similar slot arrangement as for antenna 1, good isolation ( $S_{21} < -35$  dB) across the wide impedance bandwidths has been observed. In addition to the high isolation, low cross-polarization for the two orthogonal linear polarizations has been observed.

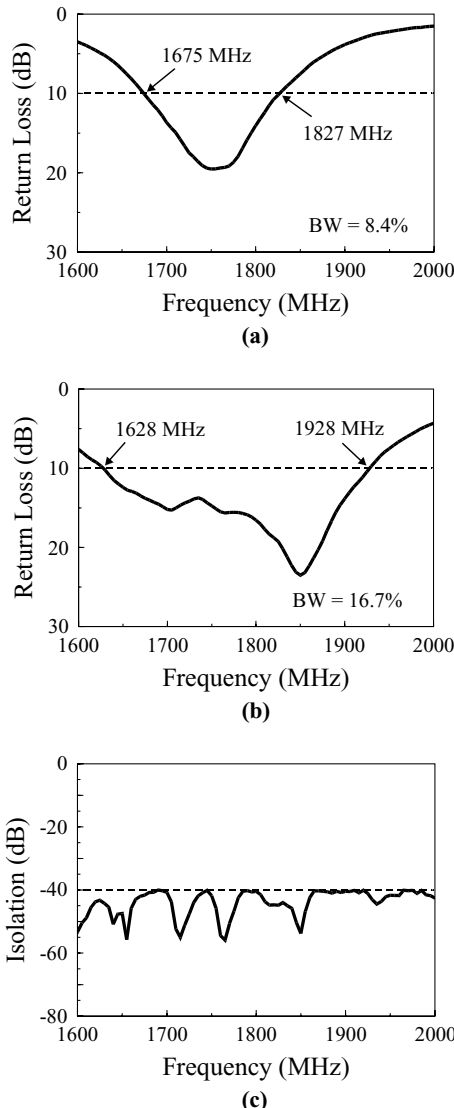


**FIGURE 8.7** Measured return loss for (a) port 1 excitation and (b) port 2 excitation of antenna 1 shown in Figure 8.6; (c) measured isolation  $S_{21}$  between ports 1 and 2 for antenna 1;  $L = 60$  mm,  $h = 12.8$  mm,  $H_1 = 19$  mm,  $H_2 = 21$  mm,  $t = 4$  mm, and ground-plane size =  $100 \times 100$  mm $^2$ .

Figure 8.8 plots the measured radiation patterns at 1800 MHz for antenna 1. It is seen that good broadside radiation patterns are obtained, and good cross-polarization radiation ( $<-20$  dB) for the two linear polarizations is seen. The measured antenna gains in the broadside direction for port 1 and port 2 excitation of antenna 1 are both about 7.5 dBi.

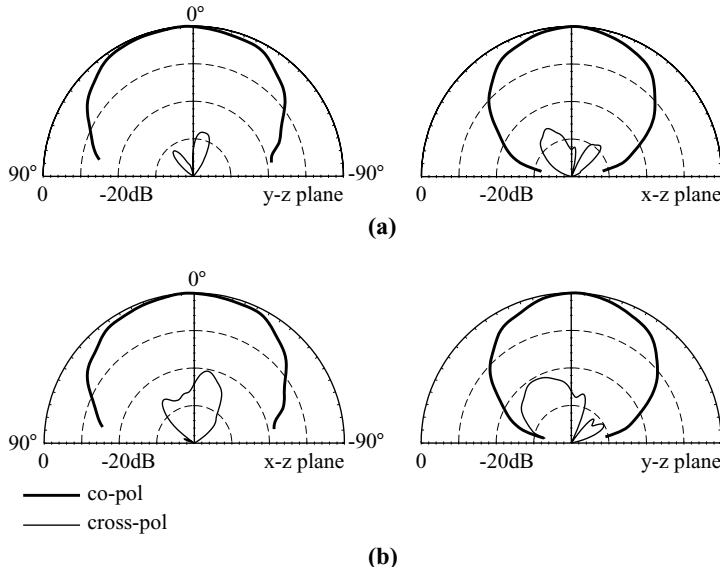


**FIGURE 8.8** Measured radiation patterns for antenna 1 shown in Figure 8.6;  $f = 1800$  MHz. (a) Port 1 excitation, (b) port 2 excitation.

### 8.3.2 Use of a Gap-Coupled Probe Feed and An H-Slot Coupled Feed

Hybrid feeds using a gap-coupled probe feed and an H-slot coupled feed (see Figure 8.9) are very effective in obtaining high isolation ( $<-30$  dB) between the two feeding ports of the antenna over the entire impedance bandwidth. Since there is no backward radiation for the gap-coupled probe feed, the coupling below the ground plane between the gap-coupled probe feed and the H-slot coupled feed can

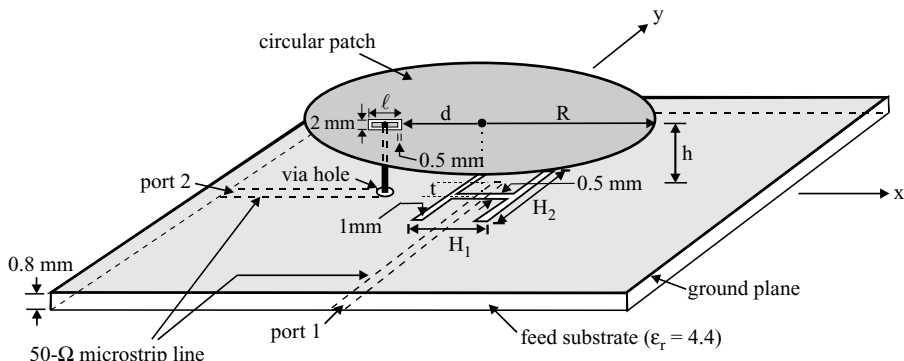


**FIGURE 8.9** Geometry of a broadband dual-polarized circular microstrip patch antenna fed by a gap-coupled probe feed and an H-slot coupled feed. (From Ref. 6, © 2000 John Wiley & Sons, Inc.)

be ignored when a reflecting plate is added to the proposed antenna for practical applications.

As shown in Figure 8.9, the circular patch has a radius  $R$  and is supported by nonconducting posts (not shown) a distance  $h$  above the ground plane of a grounded substrate (feed substrate) of thickness 0.8 mm and relative permittivity 4.4. Port 1 is the aperture-coupled feed with an H-slot cut in the ground plane to couple the electromagnetic energy from the  $50\text{-}\Omega$  microstrip line printed on the feed substrate to the circular patch. The H-slot is centered below the circular patch; the dimensions of its central arm and two side arms are  $0.5 \text{ mm} \times H_1$  and  $1 \text{ mm} \times H_2$ , respectively. Port 2 has a gap-coupled probe feed. One end of the feed is connected to a  $50\text{-}\Omega$  microstrip line through a via hole in the ground plane, and the other end is directly connected to the circular patch with a rectangular ring gap cut around the feed point. The rectangular ring gap is used to compensate the large probe inductance owing to the longer probe pin in the thick air substrate. The gap has dimensions of  $2 \text{ mm} \times \ell (\ell > 2 \text{ mm})$  and a gap width of 0.5 mm and is a distance  $d$  from the patch center. The longer side of the gap is placed parallel to the excitation direction of port 2 in order to minimize possible perturbations on the excited patch surface current.

A prototype was constructed with a designed center frequency at 1800 MHz. The radius of the circular patch was 35 mm and the air-substrate thickness was 13.6 mm, or about 8% of the wavelength of the center frequency. Figure 8.10 shows the measured return loss for the port 1 (H-slot coupled feed) and port 2 (gap-coupled probe feed) excitation. For port 1 excitation (polarization  $E$ -plane is the  $y-z$  plane), the 10-dB impedance bandwidth is 183 MHz (1712–1895 MHz), or about 10.2% referenced to 1800 MHz. For port 2 excitation (polarization  $E$ -plane is the  $x-z$  plane), the impedance bandwidth is 332 MHz (1620–1952 MHz), or about 18.4% with respect to 1800 MHz. Both impedance bandwidths for the two orthogonal polarizations are greater than 10%. Figure 8.11 shows the isolation between the two feeding ports. It is seen that the isolation for operating frequencies within the entire impedance bandwidths of ports 1 and 2 is less than  $-32$  dB, and the isolation at the center frequency is about  $-40$  dB. Figures 8.12 and 8.13 present the measured radiation patterns in two orthogonal planes at 1800 MHz for the H-slot coupled feed and the gap-coupled probe feed, respectively. In general, good cross-polarization levels are obtained. The cross-polarization levels are all larger than or about 20 dB, except that (about 14 dB) in the  $H$ -plane ( $y-z$  plane) pattern of the gap-coupled probe feed. The antenna gain for the two polarizations was 7.0 and 8.2 dBi in the broadside direction for port 1 and port 2 excitation, respectively. When a reflecting plate was added below the ground plane, the measured isloation between the two feeding ports was almost unchanged.

### 8.3.3 Use of an L-Strip Coupled Feed and an H-Slot Coupled Feed

The characteristics of a broadband dual-polarized microstrip patch antenna using the hybrid feed of an L-strip coupled feed and an H-slot coupled feed have been studied. Figure 8.14 shows the antenna geometry. Port 1 is the aperture-coupled feed with an

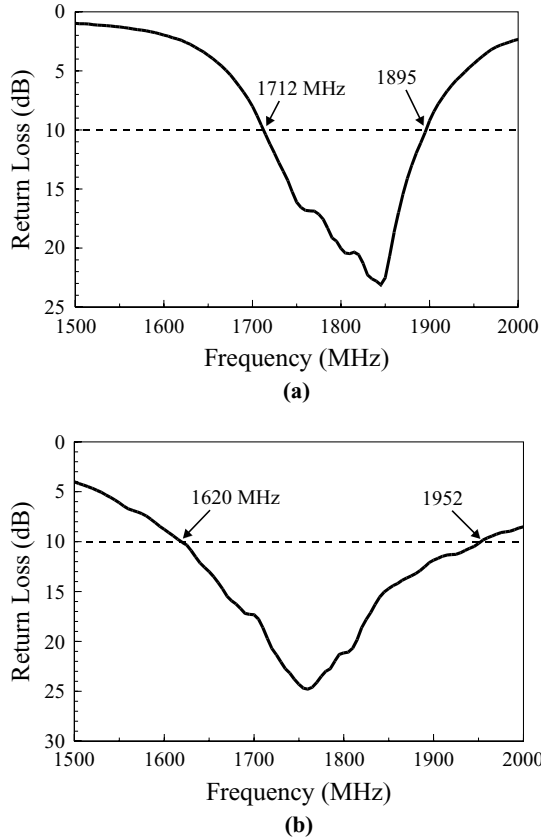


**FIGURE 8.10** Measured return loss for the antenna shown in Figure 8.9;  $R = 35$  mm,  $h = 13.6$  mm,  $d = 6.5$  mm,  $\ell = 7$  mm,  $H_1 = 10$  mm,  $H_2 = 30$  mm,  $t = 3.5$  mm, and ground-plane size =  $100 \times 100$  mm $^2$ . (a) H-slot coupled feed (port 1); (b) gap-coupled probe feed (port 2). (From Ref. 6, © 2000 John Wiley & Sons, Inc.)

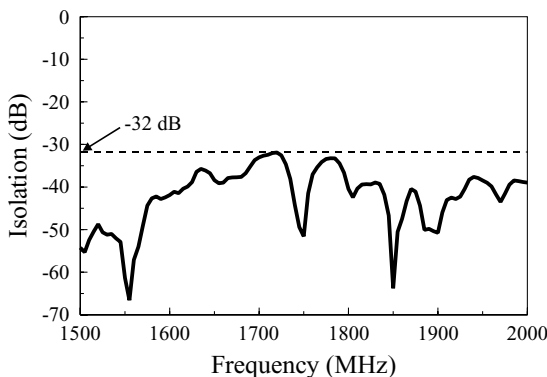


**FIGURE 8.11** Measured isolation  $S_{21}$  for the antenna studied in Figure 8.10. (From Ref. 6, © 2000 John Wiley & Sons, Inc.)

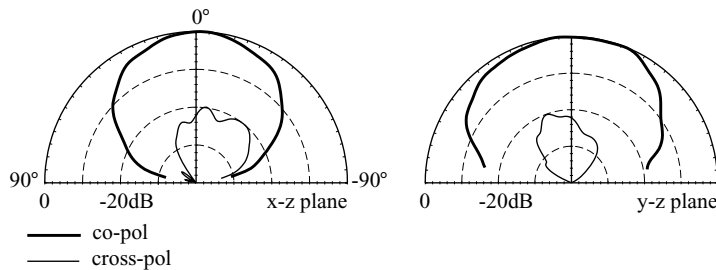


**FIGURE 8.12** Measured radiation patterns at 1800 MHz for port 1 excitation (H-slot coupled feed) of the antenna studied in Figure 8.10. (From Ref. 6, © 2000 John Wiley & Sons, Inc.)

H-shaped coupling slot, similar to those shown in Sections 8.3.1 and 8.3.2. Port 2 has an L-strip coupled feed. A conducting strip of width 1 mm and length  $\ell$  ( $\ell \gg 1$  mm) is placed parallel to and below the radiating patch at a distance of  $g$ , and couples the electromagnetic energy to the radiating patch from a  $50\text{-}\Omega$  microstrip line through a via hole in the ground plane. The conducting strip is supported by a conducting post which is a distance  $d$  from the center axis of the patch and is connected to the  $50\text{-}\Omega$  microstrip line at port 2.

A prototype of the antenna shown in Figure 8.14 was constructed and measured. The designed center frequency was 1800 MHz. The radius of the circular patch was 35 mm, and the antenna height or the air-substrate thickness was 13.6 mm, or about 8% of the wavelength of the center frequency. Figure 8.15 shows the measured return loss and isolation. The measured  $E$ - and  $H$ -plane radiation patterns for the two polarizations at 1800 MHz are plotted in Figure 8.16. For port 1 excitation, the obtained 10-dB return-loss bandwidth is 268 MHz, or about 14.9%, while that for port-2 excitation is 14.2%. The isolation between ports 1 and 2 is less than  $-30$  dB for the entire impedance bandwidths of the two polarizations. The results in Figure 8.16 show that good cross-polarization levels are in general obtained, except that the cross-polarization in the  $H$ -plane ( $y$ - $z$  plane) pattern of port 2 excitation is only about 14.4 dB. Measured antenna gain in the broadside

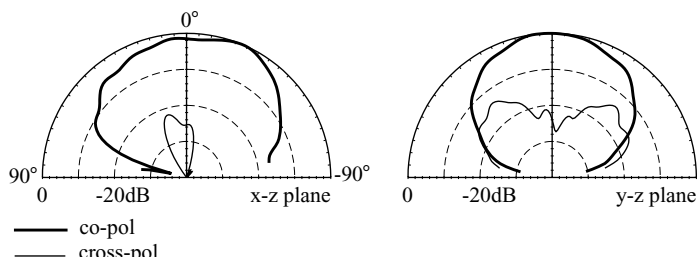


**FIGURE 8.13** Measured radiation patterns at 1800 MHz for port 2 excitation (gap-coupled probe feed) of the antenna studied in Figure 8.10. (From Ref. 6, © 2000 John Wiley & Sons, Inc.)

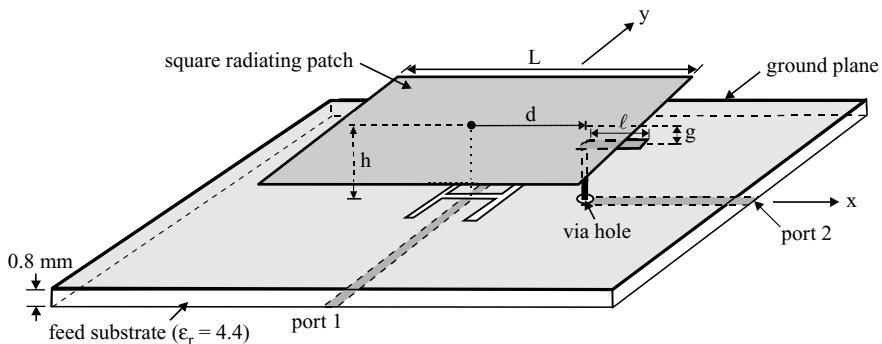


**FIGURE 8.14** Geometry of a broadband dual-polarized square microstrip patch antenna fed by an L-strip coupled feed and an H-slot coupled feed.

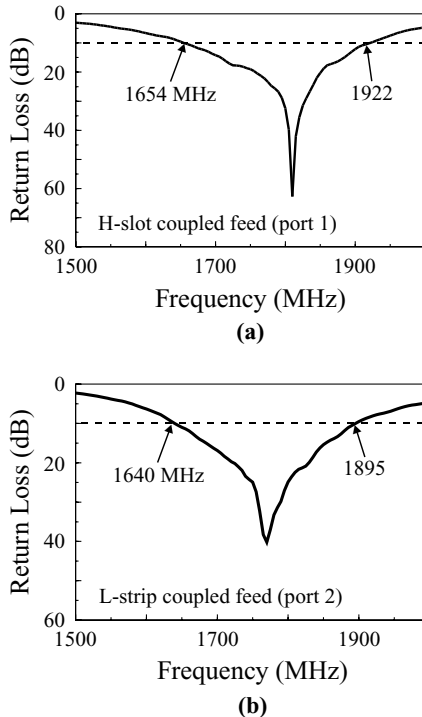


**FIGURE 8.15** Measured return loss and isolation for the antenna shown in Figure 8.14;  $L = 57.5$  mm,  $h = 13.6$  mm,  $d = 22$  mm,  $\ell = 20$  mm,  $g = 3.2$  mm, slot's center-arm dimensions =  $1 \times 20$  mm $^2$ , slot's side-arm dimensions =  $1 \times 19$  mm $^2$ , tuning-stub length = 6 mm, and ground-plane size =  $100 \times 100$  mm $^2$ . (a) Return loss for H-slot coupled feed (port 1), (b) return loss for L-strip coupled feed (port 2),

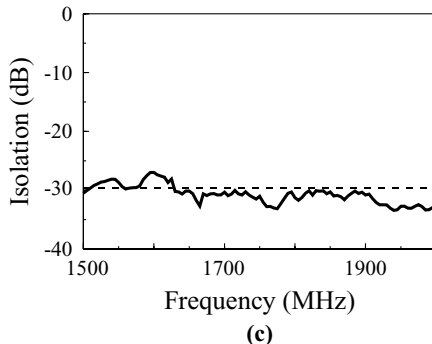


**FIGURE 8.15** (Continued.) (c) isolation between ports 1 and 2.

direction for ports 1 and 2 at 1800 MHz is also observed to be the same (about 7.4 dBi). It was observed that the measured isolation and return loss of ports 1 and 2 were almost unchanged when a reflecting conducting plate was added below the ground plane for the proposed antenna to be usable for practical applications. This also confirms the prediction that no coupling exists between the L-strip coupled feed and the H-slot coupled feed in the region between the ground plane and the reflecting plate.

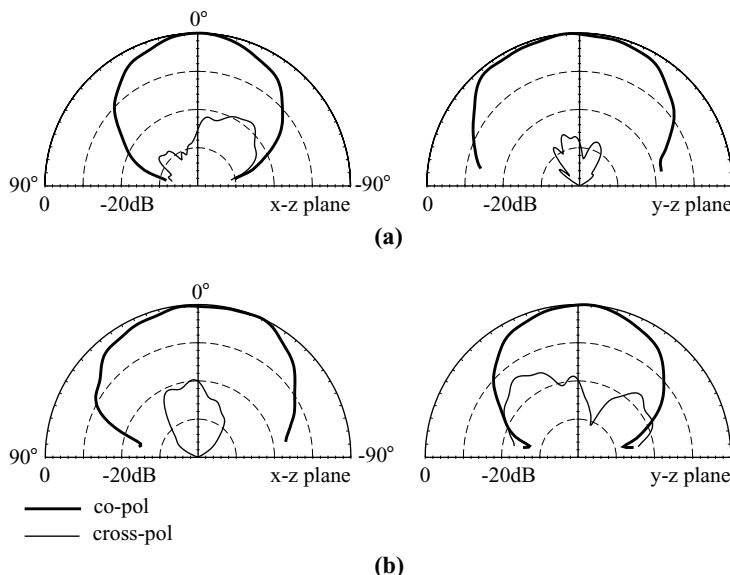


**FIGURE 8.16** Measured radiation patterns at 1800 MHz for the antenna studied in Figure 8.15. (a) H-slot coupled feed (port 1), (b) L-strip coupled feed (port 2).

## REFERENCES

1. S. Tarvas and A. Isohatala, "An internal dual-band mobile phone antenna," in *2000 IEEE Antennas Propagat. Soc. Int. Symp. Dig.*, pp. 266–269.
2. C. R. Rowell and R. D. Murch, "A compact PIFA suitable for dual-frequency 900/1800-MHz operation," *IEEE Trans. Antennas Propagat.* **46**, 596–598, April 1998.
3. Z. D. Liu, P. S. Hall, and D. Wake, "Dual-frequency planar inverted-F antenna," *IEEE Trans. Antennas Propagat.* **45**, 1452–1458, Oct. 1997.
4. K. M. Luk, C. H. Lai, and K. F. Lee, "Wideband L-probe-fed patch antenna with dual-band operation for GSM/PCS base stations," *Electron. Lett.* **35**, 1123–1124, July 8, 1999.
5. C. L. Tang, C. W. Chiou, and K. L. Wong, "Broadband dual-frequency V-shape patch antenna," *Microwave Opt. Technol. Lett.* **25**, 121–123, April 20, 2000.
6. T. W. Chiou, H. C. Tung, and K. L. Wong, "A dual-polarization wideband circular patch antenna with hybrid feeds," *Microwave Opt. Technol. Lett.* **26**, 37–39, July 5, 2000.
7. S. Hienonen, A. Lehto, and A. V. Raisanen, "Simple broadband dual-polarized aperture-coupled microstrip antenna," in *1999 IEEE Antennas Propagat. Soc. Int. Symp. Dig.*, pp. 1228–1231.
8. B. Lindmark, "A novel dual polarized aperture coupled patch element with a single layer feed network and high isolation," in *1997 IEEE Antennas Propagat. Soc. Int. Symp. Dig.*, pp. 2190–2193.
9. I. Nystrom and D. Karlsson, "Reduction of back radiation and cross-coupling in dual polarized aperture coupled patch antennas," in *1997 IEEE Antennas Propagat. Soc. Int. Symp. Dig.*, pp. 2222–2225.
10. J. R. Sanford and A. Tengs, "A two substrate dual polarized aperture coupled patch," in *1996 IEEE Antennas Propagat. Soc. Int. Symp. Dig.*, pp. 1544–1547.
11. P. Brachat and J. M. Baracco, "Printed radiating element with two highly decoupled input ports," *Electron. Lett.* **31**, 245–246, Feb. 16, 1995.
12. J.-F. Zuercher, Ph. Gay-Balmaz, R. C. Hall, and S. Kolb, "Dual polarized, single- and double-layer strip-slot-foam inverted patch (SSFIP) antennas," *Microwave Opt. Technol. Lett.* **7**, 406–410, 1994.
13. M. El Yazidi, M. Himdi, and J. P. Daniel, "Transmission line analysis of nonlinear slot coupled microstrip antenna," *Electron. Lett.* **28**, 1406–1408, July 16, 1992.

## CHAPTER NINE

---

# Broadband and Dual-Band Circularly Polarized Microstrip Antennas

---

### 9.1 INTRODUCTION

The CP operation of microstrip antennas can be achieved by using either single-feed or two-feed designs. The single-feed design has the advantage of a simple feed structure, and in addition, no external phase shifter is required. Many single-feed designs have been described in Chapter 5. However, single-feed designs usually have a narrow CP bandwidth (3-dB axial ratio) of about 1% for a microstrip antenna with a dielectric substrate. To enhance the CP bandwidth for a single-feed design, an aperture-coupled microstrip antenna using an inclined nonlinear coupling slot has been reported [1]. Details of the experimental results are given in Section 9.2. In this study, the CP bandwidth is broadened to about 2.1 times that obtained using a simple inclined coupling slot for CP operation. When a thick air or foam substrate is used, the CP bandwidth of a microstrip antenna with a single-feed design can be further enhanced. In this case, a single-feed aperture-coupled circular microstrip antenna with a slit and two stubs and having a CP bandwidth of about 7.2% has been reported [2].

For two-feed designs, single-layer, broadband CP microstrip antennas with a large CP bandwidth greater than 20% have been reported [3–5]. These broadband CP designs mainly have a thick foam or air substrate; to achieve good impedance matching, feed methods using two three-dimensional microstrip transition feed lines [3] and two aperture-coupled feeds [4, 5] have been used. Recently, two-feed designs using two gap-coupled probe feeds [6] and two capacitively coupled feeds [7] have been presented. For the former design with a thick air substrate, experimental results show that a 65% impedance bandwidth (1:2 VSWR) and a 46% 3-dB axial-ratio CP bandwidth are achieved [6]. Within the CP bandwidth, the gain bandwidth, defined

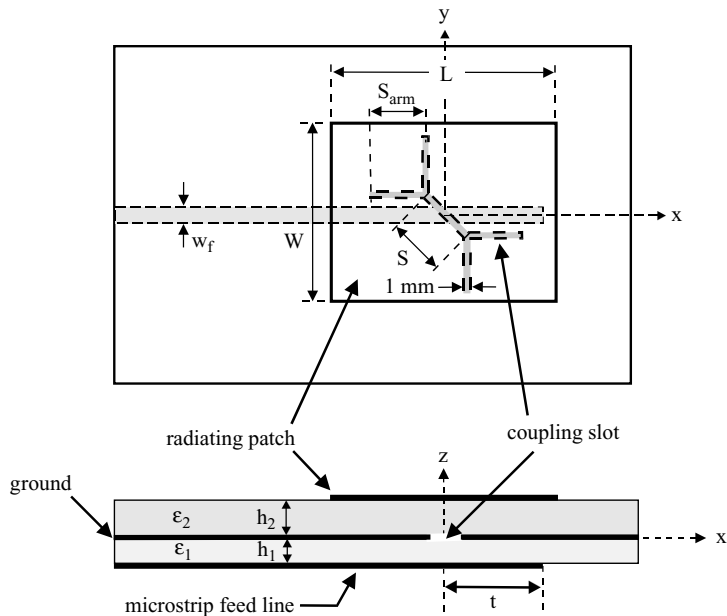
to be within 3 dB of the peak antenna gain (about 6.0 dBi), is 44.6%. For the latter case, using two capacitively coupled feeds, an impedance bandwidth (1:2 VSWR) of about 49% and a 3-dB axial-ratio bandwidth of about 35% have been achieved [7]. In this case, the 1-dB gain bandwidth is 28%, with the antenna gain level at about 7.0 dBi. The experimental results and design considerations are given in Section 9.3. For obtaining improved CP quality over a wide coverage angle for frequencies within the CP bandwidth, a four-feed design using 0°, 90°, 180°, and 270° phase shifts provided by a feed network consisting of Wilkinson power dividers is described in Section 9.4.

In the last half of this chapter, dual-band CP operations of microstrip antennas are discussed. Typical dual-band CP microstrip antennas that have been reported include a design using an aperture-coupled stacked microstrip antenna [8] and one using a spur-line filter technique [9]. In Section 9.5, some new and promising designs for obtaining dual-band CP radiation of a single-feed microstrip antenna are presented. These dual-band CP designs use a probe-fed circular patch with two pairs of arc-shaped slots [10], a probe-fed square patch with a center slot and inserted slits [11], and a probe-fed stacked elliptic patch [12]. Details of the dual-band CP performance are presented and discussed.

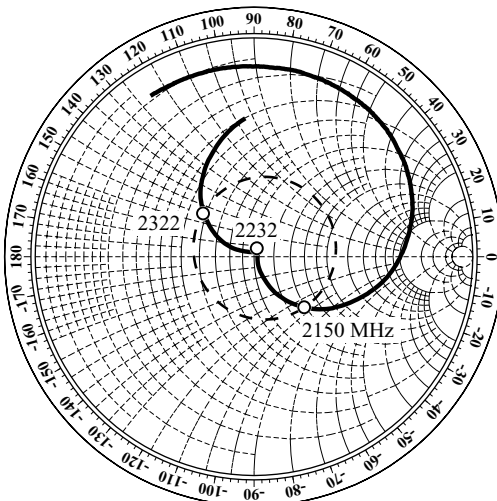
## 9.2 BROADBAND SINGLE-FEED CIRCULARLY POLARIZED MICROSTRIP ANTENNAS

Figure 9.1 shows the geometry of an aperture-coupled microstrip antenna with an inclined nonlinear coupling slot for CP bandwidth enhancement. The nonlinear coupling slot in the ground plane is centered below the patch and has a linear portion of length  $S$  and two end-loading V slots of equal arm length  $S_{\text{arm}}$ . This nonlinear coupling slot is selected to be narrow (1 mm) and is inclined with respect to the microstrip line with an angle of 45°. The two arms of each of the end-loading V slots are perpendicular to each other and are aligned parallel to both sides of the patch. With the proposed nonlinear coupling slot, the fundamental resonant mode of a nearly square patch with a relatively larger aspect ratio (greater than 1.1) can be split into two near-degenerate resonant modes with equal amplitudes and a 90° phase difference, which results in broadband CP operation. For  $L > W$ , as shown in Figure 9.1, the proposed antenna will radiate a right-hand circularly polarized wave; if  $L < W$ , left-hand CP operation is obtained.

The proposed antenna was implemented. Measured input impedance on a Smith chart is shown in Figure 9.2. The patch is selected to have dimensions of  $33.5 \times 30 \text{ mm}^2$  ( $L/W \cong 1.117$ ). The microstrip feed line has a  $50\text{-}\Omega$  characteristic impedance, and the tuning-stub length  $t$  for impedance matching is adjusted to be 23 mm for the case studied here. The dimensions of the nonlinear coupling slot are  $S = 5 \text{ mm}$  and  $S_{\text{arm}} = 6.2 \text{ mm}$ . The results show that two near-degenerate orthogonal modes with good impedance matching are excited for the parameters selected. The impedance bandwidth (1:2 VSWR) is 171 MHz, or about 7.7% with respect to



**FIGURE 9.1** Geometry of a slot-coupled microstrip antenna for broadband CP operation. (From Ref. 1, © 1998 IEE, reprinted with permission.)



**FIGURE 9.2** Measured input impedance on a Smith chart for the antenna shown in Figure 9.1;  $\epsilon_1 = \epsilon_2 = 4.4$ ,  $h_1 = 0.8$  mm,  $h_2 = 1.6$  mm,  $w_f = 1.5$  mm,  $t = 23$  mm,  $S = 5$  mm,  $S_{\text{arm}} = 6.2$  mm,  $L = 33.5$  mm, and  $W = 30$  mm. (From Ref. 1, © 1998 IEE, reprinted with permission.)

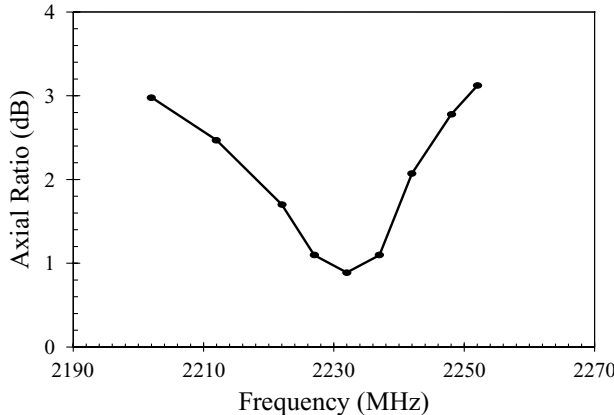


**FIGURE 9.3** Measured axial ratio for the antenna studied in Figure 9.2. (From Ref. 1, © 1998 IEE, reprinted with permission.)

the center frequency at 2232 MHz, at which the minimum axial ratio is observed (see Figure 9.3 for the measured axial ratio of the CP radiation). From the measured axial ratio, the CP bandwidth, determined from the 3-dB axial ratio, is 49 MHz, or 2.2%. This CP bandwidth is 2.1 times that (1.05%) obtained for the case using a simple inclined coupling slot (see Table 9.1). The reason the proposed coupling slot is capable of achieving broadband CP operation is probably that the required slot size of the present design for the excitation of two near-degenerate orthogonal modes for CP operation is larger [29.8 mm ( $= S + 4S_{\text{arm}}$ ) for the proposed design compared to 14 mm ( $= S$ ;  $S_{\text{arm}} = 0$ ) for the case using a simple inclined slot]. Owing to the larger slot cut in the ground plane, the electromagnetic energy within the cavity between the microstrip patch and ground plane will be less confined, which lowers the quality factor of the cavity and results in a larger impedance bandwidth.

Moreover, the patch's aspect ratio (about 1.117) in the present design is greater than those using a simple inclined coupling slot (about 1.027). Such a larger aspect ratio gives the proposed design a relaxed manufacturing tolerance. The measured

**TABLE 9.1** CP Performance of Antennas with Coupling Slot (Antenna 1) and Simple Inclined Coupling Slot without End-Loading Slots (Antenna 2) [1]<sup>a</sup>

	Patch Size (mm <sup>2</sup> )	Aspect Ratio $L/W$	$f_c$ (MHz)	1:2 VSWR Bandwidth (%)	3-dB Axial-Ratio CP Bandwidth (%)
Antenna 1	33.5 × 30	1.117	2232	7.7	2.20
Antenna 2	30.8 × 30	1.027	2340	3.8	1.05

<sup>a</sup> Antenna parameters are given in Figure 9.2.

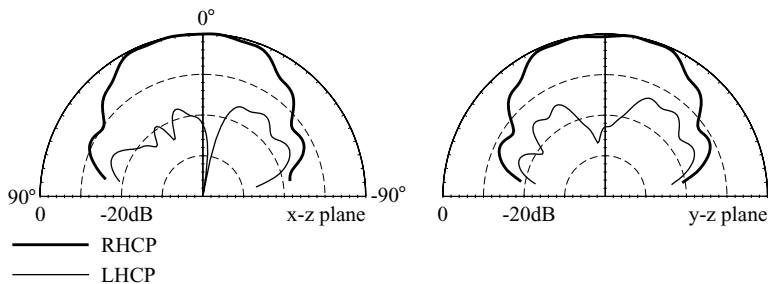


**FIGURE 9.4** Measured radiation patterns at 2232 MHz for the antenna studied in Figure 9.2. (From Ref. 1, © 1998 IEE, reprinted with permission.)

radiation patterns in two orthogonal planes at 2232 MHz for the proposed design are plotted in Figure 9.4; good right-hand CP radiation can be seen.

### 9.3 BROADBAND TWO-FEED CIRCULARLY POLARIZED MICROSTRIP ANTENNAS

#### 9.3.1 Use of Two Gap-Coupled Probe Feeds with a Wilkinson Power Divider

Figure 9.5 shows a broadband CP design with a thick air layer between the radiating patch and the ground plane. Two gap-coupled probe feeds placed in orthogonal directions are used for the excitation of the proposed antenna. The large probe inductance, owing to the thick air substrate, for the two probe feeds is tuned out by embedding a concentric annular-ring slot around each feed in the radiating patch. By further incorporating a Wilkinson power divider with a  $90^\circ$  phase shift between its two outputs to provide good equal input powers and a  $90^\circ$  phase shift for the two feeds, the present CP design can have a 3-dB axial-ratio CP bandwidth greater than 40%. Note that, in Figure 9.5, point A leads point B by  $90^\circ$ , and in this case, left-hand CP radiation is obtained. When points A and B are interchanged, right-hand CP radiation is obtained.

Measured input impedance on a Smith chart for a constructed prototype is shown in Figure 9.6, and the measured axial ratio in the broadside direction is presented in Figure 9.7. The impedance bandwidth (1:2 VSWR) is 1312 MHz (1544–2856 MHz) and, within the impedance bandwidth, the 3-dB axial-ratio CP bandwidth is 930 MHz (1550–2480 MHz). With respect to the center frequency at 2015 MHz, defined to be the average of the measured lower and upper frequencies with 3-dB axial ratio, the impedance and CP bandwidths are 65% and 46%, respectively. The measured antenna gain within the CP bandwidth is shown in Figure 9.8. The peak antenna gain is about 6 dBi and the gain bandwidth, defined to be within 3 dB of the peak antenna gain, is 44.6%, which is almost the same as the CP bandwidth. Figure 9.9 plots the measured radiation patterns at 1750 and 2100 MHz for the antenna studied; good left-hand CP radiation is observed.

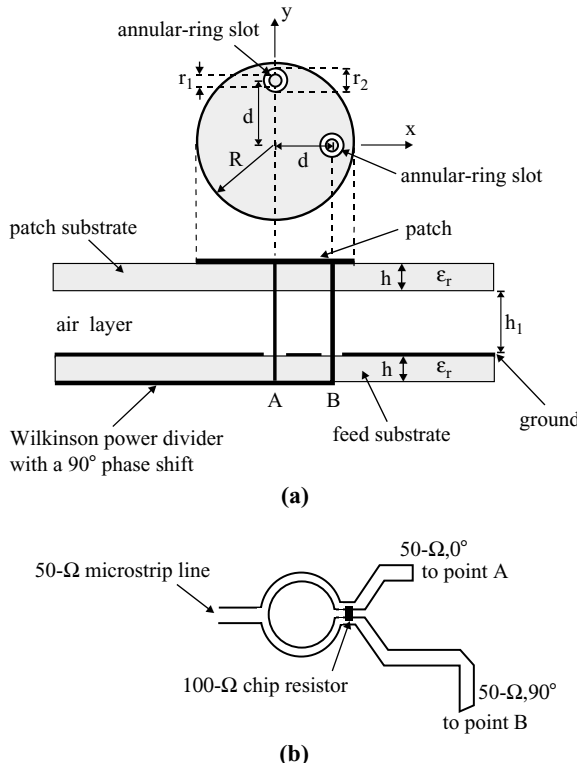


**FIGURE 9.5** (a) Geometry of a single-layer, broadband circularly polarized microstrip antenna with two gap-coupled probe feeds; (b) the Wilkinson power divider with two outputs having a 90° phase shift for feeding the antenna. (From Ref. 6, © 2000 John Wiley & Sons, Inc.)

### 9.3.2 Use of Two Capacitively Coupled Feeds with a Wilkinson Power Divider

Broadband CP operation with the use of two capacitively coupled feeds has been shown [7]. The antenna geometry is shown in Figure 9.10. By using the present capacitively coupled feeds, larger values of  $S_1$  (i.e., the air-layer thickness) can be chosen and a much wider CP bandwidth can be obtained. When the value of  $S_1$  is increased to about  $0.08\lambda_0$  ( $\lambda_0$  is the free-space wavelength of the CP center frequency), an optimal CP bandwidth is obtained. The impedance matching of the proposed antenna can be achieved by selecting the proper capacitor-plate size for the two feeds and adjusting the distance  $S_2$  between the feeds and the patch substrate. From the experiments, the optimal value of  $S_2$  for good impedance matching is about 20% of the air-layer thickness (i.e.,  $S_2 \cong 0.2S_1$ ). The Wilkinson power divider in Figure 9.10 has one arm of its outputs (point A) a quarter-wavelength longer than the other (point B) to provide good equal input powers and a 90° phase shift for the two capacitively coupled feeds. In this case, left-hand CP radiation is obtained.

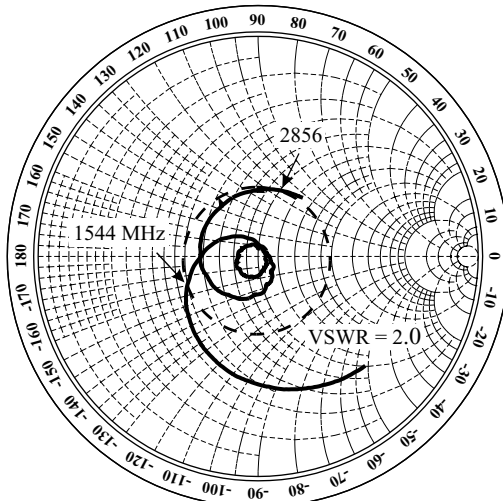


**FIGURE 9.6** Measured input impedance on a Smith chart for the antenna shown in Figure 9.5;  $\epsilon_r = 4.4$ ,  $h_1 = 12.8$  mm,  $h = 0.8$  mm,  $R = 26.25$  mm,  $d = 11$  mm,  $r_1 = 4$  mm,  $r_2 = 4.5$  mm, and ground-plane size =  $100 \times 100$  mm $^2$ . (From Ref. 6, © 2000 John Wiley & Sons, Inc.)

The proposed antenna has been implemented. To demonstrate how to achieve CP radiation of the proposed antenna, the measured input impedance on a Smith chart for the case with a single capacitively coupled feed is presented in Figure 9.11. The single-feed case corresponds to the proposed antenna shown in Figure 9.10 without the Wilkinson power divider and with one feed only; that is, the excitation of the antenna is provided by a simple microstrip feed line, through a via hole at point *A* or *B*, connected to a capacitor-plate-loaded feed. For convenience, we used the same inexpensive FR4 substrates (thickness 0.8 mm and relative permittivity 4.4) for the

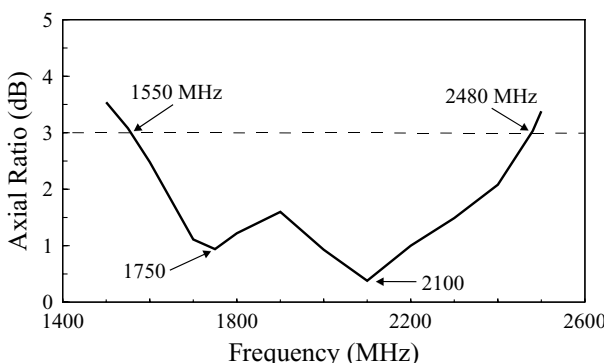


**FIGURE 9.7** Measured axial ratio for the antenna studied in Figure 9.6. (From Ref. 6, © 2000 John Wiley & Sons, Inc.)

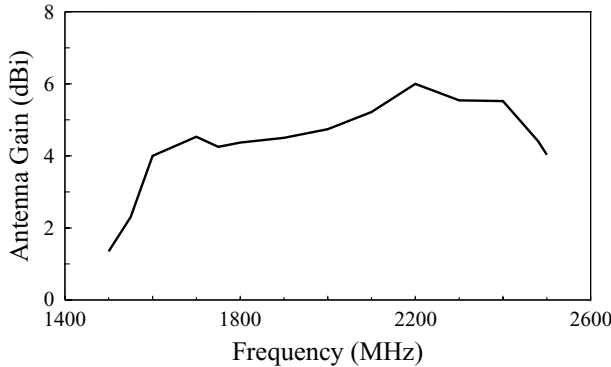


**FIGURE 9.8** Measured antenna gain for the antenna studied in Figure 9.6. (From Ref. 6, © 2000 John Wiley & Sons, Inc.)

patch and feed substrates. The circular radiating patch has a radius of 28.75 mm and the air-layer thickness is 12.8 mm. The total distance between the radiating patch and the ground plane of the feed substrate is 13.6 mm. The capacitor plate has a radius of 4.5 mm (about 0.16 times the patch radius) and is 2.4 and 22 mm from the patch substrate and  $z$  axis, respectively. In this case, the impedance curve shows a simple loop and the impedance bandwidth (1:2 VSWR) is 940 MHz, or 42.7% with respect to the center frequency at 2200 MHz.

When an additional feed of the same size is added in the orthogonal direction to the existing one and a Wilkinson power divider is used as shown in Figure 9.10, the

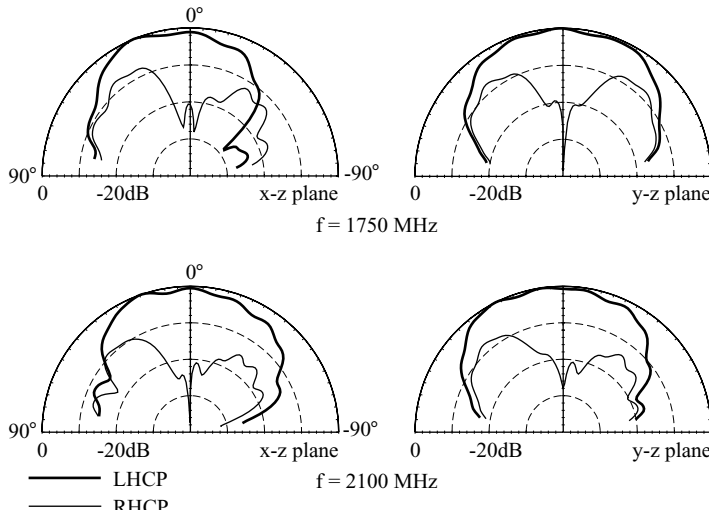


**FIGURE 9.9** Measured radiation patterns at 1750 and 2100 MHz for the antenna studied in Figure 9.6. (From Ref. 6, © 2000 John Wiley & Sons, Inc.)

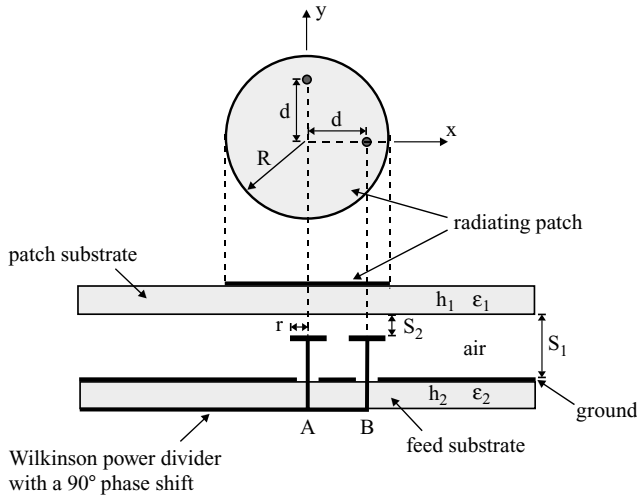


**FIGURE 9.10** Geometry of a broadband, single-patch, circularly polarized microstrip antenna with dual capacitively coupled feeds and a Wilkinson power divider. (From Ref. 7, © 2000 IEEE, reprinted with permission.)

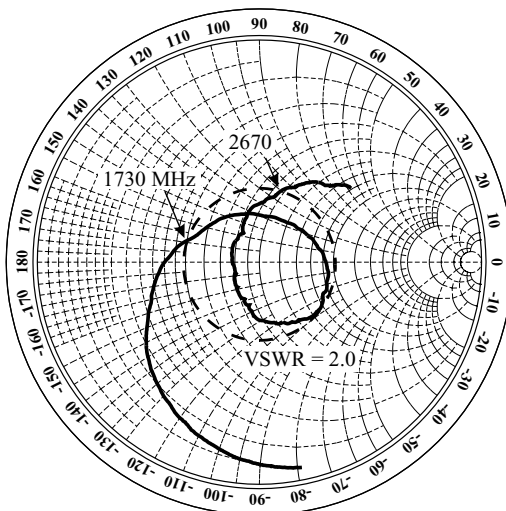


**FIGURE 9.11** Measured input impedance on a Smith chart for the antenna shown in Figure 9.10 with one feed only (either feed A or feed B) and without the Wilkinson power divider;  $\epsilon_1 = \epsilon_2 = 4.4$ ,  $h_1 = h_2 = 0.8$  mm,  $S_1 = 12.8$  mm,  $S_2 = 2.4$  mm,  $R = 28.75$  mm,  $r = 4.5$  mm,  $d = 22$  mm, and ground-plane size =  $100 \times 100$  mm $^2$ . (From Ref. 7, © 2000 IEEE, reprinted with permission.)

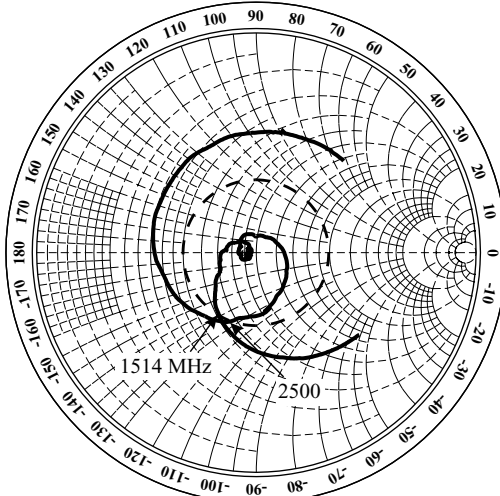


**FIGURE 9.12** Measured input impedance on a Smith chart for the antenna shown in Figure 9.10;  $\epsilon_1 = \epsilon_2 = 4.4$ ,  $h_1 = h_2 = 0.8$  mm,  $S_1 = 12.8$  mm,  $S_2 = 2.4$  mm,  $R = 28.75$  mm,  $r = 4.5$  mm,  $d = 22$  mm, and ground-plane size =  $100 \times 100$  mm $^2$ . (From Ref. 7, © 2000 IEEE, reprinted with permission.)

measured input impedance of the proposed antenna is as presented in Figure 9.12. It is clearly seen that a very small loop occurs near the center of the Smith chart or the center of the simple loop shown in Figure 9.11. The small loop indicates that two resonant modes are excited at close frequencies, and this condition can be achieved by fine adjusting the feed position  $d$  and the distance  $S_2$  between the two feeds and the patch substrate. Note that the size of the capacitor plates and other antenna parameters are the same as used for the linear polarization (LP) design in Figure 9.11. Since the two feeds have a  $90^\circ$  phase difference, this impedance curve suggests that good CP radiation can be achieved. From the results shown in Figure 9.12, the impedance bandwidth is 986 MHz, or 49% with respect to the center frequency at 2007 GHz. The impedance bandwidth is even greater than that for the LP design in Figure 9.11, largely owing to the condition that two resonant modes are excited for the CP design shown in Figure 9.12. It is also observed that the obtained center frequency is lowered by about 200 MHz or about 10% when the CP design is compared to the LP case. This suggests that capacitively coupled feeds can affect the resonant frequency of the proposed antenna.

Figure 9.13 shows the measured axial ratio for the proposed CP design. The 3-dB axial-ratio bandwidth is 635 MHz, or about 35% referenced to the center frequency at 1843 MHz. In this case, the distance (13.6 mm) between the radiating patch and the ground plane is about 0.84 times the wavelength of the center operating frequency at 1843 MHz. Also note that the CP bandwidth is within the impedance bandwidth (1514–2500 MHz) shown in Figure 9.12. The phase difference between the two

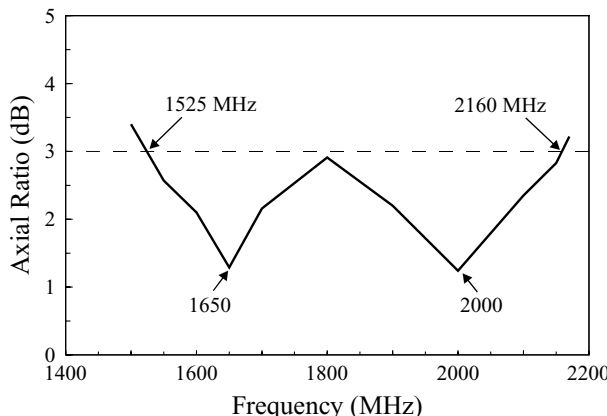


**FIGURE 9.13** Measured axial ratio for the antenna studied in Figure 9.12. (From Ref. 7, © 2000 IEEE, reprinted with permission.)

outputs (points *A* and *B*) of the Wilkinson power divider within the CP bandwidth (1525–2160 MHz) was also measured and found to increase monotonically from  $76^\circ$  to  $100^\circ$ . On the other hand, the difference in the magnitude of the output powers of points *A* and *B* was less than 0.1 dB across the CP bandwidth. Thus, although the  $90^\circ$  phase difference between the two feeds of the proposed design is not quite good, broadband CP radiation was still achieved owing to the very good equal input powers obtained.

The antenna gain in the broadside direction within the CP bandwidth was measured and is presented in Figure 9.14. The obtained antenna gain in the entire CP bandwidth is within a range of less than 3 dBi, and the peak antenna gain is about 7.2 dBi. When

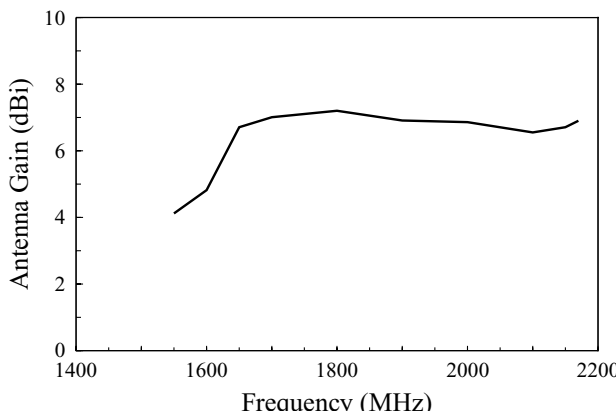


**FIGURE 9.14** Measured antenna gain for the antenna studied in Figure 9.12. (From Ref. 7, © 2000 IEEE, reprinted with permission.)

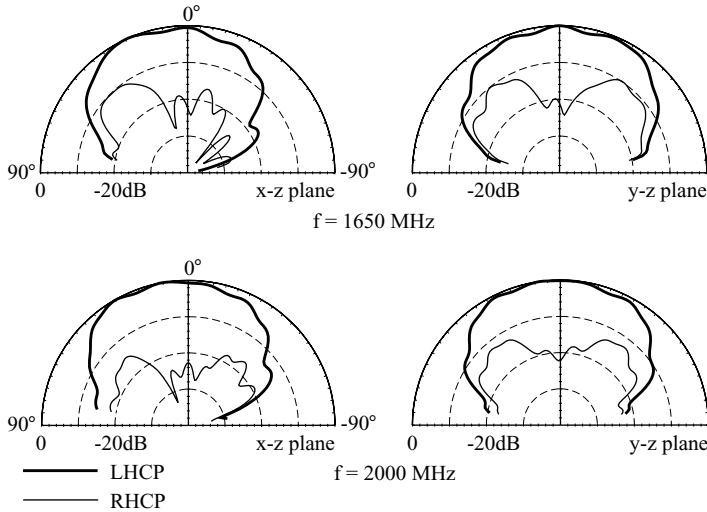


**FIGURE 9.15** Measured radiation patterns at 1650 and 2000 MHz for the antenna studied in Figure 9.12. (From Ref. 7, © 2000 IEEE, reprinted with permission.)

considering the 1-dB gain variation, the proposed antenna has a gain bandwidth of about 28% (1630–2160 MHz). The radiation patterns measured at 1650 and 2000 MHz are plotted in Figure 9.15; good left-hand CP radiation is seen.

### 9.3.3 Use of Two Capacitively Coupled Feeds with a Branch-Line Coupler

By using two capacitively coupled feeds and a three-section branch-line coupler to provide two equal input powers with a  $90^\circ$  phase difference, a broadband circularly polarized patch antenna with good radiation characteristics has been obtained. Experimental results show that, with the on-axis axial ratio less than 3 dB and gain variation within 1 dBi, the obtained circular polarization (CP) bandwidth is greater than 40%. Figure 9.16 shows the proposed antenna geometry with a circular patch. The two capacitively coupled feeds used in the study are top-loaded with a small disk plate of radius  $r$  ( $r$  is much smaller than  $R$  and is usually selected to be less than  $0.2R$ ). The choice between a three-section branch-line coupler instead of a one-section or two-section coupler was decided by experiments in which it was found that the design with a three-section coupler has much improved CP radiation characteristics than the case with a one-section or two-section coupler. This is largely because much better equal powers with a  $90^\circ$  phase difference can be obtained from the two outputs of the three-section branch-line coupler. Note that the characteristic impedance of each branch in the coupler shown in Figure 9.16 is determined by following the design method in Ref. 13, and the length of each branch is selected to be a quarter guided wavelength of the wave propagating in the feed substrate at the designed center operating frequency.

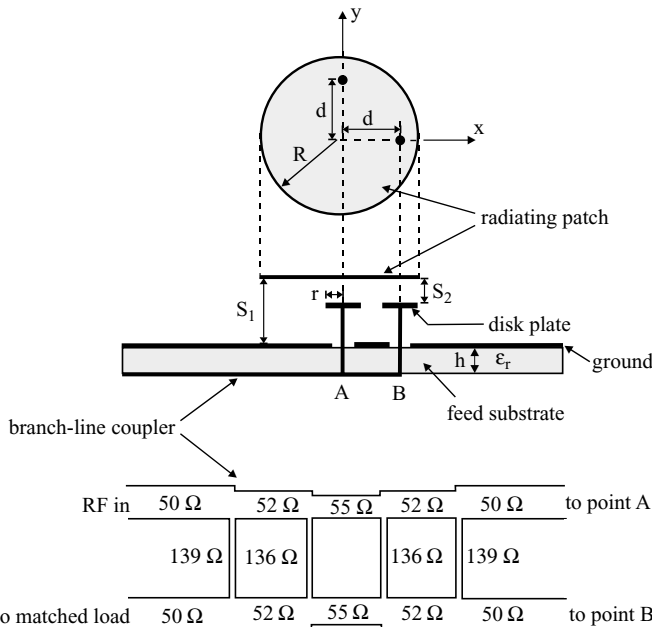


**FIGURE 9.16** Geometry of a broadband circularly polarized patch antenna with dual capacitively coupled feeds and a branch-line coupler.

For achieving broadband CP radiation, the air-substrate thickness  $S_1$  is chosen to be about 0.1 times the free-space wavelength of the center operating frequency. For the feed arrangement shown in Figure 9.16, the proposed antenna radiates a left-hand circularly polarized (LHCP) wave. Simply by interchanging the feed points A and B in the figure, the proposed antenna will have a right-hand circularly polarized (RHCP) wave. For achieving good impedance matching, the optimal feed positions are usually found to be those for  $d$  greater than  $0.7R$  and  $S_2$  less than  $0.3S_1$ . The measured input impedance on a Smith chart for a constructed prototype is shown in Figure 9.17. The RHCP radiation was studied, and the center operating frequency is designed at 2200 MHz. Thus, the radius of the circular radiating patch is selected to be 28.75 mm and the thickness of the air substrate is chosen to be 13.6 mm, which corresponds to about 0.1 times the free-space wavelength at 2200 MHz. Other design parameters are given in Figure 9.17. From the input impedance results, the impedance bandwidth (1:2 VSWR) is 1794 MHz (1484–3278 MHz), or about 81% referenced to the designed center frequency at 2200 MHz. Figure 9.18 presents the measured axial ratio in the broadside direction of the antenna; the obtained 3-dB axial-ratio bandwidth is 1385 MHz (1700–3085 MHz), or about 63%. Figure 9.19 shows the measured antenna gain against frequency. The peak antenna gain is about 6.7 dBi, and the 1-dB gain bandwidth is 930 MHz (1700–2630 MHz), or about 42%. Measured radiation patterns in two orthogonal planes at 2200 MHz are plotted in Figure 9.20, which shows good left-hand CP radiation.

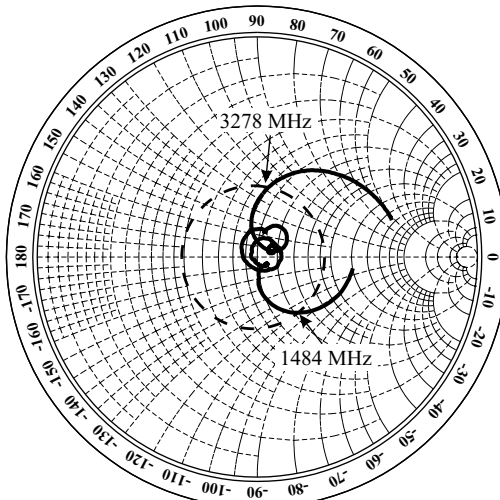


**FIGURE 9.17** Measured input impedance on a Smith chart for the antenna shown in Figure 9.16;  $\epsilon_r = 4.4$ ,  $h = 1.6$  mm,  $S_1 = 13.6$  mm,  $S_2 = 3.2$  mm,  $R = 28.75$  mm,  $d = 22$  mm,  $r = 4.5$  mm, and ground-plane size =  $200 \times 100$  mm $^2$ .

#### 9.4 BROADBAND FOUR-FEED CIRCULARLY POLARIZED MICROSTRIP ANTENNAS

A promising design with a large CP bandwidth (2-dB axial-ratio bandwidth  $>35\%$ ) and improved CP quality over a wide coverage angle for frequencies within the

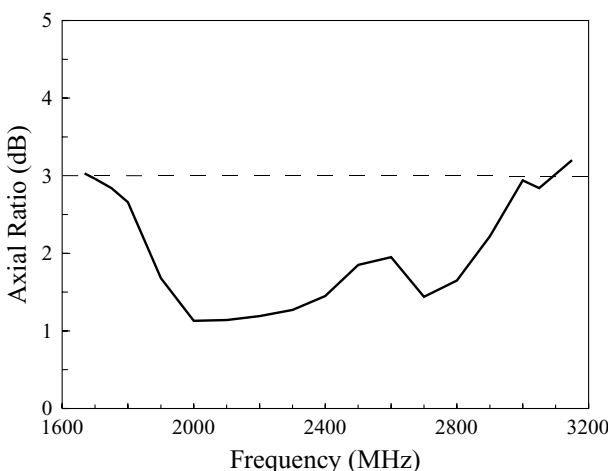


**FIGURE 9.18** Measured axial ratio for the antenna studied in Figure 9.17.

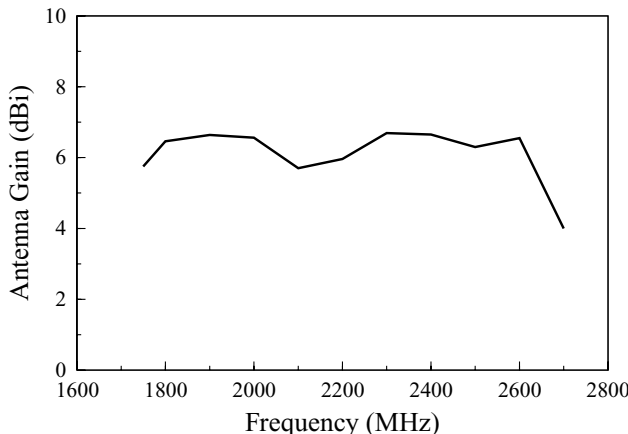


**FIGURE 9.19** Measured antenna gain for the antenna studied in Figure 9.17.

CP bandwidth is presented in Figure 9.21. This design is achieved by using four capacitively coupled feeds of equal input powers and  $0^\circ$ ,  $90^\circ$ ,  $180^\circ$ , and  $270^\circ$  phase shifts, provided by a feed network consisting of Wilkinson power dividers, for the excitation of a patch antenna with a thick air substrate. Experimental results show that for a prototype with designed center frequency at 2200 MHz (the radius of the circular patch was chosen to be 27.5 mm, and the air substrate thickness was 16 mm, about 11.7% of the free-space wavelength at 2200 MHz), the 10-dB return-loss impedance bandwidth is 2340 MHz, or greater than 100% referenced to the center frequency, and the CP bandwidth, determined by 2-dB axial ratio, is about 38% [14]. The peak antenna gain of the constructed prototype is 7.6 dBi, with gain variations less than 2 dBi within the CP bandwidth. Good CP quality for frequencies within the CP bandwidth has also been observed, which shows a slow degradation of the axial ratio from the broadside direction ( $\theta = 0^\circ$ ) to large angles.

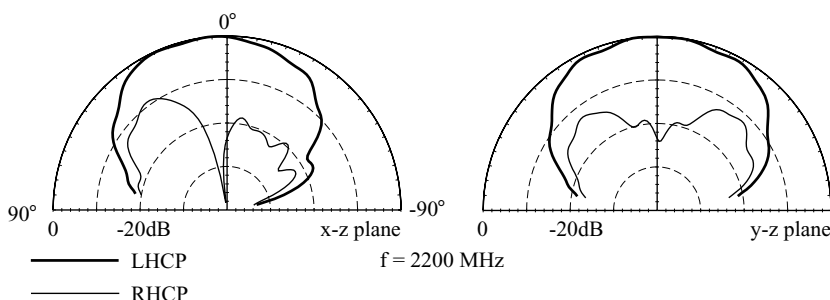


**FIGURE 9.20** Measured radiation patterns at 2200 MHz for the antenna studied in Figure 9.17.

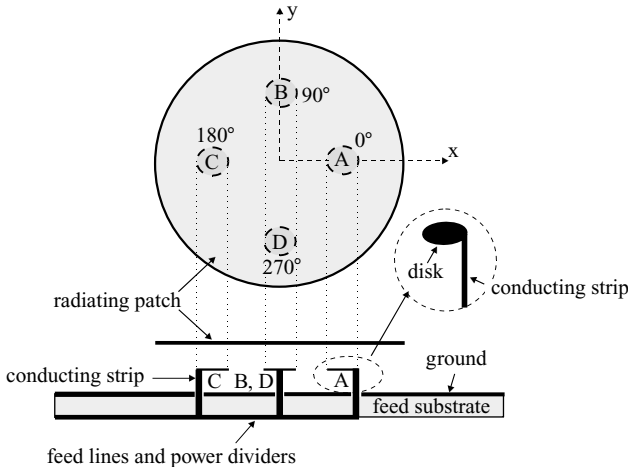


**FIGURE 9.21** Geometry of a broadband circularly polarized patch antenna with improved CP quality.

## 9.5 DUAL-BAND CIRCULARLY POLARIZED MICROSTRIP ANTENNAS

### 9.5.1 A Probe-Fed Circular Patch with Two Pairs of Arc-Shaped Slots

A novel technique for obtaining dual-band CP radiation with a single-feed circular microstrip antenna has been proposed [10]. By embedding two pairs of arc-shaped slots of appropriate lengths close to the boundary of a circular patch and protruding one of the arc-shaped slots with a narrow slot, the circular microstrip antenna can be used for dual-band CP radiation using a single probe feed. The proposed antenna geometry is shown in Figure 9.22. Two pairs of arc-shaped slots, having a narrow width of 1 mm, are placed close to the boundary of the circular patch at a distance of 1 mm.

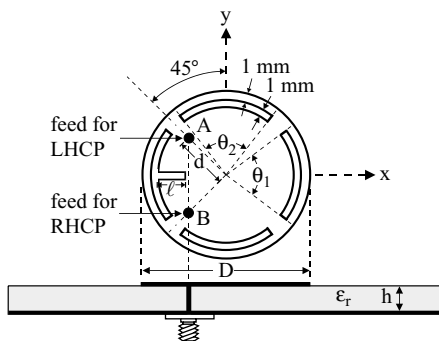
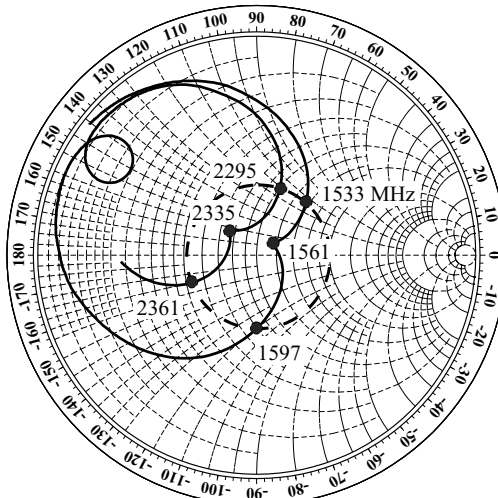


**FIGURE 9.22** Geometry of a single-feed, slotted circular microstrip antenna for dual-band CP operation. (From Ref. 10, © 1998 IEE, reprinted with permission.)

These two pairs of slots are centered with respect to the centerlines ( $x$  and  $y$  axes) of the circular patch. The pair of arc-shaped slots centered on the  $x$  axis is subtended by an angle  $\theta_1$ , and its left-hand-side slot has a radial protruding slot of length  $\ell$ . The other pair of arc-shaped slots centered on the  $y$  axis is subtended by an angle  $\theta_2$  ( $\theta_2 \neq \theta_1$ ). It should first be noted that, for each pair of arc-shaped slots, dual-frequency operation with the same polarization planes and broadside radiation patterns can be obtained by feeding the patch using a single probe feed along the centerline between the two slots. This dual-frequency characteristic is similar to that reported for a dual-frequency rectangular microstrip antenna with a pair of narrow slots [15] in which the perturbed  $\text{TM}_{10}$  and  $\text{TM}_{30}$  modes are excited for dual-frequency operation. For the present proposed structure, the two operating modes are associated with the  $\text{TM}_{11}$  and  $\text{TM}_{12}$  modes of the unslotted or simple circular microstrip antenna. With the presence of two pairs of arc-shaped slots of slightly different subtending angles in the proposed design, it is expected that the first two operating modes can both consist of two near-degenerate orthogonal resonant modes if a single probe feed is placed along the direction  $45^\circ$  to the centerlines of the circular patch.

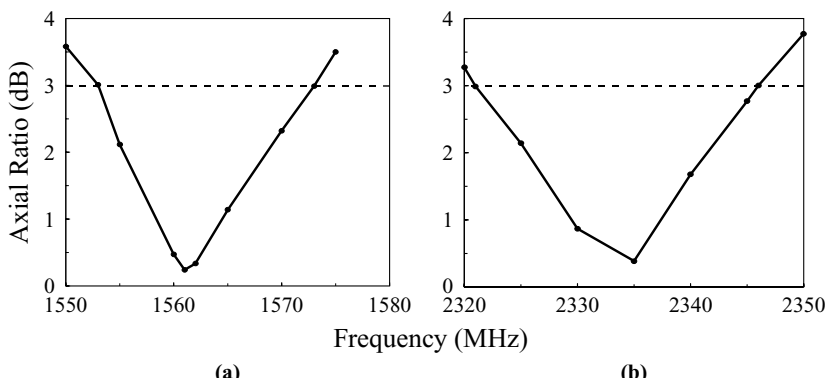
The experiments show that the resonance of the first (lower) operating mode (the perturbed  $\text{TM}_{11}$  mode) is very slightly affected by the variation in the subtending angle. On the other hand, the resonant frequency of the second (upper) operating mode (the perturbed  $\text{TM}_{12}$  mode) is significantly decreased with increasing subtending angle. Therefore, by adjusting the subtending angles, two near-degenerate orthogonal modes with equal amplitudes and a  $90^\circ$  phase shift for CP operation can be excited for the upper operating mode. To fine tune the two near-degenerate orthogonal modes of the lower operating mode to have equal amplitudes and a  $90^\circ$  phase difference for CP operation, a radial narrow slot is protruded from one of the arc-shaped slots (see Figure 9.22). It is found that, with the perturbation of the protruding slot, the desired CP operation for the lower operating mode can be achieved, while the CP performance of the upper operating mode is very slightly affected by the protruding slot. That is, by carefully selecting the subtending angles of the arc-shaped slots and the length of the protruding slot, dual-band CP operation of microstrip antennas can be obtained. For the single probe feed placed at point  $A$ , which is a distance  $d$  from the patch center and along a direction  $45^\circ$  to the  $y$  axis, dual-band left-hand CP operation is achieved. When the feed position is moved to point  $B$  (see Figure 9.22), dual-band right-hand CP operation is obtained.

Figure 9.23 shows the measured input impedance for a proposed antenna with left-hand CP operation (feed at point  $A$ ). To achieve dual-band CP operation, the radial protruding slot is adjusted to have a length of 10 mm ( $0.20D$ ), and the subtending angles  $\theta_1$  and  $\theta_2$  are adjusted to be  $88^\circ$  and  $89^\circ$ , respectively. The feed (point  $A$ ) is at a position about  $0.32D$  from the patch center. The measured axial ratio in the broadside direction is presented in Figure 9.24. The results show that two operating bands with CP radiation are excited. The CP bandwidth of the lower operating band, determined from the 3-dB axial ratio, is 20 MHz, or about 1.28% with respect to the center frequency of 1561 MHz, the frequency with a minimum axial ratio, and the CP bandwidth for the upper operating band is 25 MHz, or about 1.07% with



**FIGURE 9.23** Measured input impedance for the antenna shown in Figure 9.22 with dual-band left-hand CP operation (feed at point A);  $\epsilon_r = 4.4$ ,  $h = 1.6$  mm,  $D = 50$  mm,  $\ell = 10$  mm,  $d = 16$  mm,  $\theta_1 = 88^\circ$ , and  $\theta_2 = 89^\circ$ . (From Ref. 10, © 1998 IEE, reprinted with permission.)

respect to the center frequency of 2335 MHz. The radiation patterns in two orthogonal planes are plotted in Figure 9.25 for the operating bands at 1561 and 2335 MHz. It can be seen that good left-hand CP radiation for both bands is obtained. Finally, the frequency ratio of the two operating bands obtained here is about 1.496. By varying the subtending angles of the two arc-shaped slots and fine tuning associated parameters, different frequency ratios for the proposed dual-band CP operation can be obtained.



**FIGURE 9.24** Measured axial ratio for the antenna studied in Figure 9.23. (a) The lower band; (b) the upper band. (From Ref. 10, © 1998 IEE, reprinted with permission.)

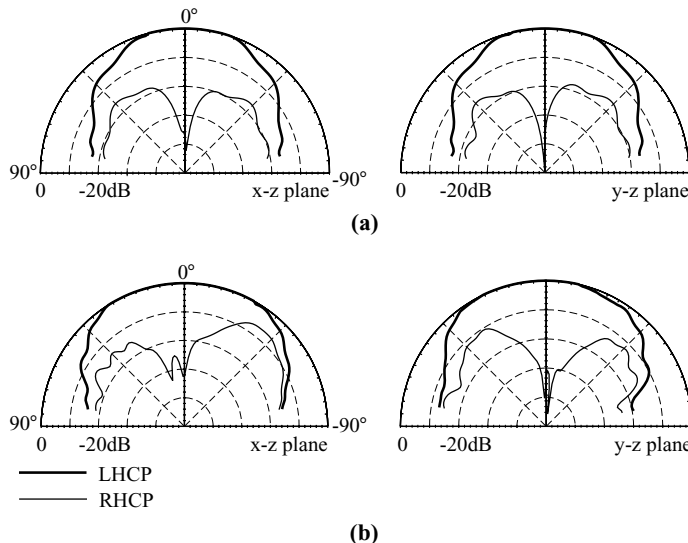


**FIGURE 9.25** Measured radiation patterns for the antenna studied in Figure 9.23. (a)  $f = 1561$  MHz; (b)  $f = 2335$  MHz. (From Ref. 10, © 1998 IEE, reprinted with permission.)

### 9.5.2 A Probe-Fed Square Patch with a Center Slot and Inserted Slits

New designs for obtaining dual-band CP radiation with a single-feed square microstrip antenna (Figure 9.26) have been proposed and experimentally studied [11]. The proposed single-feed dual-band CP designs are achieved by inserting four T-shaped slits at the patch edges or four Y-shaped slits at the patch corners of a square microstrip antenna. In the experiments, a patch size reduction of 36% for the proposed design compared to a conventional CP design without inserted slits [16] was obtained. The two resonant modes  $\text{TM}_{10}$  and  $\text{TM}_{30}$  are used for dual-band CP radiation. Due to the inserted T-shaped or Y-shaped slits, the excited patch surface current path of the  $\text{TM}_{10}$  mode is greatly lengthened, which effectively lowers its resonant frequency and gives the proposed designs a reduced patch size for the fixed lower frequency of dual-band CP radiation. For the  $\text{TM}_{30}$  mode, the inserted slits not only considerably lower its resonant frequency, but also modify its three-lobe radiation pattern [15] to become similar to that of the  $\text{TM}_{10}$  mode. By further embedding a narrow slot in the patch center and using a single probe feed at the diagonals of the slit-loaded square patch, the perturbed  $\text{TM}_{10}$  and  $\text{TM}_{30}$  modes can be split into two near-degenerate modes for dual-band CP radiation.

**9.5.2.1 Square Patch with Four T-Shaped Slits** In the slit-loaded square patch in Figure 9.26(a) (denoted design A), four T-shaped slits are inserted at the edge centers; their upper arms have the same dimensions, a narrow width  $S$  and a length  $\ell$ , and their center arms have dimensions  $d \times w$ , with the slit along the positive  $y$  axis having a different arm width  $d_T$  ( $\neq d$ ). This arrangement is very effective for fine tuning the perturbed  $\text{TM}_{30}$  mode (upper operating band in this design) into two near-degenerate modes with equal amplitudes and a  $90^\circ$  phase shift for CP radiation. The splitting

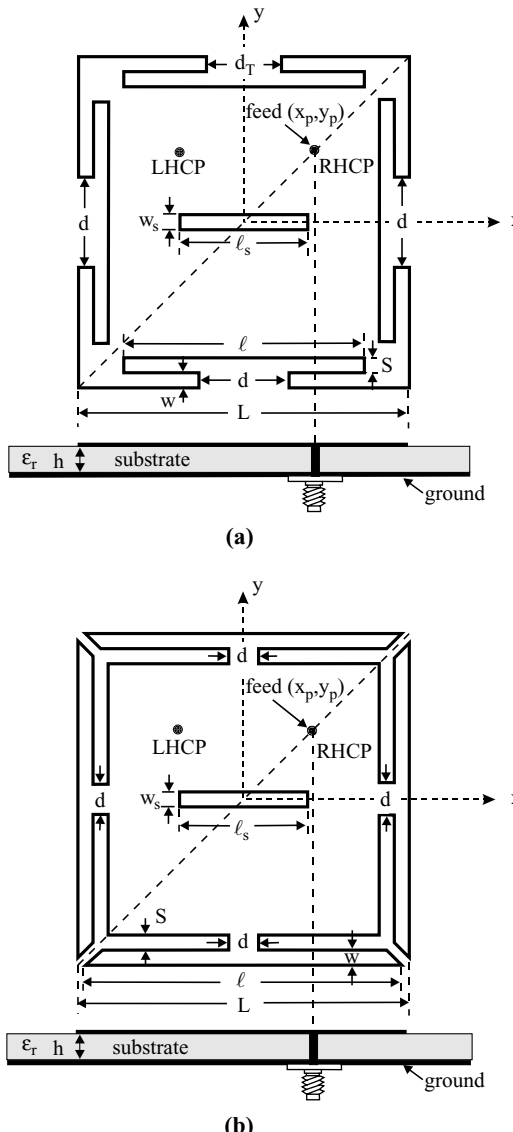


**FIGURE 9.26** Geometries of slit-loaded dual-band circularly polarized microstrip antennas. (a) Design A: a square patch with four T-shaped slits; (b) design B: a square patch with four Y-shaped slits. (From Ref. 11, © 2001 IEEE, reprinted with permission.)

of the perturbed  $\text{TM}_{10}$  mode (lower operating band) into two near-degenerate modes for CP radiation is mainly achieved by selecting suitable dimensions ( $l_s \times w_s$ ;  $l_s \gg w_s$ ) of the center slot. A single probe feed at  $(x_p, y_p)$  along the diagonals of the patch can excite right-hand or left-hand CP radiation for the two CP operating bands.

Two different antennas (antennas A1 and A2) based on design A were constructed using the same microwave substrates. Antenna A1 was designed for left-hand CP

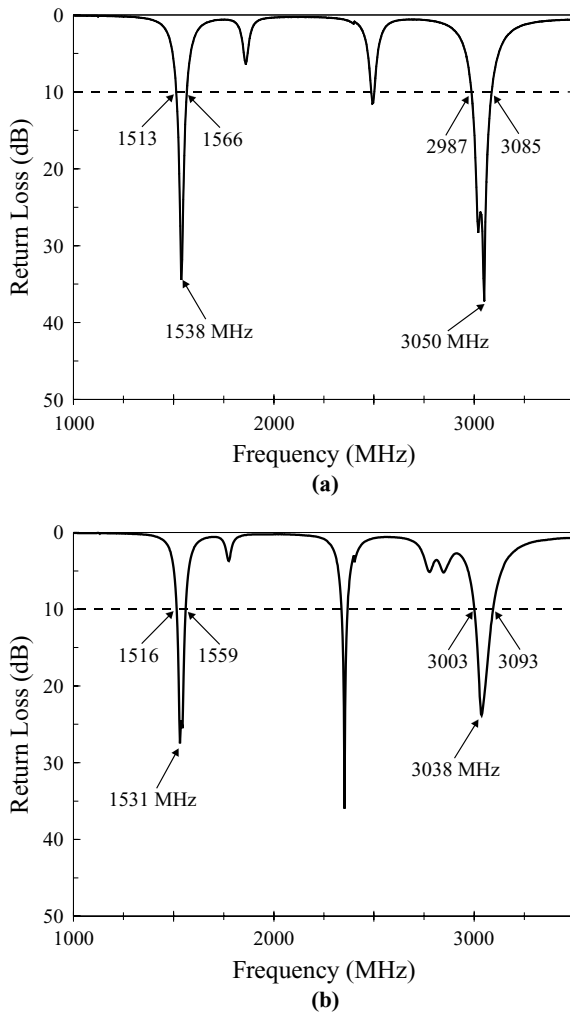


**FIGURE 9.27** Measured return loss for design A shown in Figure 9.26(a);  $\epsilon_r = 4.4$ ,  $h = 1.6$  mm, and ground-plane size =  $75 \times 75$  mm $^2$ . (a) Antenna A1 with left-hand CP radiation:  $(x_p, y_p) = (-9$  mm, 9 mm),  $L = 40$  mm,  $\ell = 32$  mm,  $d = 13.5$  mm,  $d_T = 11$  mm,  $w_s = 1$  mm,  $\ell_s = 12.5$  mm,  $S = 1$  mm, and  $w = 1$  mm; (b) antenna A2 with right-hand CP radiation:  $(x_p, y_p) = (7$  mm, 7 mm),  $L = 36$  mm,  $\ell = 28.8$  mm,  $d = 1.8$  mm,  $d_T = 3.5$  mm,  $w_s = 0.9$  mm,  $\ell_s = 13$  mm,  $S = 0.9$  mm, and  $w = 1.8$  mm. (From Ref. 11, © 2001 IEEE, reprinted with permission.)

radiation and antenna A2 radiates a right-hand CP wave. Both antennas A1 and A2 were designed to operate with dual-band CP operation. The side length of antenna A2 is chosen to be 90% of that of antenna A1; thus the patch size of antenna A2 is only about 0.81 times that of antenna A1. Results for the measured return loss are shown in Figure 9.27. The measured axial ratios in the broadside direction for antennas A1 and A2 are presented in Figure 9.28. The corresponding CP performance is listed in Table 9.2, in which the center frequencies  $f_1$  and  $f_2$  of the lower and upper CP bands

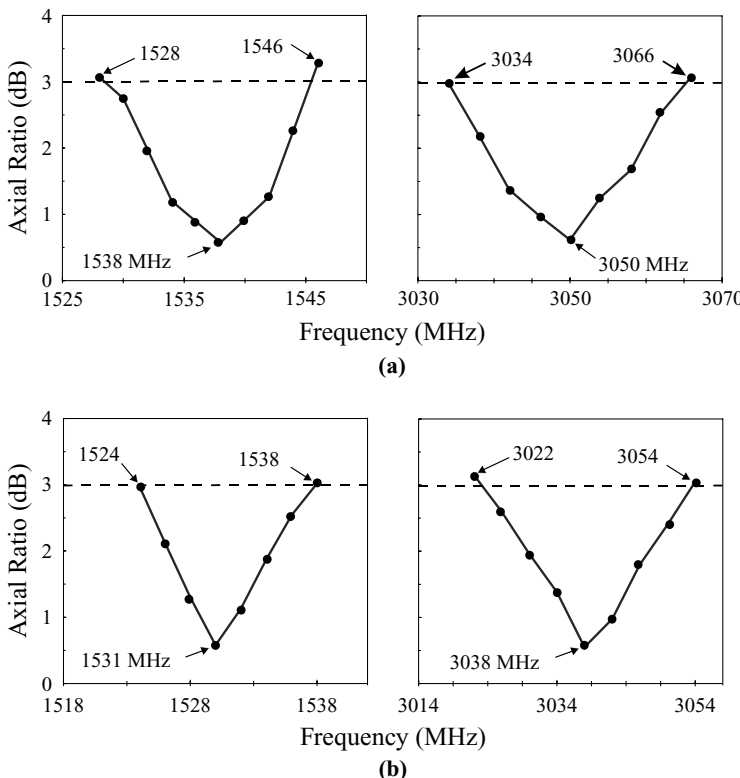


**FIGURE 9.28** Measured axial ratio of the lower and upper CP bands of (a) antenna A1 and (b) antenna A2 studied in Figure 9.27. (From Ref. 11, © 2001 IEEE, reprinted with permission.)

are defined to be the frequency at which the minimum axial ratio is observed. The obtained CP bandwidths (3-dB axial ratio) for the lower and upper operating bands are seen to be about the same. The frequency ratios for the two center frequencies for antennas A1 and A2 are almost the same, about 1.984. In comparison to the reference antenna (see Table 9.2), which requires a patch size of  $45 \times 45 \text{ mm}^2$  for operation in the 1.5-GHz band, the patch sizes of antennas A1 and A2 are, respectively, about 21% and 36% smaller. This reduction in the required patch size suggests that the antenna

**TABLE 9.2** CP Performance of the Antennas in Figures 9.26(a) and 9.26(b) [11]<sup>a</sup>

	Patch Size (mm <sup>2</sup> )	$f_1$ , CP BW (MHz, %)	$f_2$ , CP BW (MHz, %)	Frequency Ratio L/W
Antenna A1	$40 \times 40$	1538, 1.2	3050, 1.1	1.983
Antenna A2	$36 \times 36$	1531, 0.9	3038, 1.1	1.984
Antenna B	$36 \times 36$	1632, 1.1	2882, 1.0	1.766
Reference	$45 \times 45$	1550, 1.2	—	—

<sup>a</sup>Parameters of antennas A1 and A2 are given in Figure 9.27 and those of antenna B are shown in Figure 9.32. The reference antenna is constructed using a simple square patch with a diagonal slot [16].

size (or the ground-plane size) of the proposed design can be reduced accordingly [the ground plane sizes used in this study are all the same ( $75 \times 75 \text{ mm}^2$ ) for different antennas]. It is found that, when the ground-plane size is reduced by 21% for antenna A1 and 36% for antenna A2, the obtained dual-band CP performance is very slightly affected as compared to the results presented here.

The antenna gain in the broadside direction for the operating frequencies within the lower and upper CP bands was measured and is presented in Figure 9.29. For the lower operating band, it is clearly seen that the antenna gain for antenna A2 is in general about 1.0–1.5 dBi lower than that for antenna A1, which is probably due to the smaller patch size for antenna A2. On the other hand, a small gain difference between antennas A1 and A2 is observed for the upper operating band. It is observed that the antenna gain for the upper operating band is smaller than that for the lower band, which suggests that the perturbed  $\text{TM}_{10}$  mode has better radiation efficiency than the perturbed  $\text{TM}_{30}$  mode. This behavior should be considered in practical applications. The radiation patterns in two orthogonal planes for antennas A1 and A2 have been measured and are plotted in Figures 9.30 and 9.31, respectively. It can be seen that similar radiation patterns and good CP radiation characteristics for both operating bands are obtained.

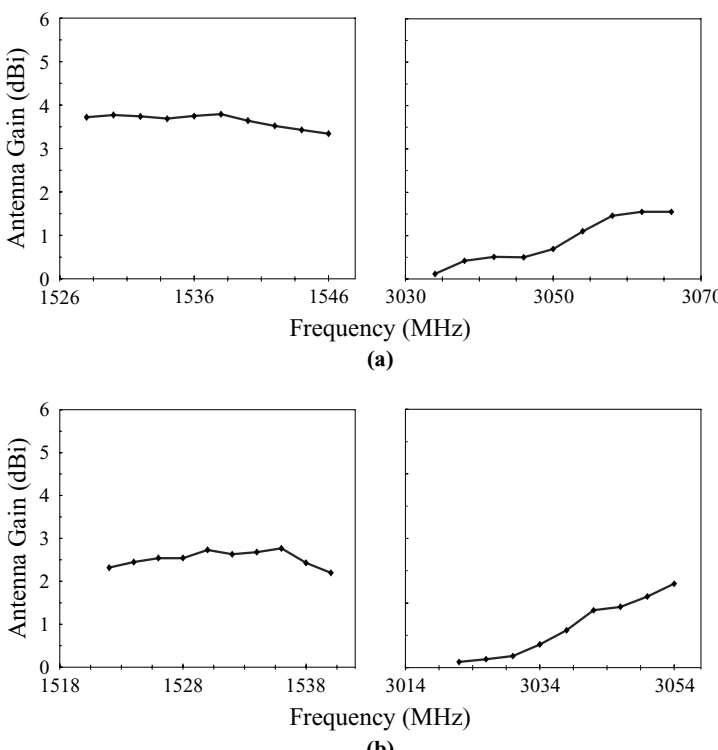


**FIGURE 9.29** Measured antenna gain for the lower and upper CP bands of (a) antenna A1 and (b) antenna A2 studied in Figure 9.27. (From Ref. 11, © 2001 IEEE, reprinted with permission.)

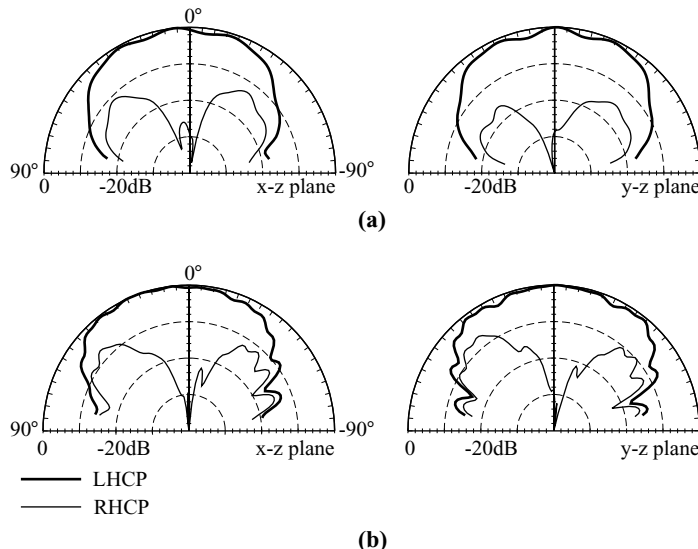


**FIGURE 9.30** Measured radiation patterns for antenna A1 studied in Figure 9.27. (a)  $f_1 = 1538$  MHz, (b)  $f_2 = 3050$  MHz. (From Ref. 11, © 2001 IEEE, reprinted with permission.)

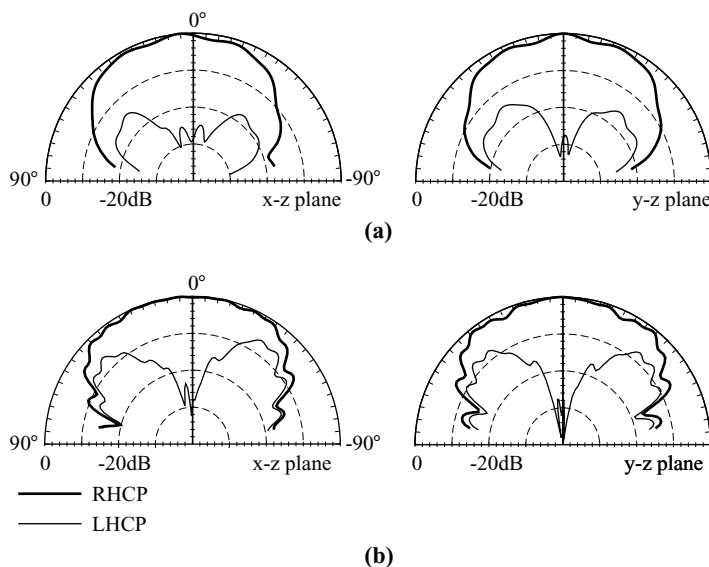


**FIGURE 9.31** Measured radiation patterns for antenna A2 studied in Figure 9.27. (a)  $f_1 = 1531$  MHz, (b)  $f_2 = 3038$  MHz. (From Ref. 11, © 2001 IEEE, reprinted with permission.)

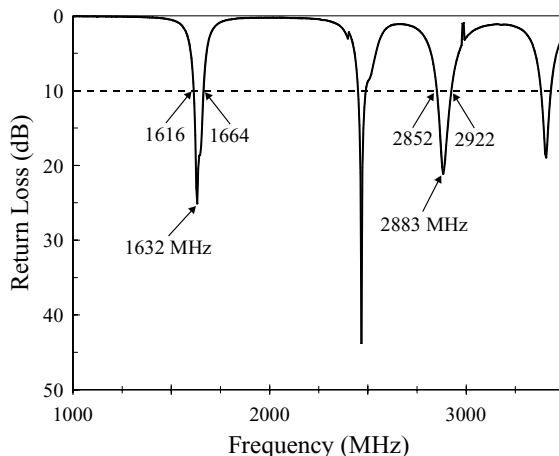


**FIGURE 9.32** Measured return loss for antenna B [design B in Figure 9.26(b) with right-hand CP radiation];  $\epsilon_r = 4.4$ ,  $h = 1.6$  mm, ground-plane size =  $75 \times 75$  mm $^2$ ,  $S = 0.9$  mm,  $w = 1.8$  mm,  $(x_p, y_p) = (7$  mm, 7 mm),  $L = 36$  mm,  $\ell = 30.6$  mm,  $d = 1.8$  mm,  $w_s = 0.9$  mm, and  $\ell_s = 12$  mm. (From Ref. 11, © 2001 IEEE, reprinted with permission.)

**9.5.2.2 Square Patch with Four Y-Shaped Slits** The design shown in Figure 9.26(b) has four Y-shaped slits inserted at the patch corners (denoted design B). Note that the four Y-shaped slits have the same dimensions, which is different from the case with four T-shaped slits (design A). In this case, the splitting of both the perturbed TM<sub>10</sub> and TM<sub>30</sub> modes into two near-degenerate modes for dual-band CP radiation can be achieved simply by selecting proper dimensions for the center slot. Based on design B, a dual-band CP antenna with right-hand CP radiation was constructed (denoted antenna B). The patch size of antenna B was selected to be the same as that of antenna A2 ( $36 \times 36$  mm $^2$ ). Figures 9.32 and 9.33 present, respectively, the measured return loss and axial ratio. The corresponding dual-band CP performance of antenna B is listed in Table 9.2. The frequency ratio of the two center frequencies, 1632 and

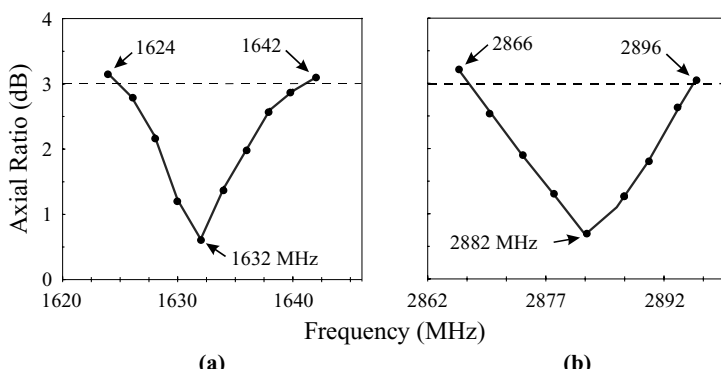


**FIGURE 9.33** Measured axial ratio for antenna B studied in Figure 9.32. (a) The lower band, (b) the upper band. (From Ref. 11, © 2001 IEEE, reprinted with permission.)

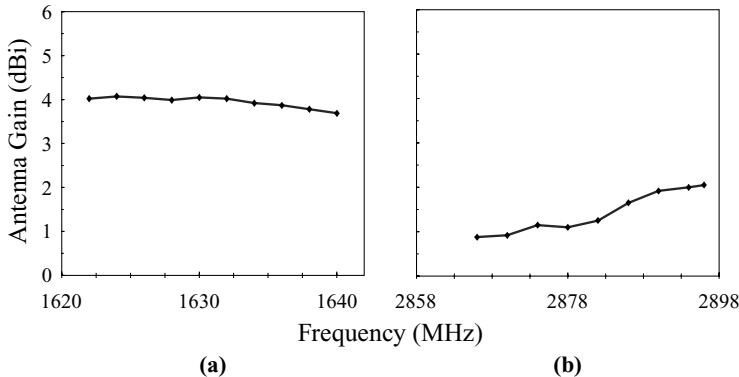


**FIGURE 9.34** Measured antenna gain for antenna B studied in Figure 9.32. (a) The lower band, (b) the upper band. (From Ref. 11, © 2001 IEEE, reprinted with permission.)

2883 MHz, is about 1.766, and the obtained CP bandwidths for lower and upper operating bands are about the same as those obtained in Section 9.5.2.1 for design A. It should be noted that for operating in the 1.6-GHz band, the required patch size using the conventional CP design [16] is about  $43 \times 43 \text{ mm}^2$ , which is much larger than that of antenna B here. This also suggests that, similar to design A in Section 9.5.2.1, design B has a reduced antenna size for fixed CP operation. Measured antenna gain for frequencies in the lower and upper operating bands are presented in Figure 9.34. Similar behavior as observed for antennas A1 and A2 in Section 9.5.2.1 is seen. Measured radiation patterns in two orthogonal planes are plotted in Figure 9.35. Good CP radiation characteristics for both operating bands are observed.

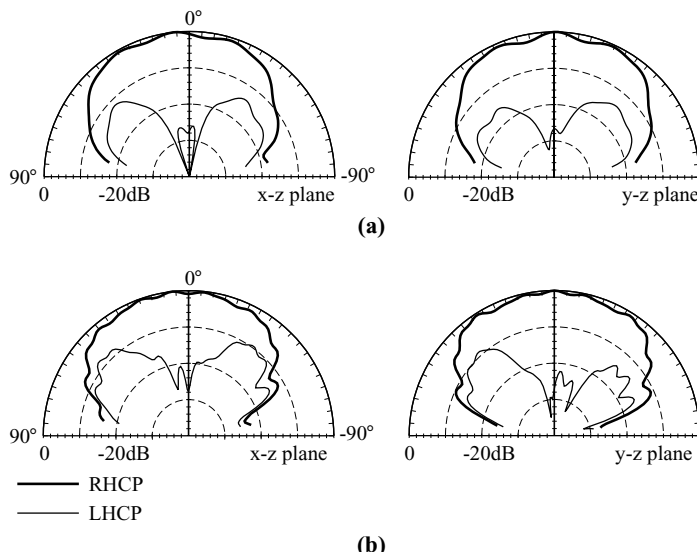


**FIGURE 9.35** Measured radiation patterns for antenna B studied in Figure 9.32. (a)  $f_1 = 1632 \text{ MHz}$ , (b)  $f_2 = 2882 \text{ MHz}$ . (From Ref. 11, © 2001 IEEE, reprinted with permission.)

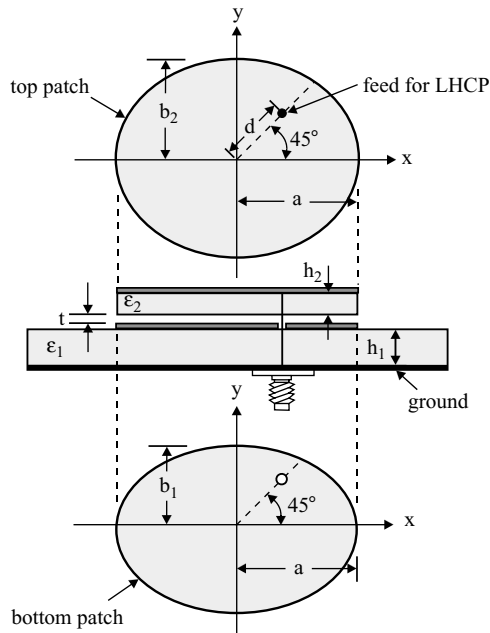


**FIGURE 9.36** Geometry of a dual-band, circularly polarized, stacked elliptic microstrip antenna. (From Ref. 12, © 2000 John Wiley & Sons, Inc.)

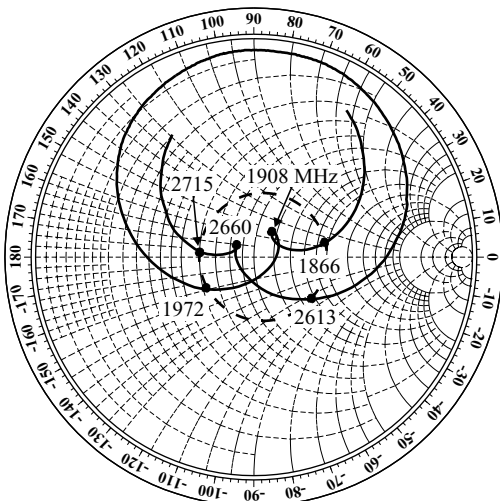


**FIGURE 9.37** Measured input impedance for the antenna shown in Figure 9.36 with left-hand CP operation;  $\epsilon_1 = \epsilon_2 = 4.4$ ,  $h_1 = 1.6$  mm,  $h_2 = 0.8$  mm,  $t = 0.5$  mm,  $a = 21.86$  mm,  $b_1/a = 0.95$ ,  $b_2/a = 0.96$ ,  $d = 12$  mm, and ground-plane size =  $75 \times 75$  mm<sup>2</sup>. (From Ref. 12, © 2000 John Wiley & Sons, Inc.)

### 9.5.3 A Probe-Fed Stacked Elliptic Patch

A probe-fed stacked elliptic microstrip antenna has been designed for obtaining dual-band CP operation [12]. The proposed design is achieved by properly selecting two elliptic patches of different axial ratios and introducing a small air-gap layer between the two patches (see Figure 9.36). The two elliptic patches are printed on separate substrates. The bottom and top elliptic patches have the same major-axis length  $a$ , but different minor-axis lengths  $b_1$  and  $b_2$ , which results in different elliptic axial ratios  $b_1/a$  and  $b_2/a$ , respectively, for the two patches. The bottom patch is centered below the top patch, and the top patch is excited by a probe feed which is connected to the top patch through a via hole in the bottom patch. The bottom patch then serves as a parasitic patch to the top patch. For ease in achieving good impedance matching of the stacked microstrip antenna and fine tuning of the operating frequencies of the

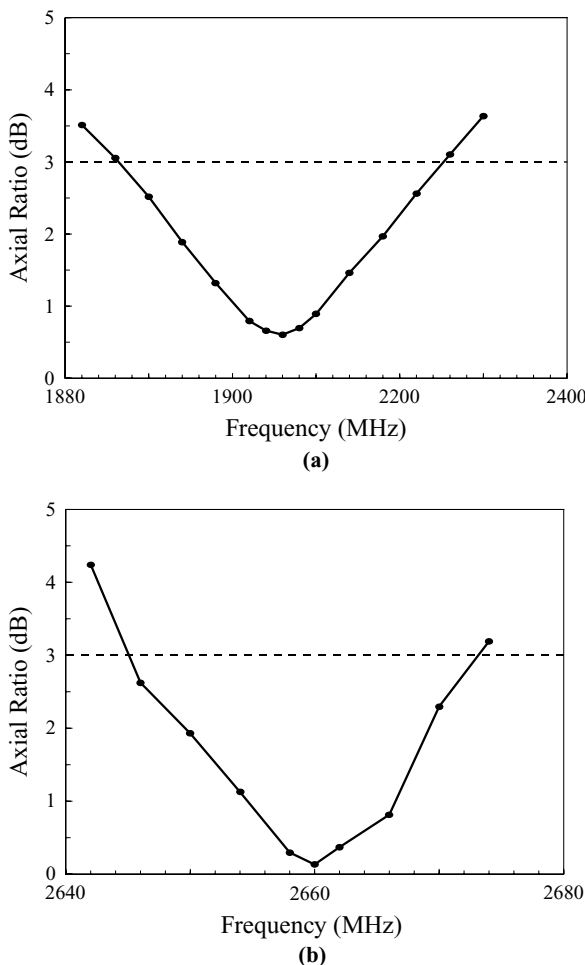


**FIGURE 9.38** Measured axial ratio for the antenna studied in Figure 9.37. (a) The lower band, (b) the upper band. (From Ref. 12, © 2000 John Wiley & Sons, Inc.)

CP modes, a small air gap of thickness  $t$  is introduced between the two patches. The feed position is placed along the  $45^\circ$  line from the major axis a distance  $d$  from the top patch's center. In this case, both operating bands of the proposed antenna have left-hand CP (LHCP) radiation. When the feed position is placed along the  $135^\circ$  line from the major axis, right-hand CP (RHCP) radiation is obtained.

In the present design, the two regions under the top and bottom patches can be treated as two different, but coupled resonant cavities, which makes possible the successful excitation of two separate operating bands for CP radiation. The first (lower) CP operating band occurs in the vicinity of the fundamental resonant frequency of the stacked microstrip antenna. From experimental results, it is found that the lower operating band is very slightly affected by variations in the axial ratios of the two patches and in the thickness of the air gap. On the other hand, the second (upper) CP operating band is strongly affected, and its operating frequency is significantly increased when the difference of the axial ratios of the two patches increases or a larger air-gap thickness is used. This suggests that, by carefully selecting the axial ratios of the two patches and the thickness of the air-gap layer, various frequency ratios between the two CP operating bands can be obtained.

Measured input impedance on a Smith chart for a constructed prototype of the proposed antenna with LHCP radiation is presented in Figure 9.37. Both the top and bottom elliptic patches are printed on inexpensive FR4 microwave substrates with relative permittivity 4.4, but different substrate thicknesses of 0.8 and 1.6 mm, respectively. The major-axis lengths of the two patches are chosen to be 21.86 mm ( $=a$ ) and their minor-axis lengths are selected such that  $b_1/a$  and  $b_2/a$  are 0.95 and 0.96, respectively. An air-gap thickness of 0.5 mm is chosen. The feed position

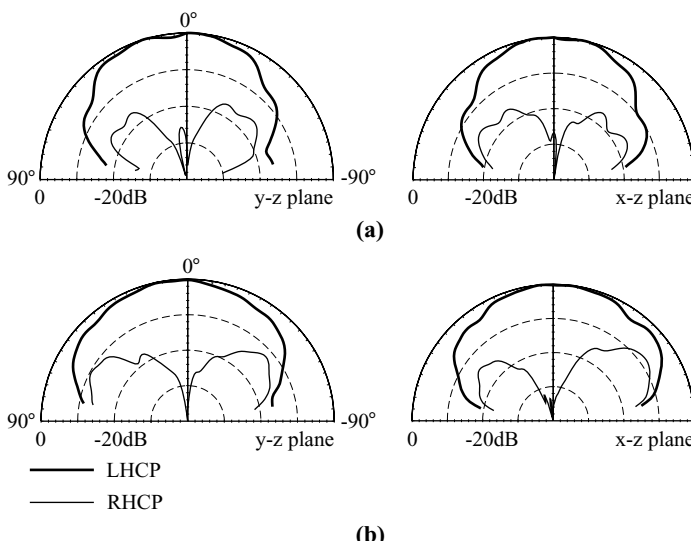


**FIGURE 9.39** Measured radiation patterns for the antenna studied in Figure 9.37. (a)  $f_1 = 1908$  MHz, (b)  $f_2 = 2660$  MHz. (From Ref. 12, © 2000 John Wiley & Sons, Inc.)

is located at  $d = 12$  mm. From the impedance results, it can be seen that there are two very small loops at 1908 and 2660 MHz, which indicates that two operating bands with CP radiation are achieved. The impedance bandwidths (1:2 VSWR) for the 1908- and 2660-MHz bands are 106 MHz (or about 5.6%) and 102 MHz (or about 3.8%), respectively. For both operating bands, the measured axial ratio in the broadside direction is presented in Figure 9.38. The CP bandwidth of the lower operating band, determined by the 3-dB axial ratio, is 40 MHz, or about 2.1% with respect to the center frequency at 1908 MHz, where a minimum axial ratio is observed. The CP bandwidth for the upper operating band is 30 MHz, or about 1.13% referenced to the center frequency at 2660 MHz. The measured radiation patterns in two orthogonal planes are plotted in Figure 9.39 for the two CP operating bands at 1908 and 2660 MHz. Good left-hand CP radiation for both operating bands is observed. The antenna gain measured for the two CP operating bands is plotted in Figure 9.40.

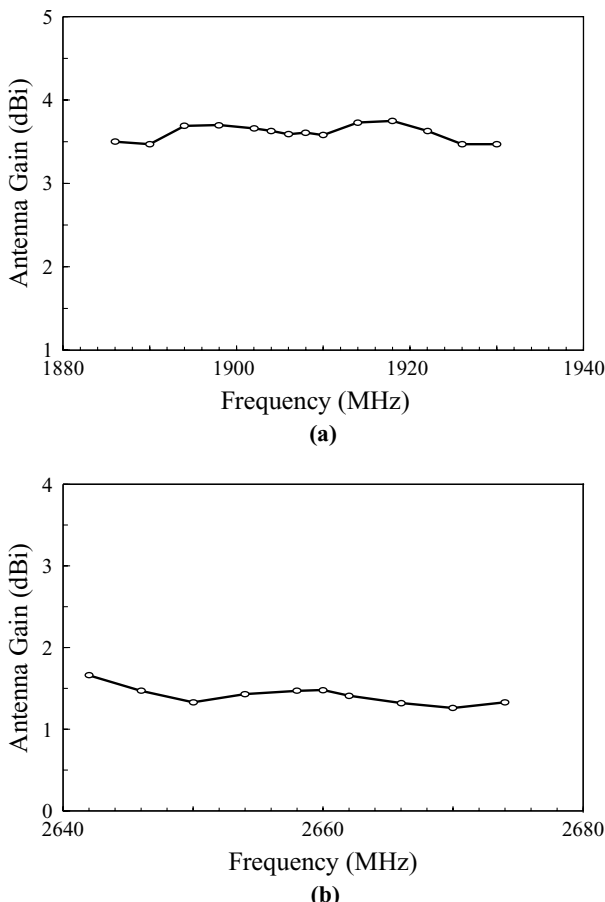


**FIGURE 9.40** Measured antenna gain for the antenna studied in Figure 9.37. (a) The lower band, (b) the upper band. (From Ref. 12, © 2000 John Wiley & Sons, Inc.)

The antenna gain variations in the CP bandwidth are less than 1 dBi for both bands, and the peak antenna gain for the lower and upper bands is about 3.7 and 1.5 dBi, respectively.

## REFERENCES

1. C. Y. Huang, J. Y. Wu, and K. L. Wong, "Slot-coupled microstrip antenna for broadband circular polarization," *Electron. Lett.* **34**, 835–836, April 30, 1998.
2. C. Wang and K. Chang, "A novel CP patch antenna with a simple feed structure," in *2000 IEEE Antennas Propagat. Soc. Int. Symp. Dig.*, pp. 1000–1003.
3. N. Hershovici, "New considerations in the design of microstrip antennas," *IEEE Trans. Antennas Propagat.* **46**, 807–812, June 1998.
4. S. D. Targonski and D. M. Pozar, "Design of wideband circularly polarized aperture-coupled microstrip antennas," *IEEE Trans. Antennas Propagat.* **41**, 214–220, Feb. 1993.
5. F. E. Gardiol and J.-F. Zuercher, "Broadband patch antennas—A SSFIP update," in *1996 IEEE Antennas Propagat. Soc. Int. Symp. Dig.*, pp. 2–5.
6. T. W. Chiou and K. L. Wong, "Single-layer wideband probe-fed circularly polarized microstrip antenna," *Microwave Opt. Technol. Lett.* **25**, 74–76, April 5, 2000.
7. K. L. Wong and T. W. Chiou, "A broadband single-patch circularly polarized microstrip antenna with dual capacitively-coupled feeds," *IEEE Trans. Antennas Propagat.* **49**, 41–44, Jan. 2000.
8. D. M. Pozar and S. M. Duffy, "A dual-band circularly polarized aperture-coupled stacked microstrip antenna for global positioning satellite," *IEEE Trans. Antennas Propagat.* **45**, 1618–1625, Nov. 1997.
9. D. Sanchez-Hernandez and I. D. Robertson, "Analysis and design of a dual-band circularly-polarized microstrip patch antenna," *IEEE Trans. Antennas Propagat.* **43**, 201–205, Feb. 1995.
10. K. B. Hsieh, M. H. Chen, and K. L. Wong, "Single-feed dual-band circularly polarized microstrip antenna," *Electron. Lett.* **34**, 1170–1171, June 11, 1998.
11. K. P. Yang and K. L. Wong, "Dual-band circularly-polarized square microstrip antenna," *IEEE Trans. Antennas Propagat.* **49**, 377–382, March 2001.
12. J. Y. Jan and K. L. Wong, "A dual-band circularly polarized stacked elliptic microstrip antenna," *Microwave Opt. Technol. Lett.* **24**, 354–357, March 5, 2000.
13. M. Muraguchi, T. Yukitake, and Y. Naito, "Optimum design of 3-dB branch-line couplers using microstrip lines," *IEEE Trans. Microwave Theory Tech.* **31**, 674–679, 1983.
14. J. S. Kuo, Novel broadband designs of microstrip antennas, Ph.D. dissertation, Department of Electrical Engineering, National Sun Yat-Sen University, Kaohsiung, Taiwan, 2001.
15. S. Maci, G. Biffi Gentili, P. Pazzesi, and C. Salvador, "Dual-band slot-loaded patch antenna," *IEE Proc. Microw. Antennas Propagat.* **142**, 225–232, June 1995.
16. P. C. Sharma and K. C. Gupta, "Analysis and optimized design of single feed circularly polarized microstrip antennas," *IEEE Trans. Antennas Propagat.* **31**, 949–955, Nov. 1983.